# GENETIC AND ENDOCRINE FACTORS INFLUENCING JUVENILE-ONSET GRANULOSA CELL TUMOURIGENESIS

by

© Kerri Nicole Smith B.Sc. (Hons.), M.Sc.

A thesis submitted to the

School of Graduate Studies

in partial fulfillment of the

requirements of the degree of

Doctor of Philosophy

Division of BioMedical Sciences (Cancer and Development)

Faculty of Medicine

Memorial University of Newfoundland

October 2020

St. John's Newfoundland and Labrador

## Abstract

Granulosa cell (GC) tumours are a rare ovarian neoplasm divided into adult and juvenile clinicopathologic subtypes. Whereas the adult-onset phenotype is attributed to an acquired mutation in the GC differentiation marker forkhead box L2 (*FOXL2*), the etiology of juvenile GC tumours is unknown. SWR/Bm (SWR) inbred strain female mice are spontaneously susceptible to the pubertal initiation of juvenile-onset GC tumours of the ovary. This heritable trait shares histological, endocrinological and malignant features with those GC tumours that appear in infants and young girls, and so the SWR strain is recognized as a model system for the identification of susceptibility genes and endocrine influences. Phenotypic mapping studies have consistently associated granulosa cell tumour susceptibility (*Gct*) loci with the GC tumour phenotype. The *Gct1* locus on distal mouse chromosome (Chr) 4 is the driver in the SWR model, whereas the *Gct4* locus on Chr X modifies tumour susceptibility in the presence of homozygous SWR-derived *Gct1* ($Gct1^{SW}$) alleles. The identity of the dehydroepiandrosterone (DHEA)-responsive *Gct1* gene remains unresolved, although substantial evidence suggests the androgen receptor (*Ar*) gene shares identity with *Gct4*. The influence of these genes on tumour initiation is confined to the ovarian GCs over a short window of susceptibility, which coincides with pubertal endocrine stimulation and the activation of the first follicle wave from the ovarian medulla. Based on the genetic and endocrine evidence and using a combination of the SWR inbred strain, congenic sublines, and engineered constructs transferred to the SWR background, we sought to: 1) elucidate *Gct1* identity using fine mapping, comprehensive genetic analyses, and *in vivo* candidate investigations; 2) delete the AR protein from the GC population to test its requirement for androgen-induced tumour initiation; and 3) lineage trace the GC tumour cell of origin using

an inducible fluorescent reporter system, with GC-specificity conferred by an engineered construct that displaced a single *Foxl2* allele.

The *Gct1* locus was resolved to 1.65 Mb and a candidate list of 18 unique annotated protein coding genes, non-coding RNA genes, and other processed transcripts with the addition of two nucleotide polymorphisms to a genetic maker panel for 12 previously phenotyped congenic mouse sublines. Complete genetic annotation of the SWR *Gct1* interval by next-generation sequencing and copy number analysis identified a splice site variant (c.460-3C>T) in the dehydrogenase/reductase (SDR family) member 3 (*Dhrs3*) gene predicted to be highly pathogenic, whereas functional analyses did not reveal any candidates capable of initiating GC tumours in SWR females or GC tumour-resistant mice. No tumours arose in ovaries that were AR protein-negative in the GC population despite the retention of homozygous $Gct1^{SW}$ alleles, suggesting that the AR is required for GC tumour initiation. SWR females carrying the engineered *Foxl2* allele were resistant to the androgen-induced GC tumour phenotype. Haploinsufficiency for *Foxl2* therefore precluded the lineage tracing experiment, but suggests that the pathway for ovarian specification involving *Foxl2* influences, or is influenced by, the activity of the *Gct1* locus. Together, these genetic investigations support a two-stage tumour susceptibility model for *Gct* allele activity, in which establishment of GC tumour susceptibility requires the *Gct1* driver locus and *Foxl2* transcription factor in the developing ovary, and GC tumour initiation in a genetically susceptible juvenile ovary requires androgenic signalling through the AR. Although the complexities of GC tumour susceptibility in the SWR mouse model have yet to be fully unraveled, the validity of the genetic contribution is clear and potentially relevant for pediatric cases of juvenile-onset GC tumours.

## Acknowledgements

First and foremost, I would like to thank my supervisor, Dr. Ann Dorward, for giving me this opportunity, having patience during my graduate training, and teaching me to think critically. I am also indebted to Dr. Dorward for helping to further my academic career by allowing me to attend conferences and apply for funding and scholarships. Her tireless efforts and great attitude towards research have not gone unnoticed.

I would like to thank my supervisory committee, Dr. Sevtap Savas and Dr. Laura Gillespie. Their valuable comments and constructive criticisms were greatly appreciated.

Thank you to the members of the Dorward lab for technical help, including Sarah Halfyard, Dr. Edward Yaskowiak, Elizabeth Chia, and Kayleigh Maxwell, among others.

I would also like to acknowledge the funding agencies that have financially supported me and this project: the Canadian Institutes of Health Research, the Research & Development Corporation of Newfoundland and Labrador, the Janeway Foundation, the Granulosa Cell Tumour Research Foundation, and the Faculty of Medicine and School of Graduate Studies of Memorial University of Newfoundland. Thanks also to the Faculty of Medicine's Office of Research and Graduate Studies, the Canadian Cancer Society, the Canadian Conference on Ovarian Cancer Research, the Canadian Institutes of Health Research, the International Mammalian Genome Society, and the Beatrice Hunter Cancer Research Institute for travel funds, as well as to Ovarian Cancer Canada for their support through the Teal Heart Award.

Finally, thank you to my friends, family, and loved ones. Your support and encouragement has been immeasurable.

## Table of Contents

## List of Tables

## List of Figures

## List of Abbreviations and Symbols

| | |
|---|---|
| + | wild type allele |
| °C | degrees Celsius |
| µL | microlitre |
| µm | micrometre |
| µM | micromolar |
| 129P2 | 129P2/OlaHsd |
| 129S1 | 129S1/Sv-*Oca2*$^{+}$*Tyr*$^{+}$*Kitl*$^{Sl\text{-}J}$ |
| 129S7 | 129S7/SvEvBrd-*Hprt*$^{b\text{-}m2}$ |
| 129X1 | 129X1/SvJ |
| 17β-HSD | 17β-hydroxysteroid dehydrogenase |
| 3H-TdR | tritium-labelled thymidine |
| 3β-HSD | 3β-hydroxysteroid dehydrogenase |
| *6330411D24Rik* | mouse RIKEN cDNA 6330411D24Rik gene |
| $A_4$ | androstenedione |
| ABC | avidin-biotin complex |
| AC | adenylyl cyclase |
| aCGH | array comparative genomic hybridization |
| *ACTB* | human actin beta gene |
| *Actb* | mouse actin, beta gene |
| ACVR1 | activin A receptor type-1 protein |
| ACVR1B | activin A receptor type-1B protein |
| ACVR2A | activin receptor type-2A protein |
| ACVR2B | activin receptor type-2B protein |
| ADAM17 | disintegrin and metalloproteinase domain-containing protein 17 |
| ADM | Aberration Detection Method |
| AF-1 | activation function 1 |
| AF1 | allele frequency |
| AF-2 | activation function 2 |
| *AKT1* | human AKT serine/threonine kinase 1 gene |
| Ala | alanine |
| ALDH | aldehyde dehydrogenase |
| AMH | anti-Müllerian hormone |
| *Amhr2* | mouse anti-Müllerian hormone type 2 receptor gene |
| AMHR2 | anti-Müllerian hormone type 2 receptor protein |
| *Amhr2*$^{cre}$ | *Amhr2*$^{tm3(cre)Bhr}$ allele |
| *Amhr2-cre* | B6;129S7-*Amhr2*$^{tm3(cre)Bhr}$/Mmnc mouse strain |
| ANOVA | analysis of variance |
| AP-1 | activator protein 1 |
| AR | androgen receptor protein |
| *AR* | human androgen receptor gene |
| *Ar* | mouse androgen receptor gene |
| ARE | androgen response element |

| | |
|---|---|
| *Areg* | mouse amphiregulin gene |
| $Ar^{flox}$ | $Ar^{tm1Verh}$ allele |
| *Ar-flox* | B6N.129-$Ar^{tm1Verh}$/Cnrm mouse strain |
| Arg | arginine |
| *ARID1A* | human AT-rich interaction domain A1 gene |
| ArKO | androgen receptor gene knockout |
| B6J | C57BL/6J |
| B6N | C57BL/6N |
| BAX | BCL2-associated X protein |
| BCL | B cell lymphoma |
| BCL2L1 | BCL2-like 1 protein |
| BLAST | Basic Local Alignment Search Tool |
| BMP | bone morphogenetic protein |
| *Bmp15* | mouse bone morphogenetic protein 15 gene |
| BMP15 | bone morphogenetic protein 15 |
| BMP2 | bone morphogenetic protein 2 |
| *Bmp2* | mouse bone morphogenetic protein 2 gene |
| BMP4 | bone morphogenetic protein 4 |
| *Bmp4* | mouse bone morphogenetic protein 4 gene |
| BMP8B | bone morphogenetic protein 8b |
| *Bmp8b* | mouse bone morphogenetic protein 8b gene |
| *Bmpr1a* | mouse bone morphogenetic protein receptor, type 1A gene |
| BMPR1A | bone morphogenetic protein receptor type-1A protein |
| BMPR1B | bone morphogenetic protein receptor type-1B protein |
| *Bmpr1b* | mouse bone morphogenetic protein receptor, type 1B gene |
| bp | base pair |
| BPES | blepharophimosis, ptosis, and epicanthus inversus syndrome |
| *BRAF* | human B-Raf proto-oncogene, serine/threonine kinase gene |
| *BRCA1* | human BRCA1 DNA repair associated gene |
| *BRCA2* | human BRCA2 DNA repair associated gene |
| *Btc* | mouse betacellulin, epidermal growth factor family member gene |
| BWA | Burrows-Wheeler Aligner |
| BWS | Beckwith-Wiedmann syndrome |
| CA | Castaneus allele |
| CAIS | complete androgen insensitivity syndrome |
| cAMP | cyclic adenosine monophosphate |
| *Casp2* | mouse caspase 2 gene |
| CAST | Castaneus |
| CBX2 | chromobox 2 protein |
| *Cbx2* | mouse chromobox 2 gene |
| CCNB1 | cyclin B1 protein |
| *CCND2* | human cyclin D2 gene |
| *Ccnd2* | mouse cyclin D2 gene |
| CCND2 | cyclin D2 protein |
| CCNE1 | cyclin E1 protein |
| CCNE2 | cyclin E2 protein |

| | |
|---|---|
| CD120a | cluster of differentiation 120a protein |
| CD120b | cluster of differentiation 120b protein |
| CD30 | cluster of differentiation 30 protein |
| CD30L | cluster of differentiation 30 ligand |
| CD99 | cluster of differentiation 99 protein |
| CDK1 | cyclin dependent kinase 1 protein |
| CDK2 | cyclin dependent kinase 2 protein |
| CDK4 | cyclin dependent kinase 4 protein |
| *Cdk4* | mouse cyclin dependent kinase 4 gene |
| CDK6 | cyclin dependent kinase 6 protein |
| *Cdkn1b* | mouse cyclin-dependent kinase inhibitor 1B gene |
| *CDKN1C* | human cyclin dependent kinase inhibitor 1C gene |
| cDNA | complementary DNA |
| *Cflar* | mouse CASP8 and FADD-like apoptosis regulator gene |
| Chr | chromosome |
| cIAP1 | cellular inhibitor of apoptosis 1 protein |
| cIAP2 | cellular inhibitor of apoptosis 2 protein |
| cm | centimetre |
| CMV | cytomegalovirus |
| CNV | copy number variation |
| $CO_2$ | carbon dioxide |
| COC | cumulus-oocyte complex |
| *Col1a2* | mouse collagen, type 1, alpha 2 gene |
| Cre | cre recombinase |
| CREB | cyclic AMP-responsive element-binding protein |
| *Ctnnb1* | mouse catenin (cadherin associated protein), beta 1 gene |
| *CTNNB1* | human catenin beta 1 gene |
| CX37 | connexin 37 protein |
| CX43 | connexin 43 protein |
| CXCL12 | C-X-C motif chemokine ligand 12 protein |
| CXCR4 | chemokine receptor type 4 protein |
| Cy | cyanine |
| CYP11A1 | cytochrome P450 family 11 subfamily A member 1 protein |
| *CYP11A1* | human cytochrome P450 family 11 subfamily A member 1 gene |
| CYP17A1 | cytochrome P450 family 17 subfamily A member 1 protein |
| *Cyp17a1* | mouse cytochrome P450 family 17 subfamily A member 1 gene |
| CYP19A1 | cytochrome P450 family 19 subfamily A member 1 protein |
| *CYP19A1* | human cytochrome P450 family 19 subfamily A member 1 gene |
| *Cyp19a1* | mouse cytochrome P450 family 19 subfamily A member 1 gene |
| Cys | cysteine |
| d | day |
| DAB | 3,3′-diaminobenzidine |
| DAX1 | dosage-sensitive sex reversal-adrenal hypoplasia congenital critical region on the X chromosome, gene 1 protein |
| *DAX1* | human dosage-sensitive sex reversal-adrenal hypoplasia congenital critical region on the X chromosome, gene 1 |

| | |
|---|---|
| *Dax1* | mouse dosage-sensitive sex reversal-adrenal hypoplasia congenital critical region on the X chromosome, gene 1 |
| DAZL | deleted in azoospermia-like protein |
| DBD | DNA-binding domain |
| dbSNP | Single Nucleotide Polymorphism Database |
| DD | death domain |
| DGVa | Database of Genomic Variants archive |
| DHEA | dehydroepiandrosterone |
| DHEA-S | sulfonated DHEA |
| DHH | desert hedgehog protein |
| DHT | 5α-dihydrotestosterone |
| *DICER1* | human dicer 1, ribonuclease III gene |
| DKK1 | dickkopf WNT signaling pathway inhibitor 1 |
| dKO | double knockout |
| *Dmrt1* | mouse doublesex and mab-3 related transcription factor 1 gene |
| *DMRT1* | human doublesex and mab-3 related transcription factor 1 gene |
| DNA | deoxyribonucleic acid |
| DND1 | DND microRNA-mediated repression inhibitor 1 protein |
| *Dnd1* | mouse DND microRNA-mediated repression inhibitor 1 gene |
| dNTP | deoxynucleotide triphosphate |
| *Dppa3* | mouse developmental pluripotency associated 3 gene |
| E | embryonic day |
| $E_1$ | estrone |
| $E_2$ | 17β-estradiol |
| ECM | extracellular matrix |
| EDTA | ethylenediaminetetraacetic acid |
| EGF | epidermal growth factor |
| EGFP | enhanced green fluorescent protein |
| EGFR | epidermal growth factor receptor protein |
| ELISA | enzyme-linked immunosorbent assay |
| *Emx2* | mouse empty spiracles homeobox 2 gene |
| EOC | epithelial ovarian cancer |
| *Erbb2* | mouse erb-b2 receptor tyrosine kinase 2 |
| *Ereg* | mouse epiregulin gene |
| $ER^{T2}$ | tamoxifen-inducible mutated estrogen receptor hormone-binding domain |
| ESE | exonic splicing enhancer |
| ESR1 | estrogen receptor 1 protein |
| *Esr1* | mouse estrogen receptor 1 gene |
| ESR2 | estrogen receptor 2 protein |
| *Esr2* | mouse estrogen receptor 2 gene |
| EST | expressed sequence tag |
| Ex1 | *Ar* exon 1 |
| Ex2 | *Ar* exon 2 |
| Ex3 | *Ar* exon 3 |
| F | filial generation |
| FADD | Fas associated via death domain protein |

| | |
|---|---|
| *Fancf* | mouse Fanconi anemia, complementation group F gene |
| FANCF | Fanconi anemia group F protein |
| FAS | Fas (TNF receptor superfamily member 6) protein |
| *Fas* | mouse Fas (TNF receptor superfamily member 6) gene |
| *Fasl* | mouse Fas ligand (TNF superfamily, member 6) gene |
| *Fblim1* | mouse filamin binding LIM protein 1 gene |
| FGF9 | fibroblast growth factor 9 protein |
| *Fgf9* | mouse fibroblast growth factor 9 gene |
| FGFR2 | fibroblast growth factor receptor 2 protein |
| FIGLA | folliculogenesis specific basic helix-loop-helix protein |
| FIGO | International Federation of Gynecology and Obstetrics |
| FOG2 | friend of GATA2 protein |
| *Foxl2* | mouse forkhead box L2 gene |
| FOXL2 | forkhead box L2 protein |
| *FOXL2* | human forkhead box L2 gene |
| *Foxo1* | mouse forkhead box O1 gene |
| FOXO1 | forkhead box O1 protein |
| *Foxo3* | mouse forkhead box O3 gene |
| FOXO3 | forkhead box O3 protein |
| fs | frameshift |
| FSH | follicle stimulating hormone |
| *FSHB* | human follicle stimulating hormone subunit beta gene |
| *Fshb* | mouse follicle stimulating hormone beta gene |
| FSHR | follicle stimulating hormone receptor protein |
| *FSHR* | human follicle stimulating hormone receptor gene |
| *Fshr* | mouse follicle stimulating hormone receptor gene |
| FST | follistatin protein |
| *FST* | human follistatin gene |
| *Fst* | mouse follistatin gene |
| FZD | frizzled protein |
| g | gram |
| *Gata4* | mouse GATA binding protein 4 gene |
| GATA4 | GATA binding protein 4 protein |
| GC | granulosa cell |
| GCE | GFP-creER$^{T2}$ |
| *Gct* | granulosa cell tumour susceptibility |
| *GDF9* | growth differentiation factor 9 protein |
| *Gdf9* | mouse growth differentiation factor 9 gene |
| gDNA | genomic DNA |
| GDP | guanosine diphosphate |
| GFP | green fluorescent protein |
| *Gja1* | mouse gap junction protein, alpha 1 gene |
| *Gja4* | mouse gap junction protein, alpha 4 gene |
| GLI1 | GLI-Kruppel family member GLI1 protein |
| Gln | glutamine |
| *GNAS* | human GNAS complex locus gene |

| | |
|---|---|
| GnRH | gonadotropin-releasing hormone |
| *GNRHR* | human gonadotropin releasing hormone receptor gene |
| GPCR | G protein-coupled receptor |
| GRCh37 | Genome Reference Consortium Human Build 37 |
| GRCh38 | Genome Reference Consortium Human Build 38 |
| GRCm38 | Genome Reference Consortium Mouse Build 38 |
| GSK3B | glycogen synthase kinase 3 beta protein |
| GTP | guanosine triphosphate |
| GUDMAP | GenitoUrinary Development Molecular Anatomy Project |
| GVBD | germinal vesicle breakdown |
| h | hour |
| H&E | hematoxylin and eosin |
| H3K27me3 | trimethylated histone 3 lysine 27 |
| H3K9me2 | dimethylation at histone 3 lysine 9 |
| *Has2* | mouse hyaluronan synthase 2 gene |
| hCG | human chorionic gonadotropin |
| HGSC | high-grade serous carcinoma |
| hnRNP | heterogeneous nuclear ribonucleoprotein |
| *Hoxa1* | mouse homeobox A1 gene |
| *Hoxb1* | mouse homeobox B1 gene |
| *hpg* | hypogonadal |
| HPG | hypothalamic-pituitary-gonadal |
| HRP | horseradish peroxidase |
| HSP | heat shock protein |
| *IDH1* | human isocitrate dehydrogenase (NADP(+)) 1, cytosolic gene |
| *IDH2* | human isocitrate dehydrogenase (NADP(+)) 2, mitochondrial gene |
| IGF1 | insulin-like growth factor 1 protein |
| *Igf1* | mouse insulin-like growth factor 1 gene |
| *Igf1r* | mouse insulin-like growth factor 1 receptor gene |
| IGF1R | insulin-like growth factor 1 receptor protein |
| IgG | immunoglobulin G |
| IHC | immunohistochemistry |
| IHH | Indian hedgehog |
| *Inha* | mouse inhibin alpha gene |
| *INHA* | human inhibin subunit alpha gene |
| INSR | insulin receptor protein |
| J | SJL allele |
| kb | kilobase |
| kDa | kilodalton |
| *Kdm5c* | mouse lysine (K)-specific demethylase 5C gene |
| *Kdm5d* | mouse lysine (K)-specific demethylase 5D gene |
| kg | kilogram |
| *Kiss1* | mouse KiSS-1 metastasis-suppressor gene |
| KIT | KIT proto-oncogene receptor tyrosine kinase protein |
| *Kit* | mouse KIT proto-oncogene receptor tyrosine kinase gene |
| KITLG | KIT ligand protein |

| | |
|---|---|
| *Kitlg* | mouse KIT ligand gene |
| KO | knockout |
| KRAB | Krüeppel-associated box |
| *KRAS* | human KRAS proto-oncogene, GTPase gene |
| *Kras* | mouse Kirsten rat sarcoma viral oncogene homolog gene |
| KREMEN1 | kringle containing transmembrane protein 1 |
| KTS | lysine-threonine-serine |
| L | litre |
| LBD | ligand-binding domain |
| Leu | leucine |
| LGR4 | leucine rich repeat containing G protein-coupled receptor 4 |
| LGR5 | leucine rich repeat containing G protein-coupled receptor 5 |
| LGR6 | leucine rich repeat containing G protein-coupled receptor 6 |
| LH | luteinizing hormone |
| *Lhb* | mouse luteinizing hormone subunit gene |
| LHB | luteinizing hormone subunit protein |
| LHCGR | LH receptor protein |
| LHX8 | LIM homeobox protein 8 |
| *Lhx8* | mouse LIM homeobox protein 8 gene |
| LHX9 | LIM homeobox protein 9 |
| *Lhx9* | mouse LIM homeobox protein 9 gene |
| Line 4-3 | SWR.SJL-X.CAST-4-3 |
| Line 4-5 | SWR.SJL-X.CAST-4-5 |
| Line 4-T | SWR.SJL-X.CAST-4-T |
| lncRNA | long intergenic non-coding RNA |
| *loxP* | locus of X-over P |
| LRP6 | low-density lipoprotein receptor related protein 6 |
| Lys | lysine |
| M | molar |
| MAPK | mitogen-activated protein kinase |
| Mb | million base pair |
| MCL1 | myeloid cell leukemia sequence 1 protein |
| MEF | mouse embryonic fibroblast |
| *Men1* | mouse multiple endocrine neoplasia 1 gene |
| Met | methionine |
| mg | milligram |
| mG | membrane-targeted EGFP |
| MGD | Mouse Genome Database |
| min | minute |
| miRNA | microRNA |
| mL | millilitre |
| mm | millimetre |
| mM | millimolar |
| MMRRC | Mutant Mouse Resource and Research Center |
| mo | month |
| MPF | maturation-promoting factor |

| | |
|---|---|
| mRNA | messenger RNA |
| mT | membrane-targeted tdTomato |
| mTNF | membrane-bound TNF |
| mTOR | mechanistic target of rapamycin protein |
| mTORC1 | mTOR complex 1 |
| *Mts1* | mammary tumour susceptibility 1 |
| MUP | major urinary protein |
| n | sample size |
| N | backcross generation |
| $NAD^+$ | nicotinamide adenine dinucleotide |
| $NADP^+$ | nicotinamide adenine dinucleotide phosphate |
| NADPH | nicotinamide adenine dinucleotide phosphate (reduced) |
| *Nanog* | mouse nanog homeobox gene |
| *Nanos3* | mouse nanos C2HC-type zinc finger 3 gene |
| NANOS3 | nanos C2HC-type zinc finger 3 protein |
| NCBI | National Center for Biotechnology Information |
| NES | nuclear export signal |
| NF-κB | nuclear factor kappa B |
| ng | nanogram |
| NGS | next-generation sequencing |
| NLS | nuclear localization signal |
| *Nobox* | mouse NOBOX oogenesis homeobox gene |
| NOBOX | NOBOX oogenesis homeobox protein |
| *Nr0b1* | mouse nuclear receptor subfamily 0 group B member 1 gene |
| *NR5A1* | human nuclear receptor subfamily 5 group A member 1 gene |
| *Nr5a1* | mouse nuclear receptor subfamily 5, group A, member 1 gene |
| NTD | N-terminal transactivation domain |
| OCT | optimal cutting temperature |
| OMIM | Online Mendelian Inheritance in Man |
| Oo | oocyte |
| P | postnatal day |
| p16/INK4A | cyclin dependent kinase inhibitor 2A protein |
| $p21^{Cip1}$ | cyclin dependent kinase inhibitor 1A protein |
| $p27^{Kip1}$ | cyclin dependent kinase inhibitor 1B protein |
| $P_4$ | progesterone |
| p53 | tumour protein p53 |
| p63 | tumour protein p63 |
| PBS | phosphate-buffered saline |
| PCOS | polycystic ovary syndrome |
| PCR | polymerase chain reaction |
| PDK1 | pyruvate dehydrogenase kinase, isoenzyme 1 protein |
| pg | picogram |
| PGC | primordial germ cell |
| *Pgr* | mouse progesterone receptor gene |
| Phe | phenylalanine |
| PI3K | phosphatidylinositide 3-kinase protein |

| | |
|---|---|
| *PIK3CA* | human phosphatidylinositol-4,5-bisphosphate 3-kinase catalytic subunit alpha gene |
| *Pik3ca* | mouse phosphatidylinositol-4,5-bisphosphate 3-kinase catalytic subunit alpha gene |
| PIS | polled intersex syndrome |
| PJS | Peutz-Jeghers syndrome |
| PKA | protein kinase A |
| PKB | protein kinase B |
| pmol | picomol |
| PMSG | pregnant mare serum gonadotropin |
| POF | premature ovarian failure |
| *Pou5f1* | mouse POU class 5 homeobox 1 gene |
| *Ppargc1b* | mouse peroxisome proliferative activated receptor, gamma, co-activator 1 beta gene |
| *Pramel5* | mouse preferentially expressed antigen in melanoma like 5 gene |
| PRDM1 | PR/SET domain 1 protein |
| PRDM14 | PR/SET domain 14 protein |
| *Prdm2* | mouse PR domain containing 2, with ZNF domain gene |
| Pro | proline |
| *PTEN* | human phosphatase and tensin homolog gene |
| *Pten* | mouse phosphatase and tensin homolog gene |
| PTGDS | prostaglandin D2 synthase protein |
| *Ptgs2* | mouse prostaglandin-endoperoxide synthase 2 gene |
| *Ptx3* | mouse pentraxin related gene |
| RA | all-*trans*-retinoic acid |
| RAL | all-*trans*-retinaldehyde |
| RAR | retinoic acid receptor |
| RAS | rat sarcoma protein |
| RB | retinoblastoma |
| *Rb1* | mouse RB transcriptional corepressor 1 gene |
| RDH10 | retinol dehydrogenase 10 (all-trans) protein |
| REC8 | REC8 meiotic recombination protein |
| *Rec8* | mouse REC8 meiotic recombination protein gene |
| RefSeq | Reference Sequence |
| RI | recombinant inbred |
| RIN | RNA integrity number |
| RIPK1 | receptor interacting serine/threonine kinase 1 protein |
| RISC | RNA-induced silencing complex |
| RNA | ribonucleic acid |
| ROL | all-*trans*-retinol |
| rpm | revolutions per minute |
| *RSPO1* | human R-spondin 1 gene |
| *Rspo1* | mouse R-spondin 1 gene |
| RSPO1 | R-spondin 1 protein |
| RT | room temperature |
| RT-PCR | reverse transcription polymerase chain reaction |

| | |
|---|---|
| *Runx1* | mouse runt related transcription factor 1 gene |
| RXR | retinoid X receptor |
| s | second |
| SCAR4 | spinocerebellar ataxia, autosomal recessive 4 |
| SCST | sex cord-stromal tumour |
| SDR | short-chain dehydrogenase/reductase |
| SDS | sodium dodecyl sulfate |
| SDSI | SRY-dependent SOX9-inducibility |
| SEM | standard error of the mean |
| Ser | serine |
| SERKAL | sex reversal and dysgenesis of kidney, adrenals and lungs |
| SERM | selective estrogen-receptor modulator |
| SF1 | steroidogenic factor 1 protein |
| SIFT | Sorting Tolerant from Intolerant |
| SJL | SJL/Bm |
| *Slc25a53* | mouse solute carrier family 25, member 53 gene |
| SLC25A53 | solute carrier family 25, member 53 protein |
| SLCT | Sertoli-Leydig cell tumour |
| *Smad1* | mouse SMAD family member 1 gene |
| SMAD1 | SMAD family member 1 protein |
| SMAD2 | SMAD family member 2 protein |
| SMAD3 | SMAD family member 3 protein |
| *Smad4* | mouse SMAD family member 4 gene |
| SMAD4 | SMAD family member 4 protein |
| *Smad5* | mouse SMAD family member 5 gene |
| SMAD5 | SMAD family member 5 protein |
| SMAD8 | SMAD family member 8 protein |
| SNP | single nucleotide polymorphism |
| snRNP | small nuclear ribonucleoprotein |
| SNV | single nucleotide variant |
| *Sohlh1* | mouse spermatogenesis and oogenesis specific basic helix-loop-helix 1 gene |
| SOHLH1 | spermatogenesis and oogenesis specific basic helix-loop-helix 1 protein |
| *Sohlh2* | mouse spermatogenesis and oogenesis specific basic helix-loop-helix 2 gene |
| SOHLH2 | spermatogenesis and oogenesis specific basic helix-loop-helix 2 protein |
| *Sox2* | mouse SRY (sex-determining region Y)-box 2 gene |
| SOX8 | SRY (sex determining region Y)-box 8 protein |
| *SOX9* | human SRY (sex determining region Y)-box 9 gene |
| *Sox9* | mouse SRY (sex determining region Y)-box 9 gene |
| SOX9 | SRY (sex determining region Y)-box 9 protein |
| SR | serine/arginine |
| SRC | Rous sarcoma oncogene |
| SRSF1 | serine and arginine rich splicing factor 1 protein |
| SRSF2 | serine and arginine rich splicing factor 2 protein |
| SRSF5 | serine and arginine rich splicing factor 5 protein |

| | |
|---|---|
| *SRY* | human sex determining region of chromosome Y gene |
| *Sry* | mouse sex determining region of chromosome Y gene |
| SRY | sex determining region of chromosome Y protein |
| SSLP | simple sequence length polymorphism |
| STAR | steroidogenic acute regulatory protein |
| *STAR* | human steroidogenic acute regulatory gene |
| STIC | serous tubal intra-epithelial carcinoma |
| *STK11* | human serine/threonine kinase 11 gene |
| sTNF | soluble TNF |
| *Stra8* | mouse stimulated by retinoic acid gene 8 gene |
| STRA8 | stimulated by retinoic acid gene 8 protein |
| SV40 | simian virus 40 |
| SW | SWR allele |
| SWR | SWR/Bm |
| SWXJ | (SWR x SJL) |
| SYCP3 | synaptonemal complex protein 3 |
| T | testosterone |
| T-ag | large T antigen |
| *Taq* | *Thermus aquaticus* |
| TAU-1 | transcriptional activation unit 1 |
| TAU-5 | transcriptional activation unit 5 |
| TBE | tris-borate-ethylenediaminetetraacetic acid |
| TC | thecal cell |
| *Tda1* | testis-determining autosomal 1 |
| tdTomato | tandem dimer tomato |
| TE | tris-ethylenediaminetetraacetic acid |
| Ter | termination codon |
| TES | testis specific enhancer of *Sox9* |
| TESCO | testis-specific enhancer of *Sox9* core element |
| *Tfm* | testicular feminization mutation |
| TGF-β | transforming growth factor beta |
| *Tgfbr1* | mouse transforming growth factor, beta receptor I gene |
| TGFBR3 | transforming growth factor, beta receptor III protein |
| Thr | threonine |
| TNF | tumor necrosis factor |
| *Tnfaip6* | mouse tumor necrosis factor alpha induced protein 6 gene |
| TNFRSF1A | tumor necrosis factor receptor superfamily member 1A protein |
| *TNFRSF1B* | human necrosis factor receptor superfamily, member 1b gene |
| *Tnfrsf1b* | mouse tumor necrosis factor receptor superfamily, member 1b gene |
| TNFRSF1B | tumor necrosis factor receptor superfamily, member 1b protein |
| *Tnfrsf8* | mouse tumor necrosis factor receptor superfamily, member 8 gene |
| TNFRSF8 | tumor necrosis factor receptor superfamily, member 8 protein |
| TNFSF8 | tumor necrosis factor (ligand) superfamily, member 8 protein |
| *TP53* | human tumor protein p53 gene |
| TRADD | TNFRSF1A associated via death domain |
| TRAF2 | TNF receptor associated factor 2 |

| | |
|---|---|
| Trp | tryptophan |
| TSC1 | tuberous sclerosis 1 protein |
| TSC2 | tuberous sclerosis 2 protein |
| TSL | transcript support level |
| UBA | ubiquitin-associated domain |
| UTR | untranslated region |
| V | volt |
| Val | valine |
| VEP | Variant Effect Predictor |
| VPS13 | vacuolar protein sorting 13 |
| *VPS13A* | human vacuolar protein sorting 13 homolog A gene |
| *VPS13B* | human vacuolar protein sorting 13 homolog B gene |
| *VPS13C* | human vacuolar protein sorting 13 homolog C gene |
| *VPS13D* | human vacuolar protein sorting 13 homolog D gene |
| *Vps13d* | mouse vacuolar protein sorting 13D gene |
| VPS13D | vacuolar protein sorting 13D protein |
| wk | week |
| *Wnt3* | mouse wingless-type MMTV integration site family, member 3 gene |
| WNT3 | Wnt family member 3 protein |
| *WNT4* | human Wnt family member 4 gene |
| *Wnt4* | mouse wingless-type MMTV integration site family, member 4 gene |
| WNT4 | Wnt family member 4 protein |
| WSI | Wellcome Sanger Institute |
| WT | wild type |
| *WT1* | human WT1 transcription factor gene |
| *Wt1* | mouse Wilms tumour 1 homolog gene |
| WT1 | Wilms tumour 1 homolog protein |
| *Xiap* | mouse X-linked inhibitor of apoptosis gene |
| yr | year |
| ZNF | zinc finger |

## List of Appendices

## Preamble for Dissertation Layout and Content

This dissertation is presented in traditional format according to the guidelines of Memorial University, incorporating a full introduction to the background literature and mouse model system explored, followed by three novel research chapters and a summary chapter with suggested future directions. In order to place more detailed introductory material in context, each research chapter has a shorter, more specific introduction section that is relevant to the research topic of the chapter, followed by methods, results and conclusions on the research outcomes. It is important for the reader to recognize that the first research chapter (Chapter 2) presents cumulative knowledge and builds on a genetic mapping refinement strategy for a specific locus on mouse chromosome 4, which was originally investigated during the course of my MSc (Medicine) program completed at Memorial University in the laboratory of Dr. Ann Dorward. This previous material is published in my MSc thesis (Smith 2011) and as a peer-reviewed scientific article (Smith *et al*. 2013; *Mammalian Genome* 24(1-2):63-71). Specifically, the work published in my MSc thesis described the phenotype-driven refinement of the *Gct1* interval using 12 subcongenic mouse lines to 1.86 Mb, whereas this dissertation details my efforts to create additional subcongenic animals and further refines the 1.86 Mb interval to 1.65 Mb. Chapter 2 also includes other novel and previously unpublished research strategies focused on resolving the identity of *Gct1*. Working on the same mouse model system and ovarian phenotype for my PhD as my MSc, all efforts were made to update the introductory and methodology descriptions that accompany the novel research results obtained during my PhD program, and the MSc thesis and *Mammalian Genome* publication are cited where appropriate. Chapter 3 and

Chapter 4 represent entirely unique research objectives for my PhD, in addition to the new findings presented in Chapter 2.

# 1. General Introduction

## 1.1 Ovarian Physiology

### 1.1.1 Overview of Ovarian Structure and Function

The mammalian ovary functions as the female reproductive organ and as such is primarily responsible for gametogenesis and steroidogenesis; together, these processes result in the production of competent germ cells capable of fertilization and embryo implantation. The ovaries are paired intra-abdominal organs that sit within the pelvic cavity. The mature ovary consists of an inner medulla and an outer cortex (Figure 1.1). The medulla is comprised mainly of lymphatic, nervous, vascular, and connective tissue. The cortex is covered by the surface epithelium, a specialized mesothelium, under which lies a dense band of connective tissue termed the tunica albuginea. Within the cortex and under the tunica albuginea are the follicles, which are composed of a single oocyte surrounded by the somatic granulosa cells (GCs) and thecal cells (TCs). The follicles form the functional units of the ovary, as they nourish the oocyte throughout development and are a major source of steroid hormones. Normal follicle development is regulated by the hypothalamic-pituitary-gonadal (HPG) axis (Figure 1.2), in which gonadotropin-releasing hormone (GnRH) secreted by the hypothalamus stimulates the gonadotrope cells of the anterior pituitary to release follicle stimulating hormone (FSH) and luteinizing hormone (LH). These gonadotropins are subject to cyclic regulation through positive and negative feedback from the ovarian follicles. These endocrine influences, in addition to the autocrine and paracrine factors that signal within the ovary, function to stimulate follicular growth and development, ultimately resulting in the ovulation of mature oocytes.

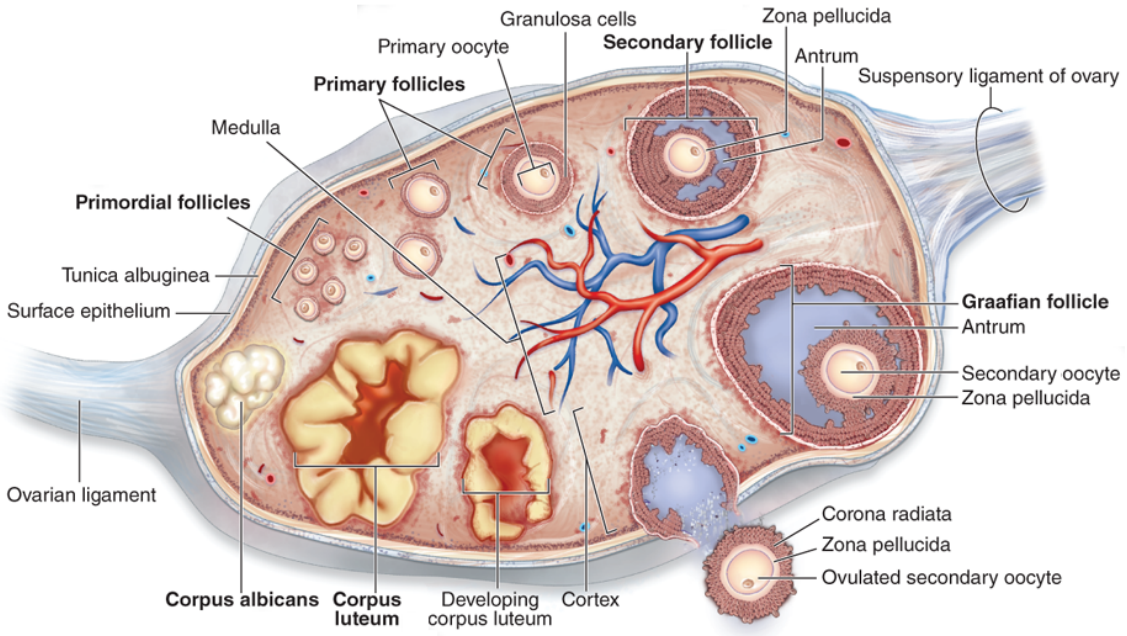


**Figure 1.1 Ovarian anatomy and cellular components**

The mammalian ovary is a bilateral endocrine and reproductive organ in the fertile female. A surface epithelium covers the tunica albuginea, which surrounds a cortex of follicles at different stages of maturation. The inner ovary, or medulla, is an area of vascular concentration. Each growing follicle consists of a developing oocyte and companion GCs, surrounded by a basement membrane and a TC layer. Post-ovulation, remaining GCs luteinize to produce the steroidogenic corpus luteum. In the absence of pregnancy, the corpus luteum regresses to a corpus albicans. Republished in adapted form with permission of McGraw-Hill Education, from Junqueira's Basic Histology: Text and Atlas, Mescher, 15th edition, copyright 2018; permission conveyed through Copyright Clearance Center, Inc.

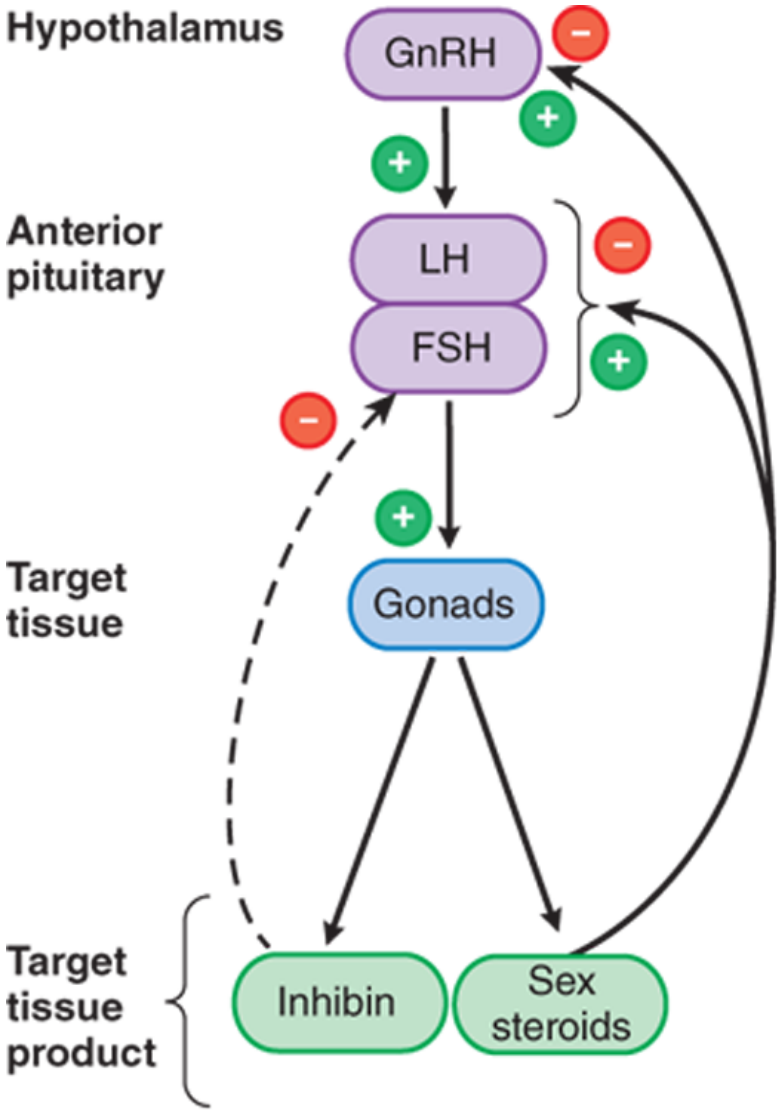


**Figure 1.2 The hypothalamic-pituitary-gonadal axis**

Reproductive cyclicity is controlled by the HPG axis. The hypothalamus secretes GnRH, which functions to stimulate the gonadotrope cells within the anterior pituitary to release FSH and LH into the systemic circulation. Together, these gonadotropins stimulate follicle growth and steroidogenesis in the ovary. The net effect of steroid and inhibin production by ovarian cells under the influence of gonadotropins has both positive and negative feedback effects at the hypothalamus and the anterior pituitary. Republished in adapted form with permission of McGraw-Hill Education, from Goodman and Gilman's: The Pharmacological Basis of Therapeutics, Molitch & Schimmer, 13th edition, copyright 2018; permission conveyed through Copyright Clearance Center, Inc.

### 1.1.2 Ovarian Development

The complex process of female gonad specification is crucial for the formation of functional gonads capable of producing competent gametes and sex steroid hormones. Ovarian development begins in the early embryo with the specification and proliferation of primordial germ cells (PGCs) and their migration to the genital ridge, the formation of the gonad from precursor embryonic tissue, and the organization of germ cells and somatic cells into ovarian follicles (reviewed by Smith, Wilhelm & Rodgers 2014). At its outset, the primitive embryonic gonad is sexually undifferentiated and maintains the potential to differentiate into the testes or ovaries. Similarly, the PGCs, which are the precursors of oogonia and spermatogonia, are initially indistinguishable in female and male embryos. The earliest stages of gonad specification thus occur in a manner irrespective of chromosomal sex; this bipotential nature is unique among all mammalian cells and tissues. PGC and gonad differentiation are dictated only by specific signalling events from the third to sixth week (wk) of gestation in humans, equivalent to approximately embryonic day (E) 6.0 to E10.5 in the mouse as a model system (De Felici 2016). The factors that influence the specification process have been highly characterized through analyses of gene function, as well as insights from knockout (KO) mouse models and human disorders of sexual development.

#### 1.1.2.1 Primordial Germ Cell Specification and Migration

PGC specification begins with the induction of a small population of somatic, proximal epiblast cells to become competent for PGC formation (Figure 1.3). This process is regulated by the bone morphogenetic protein (BMP) family members BMP2, BMP4 and BMP8B (Lawson *et al*. 1999; Ying *et al*. 2000; Ying & Zhao 2001), which are secreted from the extra-embryonic

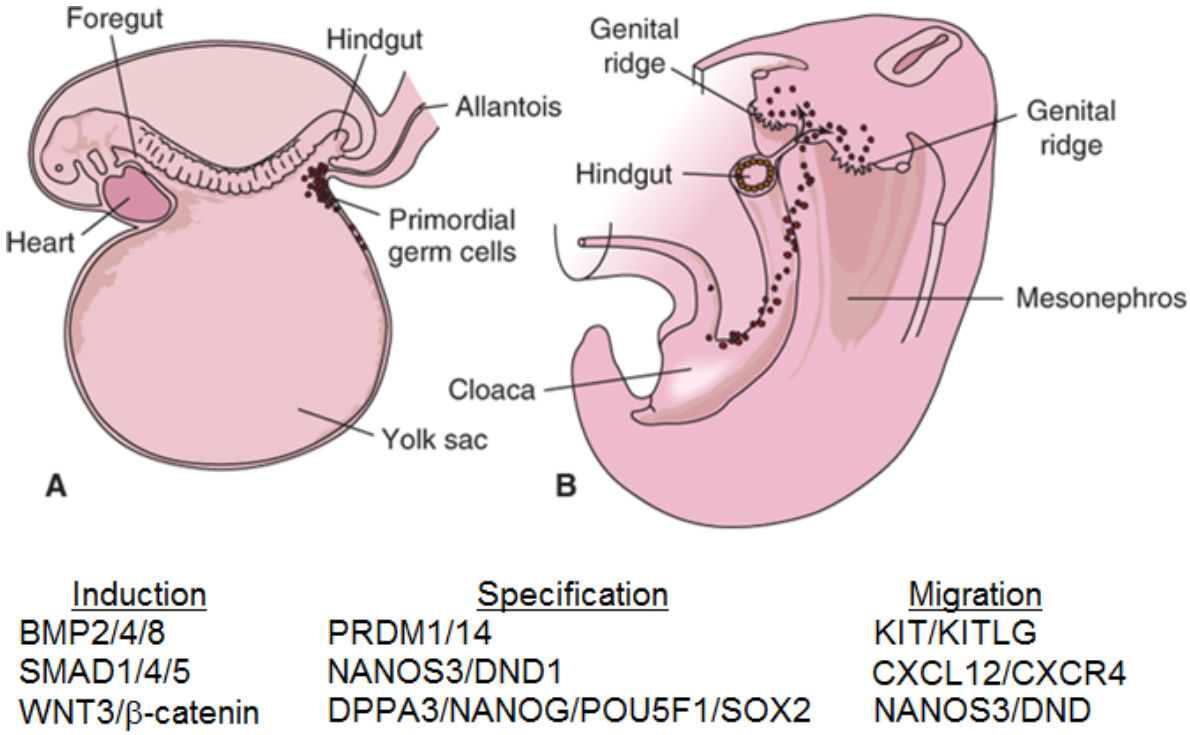


**Figure 1.3 Regulation of primordial germ cell specification and migration**

(A) PGC specification occurs from epiblast-derived cells present in the yolk sac near the base of the allantois. (B) Following their specification, PGCs migrate through the hindgut and into the bipotential genital ridge. Molecular markers and required factors are noted. Republished in adapted form with permission of McGraw-Hill Education, from Greenspan's Basic and Clinical Endocrinology, Rosen & Cedars, 10th edition, copyright 2018; permission conveyed through Copyright Clearance Center, Inc.

ectoderm and visceral endoderm prior to gastrulation (Chuva de Sousa Lopes, Hayashi & Surani 2007). The BMPs are members of the transforming growth factor beta (TGF-β) superfamily and transduce their signals through the SMAD family member 1 (SMAD1), SMAD5 and the SMAD4 common Smad transcription factors (Chang & Matzuk 2001; Tremblay, Dunn & Robertson 2001; Hayashi *et al*. 2002a; Chu *et al*. 2004), and act between E5.5 and E6.0 in the mouse to discriminate pluripotent cells near the embryonic yolk sac to become PGC precursors. PGC induction is also dependent on Wnt family member 3 (WNT3) signalling through β-catenin (Ohinata *et al*. 2009; Tanaka *et al*. 2013), which provides epiblast cells with the ability to respond to induction by BMP signals. Mice null for either *Bmp2* (Ying & Zhao 2001), *Bmp8b* (Ying *et al*. 2000), *Smad1* (Tremblay, Dunn & Robertson 2001; Hayashi *et al*. 2002a) or *Smad5* (Chang & Matzuk 2001) have a reduced population of PGCs, whereas mice null for *Bmp4* (Lawson *et al*. 1999), *Smad4* (Chu *et al*. 2004), *Wnt3* (Ohinata *et al*. 2009) or catenin (cadherin associated protein), beta 1 (*Ctnnb1*; Aramaki *et al*. 2013), which encodes β-catenin, lack them entirely.

Early PGC specification begins at approximately E6.25 in the mouse, when this discrete population of BMP- and WNT3-induced cells upregulates the expression of PR/SET domain 1 (PRDM1) and PRDM14 (Ohinata *et al*. 2005; Yabuta *et al*. 2006). Both of these transcriptional regulator proteins are essential for PGC specification, and their ablation leads to a nearly complete absence of PGCs; those that are present fail to proliferate or migrate to the genital ridge (Ohinata *et al*. 2005; Vincent *et al*. 2005; Yamaji *et al*. 2008). By E7.5, the population of PRDM1- and PRDM14-expressing PGC precursors has expanded from just six induced cells into a cluster of approximately 40 cells at the base of the allantois adjacent to the extraembryonic

ectoderm (Lawson & Hage 1994). These cells have completed the specification process and form the founder population of PGCs.

Concomitant with PGC specification is the suppression of somatic cell gene expression and the induction of PGC-specific and pluripotency-associated genes. Included among those suppressed somatic genes are homeobox A1 (*Hoxa1*) and *Hoxb1*, which encode transcription factors that are involved in morphogenesis during embryonic development (Saitou, Barton & Surani 2002). The inhibition of *Hoxa1* and *Hoxb1* expression has been found to be dependent on PRDM1 in the mouse (Ohinata *et al*. 2005). Expression of PGC-specific genes, such the ribonucleic acid (RNA)-binding protein nanos C2HC-type zinc finger 3 (*Nanos3*) and DND microRNA-mediated repression inhibitor 1 (*Dnd1*), is induced simultaneously with somatic gene repression (Sakurai *et al*. 1995; Suzuki *et al*. 2008). Additionally, several pluripotency marker genes, including developmental pluripotency associated 3 (*Dppa3*), nanog homeobox (*Nanog*), POU class 5 homeobox 1 (*Pou5f1*), and SRY (sex-determining region Y)-box 2 (*Sox2*) are re-expressed in PGCs at this time (Yamaguchi *et al*. 2005; Kurimoto *et al*. 2008). PGCs are subjected to genome-wide epigenetic reprogramming beginning at approximately E7.5. Specified PGCs in chromosome (Chr) XX embryos initially exhibit a randomly inactivated X chromosome (McMahon, Fosten & Monk 1981) and are transcriptionally repressed due to deoxyribonucleic acid (DNA) methylation, dimethylation at histone 3 lysine 9 (H3K9me2) and low levels of trimethylated histone 3 lysine 27 (H3K27me3). However, shortly after their specification, PGCs undergo widespread DNA demethylation (Guibert, Forne & Weber 2012) and chromatin modifications characterized by increasing levels of H3K27me3 and erasure of H3K9me2 methylation marks (Seki *et al*. 2005; Seki *et al*. 2007; Hajkova *et al*. 2008), as well as X chromosome reactivation in females (Sugimoto & Abe 2007; Chuva de Susa Lopes *et al*. 2008).

By approximately E8.5, the PGCs have become transcriptionally silent and arrest at the $G_2$ phase of the cell cycle (Seki *et al*. 2007). These epigenetic changes act to suppress the somatic cell gene program and erase parental epigenetic marks so as to confer totipotent potential to the future germ cells.

Concurrent with these changes in epigenetic programming is the migration of the PGCs from the base of the allantois through the hindgut and into the genital ridge, a bipotential region of embryonic tissue that will form the future gonad. The process of PGC migration begins at approximately E7.5 in the mouse, when β-catenin-mediated signalling down-regulates the cell adhesion molecule E-cadherin, resulting in a decrease in PGC-to-PGC contact and therefore enhancing their motility and migration ability (Bendel-Stenzel *et al*. 2000; Di Carlo & De Felici 2000). PGCs also exhibit changes in their cellular polarity and extend cytoplasmic protrusions just prior to migration (Anderson *et al*. 2000). Chemoattractant signalling directs the migration of individual PGCs through an extracellular matrix (ECM) gradient around E8.0. Somatic hindgut cells secrete the KIT ligand (KITLG) growth factor, which mediates PGC motility by binding to KIT proto-oncogene receptor tyrosine kinase (KIT) expressed on PGCs (Farini *et al*. 2007; Gu *et al*. 2009). Signalling via the KIT/KITLG pathway is also required for PGC survival during migration (Dolci *et al*. 1991; Godin *et al*. 1991; Matsui *et al*. 1991), and mutations at the *Kit* and *Kitlg* loci have been shown to significantly reduce the genital ridge PGC population (Bennett 1956; Mintz & Russell 1957; McCoshen & McCallion 1975; Buehr *et al*. 1993; Mahakali Zama, Hudson & Bedell 2005). The bilateral migration of PGCs into the genital ridge at approximately E10.5 is directed by the secretion of C-X-C motif chemokine ligand 12 (CXCL12) from the future gonad, which binds to chemokine receptor type 4 (CXCR4) on PGCs (Doitsidou *et al*. 2002; Knaut *et al*. 2003; Molyneaux *et al*. 2003). An overly robust ECM

gradient will impede PGC migration, whereas enhanced migration will occur through a weakened ECM, such as due to a reduction in collagen type 1 levels following transforming growth factor, beta receptor I (*Tgfbr1*) KO in the mouse (Chuva de Sousa Lopes *et al*. 2005). The PGC-specific proteins NANOS3 and DND1 are required for PGC survival during migration in addition to KIT-mediated signalling (Tsuda *et al*. 2003; Youngren *et al*. 2005). By E11.5, most PGCs have colonized the genital ridges (Molyneaux *et al*. 2001); those that have failed to properly migrate into the ridges are considered ectopic and die by intrinsic apoptotic mechanisms (Stallock *et al*. 2003). Once the PGCs have entered the genital ridge, they lose their ability to migrate. Active mitotic proliferation of the PGCs during migration and gonad colonization expands their population to over 20,000 cells by E13.5 (Tam & Snow 1981).

#### 1.1.2.2 Gonad Development

*Formation of the Biopotential Gonad*

Development of the bipotential gonad begins with the thickening of coelomic epithelium on the ventromedial surface of the transient embryonic kidney, or mesonephros, between E9.5 and E10.5 in the mouse (Figure 1.4; Harikae, Miura & Kanai 2013). The indifferent gonad initially contains only somatic cells derived from the coelomic epithelium and mesonephros, and lies adjacent to the primitive Müllerian and Wolffian ducts. In females, the Müllerian ducts form the oviducts, uterus, cervix and upper vagina, and the Wolffian ducts regress, whereas in males, the Wolffian ducts form the epididymis, vas deferens and seminal vesicles, and the Müllerian ducts regress. During the indifferent stage, the genital ridge epithelium proliferates and extends into the loose connective mesenchymal tissue above it, forming the sex cords that will surround the PGCs around E11.5 (Molyneaux *et al*. 2001). These primitive sex cords are eventually

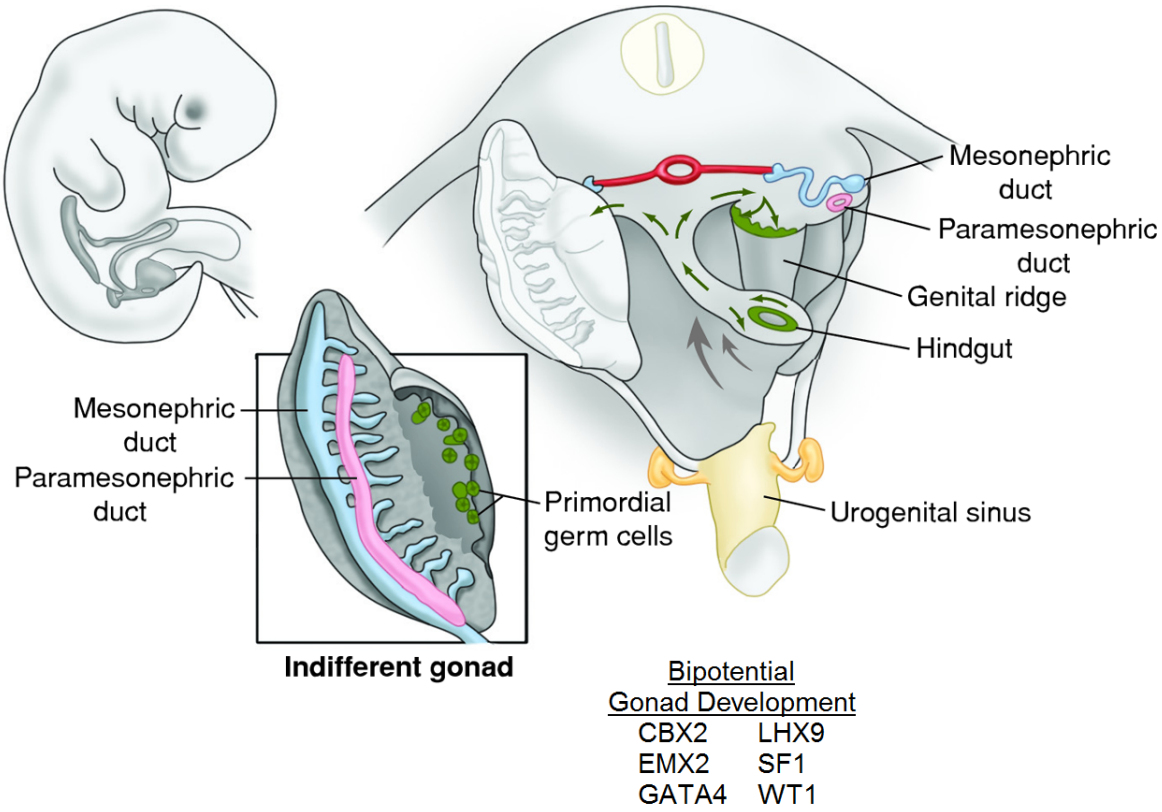


**Figure 1.4 Development of the bipotential gonad at the genital ridge**

The bipotential gonads develop as bilateral thickenings of coelomic epithelium at the genital ridge, a region on the ventromedial surface of the mesonephros. The indifferent gonad initially contains only somatic cells derived from the coelomic epithelium and mesonephros, and lies adjacent to the primitive Müllerian (paramesonephric) and Wolffian (mesonephric) ducts. During the indifferent stage, the genital ridge epithelium proliferates and extends into the loose connective mesenchymal tissue above it, forming the sex cords that will surround the PGCs. Factors required for bipotential gonad development are noted. Republished in adapted form with permission of McGraw-Hill Education, from Williams Gynecology, Hoffman, Schorge, Bradshaw, Halvorson, Schaffer & Corton, 3rd edition, copyright 2016; permission conveyed through Copyright Clearance Center, Inc.

replaced by the cortical (also known as ovigerous) sex cords in Chr XX gonads, which will contribute to the cells surrounding the germ cell as part of the ovarian follicles. A number of genes are involved in the initial development of the bipotential gonad. The empty spiracles homeobox 2 gene (*Emx2*) appears to function early in this process. Absence of this transcription factor in mice prevents the thickening of the coelomic epithelium due to defects in epidermal growth factor receptor (EGFR) signalling, resulting in the absence of the gonads as well as the Müllerian and Wolffian duct derivatives (Miyamoto *et al*. 1997; Kusaka *et al*. 2010). Loss of the Wilms tumour 1 homolog (WT1) zinc finger transcription factor also leads to a reduction of coelomic thickening and therefore gonad absence in mice (Kreidberg *et al*. 1993), and deleterious mutations within the *WT1* gene are associated with several human syndromes characterized by genitourinary abnormalities and 46,XY male-to-female sex reversal (Barbaux *et al*. 1997). Two alternative splice variants of WT1 exist, with differential transcriptional activity (Laity, Dyson & Wright 2000). Absence of the WT1(+KTS) variant, which possess a lysine-threonine-serine (KTS) sequence that interferes with DNA binding, results in Chr XY male-to-female sex reversal in mice and reduced levels of the sex determining region of chromosome Y (SRY) transcription factor and its downstream target SRY (sex determining region Y)-box 9 (SOX9; Hammes *et al*. 2001). The WT1(+KTS) variant appears to synergistically cooperate with the GATA binding protein 4 (GATA4) transcription factor on the *SRY* promoter to induce its expression (Miyamoto *et al*. 2008). Absence of the WT1(-KTS) variant, which lacks the KTS sequence, leads to streak gonads in both male and female mice due to increased cell death (Hammes *et al*. 2001). This variant functions to regulate the expression of steroidogenic factor 1 (SF1; Wilhelm & Englert 2002), a member of the nuclear receptor family of intracellular transcription factors. LIM homeobox protein 9 (LHX9) also regulates SF1 in the genital ridge by

synergizing with WT1 at the promoter for nuclear receptor subfamily 5 group A member 1 (*Nr5a1*), which encodes SF1 (Wilhelm & Englert 2002). Although PGCs are able to migrate into the genital ridge in *Lhx9*-null mice, no further development occurs and all adults lack gonads and are phenotypically female (Birk *et al*. 2000). Chromobox 2 (CBX2), a polycomb complex protein that functions to remodel chromatin, also acts upstream of SF1. Loss of *Cbx2* results in Chr XY male-to-female sex reversal and defects in ovarian development in mice (Katoh-Fukui *et al*. 1998; Katoh-Fukui *et al*. 2005) and humans (Biason-Lauber *et al*. 2009). Unlike in *Emx2*-null animals, the proliferation and ingression of the coelomic epithelium is normal in *Cbx2* KO mice; however, the gonadal cells fail to proliferate properly (Katoh-Fukui *et al*. 2012). The convergence of these signalling pathways on SF1 suggests it is a critical regulator of early gonadal development. Accordingly, deleterious mutations in *NR5A1* are associated with 46,XY male-to-female sex reversal and 46,XX gonadal dysgenesis in humans (Ozisik, Achermann & Jameson 2002), whereas mice null for *Nr5a1* phenocopy *Wt1* and *Lhx9* KO animals (Luo, Ikeda & Parker 1994).

*Testis Differentiation*

The genital ridges undergo organ fate determination into either the testis or ovary between E10.5 to E11.5, around the time of gonad colonization by the PGCs (Figure 1.5). Following their role in early genital ridge development, SF1, WT1(+KTS) and the GATA4/friend of GATA2 (FOG2) complex induce transient transcription of the Chr Y gene *Sry* in pre-Sertoli cells of the Chr XY gonad (Miyamoto *et al*. 2008). SRY is the ultimate determinant of gonadal sex development, and acts through its autosomal target gene *Sox9* to trigger the differentiation of the gonad towards a testis fate (Figure 1.6; Kent *et al*. 1996; Morais

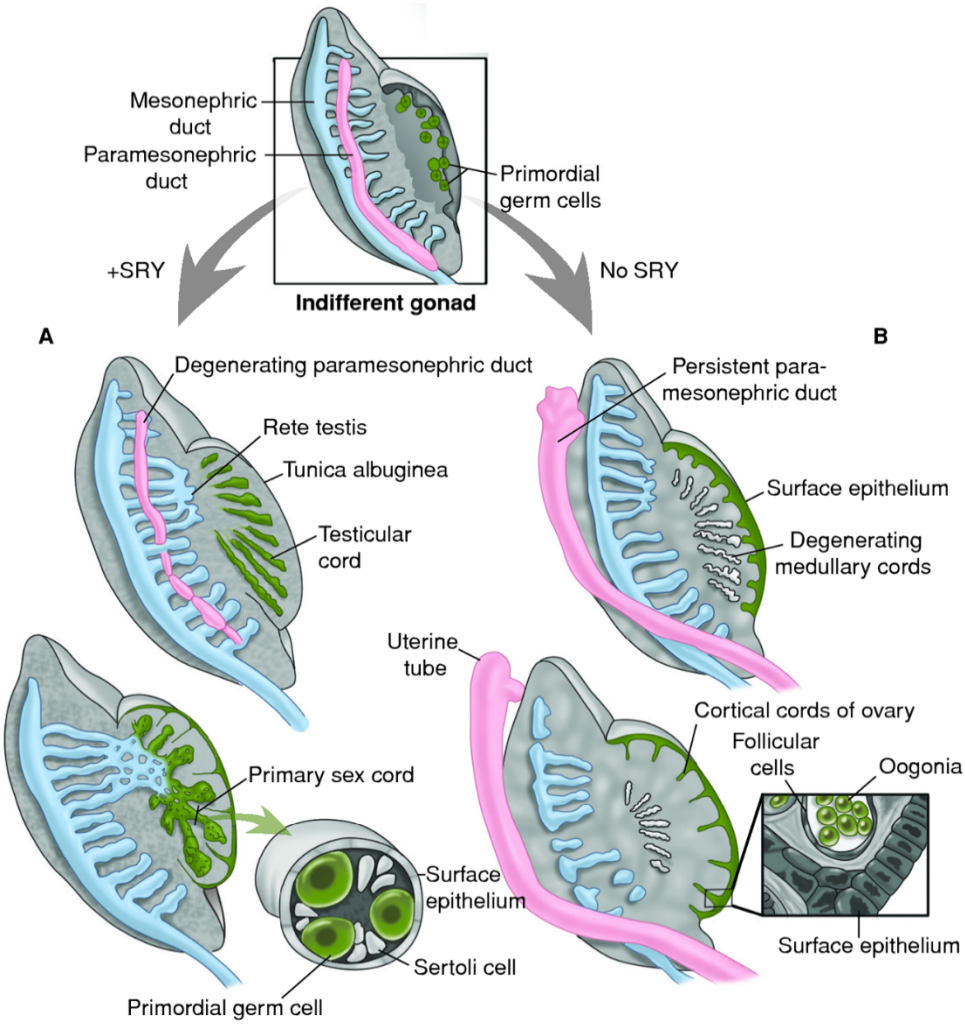


**Figure 1.5 Development of the male and female gonads from the bipotential gonad**

Development of the gonads and ductal systems in male (A) and female (B) embryos. SRY is the ultimate determinant of gonadal sex development, and acts through its autosomal target gene *Sox9* to trigger the differentiation of the gonad towards a testis fate. Historically considered the default pathway for gonad development in the absence of SRY, advances in the field have shown that ovarian differentiation is in actuality an active process regulated by discrete molecular factors. Republished in adapted form with permission of McGraw-Hill Education, from Williams Gynecology, Hoffman, Schorge, Bradshaw, Halvorson, Schaffer & Corton, 3rd edition, copyright 2016; permission conveyed through Copyright Clearance Center, Inc.

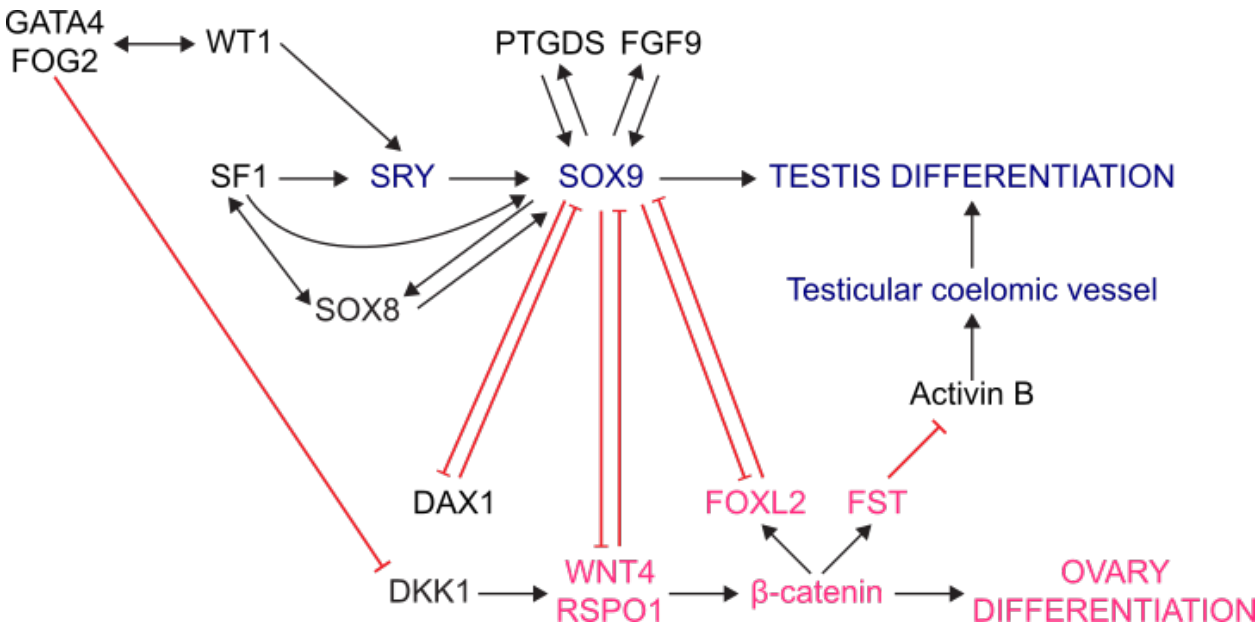


**Figure 1.6 Pathways of sex determination**

Schematic representation of the molecular mechanisms involved in determining the fate of the undifferentiated bipotential gonad. Black arrows indicate positive regulation; double arrows indicate a positive feedback loop; red lines indicate negative regulation; double red lines indicate a mutual antagonism. Adapted from Rey, Josso & Racine 2016.

da Silva *et al*. 1996; Sekido *et al*. 2004). Low levels of the SOX9 transcription factor are initially regulated by SF1 in both Chr XX and XY genital ridges (Luo, Ikeda & Parker 1994). However, at E10.5, SF1 and SRY cooperate on the testis-specific enhancer of *Sox9* core element (TESCO) in Chr XY gonads to induce high levels of SOX9 expression; in contrast, SOX9 levels are down-regulated in Chr XX gonads at this time (Kent *et al*. 1996; Morais da Silva *et al*. 1996; Sekido *et al*. 2004; Sekido & Lovell-Badge 2008). High SOX9 levels induce the differentiation of bipotential supporting cell precursors from the coelomic epithelium into the GC-analogous Sertoli cells around E11.5, a crucial event in testis development (Kent *et al*. 1996; Morais da Silva *et al*. 1996; Karl & Capel 1998). Once SOX9 levels reach a critical threshold, high SOX9 expression is maintained in Chr XY gonads through positive autoregulatory feedback loops involving continued binding of SF1 and SOX9 at TESCO (Shen & Ingraham 2002; Sekido & Lovell-Badge 2008). Fibroblast growth factor 9 (FGF9) and prostaglandin D2 synthase (PTGDS) are also involved in maintaining SOX9 expression following specification of the Sertoli cells through positive feedback loops (Kim *et al*. 2006; Wilhelm *et al*. 2007). The critical role of SOX9 in directing testis development has been demonstrated by mouse and human models. Mice null for *Sox9* in gonadal cells undergo Chr XY male-to-female sex reversal (Chaboissier *et al*. 2004; Barrionuevo *et al*. 2006; Lavery *et al*. 2011), as do 75% of human patients with campomelic dysplasia (Online Mendelian Inheritance in Man [OMIM] #114290), a skeletal disorder caused by heterozygous null mutations in *SOX9* (Houston *et al*. 1983; Foster *et al*. 1994; Wagner *et al*. 1994). Conversely, ectopic SOX9 expression in Chr XX mouse gonads is sufficient to induce the formation of testes (Bishop *et al*. 2000; Vidal *et al*. 2001), and Chr XX female-to-male sex reversal is observed in humans with duplication of *SOX9* (Huang *et al*. 1999). SOX9 remains critical to the gonad's phenotypic maintenance post-testis specification,

although the related protein SRY (sex determining region Y)-box 8 (SOX8) is also required at this time. Loss of SOX9 expression in newly specified, post-E14 Sertoli cells that lack SOX8 has been shown to induce their transdifferentiation into GC-like cells (Barrionuevo et *al*. 2009; Georg *et al*. 2012), and this SOX8/SOX9-induced protective maintenance of testis specification appears to be required into adulthood (Barrionuevo et *al*. 2016).

The differentiation of fetal Leydig cells in the Chr XY gonad around E12.5 through the expression of Sertoli cell-derived desert hedgehog (DHH; Pierucci-Alves, Clark & Russell 2001; Yao, Whoriskey & Capel 2002) in concert with SF1 signalling (Park, Tong & Jameson 2007; Karpova *et al*. 2015) leads to the production of androgenic steroid hormones and other peptides that reinforce the male-specific differentiation of the testis. Production of the TGF-β superfamily member anti-Müllerian hormone (AMH) by Sertoli cells induces degeneration of the Müllerian ducts, and testosterone (T) produced by fetal Leydig cells stimulates the differentiation of the Wolffian ducts into the male reproductive structures (Jost 1953). The PGCs that have migrated into the Chr XY genital ridge differentiate into spermatogonia, the precursors of mature spermatozoa, due to the signalling factors present in the differentiating gonad as opposed to the chromosomal constitution of the germ cells themselves. The Sertoli cells enclose the germ cells and organize into the testis cords, which eventually give rise to the seminiferous tubules. By E14.5, the majority of Chr XY germ cells have ceased their mitotic proliferation and do not divide again by mitosis or meiosis until after birth (Hilscher *et al*. 1974; Western *et al*. 2008).

*Ovary Differentiation*

Early observations of testis formation in Chr XX embryos following ectopic *Sry* expression (Koopman *et al*. 1991) and of ovary development in the absence of functional *Sry*

(Gubbay *et al*. 1992; Hawkins *et al*. 1992) lead to the hypothesis that, while testis differentiation is actively directed by SRY and SOX9, ovarian fate is the default pathway for gonad development. However, the identification of Chr XX individuals with testes but lacking the *SRY* gene suggested the existence of one or more "Z" factors that promote the ovarian differentiation pathway while actively repressing testis development (McElreavey *et al*. 1993). Recent research has shown that female gonad differentiation is indeed an active process, regulated by Wnt family member 4 (WNT4) and R-spondin 1 (RSPO1) signalling via β-catenin (Figure 1.6; Chassot *et al*. 2008; Maatouk *et al*. 2008). Prior to sex determination, both *Wnt4* and *Rspo1* are expressed in the somatic cells of the bipotential gonad and contribute to gonad development by stimulating proliferation of the coelomic epithelium (Chassot *et al*. 2012). However, their expression is down-regulated in Chr XY gonads and becomes ovary specific at approximately E11.5 in the mouse (Vainio *et al*. 1999; Parma *et al*. 2006). WNT4 ligand in the Chr XX gonads binds to a complex of the frizzled (FZD) receptor and the low-density lipoprotein receptor related protein 6 (LRP6) co-receptor (Niehrs 2012). LRP6 also interacts with the extracellular protein dickkopf WNT signaling pathway inhibitor 1 (DKK1), an inhibitor of WNT signalling that binds its receptor kringle containing transmembrane protein 1 (KREMEN1) and causes complex internalization into the cell, thus preventing LRP6 from facilitating FZD-mediated WNT4 signalling (Mao *et al*. 2001; Mao *et al*. 2002). However, RSPO1 binds to KREMEN1, inhibiting the binding of DKK1 with LRP6, preventing LRP6 internalization, and allowing LRP6 to interact with FZD and bind the co-receptor complex with WNT4 (Binnerts *et al*. 2007). RSPO1 further enhances WNT4 signalling by binding its recruitment receptors leucine rich repeat containing G protein-coupled receptor 4 (LGR4), LGR5, and LGR6, preventing WNT receptor degradation by ubiquitination (de Lau *et al*. 2011; de Lau *et al*. 2014).

The RSPO1-facilitated binding of WNT4 to the FZD/LRP6 co-receptor complex results in the transcription of WNT4 target genes via signalling through β-catenin in ovarian somatic and germ cells beginning at approximately E12.5 (Chassot *et al*. 2011; Jameson *et al*. 2012). Among the downstream targets of RSPO1/WNT4/β-catenin signalling in the Chr XX gonad is WNT4 itself and follistatin (FST; Yao *et al*. 2004), which functions to bind and antagonize activins and thus FSH secretion by the anterior pituitary (Nakamura *et al*. 1990; Section 1.1.3). The nuclear receptor subfamily 0 group B member 1 gene (*Nr0b1*), which encodes the dosage-sensitive sex reversal-adrenal hypoplasia congenital critical region on the X chromosome, gene 1 (DAX1) protein, is also a downstream target of WNT4 and β-catenin (Jordan *et al*. 2001; Mizusaki *et al*. 2003). DAX1 functions to antagonize SF1 by interacting with it at the protein level (Ludbrook *et al*. 2012). A number of mouse and human models have demonstrated that the RSPO1/WNT4-induced activation of β-catenin is an active antagonist of testis formation in the embryonic Chr XX gonad through the inhibition of SOX9 expression. Homozygous null mutations in human *WNT4* cause autosomal recessive sex reversal and dysgenesis of kidney, adrenals and lungs (SERKAL) syndrome (OMIM #611812), a disorder characterized by Chr XX female-to-male sex reversal due to increased β-catenin degradation (Mandel *et al*. 2008). Loss-of-function mutations in human *RSPO1* are associated with palmoplantar hyperkeratosis (OMIM #610644), a recessive disorder in which all individuals are phenotypic males regardless of sex chromosome constitution (Parma *et al*. 2006). Additionally, a splice site mutation in *RSPO1* that reduces β-catenin activation has been associated with Chr XX true hermaphroditism, a disorder of sexual development characterized by the presence of ovotestes, which represents a milder phenotype than the complete Chr XX female-to-male sex reversal observed in individuals will null *RSPO1* alleles (Tomaselli *et al*. 2008). Loss of *Wnt4* (Vainio *et al*. 1999; Jeays-Ward *et al*.

2003), *Rspo1* (Chassot *et al*. 2008; Tomizuka *et al*. 2008), *Ctnnb1* (Manuylov *et al*. 2008; Liu *et al*. 2009) or *Fst* (Yao *et al*. 2004) from the Chr XX mouse gonad leads to the formation of a vessel-like structure which resembles the coelomic vessel, a major artery found only in the testis. This phenotype is rescued in *Wnt4* (Maatouk *et al*. 2008; Liu, Parker & Yao 2010) and *Rspo1* (Chassot *et al*. 2008) KO mice when β-catenin is constitutively expressed in the somatic cells of the Chr XX gonad. The sex reversal of fetal ovaries from these mouse models indicates a shift towards the male determination pathway which must be repressed for normal ovarian development. Accordingly, β-catenin has been found to antagonize SOX9 expression through the inhibition of SF1-mediated TESCO transactivation, possibly by binding to TESCO itself (Bernard *et al*. 2012). Conversely, the testis differentiation pathway that occurs in Chr XY gonads functions to inhibit ovarian development by suppressing β-catenin signalling. Duplication of Chr 1p31-35, where *WNT4* and *RSPO1* reside, causes Chr XY male-to-female sex reversal in humans (Jordan *et al*. 2001), as does duplication of the Chr X region encoding *DAX1* (Bardoni *et al*. 1994). DAX1 is capable of inhibiting SF1-mediated activation of the testis specific enhancer of *Sox9* (TES), which is inclusive of the TESCO core element (Ludbrook *et al*. 2012). A similar Chr XY sex reversal phenotype is observed when DAX1 is up-regulated in mouse strains with weakly-expressed *Sry* alleles (Swain *et al*. 1998), or following β-catenin stabilization (Maatouk *et al*. 2008). β-catenin has been shown to be antagonized by SRY *in vitro* through direct interactions at the protein level that target it for degradation, therefore inhibiting β-catenin-mediated transcription (Bernard *et al*. 2008). SOX9 also physically interacts with β-catenin to cause their mutual degradation in the context of chondrocyte differentiation, leading to a reduction in β-catenin-mediated transcriptional activity (Akiyama *et al*. 2004). RSPO1 and SOX9 also mutually antagonize one another (Lavery *et al*. 2012), as do WNT4 and FGF9 (Kim

*et al*. 2006; Jameson, Lin & Capel 2012). The central role for RSPO1/WNT4 signalling via β-catenin in ovarian development suggests that β-catenin may be the "Z" factor postulated to actively stimulate the ovarian differentiation pathway and that must be inhibited in the developing testis (McElreavey *et al*. 1993). Recent investigations of *Sox9* and *Ctnnb1* (Nicol & Yao 2015) and other (Lavery *et al*. 2012; Jameson, Lin & Capel 2012) double KO (dKO) mouse models, which differentiate towards a masculinized fate, indicate that additional pro-testis genes may drive testis differentiation and that early sex determination involves redundant pathways and is an even more complex process than previously thought. Nevertheless, the testis and ovarian differentiation pathways are mutually antagonistic processes that each exhibit the active suppression of key proteins in the opposing pathway.

*Granulosa Cell Differentiation*

Commitment of the embryonic gonad to a pathway leading to an ovarian fate also sets in motion the differentiation of somatic gonadal cells into pre-GCs, the precursors of the steroidogenic, supportive GCs which surround the oocyte to form a follicle. In keeping with the gonad's bipotential ability, multiple lines of evidence indicate that GCs, the ovarian counterparts of testicular Sertoli cells, arise from a common bipotential precursor derived from the coelomic epithelium. GCs can transdifferentiate into Sertoli-like cells and vice versa in several rodent models described above and elsewhere (McLaren 1991; Couse *et al*. 1999; Colvin *et al*. 2001; Chang *et al*. 2008; Bogani *et al*. 2009; Uhlenhaut *et al*. 2009; Matson *et al*. 2011; Lindeman *et al*. 2015; Harris *et al*. 2018; Nicol *et al*. 2018; Garcia-Moreno *et al*. 2019; Nicol *et al*. 2019), and a subpopulation of Chr XX somatic cells are capable of activating the *Sry* promoter (Albrecht & Eicher 2001; Ito *et al*. 2006). Investigations into the origins of GCs in rodent models have

yielded interesting details about the dynamics of GC differentiation and their contributions to specific follicle waves, with a large body of evidence that suggests the presence of two temporally distinct GC sources that comprise discrete and spatially separated follicle populations with differential activation and growth dynamics (discussed further in Chapter 4). GC differentiation begins with the expression of the transcription factor and GC marker forkhead box L2 (*Foxl2*) in the nuclei of some somatic cells at the border between the developing ovary and the mesonephros at approximately E11.5 (Wilhelm *et al*. 2009). These cells emerge from the epithelium and move into the embryonic ovary, where they contribute to a population of medullary pre-GCs by approximately E14.5 (Mork *et al*. 2012). A second wave of pre-GCs is derived from an ovarian surface epithelium (OSE) lineage after E15.5 until shortly after birth; these cells also ingress into the ovary and upregulate *Foxl2*, where they contribute to a cortical pre-GC population (Mork *et al*. 2012).

Despite its role as an important GC differentiation marker, *Foxl2* is not required for early sex determination in mice; its deletion from fetal Chr XX ovaries results in gonadal anomalies, infertility, and the perinatal upregulation of male pathway genes including *Sox9*, *Fgf9*, and *Dhh*, but not complete sex reversal (Schmidt *et al*. 2004; Uda *et al*. 2004; Ottolenghi *et al*. 2005; Garcia-Ortiz *et al*. 2009). The ablation of *Foxl2* in combination with the deletion of *Rspo1* (Auguste *et al*. 2011), *Wnt4* (Ottolenghi *et al*. 2007), or runt related transcription factor 1 (*Runx1*; Nicol *et al*. 2019) results in a more severe female-to-male sex reversal phenotype than that observed in either single KO mouse model, indicating that *Rspo1*, *Wnt4*, *Runx1*, and *Foxl2* function complementarily during mouse ovary development. This is contrasted by the master regulatory role of *Foxl2* in goats, in which null *Foxl2* alleles cause polled intersex syndrome (PIS) characterized by the absence of horns in both sexes and Chr XX female-to-male sex

reversal (Pailhoux *et al*. 2001; Boulanger *et al*. 2014). *Foxl2* continues to be expressed in the GCs of mouse early ovarian follicles into adulthood (Pisarska *et al*. 2004). Following sex determination postnatally, ovarian β-catenin activity declines, and FOXL2 negatively regulates *Sox9* expression through direct interaction with TESCO, cooperatively with estrogen receptor 1 (ESR1) and ESR2 (Figure 1.6; Uhlenhaut *et al*. 2009). FOXL2 may also negatively regulate the male differentiation pathway through other mechanisms, including the transcriptional repression of ovarian *Nr5a1* expression through the inhibition of WT1(-KTS) (Takasawa *et al*. 2014), or the SF1-induced regulation of *Amh* (Jin *et al*. 2016). Accordingly, conditional deletion of *Foxl2* in adult female mouse GCs results in gonadal sex reversal and transdifferentiation of the GCs to Sertoli-like cells (Uhlenhaut *et al*. 2009). Complementary to the loss of *Foxl2* in adult mouse ovaries, the loss of doublesex and mab-3 related transcription factor 1 (*Dmrt1*) in adult Chr XY mouse Sertoli cells results in *Foxl2* activation, transdifferentiation of these cells into GCs, and a sex reversal phenotype (Matson *et al*. 2011); Chr XY male-to-female sex reversal is also observed in humans with deletions of Chr 9p encompassing *DMRT1* (Ottolenghi *et al*. 2000). *Foxl2* activation has also been observed in mouse models of Chr XY sex reversal following the deletion of a specific isoform of the FGF9 receptor fibroblast growth factor receptor 2 (FGFR2; Bagheri-Fam *et al*. 2017), or constitutive activation of β-catenin (Li *et al*. 2017). These investigations have revealed that gonadal identity is not irreversibly established during embryogenesis, but rather it must be maintained through mutually antagonistic pathways throughout adulthood.

*Post-Ovary Differentiation*

Following Chr XX sex determination, and in the absence of AMH and T, the Müllerian ducts differentiate into the female reproductive tract and the Wolffian ducts regress. Once gonad colonization is complete, PGCs differentiate into oogonia, the pre-meiotic germ cells, in response to external signals from ovarian somatic cells. The synchronous mitotic proliferation that drastically increases the germ cell pool at this time is characterized by incomplete cytokinesis, which results in clonal clusters of up to 30 daughter cells connected by intracellular bridges (Pepling & Spradling 1998; Lei & Spradling 2013). Although the function and physiological significance of these clusters, termed germ cell cysts, has not been clearly elucidated, they may be necessary for the development of healthy, mature oocytes through organelle and metabolite exchange between neighbouring germ cells (Pepling & Spradling 2001). Ovarian germ cell meiosis, which eventually reduces the chromosomal complement from diploid to haploid, begins between E12.5 and E13.5 (McLaren & Southee 1997). This process is initiated by all-*trans*-retinoic acid (RA), a vitamin A metabolite that diffuses from the mesonephros into the ovary in an anterior-to-posterior direction (Bowles *et al*. 2006; Koubova *et al*. 2006). RA triggers meiosis initiation by stimulating the expression of the germ cell transcription factor stimulated by retinoic acid gene 8 (*Stra8*) by binding to RA receptors (RARs) and retinoid X receptors (RXRs; Menke, Koubova & Page 2003; Baltus *et al*. 2006; Bowles *et al*. 2006; Koubova *et al*. 2006; Anderson *et al*. 2008; Mark *et al*. 2008). STRA8 is required for pre-meiotic DNA replication and the events of meiotic prophase, including chromosome condensation, cohesion, synapsis, and recombination (Baltus *et al*. 2006; Anderson *et al*. 2008). The RA-induced expression of *Stra8* requires the germ cell-specific deleted in azoospermia-like (DAZL) RNA-binding protein (Lin *et al*. 2008; Gill *et al*. 2011). DAZL also positively regulates

the translation of synaptonemal complex protein 3 (SYCP3), a component of the synaptonemal complex necessary for the recombination and segregation of meiotic chromosomes (Reynolds *et al*. 2007). In addition to *Stra8*, RA induces the expression of cohesion complex protein REC8 meiotic recombination protein (*Rec8*) in a DAZL-dependent manner (Baltus *et al*. 2006; Koubova *et al*. 2014). REC8 is required for the completion of sister chromatid cohesion, proper synapsis, and chiasmata formation during meiosis (Bannister *et al*. 2004; Xu *et al*. 2005). Following meiosis initiation, the oogonia proceed through prophase I, but arrest around E17.5 during the diplotene stage (Borum 1961). Now referred to as primary oocytes, these diploid germ cells remain perpetually quiescent in a state termed dictyate, until just prior to ovulation, when they complete the first meiotic division in response to the LH surge (discussed in Section 1.1.3). Meiosis will halt a second time after ovulation during metaphase II, and the second meiotic division is not completed in secondary oocytes until after fertilization via signals from the sperm. In females, the final product of meiosis I and II is the fertilization-ready haploid ovum, and two polar bodies that do not contribute to reproduction.

#### 1.1.2.3 Primordial Follicle Assembly

The breakdown of germ cell cysts begins immediately after birth in the mouse (Hirshfield 1991) following the perinatal invasion of elongated, pre-GCs between adjacent oocytes within the same cyst (Pepling & Spradling 2001; Lechowska *et al*. 2011). This breakdown eventually leads to the formation of primordial follicles consisting of an individual, prophase-arrested oocyte surrounded by a single layer of somatic-derived, squamous pre-GCs, with a basement membrane that separates the pre-GC layer from the surrounding stromal cells and excludes vascular networks from the inner follicle (Baker 1963; Hirshfield 1991). Germ cell cyst

breakdown begins in the ovarian medulla and spreads into the cortical region (De Felici *et al*. 2005; Mazaud *et al*. 2005; Pepling *et al*. 2010), such that the most immature germ cells are present in the cortex and progressively more mature oocytes are found in the medulla (Anderson *et al*. 2007); this pattern reflects the two temporally defined populations of GCs that contribute to discrete, spatially separated follicle waves and their activation dynamics (discussed in Chapter 4). A number of factors are known to moderate the breakdown of germ cell cysts and primordial follicle assembly, including activins (Bristol-Gould *et al*. 2006; Childs & Anderson 2009) and their negative regulator FST (Wang *et al*. 2015a); AMH (Nilsson *et al*. 2011); folliculogenesis specific basic helix-loop-helix (FIGLA; Soyal, Amleh & Dean 2000); tumor necrosis factor (TNF; Morrison & Marcinkiewicz 2002; Nilsson, Stanfield & Skinner 2006); and the steroid hormones 17β-estradiol ($E_2$) and progesterone ($P_4$; Kezele & Skinner 2003; Chen *et al*. 2007). Notch signalling appears to play an integral role in this process, as it is required for cyst breakdown (Hahn *et al*. 2005; Trombly, Woodruff & Mayo 2009; Xu & Gridley 2013), and the mechanism by which both FST and $P_4$ act in this process is due at least in part to the inhibition of Notch signalling (Guo *et al*. 2012; Wang *et al*. 2015a). Cyst breakdown is accompanied by extensive oocyte death (Pepling & Spradling 2001), with nearly 80% of all germ cells lost from the mouse ovary at this time (Lei & Spradling 2013). This apoptotic process is termed attrition, and is controlled by the caspase and B cell lymphoma (BCL) protein families. Myeloid cell leukemia sequence 1 (MCL1; Hartley *et al*. 2002; Omari *et al*. 2015) and BCL2-like 1 (BCL2L1; Rucker *et al*. 2000) protect against oocyte apoptosis, whereas BCL2-associated X protein (BAX) promotes germ cell death (Perez *et al*. 1999; Greenfeld *et al*. 2007a), and their deletion in mice results in decreased or increased initial numbers of oocytes and primordial follicles, respectively. Deletion of caspase 2 (*Casp2*), which encodes a protease that cleaves cellular proteins leading to

apoptosis, also results in an increased primordial follicle population in mice (Bergeron *et al*. 1998). Those oocytes that survive the attrition process and become enclosed within primordial follicles constitute what has traditionally been thought to be a finite and non-renewable ovarian reserve, although multiple laboratories have recently proposed that stem cells can differentiate into functional oocytes during adulthood (reviewed by Truman, Tilly & Woods 2017); however, it is unclear how or if this putative process contributes to the overall follicle reserve.

### 1.1.3 Folliculogenesis

The process of follicular development relies on autocrine, paracrine, and endocrine influences in addition to bidirectional communication between the oocyte and its adjacent somatic cells. Combined, these factors coordinate follicle recruitment, growth, and selection together with controlled follicle death (Figure 1.7; Eppig 1991; Eppig 2001). Folliculogenesis can be divided into three major stages: initiation, or the continuous recruitment of waves of primordial follicles into a growing pool; growth of a subset of these follicles to form primary, secondary, and antral follicles; and the cyclic recruitment of a cohort of antral follicles that occurs post-puberty until menopause, leading to pre-ovulatory follicle selection, maturation, and ovulation of one or more oocytes followed by the subsequent formation of corpora lutea. The GC population is subject to massive expansion over the course of follicle growth, undergoing 10 clonal divisions and expanding from approximately four pre-GCs in primordial follicles to upwards of 2,500 GCs in the mature pre-ovulatory follicle (Hirshfield & Schmidt 1987). In addition, follicular atresia begins following the formation of primordial follicles and continues throughout the reproductive lifecycle. Thus, the resting pool of primordial follicles is continuously depleted through the initiation of follicle growth, follicle degeneration by atresia,

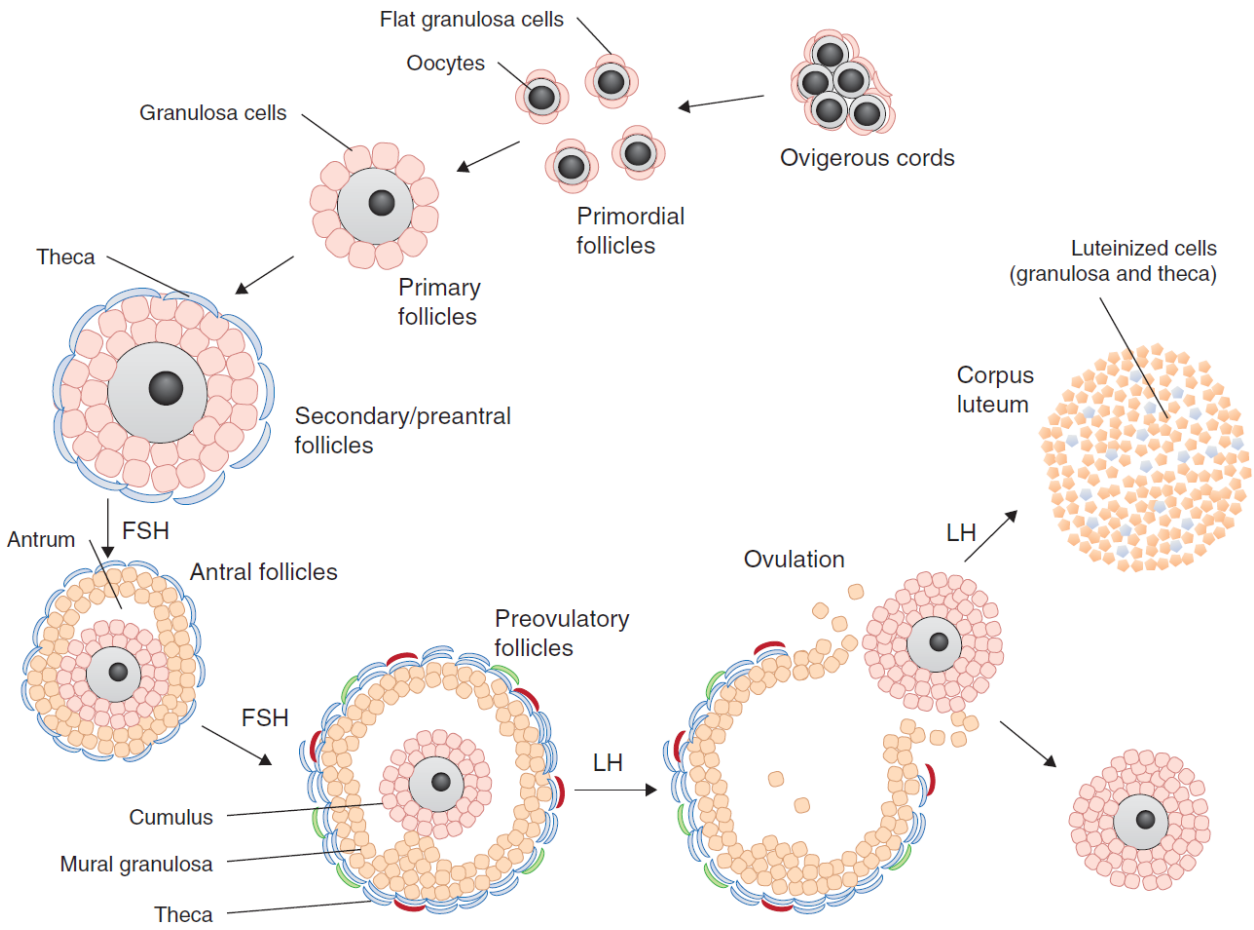


**Figure 1.7 Ovarian folliculogenesis**

Ovarian follicle maturation is a coordinated and selective process that proceeds from puberty until menopause. Primordial follicles encompass individual oocytes surrounded by a layer of flat GCs, having formed from the embryonic oocyte cluster (ovigerous cords). Primary follicles are recruited for growth from the quiescent primordial pool and progress through the secondary, antral, and pre-ovulatory stages under the influence of local and endocrine factors. The cumulus GCs are ovulated with the oocyte, while mural GCs and TCs remain in the ovary to form the corpus luteum. Republished in adapted form with permission of BioScientifica Limited, from Journal of Molecular Endocrinology, Vol 52, Georges *et al*., FOXL2: a central transcription factor of the ovary, p. R17-R33, copyright 2014; permission conveyed through Copyright Clearance Center, Inc.

and ovulation, resulting in substantial germ cell loss over the reproductive lifespan until the exhaustion of the follicular complement initiates menopause.

#### 1.1.3.1 Primordial Follicle Activation

Although the precise molecular mechanisms controlling initial follicle recruitment into the growing population have yet to be deciphered, a balance between inhibitory and activating intra- and extra-oocyte factors has been implicated. Follicles in mice null for either of the oocyte-specific transcription factors NOBOX oogenesis homeobox (*Nobox*; Rajkovic *et al*. 2004), spermatogenesis and oogenesis specific basic helix-loop-helix 1 (*Sohlh1*) or *Sohlh2*, or LIM homeobox protein 8 (*Lhx8*; Pangas *et al*. 2006; Choi *et al*. 2008; Choi, Yuan & Rajkovic 2008; Ren *et al*. 2015) cannot progress past the primordial stage. NOBOX, SOHLH1/2 and LHX8 appear to regulate several important oocyte-specific genes expressed in primary follicle germ cells, including the TGF-β superfamily members growth differentiation factor 9 (*Gdf9*) and bone morphogenetic protein 15 (*Bmp15*), which function throughout folliculogenesis to stimulate follicle growth and development. Primordial follicle activation is also initiated by KIT/KITLG. Down-regulation of *Kitlg* during early mouse folliculogenesis results in a diminished growing follicle pool (Kuroda *et al*. 1988; Huang *et al*. 1993; Bedell *et al*. 1995), and inhibition of KIT/KITLG signalling results in a block at the primordial stage of follicle development (Yoshida *et al*. 1997); the reverse is observed with recombinant KITLG treatment (Parrott & Skinner 1999). Both the LHX8 and KIT/KITLG signalling pathways have been shown to modulate the phosphatidylinositide 3-kinase (PI3K)/protein kinase B (PKB, or AKT)/mechanistic target of rapamycin (mTOR) pathway in oocytes (Reddy *et al*. 2005; Ren *et al*. 2015), which negatively regulates primordial follicle activation. Conditional deletion of the PI3K-negative regulator

phosphatase and tensin homolog (*Pten*) from oocytes causes activation of the entire primordial follicle pool, leading to premature ovarian failure (POF; Reddy *et al*. 2008; John *et al*. 2008). A similar phenotype is observed following the oocyte-specific loss of forkhead box O3 (*Foxo3*), a transcription factor and central downstream target of the PI3K pathway, that, when active, inhibits primordial follicle activation from the resting pool (Castrillon *et al*. 2003). Genetic investigations of other PI3K/AKT/mTOR pathway mediators in oocytes, including pyruvate dehydrogenase kinase, isoenzyme 1 (PDK1; Reddy *et al*. 2009), cyclin dependent kinase inhibitor 1B ($p27^{Kip1}$; Rajareddy *et al*. 2007) and tuberous sclerosis 1 (TSC1) and TSC2 (Adhikari *et al*. 2009; Adhikari *et al*. 2010) have corroborated the role of this pathway in resting follicle activation. Additionally, activation of mTOR complex 1 (mTORC1) in the pre-GCs surrounding primordial follicles triggers their activation via the stimulation of germ cell KITLG signalling (Zhang *et al*. 2014), indicating that communication between oocytes and their surrounding somatic cells is required during early folliculogenesis. The GCs also control primordial follicle activation through the production of AMH, which is produced by the GCs of growing follicles and inhibits primordial follicle growth and their transition to the primary stage; in its absence, the ovarian reserve is quickly depleted (Durlinger *et al*. 1999), whereas treatment with recombinant AMH is associated with reserve conservation (Hayes *et al*. 2016). The role of AMH in suppressing primordial follicle recruitment and its correlation with the size of the follicle pool has led to its clinical utility as a biomarker of the ovarian reserve (Visser *et al*. 2006). Primordial follicles that initiate growth progress to the primary stage, which is marked by oocyte enlargement, mitotic proliferation of the surrounding single pre-GC layer, and a transition of these cells from a squamous to cuboidal morphology to form mature GCs (Hirshfield 1991). This morphological change requires FOXL2, as *Foxl2*-null mouse ovaries contain only slow

growing, flat GCs, do not form primary follicles, and display premature follicle depletion due to global activation and subsequent oocyte atresia (Schmidt *et al*. 2004; Uda *et al*. 2004). Although the mechanism by which FOXL2 mediates this change has yet to be determined, a recent report has implicated a role for the transcription factor in mediating ECM remodelling through the regulation of collagen, type 1, alpha 2 (*Col1a2*) gene expression in perinatal mouse ovaries (Marongiu *et al*. 2016). The ECM is essential for follicle development (Harlow *et al*. 2007), and its modulation is required for follicle growth (Woodruff & Shea 2007). Regardless of the positive and negative influences on their activation, the vast majority of primordial follicles recruited into the growing pool are not destined for further growth or ovulation, but will instead die from atresia. Notably, it has not yet been determined if the factors governing the activation and growth of the first wave of medullary primordial follicles immediately after birth differ from those responsible for the activation and growth of subsequent cortical primordial follicle waves.

#### 1.1.3.2 Early Follicle Growth

In addition to their morphological GC changes, follicles committed for growth develop a glycoprotein-rich matrix, termed the zona pellucida, between the oocyte and GC layer. Cellular communication between adjacent GCs of the same follicle is achieved via gap junctions composed of homologous connexin complexes organized to form a connexon structure with a central channel. GCs also extend cytoplasmic transzonal projections through the zona pellucida to contact the oocyte via heterologous connexins. These gap junction networks allow for bi-directional communication between the oocyte and GCs through the transfer of ions, metabolites and small molecules, and are essential for continued follicle growth as well as maturation of the germ cell (Eppig 1991). Two connexins, connexin 37 (CX37) and CX43, which are encoded by

the gap junction protein, alpha 4 (*Gja4*) and *Gja1* genes, respectively, are of particular importance in the ovary. CX37 contributes to transzonal oocyte-GC gap junctions, beginning at the primary stage (Simon *et al*. 1997) whereas CX43 forms GC-GC gap junctions throughout folliculogenesis (Juneja *et al*. 1999). Ovaries from mice deficient in *Gja4* lack CX37, and are characterized by oocytes with growth deficiencies and meiotic defects due to an inability to communicate with GCs (Carabatsos *et al*. 2000). Mice null for *Gja1*, and thus CX43, exhibit ovaries with follicles that arrest at the primary stage due to a lack of GC proliferation and oocyte growth (Juneja *et al*. 1999; Ackert *et al*. 2001). The necessity of these gap junctional communication networks emphasizes the importance of crosstalk between the follicle cells for the exchange of metabolites and paracrine factors and thus normal folliculogenesis.

The onset of the secondary, or pre-antral, follicle stage is marked by proliferation of the GCs to form a double layer as well as growth of the oocyte. GDF9 is required for primary follicle progression to the secondary stage via stimulation of GC proliferation (Dong *et al*. 1996; Elvin *et al*. 1999a); the related protein BMP15 may play a role redundant to that of GDF9 at this stage of folliculogenesis (Yan *et al*. 2001). Pre-antral follicles are also characterized by the recruitment of an outer TC layer that differentiates from surrounding stromal cells. These TCs are separated from the outermost GC layer by a basement membrane, although they will eventually synthesize androgens as substrates for GC estrogen production in response to LH stimulation. Much like the differentiation of GCs from two temporally and spatially defined populations, TCs are derived from two distinct sources at different time points (Liu *et al*. 2015a). The majority of TCs in the adult mouse ovary are derived from WT1-positive progenitors derived from the coelomic epithelium of the bipotential gonad prior to sexual differentiation around E11.5. Conversely, a small percentage of TCs in the adult ovary originate from a

mesonephros-derived progenitor population positive for the TC-specific marker GLI-Kruppel family member GLI1 (GLI1) that arises just prior to birth; these TCs are first observed in the ovarian medulla, and give rise to a cohort of steroidogenic cells located immediately adjacent to the basal membrane separating TCs from GCs (Liu *et al*. 2015a). Although the authors speculated that this specification pattern may be reflective of the dual differentiation of GCs, it remains to be determined if these discrete progenitor sources differentiate into TCs with unique functions and/or contribute to distinct follicle populations (Liu *et al*. 2015a).

It has been hypothesized that, given their proximity to the GCs of growing follicles, TC recruitment from the stroma is likely regulated by one or more GC-produced paracrine factors (Kotsuji *et al*. 1990; Orisaka *et al*. 2006). Indeed, treatment of putative thecal stem cells with GC-conditioned media *in vivo* is sufficient to differentiate functional TC-like cells (Magarelli, Zachow & Magoffin 1996; Honda *et al*. 2007). A number of GC-derived molecules have been implicated in TC recruitment and differentiation, including insulin-like growth factor 1 (IGF1) and KITLG, which are also able to stimulate the differentiation of TC-like cells when individually administered to precursors *in vitro* (Honda *et al*. 2007); conversely, inhibition of these factors with neutralizing antibodies results in a significant decrease in TC differentiation rates. IGF1 has been shown to increase the expression of TC-specific proteins (Huang *et al*. 2001), and although pre-antral follicles from *Igf1*-null mice develop a thecal layer, it fails to proliferate and the follicles arrest at this stage (Baker *et al*. 1996). Furthermore, the addition of KITLG to GCs treated with IGF1 induces the expression of additional TC-specific markers (Huang *et al*. 2001). The hedgehog family of growth factors are also GC-derived TC differentiation candidates, as DHH and Indian hedgehog (IHH) produced in the GCs are able to stimulate expression of the downstream hedgehog target and TC marker GLI1 (Wijgerde *et al*.

2005; Liu *et al*. 2015a). The production of hedgehog ligands in GCs appears to be induced by oocyte-derived GDF9 (Liu *et al*. 2015a), and treatment of cultured GCs with recombinant GDF9 leads to the up-regulation of IGF1 (Varani *et al*. 2002; Pangas, Jorgez & Matzuk 2004). Accordingly, TCs do not form around follicles in the ovaries of mice (Dong *et al*. 1996) or sheep (Nicol *et al*. 2009) null for *Gdf9*, indicating an indirect role for this oocyte-specific growth factor in TC differentiation. In addition, GDF9 may also modulate the expression of ECM proteins that contribute to a scaffold on which TCs can attach (Burns *et al*. 2002).

Continued growth of the pre-antral follicle sees the development of multiple small, fluid-filled cavities interspersed between the GCs, which have proliferated significantly. Progression to the antral stage is marked by the aggregation of these spaces into the antrum, which is filled with follicular fluid containing steroid hormones, growth factors, electrolytes, proteoglycans, cytokines, and hyaluronic acid necessary for proper oocyte maturation and ovulation. Concurrent with antrum formation is the proliferation of the theca and its differentiation into two distinct layers termed the theca interna and theca externa. The theca interna is vascularized, and contains TCs rich in mitochondria with tubular cristae, smooth endoplasmic reticulum and lipid vesicles, consistent with their role in androgen production from cholesterol precursors. Conversely, theca externa cells include fibroblasts, smooth muscle-like cells and macrophages that are necessary for ovulation (Magoffin 2005). The GCs of antral follicles can also be subdivided into distinct populations with different morphological and functional properties. The mural GCs line the follicle wall and are involved in steroidogenesis and ovulation, whereas the cumulus GCs surround the oocyte and ensure its growth and competence via transzonal oocyte-GC projections (Hirshfield 1991).

#### 1.1.3.3 Antral and Pre-Ovulatory Folliculogenesis

Whereas the follicular stages prior to and inclusive of secondary follicle formation are largely independent of the anterior pituitary hormones FSH and LH, these gonadotropins are required for the proper development of antral follicles and oocyte ovulation. FSH is necessary for antral follicle survival and GC proliferation, as well as the production of estrogens through the modulation of steroidogenic GC enzyme expression and the eventual expression of LH receptors (LHCGRs) on GCs. Conversely, LH is essential for the expression of enzymes and other proteins required for androgen synthesis in TCs, and is the key ovulatory stimulus. Mice lacking both gonadotropins via GnRH deficiency (Cattanach *et al*. 1977), the FSH receptor (FSHR; Dierich *et al*. 1998; Abel *et al*. 2000), or a subunit composing FSH (Kumar *et al*. 1997) have normal pre-antral follicle growth but are infertile due to defective antral folliculogenesis. TC differentiation is also gonadotropin independent, as thecal precursor cells lack LHCGRs and the enzymes necessary for TC steroidogenesis (Magoffin & Weitsman 1994), and the theca layer forms in FSH-deficient mice (Kumar *et al*. 1997). However, the vascularization of the theca interna surrounding antral follicles establishes a means of communication between the follicle and endocrine influences, such that the transition from pre-antral to antral at the pubertal onset marks the start of follicular regulation by the HPG axis.

FSH, LH, and the related hormone human chorionic gonadotropin (hCG) are heterodimeric glycoproteins composed of a common α but unique β subunits (Pierce & Parsons 1981). The gonadotropins exert their functions by acting on G protein-coupled receptors (GPCRs); the distinct gonadotropin β subunits confer their specific biological actions, and are responsible for the specificity of their interaction with the appropriate receptor (Pierce & Parsons 1981). Due to similarities between the LH and hCG β subunits, the LHCGR also serves as the

hCG receptor and the two are analogues despite unique functions (Casarini *et al*. 2012). GPCRs transduce signals through associated cytoplasmic, heterotrimeric G proteins consisting of α, β and ɣ subunits (Sprang 1997). In the absence of gonadotropin signalling, the Gα subunit is reversibly bound to guanosine diphosphate (GDP) and thus in an inactive state. Gonadotropin binding to the LHCGR or FSHR on the cell surface induces a conformational change in the receptor that facilitates the exchange of a molecule of GDP for guanosine triphosphate (GTP; Sprang 1997). Now active, the Gα-GTP subunit dissociates from the β and ɣ subunits, initiating the linear adenylyl cyclase (AC)/cyclic adenosine monophosphate (cAMP)/protein kinase A (PKA) classical signalling cascade, in which cAMP acts as an intracellular second messenger to induce the phosphorylation of target proteins such as the cAMP-responsive element-binding protein (CREB) transcription factor. Phosphorylated CREB binds DNA at cAMP response elements within target gene promoter regions, and together with a CREB-binding protein co-activator, activates gene transcription (Borrelli *et al*. 1992). Other AC/cAMP/PKA-independent pathways may be initiated following gonadotropin binding, such as the PI3K/AKT, rat sarcoma (RAS), Rous sarcoma oncogene (SRC) tyrosine kinase, or glycogen synthase kinase 3 beta (GSK3B) signalling cascades, depending on the follicular context (Gonzalez-Robayna *et al*. 2000; Wayne *et al*. 2007; Fan *et al*. 2008a).

FSH and LH receptors begin to be expressed on the surface of GCs and TCs, respectively, in early antral follicles, and their signals result in sex steroid synthesis due to differential enzyme expression and activity within these cells (Figure 1.8). The cell-specific restriction of gonadotropin receptors and steroidogenic enzymes forms the basis of the two-cell, two-gonadotropin theory (Hillier, Whitelaw & Smyth 1994). Pituitary LH stimulates the production of steroidogenic acute regulatory protein (STAR) in TCs, which facilitates the

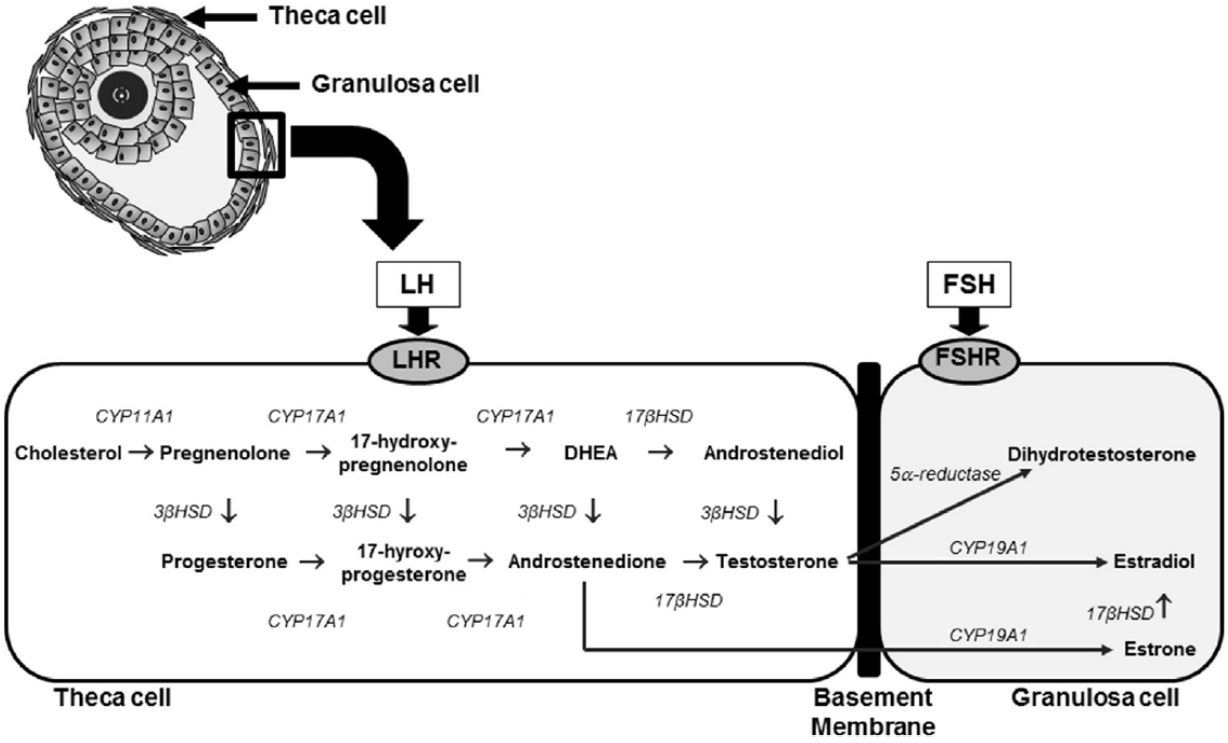


**Figure 1.8 The two-cell, two-gonadotropin theory of follicle hormone regulation and production**

The stimulation of TCs by LH stimulates cholesterol transport into the inner mitochondrial membrane, as well as the expression of the steroidogenic enzymes required for the synthesis of androgens from cholesterol precursors. FSH stimulation of GCs results in the up-regulation of aromatizing enzymes that convert androgens to estrogens. FSH is also essential for the expression of LHCGRs on the surface of the GCs later in folliculogenesis. Reprinted in adapted form with permission from Elsevier, from Molecular and Cellular Endocrinology, Vol 465, Walters & Handelsman, Role of androgens in the ovary, p. 36-47, copyright 2018; permission conveyed through Copyright Clearance Center, Inc.

transfer of cholesterol to the inner mitochondrial membrane. LH also stimulates the production of cholesterol side-chain cleavage enzyme (cytochrome P450 family 11 subfamily A member 1; CYP11A1), steroid 17α-hydroxylase/17,20-lyase (cytochrome P450 family 17 subfamily A member 1; CYP17A1), and 3β-hydroxysteroid dehydrogenase (3β-HSD) in these cells. CYP11A1 functions to cleave cholesterol to produce pregnenolone in the inner mitochondria matrix in a rate limiting reaction (Stocco & Clark 1996). Pregnenolone is converted to 17-hydroxypregnenolone and then dehydroepiandrosterone (DHEA) by CYP17A1 in the smooth endoplasmic reticulum, which is in turn metabolized to androstenedione ($A_4$) by 3β-HSD in the same location. Conversely, FSH functions to upregulate the aromatase (cytochrome P450 family 19 subfamily A member 1; CYP19A1) and 17β-hydroxysteroid dehydrogenase (17β-HSD) enzymes via the AC/cAMP/PKA pathway in GCs. The FSH-induced, GC-specific production of $E_2$ by these enzymes requires androgenic precursors that originate in the TCs. Accordingly, TC-derived $A_4$ diffuses across the basement membrane to the GCs, where it is converted to estrone ($E_1$) by aromatase and subsequently to $E_2$ by 17β-HSD. Alternatively, $A_4$ can be converted to T by 17β-HSD, which can be converted to $E_2$ by aromatase or to 5α-dihydrotestosterone (DHT) by the 5α-reductases following its diffusion into GCs (Miller 1988). In addition to the enzymes involved in steroidogenesis, both gonadotropins upregulate the expression of low-density lipoprotein receptors on the cell surface (Golos, Strauss & Miller 1987; Veldhuis 1988; LaVoie *et al*. 1999), facilitating cholesterol uptake for steroid synthesis, while LH upregulates the expression of its own receptor on TCs (Magoffin 2005).

Following its gonadotropin-induced synthesis in GCs, $E_2$ feeds back to the HPG axis to regulate FSH and LH secretion, and thus its own production, over the course of the estrous cycle. Pituitary FSH secretion is also cyclically modulated by FST and the activins and inhibins,

dimeric peptide growth factors that are members of the TGF-β superfamily. The activins and inhibins are composed of α and/or β subunits; inhibin A and inhibin B are comprised of an α subunit and a βA or βB subunit, respectively, whereas activin A, activin B, and activin C each consist of either two βA subunits, two βB subunits, or a βA and βB subunit, respectively. These subunits are derived from distinct precursor polypeptides encoded by individual genes (Ying 1988). Inhibin production by ovarian GCs increases during antral folliculogenesis in response to FSH, and functions to selectively suppress FSH secretion by the pituitary through negative feedback endocrine signalling. The activins act in opposition to the inhibins, and are produced in numerous tissues including the anterior pituitary, where they stimulate FSH production. The activins transduce positive effects on FSH synthesis by binding to the type II TGF-β receptors activin receptor type-2A (ACVR2A) or ACVR2B, which then associate with the TGF-β type I receptor activin A receptor type-1B (ACVR1B) and signal through SMAD family member 2 (SMAD2), SMAD3 and the common SMAD4 partner (Massagué 1998). In contrast, the inhibins bind to ACVR2A as a complex with transforming growth factor, beta receptor III (TGFBR3), preventing the binding of activins and increasing inhibins' functionality (Lewis *et al*. 2000). FST also functions to antagonize activins by directly binding to them, reversing activin-induced responses and inhibiting FSH secretion (Knight 1996). These proteins also act locally in the ovary in autocrine and paracrine manners to regulate late follicular development. Inhibins are capable of increasing pre-ovulatory follicle TC responsiveness to LH, thus enhancing the synthesis of androgens for their use as substrates in $E_2$ production. Additionally, intra-ovarian activins up-regulate FSHRs on GCs, stimulate GC proliferation, $E_2$ synthesis and oocyte maturation, and counteract the action of inhibins on TC androgen production (Knight, Satchell & Glister 2012). The inhibitory paracrine action of GC-derived activins on TC androgen synthesis

is necessary in pre-antral and early antral follicles, which do not yet require $E_2$ but possess LHCGRs and so could respond to LH by producing $A_4$ (Hillier *et al*. 1991; Zachow & Magoffin 1995). In addition, $A_4$ production may also be inhibited by TC growth factors with autocrine effects produced in response to GC-derived KITLG (Weitsman & Magoffin 1993; Fournet *et al*. 1996; Zachow, Weitsman & Magoffin 1997).

In addition to its role in stimulating steroid synthesis, FSH also promotes the proliferation of GCs and the maturation of follicles from pre-antral to pre-ovulatory through the modulation of the positive cell cycle regulator cyclin D2 (CCND2). CCND2 functions to promote the $G_1$/S transition during cell cycle progression by binding to cyclin dependent kinase 4 (CDK4) or CDK6, leading to hyperphosphorylation of retinoblastoma (RB) protein and thus the release of inhibition on transcription factors (Santamaria & Ortega 2006; Musgrove *et al*. 2011). Ovarian CCND2 is mainly expressed in the GCs and is induced by FSH signalling (Sicinski *et al*. 1996; Dierich *et al*. 1998; Robker & Richards 1998; Burns *et al*. 2001) via both PI3K- and PKA-mediated mechanisms (Han, Xia & Tsang 2013). *Ccnd2*-null mice are sterile due to follicular arrest at the pre-antral stage secondary to impaired GC proliferation (Sicinski *et al*. 1996), whereas GCs from mice lacking *Cdk4* proliferate in response to FSH, suggesting redundancy among the GC cell cycle regulators (Moons *et al*. 2002). The E-type cyclins (cyclin E1 [CCNE1] and E2 [CCNE2]), which bind to cyclin dependent kinase 2 (CDK2) and regulate the $G_1$/S transition in addition to CCND2 and CDK4/CDK6 complexes, may also mediate GC proliferation following gonadotropin stimulation (Cannon *et al*. 2007). Notably, the expression of *CCND2* is inhibited by FOXL2 via transcriptional repression (Bentsi-Barnes *et al*. 2010). Following Chr XX sex determination, FOXL2 continues to be expressed in the GCs of early stage follicles but decreases with advancing folliculogenesis (Pisarska *et al*. 2004), consistent

with its role in the primordial to primary transition (Schmidt *et al*. 2004; Uda *et al*. 2004) and in the continued maintenance of GC identity (Uhlenhaut *et al*. 2009). The follicle stage-specific pattern of FOXL2 expression may therefore serve to inhibit the premature proliferation of GCs via *Ccnd2* repression, perhaps so as to limit the number of growing follicles.

FSH is not only necessary for the production of $E_2$ by GCs and their proliferation through the mechanisms described above, but is also required during antral folliculogenesis for the prevention of GC apoptosis and follicle atresia (Peluso & Steger 1978; Chun *et al*. 1994; Chun *et al*. 1996). GCs stimulated with FSH secrete anti-apoptotic factors, including X-linked inhibitor of apoptosis (*Xiap*) and CASP8 and FADD-like apoptosis regulator (*Cflar*), whereas in the absence of FSH, GCs express the pro-apoptotic Fas (TNF receptor superfamily member 6) (*Fas*) death receptor and its ligand *Fasl* (Kim *et al*. 1998; Wang, Asselin & Tsang 2002). Recent investigations have shown that FSH also regulates GC autophagy, a type of programmed cell death involving self-digestion and degradation of cellular constituents that may play a role in follicular atresia in addition to apoptosis (Choi *et al*. 2010). FSH represses autophagy in ovarian GCs (Choi *et al*. 2010), and may be particularly important in suppressing autophagic processes following oxidative stress (Shen *et al*. 2016; Shen *et al*. 2017). The function of FSH as a critical GC survival factor may be mediated by the inhibition of forkhead box O1 (FOXO1), a transcription factor related to FOXO3; FOXO1 induces cell cycle arrest and cell death when activated (Shen *et al*. 2014; Shen *et al*. 2017).

FSH is not the only positive regulator of GC proliferation and survival in late-stage follicles. $E_2$ produced by GCs in response to gonadotropins induces GC proliferation (Rao, Midgley & Richards 1978; Robker & Richards 1998), prevents follicular atresia (Dupont *et al*. 2000), promotes GC survival by inhibiting pro-apoptotic gene expression (Billig, Furuta &

Hsueh 1993; Lund *et al*. 1999; Toda *et al*. 2001; Quirk, Cowan & Harman 2006), and enhances the responsiveness of ovarian follicles to gonadotropin stimulation (Richards 1979). $E_2$ mediates its effects on folliculogenesis through ESR1 and ESR2, steroid hormone receptors and members of the nuclear receptor superfamily of transcription factors (Mangelsdorf *et al*. 1995). ESR1 is the predominant $E_2$ receptor in the ovary, with expression localized to the TCs and interstitial cells, whereas ovarian ESR2 is mainly expressed in the GCs of growing follicles (Jefferson *et al*. 2000; Mowa & Iwanaga 2000). Deletions of these receptors in the mouse have helped to elucidate their roles in the ovary: *Esr1* KO mice display normal antral folliculogenesis but are infertile due to an inability to ovulate (Lubahn *et al*. 1993); *Esr2* KO mice are subfertile secondary to reduced ovulation rates (Krege *et al*. 1998); and *Esr1/2* dKO mice are infertile, with seminiferous tubule-like ovarian structures housing sex-reversed follicles composed of Sertoli-like cells (Couse *et al*. 1999; Dupont *et al*. 2000). Like $E_2$, IGF1 is also critical for normal folliculogenesis (Baker *et al*. 1996), and represses GC apoptosis (Chun *et al*. 1994; Chun *et al*. 1996) and promotes GC proliferation and survival (Richards *et al*. 2002a; Richards *et al*. 2002b). IGF1 enhances the responsiveness of GCs to FSH, likely by regulating the expression of *Fshr* on the surface of GCs (Zhou *et al*. 1997), and increases TC steroidogenesis through the upregulation of steroidogenic enzymes (McAllister, Byrd & Simpson 1994) and LHCGRs (Cara & Rosenfield 1988; Cara *et al*. 1990; Magoffin & Weitsman 1994). Insulin, signalling through the insulin receptor (INSR), has similar effects on steroid production in follicle cells (Barbieri *et al*. 1986; Hernandez *et al*. 1988; Cara & Rosenfield 1988; McAllister, Byrd & Simpson 1994; Willis & Franks 1995; Willis *et al*. 1996; Munir *et al*. 2004; Du, Rosenfield & Qin 2009). As in the case of FSH, the signalling cascades induced by $E_2$ and IGF1 control antral GC proliferation via CCND2 (Robker & Richards 1998). In contrast to the actions of these growth factors on follicle

cells, androgens produced by the TCs and which signal through the androgen receptor (AR) have been shown to enhance GC apoptosis (Billig, Furuta & Hsueh 1993); the complex actions of ovarian androgens and the AR during folliculogenesis will be discussed further in Chapter 3.

#### 1.1.3.4 Ovulation and Luteinization

The cyclic recruitment of a small cohort of antral follicles for further growth to the pre-ovulatory stage occurs after the onset of puberty. FSH and LH are secreted by the gonadotrope cells of the anterior pituitary in response to differential frequencies of pulsatile stimulation from hypothalamic GnRH, with low frequency GnRH pulses leading to FSH release and high frequency GnRH pulses leading to LH release (Belchetz *et al*. 1978). Towards the end of the luteal phase of the estrous cycle, slow pulses of GnRH cause pituitary FSH secretion while LH levels remain low. Increasing levels of FSH initiate a wave of recruitment of multiple antral follicles that compete with each other for dominance and eventual ovulation; all unselected antral follicles are subject to atresia. Low levels of $E_2$ secreted by the GCs of cyclically recruited maturing follicles in response to FSH inhibit follicle release through negative endocrine signalling. This suppression of hypothalamic GnRH and pituitary FSH prevents the FSH-induced development of new antral follicles within the same cycle. The typical result in humans is the selection of a single follicle from the antral cohort for dominance and subsequent ovulation, whereas in multiovulatory species such as mice, selection for and ovulation of multiple follicles occurs during every cycle. The regulation of follicle selection and dominance is likely attributable to a higher threshold of responsiveness to FSH, despite falling FSH levels caused by negative feedback from $E_2$, via higher FSHR expression in those follicles that become pre-ovulatory (Fauser & van Heusden 1997). Those antral follicles that are not selected and die by

atresia may therefore become atretic due to the relative lack of FSHRs on their GCs and the concomitant decrease in FSH. Additionally, the dominant follicle contains more GCs than subordinate follicles, acquires LHCGRs on the surface of the mural GCs in response to FSH and $E_2$, expresses more IGF1 resulting in increased steroidogenesis, and may be subject to increased vascularization leading to higher gonadotropin concentrations (Baerwald, Adams & Pierson 2012). Rising levels of $E_2$ peak shortly before ovulation and positively regulate the rate of GnRH pulses, which increase in frequency during the follicular phase and act directly on the pituitary to stimulate LH secretion. Dramatically increased levels of LH production lead to the LH surge at mid-cycle, whereas FSH secretion is negatively regulated by GC-derived inhibins from the dominant follicle. The surge in LH at the end of the follicular phase signals through the FSH-induced LHCGRs on the surface of the mural GCs within the dominant follicle (Peng *et al*. 1991), resulting in a cascade of events that eventually leads to the ovulation of the cumulus-oocyte complex (COC), a structure composed of the fertilizable oocyte and its surrounding cumulus GC layer. Proper ovulation requires the LH surge-induced expansion of the cumulus GCs on a hyaluronan-rich ECM, mediated by epidermal growth factor (EGF) family members including amphiregulin (*Areg*), epiregulin (*Ereg*), and betacellulin, epidermal growth factor family member (*Btc*) in mural GCs (Park *et al*. 2004). These EGF family members bind to tyrosine kinase EGFRs, resulting in the induction of mitogen-activated protein kinase (MAPK) signalling (Su *et al*. 2002; Fan *et al*. 2009). Mural GC MAPK signalling leads to the stimulation of cumulus expansion in part through the induction of genes whose protein products contribute to hyaluronan ECM formation, including hyaluronan synthase 2 (*Has2*), tumor necrosis factor alpha induced protein 6 (*Tnfaip6*), pentraxin related gene (*Ptx3*) and prostaglandin-endoperoxide synthase 2 (*Ptgs2*; Park *et al*. 2004). Accordingly, the expression of these genes is down-

regulated and gonadotropin-induced cumulus expansion is inhibited in mice null for *Areg* or *Ereg* (Hsieh *et al*. 2007). The oocyte also appears to play an active role in cumulus GC expansion following the LH surge (Buccione *et al*. 1990; Salustri, Yanagishita & Hascall 1990). Candidates for the oocyte-derived cumulus expansion-enabling factor(s) include GDF9 (Elvin *et al*. 1999b; Varani *et al*. 2002; Gui & Joyce 2005) and/or BMP15 (Yan *et al*. 2001; Yoshino *et al*. 2006; Su *et al*. 2004a). GDF9 signals at least in part through SMAD2/SMAD3 to induce cumulus expansion (Dragovic *et al*. 2007; Li *et al*. 2008a), whereas BMP15 signals through the bone morphogenetic protein receptor type-1B (BMPR1B) to activate SMAD1/SMAD5/SMAD8 (Moore, Otsuka & Shimasaki 2003).

In addition to stimulating cumulus expansion, the LH surge also initiates the resumption of meiosis within the germ cell of the dominant follicle(s) through the actions of the oocyte-synthesized maturation-promoting factor (MPF), a complex composed of cyclin dependent kinase 1 (CDK1) and cyclin B1 (CCNB1) that regulates the $G_2$/M transition of the cell cycle (Doree & Hunt 2002). The MPF is kept in an inactive state through the activation of PKA signalling and high levels of oocyte cAMP derived from the mural GCs, leading to the phosphorylation and thus inhibition of CDK1. The LH surge serves to reduce cAMP levels and PKA activity, activating the MPF and resulting in the resumption of meiosis such that the diploid primary oocyte becomes a haploid secondary oocyte (Adhikari & Liu 2014). Meiosis resumption is first characterized by the dissolution of the oocyte's nuclear envelope in a process termed germinal vesicle breakdown (GVBD). Meiosis will halt a second time after ovulation during metaphase II through stabilization of the MPF, and the completion of meiosis II does not occur until after fertilization via signals from the sperm that cause its degradation (Nixon *et al*. 2002; Saunders *et al*. 2002). Following cumulus expansion and meiotic resumption, the LH surge

results in the rupture of the OSE and ovulation of the COC into the fallopian tube. Specifically, ovulation involves proteolytic degradation of collagen in the follicular wall, the prostaglandin-induced contraction of ovarian smooth muscle cells, and an inflammatory and immune-like response that leads to the extrusion of the COC (Richards, Liu & Shimada 2008). The ovulatory process marks the end of the follicular phase of the estrous cycle.

Post-ovulation, LH is responsible for the luteinization of the GCs and TCs of the ruptured follicle remnants through terminal differentiation (Richards, Hedin & Caston 1986). This morphological and biochemical remodeling process forms the corpus luteum, a transient and highly vascularized tissue that primarily functions to secrete $P_4$. Luteinized GCs and TCs are characterized by their eosinophilic cytoplasm, large size, and prominent nucleolus. The GCs of the pre-ovulatory follicle stop dividing in response to the LH surge due to cell cycle arrest (Rao, Midgley & Richards 1978; Hirshfield 1991), which involves elevated levels of cyclin dependent kinase inhibitors such as cyclin dependent kinase inhibitor 1A ($p21^{Cip1}$) and $p27^{Kip1}$, and the loss of positive cell cycle regulators like CDK2 and cyclins D2 and E1 (Stocco, Telleria & Gibori 2007). Corpus luteum-produced $P_4$ and $E_2$ negatively regulate GnRH pulsatility, suppressing LH levels but stimulating FSH production during the luteal phase and leading to the re-initiation of the estrous cycle (Nippoldt *et al*. 1989). In the case of oocyte fertilization and embryo implantation, the corpus luteum is maintained by placental hCG, whereas in the absence of pregnancy it is degraded to the corpus albicans through luteolysis, marking the end of the luteal phase. In these ways, the gonadotropins FSH and LH, the steroid sex hormones they induce, and other intra-ovarian factors, ensure the ovulation of competent oocytes as well as the preparation of the female sex organs for potential implantation and pregnancy. Folliculogenesis results in the continuous recruitment of follicle cohorts into the growing pool, such that following ovulation,

additional antral follicles are prepared for potential ovulatory dominance through cyclic recruitment. Thus the processes of initial follicle recruitment, growth, and cyclic recruitment, accompanied by oocyte attrition and follicular atresia which ensure that most follicles never ovulate, create a balance of follicle survival and loss that results in the complete exhaustion of the ovarian reserve at the end of the reproductive lifespan.

## 1.2 Ovarian Pathologies

As discussed in Section 1.1, the robust parallels that exist between divergent mammalian species, such as rodents and humans, have led to the identification of genes important for the normal development and regulation of the mammalian ovary. Further parallels can be drawn between species in terms of reproductive disease processes, such that ovarian disease models can be used to identify previously unknown genetic determinants, interrogate causal candidate genes and pathways, and investigate interactions between genetic, endocrine, and environmental influences. Two ovarian pathologies relevant to this dissertation are: 1) polycystic ovary syndrome (PCOS), a complex disorder affecting the reproductive, endocrine, and metabolic systems; and 2) ovarian cancer, a heterogeneous disease which encompasses many unique neoplasms that are stratified by the cell type of origin, their specific histotype, and a number of defining molecular characteristics.

### 1.2.1 Polycystic Ovary Syndrome

PCOS is one of the most frequent endocrine disorders of reproductive-aged women, with a prevalence of over 10% in this population (Goodarzi *et al*. 2011). PCOS generally presents

around puberty (Franks 2002) and is characterized by hyperandrogenism and menstrual dysfunction leading to subfertility, with or without cystic ovaries (Adams, Polson & Franks 1986). Many PCOS patients also present with obesity (particularly visceral obesity; Lim *et al*. 2012), insulin resistance (Burghen, Givens & Kitabchi 1980), and metabolic syndrome (Behboudi-Gandevani *et al*. 2017), a cluster of endocrine and metabolic disturbances that includes hyperglycemia, insulin resistance, visceral obesity, dyslipidemia and hypertension (Huang 2009). The symptoms of PCOS and its co-morbidities may predispose patients to infertility (Kousta, White & Franks 1997), type 2 diabetes (Moran *et al*. 2010), cardiovascular disease, and cancer of the endometrium, ovary, and/or breast (Fauser *et al*. 2012). The diagnosis of PCOS is difficult and relies on the exclusion of other conditions (The Rotterdam ESHRE/ASRM-sponsored PCOS consensus workshop group 2004), and while evidence of a genetic predisposition is apparent (Legro *et al*. 1998) and genome-wide association studies have linked myriad loci with PCOS (Welt & Duran 2014), no single cause has been defined. Instead, a combination of genetic, endocrine and lifestyle factors are likely responsible. Despite the complexities driving this polygenic disorder, the underlying cause is thought to depend on a dysfunctional HPG axis in which LH released from the anterior pituitary leads to abnormally increased androgen production by ovarian TCs (Waldstreicher *et al*. 1988). Elevated circulating androgens, including DHEA, subsequently support visceral adiposity, hirsutism, and chronic, low-grade inflammation in a detrimental feedback loop (Deligeoroglou *et al*. 2012). Evidence of abnormal follicular development prior to the initiation of endocrine cycling in PCOS patients suggests the ovary itself is the source of PCOS susceptibility (Franks, McCarthy & Hardy 2006), and recent studies have indicated that an intrinsic TC defect in combination with dysfunctional GCs contribute to disordered folliculogenesis and androgen overproduction (Rosenfield &

Ehrmann 2016). The high levels of insulin found in some PCOS patients also stimulate TC steroidogenesis despite the presence of insulin resistance in other tissues, further contributing to hyperandrogenism and HPG dysfunction (Nestler *et al*. 1998; Wu *et al*. 2014). The excessive androgens produced by TCs signal through the AR (discussed in Chapter 3), which has also been implicated in PCOS development (Wang *et al*. 2015b; Yuan *et al*. 2015; Caldwell *et al*. 2015; Caldwell *et al*. 2017). It is evident from the data gathered to date that PCOS is a complex trait, the development of which requires an interaction of genetic, endocrine, and environmental factors and that has serious implications on patient health and quality of life.

### 1.2.2 Ovarian Cancer

Ovarian cancer is the second most common gynecological malignancy and the eighth deadliest cancer among Canadian women. The lifetime probability of developing ovarian cancer is 1.3% (1 in 75 women), while the lifetime probability of death from this disease is 1.1% (1 in 90 women; Canadian Cancer Society's Steering Committee on Cancer Statistics 2019). As ovarian cancer symptoms are generally absent or non-specific and reliable biomarkers are lacking, the majority of patients are diagnosed with late stage tumours that show resistance to traditional chemotherapeutic methods and often recur. The overall five-year (yr) relative survival rate for such late stage cases is approximately 30%, though this figure increases to over 90% for those diagnosed early when the cancer is localized to the ovaries (American Cancer Society 2018). The majority of ovarian cancer cases are diagnosed during the fifth and sixth decades of life, although ovarian cancer occurs in all age groups (Koonings *et al*. 1989).

The histological stratification of human ovarian tumours was traditionally based on the assumed ovarian cell of origin, and as such they are divided into three major classes. The

majority (80-90%) of ovarian tumours have historically been thought to arise from the OSE, and as such are termed epithelial ovarian cancers (EOC). Sex cord-stromal tumours (SCSTs) derived from steroid-producing cells, including the GCs and TCs that compose ovarian follicles, account for approximately 8% of ovarian neoplasms. Approximately 1-2% of ovarian cancers are germ cell tumours derived from the PGCs, with the remainder attributed to metastases from extraovarian primary tumours (Jamieson & Fuller 2012). These three tumour types are further subclassified by histology and characteristic mutational signatures, and accordingly, recent research and management strategies have increasingly focused on the recognition of individual histotypes as separate diseases (Rojas *et al*. 2016).

The high incidence of EOC in the human population has led to a focus in the ovarian cancer research field on this tumour histotype. These tumours generally present in post-menopausal women at a time when the ovary is devoid of follicles (Scully, Young & Clement 1998). Tumours of the EOC class can be subdivided into two broad categories termed type I and type II (Shih & Kurman 2004). Type I tumours are typically indolent and localized to the ovary, and include low-grade serous, mucinous, endometrioid, clear cell, and transitional cell carcinomas. The origins of these Type I tumours can be traced back to benign precursor lesions in the ovary (Kurman & Shih 2011; Rojas *et al*. 2016). Type II tumours tend to be clinically aggressive and present at advanced stages, and mainly include high-grade serous carcinoma (HGSC), the single most common subtype of ovarian cancer in Canadian women (Köbel *et al*. 2010). Unlike Type I EOC, the identification of benign HGSC precursor lesions has been less evident. Historically, the most accepted theory of ovarian cancer origin was that of "incessant ovulation" (Fathalla 1971), which attributed tumour susceptibility to the accumulation of deleterious mutations concomitant with the proliferative repair of the OSE following ovulation.

Observations that early menarche and late menopause increase EOC risk, and that ovulation-blocking interventions, including oral contraceptive use, pregnancy, and breastfeeding are protective (Casagrande *et al*. 1979; Purdie *et al*. 2003), supported this hypothesis. However, elegant experimentation in recent years has shown that ovarian HGSC are in fact secondary cancers arising from malignant lesions in the nearby distal fallopian tube (Kurman & Shih 2010; Karst, Levanon & Drapkin 2011; Perets & Drapkin 2016). The development of HGSC as a malignancy derived from the latter source has been hypothesized to occur in a three-step process, beginning with the development of strong tumour protein p53 (p53) expression in secretory fallopian tube epithelial cells that are otherwise benign (Lee *et al*. 2007; Folkins *et al*. 2008). The p53 tumour suppressor is critical for the maintenance of the genome's integrity through its role in DNA damage repair (Lane 1992), and while these p53 signature foci have low proliferative activity, they are subject to DNA damage, cell cycle arrest, and the accumulation of mutations in the p53 gene (*TP53*). Additional genetic perturbations in the absence of functional p53 leads to the development of a serous tubal intra-epithelial carcinoma (STIC) from p53 signature sites. STICs are characterized by morphologically atypical cells derived from the secretory fallopian tube epithelium, which possess a high proliferative index, show signs of DNA damage, and accumulate mutant p53 (Crum *et al*. 2007; Lee *et al*. 2007; Shaw *et al*. 2009; Medeiros *et al*. 2006; Chene *et al*. 2015). These STICs evolve into HGSC when highly aggressive subclones expand and invade into the nearby ovarian surface (Crum *et al*. 2007). A large body of evidence has been accumulated that supports this model of HGSC origin, including the presence of identical *TP53* mutations in contiguous p53 signatures and STICs (Lee *et al*. 2007) and STICs and their corresponding ovarian carcinomas (Kindelberger *et al*. 2007). That salpingo-oophorectomy reduces ovarian cancer risk, particularly in women at high risk due to mutations in

the BRCA1 DNA repair associated (*BRCA1*) and *BRCA2* tumour suppressor genes, also supports this hypothesis (Kauff *et al*. 2002; Rebbeck *et al*. 2002), and indicates salpingectomy followed by delayed oophorectomy for those women at high risk of HGSC may be a viable prophylactic option (Kwon *et al*. 2013). The similar frequencies of p53 signatures in *BRCA1/BRCA*2 mutation carriers and non-carriers (Lee *et al*. 2007; Folkins *et al*. 2008; Shaw *et al*. 2009), but the increased incidence of STICs identified in carriers (Shaw *et al*. 2009; Mingels *et al*. 2012; Reitsma *et al*. 2013) indicates that loss of *BRCA1/BRCA*2 may be an early requirement for the progression of a benign p53 signature to a malignant STIC. The tubal source of HGSC correlates well with an updated hypothesis of incessant ovulation, in which the inflammatory environment characteristic of ovulation assaults secretory fallopian tube epithelial cells and leads to the development of a p53 signature followed by STIC formation (reviewed by Tone 2017).

Despite the recent advances into the etiology of HGSC, it should be noted that neither of the theories discussed above account for the malignant mechanisms that predispose to SCST or germ cell tumours, which are derived from distinct and specialized cell types located below the OSE. Likewise, despite the association of multiple tumour suppressor genes and oncogenes with EOC initiation and progression (including those listed above and HGSC; KRAS proto-oncogene, GTPase (*KRAS*), B-Raf proto-oncogene, serine/threonine kinase (*BRAF*) and low-grade serous carcinoma; *KRAS* and mucinous carcinoma; *CTNNB1*, AT-rich interaction domain A1 (*ARID1A*), *PTEN*, phosphatidylinositol-4,5-bisphosphate 3-kinase catalytic subunit alpha (*PIK3CA*) and endometrioid carcinoma; and *ARID1A* and clear cell carcinoma), mutations in these genes have generally not been identified in tumours derived from other ovarian cell types (Gilks 2010; Rescigno *et al*. 2013). Lastly, the cumulatory risk conferred by ovulation over the

reproductive lifespan is not applicable to juvenile ovarian cancer subtypes, suggesting one or more significant genetic factors govern susceptibility in such cases.

#### 1.2.2.1 Granulosa Cell Tumours of the Ovary

*Overview*

SCSTs arising from the steroid and stromal cell components of the ovary are further sub-classified based mainly on histology, and include granulosa-stromal cell tumours, Sertoli-stromal cell tumours, mixed and unclassified SCSTs, and steroid cell tumours (Scully 1987). The precise diagnosis of these subtypes can be challenging due to morphological overlap between types and/or ambiguous histological presentation in some cases, such that there is a need for accurate molecular diagnostic assays that distinguish between subtypes. Approximately 5% of all ovarian cancers and 90% of SCSTs are GC tumours belonging to the granulosa-stromal cell tumour subclass (Jamieson & Fuller 2012), which are defined by the World Health Organization Classification of Gynecologic Tumours as SCSTs comprised of a 10-100% GC component (Tavassoli *et al*. 2003). The annual incidence of GC tumours in developed countries ranges from 0.4-1.7 cases per 100,000 women (Schumer & Cannistra 2003). GC tumours are further divided into the adult and juvenile clinicopathologic subtypes, with subtype stratification traditionally based on histology and age at tumour diagnosis. Unlike the usual post-menopausal presentation of EOC, GC tumours occur at both ends of the reproductive spectrum. Adult GC tumours occur more frequently than the juvenile subtype, accounting for approximately 95% of all GC tumours. This subtype typically occurs in peri- and post-menopausal women between the ages of 50-54 yr of age, though it may be observed in all age groups (Schumer & Cannistra 2003). Juvenile GC tumours most commonly affect young girls from newborns through adolescence; in the largest

cohort examined to date, 44% of cases occurred in the first decade, 34% in the second, 18% in the third, and only 3% after age 30 (Young, Dickerson & Scully 1984). The median age at juvenile GC tumour diagnosis for pediatric patients has been reported to be 7-8 yr of age (Vassal *et al*. 1988; Calaminus *et al*. 1997).

*Clinical Presentation and Pathology*

Most juvenile GC tumour cases present with acute endocrine symptoms, with or without a palpable abdominal mass accompanied by abdominal pain and swelling. Ascites are a rare complication observed in approximately 10% of cases. The majority of tumours are estrogenic due to functioning GCs, with symptoms that vary and depend on the patient's reproductive status. Over 80% of female infants and pre-pubertal children present with isosexual pseudoprecocity, mainly characterized by breast development, uterine bleeding, and vaginal discharge, as well as accelerated somatic and skeletal growth and the production of pubic and/or axillary hair. In contrast, the most common endocrine symptoms observed in adolescent girls and adult women with juvenile GC tumours are amenorrhea and irregular uterine bleeding caused by endometrial hyperplasia following estrogenic stimulation (Young, Dickerson & Scully 1984). Androgenic juvenile GC tumours resulting in virilization, while rarer than their estrogenic counterparts, have been reported (Nakashima, Young & Scully 1984; Young, Dickerson & Scully 1984; Betta & Bellingeri 1985; Merras-Salmio *et al*. 2002; Larizza *et al*. 2006; Nomelini *et al*. 2007; Kalfa *et al*. 2010; Kumar *et al*. 2014; Bús *et al*. 2017), suggesting that the conversion of androgens to estrogens in tumourigenic GCs has been compromised. Accordingly, aromatase protein expression has been shown to be absent or reduced in juvenile GC tumours from patients with hyperandrogenism (Kalfa *et al*. 2010). In addition to estrogens or androgens, most tumours

also secrete excessive levels of inhibin, and serum inhibins (particularly inhibin B) and AMH are useful tumour biomarkers (Silverman & Gitelman 1996; Mom *et al*. 2007).

The majority of juvenile GC tumour cases are unilateral, although bilateral tumours have been reported, and on average display a diameter of 12.5 cm. Macroscopically, most tumours are uniformly solid and/or cystic and may exhibit localized areas of necrotic or hemorrhagic tissue (Young, Dickerson & Scully 1984; Scully, Young & Clement 1998). Microscopically, juvenile GC tumours are characterized by a distinct nodular or diffuse pattern of neoplastic GCs. Large oval or round rudimentary follicles containing eosinophilic or basophilic fluid may be present. The tumourigenic GCs are present in a fibrothecomatous background and may be luteinized. In contrast to adult GC tumours, the juvenile subtype usually lacks Call-Exner bodies (small pockets of eosinophilic fluid between GCs) and has GCs with abundant cytoplasm and immature, hyperchromatic and round nuclei lacking grooves and with a comparatively higher mitotic activity (Scully, Young & Clement 1998; Young 2005). Immunohistochemically, juvenile GC tumours exhibit positive staining for AMH, inhibin, calretinin, cluster of differentiation 99 (CD99) antigen, FOXL2, and SF1; these markers are useful for distinguishing juvenile GC tumours from other ovarian neoplasm, including germ cell tumours and other SCST subtypes (Matias-Guiu, Pons & Prat 1998; McCluggage & Maxwell 2001; Al-Agha *et al*. 2011; Bai *et al*. 2012).

*Prognosis and Treatment*

Although they are characterized by a pattern of slow, indolent progression, the unique hormonal profile of juvenile GC tumours means that the majority (90%) of cases are diagnosed at International Federation of Gynecology and Obstetrics (FIGO) stage I, and are therefore

considered to be low-grade malignancies with favourable prognoses (Schneider *et al*. 2003). However, the disease tends to recur and is almost always fatal at advanced stages (Young, Dickerson & Scully 1984). Treatment at the earliest stages usually consists of fertility-sparing surgical debulking (i.e. unilateral salpingo-oophorectomy) alone, which is combined with adjuvant platinum-based chemotherapy (e.g. cisplatin) in advanced and/or recurrent cases. Those tumours that recur tend to do so within three yr following initial diagnosis, with metastatic recurrence more common in the juvenile subtype than in the adult condition (Young, Dickerson & Scully 1984; Geetha & Nair 2010). Metastases within the pelvic and abdominal cavities and to the liver, lungs, lymph nodes and other sites have been reported (Young, Dickerson & Scully 1984; Wessalowski *et al*. 1995; Benesch *et al*. 2015; Cheong *et al*. 2016).

*Genetics*

Investigations into the etiology of juvenile GC tumours have been largely precluded by their rarity in the human population, although some germline and somatic mutations, including those causing cancer predisposition syndromes, have been loosely associated. Juvenile GC tumours have been reported in patients with Ollier disease (OMIM #166000) and Maffucci syndrome (OMIM #614569), which are diseases characterized by the development of multiple enchondromas or enchondromas and hemangiomas, respectively (Young, Dickerson & Scully 1984). These conditions are thought to arise from somatic mosaic mutations in the isocitrate dehydrogenase (NADP(+)) 1, cytosolic (*IDH1*) or isocitrate dehydrogenase (NADP(+)) 2, mitochondrial (*IDH2*) genes (Amary *et al*. 2011; Pansuriya *et al*. 2011), which code for tricarboxylic acid cycle enzymes that catalyze the formation of α-ketoglutarate from isocitrate. Despite the appearance of GC tumours in patients with Ollier disease and Maffucci syndrome,

analyses of sporadic GC tumours have failed to identify *IDH1* or *IDH2* mutations (Aitken *et al*. 2015).

Juvenile GC tumours can also develop in females with Peutz-Jeghers syndrome (PJS; #OMIM 175200), a hamartomatous disease characterized by polyps of the gastrointestinal tract and melanin spots of the lips, buccal mucosa, and digits, and that predisposes patients to an increased risk of various neoplasms (Dozois *et al*. 1970). PJS is caused by germline mutations in the serine/threonine kinase 11 (*STK11*) gene (Hemminki *et al*. 1998; Jenne *et al*. 1998), a cell polarity regulator and tumour suppressor located on human Chr 19p13.3. However, *STK11* mutations have not been associated with sporadic GC tumours in patients without PJS (Avizienyte *et al*. 1999; Kato *et al*. 2004; Wang *et al*. 1999), although loss-of-heterozygosity near the *STK11* locus was observed in 50% of sporadic juvenile and adult GC tumours examined, indicating that loss of the wild type (WT) *STK11* allele may be a consequence of sporadic tumour progression (Kato *et al*. 2004). Furthermore, the SCSTs affecting women with PJS generally exhibit a distinctive morphology that has been described as intermediate between that of GC and Sertoli cell tumours termed "sex cord-stromal tumour with annular tubules" (Young *et al*. 1982); these tumours may therefore represent a unique ovarian neoplasm distinct from juvenile GC tumours that warrants a separate classification (Young 2005).

Germline dicer 1, ribonuclease III (*DICER1*) mutations have also been identified in patients with juvenile GC tumours (Schultz *et al*. 2011; Heravi-Moussavi *et al*. 2012; Goulvent *et al*. 2016). *DICER1* encodes an endoribonuclease that cleaves precursor microRNA (miRNA) into mature miRNA prior to their loading into the RNA-induced silencing complex (RISC). Germline mutations in this gene are associated with DICER1 syndrome (OMIM #601200), also known as pleuropulmonary blastoma familiar tumour and dysplasia syndrome, which is

characterized by pleuropulmonary blastoma, cystic nephroma, and multinodular goiter of the thyroid. Recent investigations into the etiology of another SCST subtype, Sertoli-Leydig cell tumours (SLCTs), have identified recurrent somatic *DICER1* mutations in up to 63% of cases examined (Heravi-Moussavi *et al*. 2012; Kim *et al*. 2013; Witkowski *et al*. 2013; Conlon *et al*. 2015; Goulvent *et al*. 2016). SLCTs are also known to occur in patients with DICER1 syndrome, although the frequency of germline *DICER1* mutations in sporadic SLCT cases is unknown. Considering the small number of juvenile GC tumours found to possess somatic *DICER1* mutations, the consistent presence of *DICER1* mutations in SLCTs, and the morphological overlap between these two subtypes, those mutation-positive juvenile GC tumours may in actuality be misdiagnosed SLCTs.

Activating somatic mutations in the GNAS complex locus (*GNAS*) gene, which encodes the stimulatory α subunit of the heterotrimeric G-protein that facilitates GPCR signal transduction, were identified in 30% of juvenile GC tumours in one investigation (Kalfa *et al*. 2006). Activating mutations in *GNAS* cause McCune-Albright syndrome (OMIM #174800), a clinically heterogeneous disorder that predominantly features fibrous dysplasia of the bone, café-au-lait skin pigmentation, and peripheral precocious puberty due to hyperestrogenism secondary to ovarian cysts (Boyce *et al*. 1993). While activating *GNAS* mutations could potentiate FSHR-mediated signalling pathways, other investigations have failed to identify *GNAS* mutations in juvenile GC tumours (Hannon *et al*. 2002; Bessière *et al*. 2015), and their presence in this tumour type has not been verified in other tumour series despite the high prevalence found by Kalfa and colleagues. Notably, no deleterious or activating somatic mutations of the *FSHR* have been identified in juvenile GC tumours to date (Kotlar *et al*. 1998; Hannon *et al*. 2002).

Somatic mutations, including in-frame duplications and point mutations of unknown significance, have also been identified in the AKT serine/threonine kinase 1 (*AKT1*) gene in a single series of juvenile GC tumours (Bessière *et al*. 2015). As in the cohort tested for *GNAS* mutations described above, this tumour series was comprised of juvenile GC tumours categorized as such on the basis of histology only. Subsequent transcriptomic analyses of the same tumour series identified a large number of differentially regulated genes in these tumours, particularly those involved in pluripotency and proliferation (Auguste *et al*. 2015). Somatic *AKT1* mutations may be of particular importance given the role of PI3K/AKT-mediated signalling downstream of FSH; however, while a subset of *AKT1* duplications have been shown to lead to AKT hyperactivity (Bessière *et al*. 2015), it is as yet unclear if the somatic *AKT1* mutations identified in juvenile GC tumours are the result of tumour progression or drivers of tumourigenesis. Importantly, and as in the case of the *GNAS* investigation described above (Kalfa *et al*. 2006), these results have not been replicated in independent cohorts of juvenile GC tumours.

A single case of a juvenile GC tumour has been identified in a patient with Beckwith-Wiedmann syndrome (BWS; #OMIM 130650), a pediatric overgrowth disorder that, like PJS, predisposes patients to tumour development (Lamas-Pinheiro *et al*. 2016). BWS usually occurs sporadically or by maternal transmission, and results from mutations or deletions of imprinted genes on the short arm of Chr 11 such as the negative cell cycle regulator and suspected tumour suppressor cyclin dependent kinase inhibitor 1C (*CDKN1C*). This case of BWS was associated with a deletion in *CDKN1C*; however, the diagnosis of BWS in this particular instance is of debate (Brioude & Netchine 2017). Similarly, a juvenile GC tumour has been described in a patient with Li-Fraumeni syndrome (OMIM #151623), a familial cancer predisposition

syndrome characterized by the early onset of multiple tumours due to heterozygous germline mutations in *TP53* (Nogales *et al*. 2004), as well as in an infant with germline mutations in both *TP53* and *PTEN* (Plon *et al*. 2008). Juvenile GC tumours have also been reported in patients with Meigs' syndrome, which is defined as the triad of benign ovarian tumour, ascites, and plural effusion and which has not been associated with any genetic determinants (Kaur *et al*. 2009; Ciftci, Pirgon & Unlu 2013).

*Cytogenetics*

GC tumours exhibit relatively stable karyotypes in comparison with EOCs, with approximately 5-20% displaying some degree of aneuploidy (Jamieson & Fuller 2012). Trisomy of Chr 12 and/or monosomy of Chr 22 and X have been detected in some human juvenile GC tumours; however, these cytogenetic aberrations are thought to be the consequence of tumour progression rather than a requirement for tumour initiation (Schofield & Fletcher 1992; Shashi *et al*. 1994; Kemp, Silva & Elnaggar 1995; Lindgren, Waggoner & Rotmensch 1996; Mayr *et al*. 2002).

*Granulosa Cell Tumours and Foxl2*

In 2009, Shah and colleagues identified a recurrent, somatic missense mutation in *FOXL2* in 97% of adult GC tumours using whole-transcriptome sequencing. This heterozygous C>G mutation at nucleotide 402 (NM_023067.4) results in the substitution of cysteine (Cys) with tryptophan (Trp) at residue 134. Notably, the c.402C>G *FOXL2* mutation has not been reported in the germline and is absent from other tumour types, as well as from the vast majority of

juvenile GC tumours diagnosed on the basis of age and histology (Schrader *et al*. 2009; Shah *et al*. 2009; Benayoun *et al*. 2010; Jamieson *et al*. 2010; Kim *et al*. 2010; Al-Agha *et al*. 2011). This mutational pattern has been replicated in a number of other tumour series, confirming the specificity of the p.Cys134Trp mutation to approximately 92% of adult GC tumours (784 mutation-positive tumours/851 total tumours; Jamieson *et al*. 2010; Kim *et al*. 2010; Al-Agha *et al*. 2011; D'Angelo *et al*. 2011; Rosario *et al*. 2013; Kommoss *et al*. 2014; Maillet *et al*. 2014; Goulvent *et al*. 2016; McConechy *et al*. 2016; Zannoni *et al*. 2016; Buza, Wong & Hui 2017). The identification of this highly sensitive and specific marker has altered the diagnostic paradigm for adult GC tumours, and has been incorporated into the differential diagnosis of SCSTs and other histologically ambiguous ovarian tumours (McConechy *et al*. 2016). Although the exact influence of the p.Cys134Trp mutation on adult GC tumour initiation remains unknown, its notable absence from juvenile GC tumours indicates the two subtypes have distinct genetic etiologies. Absent or reduced expression of *FOXL2* has been associated with aggressive juvenile GC tumours, suggesting a role for FOXL2 as a suppressor of juvenile GC tumour progression rather than a requirement for tumour initiation (Kalfa *et al*. 2007). While significant *FOXL2* hypermethylation has been observed in a cohort of GC tumours not distinguished by histology or mutation status (Xu *et al*. 2016), the role of epigenetic *FOXL2* regulation in the juvenile subtype, if any, is currently unknown.

*FOXL2* is a single-exon gene located on Chr 9 in the mouse and the long arm of Chr 3 (3q22.3) in humans. The *FOXL2* gene encodes a highly conserved member of the forkhead-winged-helix family of transcription factors, which regulate the expression of genes involved in cell growth, proliferation, and differentiation, with particularly important roles in determining cell fate during embryogenesis. Forkhead box (FOX) proteins are defined by the presence of a

conserved forkhead or winged-helix domain, a sequence motif of approximately 100 amino acids consisting of three α helices and two large loops that function to bind DNA. In addition to the N-terminal FOX domain, FOXL2 also contains an alanine- (Ala) and proline- (Pro) rich C-terminal region that functions as a transrepression domain (Pisarska *et al*. 2004; Bentsi-Barnes *et al*. 2010). Although FOXL2 is capable of forming homodimers (Lamba *et al*. 2009), it is not known whether this protein binds DNA and carries out its transcriptional functions as a monomer or multimer (Georges *et al*. 2013). FOXL2 is specifically expressed in the mesenchyme of the developing eyelids, the pituitary from development through adulthood, and fetal and adult ovarian GCs with a nuclear localization pattern (Cocquet *et al*. 2002; Ellsworth *et al*. 2006).

Previous investigations into the function of the FOXL2 transcription factor in the ovary have shown it is a key transcriptional regulator in GCs, as discussed throughout Section 1.1. FOXL2 is a marker of GC differentiation and is required for their transition from a squamous to cuboidal morphology, such that it is necessary for the progression of primordial to primary follicles; massive follicular atresia and infertility occur in its absence. Homozygous germline deletion of *Foxl2* in mice results in smaller animals with craniofacial defects (including absence of the upper eyelid), disorganized ovaries lacking mature GCs, and a high degree of perinatal lethality (Schmidt *et al*. 2004; Uda *et al*. 2004). FOXL2 is also required for the postnatal maintenance of GC differentiation into adulthood through the continuous repression of *Sox9*, thus preserving the ovarian determination pathway following the organ's specification (Uhlenhaut *et al*. 2009). In humans, heterozygous germline mutations in *FOXL2* have been associated with blepharophimosis, ptosis, and epicanthus inversus syndrome (BPES; OMIM #110100), a rare disorder characterized by malformation of the eyelid that is usually inherited in an autosomal dominant pattern (Crisponi *et al*. 2001). BPES is sub-classified into two clinical

subtypes, Types I and II; Type II displays only symptoms affecting the eyelids, whereas Type I is distinguished as BPES with POF, defined as menopause before the age of 40 (Zlotogora, Sagi & Cohen 1983). Over 100 mutations in *FOXL2* have been associated with BPES, although the genotype-phenotype correlation between individual *FOXL2* mutations and BPES subtypes has not been clearly determined. Unlike the recurrent and somatic p.Cys134Trp mutation identified in adult GC tumours, which is located within the second wing of the FOX domain, the germline *FOXL2* mutations present in BPES patients are spread across the gene (Beysen, Paepe & Baere 2009). Generally, it is thought that *FOXL2* loss-of-function mutations, whether due to protein truncation or missense mutations that decrease transcriptional activity, cause type I BPES with POF, whereas mutations with a less severe effect on transcriptional activity cause type II BPES (Dipietromaria *et al*. 2009). Functional investigations of some BPES-associated mutant FOXL2 proteins have shown that they affect protein localization and induce protein aggregation (Beysen *et al*. 2008; Todeschini *et al*. 2011), although these features do not correlate with BPES type (Dipietromaria *et al*. 2009). Despite the association of *FOXL2* mutations with BPES, no GC tumours have been reported in patients with either form of the syndrome.

Two GC tumour cell lines have been established that have been helpful in the interrogation of FOXL2's contribution to GC tumourigenesis. The KGN GC tumour cell line is heterozygous for the p.Cys134Trp *FOXL2* mutation (Schrader *et al*. 2009) and expresses FOXL2 messenger RNA (mRNA) and protein (Batista *et al*. 2006; Jamieson *et al*. 2010). The KGN cell line was derived from an invasive, recurrent adult GC tumour that had metastasized to the pelvic region of a 73 yr old woman (Nishi *et al*. 2001). In contrast, the COV434 GC tumour cell line, which was isolated from a primary metastatic GC tumour from a 27 yr old woman (van den Berg-Bakker *et al*. 1993; Zhang *et al*. 2000), has WT *FOXL2* alleles but no detectable *FOXL2*

mRNA or protein expression (Jamieson *et al*. 2010). The KGN and COV434 GC tumour cell lines are therefore recognized as representative of adult and juvenile GC tumours, respectively. These two cell lines present a unique opportunity to study the effect of the p.Cys134Trp mutant FOXL2 protein, and the mechanisms of adult versus juvenile GC tumourigenesis in general.

The mechanisms by which the FOXL2 p.Cys134Trp mutation contributes to adult GC tumour initiation and progression remain to be elucidated. Shah and colleagues (2009) postulated that interactions between mutant FOXL2 and its binding partners may be disrupted, as protein modelling indicated the mutation did not disrupt the FOX domain's conformation or DNA binding ability, and no mislocalization of FOXL2 was identified in mutant GC tumour samples. The p.Cys134Trp mutant FOXL2 protein also does not form large protein aggregates as do other FOXL2 mutant proteins found in BPES patients (Benayoun *et al*. 2010). The FOXL2 transcription factor is involved in the activation of a number of genes that are critical for normal ovarian function, including *CYP19A1* (Pannetier *et al*. 2006), the FSH subunit beta (*FSHB*; Lamba *et al*. 2009), gonadotropin releasing hormone receptor (*GNRHR*; Ellsworth *et al*. 2003), *FST* (Nonis, McTavish & Shimasaki 2013), and *AMH* (Park *et al*. 2014). Furthermore, FOXL2 is able to suppress the promoter activity of *NR5A1* (Takasawa *et al*. 2014), *FST* (McTavish *et al*. 2013), *STAR* (Pisarska *et al*. 2004), *CCND2*, *CYP11A1*, and *CYP19A1* (Bentsi-Barnes *et al*. 2010), and it appears to partner with other transcription factors to co-regulate gene transcription, including activator protein 1 (AP-1; Ellsworth *et al*. 2003; Kim *et al*. 2009), SF1 (Park *et al*. 2010), and SMAD3 (Nonis, McTavish & Shimasaki 2013; Roybal *et al*. 2014). *In vitro* assessments of the p.Cys134Trp FOXL2 mutant's ability to promote transcription indicate it may increase stimulation of *CYP19A1* expression two-fold higher than WT FOXL2, but has no differential effect on *STAR* expression and does not alter the protein's interaction with SF1

(Fleming *et al*. 2010). Compared to WT FOXL2, the mutant protein also has a stronger repressive effect on the GDF9- and activin A-induced transcriptional activation of *FST* via SMAD3 (McTavish *et al*. 2013; Nonis, McTavish & Shimasaki 2013). The suppression of FST production by mutant FOXL2 has been shown to lead to upregulated activin-induced proliferation in KGN cells (Cheng *et al*. 2014). The p.Cys134Trp allele is also inferior at promoting apoptosis compared to the WT protein *in vitro* (Kim *et al*. 2011; L'Hôte *et al*. 2012), in part through its actions on the *GNRHR* promoter (Cheng, Klausen & Leung 2013), the induction of lower levels of caspase 3/7 activity (Anttonen *et al*. 2014), and decreased activation of caspase 8, the tumor necrosis factor receptor superfamily member 1A (TNFRSF1A) death receptor and FAS (Kim *et al*. 2011). GC *FOXL2* expression is rapidly up-regulated following cellular exposure to oxidative stress and heat shock (Benayoun *et al*. 2009), and the protein protects cells by delaying cell cycle progression through the $G_1$ phase, partially through its repression of *CCND2* (Bentsi-Barnes *et al*. 2010) and induction of the cyclin dependent kinase inhibitor p16/INK4A (Benayoun *et al*. 2011). Mutant FOXL2 is unable to transactivate p16/INK4A *in vitro* in some cellular contexts (Benayoun *et al*. 2011). The p.Cys134Trp mutant FOXL2 protein may therefore favour GC tumourigenesis through deregulation of its ability to provoke apoptosis, negatively regulate the cell cycle, and/or induce proliferation. These differential activities may be due to altered protein-protein interactions between the p.Cys134Trp mutant FOXL2 protein and its promoter binding partners (L'Hôte *et al*. 2012). FOXL2 has been shown to heterodimerize with BPES-derived mutant FOXL2 (p.Gln219Ter) with greater affinity than to WT FOXL2, resulting in a dominant negative effect (Kuo *et al*. 2011), and it has been speculated that the p.Cys134Trp mutant FOXL2 protein may bind WT FOXL2 with similar consequences (Benayoun *et al*. 2010; Fleming *et al*. 2010). The diminished ability of the

p.Cys134Trp FOXL2 protein to induce apoptosis and inhibit cell cycle progression suggests FOXL2 is a tumour suppressor; however, loss of the WT *FOXL2* allele in adult GC tumours, as would be expected for a tumour suppressor gene, is rarely observed. Conversely, the single, recurrent heterozygous p.Cys134Trp mutation suggests an oncogenic, activating or gain-of-function mutation (Rosario, Cohen & Shelling 2014). The association of the p.Cys134Trp mutation with adult GC tumours is curious given the wide range of germline *FOXL2* mutations associated with BPES types I and II, and suggests that the induction of a specific and unique pathway leads to tumour initiation. Further work is necessary to characterize the mechanism(s) by which the somatic *FOXL2* p.Cys134Trp mutation induces the tumourigenic pathway in GCs at the end of the reproductive spectrum.

*Summary*

The high prevalence and specificity of the *FOXL2* p.Cys134Trp mutation in adult GC tumours indicates it is an early and perhaps necessary initiating step in adult GC tumourigenesis, while also providing a new avenue for molecular diagnostic criteria with promising implications for histologically challenging SCSTs. As the historical literature examining juvenile GC tumours did not benefit from this enhanced diagnostic paradigm, previous conclusions may be confounded by sample misdiagnosis. Likewise, single-series findings have poor replication, and so juvenile GC tumours remain at a disadvantage for consistent molecular diagnosis and subsequent mechanistic investigations. Given the lack of a defined genetic etiology for juvenile GC tumours, the clinician's ability to accurately predict susceptibility, effectively treat primary and recurrent cases, and estimate patient survival is obstructed. That juvenile GC tumours appear in infants and young girls prior to normal follicle recruitment at a time when the ovarian reserve

is fully replete, and that the somatic *FOXL2* mutation found in adult GC tumours is absent, suggests that these two clinicopathologic subtypes have distinct genetic origins. Accordingly, investigations into the genetic determinants underlying juvenile GC tumour initiation have capitalized on animal model systems with a goal for translation to the human condition.

### 1.3 Animal Models of Granulosa Cell Tumourigenesis

GC tumours are the most frequent spontaneous ovarian neoplasm occurring in laboratory rodents (Greenacre 2004; Thayer & Foster 2007). Although these tumours occur at variable frequencies in different strains of inbred mice, animals at advanced ages are most commonly affected. Inbred CE/Wy mice are spontaneously susceptible to GC tumours, with up to 34% of females affected by ovarian tumours, including GC-type SCSTs, by 22 months (mo) of age (Dickie 1954). C3HeB/De inbred females are also susceptible to GC tumour initiation at frequencies ranging from 13-23% by approximately 24 mo of age (Deringer 1959). A high incidence of ovarian tumours, including GC tumours, occurs in aged (24 mo) C3H/HeNctr inbred mice (Frith, Zuna & Morgan 1981). Aged (> 30 mo) CF-1 inbred mice are naturally susceptible to ovarian tumours at a frequency of 17%, although tumour subtype classification has not been reported (Breslow *et al*. 1974). NZC/Bl, NZO/Bl, and NZY/Bl inbred female mice also spontaneously develop GC tumours at advanced ages with frequencies ranging from 2-33% (Bielschowsky & D'Ath 1973), as do 3% of aged CBA/J inbred female mice (Tillmann, Kamino & Mohr 2000). Despite the numerous inbred mouse strains that are spontaneously susceptible to GC tumours, no genes that confer resistance or susceptibility to this trait have been identified to date. Furthermore, the late onset of the GC tumour phenotype in these mouse strains at a time

when the ovarian reserve has been depleted is characteristic of the adult GC tumour subtype and not the juvenile disease.

The genetic alteration of oncogenes and tumour suppressor genes, genes required for normal ovarian and endocrine function, and/or genes expressed exclusively in ovarian cell compartments has revealed insights into the genetic pathways underlying GC tumourigenesis (Table 1.1). Female mice with a single copy of the multiple endocrine neoplasia 1 (*Men1*) gene develop tumours of the endocrine system, including ovarian SCSTs comprised mainly of GCs, with 50% of mice affected by 19-26 mo of age (Bertolino *et al*. 2003). A small cohort of aged female mice examined following deletion of the Fanconi anemia, complementation group F (*Fancf*) gene were found to be susceptible to GC tumours at a frequency of 71% (Bakker *et al*. 2012). The FANCF protein complexes with other Fanconi anemia family members to regulate DNA damage repair in a *BRCA1/BRCA2*-associated pathway (Olopade & Wei 2003). Over 90% of female mice null for the *Fshr* gene spontaneously develop ovarian neoplasms including mixed SCSTs by 1 yr of age (Danilovich, Roy & Sairam 2001). The introduction of a constitutively active LH beta (LHB) subunit that elicits chronic LH hypersecretion causes GC tumour development in 100% of female mice by 5 mo of age (Risma *et al*. 1995). This trait was originally observed in transgenic mice in a CF-1 inbred strain background; however, the introduction of new alleles by crossing transgene carriers to other inbred strains resulted in the development of luteomas rather than GC tumours, suggesting additional strain-specific modifier genes influence the phenotype (Keri *et al*. 2000). Mice null for *Esr2* exhibit GC tumours and undifferentiated SCSTs with complete penetrance beginning at 15 mo of age (Fan *et al*. 2010). Tumour initiation in the absence of ESR2 requires the action of ESR1, as *Esr1* KO or *Esr1/2* dKO female mice do not develop either tumour type at any age. In addition, overactive TGF-β

**Table 1.1 Genetically engineered mouse models of sex cord-stromal tumours.** The affected genes and their Chr, the nature of the mutation and Cre driver where applicable, and the tumour type, frequency, and age of onset are shown. CAct: constitutive activation; Het: heterozygous; n/a: not applicable; OE: overexpression; Oo: oocyte; SC: stromal cell

| Affected Gene(s) | Chr (mouse) | Nature of Mutation | Cre Driver | Tumour Type | Tumour Frequency (%)[a] | Age of Onset (mo)[b] | Reference |
|---|---|---|---|---|---|---|---|
| *Bmpr1a/Bmpr1b* | 14/3 | GC dKO | *Amhr2* | GC | 90 | 8 | Edson *et al*. 2010 |
| *Ctnnb1* | 9 | GC CAct | *Amhr2* | GC | 57 | 6 | Boerboom *et al*. 2005 |
| *Esr2* | 12 | KO | n/a | GC | 100 | 15 | Fan *et al*. 2010 |
| *Fancf* | 7 | KO | n/a | GC | 71 | 13 | Bakker *et al*. 2012 |
| *Foxo1/Foxo3* | 3/12 | GC dKO | *Amhr2/Cyp19a1* | GC | 20 | 6-8 | Liu *et al*. 2015b |
| *Fshr* | 17 | KO | n/a | Mixed | 92 | 12 | Danilovich, Roy & Sairam 2001 |
| *Inha* | 1 | KO | n/a | Mixed | 100 | 1 | Matzuk *et al*. 1992 |
| *Lhb* | 7 | CAct | n/a | GC | 100 | 4 | Risma *et al*. 1995 |
| *Men1* | 19 | Het KO | n/a | Mixed | 50 | 13-18 | Bertolino *et al*. 2003 |
| *Pik3ca* | 3 | Oo KO | *Gdf9* | GC | 100 | 2 | Kim *et al*. 2016 |
| *Pten* | 19 | GC KO | *Amhr2* | GC | 7 | 2 | Laguë *et al*. 2008 |
| *Rspo1* | 4 | SC OE | *Nr5a1* | GC | 100 | 1 | De Cian *et al*. 2017 |
| *Smad1/Smad5* | 8/13 | GC dKO | *Amhr2* | GC | 100 | 3 | Pangas *et al*. 2008 |
| *Tgfbr1* | 4 | GC CAct | *Amhr2/Cyp19a1/Gdf9* | GC | 100 | 2 | Gao *et al*. 2016; 2017 |

[a]The approximate frequency of animals with tumours at the latest endpoint examined; [b]The earliest approximate age or range of ages at which tumours were first reported to be observed.

pathway signalling, as evidenced by high GC expression of phosphorylated SMAD2/SMAD3, appears to play a role in the tumourigenic mechanism observed in this model (Fan *et al*. 2010). Mice null for the inhibin alpha (*Inha*) gene lack inhibins, and therefore the normal negative feedback regulation necessary for FSH suppression is abolished, leading to the development of bilateral, mixed or incompletely differentiated SCSTs in both male and female mice as early as 1 mo of age with 100% penetrance (Matzuk *et al*. 1992). In addition to the appearance of invasive SCSTs, *Inha*$^{-/-}$ mice also develop a fatal cancer cachexia-like wasting syndrome caused by significantly increased levels of circulating activins that signal through ACVR2A (Matzuk *et al*. 1994; Coerver *et al*. 1996). *Inha*$^{-/-}$ mice have been bred with other KO mouse strains to provide insights into the role of other genes in the pathogenesis of SCSTs. The deletion of *Inha* in hypogonadal (*hpg*) mice devoid of gonadotropins and therefore sex steroids results in the development of pre-malignant ovarian lesions but no SCSTs or cachexic phenotype (Kumar, Wang & Matzuk 1996). Although mice null for *Inha* and either *Fshb* (Kumar *et al*. 1999) or *Lhb* (Nagaraja *et al*. 2008) develop SCSTs, they occur with significant delays in tumour development and progression. Further examinations of *Inha*-null mice have confirmed that ovarian GCs inappropriately respond to gonadotropins in the absence of inhibins, leading to SCST initiation (Nagaraja *et al*. 2010). *Inha*-null mice that overexpress the activin inhibitor *Fst* also display a delayed tumour progression course and are protected from developing cachexia (Cipriano *et al*. 2000), and a less aggressive tumour phenotype is also observed in *Inha*$^{-/-}$ mice lacking the positive cell cycle regulator CCND2 (Burns *et al*. 2003a) or SMAD3 (Li *et al*. 2007; Looyenga & Hammer 2007) but not SMAD2 (Rajanahally *et al*. 2010). Treatment of *Inha*-null mice with flutamide, a non-steroidal antagonist of the AR and therefore an inhibitor of androgenic signalling, also results in a more favourable outcome although all mice eventually succumb to

disease (Burns *et al*. 2003b). In contrast, deletion of the RB transcriptional corepressor 1 (*Rb1*) gene that encodes the negative cell cycle regulator RB (Andreu-Vieyra, Chen & Matzuk 2007), the cyclin-dependent kinase inhibitor 1B gene (*Cdkn1b*) that encodes $p27^{Kip1}$ (Cipriano *et al*. 2001), or *Esr1* (Burns *et al*. 2003b), results in accelerated tumour progression, an earlier onset of cachexia, and decreased survival rates.

The targeted mutation of genes in specific ovarian cell types has been accomplished by driving allele expression using gene promoters as well as cre recombinase (Cre)/locus of X-over P (*loxP*) technology, with a particular focus on genes involved in the TGF-β, PI3K/AKT, and sex determination pathways. Expression of the simian virus 40 (SV40) large T antigen (T-ag) under the control of the *Inha* promoter in ovarian stromal cells results in complete bilateral GC tumour penetrance in mice between 5-8 mo of age (Kananen *et al*. 1995). GC tumours also appear in mice that express the SV40 T-ag driven by the anti-Müllerian hormone type 2 receptor (*Amhr2*) promoter, with frequencies ranging from 16.7-100% by 8 mo of age (Dutertre *et al*. 2001). Conditional dKO of *Smad1* and *Smad5* in GCs via *Amhr2-cre* results in the complete penetrance of metastatic GC tumours or SLCTs in female and male mice, respectively, by 3 mo of age (Pangas *et al*. 2008). The absence of a tumour phenotype in mice individually null for either *Smad1* or *Smad5* indicates that these genes have redundant tumour suppressor functions in the mouse gonad. A high soy diet significantly promotes the rate of GC tumour growth and progression in these animals (Mansouri-Attia *et al*. 2014a), whereas deletion of *Smad4* leads to a favourable disease course due to the inhibition of TGF-β signal propagation (Mansouri-Attia *et al*. 2014b). GC tumours also develop in mice with *Amhr2-cre* driven deletion of the BMP type I receptors bone morphogenetic protein receptor, type 1A (*Bmpr1a*) and *Bmpr1b* in GCs, which transduce signals to SMAD1/SMAD5/SMAD8 (Edson *et al*. 2010). In contrast to the

*Smad1/Smad5* dKO model, less than 50% of *Bmpr1a/Bmpr1b* dKO females develop GC tumours by 8 mo of age, although bilateral tumours are apparent in nearly all animals by 16 mo. The constitutive activation of the TGF-β family member receptor *Tgfbr1* in mouse GCs using either *Amhr2*- or *Cyp19a1-cre* results in the initiation of GC tumours with complete penetrance at 2 mo of age (Gao *et al*. 2016). A similar phenotype is observed when an activated *Tgfbr1* allele is targeted to the oocyte using *Gdf9-cre* (Gao *et al*. 2017), adding weight to the body of evidence that signals transduced by TGF-β and BMP ligands are likely regulators of GC tumour development. The use of *Gdf9-cre* to express constitutively active *Pik3ca* in oocytes also leads to completely penetrant bilateral GC tumour development at approximately 2 mo of age (Kim *et al*. 2016). The *Pik3ca* gene encodes the catalytic subunit of the PI3K heterodimer complex and is therefore upstream of the PI3K/AKT signalling pathway. GC-specific deletion of the PI3K negative regulator *Pten* using an *Amhr2-cre* driver results in the development of poorly differentiated and metastatic GC tumours in approximately 7% of female mice beginning at approximately 2 mo of age (Laguë *et al*. 2008). The low GC tumour frequency observed in *Pten*-null mice is significantly increased to 47% at 11-13 mo of age when combined with constitutively active *Pik3ca* and targeted to multiple ovarian cell types using an intrabursal adenoviral-cre system; the remaining 53% of females develop other ovarian abnormalities (Kinross *et al*. 2012). Similarly, approximately 20% of mice null for both *Foxo1* and *Foxo3* develop GC tumours by 6-8 mo of age using *Amhr2*- or *Cyp19a1-cre*; however, when combined with a *Pten*-null allele, triple KO mice are susceptible to a more aggressive disease course and a GC tumour frequency of approximately 60% (Liu *et al*. 2015b). These mouse models provide evidence that mutation of the PI3K/AKT pathway is another mechanism by which GC tumours can develop. The *Amhr2-cre* system has also been used to express GC-targeted constitutively

active *Ctnnb1*, leading to GC tumour development in 57% of female mice by 7.5 mo (Boerboom *et al*. 2005). As in other GC tumour models described above, when combined with a null *Pten* allele, female mice expressing activated *Ctnnb1* exhibit a synergistic, aggressive phenotype characterized by the perinatal development of metastatic GC tumours with complete penetrance (Laguë *et al*. 2008; Richards *et al*. 2012). The introduction of an activated *Kras* allele to the transgenic *Ctnnb1* model using *Cyp19a1-cre* results in a similar phenotype (Richards *et al*. 2012). Finally, the overexpression of *Rspo1* in gonadal stromal cells driven by *Nr5a1-cre* results in the complete penetrance of GC tumours, with ovarian abnormalities observed beginning at 1 mo of age (De Cian *et al*. 2017). These GC tumours appear to arise from the mural GCs of antral follicles that fail to terminally differentiate and ovulate when stimulated with the LH analogue hCG, indicating that the down-regulation of *Rspo1* is likely required for normal ovulation (De Cian *et al*. 2017).

That the genetic alteration of tumour suppressors and genes critical for normal GC and ovarian physiology cause SCST development in a species with innate SCST susceptibility suggests the pathways described above may contribute to GC tumour initiation or progression in women. Examinations of a limited number of these candidates (e.g. *FSHR*, *INHA*) in human adult GC tumours have not identified causative mutations (Watson *et al*. 1997; Fuller *et al*. 1998; Bas, Pescovitz & Steinmetz 2009), although epigenetic influences governing the expression of these genes have not been investigated. Whereas a highly specific somatic mutation in *FOXL2* is the most significant mutation reported to date in human adult GC tumours, little to no genetic evidence has been accumulated with regards to the juvenile subtype. This research dissertation has focused on the spontaneous SWR mouse model of juvenile-onset GC tumour development as a strategy for the identification of genetic loci that confer pubertal GC tumour susceptibility, and

for the identification of the ovarian GC wave from which these tumours originate, so as to illuminate the genetic and endocrine pathways underlying juvenile-onset GC tumourigenesis.

### 1.3.1 The SWR/Bm Mouse Model of Juvenile Granulosa Cell Tumourigenesis

#### 1.3.1.1 Model Overview

The SWR/Bm (SWR) inbred mouse strain is unique in its heritable and spontaneous susceptibility to juvenile-onset GC tumours, which occur in ≤ 1% to approximately 25% of females, depending on strain background and hormonal stimulation (Beamer, Hoppe & Whitten 1985). This phenotype initiates during a restricted window during puberty at 3 to 4 wk of age as pre-neoplastic blood-filled follicles (Tennent *et al*. 1990). Females that remain unaffected through the susceptibility window stay tumour-free, retain normal fertility, and age normally without the occurrence of other tumours or reproductive pathologies. The pre-neoplastic follicular lesions that appear at 3 to 4 wk of age are composed of irregular masses of GCs and hypertrophied TCs, with degenerating oocytes within a large fluid- or erythrocyte-filled antrum. By 6 to 8 wk of age, these lesions have progressed to highly vascularized, cystic or hemorrhagic masses homogenously composed of GCs and enclosed within the ovarian bursa, with luteinized or necrotic areas occasionally present (Figures 1.9 and 1.10; Beamer, Hoppe & Whitten 1985; Tennent *et al*. 1990). The SWR GC tumours may be unilateral or bilateral and have malignant potential (Beamer, Hoppe & Whitten 1985). By 6 to 9 mo, approximately 42% of mice with primary GC tumours exhibit metastases to organs within the abdominal and thoracic cavities, including the liver, lungs and renal lymph nodes (Tennent *et al*. 1990). As in human juvenile GC tumours, the mouse tumours secrete high levels of estrogens and inhibins (Gocze *et al*. 1997). Excessive estrogen production results in significantly increased uterine weights and percentages

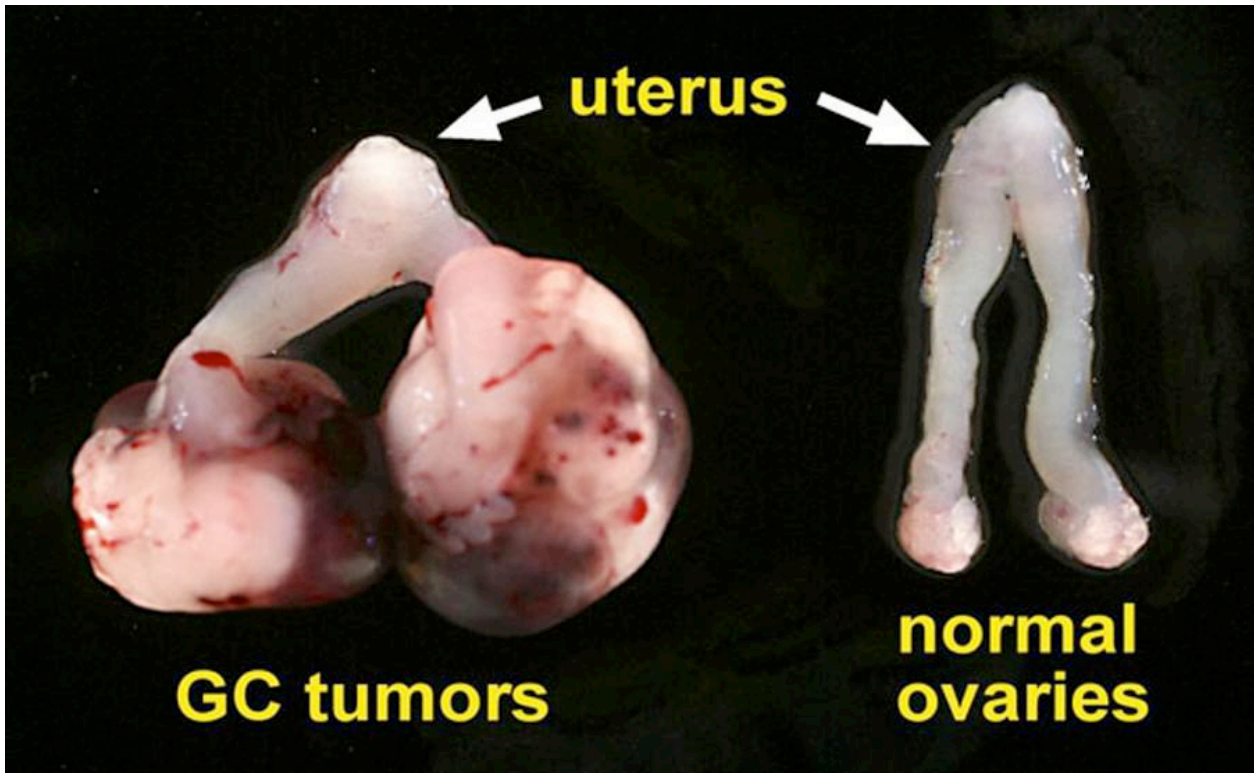


**Figure 1.9 Bilateral GC tumours isolated from a genetically susceptible female mouse**

Left: the bilateral GC tumours and uterus were removed at 8 wk of age from an SWR-derived female. Right: the normal ovaries and uterus from an age-matched littermate are shown for comparison. Reprinted from Smith 2011.

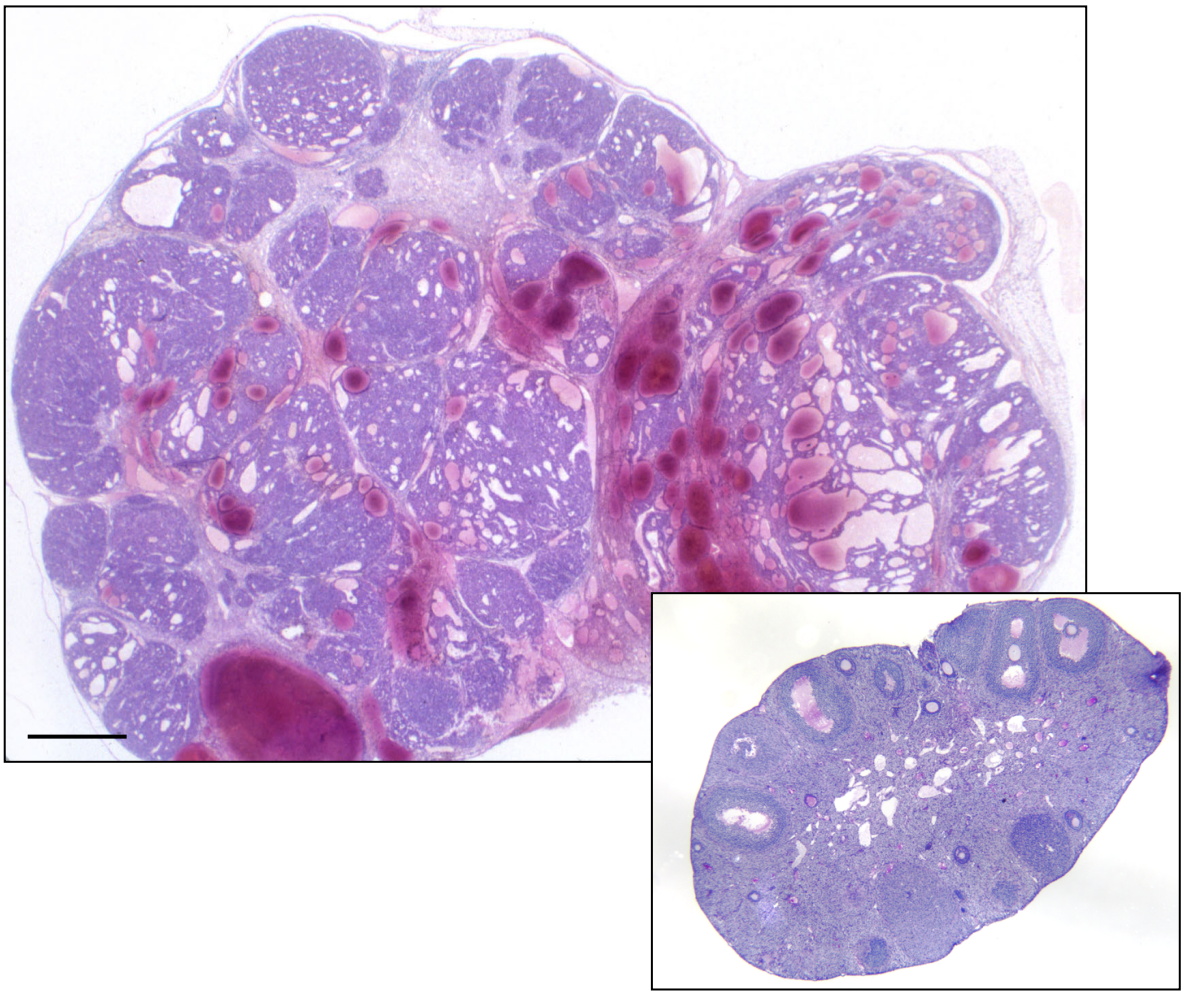

**Figure 1.10 GC tumour and normal ovary histology**

A hematoxylin and eosin (H&E)-stained GC tumour from an SWR-derived mouse necropsied at 8 wk of age. Inset: an H&E-stained, SWR-derived whole mouse ovary exhibiting normal ovarian cellular organization is shown for comparison. Magnification: 10X. Scale bar: 500 µm.

of cornified vaginal cells (Beamer, Shultz & Tennent 1988). In unilateral cases, high estrogen levels also functionally suppress the contralateral ovary, which ceases ovulation (Beamer, Hoppe & Whitten 1985). Affected females exhibit decreased levels of pituitary FSH and LH, and serum FSH, $P_4$, DHT, and T (Beamer 1986). As this unique, heritable, and early-onset spontaneous trait occurs at puberty, prior to ovarian reserve exhaustion, and demonstrates robust parallels with human juvenile GC tumours, the SWR mouse model is useful for the identification of candidate genes and pathways underlying GC tumour initiation in infants and young girls.

The GC tumour phenotype observed in SWR mice is endocrine-sensitive. An intact HPG axis is required for GC tumour development, as the transfer of pre-pubertal, genetically-susceptible ovaries to *hpg* host mice incapable of gonadotropin hormone synthesis and thus sex steroid production do not undergo GC tumour initiation (Beamer *et al*. 1993). GC tumour frequency is significantly increased with exogenous administration of the functional LH analog hCG at puberty. Similarly, treatment with the downstream androgens DHEA and T, which are synthesized by TCs in response to LH during the pubertal transition, also increases trait penetrance in the SWR model (Beamer, Shultz & Tennent 1988; Tennent, Shultz & Beamer 1993; Dorward, Shultz & Beamer 2007). Notably, these hormones do not stimulate GC tumour initiation when administered following puberty, outside of the restricted window of susceptibility (Beamer *et al*. 1993). Likewise, pubertal exposure to exogenous $E_2$ before, but not after, the initiation of pre-neoplastic follicular lesions inhibits GC tumour development (Dorward, Shultz & Beamer 2007), indicating that the windows of tumour initiation and prevention overlap. This endocrinological evidence suggests that the first pubertal wave of LH and subsequent downstream androgenic signalling stimulates GC tumour initiation, whereas the $E_2$-induced suppression of initiation occurs due to the inhibition of LH release from the anterior pituitary. In

a clear phenotypic switch from the hormone-dependent growth of early GC tumours, metastatic GC tumour grafts have the potential for growth in *hpg* mouse hosts and no longer depend upon reproductive hormonal stimulation (Dorward, unpublished data). Following initiation, SWR-derived GC tumour cells are capable of responding to FSH and hCG, as well as the growth factors IGF1 and EGF, as indicated by increased steroid production (Gocze *et al*. 1997). Immunoblotting analyses of spontaneous GC tumour lysates have revealed alterations in protein expression compared to normal SWR-derived mouse ovaries, including significantly higher levels of SOX9 and EGFR and significantly lower levels of ESR2, although it is not clear what cell types contribute to these protein differences. The mouse GC tumours also retain low levels of FOXL2 expression (Lewis 2018).

#### 1.3.1.2 Genetics

The juvenile-onset GC tumour phenotype unique to SWR females is polygenic, with multiple influential autosomal and X-linked loci associated with GC tumour susceptibility identified to date (Table 1.2). These loci, termed granulosa cell tumour susceptibility (*Gct*) loci, function autonomously within the ovary, as ovaries from genetically-susceptible females transferred to endocrinologically normal, pre-pubertal and genetically-resistant female hosts can undergo GC tumour development (Beamer *et al*. 1993). Further investigations into the genetic source of susceptibility using a grafting model and chimeric follicles composed of pure GCs isolated from tumour-susceptible or -resistant mice have shown that the GCs themselves possess the susceptibility property (Beamer 2011). Despite the clear phenotype observed in SWR females, the GC tumour susceptibility alleles impart no apparent effects on SWR males.

Although GC tumour susceptibility is a complex and polygenic trait, significant genetic

**Table 1.2 Autosomal and X-linked loci associated with GC tumour susceptibility in SWR mice.** The loci and their Chr, and the mapping cross partner strains used to map them are shown. Adapted from Smith 2011.

| Locus | Chr | Mapping Cross Partner Strains | Reference |
|---|---|---|---|
| *Gct1* | 4 | SWR/SJL | Beamer *et al*. 1988 |
| | | SWR/SJL | Beamer *et al*. 1998 |
| | | SWXJ-9/CAST | Dorward *et al*. 2005 |
| *Gct2* | 12 | SWR/SJL | Beamer *et al*. 1998 |
| *Gct3* | 15 | SWR/SJL | Beamer *et al*. 1998 |
| *Gct4* | X | SWR/SJL | Beamer *et al*. 1998 |
| | | SWR/CAST | Dorward *et al*. 2003 |
| | | SWR/CAST | Dorward *et al*. 2013 |
| *Gct5* | 9 | SWR/SJL | Beamer *et al*. 1998 |
| *Gct6* | X | SWR/CAST | Dorward *et al*. 2003 |
| | | SJL/CAST | Rabie 2015 |
| *Gct7* | 1 | SWXJ-9/CAST | Dorward *et al*. 2005 |
| *Gct8* | 2 | SWXJ-9/CAST | Dorward *et al*. 2005 |
| *Gct9* | 13 | SWXJ-9/CAST | Dorward *et al*. 2005 |

evidence suggests the *Gct1* locus on distal Chr 4 is fundamental for spontaneous tumour initiation. *Gct1* susceptibility alleles contributed by the SWR strain (*Gct1*$^{SW}$) have been consistently associated with the spontaneous GC tumour phenotype across three independent mapping crosses. Investigations of a series of 14 recombinant inbred (RI) SWXJ strains (SWXJ-1 through 14) generated from SWR and the GC tumour-resistant inbred strain SJL/Bm (SJL) identified significant linkage of spontaneous and androgen-induced GC tumour occurrence with SWR genome at distal Chr 4 (Beamer *et al*. 1988). A subsequent two-generation reciprocal intercross using (SWR x SJL)$F_2$ mice confirmed the necessity of the *Gct1* locus for spontaneous susceptibility and refined its location to within the vicinity of the simple sequence length polymorphism (SSLP) DNA marker *D4Mit232* (Beamer *et al*. 1998). A third mapping cross using an $N_2F_1$ backcross strategy, GC tumour susceptible SWXJ-9 mice, and the GC tumour resistant Castaneus (CAST) mouse strain was conducted to improve *Gct1* mapping resolution and to confirm linkage between autosomal loci and spontaneous tumour initiation (Dorward *et al*. 2005). The CAST strain is an excellent and widely used partner for mouse mapping crosses, due to its genomic divergence from more common laboratory mouse strains and the subsequent potential for higher genetic resolution (Petkov *et al*. 2004). This investigation further supported a link between *Gct1*$^{SW}$ alleles at *D4Mit232* and spontaneous GC tumour development (Dorward *et al*. 2005). Although these mapping crosses identified multiple associations between the GC tumour phenotype and other susceptibility loci, the lack of consistent linkage of other autosomal loci besides *Gct1* across multiple mapping crosses suggests their influence is likely contingent upon strain background and epistatic interactions. Heterozygosity for the *Gct1*$^{SW}$ allele is sufficient for tumourigenesis, whereas *Gct1*$^{SW}$ homozygosity confers enhanced tumourigenic

support (Dorward *et al*. 2005); these observations suggest that *Gct1* acts as an oncogenic influencer in SWR mice.

As described above, androgenic stimulation of the pre-pubertal, genetically-susceptible SWR mouse ovary significantly increases GC tumour frequency (Beamer, Shultz & Tennent 1988). Inherent GC tumour frequency in inbred SWR female mice is ≤ 1%, but increases to ≥ 20% with exogenous DHEA or T administration during the pubertal transition (Beamer, Shultz & Tennent 1988). Although DHEA is an upstream metabolite of the androgenic steroids (Figure 1.8), an investigation using the SWXJ RI strain set has shown that DHEA supplementation is not simply a substitute for T administration in this model (Tennent, Shultz & Beamer 1993). The eight SWXJ RI lines with $Gct1^{SW}$ alleles can be phenotypically segregated upon androgen administration: four strains exhibit low spontaneous GC tumour incidence that is significantly increased with either DHEA or T exposure, whereas another four "DHEA-dependent" RI strains that are naturally resistant to spontaneous GC tumour initiation only respond to DHEA, and not T, treatment (Table 1.3). The $Gct1^{SW}$ locus is therefore described as DHEA-responsive, and DHEA stimulation has been used to further map the genetic regions conferring GC tumour susceptibility.

In addition to *Gct1*, two other independent loci on the X chromosome, *Gct4* and *Gct6*, function as robust modifiers and suppressors of GC tumour susceptibility, respectively. The *Gct4* locus was identified using an (SWR x SJL)$F_2$ two-generation reciprocal intercross designed to test the contribution of parental sex on GC tumour susceptibility, whereas *Gct6* was identified using a recombinant progeny test mapping strategy (Beamer *et al*. 1998; Dorward *et al*. 2003). *Gct4* was originally identified in the SJL inbred strain that served as a GC tumour-resistant mapping partner for SWR, whereas *Gct6* was inadvertently revealed when CAST alleles were

**Table 1.3 GC tumour incidence in SWR and SWXJ RI female mice treated with DHEA or T.** RI strains are categorized as spontaneous, DHEA-dependent, or GC tumour resistant. Data are from Tennent, Shultz & Beamer 1993.

| Strain | Spontaneous GC Tumour Frequency (%) | T-Induced GC Tumour Frequency (%) | DHEA-Induced GC Tumour Frequency (%) |
|---|---|---|---|
| Spontaneous | | | |
| SWR | 2.5 | 17.4 | 24.3 |
| SWXJ-1 | 2.5 | 8.7 | 18.4 |
| SWXJ-4 | 1.2 | 11.8 | 8.1 |
| SWXJ-8 | 0.4 | 10.8 | 44.1 |
| SWXJ-9 | 10.3 | 34.3 | 40.5 |
| DHEA-dependent | | | |
| SWXJ-6 | 0 | 0 | 10.7 |
| SWXJ-7 | 0 | 0 | 13.5 |
| SWXJ-10 | 0 | 0 | 2.8 |
| SWXJ-12 | 0 | 0 | 8.3 |
| Resistant | | | |
| SWXJ-2 | 0 | 0 | 0 |
| SWXJ-3 | 0 | 0 | 0 |
| SWXJ-5 | 0 | 0 | 0 |
| SWXJ-11 | 0 | 0 | 0 |
| SWXJ-13 | 0 | 0 | 0 |
| SWXJ-14 | 0 | 0 | 0 |
| SJL | 0 | 0 | 0 |

introduced at *Gct4* and distal Chr X during the fine mapping of this locus. Notably, the GC tumour-supportive action of these loci requires the $Gct1^{SW}$ allele. In the presence of an autosomal SWR background with homozygous $Gct1^{SW}$ alleles, allelic variation at *Gct4* modifies GC tumour incidence such that phenotypic penetrance is increased from ≤1% to approximately 20% spontaneous tumour incidence in the absence of exogenous androgenic intervention. The SWR allele of *Gct4* ($Gct4^{SW}$) is a low incidence allele, whereas the CAST ($Gct4^{CA}$) and SJL ($Gct4^{J}$) alleles are strong modifiers that support increased tumour penetrance (Beamer *et al*. 1998; Dorward *et al*. 2013). In contrast, allelic variation at *Gct6* is either permissive or suppressive for spontaneous GC tumour initiation, with tumour suppressor action contributed by the CAST allele but tumour permissive activity contributed by SWR and SJL. In the presence of the highly GC tumour supportive $Gct4^{CA}$ allele, $Gct6^{SW}$ and $Gct6^{J}$ confer spontaneous tumour incidence at a frequency of approximately 20% (Beamer *et al*. 1998; Dorward *et al*. 2013). This equivalency in the effects of $Gct6^{SW}$ and $Gct6^{J}$ alleles on GC tumour penetrance prevented the identification of this locus in the earliest (SWR x SJL)$F_2$ mapping cross. The *Gct4* and *Gct6* loci are also influenced by robust parent-of-origin effects associated with the paternal allele, such that paternal, but not maternal, inheritance of susceptibility alleles results in increased tumour penetrance (Beamer *et al*. 1998; Dorward *et al*. 2003; Dorward *et al*. 2013). The high GC tumour frequency and parent-of-origin effects associated with these alleles have accelerated the fine mapping of these two loci. *Gct4* and *Gct6* have been finely-mapped to 1.345 million base pairs (Mb) and 1.019 Mb, respectively (Dorward *et al*. 2013; Rabie 2015), although the precise identities of these genes remain to be elucidated. The endocrine sensitivity of the GC tumour phenotype has distinguished the *Ar* as the primary candidate for *Gct4*, although no protein coding variants have been identified in SWR or SJL mice compared to the reference sequences

of the C57BL/6J (B6J) or BALB/c strains (Dorward *et al*. 2013). Instead, the robust paternal parent-of-origin effect influencing these X-linked loci suggests epigenetic regulation, and that allelic differences at the level of gene expression rather than protein sequence underlie their modifying and suppressing activities. Accordingly, the low GC tumour penetrance allele of the SWR strain correlates with significantly reduced *Ar* transcript levels in the pubertal female ovary (Dorward *et al*. 2013). This differential expression of *Ar* is likely overcome by the administration of exogenous androgens to SWR mice at puberty, equalizing trait penetrance with the $Gct4^{J}$ or $Gct4^{CA}$ alleles. The AR protein functions within the GCs to regulate ovarian follicle maturation over the reproductive lifespan of the mouse (Sen & Hammes 2010; Walters *et al*. 2012). The SWR model suggests that the AR plays a similar role in the unique follicle cohort that has the potential for GC tumour initiation, which will be discussed further in Chapter 3. The primary candidate for identity with the *Gct6* tumour suppressor is the solute carrier family 25, member 53 (*Slc25a53*) gene, an orphan mitochondrial solute carrier with no known function or ascribed substrate. Sequencing analysis identified a 28 base pair (bp) deletion within the SWR *Slc25a53* allele, although the effect of this deletion on SLC25A53 function and the protein's contribution to the GC tumour phenotype remains to be elucidated (Rabie 2015; Cruickshank, in progress).

### 1.4 Summary

The consistent identification of *Gct1* across three independent mapping crosses, as well as the necessity of SWR-derived susceptibility alleles at this locus for both spontaneous and androgen-induced GC tumourigenesis, suggests the $Gct1^{SW}$ allele is the fundamental oncogenic driver underlying this complex and developmentally-restricted ovarian tumour phenotype. As no *Gct1* alleles from other inbred mouse strains have been reported to predispose to spontaneous or

androgen-induced GC tumour susceptibility, a unique genetic variant causes tumour initiation in SWR mice, and the *Gct1*$^{SW}$ allele will be identifiable by genetic comparison to other mouse strains (Beamer *et al*. 1988). Robust phenotypic mapping combined with the evidence for hormonal sensitivity and a significant quantitative expression difference indicates that the *Ar* acts alongside *Gct1* to modify GC tumour susceptibility, with interstrain allelic differences likely due to a regulatory variant affecting *Ar* transcript expression. Notably, genes associated with sporadic human GC tumour appearance (e.g. *FOXL2*) or engineered mouse models of GC tumourigenesis (e.g. *Inha*) do not overlap with the *Gct1* or *Gct4* regions (Tables 1.1 and 1.2); these loci thus encode unique genetic entities that predispose to GC tumour susceptibility, although it is possible that the mechanistic pathways initiated by *Gct1* and *Gct4* may directly influence these previously reported pathways. The precise pubertal timeframe in which these genes act indicates that the mouse GC tumours arise from the first wave of ovarian GCs, and that these cells have a unique molecular profile different from subsequent waves and that targets them for GC tumourigenesis following normal endocrine stimulation. Resolution of the identity of *Gct1*, *Gct4*, and the susceptible GC cohort in the SWR mouse model will provide candidate genes and mechanistic pathways for translation to the juvenile-onset GC tumourigenesis phenotype in humans. This dissertation is divided into three research chapters that endeavour to experimentally address these questions, with specific background provided to support the research objectives outlined in each chapter.

# 2. Investigating the Oncogenic Driver *Gct1*

## 2.1 Introduction

The consistent linkage of SWR-derived *Gct1* alleles with pubertal GC tumour susceptibility suggests this DHEA-responsive locus is the oncogenic initiator of tumourigenesis. Phenotypic mapping and investigations at the level of candidate genes have been undertaken and shown to be promising strategies to aid in the identification of *Gct1*.

### 2.1.1 Previous Strategies to Identify *Gct1*

Positional cloning using congenic and subcongenic strains is a traditional strategy used to resolve genetic loci underlying polygenic traits independently from the influences of other loci. Congenic strains are established by first outcrossing two inbred strains, with the resulting heterozygous offspring being backcrossed to the inbred paternal strain for 10 or more generations; heterozygosity at a selected locus is maintained throughout backcrossing by marker-assisted breeding (Figure 2.1; Silver 1995). The result in an exchange of donor strain alleles at the locus of interest onto a recipient strain background, which achieves 99.8% homozygosity following 10 backcross generations (Flaherty 1981). *Gct1* was initially isolated in a double congenic strain named SWR.SJL-X.CAST-4-T (Line 4-T), which maintained an SWR genome on all chromosomes with the exception of distal Chr 4 and a central portion of Chr X that harboured $Gct1^{CA}$ and $Gct4^{J}$ alleles, respectively. Line 4-T mice are resistant to both spontaneous and androgen-induced GC tumour development, and as such were suitable for phenotypic mapping of the GC tumour trait (Smith 2011). Line 4-T was thus used to create ten informative

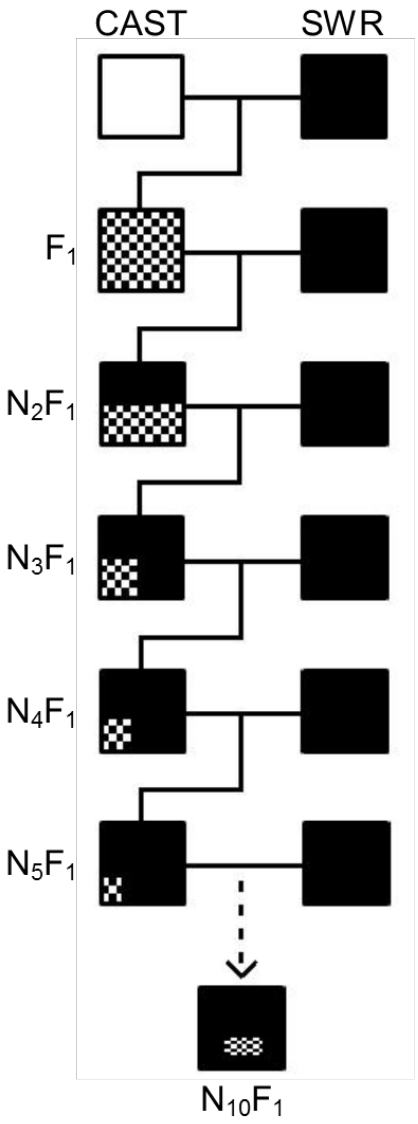


**Figure 2.1 Isolating *Gct1* in a congenic strain**

Congenic mouse strains are developed through consecutive, marker-assisted breeding between a donor and recipient strains. Sequential generations of backcrossing replaces the genome of the recipient strain at all loci with the exception of a selected genomic region. In the case of this project, CAST alleles around the *Gct1* locus ($Gct1^{CA}$) were exchanged for SWR alleles ($Gct1^{SW}$), and SWR genomic background reconstitution approximated 99.8% after 10 generations of breeding. At the $N_{10}F_1$ generation, animals were intercrossed to achieve donor (CAST) segment homozygosity (not shown). Black: SWR alleles; white: CAST alleles; checkboard pattern: heterozygous alleles. Adapted from Flaherty 1981; reprinted in adapted form from Smith 2011.

recombinant subcongenic lines (SWR.SJL-X.CAST-4-1 through 10) by fragmenting the large Chr 4 region inclusive of *Gct1*, breeding to homozygosity, and testing for androgen-induced GC tumour susceptibility (Figure 2.2). An initial round of phenotypic mapping using these subcongenic lines refined *Gct1* to a 6.69 Mb interval containing approximately 300 pseudo-, protein coding, and non-coding RNA genes. SWR.SJL-X.CAST-4-3 (Line 4-3) retained resistance to GC tumour initiation and possessed a smaller portion of the homozygous CAST genomic segment than Line 4-T (Smith 2011). A second round of phenotypic mapping using Line 4-3 as the starting donor generated an additional series of six nested subcongenic lines to improve mapping resolution at *Gct1* (Figure 2.3). In all, the 12 most informative subcongenic lines refined the *Gct1* interval from 6.69 Mb to 1.86 Mb between markers *D4sjh10* and *D4kns1*, and a shortlist of 22 candidate genes (Table 2.1; Smith 2011; Smith *et al*. 2013)[1].

The distal end of the 1.86 Mb *Gct1* interval is characterized by a highly repetitive DNA sequence that is not amenable to fine mapping with specific genetic markers. Two large, unresolved gaps in the GRCm38 genome assembly are present in *Gct1*, which await experimental sequencing and currently prevent full annotation of the interval. This region also houses an assembly exception, or an alternate sequence that differs from that on the B6J primary assembly. Distal mouse Chr 4 is also a deletion hotspot (Pötter *et al*. 2001) and is one of the most unstable regions of the mouse genome, as demonstrated by significant loss-of-heterozygosity levels in tumour tissue (Radany *et al*. 1997; Cool & Jolicoeur 1999); this lack of stability

[1] The genome coordinates and interval sizes presented in this dissertation correspond to the Genome Reference Consortium Mouse Build 38 (GRCm38), whereas those presented in my MSc thesis (Smith 2011) and published manuscript (Smith *et al*. 2013) are annotated according to the NCBI Build m37 genome assembly. Discrepancies between these documents in regards to genome coordinates and interval sizes are due to differences in annotation between these assemblies.

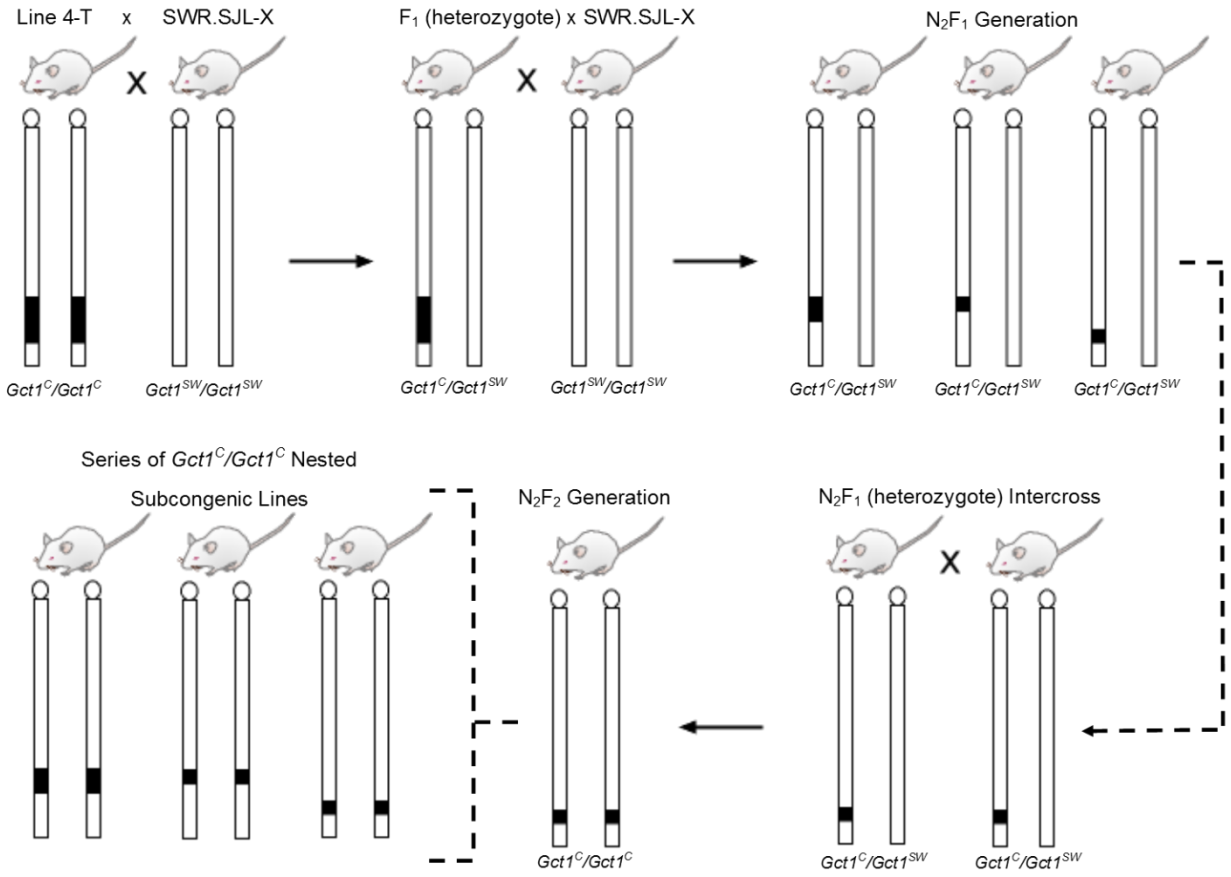


**Figure 2.2 Creating subcongenic strains to map *Gct1***

Trait mapping with congenic strains is maximized through the development of subcongenic lines that carry overlapping, nested segments of donor genome. Subcongenic lines were generated using an $N_2F_1$ backcross breeding scheme, selecting for unique combinations of the CAST and SWR genomes across the *Gct1* locus after meiotic recombination. $N_2F_1$ generation male or female mice with informative, novel recombinations across the *Gct1* locus were chosen for breeding expansion to create a series of homozygous subcongenic lines. Female offspring from subcongenic mating pairs were then examined for GC tumour susceptibility to refine the genomic location of *Gct1*. Reprinted in adapted form from Smith 2011.

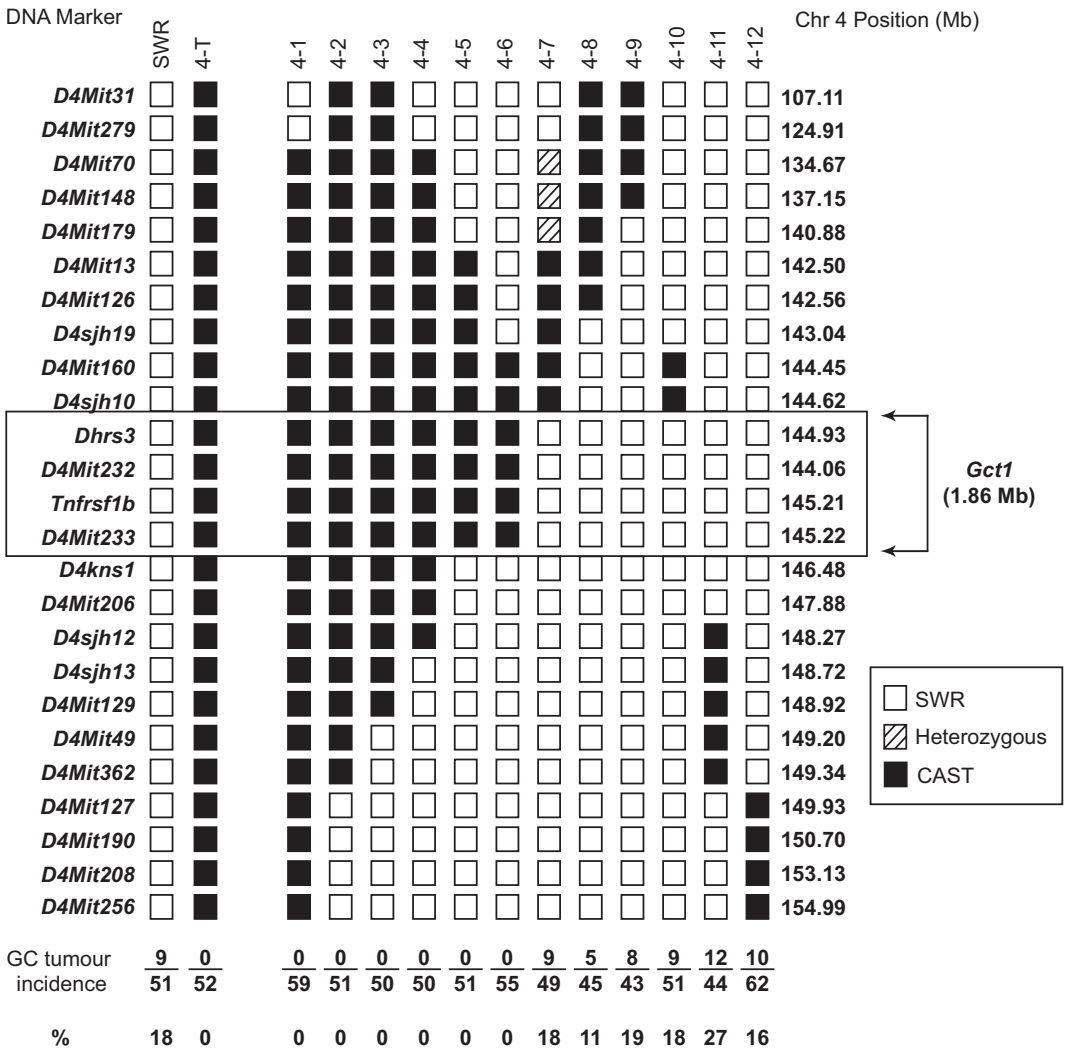


**Figure 2.3 Chr 4 haplotypes of SWR and Line 4-T subcongenic mouse lines at *Gct1* following two rounds of phenotypic mapping**

Females from the Line 4-T recombinant subcongenic Lines 4-7 through 4-12 have a significantly higher GC tumour incidence than Line 4-T and Lines 4-1 through 4-6 females. Lines 4-7 through 4-12 therefore carry the $Gct1^{SW}$ allele, whereas Lines 4-1 through 4-6 do not, and *Gct1* resides in the approximately 1.86 Mb interval between *D4sjh10* and *D4kns1*. Note that Line 4-7 is heterozygous for SWR and CAST alleles in the region between markers *D4Mit70* and *D4Mit179*, but this region does not interfere with the *Gct1* boundary determinations. Reprinted in adapted form from Smith *et al*. 2013.

**Table 2.1 Summary of the genetic determinants within the 1.86 Mb *Gct1* interval.** Gene name, location on Chr 4, strand, gene type, and the number of unique transcripts per gene are shown. Data is from Ensembl release 95 (January 2019; Zerbino *et al*. 2018). AS: antisense; LR: long intergenic non-coding RNA; PC: protein coding; PT: processed transcript; SN: small nuclear RNA; TEC: manually annotated expressed sequence tag, to be experimentally confirmed; +: forward; -: reverse

| Gene | Official Name | Location on Chr 4 (bp) | Strand | Gene Type | Unique Transcripts |
|---|---|---|---|---|---|
| *Gm436* | predicted gene 436 | 144,669,937 | - | PC | 1 |
| *Gm13178* | predicted gene 13178 | 144,703,191 | - | PC | 2 |
| *Gm25938* | predicted gene, 25938 | 144,765,627 | - | SN | 1 |
| *Gm438* | predicted gene 438 | 144,777,204 | - | PC | 1 |
| *Dhrs3* | dehydrogenase/reductase (SDR family) member 3 | 144,892,827 | + | PC | 7 |
| *Gm38074* | predicted gene, 38074 | 144,957,155 | - | TEC | 1 |
| *Vps13d* | vacuolar protein sorting 13 D | 144,972,622 | - | PC | 10 |
| *Tnfrsf1b* | tumor necrosis factor receptor superfamily member 1b | 145,213,463 | - | PC | 2 |
| *Tnfrsf8* | tumor necrosis factor receptor superfamily member 8 | 145,267,137 | - | PC | 2 |
| *Platr16* | pluripotency associated transcript 16 | 145,410,245 | + | PT | 2 |
| *Zfp990* | zinc finger protein 990 | 145,510,759 | + | PC | 4 |
| *Gm13212* | predicted gene 13212 | 145,585,166 | + | PC | 3 |
| *Gm26763* | predicted gene, 26763 | 145,601,963 | - | LR | 1 |
| *Zfp980* | zinc finger protein 980 | 145,670,685 | + | PC | 2 |
| *Gm13236* | predicted gene 13236 | 145,762,929 | + | LR | 1 |
| *Zfp986* | zinc finger protein 986 | 145,868,794 | + | PC | 2 |
| *Zfp987* | zinc finger protein 987 | 146,097,298 | + | PC | 3 |
| *Gm26573* | predicted gene, 26573 | 146,153,456 | - | LR | 1 |
| *Zfp600* | zinc finger protein 600 | 146,156,824 | + | PC | 4 |
| *Gm13165* | predicted gene 13165 | 146,167,522 | - | AS | 2 |
| *Gm13166* | predicted gene 13166 | 146,251,829 | + | LR | 5 |
| *Zpf992* | zinc finger protein 992 | 146,449,023 | + | PC | 1 |

has been shown to be governed by strain-specific effects (Radany *et al*. 1997). These aspects precluded further refinement of the distal end of *Gct1* beyond that achieved by the second round of phenotypic mapping (Smith 2011; Smith *et al*. 2013).

### 2.1.2 Prioritized Candidates for *Gct1*

In an attempt to prioritize candidate genes within the 1.86 Mb *Gct1* interval for further investigation, a qualitative expression assessment of these genetic determinants was conducted within the pubertal ovary of SWR and Line 4-T mice (Smith 2011). This analysis examined not only pubertal ovarian expression, which we hypothesize is a requirement for *Gct1* tumourigenic action, but also differential expression between GC tumour-susceptible SWR mice and the GC tumour-resistant CAST strain. Notably, this analysis assayed qualitative gene expression in the ovary as a whole and was not GC-specific, and was successfully conducted for only 11 of the 22 *Gct1* candidates due in part to an inability to design transcript-specific primers because of the repetitive nature of the interval. None of the tested genes could be excluded from *Gct1* candidacy by this strategy, as all 11 were expressed in SWR and Line 4-T pubertal ovary complementary DNA (cDNA) pools, with no qualitative expression differences evident between strains. A second prioritization strategy for the interval's gene candidates focused on the known genes that were also present in the homologous human interval on Chr 1p36.21-22: *Dhrs3*, *Vps13d*, *Tnfrsf8*, and *Tnfrs1b*. Publicly available microarray data (Su *et al*. 2004b) indicated that while all four genes are expressed in the mouse and human ovary, *Dhrs3* and *Tnfrsf1b* are present in considerably greater abundance in the mouse ovary than in the testis (23.85 and 8.59 fold, respectively; Smith 2011). Given their known expression patterns and functions (described below), these genes are considered the two main candidates for shared identity with *Gct1*.

#### 2.1.2.1 *Tnfrsf1b*

Formerly known as *Tnfr2*, tumor necrosis factor receptor superfamily, member 1b (*Tnfrsf1b*) is a 10 exon gene that encodes the TNFRSF1B protein (also known as cluster of differentiation 120b [CD120b]). Along with TNFRSF1A (CD120a), TNFRSF1B is a member of the TNF receptor superfamily, a group of type I transmembrane glycoprotein cell surface receptors that bind TNF or other similar cytokines. TNF functions as a major mediator of inflammatory and immunological processes, as well as carcinogenesis and cancer progression (reviewed by Ham *et al*. 2016). Unlike the near-ubiquitous expression of TNFRSF1A, TNFRSF1B expression is restricted to astrocytes, cardiac myocytes, endothelial cells, human mesenchymal stem cells, microglia, oligodendrocytes, T cells, a subset of neurons, and thymocytes (Borghi, Verstrepen & Beyaert 2016). TNFRSF1B expression has also been noted in human oocytes and cumulus GCs (Naz, Zhu & Menge 1997), peri- and post-natal rat ovaries (Balchak & Marcinkiewicz 1999), and in the cytoplasm of oocytes within post-natal mouse ovaries (Greenfeld *et al*. 2007b). TNFRSF1A and TNFRSF1B consist of similar TNF-binding extracellular structures characterized by repeated cysteine-rich motifs, but differ in their cytoplasmic domains, which relates to their different modes of action (Figure 2.4). Binding of the TNF receptors to their ligand exhibits a three:three stoichiometry, in which three TNF molecules bind three receptors (Banner *et al*. 1993). The conformational change in the receptors' cytoplasmic tails following ligand binding results in signal transduction (Chan *et al*. 2000). Following TNF ligand binding, TNFRSF1A binds the TNFRSF1A associated via death domain (TRADD) and receptor interacting serine/threonine kinase 1 (RIPK1) proteins through its intracellular death domain (DD). TRADD then recruits the TNF receptor associated factor 2 (TRAF2) adapter protein, and one of two TNFRSF1A signalling complexes then forms.

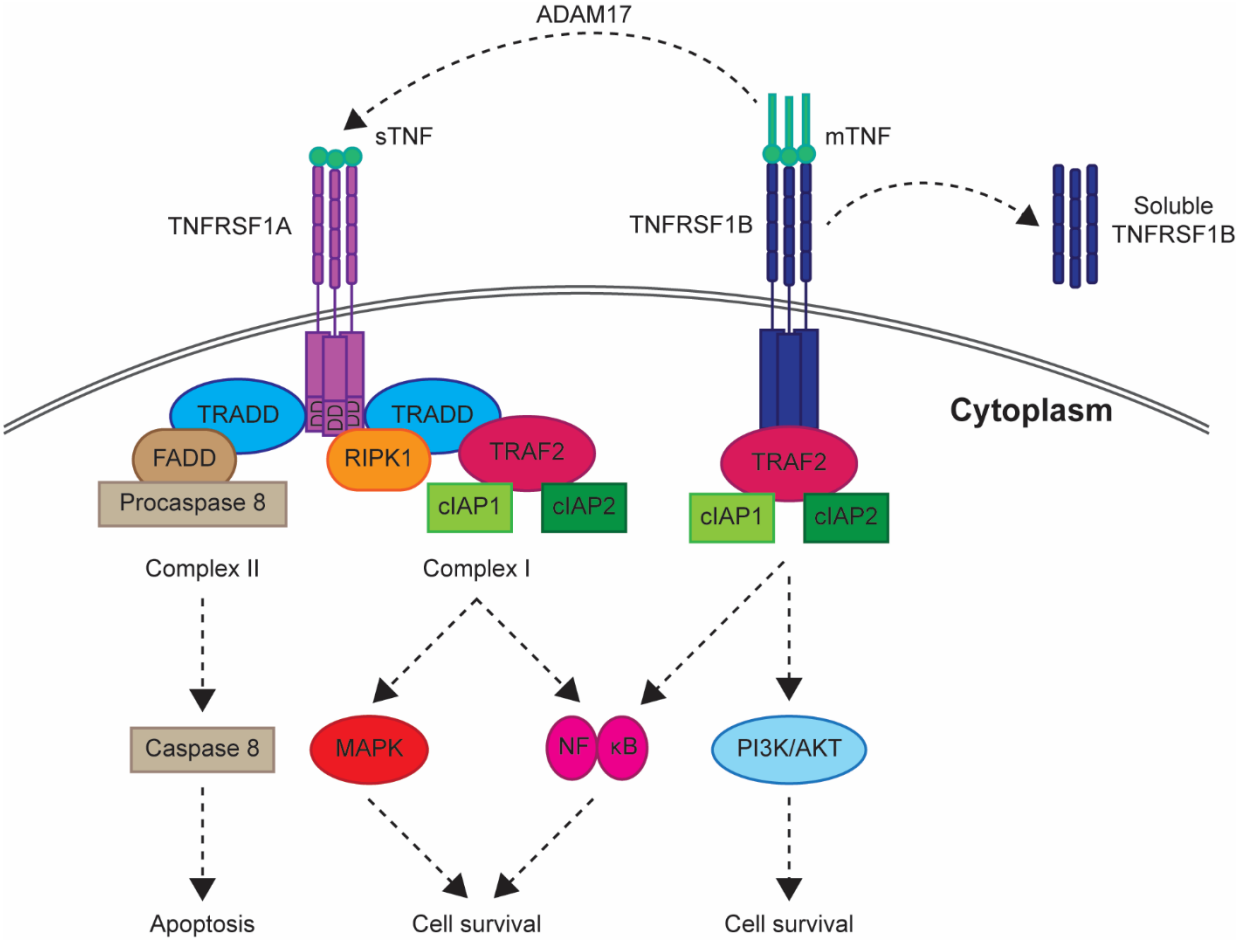


**Figure 2.4 The TNF signalling pathway**

Soluble TNF (sTNF)-bound TNFRSF1A binds TRADD and RIPK1 through its DD. TRADD recruits TRAF2 and forms complex I, which includes cIAP1 and cIAP2 and leads to cell survival via the NF-κB and MAPK signalling pathways, or complex II, in which TRADD recruits FADD and procaspase 8, leading to apoptosis. TNFRSF1B lacks a DD, and instead directly binds TRAF2 when activated by membrane-bound TNF (mTNF). cIAP1 and cIAP2 recruitment leads to the induction of the NF-κB or the PI3K/AKT signalling pathways, resulting in cell survival. Additionally, membrane-bound TNF receptors can be cleaved to form soluble TNFRSF1A (not shown) and TNFRSF1B, whereas mTNF, which preferentially binds to TNFRSF1B, is cleaved by disintegrin and metalloproteinase domain-containing protein 17 (ADAM17) to form sTNF.

Complex I, which includes the E3 ubiquitin ligases cellular inhibitor of apoptosis 1 (cIAP1) and cIAP2, activates the classical nuclear factor kappa B (NF-κB) and MAPK signalling pathways, leading to cell survival, pro-inflammatory, and anti-apoptotic gene expression. When complex I is destabilized, TRADD can recruit Fas associated via death domain (FADD) and procaspase 8, forming complex II and leading to caspase 8 activation and eventual apoptotic cell death via the caspase cascade. In contrast, TNFRSF1B lacks a DD in its intracellular region, and instead directly binds TRAF2 when activated by TNF ligand. The result is the recruitment of cIAP1 and cIAP2 and the induction of the canonical and non-canonical NF-κB signalling pathways. TNFRSF1B can also induce the PI3K/AKT signalling pathway following TNF binding, leading to cell adhesion, migration, survival and proliferation (reviewed by Yang *et al*. 2018). TNF-induced signalling is further complexified by the roles of membrane-bound and soluble forms of both TNF ligand and its receptors. TNF is synthesized as a 26 kDa type II transmembrane protein which forms a membrane-bound homotrimer (Kriegler *et al*. 1988). Precursor mTNF can be cleaved by the ADAM17 enzyme to form a 17 kDA sTNF (Black *et al*. 1995; Moss *et al*. 1997). Both mTNF and sTNF are biologically active (Decoster *et al*. 1995). TNFRSF1B has higher affinity for mTNF, whereas TNFRSF1A binds both forms (Grell *et al*. 1995); thus, sTNF typically triggers apoptotic and pro-inflammatory signals via TNFRSF1A, whereas mTNF is associated with cell survival via TNFRSF1B. The two TNF receptors can also be cleaved from their membrane-bound precursors to form soluble receptors composed solely of their extracellular domain, which can act as a biological ligand sink and regulate TNF signalling levels (Wallach *et al*. 1991). Furthermore, the TNF receptors can partake in functional crosstalk through the passing of ligand from TNFRSF1B to TNFRSF1A, such that the normally pro-survival effects mediated by TNFRSF1B are instead pro-apoptotic via TNFRSF1A (Tartaglia,

Pennica & Goeddel 1993). These factors combine to make TNF signalling a complex and often conflicting process, with effects that depend on the ligand and receptor isoforms, whether TNFRSF1A or TNFRSF1B is activated, and cellular context.

TNF is known to regulate a number of processes in the mammalian ovary, including germ cell cyst breakdown and primordial follicle assembly (Morrison & Marcinkiewicz 2002; Nilsson, Stanfield & Skinner 2006), the inhibition of gonadotropin-stimulated steroidogenesis (Terranova 1997) and ovulation (Yamamoto *et al*. 2015), and the induction of GC proliferation (Son *et al*. 2004) and death (Kaipia *et al*. 1996; Sasson *et al*. 2002). The actions of TNF on ovarian steroidogenesis and GC proliferation are thought to be mediated by TNFRSF1A (Roby, Son & Terranova 1999; Son *et al*. 2004), although a complementary, overlapping or potentiating role for TNFRSF1B in these processes has not been excluded. In the mouse ovary, TNFRSF1B-mediated TNF signalling triggers the death of immature oocytes, and loss of TNFRSF1B results in an expansion of the primordial follicle pool and an increase in the number of growing follicles (Greenfeld *et al*. 2007b). Multiple *TNFRSF1B* variants have been associated with disease in humans, particularly chronic disorders with inflammatory components. A variant in *TNFRSF1B* (c.676T>G) that causes the non-conservative substitution of arginine (Arg) for methionine (Met) at residue 196 is significantly associated with hyperandrogenism and PCOS in women (Peral *et al*. 2002). The p.Met196Arg variant demonstrates less TRAF2 recruitment, and significantly lowers TNFRSF1B-mediated NF-kB activation and subsequent anti-apoptotic and pro-inflammatory target gene expression, without affecting TNF binding kinetics (Till *et al*. 2005). Residue 196 is in the fourth cysteine-rich motif of the protein's extracellular domain, which is closest to the cell membrane and near the site (p.Pro211) of enzymatic cleavage required for the shedding of soluble TNFRSF1B (Herman & Chernajovsky 1988). While it has been speculated

that p.Met196Arg confers higher levels of soluble TNFRSF1B (Till *et al*. 2005), the p.Met196Arg variant is not associated with soluble TNFRSF1B levels in women with PCOS (Peral *et al*. 2002).

Given its known role in the regulation of follicle growth in the mouse ovary, and an association with hyperandrogenism and PCOS in women, *Tnfrsf1b* was chosen for further investigation in the SWR model of GC tumourigenesis. *Tnfrsf1b* mRNA expression was quantitatively compared between pubertal ovary pools from DHEA-treated SWR mice and either DHEA-treated Line 4-T or control-treated mice, and its genomic sequence was examined by Sanger sequencing. Although no expression differences were evident in either comparison, 12 single nucleotide polymorphisms (SNPs) and two dinucleotide deletions were identified in the distal coding and 3′ untranslated region (UTR) in SWR compared to Line 4-T and the published B6J mouse reference genome (Smith 2011). All 12 SNPs, which included four silent mutations and a single missense mutation (c.1148T>C; p.Phe360Ser), are known variants that are not unique to the SWR strain. Notably, no variants were identified at the coding site analogous to the human p.Met196Arg variant, although this residue is not conserved between mouse and human. While the two dinucleotide deletions present in the 3′ UTR are novel and appear to be unique to SWR, this region is minimally conserved between mouse and human and their significance remains unclear.

#### 2.1.2.2 *Dhrs3*

Dehydrogenase/reductase (SDR family) member 3 (*Dhrs3*) is a six exon gene that encodes a short-chain dehydrogenase/reductase (SDR). Other SDR family members, including 3β-HSD and 17β-HSD, catalyze the conversion of steroid hormones in the ovarian GCs and TCs

(Figure 1.8). DHRS3 function was initially investigated in the context of vision, where it reduces the vitamin A metabolite all-*trans*-retinaldehyde (RAL) to all-*trans*-retinol (ROL) using reduced nicotinamide adenine dinucleotide phosphate (NADPH) as a cofactor (Figure 2.5; Haeseleer *et al*. 1998). These metabolites are intermediates between retinyl esters, the storage form of vitamin A found in lipid droplets, and the biologically active signalling molecule RA. This reversible redox reaction is necessary for photoreception, although several SDRs in addition to DHRS3 are capable of reducing RAL in the retina (Kiser *et al*. 2012). The reciprocal reaction of ROL oxidation is catalyzed by retinol dehydrogenase 10 (all-trans) (RDH10; Sandell *et al*. 2007), another SDR that uses nicotinamide adenine dinucleotide ($NAD^+$) as a cofactor (Belyaeva, Johnson & Kedishvili 2008). The direction of this reaction depends on substrate and cofactor availability (Metzler & Sandell 2016). DHRS3 and RDH10 physically interact and function as part of a codependent complex, mutually stabilizing and enhancing each other's catalytic activity (Adams *et al*. 2014; Belyaeva *et al*. 2017). *Dhrs3* is induced by RA (Cerignoli *et al*. 2002; Zolfaghari, Chen & Ross 2012), and thus controls retinoid homeostasis via an RA-induced negative feedback loop in which it inhibits the molecule's biosynthesis by decreasing its immediate precursor. Expression analyses determined that DHRS3 is present in multiple tissues other than the retina, with widespread expression in human (Cerignoli *et al*. 2002) and rodent (Zolfaghari, Chen & Ross 2012) fetal and adult tissues, suggesting a role for this enzyme outside of the visual cycle. The spatial and temporal pattern of *Dhrs3* expression in many of these tissues overlaps with that of RA signalling during early development, and accordingly, *in vivo* analyses have determined that *Dhrs3* is critical for normal embryogenesis. Mouse embryos null for *Dhrs3* die in late gestation after E17.5 secondary to craniofacial, cardiac, and skeletal abnormalities due to an excess of teratogenic RA (Billings *et al*. 2013; Wang *et al*. 2018). Similarly, knockdown of

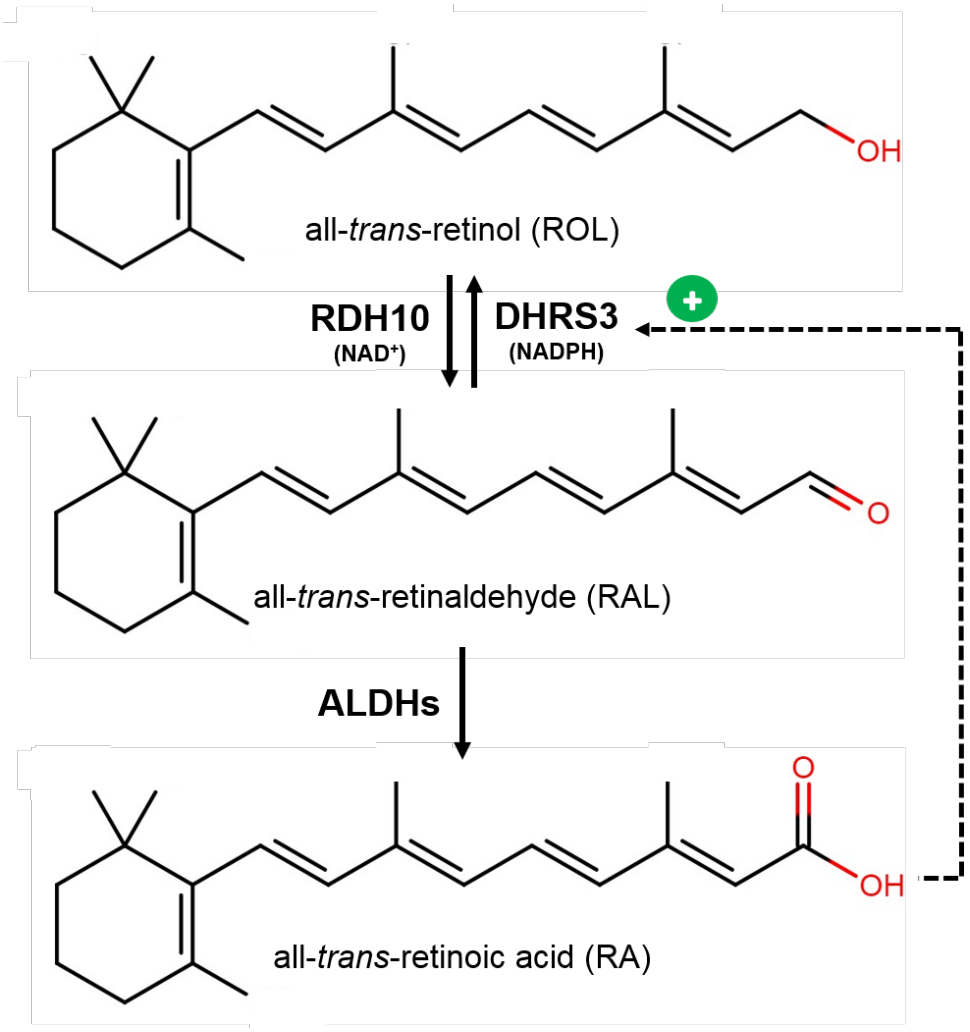


**Figure 2.5 RA metabolism and feedback regulation**

RA is synthesized via the reversible oxidation of ROL to RAL by RDH10, followed by the irreversible oxidation of RAL by the aldehyde dehydrogenases (ALDHs; Niederreither *et al*. 1999; Fan *et al*. 2003; Dupe *et al*. 2003). RA induces *Dhrs3* as part of a negative feedback loop in which DHRS3 catalyzes the reduction of RAL to ROL. DHRS3 functions with RDH10 as part of a codependent complex that mutually stabilizes and enhances both proteins' catalytic activity.

the *Dhrs3* homologues in zebrafish (Feng *et al*. 2010) and *Xenopus* (Kam *et al*. 2013) causes an excess of RA and embryogenesis defects. Further investigations focused on DHRS3 determined that it is a membrane-bound endoplasmic reticulum protein (Deisenroth *et al*. 2011; Lundova *et al*. 2015) that also associates with lipid droplets and mitochondria (Deisenroth *et al*. 2011; Belyaeva *et al*. 2017). In addition to RA, *DHRS3* is induced by the tumour suppressor p53 and the related tumour protein p63 (p63) *in vitro* (Kirschner *et al*. 2010), and by the mineralcorticoid receptor in cultures of decidualizing human endometrial stromal cells (Kuroda *et al*. 2013; Ozaki *et al*. 2017). DHRS3 may promote osteoblast differentiation (Zhang *et al*. 2018), and has been associated with inflammation-linked disorders; *DHRS3* is upregulated in the monocytes of patients with some diabetes subtypes (Padmos *et al*. 2008; Bevan *et al*. 2010; van der Heul-Nieuwenhuijsen *et al*. 2010; Baldeón *et al*. 2015), whereas it is down-regulated in cells from rheumatoid arthritis patients (Wang *et al*. 2017). *DHRS3* is somatically amplified and its expression up-regulated in papillary thyroid carcinomas (Oler *et al*. 2008; Passon *et al*. 2015), but it is aberrantly methylated in human melanoma (Furuta *et al*. 2006) and neuroblastoma (Carén *et al*. 2011) cell lines and significantly down-regulated in triple-negative breast cancer metastases (Merino *et al*. 2018).

Perhaps the most intriguing aspect of DHRS3 function with regards to this dissertation is its potential for steroid metabolism. Considering the broad substrate specificities of SDRs (Haeseleer & Palczewski 2000) and the structural similarities of DHRS3 to other steroid-metabolizing SDRs (Bray, Marsden & Oppermann 2009; Albalat *et al*. 2011), multiple studies have assayed the enzymatic action of this protein towards steroids using insect cell microsomes that overexpress recombinant DHRS3. Although one study did not report significant redox activity towards any tested steroids (Haeseleer *et al*. 1998), DHRS3 was shown to possess 17β-

HSD activity in a subsequent investigation as it was able to reduce $E_1$ to $E_2$ and $A_4$ to T (Lundova *et al*. 2015). Low oxidative activity towards T using nicotinamide adenine dinucleotide phosphate ($NADP^+$) as a cofactor was also observed in this investigation. Notably, the DHRS3 steroid redox assays conducted to date did not take into account the requirement of RDH10 in DHRS3 function, nor is it known if DHRS3 has other protein partners that may assist in steroid metabolism; therefore, the full spectrum of DHRS3 substrates and its steroid redox potential may not yet be known. That *Dhrs3* functions in the homeostasis of RA, the initiator of oocyte meiosis, and that it belongs to an enzymatic family that catalyzes steroid hormone conversion and may possess such activity itself, increases this gene's standing in the prioritized ranking of *Gct1* candidate genes.

### 2.1.3 Summary and Current Work

Robust evidence gathered from androgen-induced phenotypic mapping suggests a gene within the *Gct1* interval drives the juvenile-onset GC tumour phenotype in SWR mice. Given the challenges posed by the distal end of *Gct1* on resolving the interval's boundary, the 1.86 Mb refined interval will be the focus of a third round of phenotypic mapping and further proximal fine mapping. The resolved *Gct1* interval will undergo complete genetic annotation to identify all genomic variants unique to the SWR strain. *Tnfrsf1b* and *Dhrs3* are two highly plausible *Gct1* candidates with human orthologues that have been shown to be expressed in the SWR ovary (Smith 2011). The availability of ligand (TNF) or substrate (RAL) and inducer (RA) for these candidates and the success of previous hormonal intervention studies over the pubertal period (Beamer, Shultz & Tennent 1988; Tennent, Shultz & Beamer 1993; Dorward, Shultz & Beamer 2007) suggests they are good candidates for systemic *in vivo* testing. Therefore, concurrent with

the genetic annotation of *Gct1*, the *Tnfrsf1b* and *Dhrs3* candidate genes will be the focus of functional testing in SWR mice, to support or refute these genes and/or their pathways as causative of GC tumourigenesis.

### 2.1.4 Hypothesis and Research Objectives

*Hypothesis*

A unique genetic determinant is present within the *Gct1* locus in SWR mice, which supports susceptibility to the pubertal initiation of ovarian GC tumours in a DHEA-responsive and GC-autonomous manner.

*Research Objectives*

1) Reduce the *Gct1* candidate gene interval through a third round of phenotypic mapping and by identifying polymorphic genetic variants to fine map the genomic boundaries of the recombinant subcongenic lines.

2) Completely annotate the $Gct1^{SW}$ interval using next-generation sequencing (NGS) and copy number variation (CNV) analyses, so as to identify novel variants unique to SWR and therefore prioritize gene candidates within the refined *Gct1* interval.

3) Evaluate prioritized gene candidates for shared identity with *Gct1* by *in vivo* functional assessments, based on known biological roles and the genetic analysis of the entire $Gct1^{SW}$ interval.

## 2.2 Materials and Methods

### 2.2.1 Animal Husbandry

#### 2.2.1.1 Animal Housing

All mice were maintained in a facility operated by Animal Care Services of Memorial University of Newfoundland and experimental protocols were approved by the Institutional Animal Care Committee in accordance with the guidelines of the Canadian Council on Animal Care. Mice were housed in a pathogen-free barrier under a 12:12 hour (h) light/dark cycle and provided with food and water *ad libitum*. Prior to April 2016, mice were fed Laboratory Autoclavable Rodent Diet 5010 autoclaved food pellets (28.7% protein, 13.1% fat, 58.2% carbohydrate; LabDiet, St. Louis, MO). Following an institutional diet transition period in April 2016, mice were fed Teklad Global 18% Protein Rodent Diet 2918 irradiated food pellets (24% protein, 18% fat, 58% carbohydrate; Envigo, Huntingdon, UK). The experimental phenotype of spontaneous GC tumour susceptibility was confirmed following the change in diet.

Animals were weaned at 20 to 23 days (d) of age and housed in groups of two to five animals per cage in 501 $cm^2$ Sealsafe® PLUS individually ventilated rodent cages (Tecniplast, West Chester, PA). Mouse cages contained Bed-o'Cobs® corn-cob bedding material (The Andersons Inc., Maumee, OH), nestlets (Ancare, Bellmore, NY), and a Mouse House™ Enrichment Device (Tecniplast).

#### 2.2.1.2 Mouse Strains

SWR, Line-4-T, and 12 recombinant subcongenic lines (Lines 4-1 to 4-12) derived from Line 4-T or Line 4-3 were used to refine the *Gct1* interval using genotypic mapping. SWR and

SWR.SJL-X.CAST-4-5 (Line 4-5) were used for all sequence and functional analyses. Line 4-5 is resistant to GC tumour initiation due to the presence of CAST-derived genome at *Gct1*, and has the smallest portion of CAST-derived genome of any maintained recombinant subcongenic strain (Figure 2.3). Line 4-5 was therefore used as the starting donor for recombination between $Gct1^{CA}$ and $Gct1^{SW}$ alleles in a third round of phenotypic mapping.

#### 2.2.1.3 Surgical Capsule Implantation

Exogenous DHEA was administered to mice at puberty for two purposes: 1) for functional analyses of *Gct1* candidate genes in tandem with protein ligand, substrate/inducer, or vehicle control in SWR and Line 4-5 mice; and 2) to positively identify granulosa cell (GC) tumour-susceptible SWR mice, and as a corresponding control treatment for Line 4-5 mice, for CNV analysis of the *Gct1* interval. Mice were anesthetized with isoflurane (2-chloro-2-(difluoromethoxy)-1,1,1-trifluoro-ethane; Fresenius Kabi Canada Ltd., Richmond Hill, ON) and subcutaneously implanted with a steroid-filled capsule via a small dorsal incision between the scapula at 3 wk of age. Capsules were composed of 10 mm long Silastic® silicone laboratory tubing (1.98 mm inner diameter; Dow Corning, Midland, MI) filled with approximately 150 mg of powdered DHEA (5-androsten-3β-ol-17-one; A8500-000, Steraloids Inc., Newport, RI) and were sealed at each end with a 3 mm glass bead (Thermo Fisher Scientific, Waltham, MA). Control capsules were empty capped lengths of Silastic® tubing. The incision area was sanitized with a solution of 0.5% chlorhexidine in alcohol (Perrigo, Perth, Australia) followed by 70% isopropyl alcohol (Laboratoire Atlas Inc., Montreal, QC) and Prepodyne® scrub (West Penetone Inc., Montreal, QC). Surgical instruments were sterilized between surgeries by heating to 250 °C in a Steri 350 dry bead sterilizer (Inotech Biosystems International Inc., Brandon, FL). Incisions

were closed using a 9 mm AutoClip® stainless steel wound clip (MikRon Precision Inc., Gardena, CA). Mice were subcutaneously injected with 0.1 mL 0.5 ng/mL (5 mg/kg) Rimadyl (carprofen; Pfizer Animal Health, Kirkland, QC) analgesic preoperatively. Wound clips were removed from mice approximately 1 wk after surgery.

#### 2.2.1.4 Animal Examination

Mice were euthanized with $CO_2$ gas at 8 wk of age, and GC tumour development was assessed by macroscopic examination of the ovaries in mice with present and intact DHEA capsules. Mice with palpable GC tumour masses were necropsied earlier than 8 wk. Where applicable, kidneys, ovaries and uteri were removed at the time of necropsy.

### 2.2.2 Genotypic Mapping

Genotyping markers used were SSLPs and SNPs empirically determined to be polymorphic between the SWR and CAST genomes. SSLPs and their primer sequences were annotated in the Mouse Genome Database (MGD; Smith *et al*. 2018; informatics.jax.org) or were identified by the Computational Sciences group at The Jackson Laboratory and designed in-house. SNPs were annotated in the National Center for Biotechnology Information (NCBI) Single Nucleotide Polymorphism Database (dbSNP) build 151 (Sherry *et al*. 2001; ncbi.nlm.nih.gov/snp). Because the SWR strain has not been re-sequenced, annotated SNPs were chosen on the basis of differences between CAST alleles and the alleles of other common inbred strains, particularly Swiss-derived strains which are phylogenetically related to SWR (Petkov *et al*. 2004). SSLP markers were amplified from tail tip genomic DNA (gDNA) and assessed for

allele size by horizontal agarose gel electrophoresis, whereas SNP markers were amplified from tail tip or kidney gDNA and assessed for nucleotide changes by cycle sequencing. New $N_2F_1$ individuals were tested for recombinations against a panel of SSLP and SNP markers to establish Chr 4 haplotype patterns. SNPs were identified in at least two individuals from each recombinant subcongenic line. Novel genotyping primer sequences were designed using Primer3 version 4.1.0 (Koressaar & Remm 2007; Untergasser *et al*. 2012; bioinfo.ut.ee/primer3) and were analyzed for target specificity using the NCBI Primer Basic Local Alignment Search Tool (BLAST; Ye *et al*. 2012; ncbi.nlm.nih.gov/tools/primer-blast) program. Genotyping marker primer sequences, relative SSLP sizes for CAST and SWR, and their locations on Chr 4 are shown in Table 2.2.

#### 2.2.2.1 Genotyping by Simple Sequence Length Polymorphisms

*Tail Tip Biopsy and Genomic DNA Extraction*

Approximately 2 mm of tissue was removed from the tail tip using scissors upon necropsy or before mice reached 3 wk of age. The cut tail tips of live mice were dipped in Kwik Stop® Styptic Powder (Gimborn Pet Specialties, Atlanta, GA). Tail samples were placed in a 1.5 mL microcentrifuge tube with 500 µL of 50 mM sodium hydroxide (BHD Inc., Toronto, ON). The tubes were placed on an Isotemp™ heat block (Thermo Fisher Scientific) for 10 minutes (min) at 95 °C, after which 50 µL of 1 M tris-hydrochloric acid pH 8.0 (Sigma-Aldrich Inc., St. Louis, MO; Thermo Fisher Scientific) was added. The samples were centrifuged at 10,000 g for 30 seconds (s), and 500 µL of supernatant was transferred to a 1.5 mL microcentrifuge tube. The gDNA samples were stored at -20 °C until assayed.

**Table 2.2 SSLP and SNP genotyping markers.** Primer sequences used to amplify SSLPs and SNPs for genotypic mapping of *Gct1* by polymerase chain reaction (PCR), their genomic location on Chr 4, and relative SSLP allele sizes are shown. Data is from Ensembl release 95 (January 2019; Zerbino *et al*. 2018). Relative SSLP sizes were determined from horizontal agarose gel electrophoresis. CA: CAST allele; SW: SWR allele

| Marker Symbol | Forward Sequence (5′→3′) | Reverse Sequence (5′→3′) | Start of Amplified Region (bp) | Assay Type | Relative SSLP Allele Size |
|---|---|---|---|---|---|
| *D4sjh10* | GCAGAAATGGCACAGGAGAT | CCCACATTTGAAACCACCTC | 144,618,919 | SSLP | CA > SW |
| *Dhrs3* | ACATCTGGTTGTGGGAGACGGAAA | AGCCAGAGATGCTTAGGTCTGTGT | 144,928,064 | SNP | n/a |
| *D4Mit232* | GCGTCACCACACTGCTCTT | ACTCAGAGTCCCCTGGCC | 145,057,656 | SSLP | CA > SW |
| *D4Mit233* | TGGTCATGTGTGTCCATGC | ACTTCATGTAGCCAGGTGGG | 145,224,944 | SSLP | CA > SW |

*Polymerase Chain Reaction*

SSLP genotyping markers were amplified by PCR using a Master*Taq* Kit (5 PRIME Inc., Gaithersburg, MD) from gDNA extracted from Line 4-5 $N_2F_1$ backcross mice tail samples, and from SWR, Line 4-5 and (SWR x Line 4-5)$F_1$ genotyping standards. The following reagents were combined in a 0.2 mL PCR tube (Bio-Rad Laboratories, Hercules, CA): 5.35 µL of distilled water, 2 µL of 5X *Taq*Master PCR Enhancer heated to 65 °C, 1 µL of 10X Reaction Buffer, 0.2 µL of 10 mM deoxynucleotide triphosphates (dNTPs; Invitrogen, Carlsbad, CA), 0.2 µL of 10 µM forward and reverse primers (Integrated DNA Technologies, Coralville, IA), 0.05 µL of *Taq* DNA polymerase, and 1 µL of gDNA template. A negative control was included with each PCR with distilled water in place of gDNA template. The tubes were placed in a Veriti™ 96-Well Thermal Cycler (Applied Biosystems Inc., Foster City, CA) where PCR was performed using the following profile: 97 °C for 30 s; 39 cycles of 94 °C for 15 s, 55 °C for 30 s, and 72 °C for 30 s; 72 °C for 10 min. The PCR products were stored at 4 °C until gel electrophoresis.

*Gel Electrophoresis*

SSLP genotyping PCR products were separated by horizontal electrophoresis through a 4% agarose gel. PCR products (10 µL) were combined with 3 µL of gel loading buffer (OmniPur® bromophenol blue, sodium salt; EMD Millipore, Billerica, MA) in a 0.2 mL PCR tube and mixed by pipetting. The gels were comprised of 8 g of MetaPhor® agarose (Lonza, Rockland, ME), 20 mL of 10X tris-borate-ethylenediaminetetraacetic acid (EDTA) buffer (TBE; 0.89 M tris, 0.89 M boric acid [Thermo Fisher Scientific], 0.02 M EDTA [Sigma-Aldrich Inc.]) and 180 mL distilled water. The gel mixture was boiled using a microwave, and after cooling was poured into a gel electrophoresis chamber taped at both ends and containing loading well

combs. After the gel solidified the combs were removed and the PCR product/loading buffer solution (13 µL) or 8 µL of GD 100 bp DNA Ladder marker (FroggaBio, Toronto, ON) were pipetted into the wells. The gels were electrophoresed for 3 h at 120 V, after which they were post-stained in a solution of 50 µL of 10 mg/mL ethidium bromide solution (Bio Basic Inc., Markham, ON) in 1 L distilled water for approximately 30 min. The SSLP PCR products were visualized using a U:Genius GelVue UV transilluminator (302 nm; Syngene, Frederick, MD) and scored for allele size differences between SWR, CAST and $F_1$ gDNA standards.

#### 2.2.2.2 Genotyping by Single Nucleotide Polymorphisms

*Genomic DNA Extraction from Kidney*

gDNA was extracted from single whole kidneys at the time of necropsy using a salt extraction method. Kidneys were homogenized on ice in 6 mL of isotonic high pH (Iso-Hi-pH) buffer (0.14 M sodium chloride [BHD Inc., Toronto, ON], 0.01 M tris pH 8.4 [Sigma-Aldrich Inc.], 1.5 mM magnesium chloride [Sigma-Aldrich Inc.]) with 0.1% IGEPAL® CA-630 (Sigma-Aldrich Inc.) using a Dounce homogenizer. Lysates were transferred to a 15 mL centrifuge tube (Corning Incorporated, Corning, NY) and centrifuged at 800 g for 5 min at 4 °C. Supernatants were discarded and nuclear pellets resuspended in 6 mL of Iso-Hi-pH buffer with 0.1% IGEPAL® CA-630. A 300 µL aliquot of 20% sodium dodecyl sulfate (SDS; Sigma-Aldrich Inc.) and 150 µL of Proteinase K solution (10 mg/mL Proteinase K [Sigma-Aldrich Inc.], 0.05 M tris pH 8.0 [Sigma-Aldrich Inc.], 1 mM calcium chloride [Thermo Fisher Scientific]) were added to the tubes, which were immediately and repeatedly inverted and placed in a water bath (Thermo Fisher Scientific) at 37 °C for 3 h with periodic inversions. Following incubation, 2 mL of 6 M sodium chloride (BHD Inc.) was added to the tubes, which were mixed by vigorous inversion

and centrifuged at 2,000 g for 15 min at room temperature (RT). The supernatant was transferred to a 50 mL centrifuge tube (Corning Incorporated) with a wide-bore transfer pipette and the gDNA was precipitated by overlaying two volumes of 100% ethanol (Commercial Alcohols, Brampton, ON). gDNA was spooled onto a glass rod, soaked in 70% ethanol (Commercial Alcohols) for 10 min, and air dried for 10 min. The dried gDNA was resuspended in 600 µL of tris-EDTA (TE) buffer (10 mM tris pH 8.0, 1 mM EDTA [Sigma-Aldrich Inc.], pH 8.0) and mixed on a rocker (Boekel Scientific, Feasterville, PA) overnight. The gDNA stock solutions were diluted 1:9 gDNA to distilled water and stored at -20 °C.

*Polymerase Chain Reaction and Gel Electrophoresis*

SNP genotyping markers were amplified by PCR using a Master*Taq* Kit (5 PRIME Inc., Gaithersburg, MD) from gDNA extracted from SWR, Line 4-T and the recombinant subcongenic line mouse kidneys, and from the tail tip gDNA of $N_2F_1$ backcross mice as per the protocol for SSLP genotyping markers (Section 2.2.2.1). Successful amplification of SNP genotyping marker amplicons was confirmed by electrophoresis through a 1% agarose gel. PCR products (5 µL) were combined with 3 µL of gel loading buffer (OmniPur® bromophenol blue, sodium salt) in a 0.2 mL PCR tube and mixed by pipetting. The gels were comprised of 0.5 g of UltraPure™ agarose (Invitrogen), 5 mL of 10X TBE buffer, 45 mL of distilled water, and 3 µL of ethidium bromide solution (Bio Basic Inc.). The gels were cast, loaded, and PCR products visualized as per the protocol for SSLP genotyping markers (Section 2.2.2.1). The gels were electrophoresed for 30 min at 120 V.

*PCR Product Purification*

PCR products were purified using a QIAquick® PCR Purification Kit (28106; Qiagen Inc., Mississauga, ON) as per the manufacturer's standard protocol. Briefly, five volumes of Buffer PB were combined in a 1.5 mL microcentrifuge tube with one volume of PCR product, and transferred to a QIAquick spin column in a 2 mL collection tube with 10 µL of 3 M sodium acetate (Sigma-Aldrich Inc.). After centrifugation at 17,900 g for 1 min, the flow-through was discarded and 750 µL of Buffer PE was added to the QIAquick column. After two sequential centrifugations at 17,900 g for 1 min, the QIAquick column was transferred to a 1.5 mL microcentrifuge tube and 30 µL of distilled water was pipetted directly onto the filter membrane. The tubes were incubated for 1 min at RT, after which they were centrifuged at 17,900 g for 1 min to elute the PCR products. Purified PCR products were stored at -20 °C until Sanger sequencing.

*Cycle Sequencing*

All cycle sequencing reactions were performed at the Genomics and Proteomics Facility, Core Research and Equipment and Instrument Training Network, Memorial University of Newfoundland, using a BigDye® Terminator v3.1 Cycle Sequencing Kit (Applied Biosystems Inc.). The following reagents were combined in a 0.2 mL PCR tube and made up to a volume of 17.5 µL with distilled water: 2 µL of 5X Sequencing Buffer, 0.5 µL of Ready Reaction Mix, 2 µL of either 1.6 pmol/µL forward or reverse primer and 10-40 ng purified PCR product template. A control reaction was included with each sequencing run and consisted of 2 µL of 5X Sequencing Buffer, 0.5 µL of Ready Reaction Mix, 2 µL of M13 (-21) Primer, 2 µL of pGEM Control DNA, and 13.5 µL of distilled water. The tubes were placed in a GeneAmp® PCR

System 9700 Thermal Cycler (Applied Biosystems Inc.) and PCR was performed using the following profile: 25 cycles of 96 °C for 10 s, 50 °C for 5 s, and 60 °C for 4 min; and a 4 °C hold. The PCR products were stored at 4 °C until purification, when they were combined with 5 μL of 125 mM EDTA and 65 μL of 95% ethanol (Commercial Alcohols). The tubes were briefly vortexed and centrifuged, covered in foil and stored at 4°C overnight. The tubes were centrifuged at 3,000 g for 30 min at RT, and the supernatants were discarded by quickly inverting the tubes. The tubes were centrifuged at 200 g for 25-30 s, after which 150 μL of 70% ethanol was added. The tubes were vortexed briefly and centrifuged at 3,000 g for 15 min. The supernatants were discarded, and the tubes were air-dried for 15 min. The purified PCR products were resuspended in 20 μL of Hi-Di™ Formamide (Applied Biosystems Inc.) and briefly vortexed and centrifuged. The samples were then loaded into a cassette and placed in a 3130 or 3730 Genetic Analyzer (Applied Biosystems Inc.), where they were subject to capillary electrophoresis.

*Sequence Analysis*

Sequences were analyzed using Sequencher® version 5.2.4 (Gene Codes Corporation, Ann Arbor, MI). Experimental sequences were aligned to the B6J mouse reference genome, downloaded from Ensembl Mouse Genome Browser release 79 (GRCm38; March 2015; Cunningham *et al*. 2015; ensembl.org).

### 2.2.3 Next-Generation Sequencing

NGS was conducted to identify all unique single nucleotide variants (SNVs) and small nucleotide insertions and deletions within the entirety of the SWR *Gct1* interval in comparison to

the B6J mouse reference genome and other re-sequenced strains. Since *Gct1* was already mapped to a high resolution by phenotypic mapping, a targeted sequencing approach was utilized to isolate the $Gct1^{SW}$ locus prior to NGS (Simon *et al*. 2012). Array design, NGS and post-NGS informatics were performed at The Jackson Laboratory, whereas sample preparation (Appendix A), report analysis, and variant prioritization and validation were performed at Memorial University of Newfoundland.

#### 2.2.3.1 Genomic DNA Extraction

gDNA was extracted from mouse tail samples (Section 2.2.2.1) from three mouse lines with homozygous SWR alleles at *Gct1* (SWR, SWR.SJL-$X_5$, and SWR.CAST-X (n = 1/mouse line) using a phenol-chloroform extraction method. Tail tips were placed in a 1.5 mL microcentrifuge tube with 700 µL of tail buffer (50 mM tris-hydrochloric acid pH 8.0 [Sigma-Aldrich Inc.; Thermo Fisher Scientific], 100 mM EDTA pH 8.0 [Sigma-Aldrich Inc.], 100 mM sodium chloride [BHD Inc.], 1% SDS [Sigma-Aldrich Inc.]) and 50 µL of Proteinase K solution and vortexed briefly. The samples were placed in a water bath (Thermo Fisher Scientific) at 55 °C overnight and vortexed periodically, after which they were centrifuged at 15,000 g for 4 min. The supernatant was transferred to a new 1.5 mL microcentrifuge tube and 750 µL of phenol (Sigma-Aldrich) saturated with ACE buffer (50 mM sodium acetate [Sigma-Aldrich Inc.], 10 mM EDTA pH 5.9 [Sigma-Aldrich Inc.]) was added. The samples were vortexed for 10 s, after which they were centrifuged at 15,000 g for 4 min to separate the aqueous and organic phases. The clear upper aqueous phase was transferred to a new 1.5 mL microcentrifuge tube and 600 µL of chloroform:isoamyl alcohol 24:1 (Sigma-Aldrich Inc.) was added. The samples were mixed by vigorous inversion for 1 min and centrifuged at 15,000 g for 2 min. The aqueous phase was

transferred to a new 1.5 mL microcentrifuge tube and the gDNA was precipitated by overlaying 1 mL of absolute ethanol (Commercial Alcohols). The gDNA pellets were centrifuged at 15,000 g for 4 min, washed with 500 µL of 70% ethanol (Commercial Alcohols), and centrifuged at 15,000 g for 4 min. The 70% ethanol was removed by pipetting and the gDNA pellets were dried in a desiccator under vacuum for 10 min. The dried gDNA was resuspended in 150 µL of TE buffer and incubated overnight prior to incubation at 50 °C for 10 min. All steps were completed at RT unless otherwise noted. All gDNA samples had a 260/280 ratio of at least 1.85 as determined using a NanoDrop™ 1000 Spectrophotometer (Thermo Fisher Scientific), and were assessed for integrity and molecular weight by electrophoresis through a 1% agarose gel (Section 2.2.2.2) with GeneRuler™ 1 kb Plus DNA Ladder marker (Thermo Fisher Scientific). The gDNA samples were fragmented using a sonicator to produce 150-200 bp gDNA fragments prior to locus enrichment.

#### 2.2.3.2 Locus Enrichment, Next-Generation Sequencing, and Data Analysis

*Gct1* locus enrichment was accomplished using a SureSelect DNA Capture Array 1M (Agilent Technologies, Santa Clara, CA) customized to capture a generous interval of 2.3 Mb across the mapped *Gct1* locus. The array was designed with 286,707 unique 60 bp oligonucleotide probes offset by 3 bp and masked simple repeat regions, but represented all possible coding, regulatory and intronic regions within the *Gct1* locus. Enriched gDNA was sequenced on an Illumina HiSeq 2500 (Illumina, Inc., San Diego, CA) using 2 x 100 bp paired-end reads. Sequencing reads were aligned to the NCBI Build m37 B6J mouse reference genome assembly using Burrows-Wheeler Aligner (BWA) version 0.5.9 with default parameters (Li & Durbin 2009). Variant calling was performed using SAMtools mpileup version 0.1.16 with

default parameters (Li *et al*. 2009), and a custom software tool was used to insert annotations overlapping with called variants, including gene names, transcripts, exons, etc. The NGS data was converted from the NCBI Build m37 genome assembly to GRCm38 coordinates using the Ensembl Assembly Converter (Zhao *et al*. 2014). Common polymorphisms were eliminated by *in silico* comparison to genome sequences using data from dbSNP build 151 and from other re-sequenced inbred strains annotated by the Wellcome Sanger Institute (WSI) Mouse Genomes Project release 1505 (Keane *et al*. 2011; Yalcin *et al*. 2011; sanger.ac.uk/science/data/mouse-genomes-project). Variants were filtered by allele frequency (AF1) such that homozygous variants (AF1 = 1) were included and variants called as heterozygous (AF1 < 1), and therefore likely false, were excluded (Appendix B). Novel variants with AF1 = 1 were assessed using the Ensembl Variant Effect Predictor (VEP; McLaren *et al*. 2016; ensembl.org/Tools/VEP) and prioritized for empirical verification based on their quality metrics (Appendix B) and predicted impact. *In silico* variant analyses were performed using the Alamut® Visual version 2.11 (Interactive Biosoftware, Rouen, France) splicing prediction module, which includes GeneSplicer (Pertea, Lin & Salzberg 2001), MaxEntScan (Yeo & Burge 2004), and SpliceSiteFinder-like (Zhang 1998); Human Splicing Finder version 3.1 (Desmet *et al*. 2009; umd.be/HSF), which includes ESEFinder (Cartegni *et al*. 2003) and algorithms to evaluate the presence of branch points, heterogeneous nuclear ribonucleoprotein (hnRNP) motifs, and pseudoexon silencer motifs; and NetGene2 (Brunak, Engelbrecht & Knudsen 1991; cbs.dtu.dk/services/NetGene2), SpliceView (Rogozin & Milanesi 1997; bioinfo.itb.cnr.it/~webgene/wwwspliceview), CADD version 1.5 (Rentzsch *et al*. 2018; cadd.gs.washington.edu/snv), *FATHMM-XF* version 2.3 (Rogers *et al*. 2018; fathmm.biocompute.org.uk/fathmm-xf), and PhD-SNP$^{g}$ (Capriotti & Fariselli 2017;

snps.biofold.org/phd-snpg). Program inputs and interpretations are shown in Appendix C. Predicted nucleotide sequences were translated to amino acid sequences using the ExPASy Translate tool (Gasteiger *et al*. 2003; web.expasy.org/translate), and InterPro (Mitchell *et al*. 2019; ebi.ac.uk/interpro/) and UniProt (UniProt Consortium 2019; uniprot.org) were used for polypeptide analyses.

#### 2.2.3.3 Experimental Analysis of NGS Variants

*Empirical Validation of NGS Variants*

Prioritized variants were empirically verified by Sanger sequencing in SWR and Line 4-5 mice as per the protocol for SNP genotyping markers (Sections 2.2.2 and 2.2.2.2). Variant validation primer sequences and their locations on Chr 4 are shown in Table 2.3. One variant at the *Dhrs3* intron 3-exon 4 3′ acceptor splice site (c.460-3C>T) was prioritized and investigated for its effect on transcript splicing by reverse transcription PCR (RT-PCR).

*RNA Extraction from Mouse Ovaries*

Total RNA was extracted from whole ovaries of untreated, pubertal SWR and Line 4-5 mice using TRIzol® Reagent (Invitrogen). Ovary pairs were placed in a nuclease-free 1.5 mL microcentrifuge tube with 200 µL of TRIzol® Reagent and homogenized on ice using a Pellet Pestle® Cordless Motor (Kimble Chase Life Science and Research Products, Vineland, NJ) and nuclease-free Pellet Pestle® Tissue Grinders (Kimble Chase Life Science and Research Products). The samples were incubated at RT for 5 min, followed by centrifugation at 12,000 g for 5 min at 4 °C. The supernatant was transferred to a nuclease-free 1.5 mL microcentrifuge

**Table 2.3 NGS variant validation primers.** Primer sequences used to empirically validate candidate variants identified by NGS and the amplified region of Chr 4 are shown. Data is from Ensembl release 95 (January 2019; Zerbino *et al*. 2018).

| Gene | Primer Set | Forward Sequence (5′→3′) | Reverse Sequence (5′→3′) | Amplified Region of Chr 4 (bp) |
|---|---|---|---|---|
| *Dhrs3* | DHRS3-A | GCAGAGTGGATCCAACAGGT | CACCTTCCCACAGAAAGAGC | 144,895,424-144,896,156 |
| | DHRS3-B | AGGCACCTGCTCACAATCTT | TTGCCACAGCCACATGTAAT | 144,897,879-144,898,149 |
| | DHRS3-C | GCAGGGAGGGAAATTTTAGG | GATGGGCATTCATTTTGTCC | 144,899,365-144,899,755 |
| | DHRS3-D | CTGACATAAGCAGCCTGTGC | AGGCCAGAGGCTTACACTGA | 144,900,147-144,900,777 |
| | DHRS3-E | AGAGGGCAACTTCACCTTCA | GTTTGTGAGCACCAGAAGCA | 144,901,670-144,902,357 |
| | DHRS3-F | TTGCAATAACCCCACAAGGT | GGATAGTCTCCCAGGGAAGG | 144,910,205-144,910,525 |
| | DHRS3-G | TTAGGACCCACTCGTCAAGG | TCTTAAGTGAGCCGGCTGTT | 144,917,175-144,917,602 |
| | DHRS3-H | GCTTTGCATCCATCCAGAAT | GCTGGGTTGACTCAGGAGAG | 144,919,740-144,920,121 |
| *Vps13d* | VPS13D-A | TATGATTTTGGCCTGCACTG | GAGAGAGCTCCCACAACAGG | 145,007,821-145,008,388 |
| | VPS13D-B | ACTGGGCAACTGGGTCATAC | TGCACATGAGGCATCTAAGC | 145,071,422-145,071,873 |
| | VPS13D-C | GGGGTAGCACCATTCACAGT | CATCAGTGCCCTTGGAAATC | 145,166,356-145,166,570 |
| *Tnfrsf1b* | TNFRSF1B | ATAGGCTGCAGAGGCTACCA | TCAGACTCATCCCACCATCA | 145,236,787-145,237,328 |
| *Tnfrsf8* | TNFRSF8 | CACAGATGATGGAGGCTGAA | TCTGATCTGGGCACTGATTG | 145,282,736-145,282,979 |

tube, and a 40 µL aliquot of chloroform (Thermo Fisher Scientific) was added. The tubes were vigorously inverted for 15 s and incubated at RT for 3 min. The tubes were centrifuged at 12,000 g for 15 min at 4 °C to separate the aqueous and organic phases. The clear upper aqueous phase was transferred in 20 µL aliquots to a nuclease-free 1.5 mL microcentrifuge tube. A 50 µL aliquot of isopropanol (BDH Inc., Toronto, ON) was added to the solution, which was mixed by pipetting. The samples were incubated at RT for 10 min, after which they were centrifuged at 12,000 g for 10 min at 4 °C to pellet the RNA. The supernatant was removed and the RNA pellet was washed with two sequential aliquots of 100 µL of 75% ethanol, after which the tubes were centrifuged at 7,500 g for 5 min at 4 °C and the supernatant was removed. The RNA pellets were air-dried for 5 to 10 min and resuspended in 25 µL of nuclease-free water (Applied Biosystems Inc.). The RNA samples were stored at -80 °C until purification and concentration.

Ovary RNA samples were purified and concentrated using an RNeasy® MinElute® Cleanup Kit (Qiagen) and an RNase-Free DNase Set (Qiagen) as per the manufacturer's standard protocols. Briefly, total RNA samples were combined in a nuclease-free 1.5 mL microcentrifuge tube with 10 µL of Buffer RDD and 2.5 µL of DNase I stock solution, and made up to a 100 µL volume with nuclease-free water. The solution was left to incubate for 10 min at RT, after which 350 µL of Buffer RLT and 250 µL of anhydrous ethanol (Bio Basic Inc.) was added. Samples were centrifuged at 8,000 g for 15 s in a filter column in a collection tube. The filter column was placed in a new collection tube, and 500 µL of Buffer RPE was added and the tubes were centrifuged at 8,000 g for 15 s. A 500 µL aliquot of 80% ethanol (Commercial Alcohols) was added to the filter column, and the tubes were centrifuged at 8,000 g for 2 min. The filter column was transferred to a new collection tube, and the tubes were centrifuged at 8,000 g for 5 min with the lid of the filter column open. The filter column was transferred to a nuclease-free 1.5 mL

microcentrifuge tube, and 14 µL of nuclease-free water was pipetted directly onto the center of the filter membrane. The tubes were centrifuged at 8,000 g for 1 min. All centrifugations were conducted at RT. The concentrated RNA samples were stored at -80 °C until assayed for RNA integrity.

*RNA Integrity Assay*

The integrity of all RNA samples was assessed using an Agilent RNA 6000 Nano Kit (Agilent Technologies) and an Agilent 2100 Bioanalyzer (Agilent Technologies) prior to cDNA synthesis as per the manufacturer's standard protocol. Briefly, RNA samples and RNA 6000 Nano Ladder were denatured at 70 °C for 2 min using an Isotemp™ heat block (Thermo Fisher Scientific), after which they were immediately placed on ice. A gel-dye mix was prepared by adding 550 µL of RNA 6000 Nano Gel Matrix to a spin filter, which was centrifuged at 1,500 g for 10 min at RT. A 65 µL aliquot of filtered RNA 6000 Nano Gel Matrix was combined with 1 µL of RNA 6000 Nano Dye Concentrate, and the gel-dye mix was centrifuged at 13,000 g for 10 min at RT. The RNA Nano chip was loaded with 9 µL of gel-dye mix using a chip priming station. Aliquots of 5 µL of RNA 6000 Nano Marker were added to all wells of the RNA Nano chip, and 1 µL of denatured RNA or RNA 6000 Nano Ladder were added to the appropriate wells. The loaded RNA Nano chip was vortexed at 2,400 rpm for 1 min using an MS 3 Shaker (IKA Works Inc., Wilmington, NC) and electrophoresed using the Eukaryote Total RNA Nano program. All RNA samples reverse transcribed to cDNA had an RNA integrity number (RIN) ≥ 9.8.

*cDNA Synthesis*

cDNA was synthesized using a High-Capacity cDNA Reverse Transcription Kit (Applied Biosystems Inc.) as per the manufacturer's standard protocol. Briefly, a 2 µg sample of purified and concentrated total RNA was combined with 2 µL of 10X RT Buffer, 0.8 µL of 100 mM 25X dNTP Mix, 2 µL of 10X RT Random Primers, and 1 µL of MultiScribe™ Reverse Transcriptase in a 0.2 mL nuclease-free PCR tube (Bio-Rad Laboratories). The samples were made up to a 20 µL volume using nuclease-free water and the tubes were placed in a Veriti™ 96-Well Thermal Cycler (Applied Biosystems Inc.) where the samples were reverse transcribed using the following profile: 25 °C for 10 min; 37° for 120 min; 85° for 5 min. cDNA samples were stored at -20 °C until they were tested for integrity by amplification of a 154 bp mouse actin, beta gene (*Actb*) amplicon as per the protocol for SSLP genotyping markers (Section 2.2.2.1), and electrophoresed through a 1.5% agarose gel as per the protocol for SNP genotyping markers (Section 2.2.2.2; forward primer: 5′-GGC TGT ATT CCC CTC CAT CG-3′; reverse primer: 5′-CCA GTT GGT AAC AAT GCC ATG T-3′; Harvard PrimerBank ID: 6671509a1; Wang & Seed 2003; Spandidos *et al*. 2008; Spandidos *et al*. 2010; pga.mgh.harvard.edu/primerbank).

*Polymerase Chain Reaction, Gel Extraction and Cycle Sequencing*

cDNA samples were amplified by PCR as per the protocol for SNP genotyping markers (Sections 2.2.2 and 2.2.2.2). Primer sequences were designed to amplify an amplicon spanning *Dhrs3* exons 3 and 5 using cDNA template (Figure 2.6). Primer sequences are shown in Table 2.4.

Amplified PCR products were electrophoresed through a 1% low melting-point agarose

**Table 2.4 *Dhrs3* RT-PCR primers.** Primer sequences used to amplify *Dhrs3* exons 3 to 5 by PCR, their nucleotide ranges, and potential amplicon lengths are shown. Nucleotide ranges are relative to *Dhrs3* cDNA bp 1.

| Nucleotide Range | Forward Sequence (5′→3′) | Reverse Sequence (5′→3′) | Amplicon (bp) | |
|---|---|---|---|---|
| | | | Exons 3-4-5 | Exons 3-5 |
| 342 – 767 | GGGTGACATCACCATCCTGG | TGTTGCACAGCATCTACCGT | 426 | 187 |

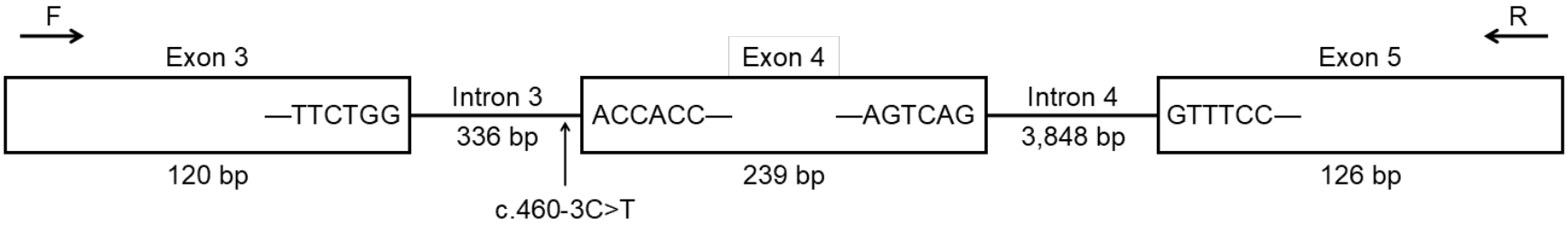


**Figure 2.6 *Dhrs3* RT-PCT primer design**

Schematic illustrating *Dhrs3* gene structure, the position of a variant at the *Dhrs3* intron 3-exon 4 3′ acceptor splice site (c.460-3C>T) prioritized for investigation, and the location of primers used to amplify cDNA by RT-PCR. Image is not to scale. Boxes: exons; lines: introns.

(Sigma-Aldrich Inc.) gel as per the protocol for SNP genotyping markers (Section 2.2.2.2). Bands were excised and purified using a QIAquick® Gel Extraction Kit (Qiagen) as per the manufacturer's standard protocol. Briefly, all gel bands were excised from the agarose gel, weighed, and combined with three volumes of Buffer QG. The samples were incubated in an Isotemp™ heat block (Thermo Fisher Scientific) at 50 °C for 10 min with intermittent vortexing. An aliquot of 10 µL of 3 M sodium acetate (Sigma-Aldrich Inc.) was added to the samples, followed by one volume of isopropanol (BDH Inc.). The samples were transferred to a QIAquick spin column in a 2 mL collection tube and centrifuged at 10,000 g for 1 min. The flow-through was discarded and 500 µL of Buffer QG was added to the samples. After centrifugation at 10,000 g for 1 min, the flow-through was discarded and 750 µL of Buffer PE was added to the QIAquick column. After two sequential centrifugations at 10,000 g for 1 min, the QIAquick column was transferred to a 1.5 mL microcentrifuge tube and 30 µL of elution buffer was pipetted directly onto the filter membrane. The tubes were incubated for 1 min at RT, after which they were centrifuged at 10,000 g for 1 min to elute the PCR products. Gel-excised and purified PCR products were stored at -20 °C until Sanger sequencing.

Gel-excised and purified PCR amplicons were Sanger sequenced and analyzed as per the protocol for SNP genotyping markers (Section 2.2.2.2), and the amplified nucleotide sequences were examined for target transcript specificity using NCBI Standard Nucleotide BLAST (Altschul *et al*. 1990; blast.ncbi.nlm.nih.gov/Blast.cgi).

### 2.2.4 Copy Number Variation Analysis

An array comparative genomic hybridization (aCGH) analysis was conducted to identify all CNVs within the resolved *Gct1* interval unique to SWR in comparison to the GC tumour-

resistant subcongenic Line 4-5. SWR and Line 4-5 mice were implanted with exogenous DHEA at puberty (Section 2.2.1.3) and necropsied for GC tumour observation and kidney collection at 8 wk of age (Section 2.2.1.4). gDNA was isolated by salt extraction from kidneys (Section 2.2.2.2) of SWR GC tumour hosts and unaffected Line 4-5 individuals (n = 4/group). All gDNA samples had a 260/280 ratio of at least 1.87 as determined using a NanoDrop™ 1000 Spectrophotometer (Thermo Fisher Scientific), and were assessed for integrity and molecular weight by electrophoresis through a 0.8% agarose gel (Section 2.2.2.2) with GeneRuler™ 1 kb Plus DNA Ladder marker (Thermo Fisher Scientific). gDNA samples (1.5-2.5 µg) were labelled with cyanine (Cy)-3 (green; reference samples; Line 4-5) or Cy-5 (red; experimental samples; SWR) prior to hybridization to a custom Agilent Mouse aCGH 4x180K Array (Agilent Technologies) in an Agilent DNA Microarray Hybridization Oven (Agilent Technologies). The experimental and reference samples were hybridized as four pairwise comparisons of unique and individual SWR and Line 4-5 samples. The four identical arrays were designed using the NCBI Build m37 assembly as the reference genome, with 174,901 unique 60 bp oligonucleotide probes and masked simple repeat regions. The *Gct1* interval was covered with 6,923 probes offset by 150 bp across a generous 2.1 Mb interval centered across the locus. The entirety of Chr 4 was also covered with 153,492 probes offset by approximately 1 kilobase (kb). The remaining probes were devoted to internal quality control features (6,563), normalization features (2,923), and biological replication features (5,000). Following hybridization, the four arrays were scanned on an Agilent DNA Microarray Scanner (Agilent Technologies) to create four TIFF files, which were converted to TXT files of aCGH data and analyzed for quality control and evaluation metrics using Agilent Feature Extraction Software version 12.0 (Agilent Technologies). aCGH data was analyzed against the NCBI Build m37 genome assembly using imported array design

files and Agilent Genomic Workbench Software version 7.0 (Agilent Technologies). Legacy centralization, which normalizes the log ratios of the most common ploidy state to zero, was applied with a stringency threshold of 10.0. The Aberration Detection Method (ADM)-2 algorithm was used to correct for aberrant intervals, with a stringency threshold of 10.0. Fuzzy zero, which applies a global error model to all aberrant intervals identified by ADM-2 analysis, was applied. CNV coordinates were converted from the NCBI Build m37 genome assembly to GRCm38 coordinates using the Ensembl Assembly Converter. CNVs were compared to structural variants annotated in the Database of Genomic Variants archive (DGVa; Lappalainen *et al*. 2013; ebi.ac.uk/dgva) following their extraction from the Ensembl Variation 94 Mouse Structural Variants dataset using Ensembl BioMart (Kinsella *et al*. 2011; ensembl.org/biomart/martview), and were assessed using the Ensembl VEP to determine their predicted impact. aCGH hybridization and scanning were performed at Genome Quebec, whereas sample preparation and data analysis (Appendix A) were performed at MUN. An illustration of the aCGH experimental outline is shown in Figure 2.7.

### 2.2.5 Functional Analyses

#### 2.2.5.1 Tumour Necrosis Factor Functional Analysis

*Tumour Necrosis Factor Administration*

A 10 µg/kg/d dose of recombinant mouse TNF (amino acids 80-235 of 235 total; 410-MT/CF; R&D Systems® Inc., Minneapolis, MN) was administered to pubertal SWR or Line 4-5 mice using 14 d release micro-osmotic pumps (0.25 µL/h; model 1002; Alzet® Osmotic Pumps,

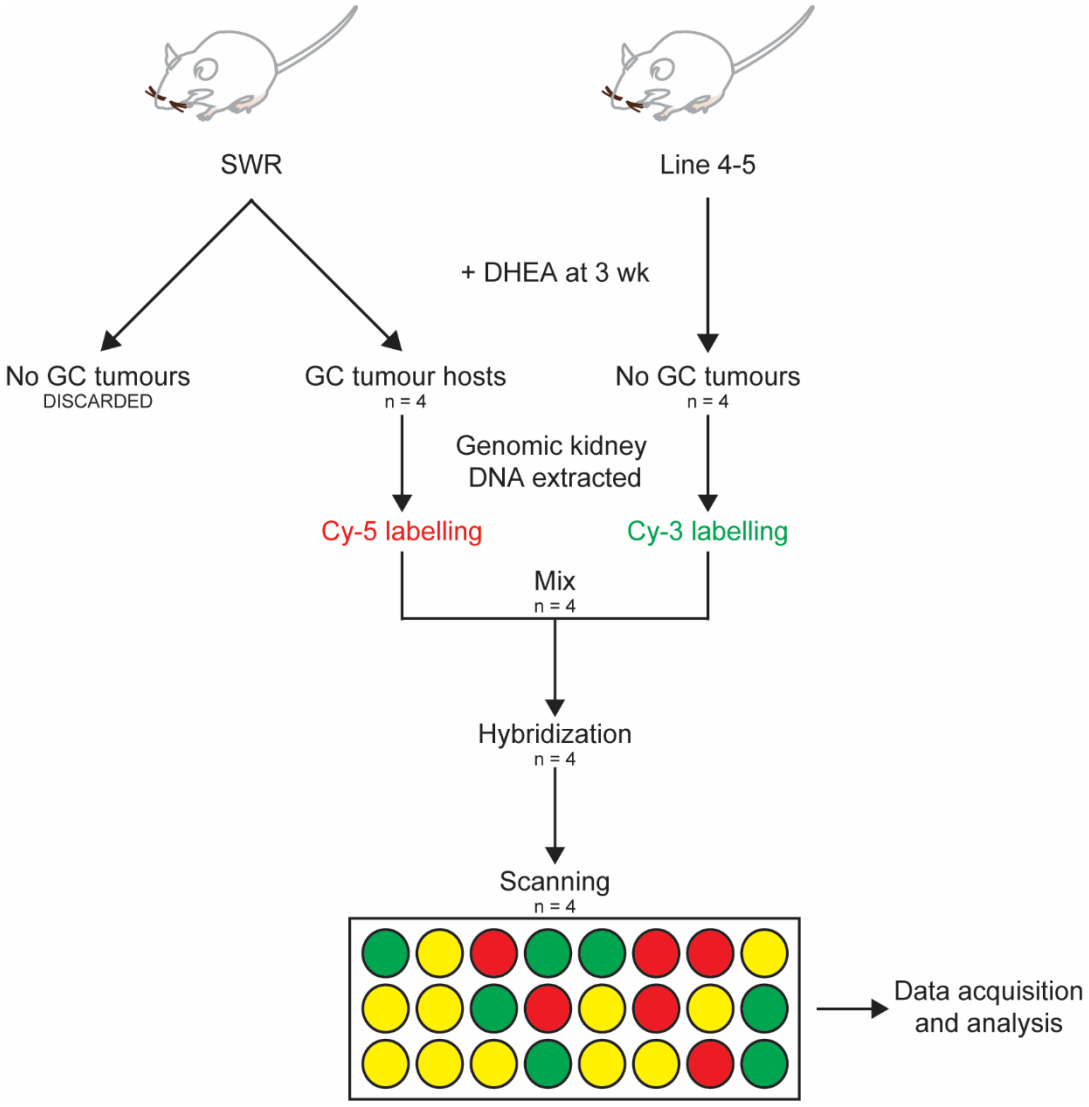


**Figure 2.7 aCGH experimental outline**

SWR and Line 4-5 females were administered DHEA at 3 wk of age. After 5 wk of treatment, gDNA was extracted from the kidneys of four SWR GC tumour hosts and four Line 4-5 females, labelled with Cy-5 or Cy-3, respectively, and hybridized as four pairwise comparisons of unique and individual SWR and Line 4-5 samples. The four arrays were scanned and data was acquired and analyzed, which included conversion of coordinates to the GRCm38 genome assembly, comparison to structural variants annotated in the DGVa, and assessment using the Ensembl VEP.

Cupertino, CA). The TNF dosing scheme was established based on the literature (Wahl *et al*. 2010a; Wahl *et al*. 2010b). The pumps were filled according to the manufacturer's protocol with either sterile saline (0.9% NaCl w/v; Kimberly-Clark, Irving, TX) or with TNF in saline under sterile conditions in a biological safety cabinet. Osmotic pumps were subcutaneously implanted in the scapular region under isoflurane anesthesia with a DHEA-filled or empty capsule as per Section 2.2.1.3.

*Serum Collection*

A subset of saline- and TNF-treated SWR females were decapitated using scissors after 8 d of treatment, and approximately 1 mL of trunk blood was collected in a 1.5 mL microcentrifuge tube. The blood samples were left on ice for 2 h to permit clotting, after which they were centrifuged at 15,000 g for 10 min. The clear upper serum phase was transferred in 100 µL aliquots to a 0.6 mL microcentrifuge tube (Thermo Fisher Scientific) and stored at -20 °C until assayed.

*Enzyme-Linked Immunosorbent Assay*

Serum TNF concentrations were assessed using a Mouse TNFα Quantikine Enzyme-Linked Immunosorbent Assay (ELISA; MTA00B; R&D Systems® Inc.). Briefly, 50 µL of Assay Diluent RD1-63 was added to each well of a 96 well Mouse TNFα Microplate. A 50 µL aliquot of Mouse TNFα Standards, Mouse TNFα Kit Control, or serum sample was added to each well and the plate was mixed gently by tapping the frame for 1 min. The plate was covered with an adhesive plate sealer and incubated for 2 h at RT, after which each well was aspirated using a

pipette and washed five times with 400 µL of Wash Buffer using a squirt bottle. The plate was inverted and blotted against clean paper towels, and 100 µL of Mouse TNFα Conjugate was added to each well. The plate was covered with an adhesive plate sealer and incubated for 2 h at RT, after which each well was aspirated and washed as per the previous step. A 100 µL aliquot of Substrate Solution was added to each well and the plate was incubated for 30 min at RT in the dark, after which 100 µL of Stop Solution was added to each well. The plate was gently tapped to ensure thorough mixing, and the plate was read within 30 min using a POLARStar OPTIMA Plate Reader (BMG LABTECH Inc., Cary, NC) at an absorbance of 450 nm. The Mouse TNFα Standards were produced by adding 900 µL of Calibrator Diluent RD6-12 to a 7,000 pg/mL stock solution of Mouse TNFα Standard. A dilution series was produced using the Calibrator Diluent RD6-12 and the stock solution, and consisted of 700, 350, 175, 84.5, 43.8, 21.9, and 10.9 pg/mL solutions. The zero standard (0 pg/mL) consisted of Calibrator Diluent RD6-12 only. All standards, samples, and the Mouse TNFα Kit Control were assayed in duplicate. The duplicate readings for each standard, control, and sample were averaged, and the average optical density of the zero standard was subtracted. A standard curve was constructed by plotting the log of the mean absorbance for each standard on the y-axis against the log of their concentrations on the x-axis in Microsoft Excel version 15.0.5075.1000 (Microsoft Corporation, Redmond, WA). Experimental sample concentrations were extrapolated from the graph.

#### 2.2.5.2 All-*Trans*-Retinaldehyde Functional Analysis

Three doses of 50 mg/kg RAL (R2500; Sigma-Aldrich Inc.) were administered to pubertal SWR or Line 4-5 mice. The RAL dosing scheme was established based on the literature (Felipe *et al*. 2004; Mercader *et al*. 2008). RAL was dissolved in 95% ethanol (Commercial

Alcohols), and 50 µL was administered subcutaneously in the flank region under isoflurane anesthesia. RAL injections were administered every second day over the course of six days. A DHEA-filled or empty capsule was subcutaneously implanted in the scapular region at the time of the first injection, as per Section 2.2.1.3. Control animals were administered an equal volume of vehicle, with a DHEA-filled capsule. Mice were necropsied as per Section 2.2.1.4.

#### 2.2.5.3 All-*Trans*-Retinoic Acid Functional Analysis

RA was administered to pubertal SWR mice using 5 mg RA 21 d release pellets (V-111; Innovative Research of America, Sarasota, FL). The RA dosing scheme was established based on the literature (Mariotti *et al*. 1987; Kogan *et al*. 2000; Minucci *et al*. 2002; Knaul *et al*. 2014). The pellets were subcutaneously implanted in the scapular region under isoflurane anesthesia with a DHEA-filled or empty capsule as per Section 2.2.1.3. Control mice were implanted with a DHEA-filled or empty capsule only. Mice were necropsied as per Section 2.2.1.4.

### 2.2.6 Statistical Analysis

The quality metrics of annotated and novel NGS variants were compared by unpaired two-tailed *t*-test, GC tumour frequencies were compared by two-tailed Fisher's exact test, and body weight and organ weight relative to body weight were compared by one-way analysis of variance (ANOVA) followed by Tukey's test (*p*-values adjusted for multiple comparisons) using GraphPad Prism version 6.07 for Windows (GraphPad Software, San Diego, CA). $p < 0.05$ was considered statistically significant. NGS quality metric and weight data is presented as mean ± standard error of the mean (SEM).

## 2.3. Results

### 2.3.1 Refining the Genetic Boundaries of *Gct1*

We sought to resolve the *Gct1* interval at the proximal boundary and as such exclude potential candidate genes. This required the identification of polymorphisms between the CAST genome and the SWR genome, recognizing that the SWR strain has not yet been re-sequenced and made publicly available. SNP-based genotyping markers were designed to amplify a single amplicon encompassing an annotated SNP with a predicted single nucleotide difference between SWR and CAST based on the known genotypes of strains phylogenetically related to SWR. These annotated SNPs were empirically tested for polymorphic base changes between CAST and SWR by Sanger sequencing. Two SNPs were identified within two markers designed to amplify single nucleotide changes in genetic segments at the proximal interval boundary in SWR and Line 4-T and 4-3 recombinant subcongenic lines (Table 2.5). The addition of *rs27597210* to the Chr 4 haplotype map resulted in a refined *Gct1* interval of 1.71 Mb, whereas the addition of *rs27633106* further refined *Gct1* to 1.65 Mb (Figure 2.8).

Line 4-5 mice were mated with SWR mice to produce $F_1$ heterozygotes at *Gct1*, which were backcrossed to SWR to produce $N_2F_1$ generation mice in an attempt to produce unique and informative SWR.SJL-X.CAST-4 recombinant subcongenic lines. This process produced 188 $N_2F_1$ males and females, which were haplotyped at informative SSLP (*D4sjh10*, *D4Mit232*, and *D4Mit233*) and SNP (*rs27597210*, *rs27633106*, and *rs32447066* and *rs33013120* upstream of the 3′ UTR of *Dhrs3*) markers across *Gct1*. One animal (female 22913) displayed a recombination of the SWR- and CAST-derived genomes at the proximal end of the *Gct1* interval. This haplotype shared the same distal boundary as Line 4-5 (*D4kns1*), but was defined by *rs27633106* proximally (Figure 2.9). Although this recombination pattern was unique and had

**Table 2.5 SSLP and SNP genotyping markers.** Primer sequences used to amplify SSLPs and SNPs for genotypic mapping of *Gct1* by PCR, their genomic location on Chr 4, and relative SSLP allele sizes are shown. Data is from Ensembl release 95 (January 2019; Zerbino *et al*. 2018). Relative SSLP sizes were determined from horizontal agarose gel electrophoresis. Entries in bold were empirically derived in-house.

| Marker Symbol | Forward Sequence (5′→3′) | Reverse Sequence (5′→3′) | Start of Amplified Region (bp) | Assay Type | Relative SSLP Allele Size |
|---|---|---|---|---|---|
| *D4sjh10* | GCAGAAATGGCACAGGAGAT | CCCACATTTGAAACCACCTC | 144,618,919 | SSLP | CA > SW |
| ***rs27597210*** | **GAAATACCAGGGGTGTGCAT** | **TAGGCATTGTGAGCCAGTTG** | **144,765,692** | **SNP** | **n/a** |
| ***rs27633106*** | **CAGTGGCCAGTTTTGGTTCT** | **CAGAGGCCAGGACTTTATGC** | **144,824,022** | **SNP** | **n/a** |
| *Dhrs3* | ACATCTGGTTGTGGGAGACGGAAA | AGCCAGAGATGCTTAGGTCTGTGT | 144,928,064 | SNP | n/a |
| *D4Mit232* | GCGTCACCACACTGCTCTT | ACTCAGAGTCCCCTGGCC | 145,057,656 | SSLP | CA > SW |
| *D4Mit233* | TGGTCATGTGTGTCCATGC | ACTTCATGTAGCCAGGTGGG | 145,224,944 | SSLP | CA > SW |

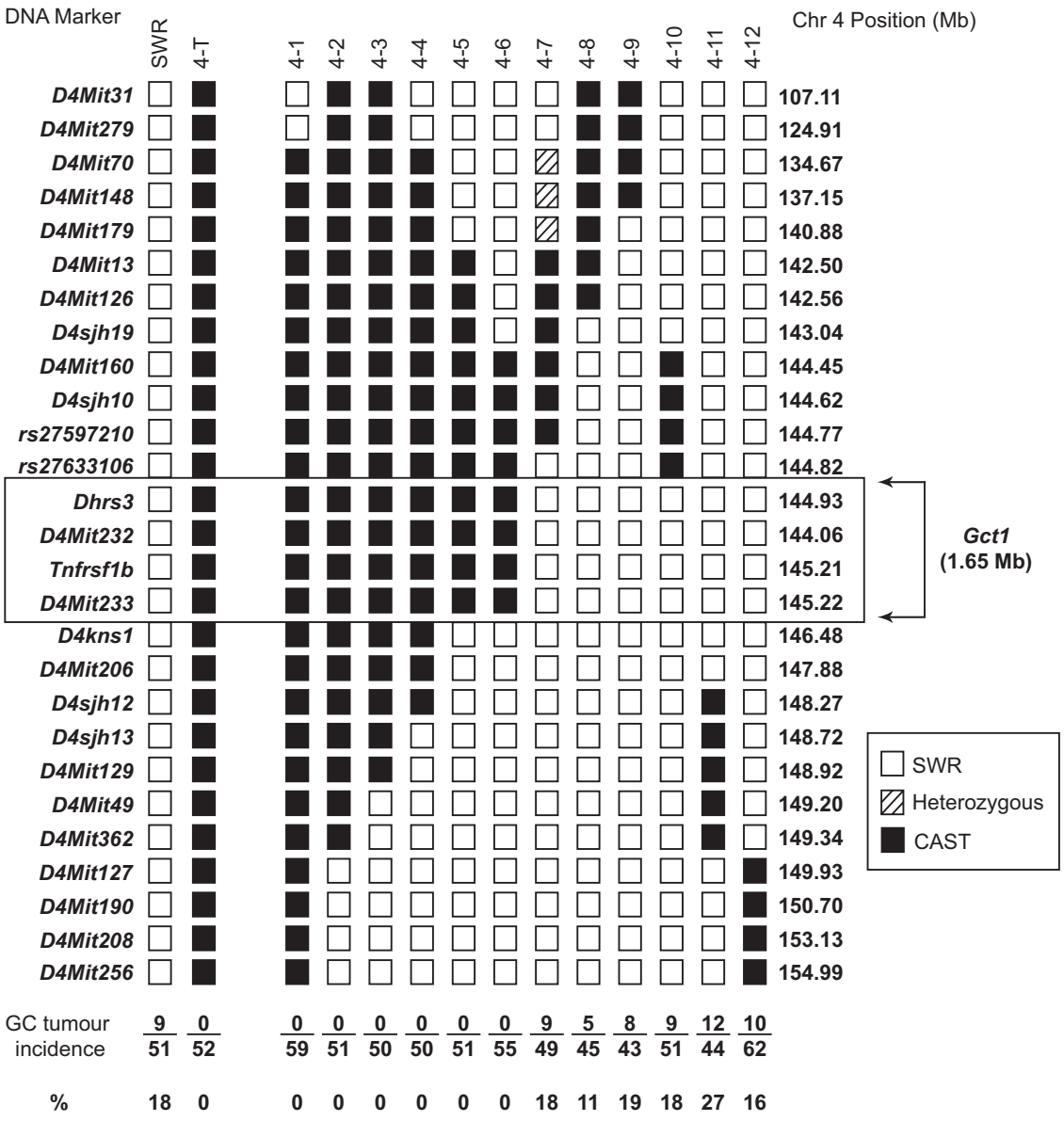


**Figure 2.8 Chr 4 haplotypes of SWR and Line 4-T and 4-3 subcongenic mouse lines at *Gct1* following fine mapping with SNP-based genotyping markers**

Line 4-T and the GC tumour susceptible subcongenic lines share common regions of SWR genetic background between markers *rs27633106* and *D4kns1*, placing *Gct1* within a minimal genetic segment of approximately 1.65 Mb. All markers were published previously with the exception of *rs27597210* and *rs27633106*. Reprinted in adapted form from Smith *et al*. 2013.

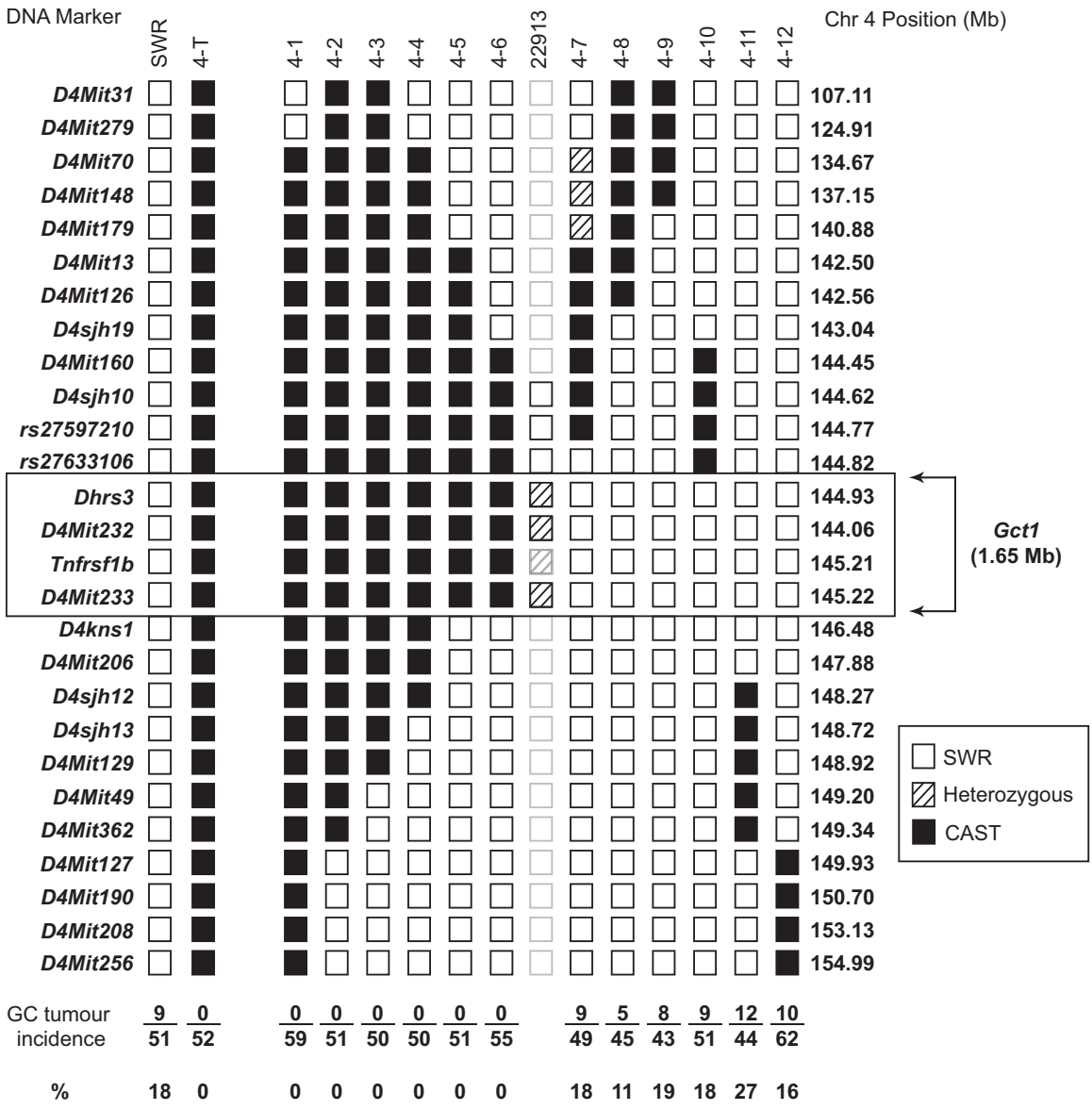


**Figure 2.9 Chr 4 haplotypes of SWR and Line 4-T and 4-3 subcongenic mouse lines at *Gct1*, showing a novel $N_2F_1$ recombinant haplotype**

The $N_2F_1$ recombinant mouse 22913 has SWR alleles at *D4sjh10*, *rs27597210* and *rs27633106*, and was heterozygous for SWR and CAST alleles at *Dhrs3*, *D4Mit232* and *D4Mit233*. All other genotypes for this mouse at Chr 4 markers are inferred (opaque boxes). Although unique among all previously generated subcongenic lines, this haplotype was ultimately uninformative. Reprinted in adapted form from Smith *et al*. 2013.

not been generated previously, it was uninformative and so was not brought to homozygosity for testing of DHEA-induced GC tumour incidence.

### 2.3.2 The Refined *Gct1* Interval

The 1.65 Mb *Gct1* interval contains 48 unique genetic determinants, including 11 protein coding genes, six non-coding transcripts (one processed transcript, one antisense, and four long non-coding RNA genes), one manually annotated expressed sequence tag (EST) that requires experimental confirmation, and 30 pseudogenes (Figure 2.10). The majority of the genetic entities in *Gct1* are located at the highly repetitive, pseudogene-rich distal end of the interval. Table 2.6 summarizes the features of the 18 genes which we hypothesize includes a genetic determinant that is causative for GC tumourigenesis. Only four of the 17 protein coding and non-coding genes – *Dhrs3*, *Vps13d*, *Tnfrsf1b* and *Tnfrsf8* – have been described in the literature with defined roles in human or mouse.

The strategies to identify *Gct1* to date succeeded in refining the *Gct1* interval to 1.65 Mb through phenotypic mapping using recombinant subcongenic lines, as well as fine mapping using empirically genotyped SNPs that differed between SWR and CAST. This is likely the smallest interval that is able to be produced using these methods, given our inability to generate new unique and informative recombinants across *Gct1* and the complexity and repetitiveness of the distal *Gct1* region. Therefore, our ensuing strategy was to completely annotate the 1.65 Mb *Gct1* interval using NGS and aCGH analyses, to find nucleotide and copy number variants that may be causative of GC tumourigenesis in SWR mice, and to interrogate prioritized candidate genes by administering exogenous ligand or substrate/inducer to pubertal SWR female mice.

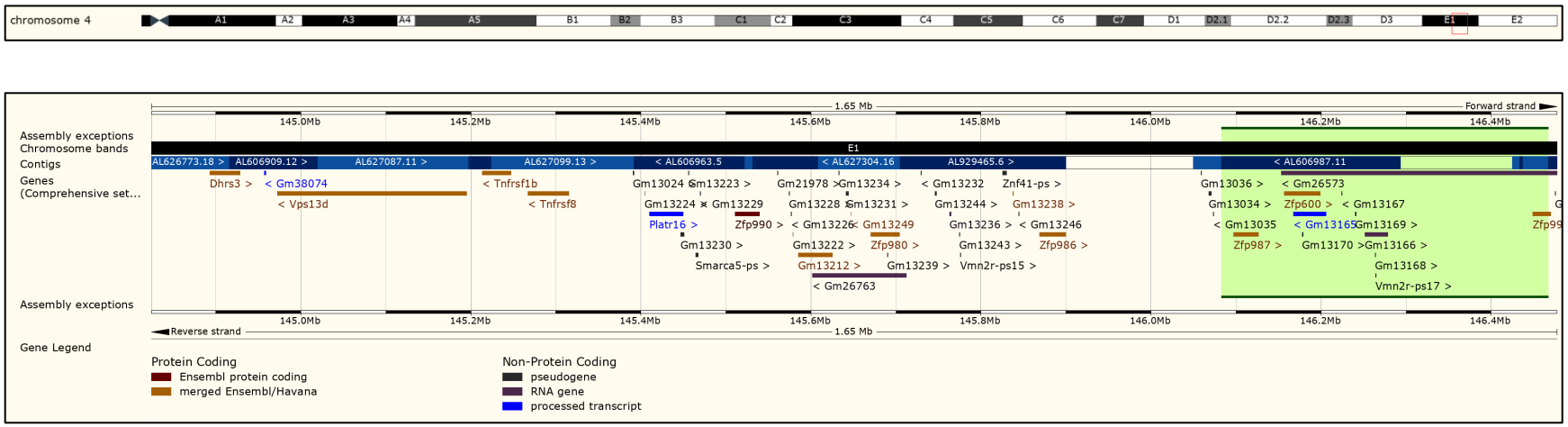


**Figure 2.10 Ensembl screenshot of the 1.65 Mb *Gct1* interval**

Top: mouse Chr 4 with the *Gct1* interval outlined in red. Bottom: the *Gct1* interval. All genetic determinants within the 1.65 Mb *Gct1* interval are shown, including protein and non-protein coding genes. Two genome assembly gaps are denoted as open spaces within the contigs track. An assembly exception in the distal region of the interval is shaded green. Images from Ensembl release 95 (January 2019; Zerbino *et al*. 2018).

**Table 2.6 Summary of the genetic determinants within the 1.65 Mb *Gct1* interval.** Gene name, location on Chr 4, strand, gene type, and the number of unique transcripts per gene are shown. Data is from Ensembl release 95 (January 2019; Zerbino *et al*. 2018). AS: antisense; LR: long intergenic non-coding RNA; PC: protein coding; PT: processed transcript; TEC: manually annotated expressed sequence tag, to be experimentally confirmed; +: forward; -: reverse

| Gene | Official Name | Location on Chr 4 (bp) | Strand | Gene Type | Unique Transcripts |
|---|---|---|---|---|---|
| *Dhrs3* | dehydrogenase/reductase (SDR family) member 3 | 144,892,827 | + | PC | 7 |
| *Gm38074* | predicted gene, 38074 | 144,957,155 | - | TEC | 1 |
| *Vps13d* | vacuolar protein sorting 13D | 144,972,622 | - | PC | 10 |
| *Tnfrsf1b* | tumor necrosis factor receptor superfamily member 1b | 145,213,463 | - | PC | 2 |
| *Tnfrsf8* | tumor necrosis factor receptor superfamily member 8 | 145,267,137 | - | PC | 2 |
| *Platr16* | pluripotency associated transcript 16 | 145,410,245 | + | PT | 2 |
| *Zfp990* | zinc finger protein 990 | 145,510,759 | + | PC | 4 |
| *Gm13212* | predicted gene 13212 | 145,585,166 | + | PC | 3 |
| *Gm26763* | predicted gene, 26763 | 145,601,963 | - | LR | 1 |
| *Zfp980* | zinc finger protein 980 | 145,670,685 | + | PC | 2 |
| *Gm13236* | predicted gene 13236 | 145,762,929 | + | LR | 1 |
| *Zfp986* | zinc finger protein 986 | 145,868,794 | + | PC | 2 |
| *Zfp987* | zinc finger protein 987 | 146,097,298 | + | PC | 3 |
| *Gm26573* | predicted gene, 26573 | 146,153,456 | - | LR | 1 |
| *Zfp600* | zinc finger protein 600 | 146,156,824 | + | PC | 4 |
| *Gm13165* | predicted gene 13165 | 146,167,522 | - | AS | 2 |
| *Gm13166* | predicted gene 13166 | 146,251,829 | + | LR | 5 |
| *Zpf992* | zinc finger protein 992 | 146,449,023 | + | PC | 1 |

#### 2.3.2.1 Next-Generation Sequencing Data

Targeted capture of the entire *Gct1* locus was successfully achieved using gDNA from three mouse lines with homozygous SWR alleles at *Gct1*. NGS of the targeted region was accomplished in all three samples, with an average read depth of 55.3X across all identified variants. The average genotype, mapping, and consensus quality scores were 110.8, 42.6, and -46.2, respectively, whereas the average AF1 was 0.833. A total of 22,362 SNVs and small nucleotide insertions and deletions were identified in the three samples prior to data filtering (Figure 2.11). When duplicates within multiple samples were removed, 9,121 unique variants remained. The sequence quality was highest for the non-repetitive, proximal region of the *Gct1* interval, while the repetitive distal region was not cleanly reassembled (Figures 2.12 and 2.13).

The 9,121 unique variants were categorized as either annotated (previously identified in other mouse strains and present within dbSNP build 151 and/or the WSI Mouse Genomes Project release 1505), or novel (unannotated in either source). A total of 8,172 and 949 variants were classified within the annotated and novel categories, respectively (Figure 2.11). The proportion of each variant category across the *Gct1* interval is shown in Figure 2.14. When data from all three samples was assessed, novel variants had significantly lower average genotype (novel: 57.16 ± 1.442; annotated: 115.3 ± 0.5197) and mapping quality (novel: 32.62 ± 0.3498; annotated: 43.47 ± 0.1014) scores than annotated variants ($p < 0.0001$) when compared by *t*-test (Figure 2.15). Novel variants also had a significantly lower average AF1 (novel: 0.6448 ± 0.0054; annotated: 0.8488 ± 0.0016), and a positive average consensus quality score that was significantly higher from that in annotated variants (novel: 17.21 ± 1.892; annotated: -51.55 ± 0.7312) when compared by *t*-test ($p < 0.0001$). The lower average AF1 and positive consensus quality scores indicate the novel variants trended towards heterozygosity. Average read depth

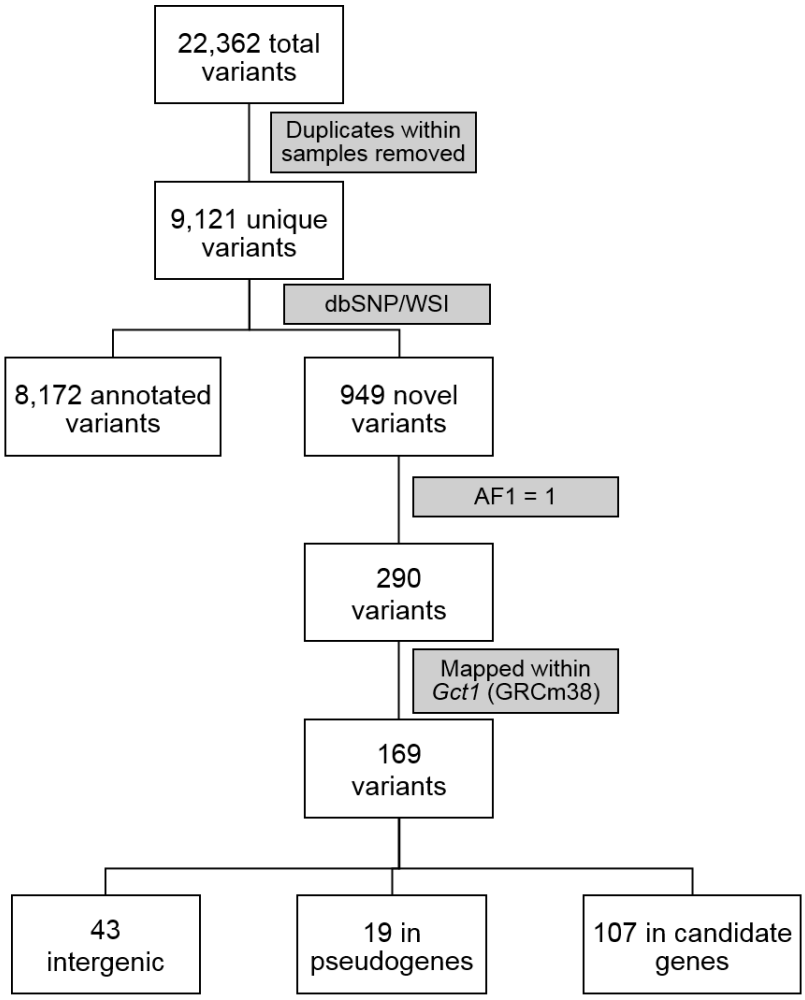


**Figure 2.11 NGS data filtering flowchart**

A total of 22,362 variants were detected across three samples with *Gct1*$^{SW}$ alleles. Following the removal of duplicate variants between samples, the 9,121 remaining unique variants were filtered against annotated variants in dbSNP build 151 and the WSI Mouse Genomes Project release 1505. The 949 novel variants were filtered by AF1, and the coordinates of the 290 variants with AF1 = 1 were converted to GRCm38 coordinates. Of the 169 remaining *Gct1* variants, 43 were intergenic, 19 were in pseudogenes, and 107 were in or within 5,000 bp of candidate genes.

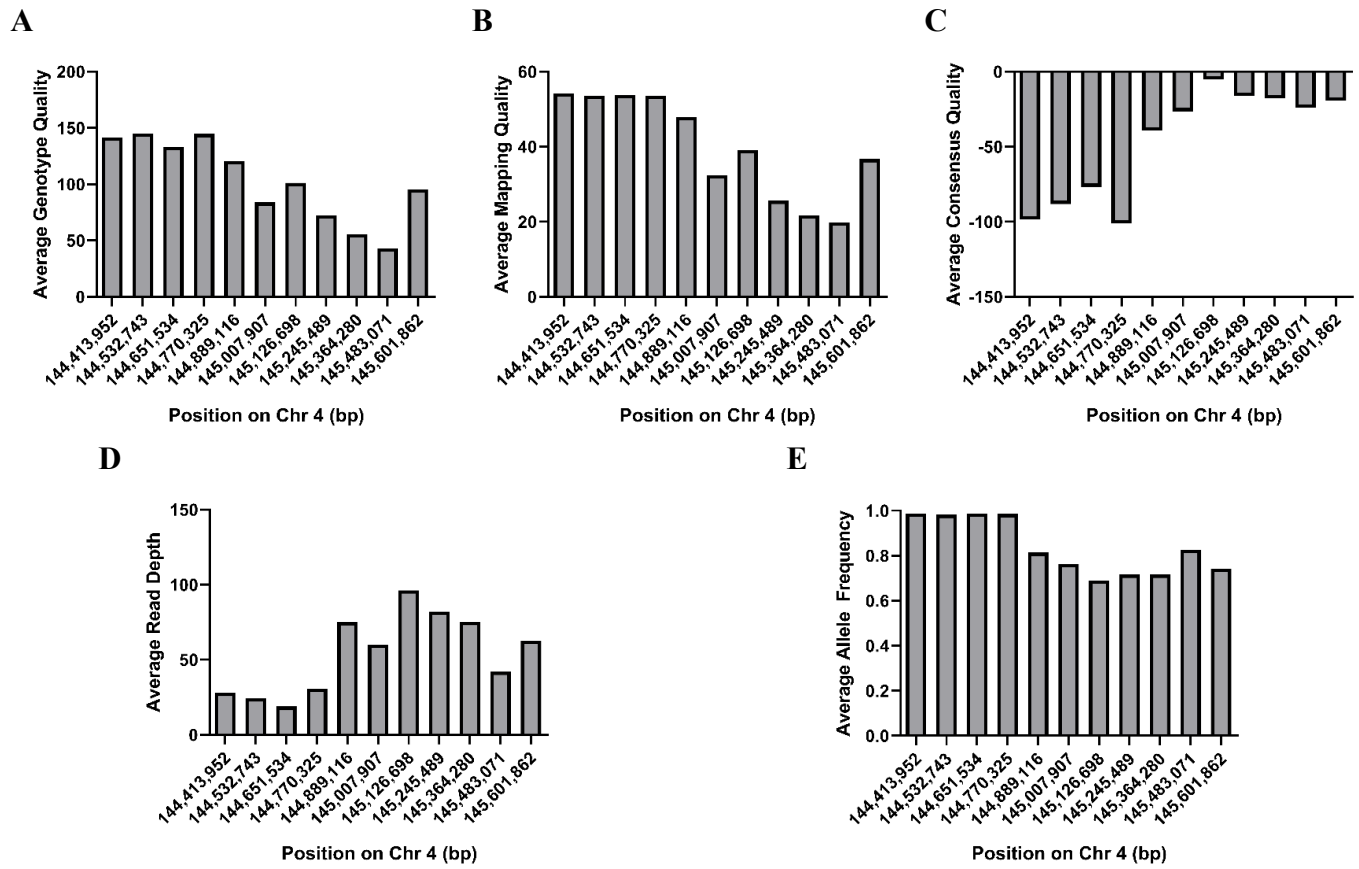


**Figure 2.12 Distribution of NGS data quality, read depth, and AF1 across the 1.65 Mb *Gct1* interval**

The mapped *Gct1* interval was divided into 11 equal bins of 118,791 bp each and the average genotype quality (A), mapping quality (B), consensus quality (C), read depth (D), and AF1 (E) per bin at all variants and across all samples were represented as frequency distributions. Base pair numbering on the X-axis represents the starting nucleotide of each bin. Coordinates are from the NCBI Build m37 mouse reference genome assembly.

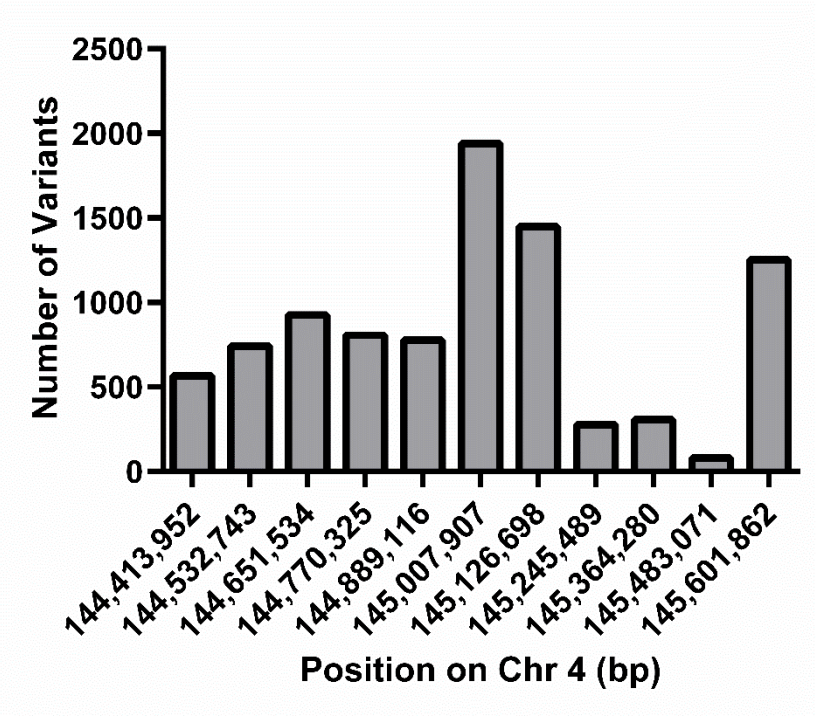


**Figure 2.13 Distribution of variants identified by NGS across the 1.65 Mb *Gct1* interval**

The mapped *Gct1* interval was divided into 11 equal bins of 118,791 bp each and the number of unique variants per bin (minus duplicates between samples) was represented as a frequency distribution. Base pair numbering on the X-axis represents the starting nucleotide of each bin. Coordinates are from the NCBI Build m37 mouse reference genome assembly.

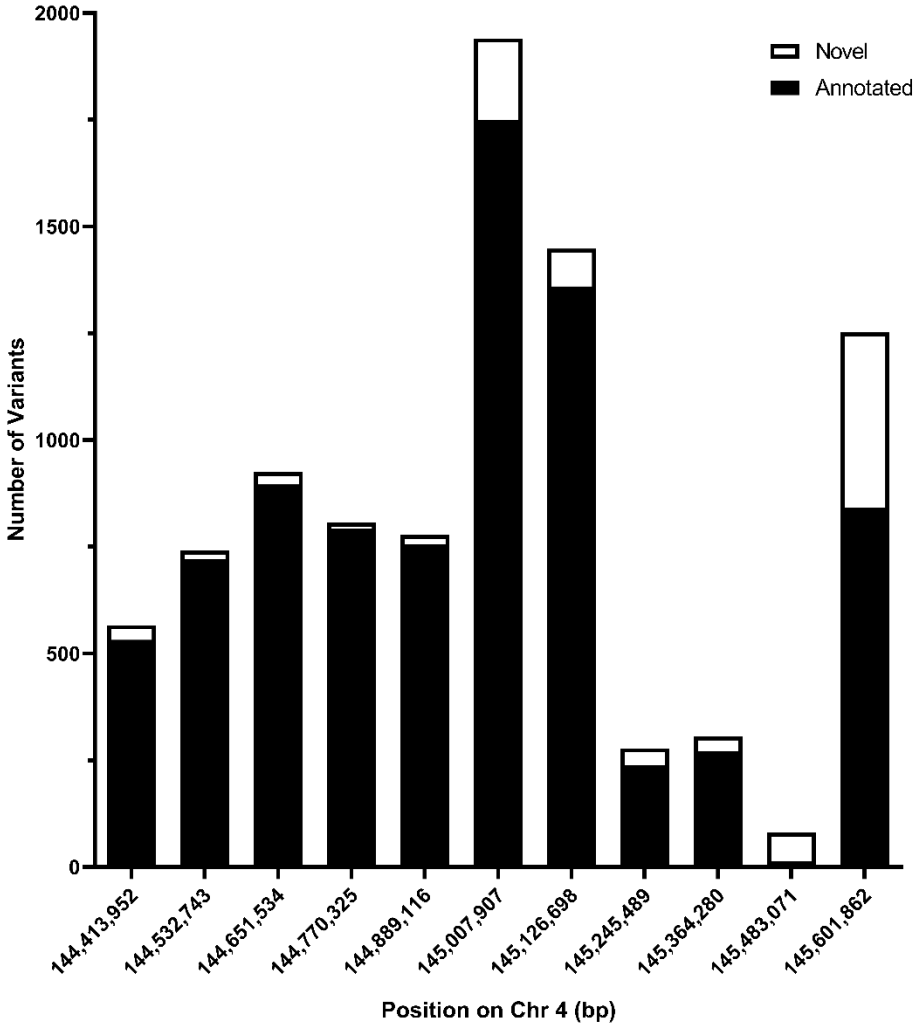


**Figure 2.14 Distribution of annotated and novel variants identified by NGS across the 1.65 Mb *Gct1* interval**

The mapped *Gct1* interval was divided into 11 equal bins of 118,791 bp each and the proportion of annotated and novel variants per bin was represented as a frequency distribution. Base pair numbering on the X-axis represents the starting nucleotide of each bin. Coordinates are from the NCBI Build m37 mouse reference genome assembly.

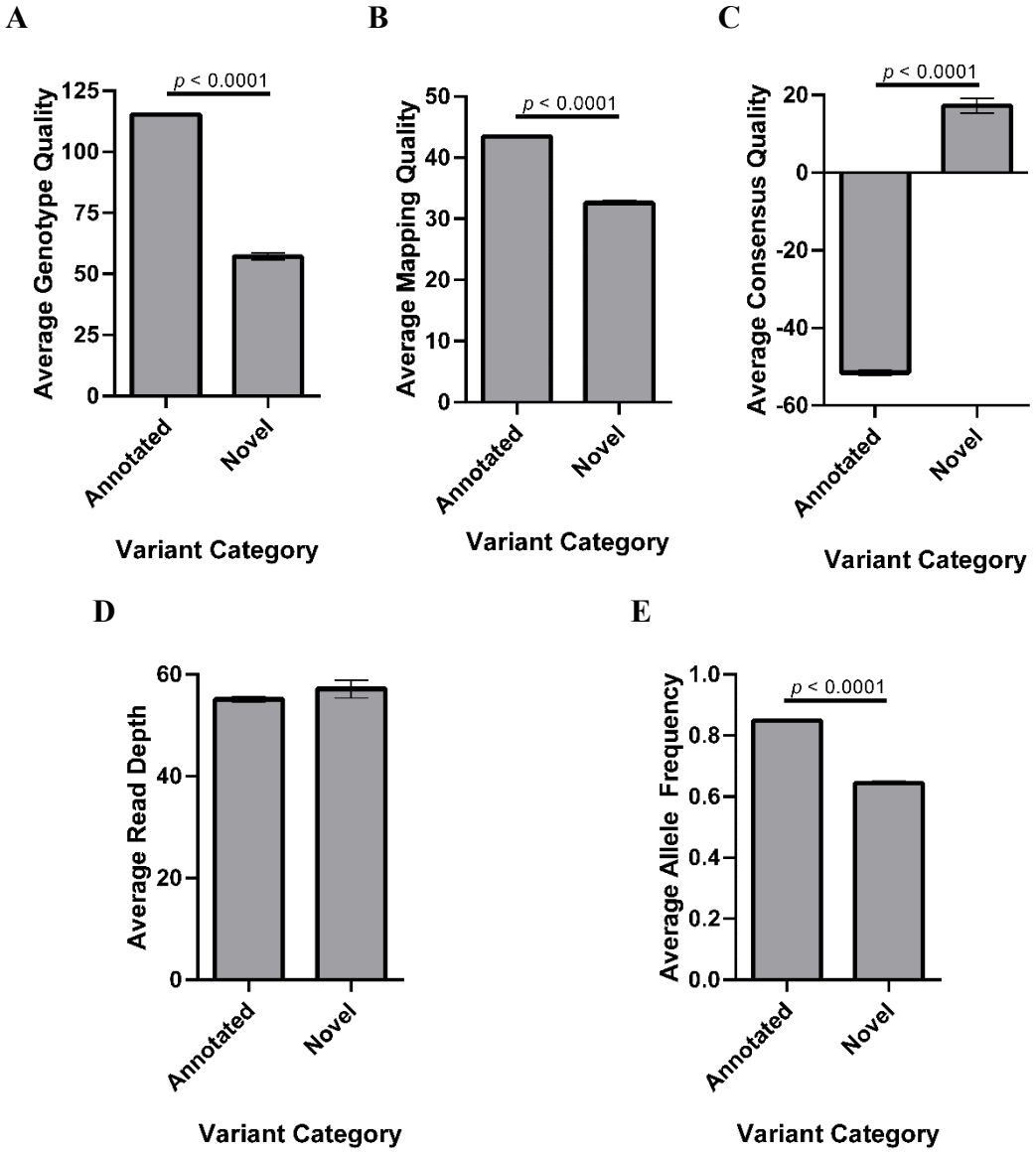


**Figure 2.15 NGS data quality, read depth, and AF1 by variant category**

Variants were categorized as annotated or novel and the average genotype quality (A), mapping quality (B), consensus quality (C), read depth (D), and AF1 (E) per category were represented as frequency distributions. Base pair numbering on the X-axis represents the starting nucleotide of each bin. Coordinates are from the NCBI Build m37 mouse reference genome assembly. Data is presented as mean ± SEM.

was not significantly different between the two categories (novel: 57.16X ± 1.781X; annotated: 55.14 X ± 0.5547X) when compared by *t*-test ($p = 0.3082$). Novel variants were filtered by AF1 such that homozygous variants (AF1 = 1) were included and variants called as heterozygous (AF1 < 1) were excluded. Of the 949 novel variants, only 290 remained when filtered for AF1. A total of 121 of these 290 variants mapped to coordinates annotated outside the *Gct1* interval following conversion to the GRCm38 genome assembly (Figure 2.11). All 169 variants within *Gct1*, including 123 SNVs and 46 small insertions and deletions, were assessed using the Ensembl VEP. Of the 169 *Gct1* variants, 43 did not overlap with any annotated transcripts and were classified as intergenic (i.e. ≥ 5,000 bp upstream or downstream of a gene). A total of 107 of the remaining 126 variants were located near (i.e. within 5,000 bp) or within one or more candidate gene transcripts; the remainder (19) were located within and around pseudogenes. None of the 107 candidate gene variants were identified within the seven genes (*Gm13236*, *Zfp987*, *Gm26573*, *Zfp600*, *Gm13165*, *Gm13166*, and *Zpf992*) that were among the eight most-distal genetic determinants in the *Gct1* interval. The majority of the 107 variants that were located near or within candidate genes were intronic (87), followed by variants within 5,000 bp upstream (13) or downstream (6) of genes. Three intronic variants overlapped transcripts from two candidate genes (one variant in both *Gm13212* and *Gm26763*, and two variants in both *Gm26763* and *Zfp980*). *Zfp990* had the most variants (48) of any candidate gene; the majority of these (40) were intronic. Only one of the 169 *Gct1* variants was present within the coding sequencing of a candidate gene (*Zfp986*; described below). A summary of the number of variants found in and around each *Gct1* candidate gene and their location category is shown in Table 2.7.

Of the 169 *Gct1* variants, 167 were categorized by the Ensembl VEP as conferring a Modifying impact. The Modifier classification is assigned to non-coding variants or variants

**Table 2.7 Summary of variants in and around *Gct1* candidate genes.** The total number of variants per gene and their location category are shown. Where a variant overlapped multiple transcripts of the same gene, the variant was categorized by its location in the gene's canonical transcript as determined by the Ensembl VEP. AS: antisense; LR: long intergenic non-coding RNA; n/a: not applicable; PC: protein coding; PT: processed transcript; TEC: manually annotated expressed sequence tag, to be experimentally confirmed

| Gene | Gene Type | Total Number of Variants | Variant Location | | | |
|---|---|---|---|---|---|---|
| | | | Upstream[a] | Coding | Intronic | Downstream[a] |
| *Dhrs3* | PC | 17 | 1 | 0 | 15 | 1 |
| *Gm38074* | TEC | 1 | 1 | n/a | 0 | 0 |
| *Vps13d* | PC | 13 | 0 | 0 | 13 | 0 |
| *Tnfrsf1b* | PC | 1 | 0 | 0 | 1 | 0 |
| *Tnfrsf8* | PC | 3 | 0 | 0 | 3 | 0 |
| *Platr16* | PT | 3 | 0 | n/a | 0 | 3 |
| *Zfp990* | PC | 48 | 6 | 0 | 40 | 2 |
| *Gm13212* | PC | 3 | 1 | 0 | 2 | 0 |
| *Gm26763* | LR | 10 | 2 | n/a | 8 | 0 |
| *Zfp980* | PC | 2 | 0 | 0 | 2 | 0 |
| *Gm13236* | LR | 0 | 0 | n/a | 0 | 0 |
| *Zfp986* | PC | 9 | 2 | 1 | 6 | 0 |
| *Zfp987* | PC | 0 | 0 | 0 | 0 | 0 |
| *Gm26573* | LR | 0 | 0 | n/a | 0 | 0 |
| *Zfp600* | PC | 0 | 0 | 0 | 0 | 0 |
| *Gm13165* | AS | 0 | 0 | n/a | 0 | 0 |
| *Gm13166* | LR | 0 | 0 | n/a | 0 | 0 |
| *Zpf992* | PC | 0 | 0 | 0 | 0 | 0 |

[a]Variants were considered as upstream or downstream of a gene if they were within 5,000 bp of the gene's beginning or end, respectively.

affecting non-coding genes, where predictions are difficult or there is no evidence of impact (Zerbino *et al*. 2018). As mentioned above, only one variant, a C to A transversion at Chr 4 genomic position 145,899,822 in *Zfp986*, was present within the coding sequence of a candidate gene. This c.1051C>A variant resulted in the substitution of a polar threonine (Thr) for a non-polar Pro at residue 351, and was classified by the Ensembl VEP as a missense variant conferring a Moderate impact on the ZFP986 protein. Moderate impact variants are defined as non-disruptive variants that might change a protein's effectiveness (Zerbino *et al*. 2018). The p.Pro351Thr variant was predicted to be deleterious (score = 0.04; range = 0.0 to 1.0, where variants scoring between 0.0 to 0.05 are considered deleterious) by the Sorting Tolerant from Intolerant (SIFT) version 5.2.2 algorithm (Sim *et al*. 2012) running within the Ensembl VEP. Residue 351 is the last residue within the sixth of eight predicted $C_2H_2$-type classical zinc finger (ZNF) domains (InterPro); these domains bind nucleic acids and zinc, and are found in zinc finger transcription factors (Iuchi 2001). The ZFP986 protein is also predicted to contain an N-terminal Krüeppel-associated box (KRAB) domain (InterPro), which have been shown to repress gene transcription (Margolin *et al*. 1994). ZFP986 may therefore function as a transcriptional regulator with repressive capability. The *Zfp986* gene has two protein coding transcripts; the c.1051C>A variant is located within exon 4 of 4 in the longer transcript only, which has been assigned an Ensembl transcript support level (TSL) of 2. TSL 2 transcripts are supported only by an mRNA that is flagged as suspect, or by multiple ESTs (Zerbino *et al*. 2018). The distal end of *Zfp986* abuts the first of two unresolved gaps in the GRCm38 genome assembly (Figure 2.10) and the gene is flagged by Ensembl with a 3′ incomplete designation, which indicates a protein coding transcript that is missing the termination codon due to incomplete evidence. The c.1051C>A variant is located only 153 bp proximally to the beginning of this gap, and the

proximity of this variant to the assembly gap prevented successful primer design for empirical verification by Sanger sequencing. *Zfp986* does not have an annotated GenBank Reference Sequence (RefSeq), a known function, or a direct human orthologue on Chr 1p36.21-22 or elsewhere in the human genome. Analyses of the quality metrics for this variant revealed a genotype quality of 3.98, a mapping quality of 20, a consensus quality of -33, and a read depth of 2X; these values were well below the averages for the NGS data set as a whole. Furthermore, this variant was identified in only one of the three samples subjected to NGS. The poor data quality values and lack of replication among independent $Gct1^{SW}$ samples suggest this variant is a false NGS finding, and strong evidence for this gene's annotation is lacking; taken together, the c.1051C>A variant within the *Zfp986* gene is not a high priority for shared identity with *Gct1*, and was not pursued further.

In the absence of any strongly-supported protein coding candidate variants, we next focused our analyses of those novel intronic variants within the four protein coding *Gct1* candidate genes that have been ascribed a known function (*Dhrs3*, *Vps13d*, *Tnfrsf1b* and *Tnfrsf8*). A subset of the 32 intronic variants within these four candidates were subjected to Sanger sequencing for empirical verification (Appendix D). Variants were pursued for validation if: 1) they were identified by NGS in at least two of the three $Gct1^{SW}$ gDNA samples; 2) they had an average read depth ≥ 10X; and 3) the sum of the average DP4 values for the alternate allele was ≥ 10X. Fourteen primer pairs were used to interrogate 14 variants by Sanger sequencing, including nine in *Dhrs3*, three in *Vps13d*, and one variant in each of *Tnfrsf1b* and *Tnfrsf8*. A fifteenth variant within intron 1 of *Tnfrsf8* could not be empirically validated despite meeting the required criteria due to a lack of specific primers. Of the 14 variants tested, all were empirically confirmed to be present in SWR but not Line 4-5 gDNA, with the exception of one variant

within *Vps13d* (Table 2.8). This variant at position 145,071,222 within *Vps13d* intron 55 was absent from the gDNA of three SWR individuals and thus was a false positive, despite being identified in all three original *Gct1*$^{SW}$ samples and having above average genotype, mapping, and consensus quality scores, albeit with a relatively low average read depth of 27.3X (Appendix D).

Among the 13 empirically validated intronic variants was one variant located at the 3′ end of the third intron of *Dhrs3*. This C to T transition at position 144,919,838 (c.460-3C>T; NM_011303.7) was the only variant among the 169 within *Gct1* that was categorized by the Ensembl VEP as conferring a Low impact, and the only variant categorized as conferring an impact more severe than Modifying except for the Moderate impact variant in *Zfp986*. Low impact variants are assumed to be mostly harmless or unlikely to change protein behaviour (Zerbino *et al*. 2018). The Ensembl VEP further classified this variant as a splice region variant, which refers to a sequence variant in which a change has occurred within the region of the splice site, either within 1-3 bases of the exon or 3-8 bases of the intron (Zerbino *et al*. 2018). The c.460-3C>T *Dhrs3* variant was identified in all three *Gct1*$^{SW}$ gDNA samples, with above average data quality values and average read depth (Appendix D). Analyses of the c.460-3C>T *Dhrs3* variant using six *in silico* splicing prediction programs confirmed this variant decreases the likelihood of correct splicing at the intron 3-exon 4 3′ acceptor site (Table 2.9). Further *in silico* analysis of the c.460-3T>C *Dhrs3* variant determined that it abolishes the binding sites of serine and arginine rich splicing factor 1 (SRSF1) and SRSF2 and decreases the likelihood of SRSF5 binding, abolishes a branch point motif and two pseudoexon silencer motifs, and creates a new binding site for the hnRNP A1 RNA-binding protein (Table 2.10). Finally, the c.460-3T>C *Dhrs3* variant was deemed to be highly pathogenic by three independent programs capable of assessing non-coding variants (Table 2.11).

**Table 2.8 Validation of NGS variants by Sanger sequencing.** Gene and variant location on Chr 4, the primer set used for variant amplification (see Table 2.3), the reference and alternate alleles, the variant's impact as predicted by the Ensembl VEP, and if the variant was confirmed by Sanger sequencing are shown. ✓: confirmed by Sanger sequencing; X: not identified by Sanger sequencing in three novel and unique SWR gDNA samples; n/a: not pursued due to a lack of specific primers

| Gene | Location on Chr 4 (bp) | Primer Set | Reference Allele | Alternate Allele | VEP Impact | Confirmed by Sanger Sequencing |
|---|---|---|---|---|---|---|
| *Dhrs3* | 144,895,554 | DHRS3-A | A | G | Modifier | ✓ |
| | 144,898,026 | DHRS3-B | C | T | Modifier | ✓ |
| | 144,899,520 | DHRS3-C | G | A | Modifier | ✓ |
| | 144,900,470 | DHRS3-D | T | C | Modifier | ✓ |
| | 144,901,872 | DHRS3-E | G | A | Modifier | ✓ |
| | 144,902,233 | DHRS3-E | G | A | Modifier | ✓ |
| | 144,910,330 | DHRS3-F | C | T | Modifier | ✓ |
| | 144,917,378 | DHRS3-G | G | C | Modifier | ✓ |
| | 144,919,838 | DHRS3-H | C | T | Low | ✓ |
| *Vps13d* | 145,008,075 | VPS13D-A | G | T | Modifier | ✓ |
| | 145,071,222 | VPS13D-B | C | T | Modifier | X |
| | 145,166,463 | VPS13D-C | T | C | Modifier | ✓ |
| *Tnfrsf1b* | 145,237,143 | TNFRSF1B | C | T | Modifier | ✓ |
| *Tnfrsf8* | 145,282,758 | TNFRSF8 | G | T | Modifier | ✓ |
| | 145,308,667 | n/a | G | T | Modifier | n/a |

**Table 2.9 *In silico* splice site analysis of the c.460-3C>T *Dhrs3* variant.** The splice site prediction program and the predicted splicing scores at the c.460 acceptor site for each c.460-3 *Dhrs3* allele are shown. Program inputs and interpretations are defined in Appendix C.

| Program | Score | |
|---|---|---|
| | c.460-3C | c.460-3T |
| Human Splicing Finder | 87.87 | 80.19 |
| GeneSplicer | 12.59 | 11.92 |
| MaxEntScan | 8.77 | 8.40 |
| NetGene2 | 0.87 | 0.17 |
| SpliceSiteFinder-like | 78.81 | 72.64 |
| SpliceView | 83 | 81 |

**Table 2.10 *In silico* splicing regulatory element analysis of the c.460-3C>T *Dhrs3* variant.** The splicing regulatory element prediction algorithm running within Human Splicing Finder, the splicing regulator element and motif affected, and the predicted scores for each c.460-3 *Dhrs3* allele are shown. The c.460-3 allele is underlined within each affected motif. Intronic nucleotides are shown in lower case and exonic nucleotides are shown in upper case. Program inputs and interpretations are defined in Appendix C. n/a: not applicable; -: binding site below threshold and absent in the presence of the c.460-3C allele or abolished in the presence of the c.460-3T allele

| Algorithm | Splicing Regulatory Element | Affected Motif | Score | |
|---|---|---|---|---|
| | | | c.460-3C | c.460-3T |
| ESEFinder | SRSF1 | cagACCA | 83.58 | - |
| | SRSF2 | gccctcag | 76.58 | - |
| | SRSF5 | tcagACC | 82.75 | 80.90 |
| Branch points | n/a | ctcagAC | 76.61 | - |
| hnRNP motifs | hnRNP A1 | tagACC | - | 76.67 |
| Silencer motifs | n/a | gccctcag | 61.64 | - |
| | n/a | cctcagAC | 61.79 | - |

**Table 2.11 *In silico* variant pathogenicity analysis of the c.460-3C>T *Dhrs3* variant.** The pathogenicity program used and the corresponding pathogenicity scores for the c.460-3C>T *Dhrs3* variant are shown. Program inputs and interpretations are defined in Appendix C.

| Program | Score |
|---|---|
| CADD | 15.27 |
| *FATHMM-XF* | 0.968994 |
| PhD-SNP[g] | 0.716 |

Loss of proper splicing at the intron 3-exon 4 3′ acceptor site would likely lead to exclusion of the 239 bp exon 4 (Abramowicz & Gos 2018), which was predicted by the ExPASy Translate tool to replace the normal DHRS3 C-terminal amino acid sequence with 65 incorrect amino acids prior to a termination codon (p.Thr154ValfsTer65). Alternatively, modulation of this acceptor site could lead to retention of the 336 bp intron 3 (Wong *et al*. 2016), which would similarly result in a termination codon following 10 incorrect amino acids (p.Thr154ValfsTer10). These protein changes would remove the inferred substrate binding site at DHRS3 residue 175, as well as three of four predicted transmembrane helices spanning residues 170 to 190, 195 to 215, and 258 to 278 (UniProt). In addition, loss of *Dhrs3* exon 4 or retention of intron 3 would abolish the highly conserved SDR active site sequence (YXXXK) at residues 188 to 192 (Adams *et al*. 2014) by substituting YCTSK for YPHYL; the likely result would be a catalytically inactive protein due to the non-conservative substitution of a positively charged, polar lysine (Lys) for a non-polar, neutral leucine (Leu) at position 5. Analysis of the potential 10 and 65 residue polypeptide sequences using InterPro did not identify any annotated domains or motifs. An alternate third scenario might involve the activation of an intronic or exonic cryptic splice site, resulting in the inclusion of an exon or intron fragment(s) (Abramowicz & Gos 2018) and potentially significant consequences on protein sequence. To determine the effect of the c.460-3C>T variant on the *Dhrs3* transcript, we conducted an RT-PCR analysis using cDNA derived from untreated pubertal SWR and Line 4-5 mouse ovaries. RT-PCR primers were designed to span *Dhrs3* exons 3 and 5, such that exons 3, 4 and 5 (normal transcript splicing; 426 bp amplicon) or exons 3 and 5 (alternate transcript splicing in the presence of the c.460-3C>T variant; 187 bp amplicon) would potentially be amplified (Figure 2.6). This primer design would also allow for the detection of intron 3 retention (762 bp amplicon), and, potentially, the

inclusion of other exon or intron fragments between exons 3 and 5. Gel electrophoresis revealed the presence of a 426 bp amplicon, corresponding to exons 3, 4 and 5, as well as a faint 187 bp amplicon, corresponding to exons 3 and 5; both amplicons were present in both the SWR and Line 4-5 samples (Figure 2.16). No evidence of a 762 bp amplicon, representing intron 3 retention, or any other amplicons, representing the inclusion of exon or intron fragments, was observed by gel electrophoresis under these conditions and following 39 cycles of PCR (data not shown). The 187 and 426 bp amplicons were sequenced and found to be identical between SWR and Line 4-5 mice, with a smooth transition between exons 3 and 5 evident in the smaller amplicon (Figure 2.16). Examination of this amplicon using NCBI Standard Nucleotide BLAST found it was specific to *Dhrs3*, indicating the primers amplified the intended alternate transcript rather than an off-target sequence.

#### 2.3.2.2 Copy Number Variation Analysis

A cohort of 38 SWR females were administered DHEA at puberty, of which 15.8% (n = 6) developed unilateral GC tumours. This GC tumour frequency was similar to that reported in SWR females administered DHEA (17.6%; Smith 2011; $p = 1.0000$ by Fisher's exact test). An additional cohort of eight Line 4-5 females were administered DHEA at puberty, and maintained resistance to GC tumour initiation as expected (0.0% GC tumour frequency). gDNA samples from four SWR GC tumour hosts and four unaffected Line 4-5 individuals were successfully hybridized as four pairwise comparisons to a custom Agilent Mouse aCGH 4x180K Array. Scanned arrays were converted to TXT files and analyzed using Agilent Feature Extraction Software. The data for all arrays was in the acceptable "good" or "excellent" ranges for all quality and evaluation metrics, with the exception of the LogRatioImbalance metric for one

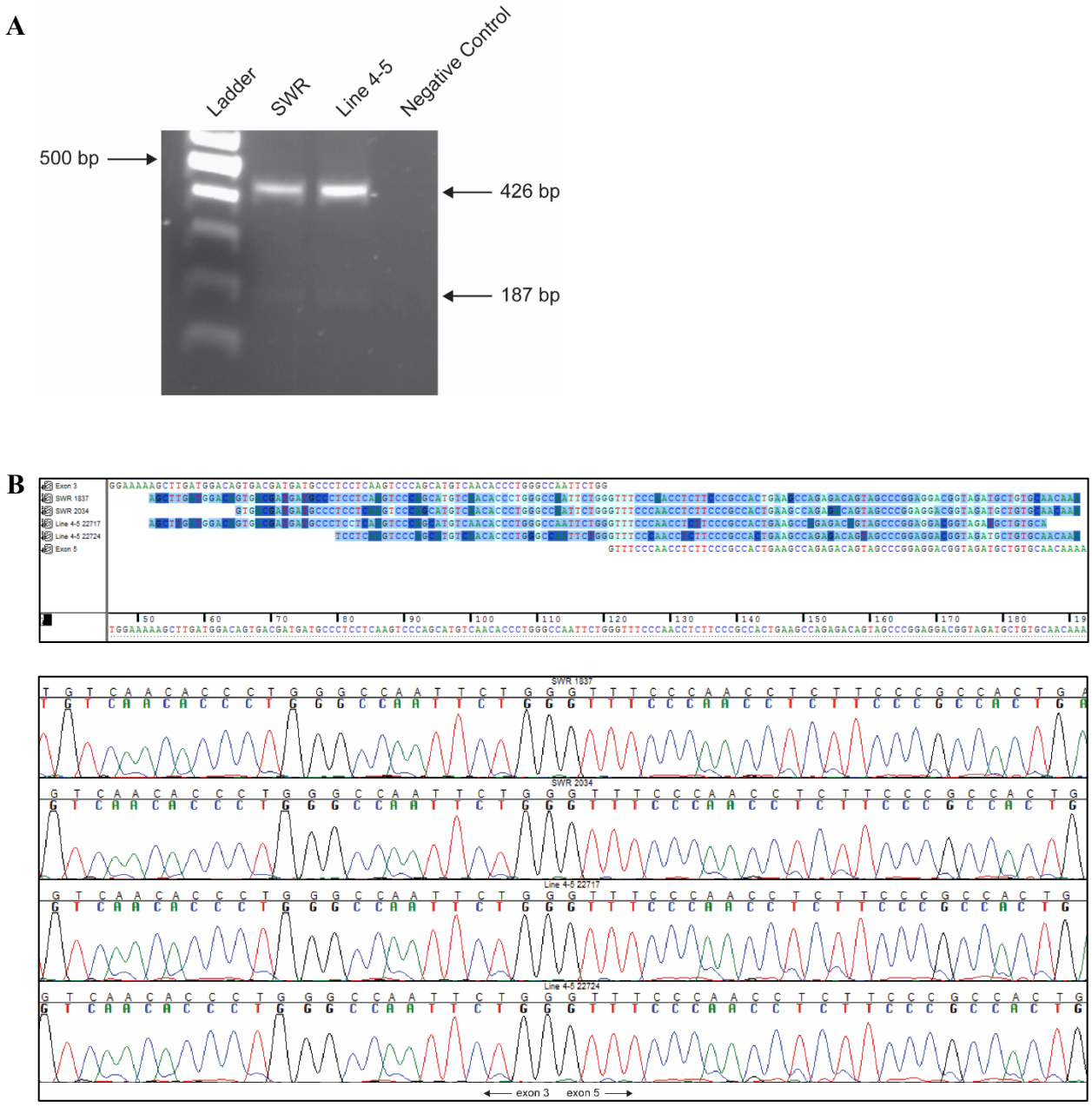


**Figure 2.16 *Dhrs3* RT-PCR analysis**

(A) Representative horizontal gel electrophoresis image of *Dhrs3* RT-PCR amplicons, showing a 426 bp and faint 187 bp amplicon in both the SWR and Line 4-5 samples. The negative control contained distilled water in place of cDNA template. (B) Sanger sequence reads (top) and electropherogram (bottom) of the 187 bp amplicon spanning *Dhrs3* exons 3 and 5 from Sequencher® version 5.2.4, showing the smooth transition between the TGG nucleotide sequence at the 3′ end of exon 3 and the GTT nucleotide sequence at the 5′ end of exon 5.

array. This metric calculates the amount of amplifications versus deletions per chromosome to determine if there is an imbalance that falls out of normal expectations (Appendix E). A value in the "evaluate" range for this metric indicates an error during gDNA hybridization; this array was therefore not included in further aCGH analysis, which did not impact the analysis of the other three independent arrays. The quality control and evaluation metrics for the four individual arrays generated by Agilent Feature Extraction Software are shown in Table 2.12.

Analysis of the aCGH data from the three acceptable arrays using Agilent Genomic Workbench Software, with the highly stringent legacy centralization and ADM-2 thresholds of 10.0 and fuzzy zero normalization applied, revealed 12 CNVs on Chr 4. These 12 CNVs included eight gains and four losses in the SWR strain relative to Line 4-5. Ten of the 12 CNVs were detected in all three samples, whereas 11 and eight CNVs had completely overlapping bp and probe fractions, respectively (i.e. the amplified or deleted areas were present in the same bp and probe regions across the samples in which they were detected). Only six CNVs were present in all three samples with completely overlapping bp and probe fractions (Figure 2.17). The coordinates of 10 CNVs were successfully converted from the NCBI Build m37 genome assembly to that of GRCm38; conversion of the two largest CNVs generated multiple, non-contiguous genomic segments. All CNVs were determined to be novel following comparison to DGVa-annotated structural variants in the Ensembl Variation 94 Mouse Structural Variants dataset, whereas all CNVs, with two exceptions (described below), were predicted by the Ensembl VEP to confer only a Modifying impact. Seven of the reported CNVs overlapped with annotated genes. The largest CNV, a 1,347,720 bp loss detected in all three samples, overlapped 16 major urinary protein (MUP) genes (*Mup1*, *Mup2*, *Mup5*, and *Mup7-19*). Protein coding transcripts for all 16 of these genes were predicted to be lost by the Ensembl VEP. All three

**Table 2.12 aCGH quality control and evaluation metrics generated by Agilent Feature Extraction Software.** The quality control and evaluation metric values for each array are shown. Data in green text are in the "excellent" range for their respective metric, whereas data in blue and red are in the "good" and "evaluate" ranges, respectively. Metrics and their value ranges are defined in Appendix E.

| Metric Name | Value | | | |
|---|---|---|---|---|
| | Array 1 | Array 2 | Array 3 | Array 4 |
| IsGoodGrid | 1.00 | 1.00 | 1.00 | 1.00 |
| AnyColorPrcntFeatNonUnifOL | 0.02 | 0.02 | 0.00 | 0.01 |
| DerivativeL_R_Spread | 0.11 | 0.13 | 0.15 | 0.24 |
| gRepro | 0.12 | 0.13 | 0.12 | 0.12 |
| g_BGNoise | 4.09 | 3.75 | 3.51 | 3.55 |
| g_Signal2Noise | 304.78 | 300.51 | 304.46 | 332.81 |
| g_SignalIntensity | 1245.66 | 1128.22 | 1060.20 | 1180.00 |
| rRepro | 0.11 | 0.12 | 0.11 | 0.12 |
| r_BGNoise | 6.51 | 6.94 | 6.67 | 5.97 |
| r_Signal2Noise | 246.39 | 239.47 | 216.25 | 239.09 |
| r_SignalIntensity | 1604.24 | 1661.06 | 1442.60 | 1428.29 |
| LogRatioImbalance | 0.00 | 0.00 | 0.00 | -1.05 |

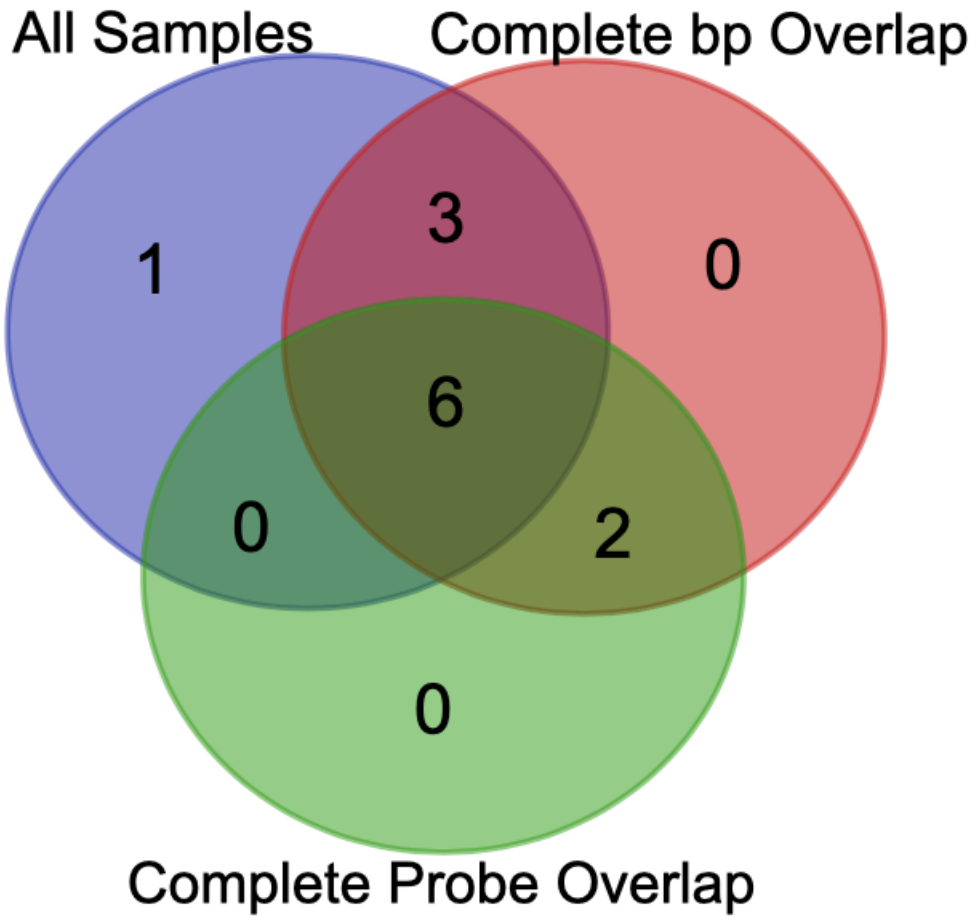


**Figure 2.17 Venn diagram of Chr 4 CNV characteristics**

Of the 12 Chr 4 CNVs that were unique to SWR, only six were identified in all three samples and had complete bp and probe overlapping fractions. Two of these six CNVs, which were both called as gains, were within the *Gct1* interval.

samples were also positive for one gain CNV that overlapped the filamin binding LIM protein 1 gene (*Fblim1*), as well as for two gain CNVs that both overlapped the RIKEN cDNA 6330411D24Rik gene (*6330411D24Rik*) and for a loss CNV overlapping the preferentially expressed antigen in melanoma like 5 gene (*Pramel5*). Both of the two *Pramel5* protein coding transcripts were predicted to be lost by the Ensembl VEP. Two samples displayed a CNV loss overlapping with the PR domain containing 2, with ZNF domain gene (*Prdm2*). Only two of the 12 CNVs, which were both called as gains in all three samples assayed with completely overlapping fractions, were within the *Gct1* interval. One of these CNVs overlapped with intron 6 of the *Gct1* candidate gene *Tnfrsf8*, whereas the other did not overlap with any *Gct1* candidates. The 12 CNVs identified on Chr 4 are summarized in Table 2.13.

#### 2.3.2.3 Functional Analyses of Candidate Genes

*Tumour Necrosis Factor*

The 10 µg/kg TNF administration paradigm was tolerated well and was non-toxic; all mice survived with no observable side-effects until scheduled necropsy and GC tumour assessment at 8 wk of age. Body weight and ovary and uterus weights as a proportion to body weight for mice given TNF are shown in Appendix F. ELISA revealed that SWR females administered exogenous TNF for 8 d had an average serum TNF concentration of 88.66 pg/mL ± 15.12 compared to 44.46 ± 8.469 pg/mL in females administered saline alone. A cohort of 19 pubertal SWR females were treated with 10 µg/kg TNF in combination with DHEA, of which 26.3% developed GC tumours (n = 2 unilateral, n = 3 bilateral). This GC tumour frequency was not significantly different from that reported in SWR females administered DHEA alone (17.6%; Smith 2011) when compared by Fisher's exact test ($p = 0.5049$). An additional cohort of 17

**Table 2.13 Chr 4 CNVs detected in SWR GC tumour hosts relative to Line 4-5 females by aCGH analysis.** The location of CNVs on Chr 4, CNV size, the number of probes amplified or deleted per CNV, the number of samples in which the CNVs were detected, their average overlap fractions, CNV type (gain or loss), the genes overlapped, and the VEP predicted impact category are shown. Data is from Ensembl release 95 (January 2019; Zerbino *et al*. 2018). The two CNVs within the *Gct1* interval are indicated by bold text. n/a: not applicable

| Location on Chr 4 (bp) | | Size (bp) | Probes | Samples | Average Overlap Fraction (bp) | Average Overlap Fraction (probes) | CNV Type | Overlapping Genes[b] | Predicted Outcome (VEP)[c] |
|---|---|---|---|---|---|---|---|---|---|
| Start | Stop | | | | | | | | |
| 60,007,640[a] | 61,857,194 | 1,347,720 | 23 | 3 | 0.81 | 0.05 | Loss | *Mup7*, *Mup2*, *Mup8*, *Mup9*, *Mup1*, *Mup10*, *Mup11*, *Mup12*, *Mup13*, *Mup14*, *Mup15*, *Mup16*, *Mup17*, *Mup18*, *Mup19*, *Mup5* | High |
| 122,290,670[a] | 122,073,598 | 175,869 | 95 | 1 | 1.0 | 1.0 | Gain | n/a | Modifier |
| 141,580,464 | 141,584,992 | 4,529 | 5 | 3 | 1.0 | 0.5 | Gain | *Fblim1* | Modifier |
| 142,858,562 | 142,861,897 | 3,336 | 6 | 3 | 1.0 | 0.33 | Gain | *6330411D24Rik* | Modifier |
| 143,018,316 | 143,019,345 | 1,030 | 3 | 3 | 1.0 | 1.0 | Gain | *6330411D24Rik* | Modifier |
| 143,146,756 | 143,147,779 | 1,024 | 3 | 2 | 1.0 | 1.0 | Loss | *Prdm2* | Modifier |
| 143,854,439 | 143,857,273 | 2,835 | 3 | 3 | 1.0 | 1.0 | Loss | n/a | Modifier |
| 144,259,612 | 144,296,091 | 36,480 | 7 | 3 | 1.0 | 0.25 | Loss | *Pramel5* | High |
| 144,494,314 | 144,494,690 | 377 | 3 | 3 | 1.0 | 1.0 | Gain | n/a | Modifier |
| 144,754,928 | 144,756,867 | 1,940 | 4 | 3 | 1.0 | 1.0 | Gain | n/a | Modifier |
| **145,289,996** | **145,290,707** | **712** | **5** | **3** | **1.0** | **1.0** | **Gain** | ***Tnfrsf8*** | **Modifier** |
| **145,349,295** | **145,350,019** | **725** | **4** | **3** | **1.0** | **1.0** | **Gain** | **n/a** | **Modifier** |

[a]CNV coordinates were not contiguous following conversion to the GRCm38 assembly; [b]Where more than one gene is encompassed by a CNV, the genes are presented in order of their location along Chr 4; [c]Where more than one impact category was predicted, only the most severe consequence (High > Moderate > Low > Modifier) is noted.

pubertal SWR females were administered 10 µg/kg TNF with an empty capsule. All 17 mice remained GC tumour-free up to 8 wk; the GC tumour frequency observed in this cohort (0.0%) was significantly different from that of SWR females treated with TNF and DHEA ($p = 0.0473$ by Fisher's exact test). Finally, a cohort of 12 pubertal Line 4-5 females were treated with 10 µg/kg TNF in combination with DHEA. Line 4-5 females maintained resistance to GC tumour initiation (0.0% GC tumour frequency) with TNF and DHEA treatment. A summary of the GC tumour frequencies observed following TNF administration is shown in Table 2.14.

*All-Trans-Retinaldehyde and All-Trans-Retinoic Acid*

The 50 mg/kg RAL administration paradigm employed in this study was moderately toxic towards pubertal mice. Two SWR mice were found dead and one was euthanized due to an adverse reaction following one, two or three RAL injections and the implantation of a DHEA capsule. This toxicity may be due to the effects of the 95% ethanol vehicle rather than exogenous RAL, as one SWR mouse given DHEA was found dead following three injections of vehicle only. This toxicity was not specific to the SWR strain, as one Line 4-5 mouse given an empty capsule was also found dead after three RAL injections. An analysis of body weight and ovary and uterus weights as a proportion to body weight revealed that RAL conferred no significant effects on these measurements (Appendix F). A cohort of 15 pubertal SWR females were administered three doses 50 mg/kg RAL in combination with DHEA, of which 6.7% (n = 1) developed unilateral GC tumours. This GC tumour frequency was not significantly different from that reported in SWR females administered DHEA alone (17.6%; Smith 2011) when compared by Fisher's exact test ($p = 0.4334$). An additional cohort of 13 pubertal SWR females were administered three doses of 50 mg/kg RAL with an empty capsule. All 13 mice remained

**Table 2.14 GC tumour incidence in SWR and Line 4-5 female mice administered 10 µg/kg TNF at puberty.** SWR females were treated with TNF alone with an empty capsule or in combination with DHEA, whereas Line 4-5 females were treated with TNF in combination with DHEA. GC tumour frequencies in 8 wk old mice are shown.

| Strain | Androgen Treatment | GC Tumour Incidence |
|---|---|---|
| SWR | DHEA | 5/19 (26.3%)[a] |
| SWR | None | 0/17 (0.0%)[b] |
| Line 4-5 | DHEA | 0/12 (0.0%) |

[a]Not significantly different from the GC tumour frequency of SWR females administered DHEA alone at puberty by Fisher's exact test ($p = 0.5049$; Smith 2011); [b]Significantly different from the GC tumour frequency of SWR females administered TNF and DHEA at puberty ($p = 0.0473$) by Fisher's exact test.

GC tumour-free up to 8 wk; the GC tumour frequency observed in this cohort (0.0%) was not significantly different from that of SWR females treated with RAL and DHEA ($p$ = 1.0000) or DHEA alone ($p$ = 0.1845) when compared by Fisher's exact test. A third cohort of 18 pubertal SWR females were administered three doses of vehicle alone in combination with DHEA. Only 5.6% (n = 1) of these 18 mice developed unilateral GC tumours; although this GC tumour frequency was lower than what has historically been observed in SWR mice administered pubertal DHEA, it was not significantly different from that reported in SWR females administered DHEA alone (17.6%; Smith 2011; $p$ = 0.2736), nor was it significantly different from that observed in SWR females administered RAL and DHEA ($p$ = 1.0000) when compared by Fisher's exact test. Finally, cohorts of pubertal Line 4-5 females were administered three doses of 50 mg/kg RAL with DHEA (n = 22), with an empty capsule (n = 25), or were administered vehicle only and DHEA (n = 2). No Line 4-5 females in any of these three cohorts developed GC tumours (0.0% GC tumour frequencies). A summary of the GC tumour frequencies observed following RAL administration is shown in in Table 2.15.

The 5 mg RA administration paradigm employed in this study was moderately toxic towards SWR mice. Three females were found dead between 5 and 6 wk of age, following implantation of the 5 mg RA pellets at puberty and prior to the 8 wk necropsy. One of these animals was implanted with a DHEA-filled capsule, whereas the other two animals were administered RA only. Upon necropsy, all females were found to have a fatty mass with yellow deposits of RA under the skin at the site of RA pellet administration. Microscopic examination of these masses determined they were infiltrated with fibroblastic-like cells (data not shown). An analysis of body weight and ovary and uterus weights as a proportion to body weight revealed that RA conferred no significant effects on these measurements (Appendix F). A cohort of 10

**Table 2.15 GC tumour incidence in SWR female mice administered three doses of 50 mg/kg RAL at puberty.** SWR and Line 4-5 females were treated with RAL or vehicle alone with an empty capsule or in the presence of DHEA. GC tumour frequencies in 8 wk old mice are shown.

| Strain | RAL Treatment | Androgen Treatment | GC Tumour Incidence |
|---|---|---|---|
| SWR | RAL | DHEA | 1/15 (6.7%)[a] |
| SWR | RAL | None | 0/13 (0.0%)[b] |
| SWR | Vehicle | DHEA | 1/18 (5.6%)[c] |
| Line 4-5 | RAL | DHEA | 0/22 (0.0%) |
| Line 4-5 | RAL | None | 0/25 (0.0%) |
| Line 4-5 | Vehicle | DHEA | 0/2 (0.0%) |

[a]Not significantly different from the GC tumour frequency of SWR females administered DHEA alone at puberty by Fisher's exact test ($p = 0.4334$; Smith 2011); [b]Not significantly different from the GC tumour frequency of SWR females administered DHEA alone ($p = 0.1845$; Smith 2011) or RAL and DHEA ($p = 1.0000$) at puberty by Fisher's exact test; [c]Not significantly different from the GC tumour frequency of SWR females administered DHEA alone ($p = 0.2736$; Smith 2011) or RAL and DHEA ($p = 1.0000$) at puberty by Fisher's exact test.

pubertal SWR females were administered 5 mg RA 21 d release pellets in combination with DHEA, of which none developed GC tumours (0.0% GC tumour frequency). This GC tumour frequency was not significantly different from that reported in SWR females administered DHEA alone (17.6%; Smith 2011) when compared by Fisher's exact test ($p = 0.3324$). An additional cohort of 9 pubertal SWR females were administered 5 mg RA 21 d release pellets alone. All 9 mice remained GC tumour-free up to 8 wk; the GC tumour frequency observed in this cohort (0.0%) was not significantly different from that of SWR females treated with RA and DHEA ($p = 1.0000$) or DHEA alone ($p = 0.3304$) when compared by Fisher's exact test. Additional cohorts of pubertal SWR females were administered DHEA alone (n = 9) or an empty capsule alone (n = 12) over the duration of the 5 mg RA 21 d release pellet paradigm. As expected, 22.2% of SWR females administered DHEA alone at puberty developed GC tumours (n = 1 unilateral, n = 1 bilateral), whereas none were observed in SWR pubertal females administered an empty capsule (0.0% GC tumour frequencies). The GC tumours frequencies of SWR females administered DHEA or an empty capsule at puberty were not significantly different from that previously reported in SWR females administered DHEA (17.6%; Smith 2011) when compared by Fisher's exact test ($p = 0.6644$ and 0.1869, respectively). A summary of the GC tumour frequencies observed following RA administration is shown in in Table 2.16.

**Table 2.16 GC tumour incidence in SWR female mice administered 5 mg RA 21 d release pellets at puberty.** SWR females were treated with 5 mg of RA with DHEA or an empty capsule, or with DHEA or an empty capsule alone. GC tumour frequencies in 8 wk old mice are shown.

| RA Treatment | Androgen Treatment | GC Tumour Incidence |
|---|---|---|
| 5 mg | DHEA | 0/10 (0.0%)[a] |
| 5 mg | None | 0/9 (0.0%)[b] |
| None | DHEA | 2/9 (22.2%)[c] |
| None | None | 0/12 (0.0%)[d] |

[a]Not significantly different from the GC tumour frequency of SWR females administered DHEA alone at puberty by Fisher's exact test ($p = 0.3324$; Smith 2011); [b]Not significantly different from the GC tumour frequency of SWR females administered DHEA alone ($p = 0.3304$; Smith 2011) or RA and DHEA ($p = 1.0000$) at puberty by Fisher's exact test; [c]Not significantly different from the GC tumour frequency of SWR females administered DHEA alone at puberty by Fisher's exact test ($p = 0.6644$; Smith 2011); [d]Not significantly different from the GC tumour frequency of SWR females administered DHEA alone at puberty by Fisher's exact test ($p = 0.1869$; Smith 2011)**.**

## 2.4. Discussion

### 2.4.1 Overview

Ovarian GC tumours appear in women at either end of the reproductive spectrum, and based on age of onset, histology, and genetics are divided into distinct adult and juvenile clinicopathologic subtypes. Whereas somatic mutation of *FOXL2* is associated with human adult GC tumours, and while genetic alteration of multiple genes results in high frequencies of SCST phenotypes in mice, no genes that confer inherent juvenile GC tumour susceptibility or resistance have been identified in humans or mice. The SWR mouse model recapitulates innate susceptibility to early-onset GC tumours at a low phenotypic frequency of ≥ 1%, with *Gct1* on distal mouse Chr 4 acting as a fundamental locus for GC tumour initiation during a restricted window of susceptibility and endocrinological sensitivity that coincides with the onset of puberty. Exogenous androgen administration has been successfully used to increase trait penetrance, and has facilitated the genetic mapping of *Gct1* while reinforcing the influence of steroid hormones on the GC tumour initiation mechanism in the complex biology of the mammalian ovary. The objective of this dissertation chapter was to reduce and completely genetically annotate the *Gct1* candidate gene interval, and to evaluate prioritized gene candidates and genomic variants for shared identity with *Gct1*.

### 2.4.2 *Gct1* Resides Within a 1.65 Mb Interval

A third round of phenotypic mapping using Line 4-5 as a starting donor was unsuccessful, as no informative recombinations were produced. However, two SNPs were identified at the *Gct1* proximal boundary that were polymorphic between CAST and SWR, and

that refined the *Gct1* interval to 1.65 Mb. This region of mouse Chr 4 contains a total of 18 protein coding genes and non-coding transcripts, as well as 30 annotated pseudogenes (Table 2.6). Successful reduction of the *Gct1* interval eliminated four candidate genes from consideration of shared identify with *Gct1*. Efforts to fine map the *Gct1* interval were focused on the proximal end of the locus due to the high degree of repetitive DNA sequence at the distal region, which has prevented the development of accurate and specific genotyping markers. Should this hurdle be overcome, a more exact boundary description at the distal *Gct1* interval would be possible from the genotyping of already phenotyped subcongenic lines, and may reduce the 1.65 Mb interval further.

### 2.4.3 Prioritizing *Gct1* Candidates: Interval Annotation and Functional Analyses

Having achieved maximum genetic resolution, we sought to thoroughly annotate the entire *Gct1* interval with two complementary technologies. NGS was conducted to identify all candidate SNVs and small nucleotide insertions and deletions, whereas aCGH was conducted to identify all candidate CNVs. A targeted sequencing approach was utilized to isolate the $Gct1^{SW}$ locus prior to NGS given the small size of the highly resolved *Gct1* interval (Simon *et al*. 2012). Targeted capture of the entire *Gct1* locus was successful and NGS identified 22,362 SNVs and small nucleotide insertions and deletions in the three samples, which was reduced to 9,121 unique variants when duplicates between samples were removed (Figure 2.11). The distal region of *Gct1* displayed poorer genotype, mapping, and consensus quality scores and lower AF1 values compared to the proximal region of the interval (Figure 2.12). Some sections of the distal region also displayed more variants, which may be false positives, or fewer variants despite high read depths, which may reflect the poor annotation of this region (Figure 2.13). The high read depths

at the distal end of the *Gct1* interval may also be due to the non-specific alignment of reads that were enriched due to this region's similarity with other areas of the genome.

The fact that no other inbred mouse strains contribute *Gct1* alleles that support GC tumour susceptibility even with androgen treatment suggests that the *Gct1* variant is unique to SWR, and so annotated variants and those identified in other mouse strains were filtered out. This step removed 8,172 annotated variants from consideration for shared identity with *Gct1* (Figure 2.11). Variants categorized as novel had significantly poorer genotype and mapping qualities compared to annotated variants, and also had lower average AF1 and positive consensus quality scores indicative of heterozygosity (Figure 2.15). It is therefore likely that a significant portion of these novel $Gct1^{SW}$ variants may in fact be false NGS findings. The remaining 949 variants were subjected to a conservative filtering strategy in which they were filtered by AF1, such that heterozygous variants identified in the any of the three mice with homozygous $Gct1^{SW}$ alleles, which are likely false, were removed; however, variants were not excluded on the basis of read depth, quality metrics, or replication between independent samples. Remapping of the remaining 290 variants from NCBI Build m37 coordinates revealed that only 169 variants are located within the *Gct1* interval as it is currently annotated within the GRCm38 genome assembly. No variants were identified in seven of the eight most distal *Gct1* genes (Table 2.7), which is unlikely and may indicate poor annotation and/or the inaccuracy of re-assembly of the highly repetitive distal portion of *Gct1*. Assessment of the 169 *Gct1* variants using the Ensembl VEP revealed that 168 were non-coding or within non-coding genes, and thus were predicted to confer a Modifying impact. One non-synonymous missense variant in *Zfp986* was predicted to confer a Moderate impact on protein function; however, incomplete gene annotation, low read depth, poor data quality, and a lack of replication between samples suggested it was a false

finding and the variant was not pursued. A subset of 15 intronic variants within *Gct1* candidate genes, including a *Dhrs3* acceptor splice site variant, were selected for independent validation by Sanger sequencing based on read depth, quality metrics, and replication between samples. Of these 15 variants pursued by Sanger sequencing, 13 were empirically confirmed to be present in SWR but not Line 4-5 gDNA; one variant within *Tnfrsf8* was unable to be confirmed due to a lack of specific primers, and one variant within *Vps13d* was absent from multiple SWR gDNA samples despite strong NGS evidence, and was thus a false positive. It is possible that the NGS reads overlapping the position of the false *Vps13d* variant in fact map to a similar region elsewhere in the genome, and have been incorrectly mapped to the *Gct1* interval.

Of the 13 empirically confirmed variants, only one was predicted by the Ensembl VEP as conferring an impact more severe than Modifying. Although the c.460-3C>T *Dhrs3* variant was not predicted to abolish the intron 3-exon 4 3′ acceptor splice site by six *in silico* splice site prediction programs, all programs predicted a decreased likelihood of correct splicing (Table 2.9). Variants within the mammalian consensus splice site sequences (AG|GTRAGT at the 5′ donor site and $Y_{10}$NCAG|G at the 3′ acceptor site, where R is a purine, Y is a pyrimidine, and N is any nucleotide; Senapathy, Shapiro & Harris 1990) have the potential to alter correct splicing by interrupting the interaction between precursor mRNA and essential splicing proteins, including components of the spliceosome (Abramowicz & Gos 2018). The spliceosome, a large protein-RNA complex that contains dozens of proteins including five core small nuclear ribonucleoproteins (snRNPs), catalyzes transcript splicing by removing introns and ligating exons to form mature mRNA (Abramowicz & Gos 2018). *In silico* algorithms also predicted the loss of binding sites for SRSF1 and SRSF2, and a decrease in the likelihood of SRSF5 binding. These classical serine/arginine (SR) RNA-binding proteins enhance splicing by binding *cis*-

regulatory elements known as exonic splicing enhancers (ESEs) and recruiting the spliceosome to the vicinity of the splice site, and as such are required for constitutive and alternative splicing activation (Long & Caceres 2009). The c.460-3C>T *Dhrs3* variant also abolishes a branch point motif; the branch point, which is required for early spliceosome formation, is located within the intron between -9 to -400 bp downstream of the 3′ acceptor splice site (Abramowicz & Gos 2018). Although the mammalian branch point consensus sequence is more degenerate than that of the 5′ and 3′ splice site sequences, a conserved adenine is necessary for initiating the first splicing reaction (Will & Lührmann 2011). In contrast, a new binding site for the hnRNP A1 RNA-binding protein was predicted to be established in the presence of the c.460-3C>T *Dhrs3* variant. hnRNPs negatively regulate splicing by binding to exonic and intronic splicing silencers (Wagner & Garcia-Blanco 2001). *In silico* analysis also predicted the loss of two silencer motifs that may repress the inclusion of pseudoexons, intronic sequences with potential 5′ and 3′ splice site sequences, in the mature transcript (Sironi *et al*. 2004). Together, a decrease in the likelihood of correct splicing at the 3′ acceptor site, the loss of two ESE binding sites, the inclusion of a new hnRNP A1 binding site, and the loss of two pseudoexon silencer motifs, suggests a significant impact on normal *Dhrs3* transcript splicing. Indeed, the c.460-3T>C *Dhrs3* variant was deemed to be highly pathogenic by three independent programs capable of assessing non-coding variants (Table 2.11). A mutant *Dhrs3* mRNA transcript lacking exon 4 or including intron 3 might be degraded by nonsense-mediated mRNA decay, or be translated into a protein with an inferior, null, new or dominant negative function. The p.Thr154ValfsTer65 and p.Thr154ValfsTer10 mutant proteins would lack a predicted substrate binding site, might mislocalize due to the loss of three of four transmembrane domains, and would be catalytically inactive due to the loss of the DHRS3 active site. Alternatively, the loss of the two silencer

motifs near the 3′ acceptor site might lead to the inclusion of a pseudoexon within intron 3, drastically altering the expected *Dhrs3* transcript.

To determine the effect of the c.460-3C>T variant on the *Dhrs3* transcript, we conducted an RT-PCR analysis using cDNA derived from untreated pubertal SWR and Line 4-5 mouse ovaries and primers spanning *Dhrs3* exons 3 and 5. Unexpectedly, an alternate *Dhrs3* transcript lacking exon 4 was present in samples prepared from Line 4-5 ovary cDNA pools as well as those from SWR mice, and so was not specific to the GC tumour-susceptible ovary. Although this RT-PCR evidence ostensibly refutes the c.460-3C>T *Dhrs3* variant as affecting ovarian transcript splicing during the mouse pubertal period, it does not exclude *Dhrs3* from sharing identity with *Gct1*. The probability of splicing is determined by the binding energy of *cis*- and *trans*-acting modulators at splice sites and regulatory elements. However, the splicing code is inherently stochastic, with variations at the donor and acceptor splice sites, branch point, silencer or enhancer sequences, and binding sites of SR proteins or hnRNPs all contributing to fluctuations in splicing efficiency (Hu *et al*. 2017a; Wan & Larson 2018). The result is a diverse array of temporally- and spatially-restricted transcripts that contribute to phenotypic variability between cells and organisms. Evidently, alternate *Dhrs3* splicing occurs in the pubertal mouse ovary, as both the SWR and Line 4-5 strains expressed a transcript lacking exon 4; however, the SWR-specific c.460-3T allele may alter usual transcript splicing under suitable conditions, and this RT-PCR analysis did not account for cell type (i.e. GCs versus whole ovary cDNA pools), spatiotemporal (i.e. first medullary versus subsequent cortical GC populations within follicle waves), or endocrine (i.e. DHEA stimulation) influences. Further elucidation of the likely complex effects of the SWR c.460-3C>T *Dhrs3* variant on transcript splicing requires further RNA analyses, such as TOPO cloning, minigene assays, or whole-transcriptome sequencing of

the early SWR versus Line 4-5 ovary, with consideration of cell type, GC wave timing, and androgen stimulation. Functional investigations of transcriptional regulation and downstream effects on retinoid and steroid metabolism could be interrogated using an *in vitro* culture system (e.g. short-term culture of mouse embryonic fibroblasts (MEFs) isolated from SWR and Line 4-5 embryos), should transcriptional profiles be altered.

A total of 12 differential Chr 4 CNVs were identified in SWR GC tumour hosts compared to Line 4-5 females (Table 2.13). Only two of these 12 CNVs are located within *Gct1*, and only one of these two gains overlaps a *Gct1* gene candidate. The implications of the 10 CNVs (six gains and four losses) detected on Chr 4 but outside the *Gct1* interval are unknown. Two of these 10 CNVs are predicted by the Ensembl VEP to confer a High impact through the loss of protein coding transcripts in all three samples, including that of 16 MUP genes and *Pramel5*. At least 21 MUP paralogues and 20 MUP pseudogenes have been identified in mice, and all are located within a 2 Mb interval on Chr 4 (Logan, Marton & Stowers 2008; Mudge *et al*. 2008). The MUP proteins are secreted in large quantities in the urine and function to transport pheromones, thus providing unique chemical signatures associated with mouse social behaviours (Novotny 2003). In contrast, *Pramel5* has no known function, although members of the preferentially expressed antigen in melanoma family are tumour antigens in humans (Epping & Bernards 2006). No KO mouse models have been created for any of these 17 genes, and there is no indication of a phenotype caused by their loss in SWR mice. These differential CNVs could be due to genetic drift between the SWR and Line 4-5 strains, which have undergone a significant number of brother-sister matings since the generation of the Line 4-5 subcongenic strain; the Line 4-5 females used in the CNV analysis were generation $N_3F_{21}$ and as such 23 generations have passed since it was first established from the Line 4-T congenic strain, which

itself was derived from SWR following 10 backcross generations. Alternatively, these CNVs could be false positives, particularly in the case of the repetitive, pseudogene-rich MUP genes. Notably, the average probe overlap fractions are poor for these CNVs. The implications of the *Tnfrsf8* CNV gain identified in all three SWR GC tumours hosts are also unclear. This 725 bp amplification within the 4,077 bp of intron 6 does not overlap with any intronic regulatory features according to the Ensembl VEP and is predicted to confer a Modifying impact only; elucidation of this CNV's effects would require analyses of *Tnfrsf8* gene and/or protein expression in GCs between SWR and Line 4-5 mice, with consideration of the temporally- and spatially-restricted, androgen-inducible GC tumour phenotype.

The wealth of data gathered to date suggests two genes as primary candidates for shared identity with *Gct1* (Section 2.1.2). *Tnfrsf1b* encodes a receptor for mTNF and usually initiates pro-survival signalling, whereas *Dhrs3* is induced by RA and its gene product reduces RAL to ROL. Given this evidence, the success of previous hormone intervention studies at puberty, and the availability of exogenous TNF, RAL and RA, we examined their effect over the short pubertal window of GC tumour susceptibility concurrently with the NGS and aCGH analyses. The TNFRSF1B ligand TNF was administered as a 10 µg/kg dose over a 14 d period via a micro-osmotic pump, whereas the DHRS3 substrate RAL was administered through three 50 mg/kg injections over a six day period and the *Dhrs3* inducer RA was administered as a 21 d release pellet. Ligand, substrate and inducer were administered to pubertal female mice with or without DHEA, and animals were necropsied at 8 wk of age to assess GC tumour incidence. A TNF ELISA confirmed that SWR females administered TNF had higher serum TNF levels on average compared to those females administered saline alone; testing for RA and its derivatives, which requires high-performance liquid chromatography, was not performed given our

uncertainties regarding toxicity and the induction of cell migration by RA pellets. These functional assays were generally not conducted with sample sizes large enough to find statistically significant differences in GC tumour frequencies between treatment cohorts, or between treatment cohorts and previously reported GC tumour frequencies. Instead, we assessed the potential of a molecule to induce GC tumours in SWR females in the absence of DHEA, or in GC tumour-resistant Line 4-5 mice with or without exogenous androgen administration, using SWR females administered DHEA as a comparator.

SWR females administered TNF with DHEA developed GC tumours at a similar frequency (26.3%; Table 2.14) to that previously observed following exogenous DHEA treatment (Smith 2011), indicating that TNF treatment permits the expected GC tumour phenotype when administered with DHEA at puberty. However, TNF alone was not capable of inducing GC tumours in SWR females without DHEA, nor was it capable of inducing GC tumours in normally resistant Line 4-5 pubertal mice with or without exogenous androgens. This data suggests that that the 10 μg/kg/d dose of recombinant mouse TNF over the pubertal period has no major influence on GC tumour initiation in the SWR mouse model. While both mTNF and sTNF are biologically active (Decoster *et al*. 1995), TNFRSF1B preferentially binds mTNF and induces cell survival (Grell *et al*. 1995). Therefore, the effects of exogenous, recombinant non-membrane-bound mouse TNF on GC tumourigenesis may have been underestimated in this experiment.

SWR females administered RAL with DHEA developed GC tumours at a frequency of 6.7% (Table 2.15). This GC tumour frequency is lower than that expected when DHEA is administered alone (Smith 2011). Our observations have shown that the spontaneous, pubertal GC tumour phenotype is sensitive to external stress, including excessive handling during the

pubertal period. As SWR mice given vehicle alone with DHEA also displayed a lower than expected GC tumour frequency of 5.6%, it appears that the decreased GC tumour frequency observed in females administered RAL with DHEA is due to the three dose injection scheme and/or the 95% ethanol vehicle, rather than the action of RAL itself. As was observed with TNF treatment, RAL alone was not capable of inducing GC tumours in SWR mice without DHEA, nor was it capable of inducing GC tumours in Line 4-5 pubertal mice with or without DHEA. DHRS3 catalyzes the reduction of RAL to ROL, thus reducing RA levels as part of a negative feedback loop (Figure 2.5; Haeseleer *et al*. 1998). While it is possible that an abundance of RAL (and/or subsequently high levels of RA) suppresses pubertal GC tumour initiation in SWR mice, these experimental questions could not be tested with the three dose injection/95% ethanol vehicle paradigm. An alternate administration method, such as intrabursal injection, could be employed to overcome the decreased GC tumour frequency attributed to the experimental paradigm.

RA was not capable of inducing GC tumours in SWR pubertal mice alone or in the presence of DHEA, albeit with small experimental samples sizes (Table 2.16). Due to resource limitations, Line 4-5 mice were not administered RA pellets. All females had a fatty mass with yellow deposits of RA and fibroblastic-like infiltrates at the site of RA pellet administration. This phenomenon has not been reported in the literature to our knowledge, and may be a phenotype unique to the SWR strain. As with RAL, intrabursal injection of RA might mitigate concerns regarding the method of RA administration. The lack of a GC tumour phenotype in SWR mice given RA and DHEA suggests that RA counteracts pubertal androgen-induced GC tumour initiation. Therefore, low levels RA may predispose SWR mice to GC tumour susceptibility. The mechanism by which RA could induce GC tumourigenesis is unclear. As RA induces *Dhrs3*

expression (Figure 2.5; Cerignoli *et al*. 2002; Zolfaghari, Chen & Ross 2012), it is plausible that SWR females possessing the c.460-3C>T *Dhrs3* variant produce too little of the normal *Dhrs3* transcript following RA stimulation during the critical GC tumour susceptibility window. *Dhrs3* induction by RA could also produce high levels of the aberrant *Dhrs3* splice variant lacking exon 4, which could be translated into DHRS3 protein incapable of reducing RAL or ROL or has a new or dominant negative function. Alternatively, the outcome of these splicing alterations on GC tumourigenesis could be due to a putative action of DHRS3 on steroid metabolism, as discussion in Section 2.4.4. Although inconclusive, these *in vivo* experiments suggest that retinoid homeostasis is precisely controlled and interference has consequences on GC tumour initiation. A survey of endogenous retinoid derivatives and *Dhrs3* mRNA and/or protein levels across space and time in the GC tumour-susceptible SWR ovary are warranted.

### 2.4.4 The *Gct1* Interval in Mouse and Human

The distal portion of mouse Chr 4 that houses *Gct1* is orthologous to human Chr 1p36.21-22, which has been implicated in a number of disorders through genome-wide association, cytogenetic, and aCGH studies (Figure 2.18). Chr 1p36 has been speculated to harbour a tumour suppressor gene for over four decades, following observations that it is frequently lost in a wide range of cancers (Bagchi & Mills 2008; Henrich, Schwab & Westermann 2012). Human Chr 1p36.22 is a susceptibility locus for hepatocellular carcinoma in patients infected with hepatitis B infection (Zhang *et al*. 2010), and for the pediatric bone and soft tissue cancer Ewing sarcoma (Postel-Vinay *et al*. 2012; Machiela *et al*. 2018). Deletions at human Chr 1p36.22 are a frequent and early event in human hepatocellular carcinoma (Nishimura *et al*. 2006; Midorikawa *et al*. 2009), and have been identified in infiltrating ductal carcinoma of the breast (Hawthorn *et al*.

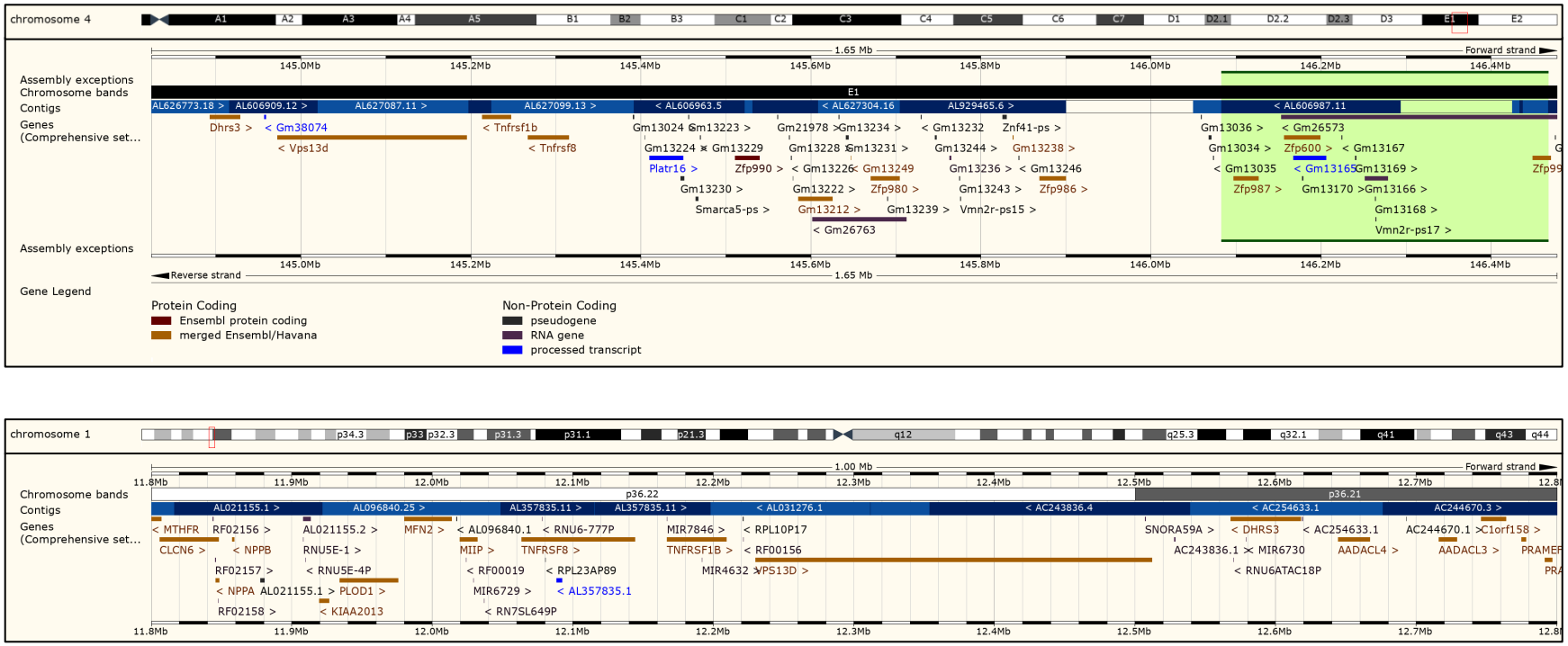


**Figure 2.18 Ensembl screenshot of the mouse *Gct1* interval and the orthologous human region Chr 1p36.21-22**

Top: mouse Chr 4 and the *Gct1* interval. Bottom: human Chr 1 and the *Gct1* orthologous region 1p36.21-22. All genetic determinants within the 1.65 Mb *Gct1* interval are shown, including protein and non-protein coding genes. Images from Ensembl release 95 (January 2019; Zerbino *et al*. 2018).

2010) and pre-menopausal breast cancers (Varma *et al*. 2005). Furthermore, *Gct1* is in close proximity to the mouse mammary tumour susceptibility 1 (*Mts1*) locus, which has shown a highly significant association with erb-b2 receptor tyrosine kinase 2 (*Erbb2*) transgene-driven mammary tumour appearance (Quan *et al*. 2012). Loss-of-heterozygosity at the Chr 1p36.2 region is often found in neuroblastoma and germ cell tumours (Ejeskär *et al*. 2001), and multiple putative tumour suppressor genes within the region, but outside *Gct1*, have been identified (Chen *et al*. 2003; Krona *et al*. 2004; Munirajan *et al*. 2008; Schlisio *et al*. 2008; Geli *et al*. 2010; Liu *et al*. 2011). Conversely, somatic amplification of Chr 1p36.22 has been identified in cervical cancer (Lee *et al*. 2014) and gastric adenocarcinoma (Liu *et al*. 2012).

In addition to its associations with malignancies described above, deletion or duplication of the Chr 1p36.21-22 region has also been identified in syndromic disorders. Chromosome 1p36 deletion syndrome (OMIM #607872) is the most common subtelomeric chromosomal deletion syndrome (Heilstedt *et al*. 2003) and is characterized by dysmorphic facial features, developmental delay/intellectual disability, muscular hypotonia, structural brain abnormalities, epilepsy and congenital heart defects, with sensorineural hearing loss, skeletal anomalies, precocious puberty and abnormalities of the external genitalia occurring in some patients (Battaglia *et al*. 2008). Although some discrete Chr 1p36 candidate loci have been associated with individual phenotypes of this syndrome (e.g. hearing loss [Wu *et al*. 1999], epilepsy [Heilstedt *et al*. 2001], and facial clefting [Colmenares *et al*. 2002]), other reports show no evidence of a genotype-phenotype correlation in which the deletion size or position correlates with the number or type of observed clinical features (Redon *et al*. 2005; Gajecka, Mackay & Shaffer 2007). Chromosome 1p36 deletion syndrome is twice as common in females as in males (Battaglia *et al*. 2008), and 60% of *de novo* Chr 1p36 deletions occur on the maternally-derived

chromosome (Wu *et al*. 1999). Although far rarer, trisomy for Chr 1p36.22 has been associated with achalasia (esophageal deformity) and epilepsy (Chen *et al*. 2006), and Chr 1p36.21-22 duplication or triplication causes Setleis syndrome (focal facial dermal dysplasia type III; OMIM #227260), a disorder characterized by dysmorphic facial features and bilateral scar-like lesions on the temples (Lee *et al*. 2015; Weaver *et al*. 2015). The identification of *Gct1* will allow for investigations of what role, if any, this GC tumour susceptibility gene might play in other diseases previously linked to Chr 1p36.21-22.

Of the 48 entities within the *Gct1* interval, only *Dhrs3*, *Vps13d*, *Tnfrsf1b*, and *Tnfrsf8* are conserved between mouse and human based on our current knowledge (Figure 2.18). As we anticipate that GC tumour susceptibility candidates identified in the SWR mouse model will translate to juvenile-onset GC tumours in young patients, these four genes have prioritized for further investigation. Previous qualitative expression analyses did not exclude any candidate genes from shared identity with *Gct1*, although *in silico* analysis determined that *Dhrs3* and *Tnfrsf1b* exhibit higher relative expression levels in the mouse ovary than in the testis (Section 2.1.2; Smith 2011); this skew in relative gonadal expression is intriguing given that male mice of the GC tumour susceptible SWR strain do not develop SCSTs at any age, and we speculate that the *Gct1* candidate gene either has ovary-specific functions and/or a GC-restricted expression pattern. *Dhrs3* and *Tnfrsf1b* were therefore of significant interest, given both their known functions and this suggestive expression pattern.

*Vps13d*

Vacuolar protein sorting 13D (*Vps13d*) is a large and complex 70 exon gene with multiple isoforms in both mouse and human. *In silico* analyses (Velayos-Baeza *et al*. 2004) have

determined that the VPS13D protein has two putative domains: a ubiquitin-associated domain (UBA), which confers protein target specificity in the ubiquitination pathway (Hofmann & Bucher 1996), and a ricin B lectin domain, which can bind simple sugars and is present in many proteins with carbohydrate-recognition abilities (Hazes 1996). The *Vps13d* gene encodes a protein belonging to the vacuolar protein sorting 13 (VPS13) gene family. In yeast, these proteins assist in membrane protein trafficking between the trans-Golgi network and the pre-vacuolar compartment (Brickner & Fuller 1997). The human VPS13 gene family has four members (*VPS13A* through *D*; Velayos-Baeza *et al*. 2004), although little is known about their function. Mutations in *VPS13A* cause choreoacanthocytosis (OMIM #200150), a rare, progressive neurodegenerative disorder that presents between the third and fifth decades of life (Rampoldi *et al*. 2001; Ueno *et al*. 2001). *VPS13B* is mutated in patients with Cohen syndrome (OMIM #216550), an uncommon, non-progressive psychomotor retardation disorder characterized by microcephaly, retinal dystrophy and distinctive facial features (Kolehmainen *et al*. 2003). Loss-of-function mutations in *VPS13C* have been associated with autosomal recessive early-onset Parkinson disease (OMIM #616840), a rare form of hereditary Parkinson disease with mitochondrial dysregulation (Lesage *et al*. 2016). Finally, deleterious compound heterozygous *VPS13D* mutations have recently been identified in patients with spinocerebellar ataxia, autosomal recessive 4 (SCAR4; OMIM #607317; Gauthier *et al*. 2018; Seong *et al*. 2018). SCAR4 is a progressive movement disorder characterized by ataxia and spasticity with a variable age of onset. Fibroblasts from SCAR4 patients demonstrate defects in mitochondrial morphology and function (Seong *et al*. 2018). Recent analyses in *Drosophila* and human cells have determined that VPS13D is essential for mitophagy and mitochondrial size, and its UBA domain is required for this regulation (Anding *et al*. 2018). The known function of VPS13D and

its association with movement disorders, as well as a lack of deleterious variants, does not immediately highlight it as a likely candidate for *Gct1*.

*Tnfrsf8*

Tumor necrosis factor receptor superfamily, member 8 (*Tnfrsf8*) is a 13 exon gene that encodes the TNFRSF8 protein (also known as cluster of differentiation 30 [CD30]). Like *Tnfrsf1b*, *Tnfrsf8* encodes a transmembrane cell surface receptor and member of the TNF receptor superfamily. However, rather than binding TNF, TNFRSF8 binds tumor necrosis factor (ligand) superfamily, member 8 (TNFSF8; also known as cluster of differentiation 30 ligand [CD30L]). Physiologic TNFRSF8 expression is restricted to the cells of the immune system, particularly activated T and B cells (Kennedy, Willis & Armitage 2006). Downstream signalling from TNFRSF8 is mainly transduced through TRAF2 and related proteins, resulting in activation of the MAPK and NF-κB pathways (Horie *et al*. 1998; Zheng *et al*. 2003). The effects of TNFRSF8 signalling depend on the cellular and stimulatory context, with proliferative and pro-survival or anti-proliferative and apoptotic effects possible (Gruss *et al*. 1994; Mir *et al*. 2000). Serum levels of soluble TNFRSF8 are increased in patients with autoimmune diseases, chronic inflammatory disorders, and those infected with hepatitis B or C, Epstein-Barr virus, or human immunodeficiency virus. TNFRSF8 expression is also up-regulated in hematological malignancies such as Hodgkin's and non-Hodgkin's lymphomas (Oflazoglu, Grewal & Gerber 2009). TNFRSF8 is also expressed in embryonal carcinomas, but not seminomas, and is used in the differential diagnosis of these germ cell tumour subtypes (Leroy *et al*. 2002). The function of TNFRSF8 and its increased expression in some cancers enhances this gene's standing as an interesting *Gct1* candidate. Although the action of *Gct1* is confined to the ovarian GCs, it is

possible that aberrant *Tnfrsf8* GC expression or downstream signalling could result in malignancy; as such, the limited expression pattern of *Tnfrsf8* on activated immune cells cannot exclude it from the list of *Gct1* candidates. The presence of a CNV amplification within *Tnfrsf8* intron 6 that is predicted to confer only a modifying impact, and the absence of any other deleterious variants, decreases its ranking in the list of likely *Gct1* candidates.

*Tnfrsf1b*

The role of TNFRSF1B in the regulation of mouse follicle growth and its association with hyperandrogenism and PCOS in women (Section 2.1.2.1) made *Tnfrsf1b* a particularly interesting candidate for *Gct1*. Previous analyses revealed a unique SWR *Tnfrsf1b* 3′ UTR haplotype, which did not appear to impact *Tnfrsf1b* mRNA expression between DHEA-treated and untreated SWR pubertal whole ovary pools, or DHEA-treated SWR and Line 4-T pubertal whole ovary pools (Smith 2011). This novel haplotype may be responsible for the SWR strain's high susceptibility to pulmonary infection with *Mycobacterium tuberculosis* (Turner *et al*. 2003), as functional *TNFRSF1B* 3′ UTR haplotypes have been significantly associated with *M. tuberculosis* in human populations (Möller *et al*. 2010). No deleterious variants were identified in SWR mice by NGS or aCGH analyses in the current investigation; similarly, functional analysis using the TNFRFS1B ligand TNF did not reveal any influence on GC tumourigenesis in pubertal SWR or Line 4-5 mice. Future work to investigate the functional impact, if any, of the unique SWR *Tnfrsf1b* 3′ UTR haplotype in the GCs of the first follicle wave would be complementary to the methods undertaken to investigate *Tnfrsf1b* to date.

*Dhrs3*

The role of *Dhrs3* in the homeostasis of RA, which functions to initiate oocyte meiosis, and that it belongs to an enzymatic family involved in the catalysis of steroid hormone conversion (Section 2.1.2.2), increased the standing of *Dhrs3* as a potential candidate for *Gct1*. We identified a highly pathogenic 3′ acceptor splice site variant in intron 3 of *Dhrs3* that would likely result in exclusion of exon 4. However, RT-PCR analyses revealed no difference between *Dhrs3* transcripts in ovary pools prepared from untreated, pubertal SWR and Line 4-5 mice, although this analysis did not account for GC-specific, temporal, and/or endocrine influences on *Dhrs3* splicing. Functional analyses of DHRS3 *in vivo* resulted in a decrease in the expected GC tumour frequency following administration of exogenous RA, whereas the effects of exogenous RAL could not be confidently examined due to the effect of the administration paradigm on the GC tumour phenotype. Although DHRS3 is required for the precise control of embryonic RA levels (Billings et *al*. 2013; Wang *et al*. 2018), it is not yet known if this enzyme metabolizes retinoids in the ovary and/or plays a role in RA-induced oocyte meiosis. Similarly, it is not yet known if DHRS3 exhibits steroid redox activity in the mouse ovary, as has been shown towards $E_1$, $A_4$ and T *in vitro* (Lundova *et al*. 2015). We propose that the c.460-3C>T *Dhrs3* variant leads to a quantitative and/or qualitative change in functional *Dhrs3* transcript expression that widens the threshold for GC tumour initiation due to either an imbalance in follicular RA regulation or steroid metabolism. Elucidation of the factors governing the endocrine induction of GC tumourigenesis and the susceptible cell population will allow the rigorous testing of these hypotheses and further interrogations of the role of *Dhrs3*.

*Other Gct1 Candidates and Considerations*

Although our investigations into the identity of *Gct1* to date have focused on the protein coding genes with human orthologues, we have not discounted the possibility that another *Gct1* determinant is responsible for initiating GC tumours in SWR mice. For example, one of the seven protein coding genes within *Gct1* without a described function may be responsible for establishing tumour susceptibility through a yet to be determined mechanism. Alternatively, the highly repetitive distal end of the interval could be acting as a cassette to induce GC tumours at puberty through an unknown mechanism. Similarly, an element in *Gct1* (e.g. a long intergenic non-coding RNA [lncRNA]) might be acting in *cis* on *Wnt4* and/or *Rspo1*, which map outside of *Gct1* but are located within approximately 7.5 and 19.8 Mb proximally of the interval, respectively. The close proximity of these two genes to *Gct1* is curious given: 1) their role in female gonad differentiation (Chassot *et al*. 2008; Maatouk *et al*. 2008); 2) the complementary role of *Wnt4* and *Rspo1* with that of *Foxl2* during ovary development (Ottolenghi *et al*. 2007; Auguste *et al*. 2011); 3) that *Foxl2* assumes antagonism of the male pathway driver *Sox9* from *Wnt4* and *Rspo1* postnatally (Uhlenhaut *et al*. 2009); 4) the association between the somatic p.Cys134Trp *FOXL2* mutation and adult-onset human GC tumours (Shah *et al*. 2009); and 5) the overexpression of *Rspo1* in mouse stromal cells results in GC tumour initiation within 1 mo of age (De Cian *et al*. 2017; Table 1.1). lncRNAs are non-coding RNAs longer than 200 nucleotides that do not overlap annotated coding genes, and function to regulate gene transcription through chromatin modulation and other mechanisms (Ransohoff, Wei & Khavari 2018). lncRNA-mediated regulation of androgen-induced AR signalling and subsequent tumour growth has been demonstrated previously (Yang *et al*. 2013). The 1.65 Mb *Gct1* interval houses four lncRNAs (*Gm26763*, *Gm13236*, *Gm26573* and *Gm13166*; Table 2.6), which do not have known functions

or human orthologues. Although 10 variants were identified within *Gm26763* by NGS (Table 2.7), none were pursued for empirical validation or functional impact at this time.

The influence of DHEA on GC tumourigenesis in SWR mice is particularly intriguing. Subcutaneous injections of 60 mg/kg DHEA to pubertal mice for 20 consecutive d is an established protocol for PCOS initiation in the mouse, and results in acyclicity, anovulation, hyperandrogenism and metabolic symptoms with strain-dependent effects that suggest genetic influences (Luchetti *et al*. 2004; Sander *et al*. 2006; Elia *et al*. 2009; Zhu *et al*. 2010; Dowling *et al*. 2013; Lai *et al*. 2014). Our research has shown that SWR mice have a unique *Gct1* allele that responds to DHEA by initiating GC tumourigenesis. The SWR mouse model of ovarian GC tumours has numerous parallels with human PCOS: 1) the phenotype is dependent on LH or androgen stimulation (Waldstreicher *et al*. 1988; Beamer, Shultz & Tennent 1988; Tennent, Shultz & Beamer 1993; Dorward, Shultz & Beamer 2007); 2) the phenotype is restricted to a developmentally sensitive window during the pubertal transition (Tennent *et al*. 1990; Beamer *et al*. 1993; Franks 2002); 3) the phenotype is polygenic (Beamer *et al*. 1988; Beamer *et al*. 1998; Dorward *et al*. 2003; Dorward *et al*. 2005; Dorward *et al*. 2013; Welt & Duran 2014); and 4) the phenotype is specifically linked to ovarian cells (Beamer *et al*. 1993; Franks, McCarthy & Hardy 2006). In humans, circulatory levels of DHEA are high at birth and reach maximal levels between the ages of 20 to 30 yr (Rutkowski *et al*. 2014), a period that overlaps with juvenile GC tumour onset. No specific nuclear receptor for DHEA has been identified, although the effects of DHEA may be mediated by the AR or ESR1/ESR2 depending on cellular context (Webb *et al*. 2006; Engdahl *et al*. 2014). The Chr 1p36.22 locus has been significantly associated with levels of DHEA fatty acid esters in human populations (An *et al*. 2001), further supporting our hypothesis that an element within *Gct1* is involved in DHEA metabolism. Additionally, Chr

1p36.22 has been linked to early-onset androgenetic alopecia (commonly known as male-pattern baldness), a multifactorial disorder likely caused by interactions among several genes and environmental influences (Li *et al*. 2012; Heilmann-Heimbach *et al*. 2017). Androgen metabolism is strongly associated with androgenetic alopecia; accordingly, the most robust genetic association between this disorder and any gene is with the AR, our foremost candidate for *Gct4* (Hillmer *et al*. 2005). As in our model of GC tumourigenesis, it appears that the Chr 1p36.22/*Gct1* locus and the AR are cooperating to promote androgen-regulated disease.

### 2.4.5 Summary

The SWR mouse model of GC tumourigenesis provides a unique opportunity to identify the oncogene driving this complex pediatric ovarian cancer subtype. Fine mapping using novel SNP-based genotyping markers has successfully resolved the *Gct1* interval to 1.65 Mb. This refined interval is relatively gene-rich, with 48 annotated genetic entities, although 30 are repetitive pseudogenes that have largely prevented resolution of the interval's distal boundary. We set out to fully genetically annotate the refined *Gct1* interval using NGS and aCGH analyses in concert with *in vivo* functional investigations of prioritized gene candidates. We identified a novel 3′ acceptor splice site variant in *Dhrs3* (c.460-3C>T) that was predicted to be highly pathogenic and to confer a significant impact on normal *Dhrs3* transcript splicing, but which could not be confirmed using standard RT-PCR techniques. The low GC tumour phenotype penetrance in this mouse model, and the absence of an obvious phenotype in SWR males, suggests a unique, subtle mutation such as the c.460-3C>T *Dhrs3* variant that obstructs normal ovarian physiology, leading to stochastic tumourigenesis in only a fraction of susceptible mice. *Dhrs3* remains the highest priority candidate for *Gct1*, and future strategies to resolve *Gct1*

identity will incorporate the influence of cellular compartment, developmental timing, and endocrine stimulation on *Dhrs3* function.

# 3. Deletion of the Androgen Receptor from Ovarian Granulosa Cells

## 3.1 Introduction

The trait of spontaneous, juvenile-type ovarian GC tumour appearance in SWR mice is polygenic, with multiple loci on the autosomes and the X Chr that act in the presence of *Gct1*$^{SW}$ alleles to influence tumour frequency (Table 1.2). Phenotypic mapping capitalizing on a paternal parent-of-origin effect has refined *Gct4* to a 1.345 Mb interval and a short-list of candidate genes inclusive of the Ar (Table 3.1; Beamer *et al*. 1998; Dorward *et al*. 2003; Dorward *et al*. 2013). The endocrine-sensitivity of the GC tumour phenotype combined with evidence from genetic mapping and gene expression analyses strongly implicates the *Ar* for shared identity with *Gct4*. Experiments using *in vitro* and *in vivo* models have investigated the AR's role in the ovary and shown that AR-mediated signalling is required for optimal ovarian function.

### 3.1.1 The Androgen Receptor

#### 3.1.1.1 Androgen Receptor Signalling

The effects of androgens are primarily mediated through the AR, a steroid hormone receptor and member of the nuclear receptor superfamily of transcription factors (Evans 1988). The AR protein is encoded by the *AR* gene, which is located on the X chromosome and is therefore present in two copies in females and one copy in males (Migeon *et al*. 1981; Lubahn *et al*. 1988). The mouse *Ar* and human *AR* genes are composed of eight exons which are translated into four distinct functional domains: an N-terminal transactivation domain (NTD); a highly conserved DNA-binding domain (DBD); a small hinge region, which contains the majority of a

**Table 3.1 Summary of the genetic determinants within the 1.345 Mb *Gct4* interval.** Gene name, location on Chr X, strand, gene type, and the number of unique transcripts per gene are shown. Data is from Ensembl release 95 (January 2019; Zerbino *et al*. 2018). *Stard8* is bisected by SSLP marker *DXamd27*. MR: microRNA; PC: protein coding; SR: small nuclear RNA; +: forward; -: reverse

| Gene | Official Name | Location on Chr X (bp) | Strand | Gene Type | Unique Transcripts |
|---|---|---|---|---|---|
| *Ar* | androgen receptor | 98,148,769 | + | PC | 1 |
| *Ophn1* | oligophrenin 1 | 98,554,277 | - | PC | 10 |
| *Gm27554* | predicted gene, 27554 | 98,727,315 | - | MR | 1 |
| *Gm26000* | predicted gene, 26000 | 98,814,775 | + | SR | 1 |
| *Yipf6* | Yip1 domain family member 6 | 98,936,316 | + | PC | 6 |
| *Stard8* | StAR related lipid transfer domain containing 8 | 99,003,248 | + | PC | 4 |

nuclear localization signal (NLS); and a C-terminal ligand-binding domain (LBD; (Figure 3.1; MacLean, Warne & Zajac 1997). In the absence of androgenic stimuli, the AR protein is sequestered in the cytoplasm in an inactive complex composed of heat shock proteins (HSPs), cytoskeletal proteins, and other molecular chaperones. Androgen binding at the LBD results in a conformational change that enables the dissociation of HSPs, exposure of the NLS, and subsequent translocation of androgen-activated AR into the nucleus. Nuclear AR homodimerizes, and two ZNF domains within the DBD facilitate DNA binding of dimerized AR at androgen response elements (AREs) in the promoters and enhancers of AR-regulated genes. The binding of AR at AREs triggers the recruitment of transcriptional co-regulators, including co-activators capable of influencing chromatin remodelling, as well as other transcription factors and components of the general transcription machinery. Non-ligand bound AR is shuttled back to the cytoplasm in a process mediated by the nuclear export signal (NES) within the LBD, or is ubiquitinated in preparation for proteosomal degradation. This classical genomic AR signalling pathway, so named because it involves gene transcription, results in the transcription of androgen-dependent genes with roles in proliferation, differentiation, and apoptosis (Figure 3.2; Bennett *et al*. 2010). Androgens and the AR are also capable of mediating non-classical actions independent of gene transcription that occur within moments after ligand binding. These non-genomic mechanisms occur at the plasma membrane or within the cytoplasm, and mainly involve increases in intracellular calcium concentrations and the activation of other second messenger pathways (Davey & Grossmann 2016). The classical genomic pathway of AR signalling is the most well-characterized, but an increasing body of evidence indicates that non-genomic AR signalling in involved in both normal development and disease processes.

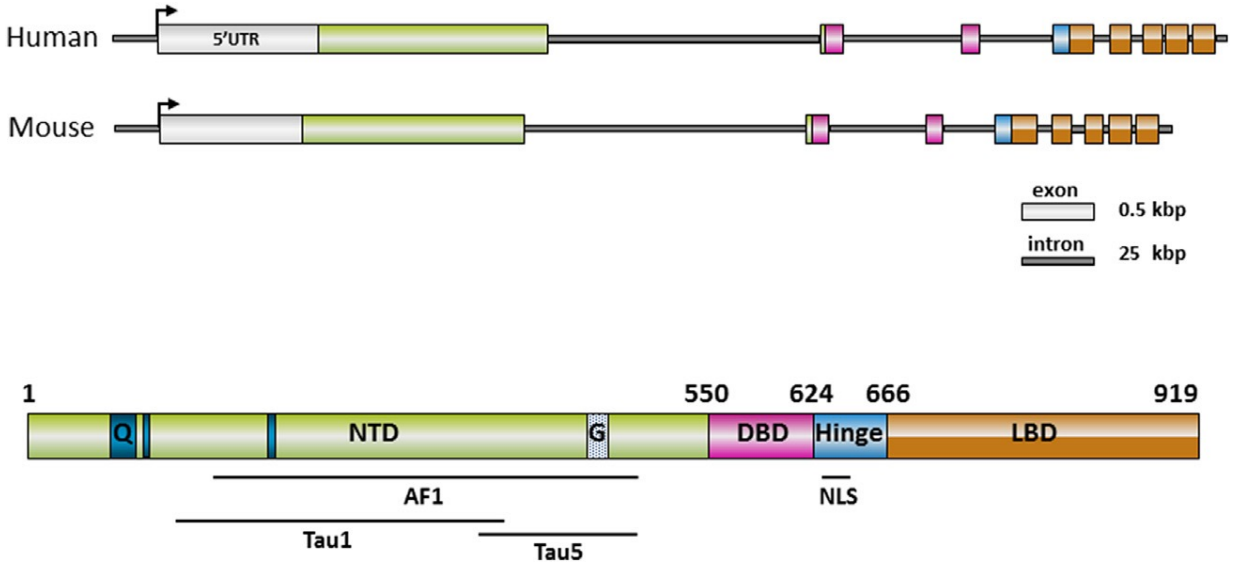


**Figure 3.1 AR gene and protein structure**

The AR is located on the X Chr. Exon 1 codes for the NTD, which contains the transcriptional activation function 1 (AF-1) domain composed of the transcriptional activation units 1 (TAU-1) and TAU-5. Exons 2 and 3 encode the first and second ZNFs of the DBD, respectively, which facilitate binding of ligand-bound AR at AREs. Exons 4 through 8 code for the hinge region, which contains the majority of an NLS, and the LBD, which contains the NES and the transcriptional activation function 2 (AF-2) domain (not shown). Reprinted in adapted form with permission from Elsevier, from Molecular and Cellular Endocrinology, Vol 465, Hunter *et al*., Tissue control of androgen action: the ups and downs of androgen receptor expression, p. 27-35, copyright 2018; permission conveyed through Copyright Clearance Center, Inc.

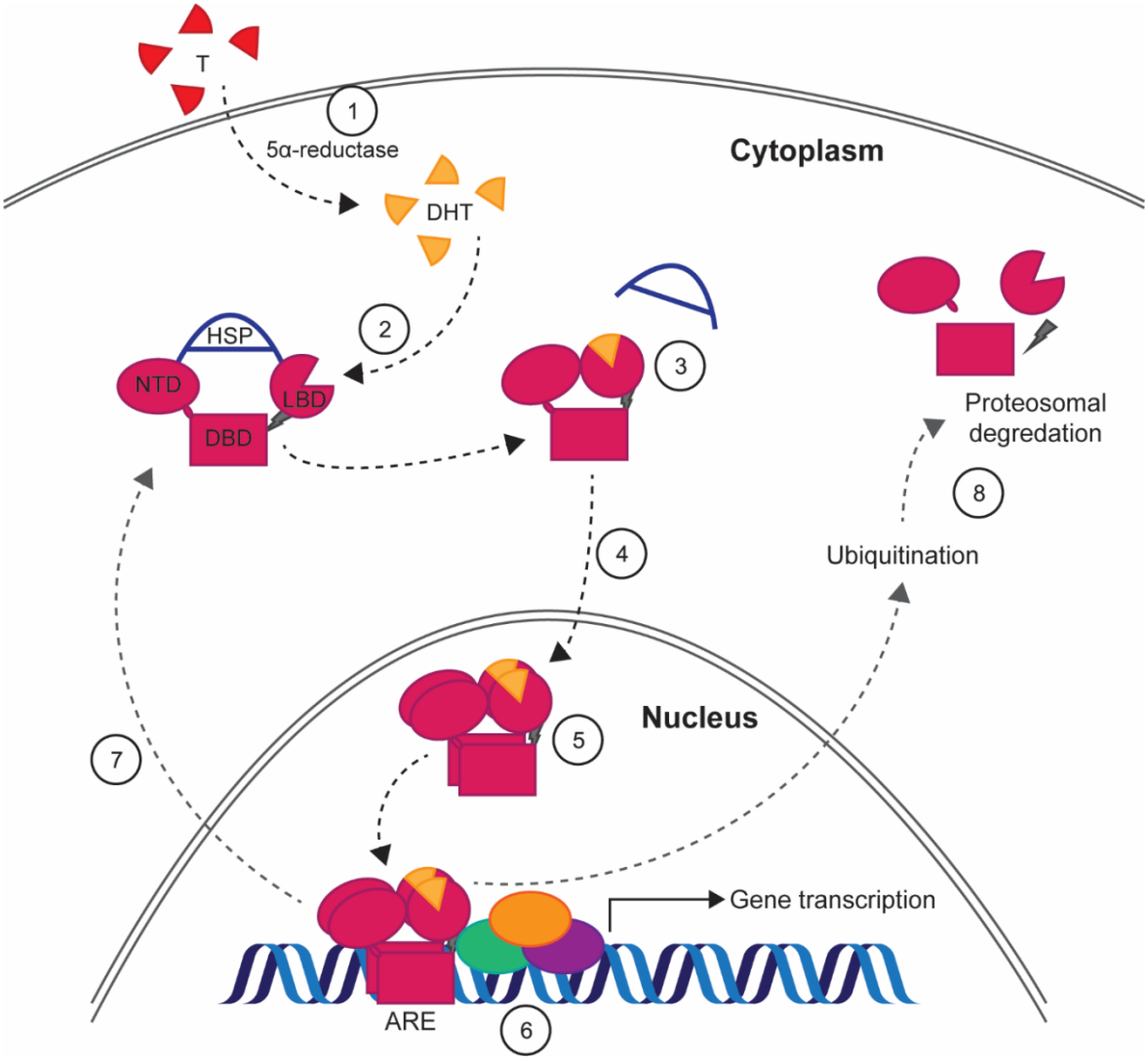


**Figure 3.2 The classical AR signalling pathway**

(1) T is converted to the more potent AR ligand DHT by 5α-reductase, which is bound by the AR (2). Ligand binding induces an AR conformational change that causes HSP dissociation (3), exposing the NLS and allowing the AR to more into the nucleus (4). Nuclear AR dimerizes (5), and AR dimers bind to AREs via the DBD and recruit transcriptional co-regulators (green), other transcription factors (purple) and components of the general transcription machinery (orange), which together promote gene transcription (6). Non-ligand bound AR is shuttled back to the cytoplasm (7), or is ubiquitinated in preparation for proteosomal degradation (8). Adapted with permission from Elsevier, from The International Journal of Biochemistry & Cell Biology, Vol 42, Bennett *et al*., Molecular cell biology of androgen receptor signalling, p. 813-827, copyright 2010; permission conveyed through Copyright Clearance Centre, Inc.

#### 3.1.1.2 Androgen Receptor Ligands

The AR directly binds and is activated by T and its non-aromatizable metabolite DHT. These steroid hormones are transported to target tissues through the bloodstream, where the majority are bound by the liver-derived proteins sex hormone binding globulin or serum albumin (Siiteri *et al*. 1982). T and DHT diffuse into target cells following dissociation from these carrier proteins and bind to the LBD of the AR with differential affinities. DHT is the most potent endogenous AR ligand, with an AR binding affinity twice that of T (Grino, Griffin & Wilson 1990). A number of androgen precursors, including $A_4$, DHEA and sulfonated DHEA (DHEA-S), are present within the circulation in addition to T and DHT. These pro-androgens require conversion to T and/or DHT in peripheral tissues to exert androgenic effects, but are present in much higher serum concentrations in both males and females (Labrie *et al*. 2005). In men, androgens are predominantly produced by the testes in the form of T, whereas in women, DHEA, DHEA-S, $A_4$ and T derive from the ovaries and adrenal glands (Burger 2002).

### 3.1.2 The Role of the Androgen Receptor in Ovarian Function

The roles of androgens in normal male physiology (e.g. phenotype development and maintenance, reproduction) and abnormal pathologies (e.g. androgen insensitivity syndrome, prostate cancer) have been well characterized. However, apart from the requirement of T for $E_2$ synthesis (Hillier, Whitelaw & Smyth 1994), much less is known about the role of androgens and AR-mediated actions in females. Evidence suggesting a role for androgens in the regulation of follicle development has been demonstrated by hyperandrogenic clinical pathologies such as PCOS (Rosenfield & Ehrmann 2016), and by the observation that androgenic stimuli prior to *in vitro* fertilization can increase the ovarian response to gonadotropins (Kim 2013). Our current

knowledge of the role of androgens in the female ovary has been expanded by *in vivo* and *in vitro* examinations using exogenous androgens and AR antagonists, and from global and cell-specific *Ar* KO (ArKO) mouse models. The accumulation of evidence has increasingly pointed to AR-mediated androgen signalling as integral to optimal ovarian function.

#### 3.1.2.1 Androgen Receptor Expression and Function throughout Folliculogenesis

The AR is expressed in all three components of the HPG axis. In the brain, AR is expressed in the gonadotrope cells of the anterior pituitary (Pelletier 2000) and multiple regions of the hypothalamus (Bakker *et al*. 1997). AR expression is present at most follicular stages in the ovary, and exhibits a distinct spatial and temporal pattern throughout folliculogenesis (Figure 3.3). This differential expression pattern reflects the specific action of AR-mediated androgens at discrete time points during follicle development.

The AR is expressed in the developing ovary of sheep (Juengel *et al*. 2006), pig (Burek *et al*. 2007) and human fetuses (Wilson & McPhaul 1996; Fowler *et al*. 2011). Human ovarian AR expression is detectable in the second trimester and is specific to the nuclei of somatic cells surrounding germ cell cysts. This expression increases throughout gestation, with the highest levels correlating with the beginning of primordial follicle formation at 17-20 wk. While these follicles express the steroidogenic enzymes necessary to synthesize androgens, the relevance of this ability in the fetal ovary remains unknown (Fowler *et al*. 2011). *In utero* inhibition of AR-mediated signalling by the AR antagonist flutamide has been shown to delay the formation of primordial follicles when administered during gestation in pigs (Knapczyk-Stwora *et al*. 2013a), possibly due to the alteration of steroidogenic enzyme expression and other factors affecting follicle formation (Knapczyk-Stwora *et al*. 2015). This evidence indicates that prenatal ovarian

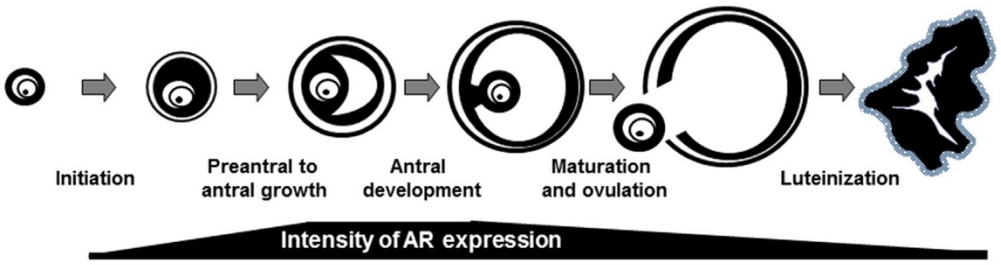


**Figure 3.3 Ovarian AR expression through folliculogenesis**

Ovarian AR expression can be detected as follicles enter the growing pool and persists throughout folliculogenesis. The AR is expressed as a gradient that increases to the antral stage and then progressively declines in the outer mural GC of antral follicles, but remains intense in the cumulus cells that surround the oocyte. Reprinted in adapted form with permission from Elsevier, from Molecular and Cellular Endocrinology, Vol 465, Walters & Handelsman, Role of androgens in the ovary, p. 36-47, copyright 2018; permission conveyed through Copyright Clearance Centre, Inc.

androgen signalling may be an important regulator of primordial follicle formation and consequently normal reproductive function into adulthood.

AR expression has not typically been detected in the primordial follicles of the postnatal mammalian ovary (Szoltys & Slomczyńska 2000; Hampton *et al*. 2004; Juengel *et al*. 2006; Hild-Petito *et al*. 1991; Rice *et al*. 2007; Suzuki *et al*. 1994; Horie *et al*. 1992). Nevertheless, androgens have been shown to stimulate the initiation of resting primordial follicles into the growing follicle pool (Vendola *et al*. 1999; Yang *et al*. 2010; Knapczyk-Stwora *et al*. 2013b; Magamage *et al*. 2010; Narkwichean *et al*. 2014), despite the apparent absence of AR in some species. In primates, this androgen-induced, AR-independent recruitment may be due to the oocyte-specific upregulation of mRNAs encoding IGF1 and the insulin like growth factor receptor (IGF1R; Vendola *et al*. 1999). A recent report identified *AR* gene expression in the GCs of human primordial follicles, with the concomitant enrichment of downstream androgen-responsive transcripts as well as insulin-like growth factor family members (Steffensen *et al*. 2018). High levels of AR protein have been detected in mouse primordial follicle cells by immunohistochemistry (IHC; Yang *et al*. 2015) and immunofluorescence (Yang *et al*. 2010; Laird *et al*. 2017), indicating that AR expression in this follicle type may be species-specific. The effect of androgens on mouse primordial follicle initiation appears to be due to the rapid (i.e. non-genomic), AR-mediated activation of the PI3K/AKT/FOXO3 pathway in oocytes, as well as the down-regulation of oocyte-specific *Gdf9* (Yang *et al*. 2010).

The AR is expressed in the primary follicles of mouse (Cheng *et al*. 2002; Yang *et al*. 2015), rat (Szoltys & Slomczyńska 2000), bovine (Hampton *et al*. 2004; Salvetti *et al*. 2012), ovine (Juengel *et al*. 2006), and primate (Hild-Petito *et al*. 1991; Horie *et al*. 1992; Rice *et al*. 2007) ovaries, suggesting that AR expression increases and/or becomes detectable as follicles

enter the growing pool. T has been shown to stimulate the transition of bovine primary follicles to the secondary stage in a dose-dependent, AR-mediated manner (Yang & Fortune 2006). T administration also increases the expression of *FSHR* mRNA in the GCs of primate primary follicles. This is complimented by significant increases in *AR* mRNA following FSH treatment in the same cells (Weil *et al*. 1999). Although FSH is associated with follicle growth and anti-atretic actions, its potential role in primary follicles following androgen treatment is not readily clear, as folliculogenesis up to and including the formation of secondary follicles is thought to be largely independent of gonadotropin control. However, a number of studies have demonstrated responsiveness to FSH in so-called gonadotropin-independent follicle types when they are cultured *in vitro* (Hsueh *et al*. 2015).

AR expression is detectable in the GCs and TCs of pre-antral follicles in a number of mammalian species (Cheng *et al*. 2002; Yang *et al*. 2015; Laird *et al*. 2017; Szoltys & Slomczyńska 2000; Lenie & Smitz 2009; Hampton *et al*. 2004; Salvetti *et al*. 2012; Juengel *et al*. 2006; Slomczyńska, Duda & Ślęzk 2001; Slomczyńska & Tabarowski 2001; Hild-Petito *et al*. 1991; Hillier, Tetsuka & Fraser 1997; Weil *et al*. 1998; Rice *et al*. 2007), and ovarian AR expression reaches its peak in pre-antral and early antral follicles. Accordingly, a large body of evidence suggests that androgens enhance the pre-antral to antral stages of follicle growth in an AR-dependent manner. Androgens have been shown to increase the number of pre-antral and small antral follicles in primate ovaries (Vendola *et al*. 1998), and stimulate pre-antral follicle growth and antrum development in multiple species (Murray *et al*. 1998; Spears *et al*. 1998; Wang *et al*. 2001; Lenie & Smitz 2009; Tarumi *et al*. 2012; Narkwichean *et al*. 2014; Laird *et al*. 2017). Additionally, androgens are regulators of ovarian connexin gene expression (Wu *et al*. 2010; Knapczyk-Stwora, Grzesiak & Slomczynska 2013; Zhang *et al*. 2016) and can protect

follicles from atresia (Vendola *et al*. 1998). The stimulatory and anti-apoptotic actions of androgens in pre-antral follicles are likely due to increases in FSH responsiveness (Wang *et al*. 2001) through the up-regulation of FSHR mRNA (Weil *et al*. 1999; Laird *et al*. 2017) or protein (Sen *et al*. 2014). Androgen-induced AR may also amplify FSH action by increasing cAMP-mediated signalling downstream of the FSHR in GCs (Hillier & Tetsuka 1997). The protective mechanism of androgens is further potentiated by their role as a substrate for the follicle survival factor $E_2$. In the mouse ovary, androgens alone are incapable of promoting pre-antral follicle progression and are not required for FSH-induced follicle development; rather, they increase follicle sensitivity to FSH, resulting in a synergistic effect that optimizes pre-antral follicle growth and transition to the antral stage (Sen *et al*. 2014). However, studies of rodent pre-antral follicles have demonstrated that high levels of androgens impair oocyte maturation and follicular development (Pradeep *et al*. 2002; Romero & Smitz 2010; Tarumi *et al*. 2012) and can induce GC apoptosis (Billig, Furuta & Hsueh 1993), suggesting that a balance of ovarian androgens is key for optimal pre-antral follicle growth.

The AR is expressed at high levels in the antral and pre-ovulatory follicles of multiple species, with expression particularly strong in the GCs (Hild-Petito *et al*. 1991; Chadha *et al*. 1994; Suzuki *et al*. 1994; Hillier, Tetsuka & Fraser 1997; Weil *et al*. 1998; Szoltys & Slomczyńska 2000; Slomczyńska, Duda & Ślęzk 2001; Slomczyńska & Tabarowski 2001; Cheng *et al*. 2002; Hampton *et al*. 2004; Juengel *et al*. 2006; Catteau-Jonard *et al*. 2008; Nielsen *et al*. 2011; Salvetti *et al*. 2012), as well as in corpora lutea at variable levels (Duffy *et al*. 1999; Shiina *et al*. 2006; Yang *et al*. 2015). AR expression exhibits a unique intensity gradient pattern in rodent antral and pre-ovulatory follicles, characterized by weak expression in the outer mural GCs and strong expression in the cumulus GCs surrounding the oocyte (Szoltys & Slomczyńska

2000; Lenie & Smitz 2009). This gradient becomes more pronounced as the follicles develop, and may be regulated by oocyte-secreted factors (Lenie & Smitz 2009). The AR and androgens play a role in antral and pre-ovulatory follicle development, oocyte maturation and ovulation. Androgens have been found to increase the growth and number of pre-ovulatory follicles in pigs (Cardenas & Pope 1994; Cardenas, Herrick & Pope 2002; Hickey *et al*. 2004) but not primates (Vendola *et al*. 1998), indicating a species-specific action. This androgen-induced proliferation is again likely due to the upregulation of FSHR and therefore increased sensitivity to FSH (Cardenas, Herrick & Pope 2002; Hickey *et al*. 2004). Conversely, androgens can promote atresia of mature antral follicles that have not been selected for ovulatory dominance, thus ensuring the ovulation of single oocytes in mono-ovulatory species (Franks & Hardy 2018). Anti-androgen treatments result in the inhibition of ovulation (Mori *et al*. 1977; Kumari, Datta & Roy 1978), whereas optimal levels of androgens have been shown to improve the ovulatory response to superovulatory conditions (Ware 1982; Sen *et al*. 2014). The effects of androgens on ovulation may be due to the AR-mediated up-regulation of ovulatory marker genes such as *Ptgs2* and *Areg*, as shown in the GCs of rodent peri-ovulatory follicles (Yazawa *et al*. 2013). The AR and androgens also affect oocyte maturation, as androgens are capable of promoting GVBD in mice (Gill, Jamnongjit & Hammes 2004), primates (Borman *et al*. 2004) and pigs (Li *et al*. 2008b), possibly through non-genomic mechanisms (Gill, Jamnongjit & Hammes 2004). Again, elevated levels of androgens were found to reduce mouse oocyte meiotic competence (Romero & Smitz 2010), indicating that a balance of ovarian androgen action is key to optimal ovulation levels.

### 3.1.2.2 Androgen Receptor Knockout Mouse Models

The first mouse models used to examine phenotypes in the absence of *Ar* were derived from mice harbouring the spontaneous testicular feminization mutation (*Tfm*) and which mimicked complete androgen insensitivity syndrome (CAIS) in humans (Lyon & Hawkes 1970). However, the production of *Ar*-null females was complicated by the sterility of *Tfm* males due to hemizygous inactivating mutations in *Ar*. The Cre/*loxP* system has been employed to produce engineered mouse models to examine the effects of *Ar* deletion on a global scale, which recapitulate CAIS models characterized before Cre/*loxP* technology, as well as in specific cell subtypes. Three different global ArKO mouse models have been created with targeted deletions of exon 1 ($ArKO^{Ex1}$; Shiina *et al*. 2006), exon 2 ($ArKO^{Ex2}$; Yeh *et al*. 2002; Hu *et al*. 2004) or exon 3 ($ArKO^{Ex3}$; Walters *et al*. 2007). Ovarian cell-specific ArKO models include the GC-restricted deletion of *Ar* exon 2 (GC-$ArKO^{Ex2}$; Sen & Hammes 2010) or exon 3 (GC-$ArKO^{Ex3}$; Walters *et al*. 2012), as well as deletions in TCs (TC-ArKO; Ma *et al*. 2017) and oocytes (Oo-ArKO; Sen & Hammes 2010). These models have significantly increased our understanding of intra- and extra-ovarian AR-mediated actions. The genotypic and phenotypic features of these seven ArKO mouse models are summarized in Table 3.2.

*Global Androgen Receptor Knockout Mouse Models*

The definitive feature of all three global ArKO mouse models is subfertility, with some phenotypic differences that have been attributed to the nature of the individual deletion constructs (Yeh *et al*. 2002; Hu *et al*. 2004; Shiina *et al*. 2006; Walters *et al*. 2007). The complete excision of exon 1 in the $ArKO^{Ex1}$ mouse model results in the insertion of a premature

**Table 3.2 Summary of global and ovarian cell-specific ArKO mouse models.** Adapted from Walters & Handelsman 2018.

Genotype and phenotype data for seven ArKO mouse models are shown. NC: no change; -: not examined; ↑: increased; ↓: decreased

| | ArKO$^{Ex1}$ | ArKO$^{Ex2}$ | ArKO$^{Ex3}$ | GC-ArKO$^{Ex2}$ | GC-ArKO$^{Ex3}$ | TC-ArKO$^{Ex2}$ | Oo-ArKO$^{Ex2}$ |
|---|---|---|---|---|---|---|---|
| Genotype data | | | | | | | |
| Excised exon | 1 | 2 | 3 | 2 | 3 | 2 | 2 |
| cre driver | *CMV-cre* | *ACTB-cre* | *CMV/Sox2-cre* | *Amhr2-cre* | *Amh-cre* | *Cyp17a1-cre* | *Gdf9-cre* |
| Strain background | B6J/CD-1 | B6J/129/SVE | B6J | B6J | B6J | B6J/CD-1/129Sv | B6J |
| Mutant *Ar* retained? | No | No | Yes | No | Yes | No | No |
| Phenotype data | | | | | | | |
| Fertility | ↓ pups/litter | ↓ pups/litter | ↓ pups/litter | ↓ pups/litter | ↓ pups/litter at 6 mo | Normal | Normal |
| Follicle populations | ↓ corpora lutea; POF by 40 wk | ↓ corpora lutea; POF by 5-6 mo | ↓ pre-ovulatory follicles and corpora lutea; no POF | ↓ antral follicles and corpora lutea at 2 and 6 mo | ↓ large pre-antral and small antral follicles at 3 mo | Normal | Normal |
| Follicle health | ↑ atretic follicles | ↓ GC thickness in antral follicles; dissociation of cumulus cells from oocyte | ↑ unhealthy follicles | ↑ atretic follicles at 2 and 6 mo | ↑ atretic and unhealthy follicles at 6 mo | - | ↓ androgen-induced GVBD |
| Ovulation | - | ↓ superovulated oocytes | ↓ naturally ovulated oocytes | ↓ naturally ovulated oocytes | ↓ cumulus expansion | - | - |
| Fertilization rate | - | - | Normal | - | ↓ | - | - |
| Gene expression | ↓ *Kitl*, *Bmp15*, *Gdf9* at pro-estrus | ↓ *Fshr*, *Igf1r* at 10 d; ↓ *Has2*, *Pgr*, *Tnfaip6* after hyperstimulation | ↓ *Cyp19a1* at estrus | - | NC | NC | - |
| Hormones and steroids | NC | - | ↓ LH, $E_2$ and $E_1$ at proestrus | - | NC | Normal | - |
| Estrus cycle length | - | ↑ | ↑ | ↑ at 6 mo | ↑ at 6 mo | Normal | Normal |

termination codon resulting in the loss of the majority of the *Ar* transcript and subsequently all AR signalling and interactions (Kato 2002). The ArKO$^{Ex2}$ mouse model was generated by complete excision of exon 2, which encodes the first ZNF domain of the DBD. The resulting frameshift inserts a premature termination codon within exon 3 that, as in ArKO$^{Ex1}$, results in a null *Ar* allele (Yeh *et al*. 2002). This exon excision replicates a spontaneous mutation found in the human population (Hellwinkel *et al*. 1999) and in mice (He, Kumar & Tindall 1991) that has been shown to cause CAIS. The ArKO$^{Ex3}$ mouse model was generated through an in-frame deletion of exon 3, which encodes the AR's second ZNF (Notini *et al*. 2005). This construct maintains a truncated mutant AR protein that is incapable of mediating genomic actions dependent on DNA binding, but retains non-classical signalling abilities and the capacity to bind ligand, co-regulators, and other transcription factors (Pang *et al*. 2012; Rana, Davey & Zajac 2014). As is the case with deletion of exon 2 in the ArKO$^{Ex2}$ model, loss of exon 3 has been associated with CAIS in humans (Quigley *et al*. 1992). The excision of these exons by Cre-mediated recombination was driven by the human cytomegalovirus (CMV) minimal promoter (*CMV-cre*) in the ArKO$^{Ex1}$ model (Schwenk, Baron & Rajewsky 1995), by the human actin beta (*ACTB*) housekeeping gene promoter (*ACTB-cre*) in the ArKO$^{Ex2}$ model (Lewandoski, Meyers & Martin 1997), and by the *CMV-cre* or *Sox2* transcription factor promoter (*Sox2-cre*) in the ArKO$^{Ex3}$ model (Hayashi *et al*. 2002b). The *CMV*-, *ACTB*- and *Sox2-cre* constructs are ubiquitously expressed and are active from the earliest stages of embryogenesis. Phenotypic differences between global ArKO models may also be due in part to strain-specific influences; the ArKO$^{Ex1}$, ArKO$^{Ex2}$, and ArKO$^{Ex3}$ models were generated and maintained on mixed B6J and CD-1, mixed B6J and 129/SVE, and B6J genetic backgrounds, respectively (Kato 2002; Yeh *et al*. 2002; Notini *et al*. 2005).

The subfertility observed in global ArKO female mice is characterized by fewer pups per litter and is primarily due to dysfunctions in late follicular dynamics and ovulation. Follicular atresia is significantly increased in all global ArKO mouse models (Yeh *et a*l. 2002; Hu *et al*. 2004; Shiina *et al*. 2006; Walters *et al*. 2007). Poor follicle health is observed in the ArKO$^{Ex3}$ model, as characterized by pyknotic GC nuclei, impaired antrum development, and oocyte degeneration (Walters *et al*. 2007; Cheng *et al*. 2013), and by a reduction in the thickness of antral follicle GC layers in ArKO$^{Ex2}$ mice (Hu *et al*. 2004). The number of pre-ovulatory follicles in ArKO$^{Ex3}$ mouse ovaries are significantly reduced (Cheng *et al*. 2013) and all three global ArKO models show reductions in the number of corpora lutea, suggesting reduced ovulation rates (Hu *et al*. 2004; Shiina *et al*. 2006; Walters *et al*. 2007; Cheng *et al*. 2013). Oocytes within pre-ovulatory follicles found in ArKO$^{Ex2}$ ovaries lose contact with the surrounding cumulus cells during ovulation, and the expression of genes required for normal cumulus expansion, such as of *Has2* and *Tnfaip6*, is significantly reduced following hyperstimulation of the ovary with pregnant mare serum gonadotropin (PMSG) and hCG (Hu *et al*. 2004). These oocytes were found to have a significantly poor maturation rate, and their associated GCs demonstrated impaired differentiation and defective mitochondrial adenosine triphosphate production and biogenesis, due to decreases in the expression of peroxisome proliferative activated receptor, gamma, co-activator 1 beta (*Ppargc1b*; Wang *et al*. 2015c). ArKO$^{Ex2}$ mouse ovaries also down-regulate the expression of the progesterone receptor (*Pgr*) following ovary hyperstimulation, which may lead to GC apoptosis in pre-ovulatory follicles during GC luteinisation (Hu *et al*. 2004). Other key folliculogenesis regulatory genes are down-regulated in global ArKO mice, such as *Fshr* and *Igf1r* in the ArKO$^{Ex2}$ model (Hu *et al*. 2004), *Kitlg*, *Bmp15*, and *Gfd9* in ArKO$^{Ex1}$ mice at pro-estrus (Shiina *et al*. 2006), and *Cyp19a1* in the ArKO$^{Ex3}$ model at estrus

(Walters *et al*. 2007). Notably, no disassociation of cumulus cells from pre-ovulatory follicle oocytes occurs in ArKO$^{Ex3}$ ovaries, which retain a mutant AR protein with non-genomic signalling ability (Walters, Allen & Handelsman 2008). Furthermore, oocytes appear to be unaffected in this model, as embryo quality and fertilization rates are unchanged and normal embryonic development occurs up to the two-cell blastocyst stage (Walters *et al*. 2007; Cheng *et al*. 2013). These observations are particularly interesting given the known role of T in the induction of GVBD oocytes *in vitro* (Gill, Jamnongjit & Hammes 2004; Li *et al*. 2008b), which has been shown to be due to transcription-independent AR signalling in the mouse (Gill, Jamnongjit & Hammes 2004). The three global ArKO models also show construct-related variation in the reproductive lifespans of homozygous *Ar*-null females. ArKO$^{Ex1}$ and ArKO$^{Ex2}$ mice initially exhibit normal follicle numbers, but rapid depletion of the follicle pool eventually leads to the development of a POF phenotype that causes infertility by 40 wk and 5-6 mo of age, respectively (Shiina *et al*. 2006; Hu *et al*. 2004). However, ArKO$^{Ex3}$ mice retain ovarian follicles up to 52 wk (Walters *et al*. 2007), indicating that AR-mediated retention of the follicle reserve is facilitated at least in part by non-genomic AR signalling and/or interactions of the mutant ArKO$^{Ex3}$ protein with AR co-factors. Interestingly, mice heterozygous for the *Ar* exon 3 deletion, but not heterozygous deletions of exons 1 or 2, exhibit an age-dependent reduction in fertility similar to that of the homozygous ArKO$^{Ex1}$ and ArKO$^{Ex2}$ models, indicating that *Ar* gene dosage effects may play a significant role in the reproductive lifespan of the female ovary (Walters *et al*. 2007).

The global nature of these ArKO models brings into question whether extra-ovarian AR deletion has consequences on the reproductive functioning of these mice, given that AR is expressed throughout the HPG axis and other reproductive-associated organs such as the uterus

(Pelletier 2000). ArKO$^{Ex2}$ and ArKO$^{Ex3}$ females exhibit abnormally long and irregular estrus cycles (Hu *et al*. 2004; Walters *et al*. 2009), and ArKO$^{Ex3}$ mice have a delay in the time of their first litter as well as reduced ovulation rates that are overcome by PMSG and hCG (Walters *et al*. 2007). ArKO$^{Ex3}$ females also exhibit increased levels of FSH and $E_2$ at estrus, have an increased sensitivity to negative $E_2$ feedback on LH secretion (Walters *et al*. 2009), and produce a decreased, shortened, and mistimed LH surge that reflects aberrant follicular steroidogenesis characterized by decreases in serum estrogens at pro-estrus (Cheng *et al*. 2013). Reciprocal ovarian transplants confirmed an extra-ovarian defect in ArKO mice, as ovariectomized WT hosts with ArKO$^{Ex3}$ ovary transplants exhibit normal estrus cycles and fertility, whereas ArKO$^{Ex3}$ hosts with WT ovary transplants have irregular estrus cycles and a subfertility phenotype similar to intact ArKO$^{Ex3}$ mice (Walters *et al*. 2009). Accordingly, hypothalamic expression of KiSS-1 metastasis-suppressor (*Kiss1*), which is necessary for the stimulation of GnRH secretion (Smith, Clifton & Steiner 2006) and the LH surge (Smith *et al*. 2006; Clarkson *et al*. 2008), is decreased in ArKO$^{Ex3}$ females, suggesting that AR actions are involved in the regulation of the ovulation-triggering kisspeptin/GnRH/LH cascade (Cheng *et al*. 2013). These findings suggest that a lack of normal AR-mediated signalling leads to neuroendocrine defects, and that the AR has an extra-ovarian role in the preparation of ovulation through the regulation of gonadotropin secretion, in addition to its intra-ovarian role in the regulation of late follicular dynamics. In addition to these neuroendocrine phenotypes, defects in uterine morphology, such as diameter and horn length, were noted in the ArKO$^{Ex2}$ and ArKO$^{Ex3}$ models (Hu *et al*. 2004; Walters *et al*. 2009). ArKO$^{Ex2}$ uteri also exhibited decreased responses to estrus and ovulation (Hu *et al*. 2004). However, these uterine defects did not affect implantation, embryo or fetal

development, or parturition in the ArKO$^{Ex3}$ model, leading the authors to conclude that AR plays an important but unnecessary role in proper uterine function (Walters *et al*. 2009).

*Ovarian Cell-Specific Androgen Receptor Knockout Mouse Models*

Multiple cell-specific ArKO models have been generated to address the intra-ovarian defects caused by *Ar* deletion on an individual cell-type basis, and without the confounding influence of *Ar* loss in the HPG axis and elsewhere. Two models have been produced that intended to completely delete the *Ar* only in GCs using GC-specific Cre drivers (Sen & Hammes 2010; Walters *et al*. 2012). GC-ArKO$^{Ex2}$ mice display complete loss of *Ar* due to excision of exon 2 driven by the *Amhr2* promoter (Jamin *et al*. 2002). This excision was achieved using a construct different from that used to generate ArKO$^{Ex2}$ mice, but still resulted in deletion of the first ZNF of the *Ar* DBD, a frameshift mutation leading to the insertion of a premature termination codon in exon 3, and subsequently a null *Ar* allele (De Gendt *et al*. 2004). As in the global ArKO$^{Ex3}$ model, GC-ArKO$^{Ex3}$ mice were generated through an in-frame deletion of *Ar* exon 3 that results in the production of a mutant AR capable of non-DNA binding activities (Notini *et al*. 2005; Rana, Davey & Zajac 2014); however, this excision was driven by the *Amh* promoter (Lécureuil *et al*. 2002). Both models were generated and maintained on B6J genetic backgrounds. As in the global ArKO models, these two models show slight differences in their ovarian and reproductive phenotypes, likely due to the nature of the *Ar* deletion constructs, as well as the specificity of the Cre drivers. The *Amhr2-cre* promoter is active exclusively in the urogenital ridge as early as E11.5, and by E12.5 this expression is specific to the gonadal somatic cells and the mesenchymal cells surrounding the epithelium of the Müllerian ducts (Jamin *et al*. 2002). Some evidence has suggested that the action of *Amhr2-cre* is predominant in the GCs of

pre-antral and small antral, but not primordial or primary, follicles (Jorgez *et al*. 2004; Boerboom *et al*. 2005; Pangas *et al*. 2006). Although the *Amhr2-cre* promoter is a well-characterized Cre driver used to delete or express genes in the GC compartment (Jorgez *et al*. 2004; Jeyasuria *et al*. 2004; Boerboom *et al*. 2005; Pangas *et al*. 2006; Andreu-Vieyra, Chen & Matzuk 2007; Fan *et al*. 2008a; Pangas *et al*. 2008; Edson *et al*. 2010), non-specific leakage has been identified in the uterus, oocytes, and TCs (Jorgez *et al*. 2004; Pangas *et al*. 2006; Hernandez Gifford, Hunzicker-Dunn & Nilson 2009). *Ar* mRNA is absent from the GCs, but not the pituitary or hypothalamus, of GC-ArKO$^{Ex2}$ mice. The absence of AR protein in the ovary is specific to GCs, and no urogenital tract morphological changes such as those identified in the global ArKO$^{Ex2}$ model were identified. Furthermore, no evidence of differential follicle-type *Amhr2-cre* action was noted in the GC-ArKO$^{Ex2}$ model (Sen & Hammes 2010). In contrast, *Amh-cre* promoter activity is absent from the prenatal ovary and is detected heterogeneously in the GCs of pre-antral and antral follicles of adult mice (Lécureuil *et al*. 2002). This activity pattern correlates with the pattern of AMH expression, which is present at its highest levels in these follicle types (Durlinger, Visser & Themmen 2002; Visser *et al*. 2006) and was exhibited in GC-ArKO$^{Ex3}$ model. Although only WT *Ar* was present in the uterus, pituitary and brain, and *Amh-cre* promoter activity was absent from TCs and oocytes, not all GCs in the ovaries of GC-ArKO$^{Ex3}$ mice expressed the mutant *Ar* transcript (Walters *et al*. 2012). The heterogeneous activity of *Amh-cre* in GCs suggests that the genomic contribution of GC-specific AR signalling may be underestimated in the GC-ArKO$^{Ex3}$ model.

Both GC-ArKO mouse models recapitulate the subfertility phenotype found in global ArKO mice and show significantly dysfunctional follicle health and development (Sen & Hammes 2010; Walters *et al*. 2012), suggesting that GC-specific AR signalling is critical for

normal ovarian function. GC-ArKO$^{Ex2}$ females exhibit a POF phenotype due to accelerated follicle depletion that mimics the ArKO$^{Ex1}$ and ArKO$^{Ex2}$ models, with reduced pups per litter and total litters born. The follicle complement of GC-ArKO$^{Ex2}$ mice is initially normal, but at both 2 and 6 mo of age their ovaries are characterized by significantly more pre-antral and atretic follicles but fewer antral follicles and corpora lutea compared to controls. Follicles from GC-ArKO$^{Ex2}$ mice also grew slower than controls when grown *in vitro*. In addition, GC-ArKO$^{Ex2}$ females naturally ovulate fewer oocytes and have longer estrus cycles at 6 mo of age compared to WT and heterozygous mice, indicating these mice have defects in ovulation and HPG signalling (Sen & Hammes 2010). GC-ArKO$^{Ex3}$ females exhibit a reduction in total litters produced over 6 mo, as well as an age-dependent reduction in the total number of pups born beginning at 6 mo of age; however, as in the global ArKO$^{Ex3}$ model and unlike in their global and GC-specific ArKO$^{Ex2}$ counterparts, GC-ArKO$^{Ex3}$ mice do not exhibit accelerated follicle depletion leading to POF. GC-ArKO$^{Ex3}$ females do, however, show estrus length abnormalities similar to that observed in the GC-ArKO$^{Ex2}$ model. Although there is no difference in GC-ArKO$^{Ex3}$ corpora lutea numbers at any age, they do have fewer large pre-antral and small antral follicles at 3 mo and significantly increased rates of follicular atresia and numbers of unhealthy follicles at 6 mo. In contrast to the GC-ArKO$^{Ex2}$ model, naturally ovulated oocyte numbers were normal in GC-ArKO$^{Ex3}$ mice, but cumulus expansion and fertilization rates were decreased compared to controls (Walters *et al*. 2012). The altered follicle population dynamics and increased atresia in both GC-ArKO models suggests a role for GC-specific AR in regulating GC growth, survival and apoptosis. Furthermore, the decreases in ovulated oocytes and corpora lutea found in GC-ArKO$^{Ex2}$ ovaries and the cumulus expansion and fertilization defects found in GC-ArKO$^{Ex3}$ mice indicate a role for GC-specific AR signalling in the peri-ovulatory process, with

the differences in phenotype correlating with the complete ablation of AR function in the GC-ArKO$^{Ex2}$ model, or with the loss of DNA binding activity only in the GC-ArKO$^{Ex3}$ model.

In contrast to the phenotypes of the two GC-ArKO mouse models, deletion of the *Ar* specifically in the TCs (Ma *et al*. 2017) or oocytes (Sen & Hammes 2010) has no effect on fertility. The complete excision of *Ar* exon 2 (Yeh *et al*. 2002; De Gendt *et al*. 2004) was driven by the TC-specific *Cyp17a1-cre* promoter (Bridges *et al*. 2008) in the TC-ArKO mouse model or by the oocyte-specific *Gdf9-cre* promoter (Lan, Xu & Cooney 2004) in the Oo-ArKO mouse model. Although neither model exhibited alterations in follicle populations, estrus cycling or ovarian morphology, excess androgen exposure was associated with impaired GVBD in Oo-ArKO mice, confirming the role of AR-mediated signalling in oocyte maturation, but a more favourable reproductive outcome in TC-ArKO mice compared to WT females. These results indicate that the GCs, but not TCs or oocytes, are the critical site of ovarian AR-mediated signalling in terms of fertility regulation, and that AR signalling in these cell types may play a role in the response to hyperandrogenic conditions such as those observed in PCOS. However, the findings of these models may underestimate the contribution of AR signalling in these cell types, as TC-ArKO and Oo-ArKO mice exhibited an approximately 4-fold reduction, rather than complete absence, of *Ar* mRNA in TCs and oocytes, respectively.

### 3.1.3 Summary and Current Work

AR-mediated androgen signalling promotes folliculogenesis and protects follicles from atresia, and cell-specific KO models have been useful in determining that fine-tuned, GC-specific AR signalling is critical for normal ovarian function. Compelling endocrine, phenotypic

mapping, and quantitative gene expression evidence gathered to date suggests the *Ar* shares identity with *Gct4*, and modifies GC tumour susceptibility when in the presence of $Gct1^{SW}$ alleles. We therefore pursued a GC-specific KO model to test the requirement of the AR for androgen-induced GC tumour initiation. We employed the $ArKO^{Ex2}$ *Ar* allele and the *Amhr2* promoter-driven Cre construct used by Sen & Hammes (2010) to interrogate the effects of *Ar* gene deletion on ovarian function. Mice with this *Amhr2-cre* construct are haploinsufficient for *Amhr2* due to allele displacement, as they carry a *cre* gene knocked into exon 5 of the *Amhr2* gene (Jamin *et al*. 2002). The combination of these constructs allows for the complete excision of *Ar* exon 2 in *Amhr2*-expressing cells; the result is a frameshift and the insertion of a premature termination codon that produces a null *Ar* allele (De Gendt *et al*. 2004). The introduction of engineered constructs to explore a spontaneous phenotype known to be influenced by allele effects and endocrine sensitivity posed several challenges to consider for experimental design and control variables, including the impact of *Ar* allelic substitution and the effect of *Amhr2* allele displacement by a promoter driver as a means to gain cell-specific expression patterns. These factors therefore necessitated that following initial backcrossing to the SWR inbred strain, we test the individual construct lines for the retention of GC tumour susceptibility prior to the experimental crosses to delete the AR from the ovarian GCs.

### 3.1.4 Hypothesis and Research Objectives

*Hypothesis*

The AR is required for GC tumour initiation in SWR mice, and its deletion from the SWR GC compartment will prevent androgen-induced GC tumourigenesis.

*Research Objectives*

1) Independently backcross the ArKO$^{Ex2}$ *Ar* and *Amhr2-cre* alleles onto the SWR inbred strain background for a minimum of six generations, and test the individual construct lines for androgen-induced GC tumour initiation at puberty.

2) Delete the AR protein from the SWR GC compartment through a two-generation cross of backcrossed mice carrying the ArKO$^{Ex2}$ *Ar* and *Amhr2-cre* alleles, assess the degree of its deletion by qualitative protein expression analysis, and test for androgen-induced pubertal GC tumour susceptibility in its absence.

3) Delete the AR protein from the GC compartment of B6J female mice as a phenotype comparison to SWR, and to determine if AR loss from the ovaries of this GC tumour-resistant strain influences androgen-induced pubertal GC tumour susceptibility.

## 3.2 Materials and Methods

### 3.2.1 Animal Husbandry

#### 3.2.1.1 Animal Housing

Animals were housed as per Section 2.2.1.1.

#### 3.2.1.2 *Ar-flox* Mouse Strain

The B6N.129-*Ar*$^{tm1Verh}$/Cnrm (*Ar-flox*) mouse strain was obtained from Dr. Stephen Hammes (University of Rochester; European Mouse Mutant Archive strain EM:02579) and the *Ar*$^{tm1Verh}$ (*Ar*$^{flox}$) allele was backcrossed onto the SWR inbred mouse strain. *Ar-flox* mice carry an *Ar* gene derived from the (129X1/SvJ [129X1] x 129S1/Sv-*Oca2*$^{+}$*Tyr*$^{+}$*Kitl*$^{Sl\text{-}J}$ [129S1])$F_1$ mouse strain in which exon 2 is floxed (i.e. flanked by *loxP*) in a C57BL/6N (B6N) mouse strain background (De Gendt *et al*. 2004).

To determine the GC tumour-supportive action of the (129X1 x 129S1)$F_1$ *Ar*$^{flox}$ allele and to generate mice used for the experimental crosses to produce GC-ArKO mice, it was backcrossed onto the SWR inbred strain for a minimum of six generations ($N_6$, approximately 96.9% SWR strain background; Silver 1995; Figure 3.4). The presence of SWR alleles at the specific mapped susceptibility *Gct* loci *Gct1* (Chr 4; *D4Mit232*), *Gct2* (Chr 12; *D12Mit172*), *Gct3* (Chr 15; *D15Mit133*), *Gct5* (Chr 9; *D9Mit17* and *D9Mit21*), and *Gct6* (Chr X; *DXamd22*) was confirmed using SSLP DNA markers at generation $N_6F_1$ prior to intercrossing and bringing the *Ar*$^{flox}$ allele to homozygosity (Section 3.2.2.4). $N_6F_3$ SWR.*Ar*$^{flox/flox}$ female mice were examined to confirm that they retained GC tumour susceptibility following pubertal DHEA and T stimulation (Section 3.2.1.5). Backcrossing of the *Ar*$^{flox}$ allele onto the SWR inbred strain was

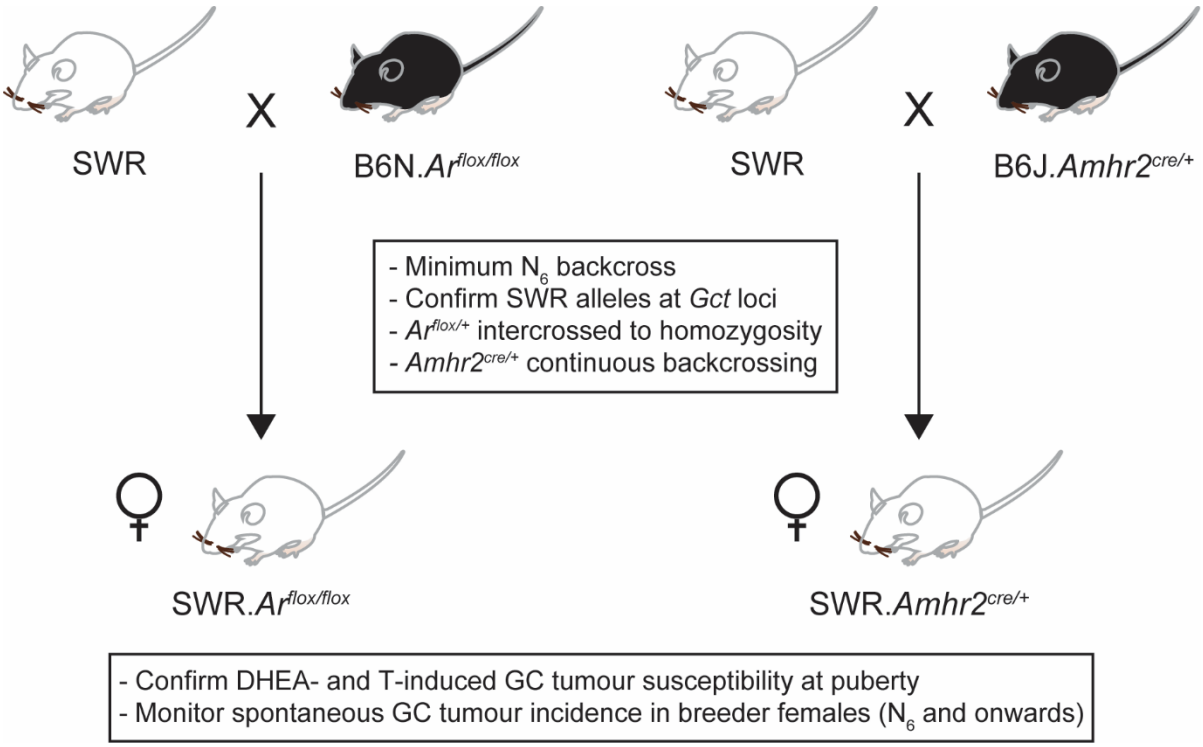


**Figure 3.4 *Ar*$^{flox}$ and *Amhr2*$^{cre}$ backcross breeding strategy**

A marker-assisted backcross strategy was employed to independently transfer the *Ar*$^{flox}$ and *Amhr2*$^{cre}$ alleles onto the SWR strain. Pubertal androgen-induced GC tumour susceptibility was assessed in SWR.*Ar*$^{flox/flox}$ and SWR.*Amhr2*$^{cre/+}$ females following a minimum of six backcross generations. Additionally, all SWR.*Ar*$^{flox/flox}$ and SWR.*Amhr2*$^{cre/+}$ breeder females were monitored for spontaneous GC tumour incidence from generation $N_6$ onwards.

continued until eight backcross generations were achieved ($N_8$, approximately 99.2% SWR strain background), and $N_8F_1$ *Ar*$^{flox}$ carrier mice were intercrossed and the allele was brought to homozygosity to produce $N_8F_3$ SWR.*Ar*$^{flox/flox}$ mice, which were maintained thereafter as brother-sister matings ($F_3$, $F_4$, etc.). The $N_8$ SWR.*Ar*$^{flox/flox}$ colony was the source for all mice used in the experimental crosses to generate GC-ArKO females. Spontaneous GC tumour incidence in SWR.*Ar*$^{flox/flox}$ breeder females was monitored from generation $N_6$ onwards.

The *Ar*$^{flox}$ allele was also independently backcrossed onto the B6J mouse strain, purchased from The Jackson Laboratory (Stock No: 000664; Bar Harbor, ME), for six generations ($N_6$, approximately 96.9% B6J strain background). $N_6F_1$ *Ar*$^{flox}$ carrier mice were intercrossed and the allele was brought to homozygosity to produce $N_6F_3$ generation B6J.*Ar*$^{flox/flox}$ mice, which were maintained thereafter as brother-sister matings ($F_3$, $F_4$, etc.). The $N_6$ B6J.*Ar*$^{flox/flox}$ colony was the source for all mice used in the experimental crosses to generate GC-ArKO mice in a B6J strain background as a phenotype comparison to SWR.

#### 3.2.1.3 *Amhr2-cre* Mouse Strain

The B6;129S7-*Amhr2*$^{tm3(cre)Bhr}$/Mmnc (*Amhr2-cre*) mouse strain was purchased from the Mutant Mouse Resource and Research Center (MMRRC; Stock No: 014245-UNC) and the *Amhr2*$^{tm3(cre)Bhr}$ (*Amhr2*$^{cre}$) allele was backcrossed onto the SWR mouse strain. *Amhr2-cre* mice carry a *cre* gene knocked into exon 5 of the *Amhr2* gene derived from the 129S7/SvEvBrd-*Hprt*$^{b-m2}$ (129S7) mouse strain in a B6J mouse strain background (Jamin *et al*. 2002).

To determine the GC tumour-supportive action of the 129S7 *Amhr2*$^{cre}$ allele and to generate mice used for the experimental crosses to produce GC-ArKO mice, it was backcrossed

onto the SWR inbred strain for a minimum of six generations ($N_6$, approximately 96.9% SWR strain background; Figure 3.4) and maintained in a heterozygous state, due to the presumed inherent inactivation of the affected *Amhr2* allele as a result of its disruption by the *cre* cassette (Jamin *et al*. 2002). The presence of SWR alleles at the specific mapped susceptibility *Gct* loci *Gct1*, *Gct2*, *Gct3*, *Gct4* (Chr X; *DXMit96*), *Gct5*, and *Gct6* was confirmed using SSLP DNA markers at $N_5F_1$ prior to further and ongoing backcrosses onto the inbred SWR strain for $Amhr2^{cre}$ maintenance (Section 3.2.2.4). $N_6F_1$ generation SWR.$Amhr2^{cre/+}$ female mice were examined to confirm that they retained GC tumour susceptibility following pubertal DHEA and T stimulation (Section 3.2.1.5). SWR.$Amhr2^{cre/+}$ mice used for the experimental crosses to generate GC-ArKO mice were minimum generation $N_6F_1$. Spontaneous GC tumour incidence in SWR.$Amhr2^{cre/+}$ breeder females was monitored from generation $N_6$ onwards.

The $Amhr2^{cre}$ allele was also independently maintained in a heterozygous state on a B6J background by breeding to in-house B6J mice. Mice used for the experimental crosses to generate GC-ArKO mice in a B6J strain background as a phenotype comparison to SWR were minimum in-house generation $N_3F_1$.

### 3.2.1.4 Generation of GC-ArKO Mice

GC-ArKO mice were generated using a two-generation breeding scheme (Figure 3.5). Female SWR.$Ar^{flox/flox}$ mice were crossed with male SWR.$Amhr2^{cre/+}$ mice to generate SWR.$Ar^{flox/+}Amhr2^{+/cre}$ mice (labelled experimental breeder cross 1). Female SWR.$Ar^{flox/+}Amhr2^{+/cre}$ mice were then backcrossed with SWR.$Ar^{flox/Y}$ male mice to generate SWR.$Ar^{flox/flox}Amhr2^{cre/+}$ GC-ArKO and SWR.$Ar^{+/flox}Amhr2^{cre/+}$ control mice heterozygous for *Ar* (hereafter designated heterozygous control mice; labelled experimental breeder cross 2). The

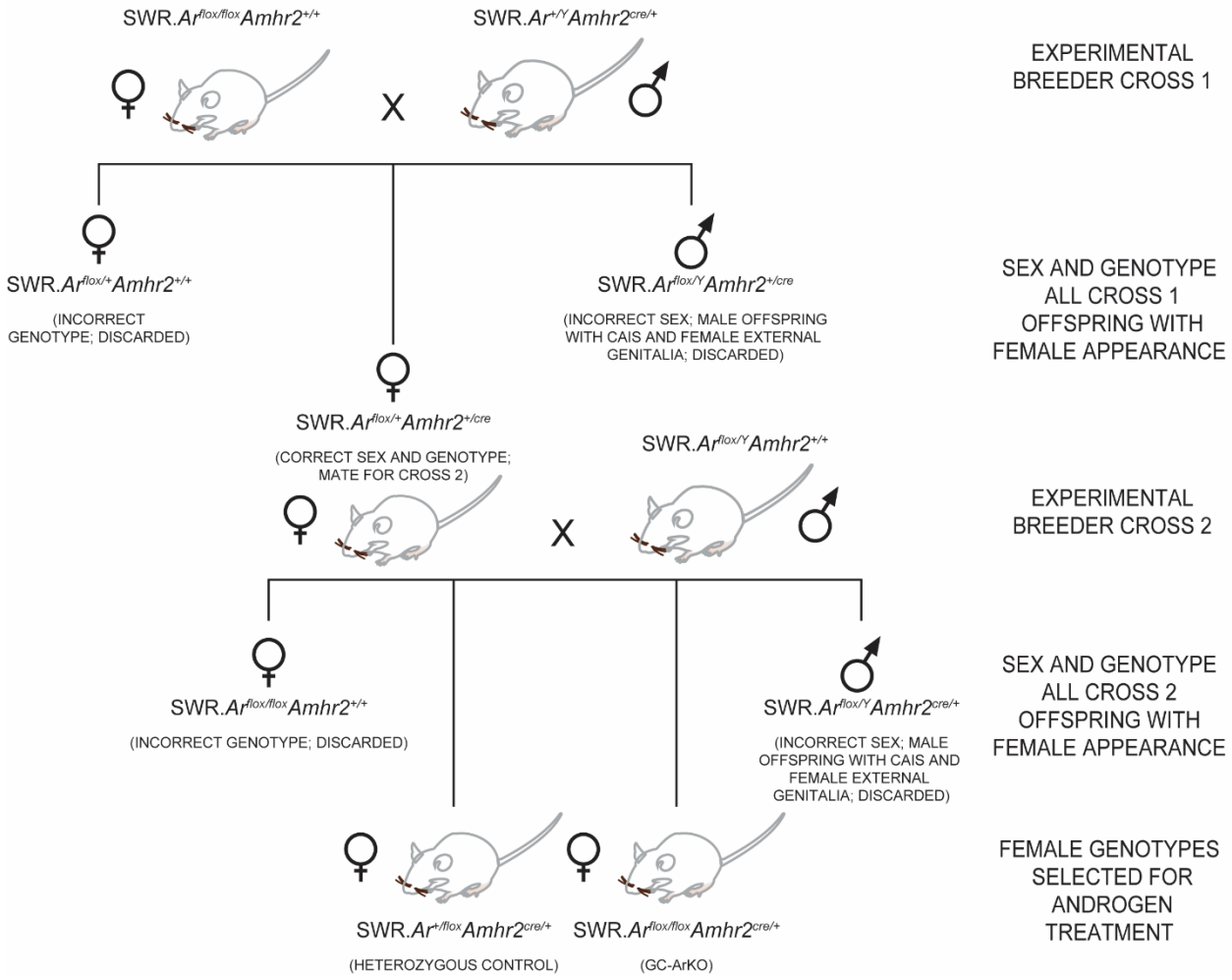


**Figure 3.5 GC-ArKO breeding scheme**

SWR.$Ar^{flox/flox}Amhr2^{+/+}$ females were crossed with SWR.$Ar^{+/Y}Amhr2^{cre/+}$ males (experimental breeder cross 1) to generate SWR.$Ar^{flox/+}Amhr2^{+/cre}$ female mice, which were backcrossed with SWR.$Ar^{flox/Y}Amhr2^{+/+}$ males (experimental breeder cross 2) to generate SWR.$Ar^{+/flox}Amhr2^{cre/+}$ control mice heterozygous for *Ar* and SWR.$Ar^{flox/flox}Amhr2^{cre/+}$ GC-ArKO females. All experimental breeder cross 1 and 2 offspring with an external female appearance were genotyped for their sex chromosome constitution and construct genotypes. The independent generation of B6J GC-ArKO mice was accomplished in the same manner.

independent generation of B6J GC-ArKO mice was accomplished in the same manner.

All pups with an external female phenotype generated from SWR or B6J experimental breeder cross 1 and 2 were genotyped for *Amhr2*$^{cre}$ and their sex chromosome complement, since the GC-ArKO breeding scheme resulted in the generation of Chr XY pseudo-hermaphrodite males with abdominal testes-like structures but an external female appearance (CAIS phenotype) due to *Amhr2*$^{cre}$-driven loss of the *Ar*$^{flox}$ allele in early development (Sections 3.2.2.2 and 3.2.2.3). Confirmed Chr XX female pups generated from SWR or B6J experimental breeder cross 2 were genotyped for their *Ar*$^{flox}$ allele status, as heterozygotes or homozygotes (Section 3.2.2.1); heterozygous females that retain GC-specific *Ar* expression from one WT *Ar* allele (*Ar*$^{+/flox}$, *Amhr2*$^{cre/+}$ genotype) are controls in this investigation, whereas homozygous females (*Ar*$^{flox/flox}$, *Amhr2*$^{cre/+}$ genotype) represent the experimental arm for GC-specific *Ar* deletion. Females of both genotypes were administered androgenic steroid capsules at puberty (Section 3.2.1.5).

### 3.2.1.5 Surgical Capsule Implantation

Exogenous DHEA or T was administered to female mice at puberty for four purposes: 1) to confirm GC tumour susceptibility was retained in the independent mouse lines carrying the *Ar*$^{flox/flox}$ and *Amhr2*$^{cre/+}$ constructs on the SWR background, particularly for the latter condition which induced hemizygosity for the *Amhr2* gene; 2) to generate androgen-treated normal ovaries and androgen-induced GC tumours in inbred SWR female mice for an analysis of ovarian AR protein expression; 3) to determine GC tumour frequency following androgenic stimulation in the absence of AR protein from GCs (GC-ArKO females) versus heterozygous controls; and 4) to investigate the specific action of DHEA versus T and its effect on the ovarian phenotype in the

absence of AR from GCs. SWR.*Ar*$^{flox}$, SWR.*Amhr2*$^{cre}$, and SWR and B6J GC-ArKO and the respective heterozygous control mice were implanted with DHEA or T capsules as per Section 2.2.1.3. T capsules were filled with approximately 150 mg of powdered T (4-androsten-17β-ol-3-one; A6950-000, Steraloids Inc.).

### 3.2.2 Genotyping

#### 3.2.2.1 *Ar*$^{flox}$

*Ar*$^{flox}$ genotyping markers were amplified by PCR using a One*Taq*® GC Reaction Buffer Pack (New England BioLabs® Ltd., Whitby, ON) from gDNA extracted from mouse tail samples (Section 2.2.2.1). The following reagents were combined in a 0.2 mL PCR tube (Bio-Rad Laboratories): 5.9375 µL of distilled water, 2.5 µL of 5X One*Taq*® Standard Reaction Buffer, 1.25 µL of One*Taq*® High GC Enhancer, 0.25 µL of 10 mM dNTPs (Invitrogen), 0.25 µL of 10 µM forward and reverse primers (Integrated DNA Technologies), 0.0625 µL of One*Taq*® DNA polymerase, and 2 µL of gDNA template. A negative control was included with each PCR with distilled water in place of gDNA template. The tubes were placed in a Veriti™ 96-Well Thermal Cycler (Applied Biosystems Inc.) where PCR was performed using the following profile: 95 °C for 1 min; 35 cycles of 95 °C for 15 s, 61 °C for 1 min, and 72 °C for 2 min; 72 °C for 7 min. The PCR products were stored at 4 °C until gel electrophoresis. *Ar*$^{flox}$ genotyping primer sequences were obtained from De Gendt *et al*. 2004 and are shown with their amplicon sizes in Table 3.3. *Ar*$^{flox}$ PCR products were separated by horizontal electrophoresis through a 1% agarose gel as per Section 2.2.2.2 and scored for allele differences as per Table 3.3.

**Table 3.3 *Ar*$^{flox}$ genotyping primers.** Primer sequences used to amplify the *Ar*$^{+}$, *Ar*$^{flox}$ and Cre-recombined (excised) alleles by PCR and the corresponding amplicon lengths are shown.

| Target Allele | Forward Sequence (5′→3′) | Reverse Sequence (5′→3′) | Amplicon (bp) | | |
|---|---|---|---|---|---|
| | | | WT | Floxed | Excised |
| *Ar*$^{+}$/*Ar*$^{flox}$ | AGCCTGTATACTCAGTTGGGG | AATGCATCACATTAAGTTGATACC | 855 | 952 | 404 |

#### 3.2.2.2 *Amhr2$^{cre}$*

*Amhr2$^{cre}$* genotyping markers were amplified by multiplex touchdown PCR using a One*Taq*® GC Reaction Buffer Pack (New England BioLabs® Ltd.) from gDNA extracted from mouse tail samples (Section 2.2.2.1). The following reagents were combined in a 0.2 mL PCR tube (Bio-Rad Laboratories): 5.9375 µL of distilled water, 2.5 µL of 5X One*Taq*® Standard Reaction Buffer, 1.25 µL of One*Taq*® High GC Enhancer, 0.25 µL of 10 mM dNTPs (Invitrogen), 0.25 µL of 10 µM WT *Amhr2* forward primer, 0.5 µL of 10 µM *Amhr2$^{cre}$* forward primer, 0.75 µL of 10 µM reverse primer (Integrated DNA Technologies), 0.0625 µL of One*Taq*® DNA polymerase, and 1 µL of gDNA template. A negative control was included with each PCR with distilled water in place of gDNA template. The tubes were placed in a Veriti™ 96-Well Thermal Cycler (Applied Biosystems Inc.) where touchdown PCR was performed using the following profile: 94 °C for 5 min; 6 cycles of 94 °C for 30 s, 66 °C-61 °C for 30 sec (-1 °C/cycle), and 72 °C for 1 min; 35 cycles of 94 °C for 30 sec, 60 °C for 30 sec, 72 °C for 1 min; 72 °C for 7 min. The PCR products were stored at 4 °C until gel electrophoresis. *Amhr2$^{cre}$* genotyping primer sequences were obtained from the MMRRC (MMRRC UNC 2013) and are shown with their amplicon sizes in Table 3.4. *Amhr2$^{cre}$* PCR products were separated by horizontal electrophoresis through a 1% agarose gel as per Section 2.2.2.2 and scored for allele differences as per Table 3.4.

#### 3.2.2.3 Karyotypic Sex

The loss of the *Ar$^{flox}$* allele from the single X chromosome of SWR and B6J GC-ArKO cross 1 and 2 Chr XY males resulted in phenotypically female pseudo-hermaphrodites, making it

**Table 3.4 *Amhr2$^{cre}$* genotyping primers.** Primer sequences used to amplify the *Amhr2*$^{+}$ and *Amhr2$^{cre}$* alleles by multiplex touchdown PCR and the corresponding amplicon lengths are shown.

| Target Allele | Forward Sequence (5′→3′) | Reverse Sequence (5′→3′) | Amplicon (bp) |
|---|---|---|---|
| *Amhr2*$^{+}$ | AGGTGGGTCAGACCCAGAGCC | ACCTAGTAGAGAGGCTGCGTTGAGTGTG | 223 |
| *Amhr2$^{cre}$* | CCGCTTCCTCGTGCTTTACGGTAT | ACCTAGTAGAGAGGCTGCGTTGAGTGTG | ~500 |

necessary to genotype all phenotypically female *Amhr2*$^{cre}$ carrier mice generated from these crosses for their X and Y constitution. Karyotypic sex was determined using genotyping markers for the Chr X and Y homologues of the lysine (K)-specific demethylase 5C (*Kdm5c*) and lysine (K)-specific demethylase 5D (*Kdm5d*) genes, respectively. *Kdm5c* and *Kdm5d* genotyping markers were amplified by PCR using a One*Taq*® GC Reaction Buffer Pack (New England BioLabs® Ltd.) from gDNA extracted from mouse tail samples (Section 2.2.2.1). The following reagents were combined in a 0.2 mL PCR tube (Bio-Rad Laboratories): 4.9375 µL of distilled water, 2.5 µL of 5X One*Taq*® Standard Reaction Buffer, 1.25 µL of One*Taq*® High GC Enhancer, 0.25 µL of 10 mM dNTPs (Invitrogen), 0.25 µL of 10 µM forward and reverse primers (Integrated DNA Technologies), 0.0625 µL of One*Taq*® DNA polymerase, and 3 µL of gDNA template. A negative control was included with each PCR with distilled water in place of gDNA template. The tubes were placed in a Veriti™ 96-Well Thermal Cycler (Applied Biosystems Inc.) where PCR was performed using the following profile: 97 °C for 30 s; 39 cycles of 94 °C for 15 s, 55 °C for 30 s, and 72 °C for 30 sec; 72 °C for 10 min. The PCR products were stored at 4 °C until gel electrophoresis. Karyotypic sex genotyping primer sequences were obtained from Mroz, Carrel & Hunt 1999 and are shown with their amplicon sizes in Table 3.5. Karyotypic sex PCR products were separated by horizontal electrophoresis through a 2% agarose gel as per Section 2.2.2.2 and scored for allele differences as per Table 3.5.

#### 3.2.2.4 SSLPs

SSLPs and their primer sequences were annotated in the MGD (Smith *et al*. 2018) or were identified by the Computational Sciences group at The Jackson Laboratory and designed in-house. SSLP genotyping markers were amplified by PCR using a Master*Taq*™ Kit from

**Table 3.5 Karyotypic sex genotyping primers.** Primer sequences used to amplify the Chr X and Y homologues of the *Kdm5c* and *Kdm5d* genes, respectively, by PCR and the corresponding amplicon lengths are shown.

| Target Allele | Forward Sequence (5′→3′) | Reverse Sequence (5′→3′) | Amplicon (bp) | |
|---|---|---|---|---|
| | | | *Kdm5c* | *Kdm5d* |
| *Kdm5c*/*Kdm5d* | TGAAGCTTTTGGCTTTGAC | CCGCTGCCAAATTCTTTGG | 330 | 301 |

gDNA extracted from mouse tail samples as per Section 2.2.2.1. Genotyping marker primer sequences, relative SSLP allele sizes for SWR, B6J and B6N, and their genomic locations are shown in Appendix G. SSLP PCR products were separated by horizontal electrophoresis through a 4% agarose gel as per Section 2.2.2.1 and scored for allele differences as per Appendix G.

### 3.2.3 Qualitative Protein Expression Analysis

#### 3.2.3.1 Tissue Collection and Processing

Mice were euthanized by exposure to $CO_2$ gas at 3 or 8 wk of age, and GC tumour development was assessed by macroscopic examination of the ovaries in mice with present and intact DHEA or T capsules. Ovary pairs and GC tumour samples were collected from androgen-treated inbred SWR mice and from androgen-treated and untreated SWR and B6J GC-ArKO and heterozygous control mice. Seminal vesicles were collected from untreated pubertal male B6J mice as a positive control tissue for AR protein expression. The tissues were dissected using scissors and tweezers and were fixed in Bouin's solution (Sigma-Aldrich Inc.) for 24 h. Samples were paraffin embedded using a Tissue-Tek VIP® 6 automatic tissue processor (Sakura Finetek USA Inc., Torrance, CA), after which a Leica RM2235 Manual Rotary Microtome (Leica Biosystems Inc., Concord, ON) was used to cut 5 µm tissue sections which were affixed to positively charged Superfrost® Plus Micro Slides (VWR International, Radnor, PA) and heated overnight in a temperature-controlled oven at 45 °C. The paraffin embedding of samples, sectioning of histology blocks, and staining of select slides with H&E was performed at the Histology Unit of the Medical Education and Laboratory Support Services of Memorial University of Newfoundland.

### 3.2.3.2 Immunohistochemistry

Slides were processed immediately the day after sectioning and were comprised of tissue sections from GC-ArKO, heterozygous control, and/or inbred SWR samples. A separate slide with seminal vesicle tissue sections was included with every assay as a technical control. Tissue sections were deparaffinized and rehydrated by two sequential washings in xylene (ACP Chemicals Inc., Montreal, QC) for 5 min, followed by decreasing concentrations of 100%, 95%, 80% and 70% ethanol (Commercial Alcohols, Brampton, ON) for 3 min each and a final wash in distilled water for 5 min. Antigen retrieval was accomplished by placing slides in a Deni® pressure cooker (Keystone Manufacturing Company, Inc., St. Catharines, ON) on the highest setting for 5 min with 15 mL of pH 6.0 100X citrate-based Vector® Antigen Unmasking Solution (Vector Laboratories, Burlingame, CA) diluted in 1600 mL of distilled water. Slides were briefly rinsed in distilled water and subsequently washed in pH 7.5 phosphate-buffered saline (PBS) for 5 min. Endogenous peroxidase activity was quenched by submerging slides in a 3% hydrogen peroxide solution (Sigma-Aldrich Inc.) for 5 min, followed by washing in distilled water for 5 min and pH 7.5 PBS for 5 min. Experimental and immunoglobulin G (IgG) isotype negative control tissue sections were separated using an ImmEdge™ Hydrophobic Barrier Pen (Vector Laboratories). All blocking, primary, and secondary antibody incubations and avidin-biotin complex (ABC) immunodetection steps were accomplished using a Rabbit IgG VECTASTAIN® Elite ABC Kit (Vector Laboratories). Tissue sections were blocked for 20 min by adding 150 µL of normal serum to 10 mL of pH 7.5 PBS. Experimental tissue sections were incubated for 30 min in a 1:200 dilution of AR (N-20) rabbit polyclonal primary antibody (200 µg/mL; sc-816, Santa Cruz Biotechnology, Inc., Dallas, TX) in blocking serum solution. The AR (N-20) antibody recognizes epitopes at the N-terminus of Ar. IgG isotype negative control tissue

sections were incubated for 30 min in a 1:200 dilution of polyclonal normal rabbit IgG primary antibody (400 µg/mL; sc-2027, Santa Cruz Biotechnology, Inc.) in blocking serum solution. Slides were submerged in pH 7.5 PBS for 5 min following the incubation period. Tissue sections were incubated in secondary antibody for 30 min by adding 100 µL of biotinylated, affinity-purified anti-IgG antibody stock to 10 mL of blocking serum solution. Antigens were detected by first incubating tissue sections for 30 min in ABC reagent, which was prepared by adding 100 µL each of Avidin DH and biotinylated horseradish peroxidase (HRP) H to 5 mL of pH 7.5 PBS and allowing the reagent to incubate for 30 min. Slides were submerged in pH 7.5 PBS for 5 min following the incubation period, after which they were briefly rinsed in distilled water. Tissue sections were incubated in a 3,3′-diaminobenzidine (DAB) substrate working solution using an ImmPACT™ DAB Peroxidase (HRP) Substrate Kit (Vector Laboratories) by adding 100 µL of ImmPACT™ DAB Chromogen concentrate to 2 mL of ImmPACT™ DAB Diluent. Tissue sections were incubated until desired stain intensity developed, approximately 25 min. Slides were submerged in distilled water for 5 min, after which tissue sections were counterstained using Vector® Hematoxylin QS Nuclear Counterstain (Vector Laboratories) heated to 30 °C for 45 s and submerged in tap water for 10 s. Tissue sections were dehydrated by dipping slides 20 times in two sequential washes of 95% ethanol, one 100% ethanol wash, and two sequential washes of xylene. Slides were coverslipped using VectaMount™ Mounting Medium (Vector Laboratories) and allowed to dry flat (Appendix A). Slides were stored at -20°C. All steps were completed at RT unless otherwise noted.

#### 3.2.3.3 Slide Imaging and Qualitative Protein Scoring

Slides were scanned at the Cold-Ocean Deep-Sea Research Facility, Ocean Sciences Centre, Memorial University of Newfoundland, using an Axio Scan.Z1 digital slide scanner (Carl Zeiss Microscopy GmBH, Oberkochen, Germany) at 20X magnification. Scanned images were saved as CZI image files and viewed using ZEN lite version 2.3 (Carl Zeiss Microscopy GmBH). Slides were blinded and individual sections were scored for AR expression and staining intensity in the GCs of primary, secondary, early antral, and pre-ovulatory follicles, as well as in oocytes, TCs, cells of the OSE and corpora lutea.

### 3.2.4 Statistical Analysis

Genotyping and sex ratios were compared by two-tailed z-test, GC tumour frequencies were compared by two-tailed Fisher's exact test, and mean pups weaned per litter were compared by one-way ANOVA followed by Tukey's test (*p*-values adjusted for multiple comparisons) using GraphPad Prism version 6.07 for Windows (GraphPad Software). $p < 0.05$ was considered statistically significant. Fertility data is presented as mean pups weaned per litter ± SEM.

## 3.3 Results

### 3.3.1 Generation of GC-ArKO Mice

#### 3.3.1.1 *Ar$^{flox}$* and *Amhr2$^{cre}$* Construct Lines

The *Ar$^{flox}$* and *Amhr2$^{cre}$* constructs were successfully backcrossed onto the inbred SWR strain background for a minimum of six generations (approximately 96.9% SWR strain background; Silver 1995), and the presence of SWR alleles was confirmed at mapped *Gct* susceptibility loci. The *Ar$^{flox}$* allele was also backcrossed onto the inbred B6J strain background for six generations (approximately 96.9% B6J strain background), but the high degree of genetic similarity between the B6J and B6N strains (approximately 99.8%) precluded an SSLP marker-assisted investigation of the success of the backcross (Mekada *et al*. 2009; Simon *et al*. 2013). Statistical analysis using the z-test determined that the *Ar$^{flox}$* and *Amhr2$^{cre}$* alleles were recovered at the expected Mendelian frequencies during the backcrossing of both constructs onto both strain backgrounds (SWR.*Ar$^{flox}$*: $p = 0.5824$; SWR.*Amhr2$^{cre}$*: $p = 0.4012$; B6J.*Ar$^{flox}$*: $p = 0.2362$; B6J.*Amhr2$^{cre}$*; $p = 0.7448$). Similarly, no statistically significant deviations from the expected 1:1 male-to-female phenotypic sex ratios were observed when analyzed by z-test (SWR.*Ar$^{flox}$*: $p = 0.4494$; SWR.*Amhr2$^{cre}$*: $p = 0.3787$; B6J.*Ar$^{flox}$*: $p = 0.4056$; B6J.*Amhr2$^{cre}$*; $p = 0.3342$). A summary of the phenotypic sex and genotype frequencies observed in the *Ar$^{flox}$* and *Amhr2$^{cre}$* backcross mouse colonies is shown in Table 3.6. No statistically significant differences in fertility were observed when the average number of pups weaned per litter were compared from the SWR.*Ar$^{flox}$*, B6J.*Ar$^{flox}$* or B6J.*Amhr2$^{cre}$* construct lines by one-way ANOVA followed by Tukey's test (Figure 3.6); however, SWR dams mated to SWR.*Amhr2$^{cre/+}$* sires (SWR x SWR.*Amhr2$^{cre/+}$*) had significantly more pups weaned per litter ($8.50 \pm 0.2693$) than inbred SWR mice ($6.98 \pm 0.1676$; multiplicity adjusted $p$ value = 0.0111).

**Table 3.6 Phenotypic sex and genotype frequencies in *Ar*$^{flox}$ and *Amhr2*$^{cre}$ backcross mouse colonies.** Phenotypic sex and allele frequencies from SWR and B6J *Ar*$^{flox}$ and *Amhr2*$^{cre}$ backcross breeding colonies are shown. Total cohort sizes are shown in brackets. Not all sex-phenotyped mice were assessed for their *Ar* and *Amhr2* allele constitutions. -: not applicable

| Backcross Colony | Phenotypic Sex | | *Ar* Alleles[a] | | *Amhr2* Alleles | |
|---|---|---|---|---|---|---|
| | Female | Male | +/+ and +/*Y* | *flox*/+ and *flox*/*Y* | +/+ | +/*cre* |
| SWR.*Ar*$^{flox}$ | 46.4% (104) | 53.6% (120) | 53.8% (57) | 46.2% (49) | - | - |
| B6J.*Ar*$^{flox}$ | 55.3% (68) | 44.7% (55) | 61.5% (32) | 38.5% (20) | - | - |
| SWR.*Amhr2*$^{cre}$ | 53.2% (198) | 46.8% (174) | - | - | 46.3% (119) | 53.7% (138) |
| B6J.*Amhr2*$^{cre}$ | 54.2% (141) | 45.8% (119) | - | - | 48.2% (82) | 51.8% (88) |

[a]For simplicity, only offspring generated from crosses between *Ar*$^{flox/+}$ females and *Ar*$^{+/Y}$ males, in which 50% of female and male offspring are expected to be heterozygous or hemizygous for the *Ar*$^{flox}$ allele, respectively, have been included in genotype frequency calculations.

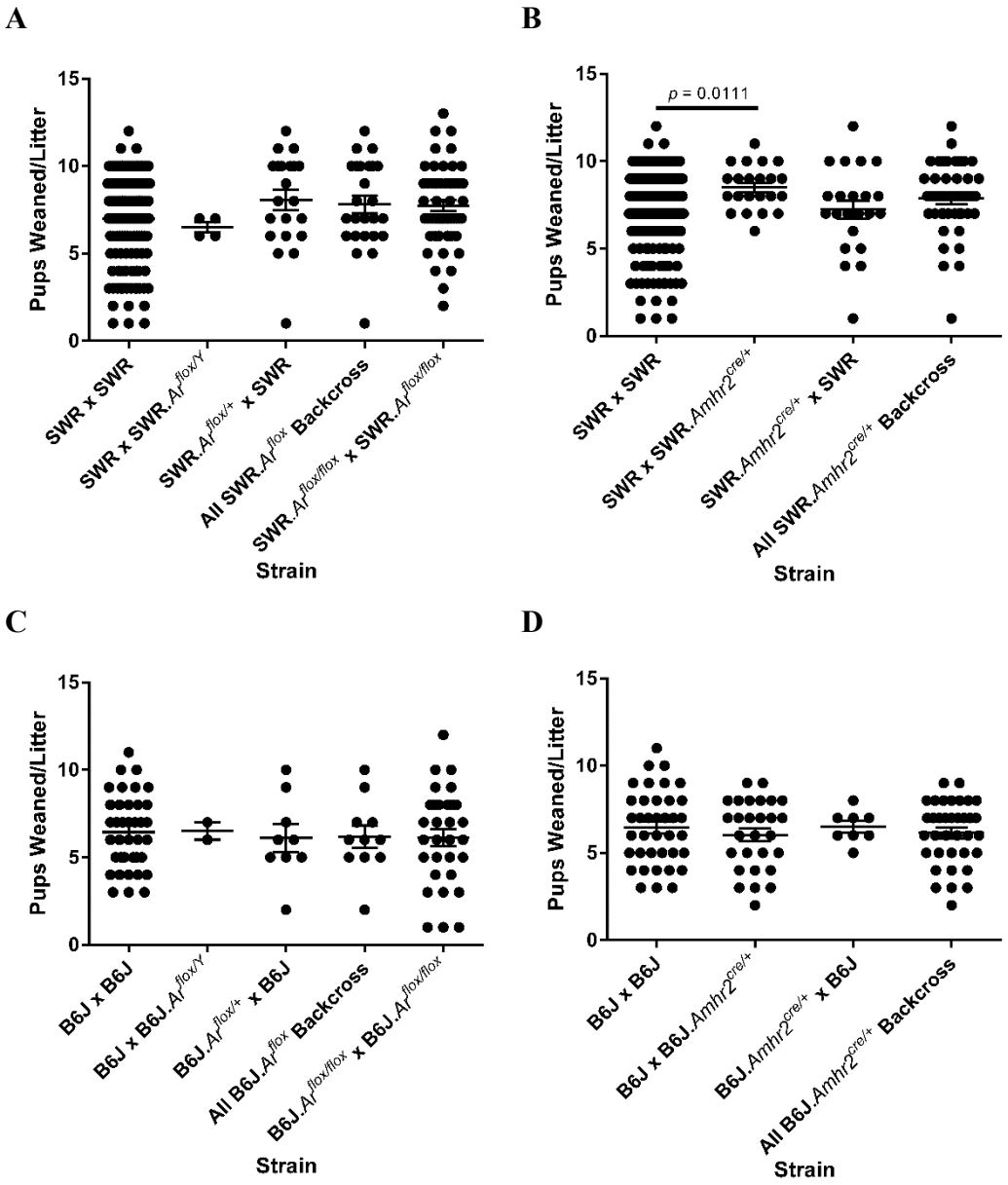


**Figure 3.6 Fertility in SWR and B6J *Ar*$^{flox}$ and *Amhr2*$^{cre}$ construct lines**

The average number of pups weaned per litter were compared from the SWR and B6J *Ar*$^{flox}$ and *Amhr2*$^{cre}$ construct lines by one-way ANOVA followed by Tukey's test. No statistically significant differences in fertility were observed with the exception of the SWR.*Amhr2*$^{cre}$ construct line (B), as SWR dams mated to SWR.*Amhr2*$^{cre/+}$ sires (SWR x SWR.*Amhr2*$^{cre/+}$) had significantly more pups weaned per litter (8.500 ± 0.2693) than inbred SWR mice (6.983 ± 0.1676; multiplicity adjusted *p* value = 0.0111). Data is presented as mean pups weaned per litter ± SEM.

Female mice carrying *Ar*$^{flox/flox}$ or *Amhr2*$^{cre/+}$ alleles in an SWR inbred strain background were tested for the retention of GC tumour susceptibility following the administration of DHEA or T at puberty, with an 8 wk endpoint for GC tumour assessment. Both construct lines were susceptible to GC tumour initiation following pubertal stimulation with either androgen at the 8 wk time point as expected (Table 3.7). Female SWR.*Ar*$^{flox/flox}$ and SWR.*Amhr2*$^{cre/+}$ mice treated with DHEA at puberty developed GC tumours within 8 wk at a frequency of 19.0% (n = 1 unilateral, n = 3 bilateral; 4/21 females or 7/42 [16.7%] ovaries with a GC tumour) and 9.1% (n = 1 bilateral; 1/11 females or 2/22 [9.1%] ovaries with a GC tumour), respectively. Pubertal T treatment also resulted in GC tumour development by 8 wk with a frequency of 5.3% in SWR.*Ar*$^{flox/flox}$ females (n = 1 unilateral; 1/10 females or 1/38 [2.6%] ovaries with a GC tumour) and 12.5% in SWR.*Amhr2*$^{cre/+}$ females (n = 1 unilateral; 1/8 or 1/16 [6.3%] ovaries with a GC tumour). The GC tumours observed in these strains resembled androgen-induced GC tumours found in inbred SWR females (data not shown).

Spontaneous GC tumour susceptibility of SWR.*Ar*$^{flox}$ females with a floxed *Ar* allele and of SWR.*Amhr2*$^{cre}$ females hemizygous for *Amhr2* was of interest, given the influence of these genes on ovarian physiology. No spontaneous GC tumours were observed in females of any line in the timeframe of colony maintenance or during the experimental crosses, including in the SWR.*Amhr2*$^{cre/+}$ colony (0/6), in the SWR.*Ar*$^{flox}$ backcross (0/9) or intercrossed (0/22) colonies, in the SWR.*Ar*$^{flox/flox}$ females used as breeders in experimental cross 1 (0/9), or in the SWR.*Ar*$^{flox/+}$*Amhr2*$^{+/cre}$ females used as breeders in experimental cross 2 (0/23). Similarly, no ovarian pathologies were noted in female breeders carrying either construct in a B6J strain background. No unexpected breeder deaths were observed in either of the SWR or B6J construct lines.

**Table 3.7 GC tumour incidence in SWR.*Ar*$^{flox}$ and SWR.*Amhr2*$^{cre}$ female mice treated with DHEA or T at puberty.** GC tumour frequencies (GC tumour hosts versus all treated mice) and the number of affected ovaries (individual GC tumours observed versus all ovaries examined) in 8 wk old mice with homozygous *Ar*$^{flox}$ alleles and a heterozygous *Amhr2*$^{cre}$ allele are shown.

| Strain | DHEA | | T | |
|---|---|---|---|---|
| | GC Tumour Hosts/ Treated Mice | Individual GC Tumours/ Ovaries Examined | GC Tumour Hosts/ Treated Mice | Individual GC Tumours/ Ovaries Examined |
| SWR.*Ar*$^{flox}$ | 4/21 (19.0%) | 7/42 (16.7%) | 1/19 (5.3%) | 1/38 (2.6%) |
| SWR.*Amhr2*$^{cre}$ | 1/11 (9.1%) | 2/22 (9.1%) | 1/8 (12.5%) | 1/16 (6.3%) |

### 3.3.1.2 Experimental Crosses to Delete the Androgen Receptor from Granulosa Cells

SWR and B6J GC-ArKO and heterozygous control mice were generated using a two-generation breeding scheme (Figure 3.5). Female $Ar^{flox/flox}Amhr2^{+/+}$ mice were first crossed with $Ar^{+/Y}Amhr2^{cre/+}$ males, and $Ar^{flox/+}Amhr2^{+/cre}$ females were selected by genotype and crossed with $Ar^{flox/Y}Amhr2^{+/+}$ males to generate $Ar^{flox/flox}Amhr2^{cre/+}$ (GC-ArKO) and $Ar^{+/flox}Amhr2^{cre/+}$ (heterozygous control) females. The phenotypic sex frequency observed in both SWR and B6J experimental breeder cross 1 and 2 litters deviated significantly from the 1:1 male-to-female ratio expected for normal litters when analyzed by z-test ($p < 0.0001$; Table 3.8). Upon necropsy, a proportion of phenotypically female mice were found to lack ovaries and uteri, and instead had small testis-like structures in the absence of seminal vesicles (data not shown). PCR genotyping revealed that 46.3 to 46.7% and 32.9 to 37.5% of phenotypically female experimental breeder cross 1 and 2 offspring genotyped for their Chr X and Y constitution possessed a Y chromosome, respectively. The SWR and B6J experimental breeder cross 2 litters did not deviate significantly from the expected proportion of genotypic males and females when analyzed by z-test ($p$ = 0.3882 and 0.1333, respectively), given the 1:1 male-to-female ratio expected in normal litters and assuming that approximately 70% of phenotypic females will have an XX Chr constitution and 30% will have an XY Chr constitution. The proportion of SWR and B6J experimental breeder cross 1 phenotypic females with a Y Chr was not compared to the expected 3:7 genotypic male-to-female ratio, as only those phenotypic females carrying an $Amhr2^{cre}$ allele were genotyped for their sex chromosome constitution.

The $Ar^{flox}$ and $Amhr2^{cre}$ alleles were recovered at the expected Mendelian frequencies (first experimental breeder cross: 1:1 $Amhr2^{+/+}$:$Amhr2^{+/cre}$; second experimental breeder cross: 1:1 $Ar^{+/flox}$:$Ar^{flox/flox}$ and $Amhr2^{+/+}$:$Amhr2^{cre/+}$) in female offspring from both experimental

**Table 3.8 Phenotypic sex and genotype frequencies in the experimental crosses to delete *Ar* from GCs.** Phenotypic and genotypic sex and $Ar^{flox}$ and $Amhr2^{cre}$ allele frequencies from the experimental breeder crosses to delete *Ar* in SWR and B6J backgrounds are shown. Total cohort sizes are shown in brackets. Not all sex-phenotyped mice were assessed for their sex Chr or *Ar* and *Amhr2* allele constitutions. -: not applicable.

| Strain | Phenotypic Sex[a] | | Sex Chr Constitution of Phenotypic Females | | *Ar* Alleles[b] | | $Amhr2^{cre}$ Alleles | |
|---|---|---|---|---|---|---|---|---|
| | Female | Male | XX | XY | *flox/flox* | *+/flox* | *+/+* | *+/cre* |
| SWR Cross 1 | 69.5% (203) | 30.5% (89) | 53.3% (48) | 46.7% (42) | - | - | 40.0% (56) | 60.0% (84) |
| SWR Cross 2 | 67.1% (617) | 32.9% (303) | 67.1% (253) | 32.9% (124) | 55.6% (90) | 44.4% (72) | 50.4% (330) | 49.6% (325) |
| B6J Cross 1 | 73.8% (93) | 26.2% (33) | 53.7% (22) | 46.3% (19) | - | - | 35.2% (19) | 64.8% (35) |
| B6J Cross 2 | 69.2% (245) | 30.8% (109) | 62.5% (105) | 37.5% (63) | 78.2% (68)[c] | 21.8% (19)[c] | 62.0% (150)[d] | 38.0% (92)[d] |

[a]Significantly different from the 1:1 male-to-female ratio expected for normal litters in all crosses by z-test ($p < 0.0001$); [b]Genotypes of Chr XX females with a heterozygous $Amhr2^{cre}$ allele only; experimental breeder cross 1 females were obligate heterozygotes for the $Ar^{flox}$ allele and so were not tested; [c]Significantly different from expected by z-test ($p = 0.0001$); [d]Significantly different from expected by z-test ($p = 0.0079$).

breeder crosses from both strains, with the exception of the B6J experimental breeder cross 2 (Table 3.8). Litters from this cross demonstrated a significantly higher than expected number of *Amhr2*$^{+/+}$ and *Ar*$^{+/flox}$ alleles when analyzed by z-test ($p$ = 0.0079 and 0.0001, respectively). No significant difference in the number of SWR.*Ar*$^{flox/flox}$*Amhr2*$^{cre/+}$ GC-ArKO and SWR.*Ar*$^{+/flox}$*Amhr2*$^{cre/+}$ heterozygous control pups generated from experimental breeder cross 2 were observed when analyzed by z-test ($p$ = 0.3166; Table 3.9); however, significantly more heterozygous control females were generated in the B6J colony than GC-ArKO females ($p$ = 0.0001) in light of the deviation from the expected *Ar*$^{flox}$ allele frequency in this colony. Upon review of breeding records, six B6J.*Ar*$^{flox/+}$*Amhr2*$^{+/cre}$ experimental cross 1 females produced heterozygous control female offspring only across 26 litters, compared to only one SWR.*Ar*$^{flox/+}$*Amhr2*$^{+/cre}$ experimental cross 1 female breeder across a single litter. No spontaneous ovarian phenotypes were observed in experimental breeder cross 1 or cross 2 offspring from either strain background, and no statistically significant differences in fertility were observed when the average number of pups weaned per litter were compared in the B6J colonies by one-way ANOVA followed by Tukey's test (Figure 3.7); however, significantly more pups were weaned per litter from the SWR experimental breeder cross 1 (8.343 ± 0.4299; multiplicity adjusted $p$ value = 0.0125) and cross 2 (8.027 ± 0.2693; multiplicity adjusted $p$ value = 0.0011) than from inbred SWR mice (6.983 ± 0.1676).

### 3.3.2 Androgen Receptor Protein Expression in SWR Ovaries and Granulosa Cell Tumours

The AR antibody employed in this investigation was first validated using seminal vesicles from untreated pubertal male B6J mice as a positive control. Mouse seminal vesicles are

**Table 3.9 Frequency of the *Ar*$^{+/flox}$*Amhr2*$^{cre/+}$ and *Ar*$^{flox/flox}$*Amhr2*$^{cre/+}$ genotypes generated from experimental breeder cross 2.** *Ar* and *Amhr2* genotypes generated from the second experimental breeder cross to delete *Ar* in SWR and B6J backgrounds are shown. Total cohort sizes are shown in brackets.

| Genotype | Frequency |
|---|---|
| SWR.*Ar*$^{+/flox}$*Amhr2*$^{cre/+}$ | 55.6% (90) |
| SWR.*Ar*$^{flox/flox}$*Amhr2*$^{cre/+}$ | 44.4% (72) |
| B6J.*Ar*$^{+/flox}$*Amhr2*$^{cre/+}$ | 78.2% (68)[a] |
| B6J.*Ar*$^{flox/flox}$*Amhr2*$^{cre/+}$ | 21.8% (19)[a] |

[a]Significantly different from expected by z-test ($p = 0.0079$).

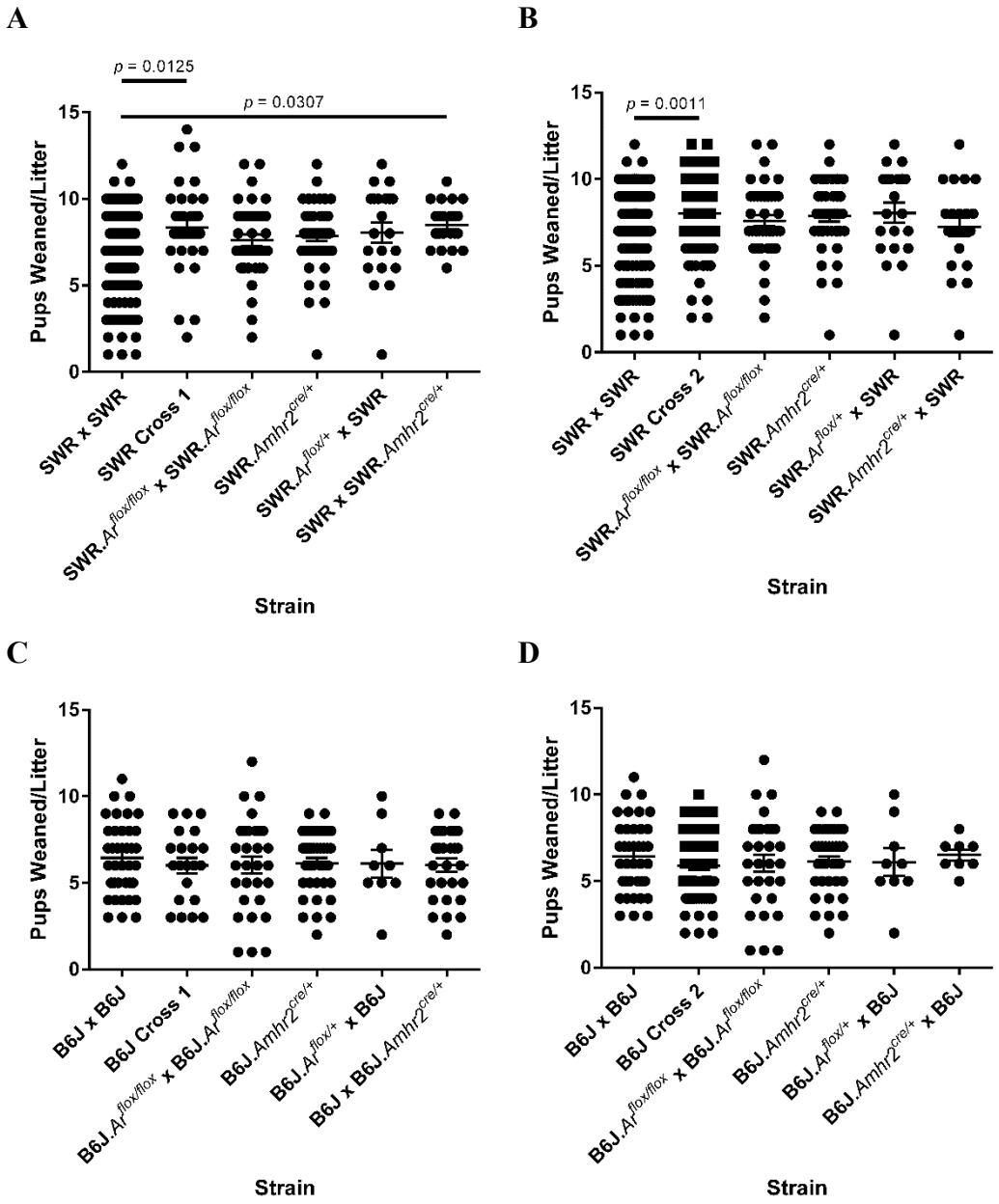


**Figure 3.7 Fertility in SWR and B6J experimental breeder cross 1 and 2 female mice**

The average number of pups weaned per litter were compared from the SWR and B6J experimental breeder crosses by one-way ANOVA followed by Tukey's test. No statistically significant differences in fertility were observed in the B6J colonies. However, significantly more pups weaned per litter were produced from SWR experimental breeder cross 1 (A; 8.343 ± 0.4299; multiplicity adjusted *p* value = 0.0125) and cross 2 (B; 8.027 ± 0.2693; multiplicity adjusted *p* value = 0.0011) than from inbred SWR mice (6.983 ± 0.1676). Data is presented as mean pups weaned per litter ± SEM.

androgen-dependent accessory glands that express high levels of AR in their pseudostratified columnar epithelium and stromal tissue by postnatal day (P) 2, with a nuclear expression pattern (Cooke, Young & Cunha 1991). The pubertal mouse seminal vesicles examined by AR IHC exhibited specific nuclear staining for AR protein in the pseudostratified columnar epithelium and stromal tissue, as compared to the non-specific IgG primary antibody that showed very little background staining (Figure 3.8). Pubertal mouse seminal vesicle tissue was included as a technical control with each AR IHC assay conducted.

Untreated inbred SWR female mice were necropsied at 8 wk of age, and normal ovaries were collected and examined for their AR expression pattern by IHC (Figure 3.9). The GCs of primary, secondary, and early antral follicles exhibited specific nuclear staining for AR protein, with the strongest expression observed in the GCs of secondary and early antral follicles. The squamous pre-GCs composing the few primordial follicles observed were positive for AR protein expression. Although the majority of GCs within pre-ovulatory follicles were negative for AR protein expression, some low- to mid-intensity AR protein-positive cells were scattered throughout the follicles. No gradient of AR protein expression between mural and cumulus GCs was noted in pre-ovulatory follicles. Corpus luteum cells showed a similar pattern of low-intensity staining for AR protein expression in sporadic cells as that observed in pre-ovulatory follicles; many corpora lutea exhibited high levels of non-specific background staining. Specific nuclear AR protein expression was observed in the TCs surrounding secondary, antral, and pre-ovulatory follicles as well as in other stromal tissue throughout the ovary. The OSE was negative for AR protein expression, as were oocytes at all stages of follicle development.

Cohorts of inbred SWR female mice were implanted with a capsule filled with DHEA (n = 20) or T (n = 10) at puberty and necropsied at 8 wk of age. No GC tumours were observed in

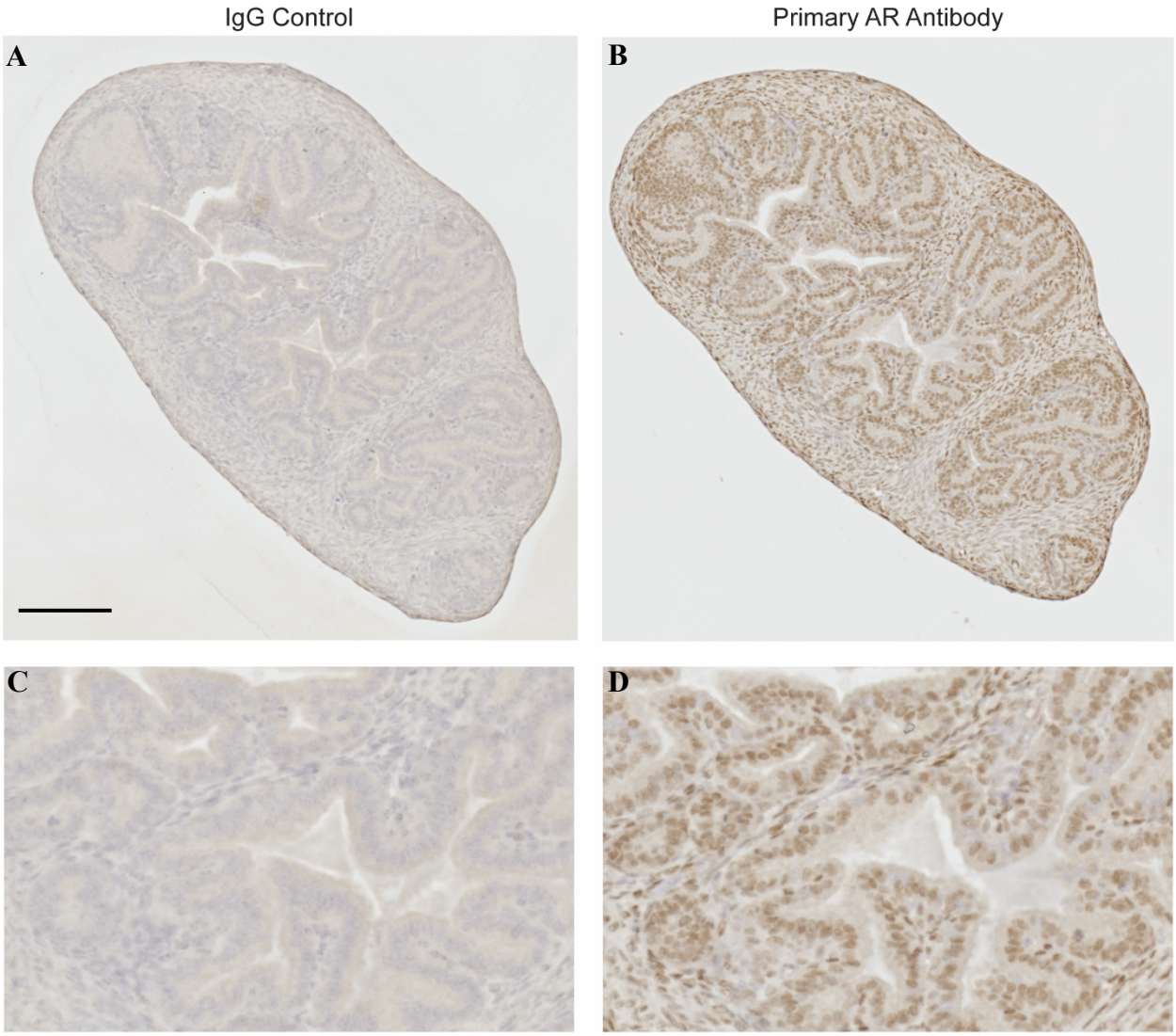


**Figure 3.8 Detection of AR protein in seminal vesicles by IHC**

Representative photos of AR IHC in pubertal mouse seminal vesicles. (A) IgG isotype negative control. (B) AR protein staining. (C) and (D) show close-ups of images (A) and (B), respectively. The pseudostratified columnar epithelium and stromal tissue of pubertal mouse seminal vesicles exhibited specific nuclear staining for AR protein, as compared to the IgG isotype control which showed no specific staining. Magnification: 20X. Scale bar: 250 μm.

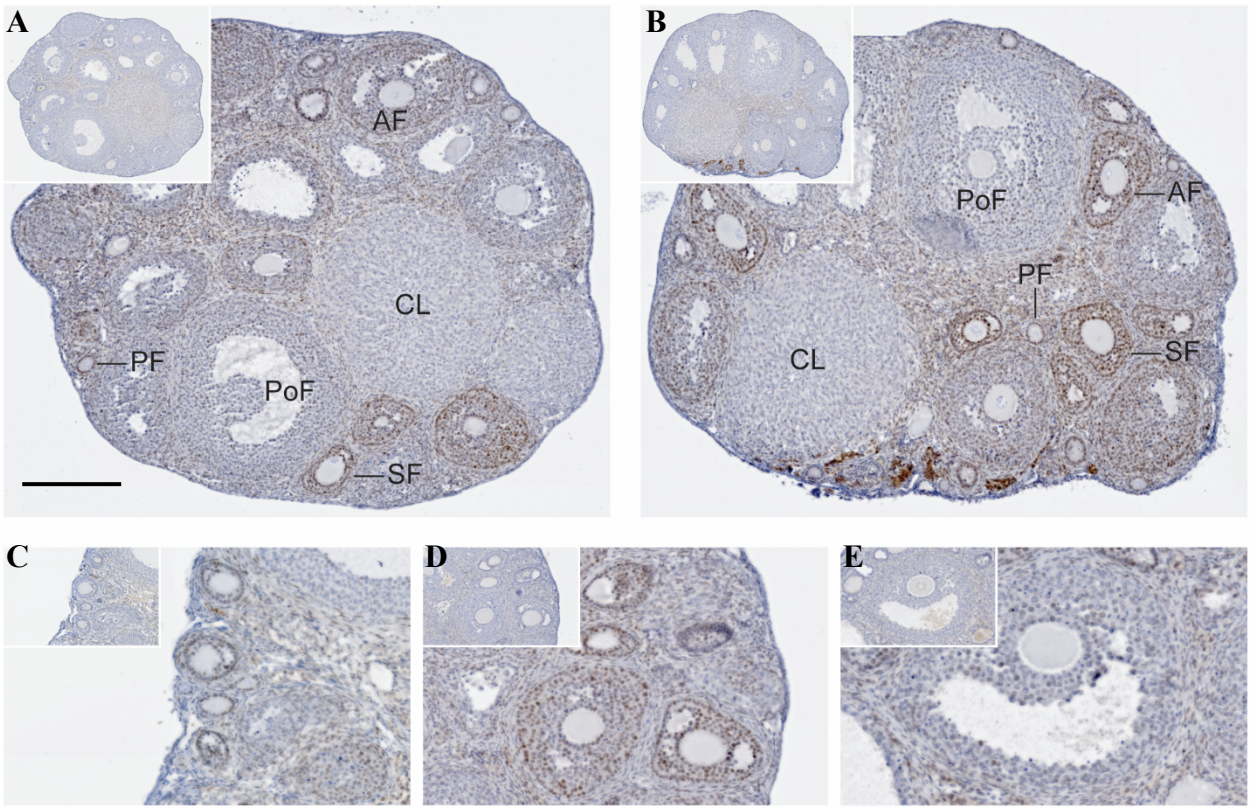


**Figure 3.9 Detection of AR protein in inbred SWR ovaries by IHC**

Representative photos of AR IHC in ovaries from untreated inbred SWR mice necropsied at 8 wk of age. (A) & (B): paired whole ovaries from an SWR female. (C), (D) & (E): close-ups of primary and secondary, antral, and pre-ovulatory follicles, respectively, from ovaries from unique SWR females. Specific nuclear AR protein expression was strongest in the GCs of secondary and early antral follicles. Insets: IgG isotype negative control. AF: antral follicle; CL: corpus luteum; PF: primary follicle; PoF: pre-ovulatory follicle; SF: secondary follicle. Magnification: 20X. Scale bar: 250 µm.

the T-treated cohort (0.0% GC tumour frequency), whereas 20.0% (n = 4) of DHEA-treated females developed unilateral GC tumours (4/40 [10.0%] ovaries with a GC tumour). DHEA- and T-treated normal ovaries and DHEA-induced GC tumours were collected and examined for their AR expression pattern by IHC (Figure 3.10). The AR protein expression pattern observed in the normal ovaries of DHEA-treated females closely resembled that of untreated SWR mice, with specific nuclear staining for AR protein present in the GCs of primary, secondary, and early antral follicles. Again, the strongest AR protein expression was observed in the GCs of secondary and early antral follicles, whereas pre-ovulatory follicles were mainly comprised of GCs that were negative for AR protein expression with sporadic low- to mid-intensity AR protein positive cells. Occasional corpus luteum cells again showed low-intensity staining for AR protein expression, with many samples exhibiting high levels of background staining. Specific nuclear AR protein expression was observed in TCs and other stromal cells, whereas the cells of the OSE and oocytes at all stages of follicle development were negative for AR protein expression. T-treated normal ovaries exhibited a similar pattern of AR protein expression to that observed in untreated and DHEA-treated ovaries, although the overall intensity of AR protein expression was consistently higher. AR protein-positive tumour cells were observed in proliferative regions of DHEA-induced GC tumours, with a specific nuclear expression pattern.

### 3.3.3 Selective Knockout of the Androgen Receptor Gene in Granulosa Cells

A cohort of 19 untreated mice generated from the two-generation breeding scheme to delete the *Ar* from the GCs of SWR mice were necropsied at 3 wk of age, and ovary pairs (n = 38) were collected and assayed for AR expression by IHC. The AR-stained slides were blinded, and ovaries were examined and categorized as either GC AR protein-positive or -negative, based

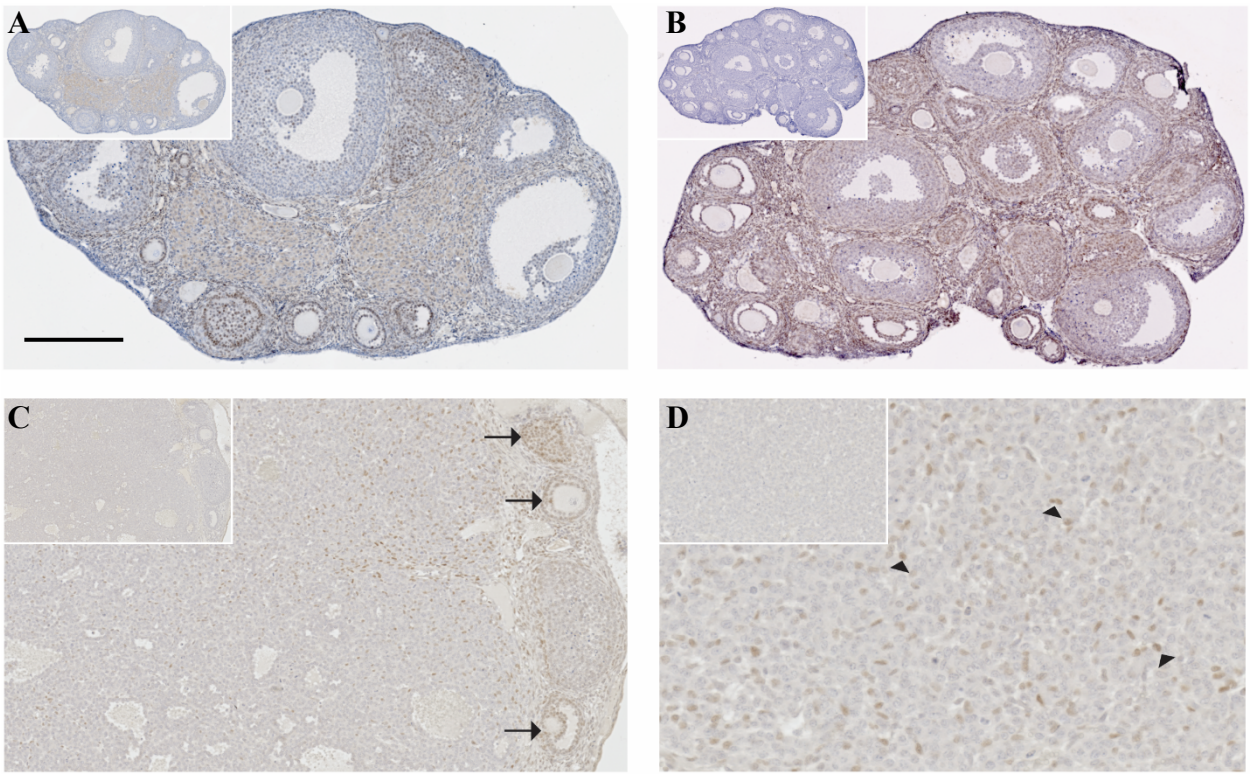


**Figure 3.10 Detection of AR protein in androgen-treated inbred SWR ovaries and androgen-induced GC tumours by IHC**

Representative photos of AR IHC in ovaries and GC tumours from androgen-treated inbred SWR mice necropsied at 8 wk of age. (A) & (B): normal ovaries from DHEA- and T-treated mice, respectively. (C): a DHEA-induced GC tumour; arrows indicate follicles with GC specific nuclear AR protein expression that have been pushed to the edge by the expanding GC tumour tissue. (D): close-up of the GC tumour shown in (C); arrowheads indicate GC tumour cells with specific nuclear AR protein expression. Insets: IgG isotype negative control. Magnification: 20X. Scale bar: 250 µm.

solely on GC AR expression and with the expectation that ovaries with AR protein-positive GCs were from SWR.$Ar^{+/flox}Amhr2^{cre/+}$ heterozygous control mice, and ovaries with AR protein-negative GCs were from SWR.$Ar^{flox/flox}Amhr2^{cre/+}$ GC-ArKO mice. The majority of ovaries (n = 28 ovaries from 14 mice) exhibited an AR protein staining pattern similar to that observed in inbred SWR mice at 8 wk of age, with specific nuclear staining in GCs and TCs, but not in oocytes or the cells of the OSE (Figure 3.11). AR protein expression was again strongest in the GCs of secondary and early antral follicles. A smaller proportion of untreated pubertal ovaries (n = 10 ovaries from five mice) displayed significantly fewer AR protein-positive GCs in the presence of AR protein-positive TCs and other stromal cells. Primary follicles in these ovaries were composed mainly of AR protein-negative GCs, with some low-intensity AR protein-positive GCs present in some follicles. While some secondary and antral follicles were similarly GC AR protein-negative, many displayed a mosaic appearance in which clustered subsets of GCs displayed mid- to high-intensity AR protein expression (Figure 3.12). The GCs of most pre-ovulatory follicles displayed low-intensity AR protein expression with either a sporadic pattern similar to that observed in inbred SWR ovaries, or a mosaic appearance similar to that observed in secondary and antral follicles; others were composed entirely of AR protein-negative GCs. Overall, the ovaries from these five mice displayed a range of variability in GC AR protein expression, although no ovaries characterized as GC AR protein-negative exhibited a complete lack of GC AR protein staining. Notably, ovary pairs from within an individual mouse displayed the same GC AR protein expression phenotype (i.e., both ovaries within an ovary pair were categorized as either GC AR protein-positive or AR protein-negative). Upon PCR genotyping, all five mice with ovaries categorized as GC AR protein-negative were found to possess an $Ar^{flox/flox}Amhr2^{cre/+}$, GC-ArKO genotype. Of the 14 ovary pairs that were scored as positive for

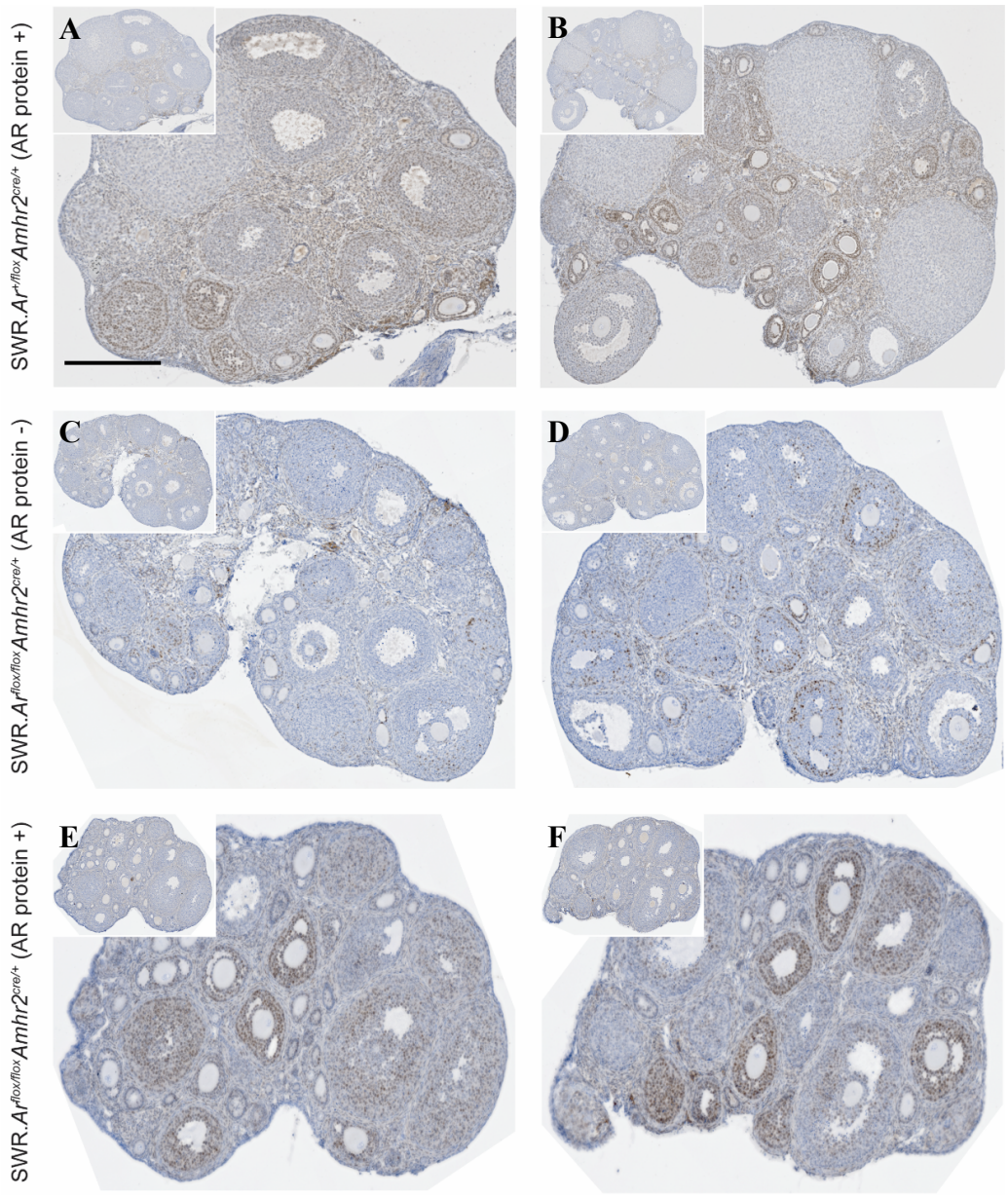


**Figure 3.11 Detection of AR protein in pubertal SWR GC-ArKO and heterozygous control ovaries by IHC**

Representative photos of AR IHC in ovaries of SWR GC-ArKO and heterozygous control mice necropsied at 3 wk of age. (A) & (B): paired ovaries from an SWR.$Ar^{+/flox}Amhr2^{cre/+}$ female scored as AR protein positive. (C) & (D): paired ovaries from an SWR.$Ar^{flox/flox}Amhr2^{cre/+}$ female scored as AR protein negative. (E) & (F): paired ovaries from an SWR.$Ar^{flox/flox}Amhr2^{cre/+}$ female scored as AR protein positive. Insets: IgG isotype negative control. Magnification: 20X. Scale bar: 250 µm.

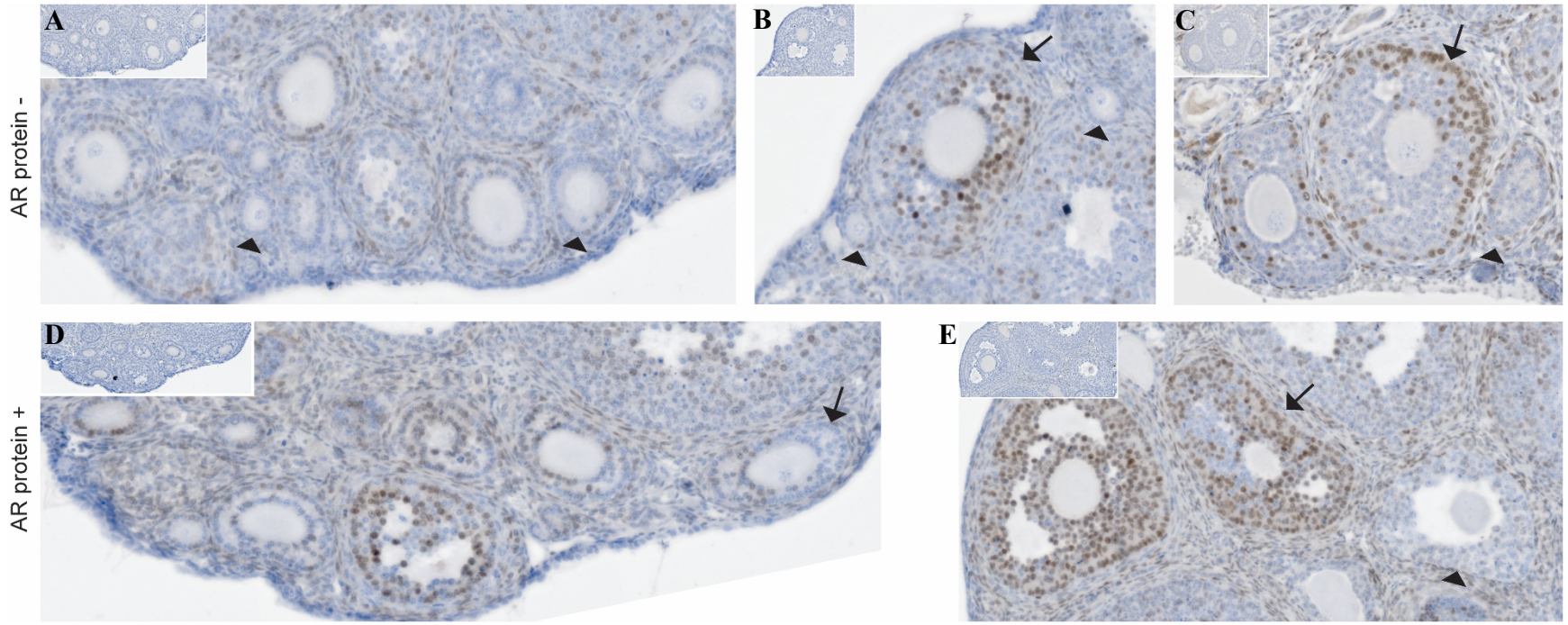


**Figure 3.12 Detection of AR protein in pubertal SWR GC-ArKO follicles by IHC**

Representative photos of AR IHC in ovarian follicles of SWR GC-ArKO mice necropsied at 3 wk of age. (A), (B) & (C): close-ups of follicles from ovaries categorized as AR protein-negative. (D) & (E): close-ups of follicles from ovaries categorized as AR protein-positive. Follicles with a mosaic pattern of GC AR protein expression (arrows) and follicles entirely or largely composed of AR protein-negative GCs (arrowheads) were frequently observed in SWR GC-ArKO ovaries. Samples shown in (A & B), (C), and (D & E) are from individual mice. Insets: IgG isotype negative control. Magnification: 20X.

GC AR expression, and were thus categorized as ovaries from heterozygous control females, 11 had an $Ar^{+/flox}Amhr2^{cre/+}$ genotype that matched the GC AR expression phenotype as expected; however, three of the 14 AR protein-positive ovary pairs were in actuality from mice with an $Ar^{flox/flox}Amhr2^{cre/+}$, GC-ArKO genotype. Therefore, ovaries from SWR GC-ArKO mice could be categorized as "good" *Ar* KOs that were hypomorphic for GC AR, albeit with a spectrum of GC AR protein expression ranging from almost none to some, or "poor" *Ar* KOs that displayed AR protein-positive GCs, and were indistinguishable from the ovaries of heterozygous control mice. Examination of blinded, AR-stained slides from a cohort of 13 untreated pubertal B6J GC-ArKO and heterozygous control mice revealed that the majority (n = 18 ovaries from nine mice) were GC AR protein-positive, whereas a smaller proportion (n = eight ovaries from four mice) were GC AR protein-negative (Figure 3.13). The GC AR protein expression patterns in B6J ovaries categorized as AR protein-positive and -negative were similar to those observed in their respective SWR counterparts. PCR genotyping revealed that all four mice with ovaries categorized as GC AR protein-negative had an $Ar^{flox/flox}Amhr2^{cre/+}$, GC-ArKO genotype, as did two of the nine mice with ovaries categorized as GC AR protein-positive; the remaining seven mice with AR protein-positive GCs had an $Ar^{+/flox}Amhr2^{cre/+}$, heterozygous control genotype.

The high degree of GC AR protein expression observed in the ovaries of some SWR and B6J GC-ArKO mice necropsied at 3 wk of age imparted uncertainty about the performance of the *Amhr2* promoter-driven deletion strategy. Although near complete GC *Ar* excision was observed in the ovaries of some females, genotype could not be confidently relied upon as an indicator of GC AR protein expression phenotype. Therefore, it was required that we examine all ovaries and GC tumours from mice with an $Ar^{flox/flox}Amhr2^{cre/+}$ genotype for their GC AR protein expression phenotype by IHC, and categorize them appropriately (i.e. AR protein-positive or

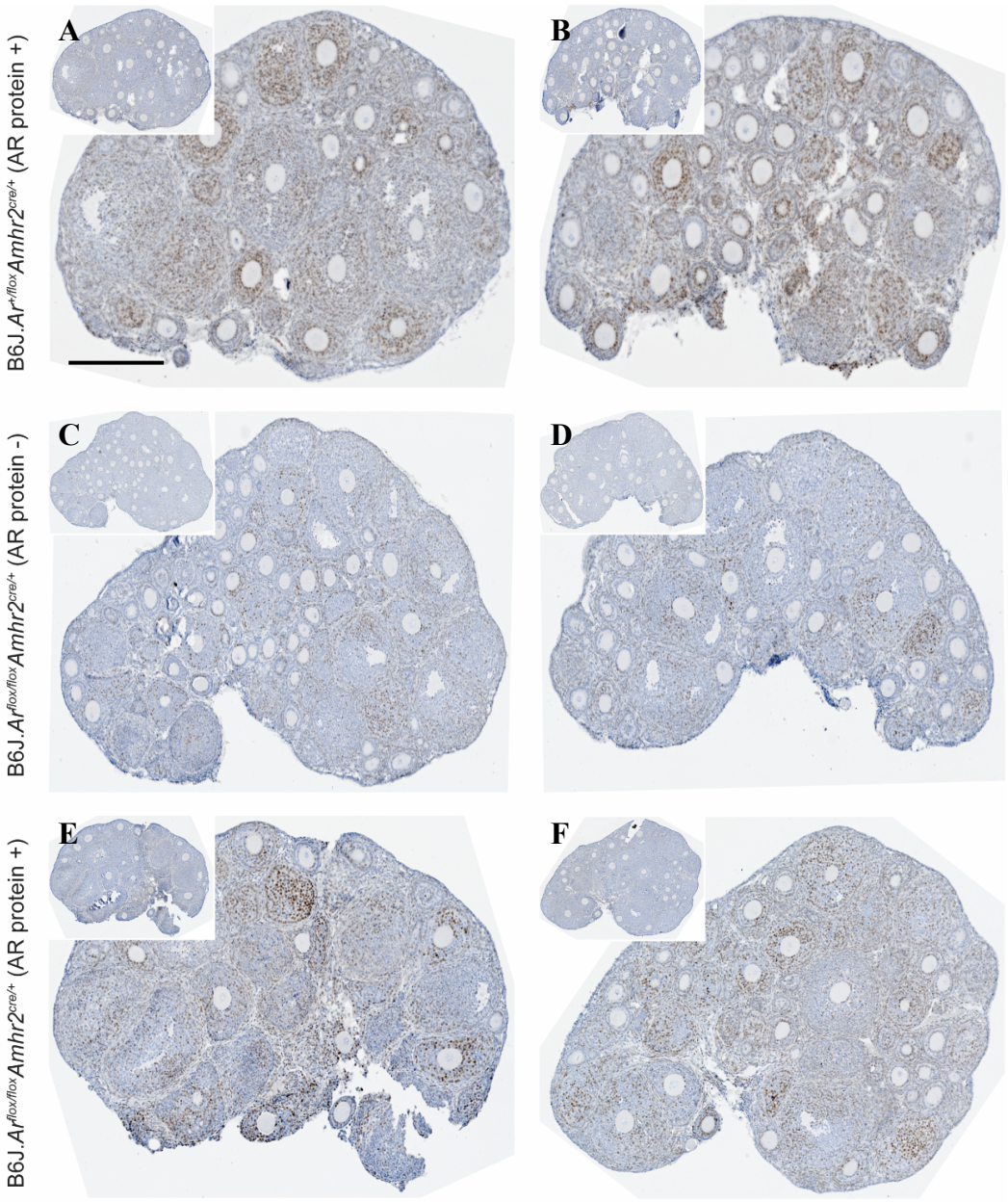


**Figure 3.13 Detection of AR protein in pubertal B6J GC-ArKO and heterozygous control ovaries by IHC**

Representative photos of AR IHC in ovaries of B6J GC-ArKO and heterozygous control mice necropsied at 3 wk of age. (A) & (B): paired ovaries from a B6J.$Ar^{+/flox}Amhr2^{cre/+}$ female scored as AR protein positive. (C) & (D): paired ovaries from a B6J.$Ar^{flox/flox}Amhr2^{cre/+}$ female scored as AR protein negative. (E) & (F): paired ovaries from a B6J.$Ar^{flox/flox}Amhr2^{cre/+}$ female scored as AR protein positive. Insets: IgG isotype negative control. Magnification: 20X. Scale bar: 250 µm.

-negative) prior to further study from this point forward in our investigation.

As part of our examination of GC tumour susceptibility with androgens in the absence of the AR (Section 3.3.4, described below), we blindly examined GC AR protein expression in ovaries from androgen-treated adult SWR GC-ArKO and heterozygous control females at 8 wk of age by IHC. As in ovaries from mice necropsied at 3 wk of age, we categorized ovary pairs as either GC AR protein-positive or -negative. Of 111 ovary pairs from androgen-treated mice, 79 were categorized as GC AR protein-positive and 32 were categorized as GC AR protein-negative (Figure 3.14). GC AR protein-positive ovaries exhibited an AR protein staining pattern similar to that observed in adult inbred SWR mice, with specific nuclear staining in GCs and TCs, but not in oocytes or the cells of the OSE. AR protein expression was again strongest in the GCs of secondary and early antral follicles. In contrast, ovaries categorized as GC AR protein-negative displayed significantly fewer AR protein-positive GCs in the presence of AR protein-positive TCs and other stromal cells. As in mice examined at puberty, follicular mosaicism in GC AR protein expression was present, and a range of variability in GC AR protein expression was observed. Again, no ovaries characterized as GC AR protein-negative exhibited a complete lack of GC AR protein staining, and ovary pairs from within an individual mouse displayed the same GC AR protein expression phenotype. Although PCR genotyping revealed that all 32 GC AR protein-negative mice had an $Ar^{flox/flox}Amhr2^{cre/+}$ genotype, 14 of the 79 GC AR protein-positive mice possessed this genotype as well. Notably, DHEA did not appear to affect GC AR protein expression, whereas T treatment, as in inbred SWR females, increased the overall AR protein staining intensity (Section 3.3.2 and Figure 3.10). Similar results were obtained following an examination of 51 DHEA-treated adult B6J GC-ArKO and heterozygous control mice (Figure 3.15); of 50 ovary pairs categorized as GC AR protein-positive, six were found to possess an

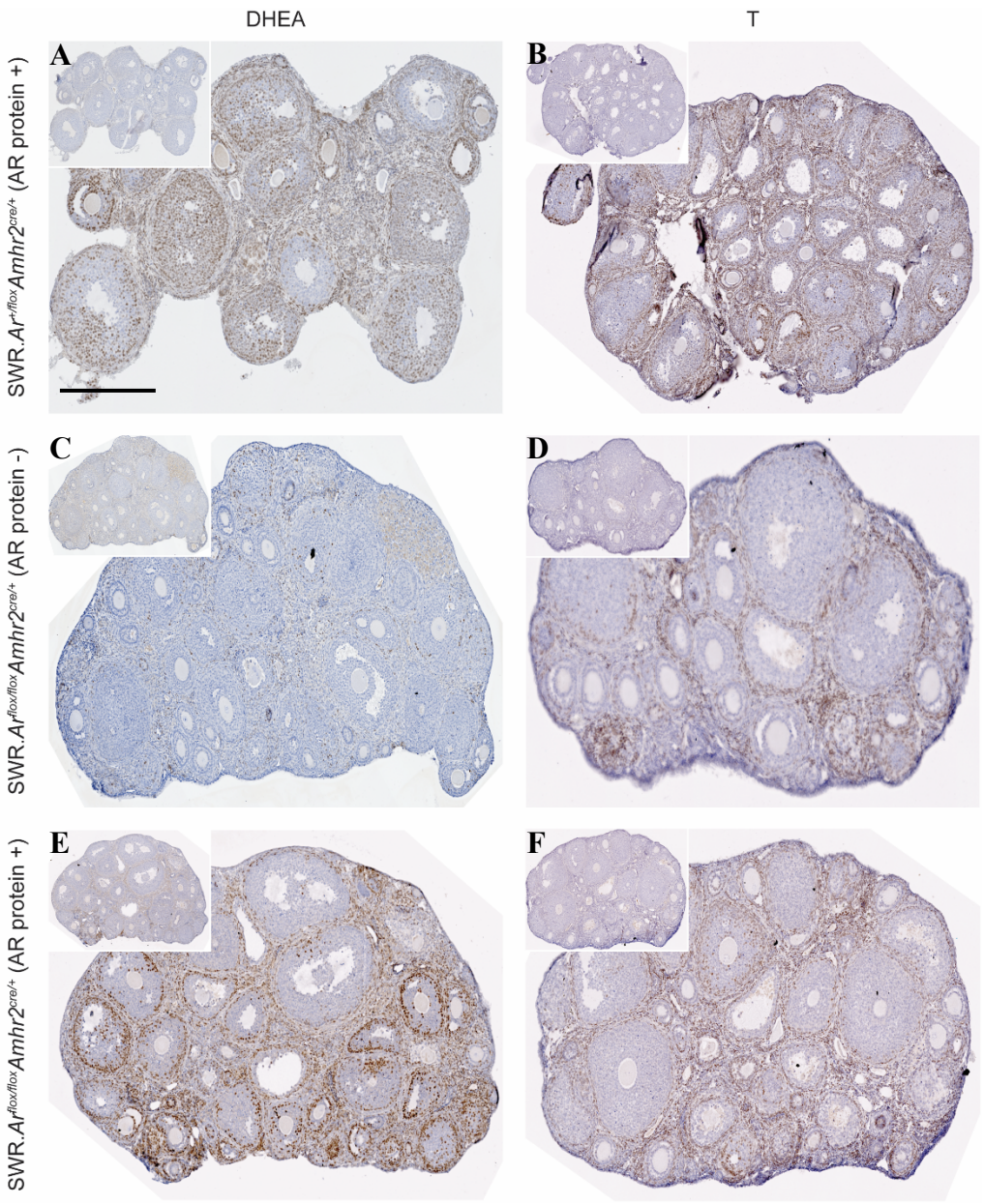


**Figure 3.14 Detection of AR protein in androgen-treated adult SWR GC-ArKO and heterozygous control ovaries by IHC**

Representative photos of AR IHC in ovaries of SWR GC-ArKO and heterozygous control mice necropsied at 8 wk of age. (A) & (B): ovaries from SWR.$Ar^{+/flox}Amhr2^{cre/+}$ females scored as AR protein positive. (C) & (D): ovaries from SWR.$Ar^{flox/flox}Amhr2^{cre/+}$ females scored as AR protein negative. (E) & (F): ovaries from SWR.$Ar^{flox/flox}Amhr2^{cre/+}$ females scored as AR protein positive. Ovaries from (A), (C), and (E), and (B), (D), and (F), were treated with DHEA and T, respectively. Insets: IgG isotype negative control. Magnification: 20X. Scale bar: 250 µm.

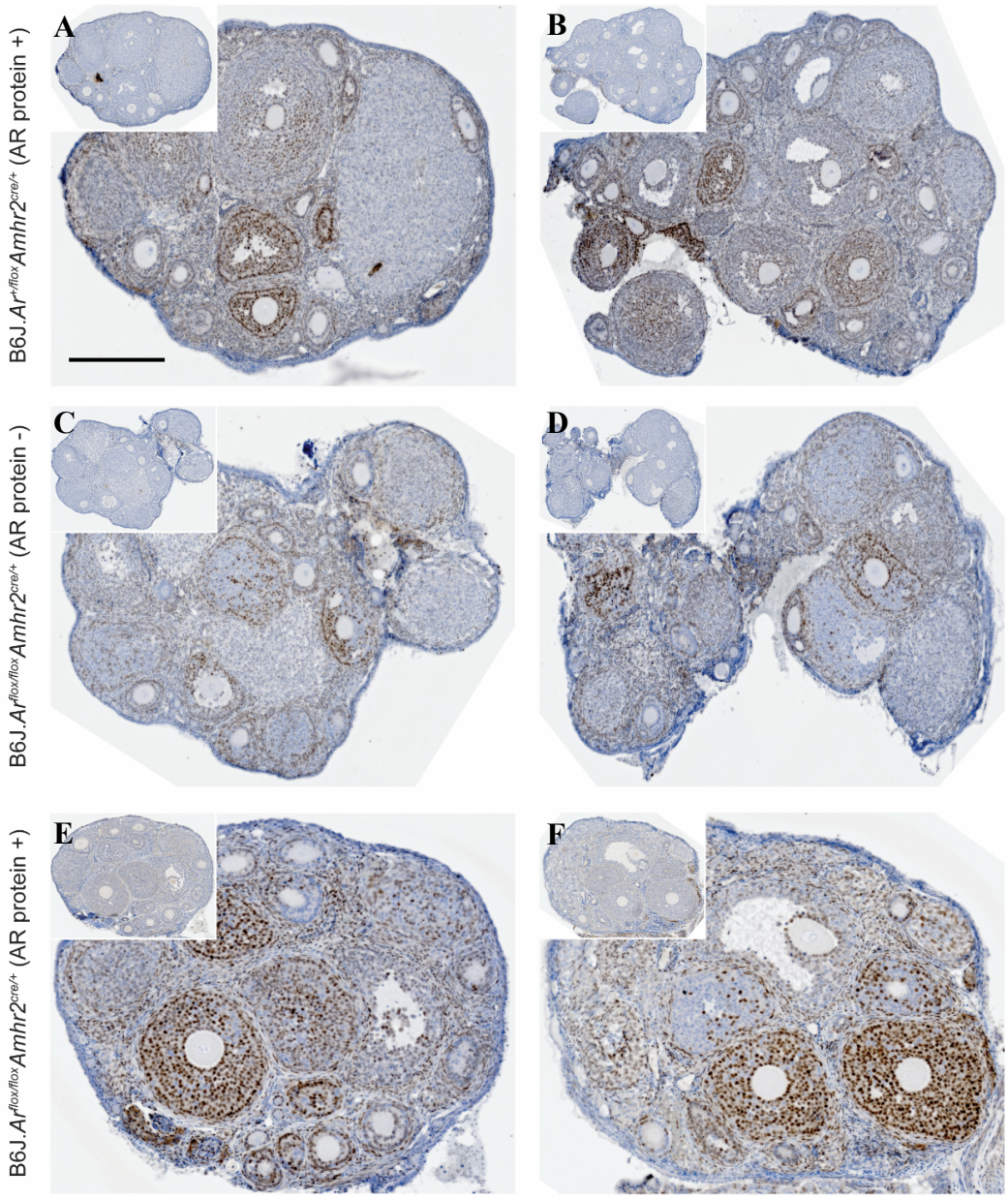


**Figure 3.15 Detection of AR protein in DHEA-treated adult B6J GC-ArKO and heterozygous control ovaries by IHC**

Representative photos of AR IHC in DHEA-treated ovaries of B6J GC-ArKO and heterozygous control mice necropsied at 8 wk of age. (A) & (B): paired ovaries from a B6J.*Ar*$^{+/flox}$*Amhr2*$^{cre/+}$ female scored as AR protein positive. (C) & (D): paired ovaries from a B6J.*Ar*$^{flox/flox}$*Amhr2*$^{cre/+}$ female scored as AR protein negative. (E) & (F): paired ovaries from a B6J.*Ar*$^{flox/flox}$*Amhr2*$^{cre/+}$ female scored as AR protein positive. Insets: IgG isotype negative control. Magnification: 20X. Scale bar: 250 µm.

*Ar*$^{flox/flox}$*Amhr2*$^{cre/+}$ genotype. This examination therefore revealed that the variability of the GC-specific AR KO observed in SWR and B6J GC-ArKO mice at 3 wk was also present at 8 wk of age.

### 3.3.4 Granulosa Cell Tumour Frequencies in GC-ArKO Mice

#### 3.3.4.1 SWR Inbred Strain Background

Female SWR GC-ArKO and heterozygous control mice were tested for GC tumour incidence following the administration of DHEA or T at puberty, with an 8 wk endpoint for GC tumour assessment. Following necropsy, all ovary pairs from mice with an *Ar*$^{flox/flox}$*Amhr2*$^{cre/+}$, GC-ArKO genotype were blinded and tested for their GC AR protein expression pattern by IHC, and were categorized as either GC AR protein-positive or -negative (Section 3.3.3, described above). All androgen-induced GC tumours were tested for AR protein expression by IHC, regardless of the host's genotype. Of the 32 GC AR protein-negative females generated, 13 were administered DHEA and 19 were administered T, whereas of the 79 GC AR protein-positive females generated, 45 were administered DHEA and 34 were administered T. Mice with AR protein-positive GCs were susceptible to GC tumour initiation following stimulation with DHEA at puberty and developed unilateral (n = 3) or bilateral (n = 5) GC tumours within 8 wk at a frequency of 17.8% (8/45 females, or 13/90 [14.4%] ovaries with a GC tumour; Table 3.10). Similarly, the administration of T at puberty led to the initiation of unilateral (n = 3) or bilateral (n = 6) GC tumours in GC AR protein-positive females at a frequency of 26.5% (9/34 females, or 15/68 [22.1%] ovaries with a GC tumour). The GC tumours that appeared in GC AR protein-positive females resembled androgen-induced GC tumours found in inbred SWR mice (data not shown). The GC tumour frequencies observed following DHEA or T supplementation were not

**Table 3.10 GC tumour incidence in SWR GC AR protein-positive and -negative female mice treated with DHEA or T at puberty.** GC tumour frequencies (GC tumour hosts versus all treated mice) and the number of affected ovaries (individual GC tumours observed versus all ovaries examined) in 8 wk old mice stratified by GC AR protein expression are shown.

| AR Protein Expression | DHEA | | T | |
|---|---|---|---|---|
| | GC Tumour Hosts/ Treated Mice | Individual GC Tumours/ Ovaries Examined | GC Tumour Hosts/ Treated Mice | Individual GC Tumours/ Ovaries Examined |
| Negative | 0/13 (0.0%) | 0/26 (0.0%) | 0/19 (0.0%) | 0/38 (0.0%) |
| Positive | 8/45 (17.8%) | 13/90 (14.4%) | 9/34 (26.5%) | 15/68 (22.1%) |

significantly different than those reported in SWR females administered DHEA (17.6%; Smith 2011; $p = 1.0000$) or fed T in the diet over the pubertal transition (17.4%; Tennent, Shultz & Beamer 1993; $p = 0.2308$) when compared by Fisher's exact test. An IHC examination of AR protein expression revealed the presence of AR staining in the nuclei of GC tumour cells throughout all androgen-induced GC tumours that arose, regardless of genotype (Figure 3.16 and data not shown). A subset of androgen-treated, matched normal contralateral ovaries from SWR GC-ArKO mice were largely GC AR protein-negative, despite the presence of nuclear AR in GC tumour cells. Many of the androgen-induced GC tumours that appeared in SWR GC-ArKO and heterozygous control mice retained follicles, which were pushed to the edges by the expanding GC tumour tissue (Figure 3.17 and data not shown). In GC tumours from SWR GC-ArKO mice, GC AR protein expression in these follicles ranged from almost none to expression in all GCs present, recapitulating the variable GC AR expression phenotype we observed in normal and androgen-treated ovaries. In contrast to mice with AR protein-positive GCs, no GC tumours were observed in the 32 mice with AR protein-negative GCs following the administration of either androgen at puberty (0.0% GC tumour frequencies; Table 3.10). This GC tumour frequency was significantly lower ($p = 0.0027$) than that observed in females with AR protein-positive GCs following administration of DHEA or T when compared by Fisher's exact test.

#### 3.3.4.2 B6J Inbred Strain Background

Female B6J GC-ArKO and heterozygous control mice were tested for GC tumour incidence following the administration of DHEA puberty, with an 8 wk endpoint for GC tumour assessment (n = 51). As with SWR mice, all ovary pairs from females with an $Ar^{flox/flox}Amhr2^{cre/+}$, GC-ArKO genotype were tested for their GC AR protein expression pattern

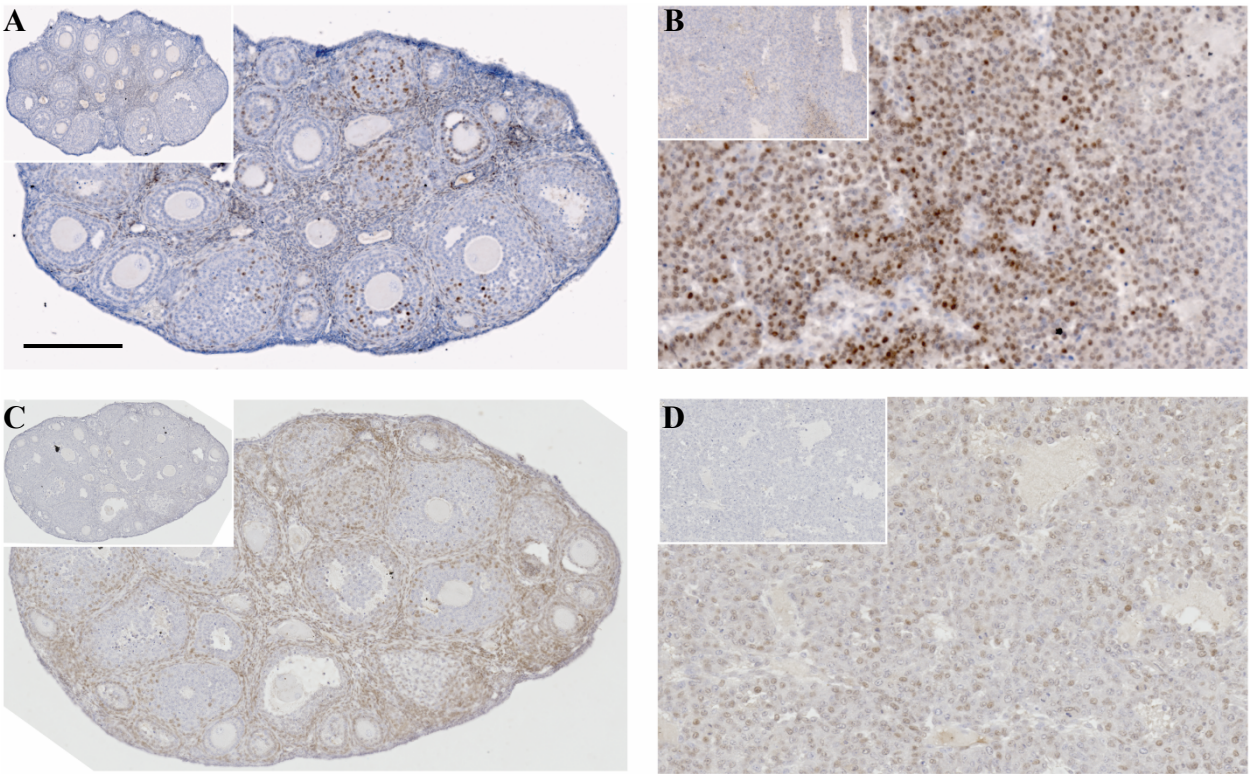


**Figure 3.16 Detection of AR protein in androgen-induced GC tumours and contralateral normal ovaries from SWR GC-ArKO mice by IHC**

Representative photos of AR IHC in DHEA- (A & B) or T- (C & D) induced unilateral GC tumours (B & D) and their respective contralateral ovaries (A & C) from SWR GC-ArKO mice necropsied at 8 wk of age. All androgen-induced GC tumours were AR protein-positive, including those that appeared in SWR-GC-ArKO (above) and heterozygous control mice (data not shown). In contrast, a subset of androgen-treated, matched normal contralateral ovaries from SWR GC-ArKO mice were largely GC AR protein-negative. Note the increased intensity of AR protein staining in the TCs and stromal tissue of the normal contralateral ovary following T administration (C). Insets: IgG isotype negative control. Magnification: 20X. Scale bar: 250 µm.

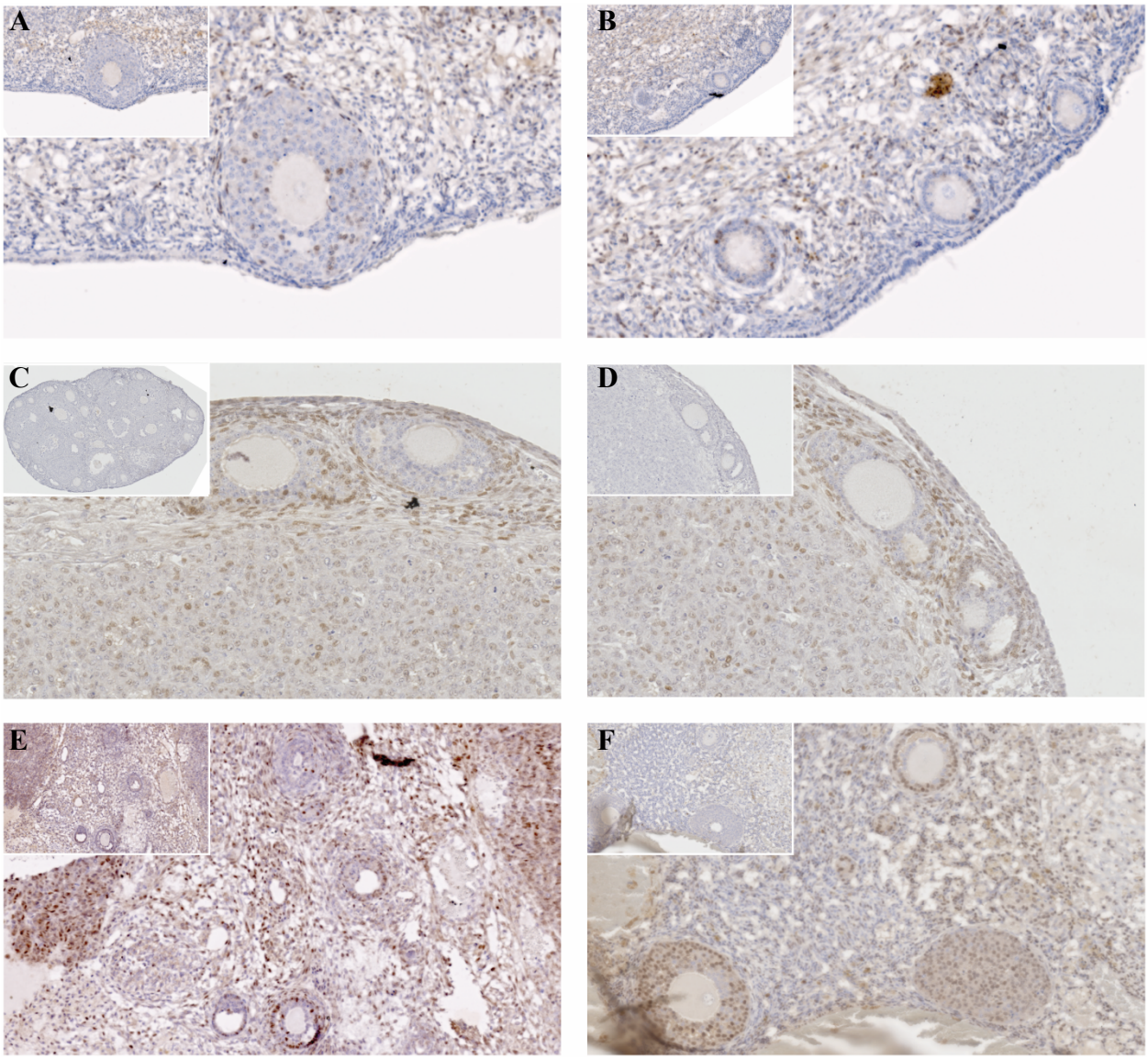


**Figure 3.17 Detection of AR protein in follicles within androgen-induced GC tumours from SWR GC-ArKO mice by IHC**

Representative photos of AR IHC in follicles within DHEA (A, B, E, & F) or T- (C & D) induced GC tumours from SWR GC-ArKO mice necropsied at 8 wk of age. Follicles that have been pushed to the edge by the expanding GC tumour tissue show various levels of GC AR protein expression, ranging from almost none to expression in all GCs. Samples shown in (A & B), (C & D), (E), and (F) are from individual mice. Insets: IgG isotype negative control. Magnification: 20X.

by IHC, and were categorized as either GC AR protein-positive or -negative. Only one GC AR protein-negative female was generated, whereas 50 GC AR protein-positive females were generated. No macroscopic ovarian phenotypes, including the appearance of GC tumours, were observed in the B6J inbred strain background, either spontaneously or when DHEA was given at puberty, regardless of classification by GC AR protein expression status (Table 3.11).

**Table 3.11 GC tumour incidence in B6J GC AR protein-positive and -negative female mice treated with DHEA at puberty.**

GC tumour frequencies (GC tumour hosts versus all treated mice) and the number of affected ovaries (individual GC tumours observed versus all ovaries examined) in 8 wk old mice stratified by GC AR protein expression are shown.

| AR Protein Expression | GC Tumour Hosts/ Treated Mice | Individual GC Tumours/ Ovaries Examined |
|---|---|---|
| Negative | 0/1 (0.0%) | 0/2 (0.0%) |
| Positive | 0/51 (0.0%) | 0/102 (0.0%) |

## 3.4 Discussion

### 3.4.1 Overview

The spontaneous trait of juvenile-onset ovarian GC tumours in SWR mice is polygenic, with the *Gct4* locus on Chr X acting in the presence of homozygous $Gct1^{SW}$ alleles to influence tumour frequency in an allele-dependent manner. Significant evidence suggests that the AR shares identity with *Gct4*, and is required for GC tumour initiation in SWR mice. The objective of this dissertation chapter was to use a GC-specific KO strategy to explore the influence of AR signalling as a trigger of spontaneous juvenile-onset GC tumourigenesis in the unique SWR model. This strategy required the transfer of individual genetic constructs and confirmation that GC tumour susceptibility was retained at every phase of the experimental design. Overall, the GC tumour phenotype was stable during the development of the engineered strains in order to complete the experimental crosses to delete the AR from the GC compartment, generating evidence to support our hypothesis that AR-mediated signalling is required for GC tumour development.

### 3.4.2 The Androgen Receptor is Required for GC Tumourigenesis in SWR Mice

#### 3.4.2.1 The AR is Expressed in SWR Mouse Ovaries and Granulosa Cell Tumours

The AR antibody employed in this investigation was first validated prior to investigations of GC AR protein expression in inbred SWR, GC-ArKO and heterozygous control ovaries (Figure 3.8). The inclusion of pubertal mouse seminal vesicle tissue as a positive technical control as well as matched IgG negative control tissues on all slides ensured confidence in the

specificity of the AR antibody, as well as its performance between individual slides and experiments.

An investigation of AR protein in the normal SWR ovary, as well as in normal androgen-treated ovaries and androgen-induced GC tumours, was completed to establish a baseline for qualitative ovarian AR protein expression. GCs displayed specific nuclear AR protein expression at all follicle stages, with expression strongest in the GCs of secondary and early antral follicles (Figure 3.9). AR protein expression was also observed in the TCs and other stromal tissue throughout the ovary, but not in the cells of the OSE or oocytes. Overall, the pattern of GC AR protein expression closely resembled that previously observed in the literature (Figure 3.3; Cheng *et al*. 2002), with some exceptions. SWR ovaries lacked a gradient of AR expression between the cumulus and mural GCs of pre-ovulatory follicles previously observed in a single investigation in the mouse (Lenie & Smitz 2009). Similarly, specific AR protein expression was not observed in oocytes, as has been reported (Gill, Jamnongjit & Hammes 2004; Li *et al*. 2008b; Sen & Hammes 2010). These deviations from the pattern of AR protein expression in the literature may be due to differences in methodology, or might represent a truly differential pattern in SWR mice compared to that found in other strains. The treatment of pubertal SWR females with DHEA did not affect AR protein localization or the intensity of its expression in ovaries at 8 wk of age (Figure 3.10). In contrast, T-treated normal ovaries exhibited consistently higher intensities of AR protein expression; qualitative increases in ovarian AR protein expression following T administration have been reported previously (Weil *et al*. 1998; Yang *et al*. 2015). Finally, AR protein-positive tumour cells were observed in proliferative regions of DHEA-induced GC tumours, with a specific nuclear expression pattern. AR protein expression varies in human GC tumours, with some showing no AR protein expression and others

exhibiting specific nuclear staining ranging from weak to strong (Chadha *et al*. 1993; Ahonen *et al*. 2000; Kato *et al*. 2001; Vang, Herrmann & Tavassoli 2004; Niwa *et al*. 2013). In the largest series examined to date, 59% (17/29) of human GC tumours expressed some level of nuclear AR protein (Mills *et al*. 2019); however, examinations of AR protein expression published to date did not incorporate the latest *FOXL2* diagnostic paradigm and do not otherwise distinguish between the adult and juvenile GC tumour subtypes.

#### 3.4.2.2 Retention of GC Tumour Susceptibility in Engineered SWR Cre/*loxP* Strains

The $Ar^{flox}$ and $Amhr2^{cre}$ constructs were backcrossed onto the SWR and/or the B6J inbred strains for a minimum of six generations, using marker-assisted progeny selection to achieve approximately 96.9% inbred strain background (Silver 1995). This "speed congenic" approach also ensured a full complement of SWR alleles at important *Gct* loci in SWR.$Ar^{flox}$ and SWR.$Amhr2^{cre}$ mice (Wong 2002). Importantly, SWR.$Ar^{flox}$ and SWR.$Amhr2^{cre}$ female mice developed GC tumours when administered DHEA or T at puberty, with a tumour onset timing and macroscopic and microscopic phenotype similar to that observed in androgen-treated inbred SWR mice (Table 3.7). GC tumour frequencies in SWR.$Ar^{flox}$ and SWR.$Amhr2^{cre}$ females were not statistically compared to each other, concurrent, or historically reported rates, as we were concerned only in ensuring that the SWR construct lines were sensitive to GC tumour development with androgen administration at puberty. Confirmation of androgen-induced GC tumour susceptibility retention in these construct lines allowed us to proceed with the experimental two-generation cross and subsequent androgen-treatment of SWR GC-ArKO and heterozygous control females.

The disruption of *Amhr2* exon 5 by the *cre* cassette is presumed to create a null *Amhr2* allele (Jamin *et al*. 2002); however, hemizygosity for *Amhr2* in an SWR background had no notable positive or negative influence on the rate of spontaneous GC tumour initiation in breeding colonies, or on the rate of androgen-induced GC tumour initiation in steroid capsule studies. AMH is secreted by the GCs of growing follicles, and mediates the assembly of primordial follicles (Nilsson *et al*. 2011) but negatively regulates primordial follicle activation (Durlinger *et al*. 1999). AMH is a member of the TGF-β superfamily, and transduces its signals via a heteromeric receptor complex composed of the type II receptor AMHR2 and either of the BMPR1A, BMPR1B, or activin A receptor type-1 (ACVR1) type I receptors (Visser 2003). The binding of AMH to these receptors activates the SMAD1/SMAD5/SMAD8 pathway, resulting in the regulation of gene transcription (Clarke *et al*. 2001). Loss of one *Amhr2* allele might therefore result in reduced levels SMAD1/SMAD5/SMAD8-transduced AMH signalling. Multiple signalling molecules downstream of AMH have been implicated in GC tumourigenesis through mouse model investigations (e.g. *Bmpr1a*/*Bmpr1b* and *Smad1*/*Smad5* GC-specific dKO models), as have other TGF-β superfamily members (e.g. global *Inha* KO, constitutive activation of *Tgfbr1* in GCs; Table 1.1). However, AMH KO mice do not develop GC tumours up to 13 mo of age (Durlinger *et al*. 1999), and although human juvenile GC tumours secrete AMH (Silverman & Gitelman 1996), it has not been implicated as an initiating factor in human cases. Instead, AMH has been shown to promote apoptosis in KGN cells and primary adult GC tumour cells (Anttonen *et al*. 2011); this inhibitory effect on GC tumour cell growth is presumably abolished in mouse models in which downstream AMH signalling molecules are deleted, resulting in tumour initiation (Anttonen *et al*. 2011). Regardless, loss of one allele of *Amhr2* in GCs and a potential decrease in AMH signalling does not appear to be influential on GC tumour

initiation in SWR mice, as no notable increase in spontaneous GC tumour frequency or inhibitory action in the case of androgen-induced GC tumour frequency were observed. No other spontaneous ovarian pathologies were observed in female breeders with an *Amhr2*$^{cre}$ allele, nor did the loss of one *Amhr2* allele result in decreases in fertility in either strain. However, a statistically significant increase in pups weaned per litter was noted when SWR dams were mated to SWR.*Amhr2*$^{cre/+}$ sires compared to inbred SWR mice (multiplicity adjusted $p$ value = 0.0111; Figure 3.6). *Amhr2* is expressed on Sertoli cells (Baarends *et al*. 1995) and Leydig cells (Racine *et al*. 1998) in the male testis, and so expression of the *Amhr2*$^{cre}$ allele would inactivate one gene copy in these cell types. AMH secreted by the Sertoli cells is responsible for the regression of the Müllerian ducts (Jost 1953), reduces aromatase activity (Rouiller-Fabre *et al*. 1998), and is a negative regulator of Leydig cell proliferation and therefore T production (Behringer, Finegold & Cate 1994). As low AMH levels have been correlated with infertility due to a lack of sperm in the semen (Xu *et al*. 2019), it is not clear how the loss of one *Amhr2* allele in SWR males could improve fertility over that of inbred SWR mice or of SWR.*Amhr2*$^{cre/+}$ dams bred to SWR sires, with no effect observed in the B6J.*Amhr2*$^{cre}$ colony. Given the minimal influences observed on fertility and the spontaneous and androgen-induced GC tumour phenotype, and the GC specificity enabled by the *Amhr2-cre* construct (Jorgez *et al*. 2004; Jeyasuria *et al*. 2004; Boerboom *et al*. 2005), it proved to be a suitable choice for our experimental strategy.

*Ar-flox* mice carry an *Ar* gene derived from the (129X1 x 129S1)$F_1$ mouse strain in which exon 2 is floxed (De Gendt *et al*. 2004). As was the case for *Amhr2* hemizygosity, the floxed (129X1 x 129S1)$F_1$ *Ar* allele had no notable positive or negative influence on the rate of spontaneous GC tumour initiation in breeding colonies, or on the rate of androgen-induced GC

tumour initiation in steroid capsule studies in an SWR background. Previous experiments designed to map *Gct4* have shown that allelic variation at this locus influences spontaneous GC tumour incidence, as SJL and CAST *Gct4* alleles increase phenotypic penetrance from ≤1% to approximately 20% in the absence of exogenous androgens when in the presence of an SWR genetic background (Beamer *et al*. 1998; Dorward *et al*. 2003). The lack of spontaneous GC tumours in female breeders from the SWR.$Ar^{flox}$ backcross or intercrossed colonies therefore suggests that the (129X1 x 129S1)$F_1$ *Ar* allele is not a strong spontaneous modifier of tumour initiation at *Gct4*, as are $Gct4^{CA}$ and $Gct4^{J}$. In addition, the presence of the floxed *Ar* allele did not result in any other spontaneous ovarian pathologies in female breeders or decreases in fertility in either strain. Thus, as with the $Amhr2^{cre}$ allele, the independent presence of the $Ar^{flox}$ allele did not significantly influence fertility or the expected GC tumour phenotype as has been previously observed, and the choice of floxed *Ar* construct was appropriate for further experimental crosses prior to testing for GC tumour incidence in mice lacking the AR in GCs.

#### 3.4.2.3 Generation of GC-ArKO Mice

SWR and B6J GC-ArKO and heterozygous control mice were successfully derived from the backcrossed construct lines using a two-generation breeding scheme (Figure 3.5). Highly significant deviations from the expected 1:1 male-to-female phenotypic sex ratio were observed in all experimental crosses from both strains, as considerably more female than male pups were noted at the time of weaning; such deviations were not observed in the individual $Ar^{flox}$ and $Amhr2^{cre}$ construct lines. Although the external phenotype of these mice resembled that of females, internal examination of a proportion of these animals revealed the absence of ovaries and uteri and the presence of testes-like structures in the absence of seminal vesicles. This

pseudo-hermaphrodite-like phenotype is reminiscent of CAIS in humans and the *Tfm* mouse model, in which mutations that inactivate the AR prevent the normal androgen response during sexual development and lead to infertility, differentiated testes that are retained in the abdomen, and a completely feminized physique (Quigley *et al*. 1995). The production of pseudo-hermaphrodites is presumably due to the deletion of the *Ar* in the *Amhr2*-expressing Sertoli cells of Chr XY genotypic males during the critical masculinization programming window hypothesized to take place between E13.5 to E17.5 in the mouse (Lehraiki *et al*. 2001). Approximately 70% of the observed phenotypic females would be expected to possess an XX Chr constitution, given the 1:1 male-to-female phenotypic sex ratio expected in typical litters. Indeed, PCR genotyping for sex chromosome constitution revealed that 62.5% to 67.1% of phenotypic females from the SWR and B6J experimental breeder cross 2 colonies, respectively, possessed an XX Chr constitution (Table 3.8). The generation of large numbers of pseudo-hermaphrodites suggests that the *Amhr2-cre* driver was operating efficiently upon *Amhr2* expression during the expected embryonic timeframe, although as phenotypic males were not genotyped for the presence of the $Amhr2^{cre}$ allele, an indirect measurement of Cre activity cannot be calculated. Likewise, the proportions of observed phenotypic females deviated from expected similarly in both the SWR and B6J strains, suggesting comparable levels of *Amhr2-cre* driver efficiency between strains.

As was the case for phenotypic sex ratios, significant deviations from the expected Mendelian frequencies were also noted for the $Ar^{flox}$ and $Amhr2^{cre}$ alleles in the female offspring of the B6J experimental breeder cross 2 (Table 3.8), and subsequently significantly more B6J heterozygous control females were generated than B6J GC-ArKO females (Table 3.9). The deviations from the expected allele frequencies were not observed in the individual B6J.$Ar^{flox}$ and

B6J.*Amhr2*$^{cre}$ construct lines, suggesting that the presence of these two constructs may induce embryonic lethality in a B6J background. Alternatively, the *Ar*$^{flox}$ allele may have been spontaneously lost from either the B6J.*Ar*$^{flox/Y}$*Amhr2*$^{+/+}$ male or B6J.*Ar*$^{flox/+}$*Amhr2*$^{+/cre}$ female experimental cross 2 breeders. Neither the intercrossed *Ar*$^{flox}$ colonies (*Ar*$^{flox/flox}$ or *Ar*$^{flox/Y}$ genotype) nor the experimental cross 1 female offspring (obligate *Ar*$^{flox}$ heterozygotes) were routinely genotyped to confirm the presence of the *Ar*$^{flox}$ allele prior to breeding to generate experimental cross 2 heterozygous control and GC-ArKO offspring. Genotyping of the six B6J experimental cross 1 breeder pairs would be required to confirm loss of the *Ar*$^{flox}$ allele. It is possible that the B6J strain tends to spontaneously lose the *Ar*$^{flox}$ allele at a higher frequency than the SWR strain, as no deviation from the expected frequency of heterozygous control and GC-ArKO female offspring was observed in an SWR strain background. We were previously aware of the possibility of spontaneous *Ar*$^{flox}$ allele loss, which occurred in the original B6N.*Ar*$^{flox}$ colony prior to the strain's transfer to our institution and significantly delayed this project. Finally, loss of one or both copies of the *Ar* did not result in any ovarian pathologies in female breeders or decreases in fertility in either strain. However, a statistically significant increase in pups weaned per litter was noted in the SWR experimental breeder cross 1 (multiplicity adjusted $p$ value = 0.0125) and cross 2 (multiplicity adjusted $p$ value = 0.0011) colonies compared to inbred SWR mice (Figure 3.7). The sire carries the *Amhr2*$^{cre}$ allele in experimental breeder cross 1, which may account for the higher number of pups weaned per litter as was observed when SWR dams were mated to SWR.*Amhr2*$^{cre/+}$ sires (Figure 3.5). In contrast, the dam contributes the *Amhr2*$^{cre}$ allele in experimental breeder cross 2; a reduction of AMH-induced inhibition on primordial follicle assembly (Durlinger *et al*. 1999) might result in higher rates of fertility.

### 3.4.2.4 Variability of the Granulosa Cell-Specific Androgen Receptor Gene Knockout

Blinded examinations of AR protein expression in a subset of pubertal and adult SWR and B6J GC-ArKO mouse ovaries revealed the near-absence of AR protein expression in GCs, with the retention of AR protein expression in TCs and other stromal tissues throughout the ovary (Figures 3.11 to 3.15); this expression pattern suggests the $Ar^{flox}$ allele was efficiently and specifically recombined in the GC compartment only. GC-specific activity of the *Amhr2-cre* driver has been described previously, although some investigations have reported *Amhr2-cre*-driven recombination in the TCs and oocytes (Jorgez *et al*. 2004; Pangas *et al*. 2006). Further examinations of GC-ArKO and heterozygous control ovaries revealed that the GC-specific *Ar* KO ranged from relatively complete ("good" KOs that were hypomorphic for GC AR, albeit with a spectrum of GC AR protein expression ranging from almost none to some) to near-incomplete ("poor" KOs that were indistinguishable from the ovaries of heterozygous control mice). We concluded that genotype could not be confidently relied upon as an indicator of GC AR protein expression phenotype, necessitating the qualitative examination of all ovaries from mice with an $Ar^{flox/flox}Amhr2^{cre/+}$ genotype for their GC AR protein expression phenotype by IHC. Many follicles in GC-ArKO mouse ovaries displayed a mosaic appearance in which clustered subsets of GCs displayed AR protein expression (Figure 3.12), suggesting the clonal expansion of non-recombined and therefore AR protein-positive GCs; the proliferation of unrecombined GCs has been reported previously in the *Amhr2-cre*-driven expression of constitutively active *Ctnnb1* (Boerboom *et al*. 2005). Multiple investigations utilizing the *Amhr2-cre* driver have reported inefficiency in recombination, leading to a hypomorphic rather than null ovarian condition similar to that which we observed (Boerboom *et al*. 2005; Pangas *et al*. 2006; Andreu-Vieyra, Chen & Matzuk 2007; Hernandez Gifford, Hunzicker-Dunn & Nilson 2009; Edson *et al*.

2010). In contrast, analyses in other models using this *Amhr2-cre* driver have demonstrated highly efficient gene deletions (Fan *et al*. 2008a; Sen & Hammes 2010). In fact, no variability in GC-specific *Ar* gene deletion was reported in a previous investigation using the same *Amhr2-cre* driver utilized here but in a B6J genetic background (Section 3.1.2.2; Sen & Hammes 2010). The success and specificity of the *Amhr2-cre*-driven *Ar* deletion was verified in this previously-published model using quantitative RT-PCR, western blot, and IHC analyses, and led us to choose these specific constructs for our own experimentation. As others have used the *Amhr2* driver to investigate gene function over the reproductive lifespan, or the effect of hypomorphic alleles on disease initiation (e.g. development of GC tumours), the imprecision of the gene deletion imparted by the *Amhr2-cre* driver is likely less influential on experimental outcomes therein in comparison to our research paradigm (i.e. inhibition of GC tumour development) using the SWR model of GC tumourigenesis. The leakiness of *Amhr2-cre* activity we and others have observed may be due to a number of factors, including strain background and the timing of *Amhr2* promoter expression. Several other Cre drivers with specific GC activity are commercially available, including those driven by *Amh* (Lécureuil *et al*. 2002), *Cyp19a1* (Fan *et al*. 2008b), *Inha* (Jorgez, De Mayo & Matzuk 2006), and *Nr5a1* (Bingham *et al*. 2006), although as with the *Amhr2-cre* driver, limitations in their use (e.g. leakiness in expression, promoter expression timing, etc.) have been reported. Pinpointing the GC tumour cell of origin could facilitate the targeting of this cell type with a spatially- and temporally-specific Cre driver for future examinations of influential genes and mechanistic pathways in the SWR model.

### 3.4.2.5 Granulosa Cell Tumour Development in GC-ArKO Mice

All GC tumours (n = 17) that appeared following androgen treatment in SWR GC-ArKO and heterozygous control mice displayed nuclear AR protein expression (Figure 3.17). The presence of AR-positive GC tumour cells in samples from SWR GC-ArKO mice, including those with GC AR protein-negative contralateral ovaries (Figure 3.17) and intratumoural follicles (Figure 3.18), suggests the clonal expansion of non-recombined, AR-positive GCs, as was observed in the follicles of normal GC-ArKO mouse ovaries (Figure 3.12). In contrast, no GC tumours arose following androgen treatment in SWR females when AR was successfully excised from ovarian GCs. Although complete loss of the *Ar* from the GC compartment of all SWR mice was hindered by the deletion strategy we employed, the presence of the AR in all GC tumours supports our hypothesis that AR-mediated signalling is required for GC tumour development.

We included an analysis of GC-specific AR deletion in B6J females as a phenotype comparison in tandem with our experiments in the SWR genetic background, to analyze the effects of DHEA administration in the absence of the AR in a GC tumour-resistant strain. No GC tumours or other macroscopic ovarian phenotypes were observed in B6J heterozygous control or GC-ArKO females, regardless of the AR protein phenotype observed following IHC. The lack of a notable influence by DHEA on ovaries of B6J mice lacking AR in the GCs suggests that the mechanism by which the AR induces GC tumour initiation is dependent on the presence of $Gct1^{SW}$ alleles. Although our data supports this theory, other genetic loci, such as the tumour suppressor locus *Gct6*, may override AR signalling and the oncogenic activity of $Gct1^{SW}$. Previous investigations have shown that (SWR x B6J)$F_1$ daughter offspring are resistant to spontaneous (Beamer, Hoppe & Whitten 1985) and DHEA-induced (Beamer *et al*. 1988) GC tumour initiation. Recent work in our laboratory using SWR.B6J-X congenic lines has shown

that paternal inheritance of a B6J *Gct6* allele significantly suppresses GC tumourigenesis, but does not confer complete GC tumour resistance as does $Gct6^{CA}$ (Rabie 2015).

The GC tumours observed in inbred SWR mice can be unilateral or bilateral; in the largest survey to date, 10.8% (n = 27) of 249 affected mice had bilateral GC tumours (276/498 [55.4%] ovaries with a GC tumour; Beamer, Hoppe & Whitten 1985). Typically, unilateral GC tumour initiation in SWR mice results in a small contralateral ovary, likely due to gonadotropin suppression resulting from the estrogenic output of the growing GC tumour (Beamer 1986). Upon review of the GC tumour frequency data, we noticed that a large proportion of the SWR heterozygous control and GC-ArKO mice given androgens at puberty developed bilateral GC tumours. Of 17 mice with androgen-induced GC tumours, 64.7% (n = 11) were bilateral cases (28/34 [82.4%] ovaries with a GC tumour). The preponderance towards bilateral GC tumours in the current investigation was significantly different than that expected when compared to the historical data by Fisher's exact test ($p < 0.0001$; Beamer, Hoppe & Whitten 1985). Although serum samples were not taken from females from the second experimental cross, we might hypothesize that reduced estrogenic output from the GC tumours that appeared in these females permitted a greater number of bilateral cases than expected. Overall, the high rate of bilateral GC tumours posed an advantage to the experimental design, and all collected GC tumours were individually examined for AR protein expression by IHC.

Due to the fixed direction of the experimental breeder crosses, SWR.$Ar^{+/flox}Amhr2^{cre/+}$ heterozygous control females were obligate carriers of the paternal $Ar^{flox}$ allele and maternal $Ar^{+}$ allele (Figure 3.5). This was of particular interest for the SWR model as the *Gct4* locus on Chr X is subject to a parent-of-origin effect, such that paternal and maternal susceptibility alleles are not equivalent in their influence on tumour penetrance when strain-dependent allele effects are

tested (Beamer *et al*. 1998; Dorward *et al*. 2003; Dorward *et al*. 2013). Should the paternal $Ar^{flox}$ allele be preferentially expressed over the maternal $Ar^{+}$ allele, the Cre-mediated excision of $Ar^{flox}$ and expression of $Ar^{+}$ might result in a lower GC tumour frequency in the heterozygous control cohort than if these parental alleles were expressed equally. Only 13.8% (n = 9/65 females, or 15/130 [11.5%] ovaries with a GC tumour) of SWR.$Ar^{+/flox}Amhr2^{cre/+}$ heterozygous control females given DHEA or T at puberty developed unilateral or bilateral GC tumours by 8 wk of age. Although this GC tumour frequency was lower than expected, it was not significantly different from frequencies historically observed in SWR mice administered pubertal DHEA or fed T in the diet over the pubertal transition T (17.4%; n = 30/172 females with GC tumour(s); Tennent, Shultz & Beamer 1993; Smith 2011; $p = 0.5617$ by Fisher's exact test). Similarly, preferential expression of the paternal $Ar^{flox}$ allele over the maternal $Ar^{+}$ allele might result in the appearance of genotypic heterozygotes as phenotypic AR protein KOs. This phenomenon was not observed, although evidence of such may have been precluded by the leakiness of the *Amhr2-cre* construct, which resulted in a spectrum of AR protein expression. Testing the parent-of-origin effect on GC tumourigenesis in the GC-ArKO model would require a much larger cohort of SWR.$Ar^{+/flox}Amhr2^{cre/+}$ heterozygous females.

### 3.4.3 Is the Androgen Receptor *Gct4*?

Our finding that the AR is required for GC tumourigenesis complements the substantial body of evidence indicating that the *Ar* shares identity with *Gct4*. No coding sequence mutations have been identified in the *Ar* gene in SWR mice (Dorward *et al*. 2003); similarly, no high-impact variants were identified by NGS of the *Gct4* interval from mice with SWR, CAST or SJL

alleles (unpublished data). The causative *Gct4* variant is likely regulatory, and given the robust, paternal parent-of-origin effect governing GC tumour susceptibility, may be epigenetic in nature.

Quantitative transcript analyses have revealed that a significant difference in *Ar* mRNA expression is present between strains with differential allele effects on GC tumour frequency (Dorward *et al*. 2013). That differences in *Ar* expression between mouse strains with inherently differential susceptibility is overcome by androgen administration at puberty suggests that ovarian AR-mediated signalling is critical for GC tumour initiation in the SWR model. Androgens have proven to be modifiers of SCST tumourigenesis in the *Inha* KO mouse model, wherein AR antagonists delay, but do not avert, tumour development (Burns *et al*. 2003b), or reduce lethality due to tumour burden (Shou, Woodruff & Matzuk 1997). As *in vivo* and *in vitro* investigations have shown that a balance of androgens is critical for optimal ovarian function, it is likely that AR expression levels are at a tipping point in the SWR ovary, with high pubertal levels detrimental when expressed in the correct context of genetic (i.e. $Gct1^{SW}$ alleles) and spatiotemporal (i.e. first medullary GC wave) susceptibility. GC tumours are the most common spontaneous ovarian neoplasm affecting laboratory rodents, whereas the incidence of GC tumours in humans is relatively low in comparison to EOC. The difference in GC tumour susceptibility between these multi- and mono-ovulatory species may be the result of differential levels of ovarian AR expression (Franks & Hardy 2018). The fact that DHEA supplementation increases *AR* expression in human GCs (Hu *et al*. 2017b) and T expression increased AR protein expression in this and other investigations (Weil *et al*. 1998; Yang *et al*. 2015) further supports the theory that endocrine stimulation is a trigger of AR-mediated SWR juvenile GC tumourigenesis. This mechanism is reminiscent of similar pathological scenarios in which endocrine stimulation increases risk above and beyond genetic context, such as in cancer of the

prostate and breast. Although there are no reports of the use of AR inhibitors in the treatment of GC tumours, *Ar* expressing tumours, including prostate cancer (Cioni, Zwart & Bergman 2018) and estrogen receptor negative breast cancer (Salvi, Bonafè & Bravaccini 2019) are the subject of AR antagonists. The SWR model of juvenile GC tumours should be investigated for AR targeting to reduce susceptibility and/or to prevent spontaneous metastases in GC tumour-bearing mice.

### 3.4.4 Summary

The SWR mouse model for GC tumourigenesis is a complex model for cancer risk at the intersection of genetics and the endocrine environment, thus reflecting the true complexity of cancer biology. We successfully established an engineered, GC-specific KO of the AR protein in an inbred SWR strain background to interrogate the influence of AR protein expression on androgen-driven GC tumour susceptibility. Our findings indicate the presence of the AR is required for GC tumour susceptibility in SWR mice, such that no GC tumours appeared when AR was successfully excised from ovarian GCs, despite the retention of fundamental $Gct1^{SW}$ homozygous alleles. Furthermore, the mechanism by which the AR induces GC tumour initiation is dependent on the presence of $Gct1^{SW}$ and tumour-supportive *Gct6* alleles, as evidenced by a lack of GC tumour susceptibility in B6J mice lacking the AR. The influence of androgens and AR-mediated signalling on GC tumour susceptibility should be analyzed in the context of the *Dhrs3* c.460-3C>T variant, the primary candidate for the oncogenic driver *Gct1*. Should the c.460-3C>T *Dhrs3* variant lead to a quantitative and/or qualitative change in functional *Dhrs3* transcript expression and subsequently an imbalance in steroid metabolism, increased levels of DHEA at puberty might lead to increased AR expression, resulting in increased rates of GC

tumour incidence. Future strategies to resolve the mechanism by which *Gct1* and *Gct4* cooperate to induce GC tumours will require considerations of the spatial and temporal context of the susceptible GC population.

# 4. Lineage Tracing the Granulosa Cell Tumour Cell of Origin

## 4.1 Introduction

It is evident that SWR GCs are unique in their capacity to undergo tumourigenic transformation in the presence of the normal endocrine stimulation of puberty or pubertal exogenous androgen exposure. Recent investigations into the origins of GCs in rodent models have yielded interesting details about the dynamics of follicle waves, and a large body of evidence suggests the presence of two distinct follicle populations with different activation and growth dynamics. These distinct follicle waves have implications for fertility as well as temporally-restricted pathologies affecting the cells of the ovarian follicle, such as juvenile-onset GC tumours found in infants and young girls, and the hormonally-initiated GC tumours that appear in SWR mice at the onset of puberty.

### 4.1.1 Dynamics and Origins of Ovarian Follicle Waves

The primitive gonad is sexually undifferentiated and bipotential, with differentiation into either the testes or ovaries directed by specific genetic determinants (Section 1.1.2.2). Following commitment of the embryonic gonad to the ovarian fate pathway is the differentiation of pre-GCs, the precursors of those GCs which surround the oocyte to form a follicle. Historically, three potential embryonic sources of GCs have been proposed, including a supporting cell precursor population present in the bipotential gonad, the OSE, and the rete ovarii, a vestigial network of cells and tubules (reviewed by Liu, Liu & Yao 2010). Multiple lines of evidence indicate GCs and their analogous counterparts in the testis, the Sertoli cells, arise from a common bipotential

precursor. The GCs can transdifferentiate into Sertoli-like cells and vice versa in several rodent models, as described in Section 1.1.2.2. Fetal ovaries grafted under the kidney capsule of adult male mice also undergo partial sex reversal, in which a subset of GCs transdifferentiate into SOX9-positive Sertoli-like cells within 15 to 20 d following transplantation (Taketo, Merchant-Larios & Koide 1984; Taketo & Merchant-Larios 1986; Morais da Silva *et al*. 1996). This process is partly influenced by sex hormones, as exogenous T and $E_2$ administered to the host mouse increase or decrease the proportion of transdifferentiated fetal ovaries, respectively (Taketo & Merchant-Larios 1986), and significantly fewer SOX9-positive Sertoli-like cells are found in fetal ovaries transplanted into castrated male hosts compared to intact males (Miura *et al*. 2019). Furthermore, a subpopulation of somatic cells in the Chr XX mouse gonad are capable of expressing enhanced green fluorescent protein (EGFP) driven by the promoter for *Sry*, the testis-determining factor that initiates male sex determination (Albrecht & Eicher 2001). Those cells capable of activating the *Sry* promoter represent a common bipotential precursor population for the supporting cell lineage from which both Sertoli cells and GCs are derived. A small subset of GCs retain this reporter activity postnatally, although the contribution of other cell types to the larger GC population found in adults was not excluded by initial experiments (Ito *et al*. 2006).

#### 4.1.1.1 Granulosa Cells Differentiate in Two Distinct Waves

It was known prior to investigations into GC origins that some primordial follicles enter the growing pool immediately after their formation, whereas others may remain quiescent for long periods. Initial hypotheses on the dynamics of primordial wave activation suggested that the oocytes formed earliest during gonad development were also ovulated earliest and those that formed later were ovulated later (Henderson & Edwards 1968), or alternatively that two different

populations of cells give rise to the GCs of primordial follicles, with each population having an inherently different threshold for entering the cell cycle (Hirshfield 1992). The use of tritium-labelled thymidine (3H-TdR) to label proliferating cells in the early rat ovary showed that both hypotheses of primordial follicle formation were in fact correct. When 3H-TdR was administered to pregnant rats, a large number of cells within the core of the developing fetal ovary failed to incorporate the label from E14 through E19, indicating they were mitotically inactive. These quiescent, unlabelled cells gave rise to the GCs of the first follicles to form, which were located in the medulla of the ovary and were also the first to begin to grow shortly after birth. Furthermore, these unlabelled cells did not contribute to the formation of follicles in the cortical region of the ovary, which were composed of heavily labelled GCs and began to grow later than those in the medulla (Hirshfield 1992). The identification of different GC lineages leading to a spatial gradient of distinct follicle populations suggests that each primordial follicle in the rodent ovary possess unique characteristics that determine the dynamics of its activation. Accordingly, the follicles composing the medullary population that are activated in a wave immediately after birth exhibit a two-fold accelerated rate of growth to the antral stage in comparison to those in the cortical population (Hirshfield 1991). This first wave of antral follicles has been thought to be destined for death or conversion to interstitial ovarian tissue rather than ovulation, due to a lack of the ovulation-stimulating gonadotropin LH (McGee *et al*. 1998; Adhikari & Liu 2009). Instead, the early activation and growth of these medullary follicles is thought to establish an individual's functional endocrine environment so as to facilitate later activation and growth of the cyclically-ovulated cortical follicles (Guigon *et al*. 2003).

The use of inducible transgenic mouse lines to lineage trace the fate of early ovarian supporting cell precursors further substantiated the hypothesis that GCs arise from two

populations in the fetal ovary (Figure 4.1). Using a tamoxifen-inducible Cre under the control of the *Foxl2* promoter (McMahon *et al*. 2008; Harding *et al*. 2011), Mork and colleagues (2012) tracked the fate of *Foxl2*-expressing cells immediately and several days after fetal ovarian differentiation. Notably, mice with this inducible Cre construct are haploinsufficient for *Foxl2*, due to allele displacement by the promoter driver (Guo *et al*. 2011). The authors found that cells within the embryonic mouse ovary that were capable of upregulating the *Sry* promoter were also able to upregulate *Foxl2* between E12.5 and 13.5, after committing to the ovarian pathway. These *Foxl2*-expressing cells are derived from the fetal OSE and give rise to the GCs of the medullary, but not cortical, follicle pool. These cells are arrested during embryonic development; mitotic arrest persisted until after birth, when the GCs in activated medullary follicles resumed cycling while those in cortical follicles remained arrested. This indicated, as Hirshfield (1992) had observed, that ovarian GCs are produced in two waves, the first of which is derived from *Foxl2*-positive cells originating from the bipotential supporting cell precursors and which surround medullary follicles by E14.5. The GCs of medullary follicles are subject to a short period of mitotic arrest that begins with their embryonic specification and lasts until activation of these follicles shortly after birth. A second wave of GCs is derived from an OSE lineage, which upregulate *Foxl2* and ingress into the ovarian cortex between E15.5 until P7, where they are incorporated into cortical follicles. These GCs enter mitotic arrest as they are assembled into follicles, a state in which they remain until their activation into the growing pool throughout reproductive life. The precursor lineage for this second GC wave is marked as early as E13.5 by the RSPO1 recruitment receptor LGR5, the expression of which is downregulated as the cells begin to express FOXL2 and differentiate into GCs (Rastetter *et al*. 2014). As discussed in Section 1.1.2.2, LGR5 binds RSPO1 and facilitates WNT4 receptor binding, resulting in β-

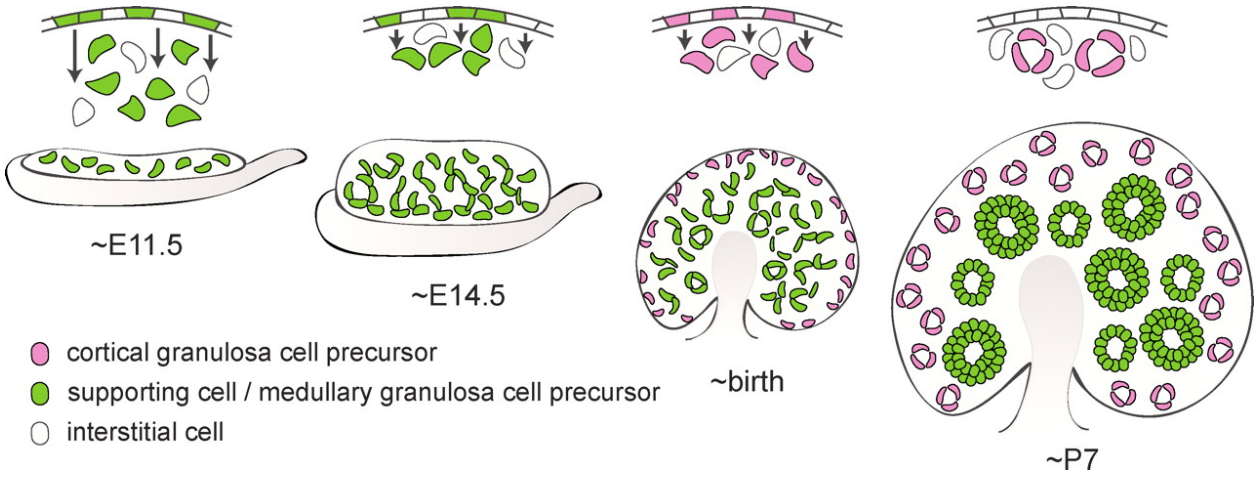


**Figure 4.1 Origin of ovarian granulosa cells**

Cells in the surface epithelium of the bipotential gonad (E11.5) produce supporting cell precursors (green) that move deep into the ovary and differentiate into GCs in the medullary follicles, which are activated immediately after their assembly at birth. As the ovary differentiates (E14.5), the surface epithelium contributes more cells to the GC population, which remain close to the ovarian surface and compose the cortical follicles (birth) that are activated throughout adulthood. Follicle assembly and the movement of surface epithelial cells into the ovary are complete by P7. Reprinted in adapted form with permission from Oxford University Press, from Biology of Reproduction, Vol 86, Mork *et al*., Temporal differences in granulosa cell specification in the ovary reflect distinct follicles fates in mice, p. 1-9, copyright 2012; permission conveyed through Copyright Clearance Centre, Inc.

catenin-mediated WNT4 gene transcription and female gonad differentiation. LGR5-positive OSE cells contribute to the regenerative repair of the ovarian surface following ovulation (Ng *et al*. 2014), and although loss of LGR5 results in a delay in the differentiation of germ cells within cortical follicles, the significance of its functional role in the GCs of the second follicle wave is unclear. Additional investigations using a heat-shock inducible *Sry* transgene have shown that a small population of medullary pre-GCs near the mesonephros and that contribute to the first follicle wave maintain the ability to express *Sox9* throughout fetal development until approximately P14 (Hiramatsu *et al*. 2009; Harikae *et al*. 2013). This *Sox9* expression potential, termed SRY-dependent SOX9-inducibility (SDSI), is absent from the pre-GCs that contribute to cortical follicles, and its regulation in medullary follicle GCs is independent of FOXL2, WNT4, and RA (Harikae *et al*. 2013). This data indicates that a portion of GCs in the first wave of folliculogenesis retain sexual bipotentiality, whereas GCs in subsequent waves do not possess this phenotypic plasticity (Harikae *et al*. 2013).

#### 4.1.1.2 Characteristics of First Wave Follicles

In addition to their distinct cellular origins, the first wave of ovarian follicles exhibit several properties that distinguish them from the follicles of subsequent waves. Medullary follicles are subject to an accelerated rate of growth (Hirshfield 1991) and possess distinct morphological features including differences in GC number and size (Hirshfield & DeSanti 1995). The medullary follicles are also characterized by aberrant steroidogenic enzyme and steroid receptor protein expression compared to subsequent follicle waves, including delayed onset and lower expression of the TC-specific enzyme CYP17A1 (resulting in decreased $E_2$ production and a lack of the ovulation-inducing LH surge), and an absence of GC-specific AR

expression until the pre-antral stage (Galas *et al*. 2012). The differential dynamics of follicular activation between these two populations was confirmed and further explored using additional transgenic mouse strains (Zheng *et al*. 2014). Using a novel tamoxifen-inducible *Foxl2-cre* that maintains *Foxl2* diploidy in combination with a fluorescent reporter strain (Muzumdar *et al*. 2007), Zheng and colleagues (2014) confirmed the presence of two discrete follicle populations with distinct activation timings, and also mapped the delayed progression of cortical follicles through the stages of folliculogenesis in comparison to medullary follicles. Notably, the authors suggested that a proportion of the medullary wave of follicles activated shortly after birth may in fact contribute to reproduction as indicated by the presence of corpora lutea (Zheng *et al*. 2014). However, no direct evidence of ovulation, such as labelled COCs in the fallopian tube, was presented, nor did the authors attempt to reconcile previous reports of altered medullary follicle steroidogenesis consistent with anovulation. Despite the differences in morphology, gene and protein expression, and growth dynamics described above, mouse oocytes from medullary follicles are competent to produce normal offspring when used for *in vitro* fertilization (O'Brien, Pendola & Eppig 2003; Eppig *et al*. 2009).

Interestingly, female mice with a single X chromosome (XO) are subject to a defect in the medullary follicle population (Miura *et al*. 2017). Chr XO mice, which lack the maternal X Chr copy, are a model of human Turner Syndrome. Women with this rare disorder lack some or all of an X Chr, resulting in short stature and other physical malformations, and often exhibit gonadal dysgenesis and are infertile (Sybert & McCauley 2004). Although Chr XO mouse ovaries undergo the normal formation of cortical follicles, they do not form medullary follicles or display the first folliculogenesis wave (Miura *et al*. 2017). No GC tumours have been reported in Chr XO mice, lending indirect evidence in support of the restriction of juvenile mouse GC

tumours to the first follicle wave. Further investigations into the mechanisms of medullary versus cortical follicle activation, their differential gene and protein expression patterns, and the fate of medullary follicles – whether they are lost to atresia or a subset is ovulated, and the mechanisms leading to these fates – are warranted.

### 4.1.2 Summary and Current Work

The spontaneous GC tumours that appear in SWR female mice are developmentally restricted, despite lifelong maintenance of the *Gct* susceptibility alleles and appropriate endocrine conditions over the reproductive lifespan. The only window of susceptibility is the onset of puberty in the female mouse (Section 1.3.1.1), strongly suggesting that genetic susceptibility is restricted to the first follicle wave. We set out to explore this concept with a tissue-specific, engineered fluorescence reporter construct to trace juvenile GC tumour origins in the SWR mouse model. We employed the *Foxl2* promoter-driven, tamoxifen-inducible Cre construct used by Mork and colleagues (2012), available through the GenitoUrinary Development Molecular Anatomy Project (GUDMAP) consortium (McMahon *et al*. 2008; Harding *et al*. 2011). Mice with this construct are haploinsufficient for *Foxl2* due to allele displacement, as they carry a *GFP-creER*$^{T2}$ (GCE) cassette knocked into exon 1 of the *Foxl2* gene (Guo *et al*. 2011). The GCE cassette consists of three components: 1) a green fluorescent protein (GFP) coding sequence; 2) a *cre* gene; and 3) a tamoxifen-inducible mutated estrogen receptor hormone-binding domain (*ER*$^{T2}$). Together these components function to drive *cre* expression in *Foxl2*-expressing cells following tamoxifen exposure. We paired this *Foxl2*-driven construct with the fluorescent reporter mouse strain used by Zheng and colleagues (2014) to investigate the differential dynamics of medullary and cortical follicle activation. This strain

carries a *cre*-excisable membrane-targeted tandem dimer Tomato (tdTomato) (mT) coding sequence and expresses tdTomato, a red fluorescent protein, with membrane localization in all tissues and cell types examined (Muzumdar *et al*. 2007). Cre-mediated recombination results in the excision of the mT cassette, allowing instead for the expression of a membrane-targeted EGFP (mG) cassette and therefore EGFP expression with membrane localization in *cre*-expressing tissue(s). The combination of these two constructs in a single mouse strain allows for a switch from red to green fluorescence in *Foxl2*-expressing, *cre*-recombined cells, with a temporal specificity restricted by tamoxifen administration. *Foxl2* is first detected in the nuclei of some somatic cells at the border between the developing ovary and the mesonephros at approximately E11.5 (Wilhelm *et al*. 2009); by E14.5, they have been incorporated into the medullary pre-GC population (Mork *et al*. 2012). The administration of tamoxifen to SWR mice with both constructs at E12.5 would therefore label the GCs of the first follicular wave with mG fluorescence, while maintaining mT fluorescence in all other ovarian cells, including those that up-regulate *Foxl2* and begin to differentiate into the pre-GCs of cortical follicles around E15.5 until approximately P7. Should the GC tumour cell of origin arise from the first follicular wave as we suspect, all tumour cells that proliferate by clonal expansion from this cell will be labelled with mG fluorescent protein. This experimental design gave rise to two main challenges, namely, the effect of *Foxl2* haploinsufficiency and the influence of tamoxifen on the spontaneous, endocrine-responsive GC tumour phenotype. Unfortunately, we were unable to acquire the tamoxifen-inducible *Foxl2* construct utilized by Zheng and colleagues (2014); this construct maintains a *Foxl2* diploid state, but is not commercially available and our request for use was declined.

Although *FOXL2* has not been implicated in human juvenile GC tumours, its role in adult GC tumourigenesis (Shah *et al*. 2009) as well as its critical function in the maintenance of GC differentiation and ovarian gonadal identity in adulthood (Uhlenhaut *et al*. 2009) necessitated that we ensured the retention of the GC tumour phenotype in mice lacking one copy of the *Foxl2* allele. Furthermore, the influence of the selective estrogen-receptor modulator (SERM) tamoxifen on the GC tumour susceptibility trait was of concern. Although tamoxifen induction of cell-specific *cre*-mediated recombination is well described (Feil, Valtcheva & Feil 2009), its use here in the context of an endocrine-sensitive, spontaneous ovarian phenotype required caution. Adult GC tumours have been reported in women prescribed tamoxifen (20 mg/d for 5 y) for estrogen receptor positive breast cancer (Gherman, Parker & Macri 1994; Arnould *et al*. 2002; Abahssain *et al*. 2010; Tanaka, Kato & Ohmichi 2012), although the overall incidence rate is rare in relation to the large number of women prescribed tamoxifen for this use. In contrast, tamoxifen has been utilized as a treatment for GC tumours, with limited success (van Meurs *et al*. 2014). *In utero* tamoxifen administration has been shown to induce malignant GC tumours in aged CD-1 female offspring (Diwan, Anderson & Ward 1997); unlike some other mouse strains (Section 1.3), CD-1 mice are not susceptible to high rates of GC tumour initiation with age (Giknis & Clifford 2005). Finally, tamoxifen treatment increases levels of *Sox9* and *Fgf9* while decreasing levels of *Foxl2* and *Wnt4* in Chr XX fetal and adult mouse gonads, suggesting a switch from the female differentiation pathway to a male fate (Yu *et al*. 2014; Yu *et al*. 2015). As in the experimental design for the GC-specific deletion of the AR described in Chapter 3, these factors necessitated that we test the individual construct lines for the retention of GC tumour susceptibility following initial backcrossing to the SWR inbred strain and prior to the experimental crosses to lineage trace GC tumour cells. Similarly, an independent tamoxifen

challenge of inbred SWR and Line 4-5 pubertal female mice was necessary to determine the influence, if any, on these respectively GC tumour-susceptible and -resistant mouse strains.

### 4.1.3 Hypothesis and Research Objectives

*Hypothesis*

The GC tumours that appear in SWR mice originate from GCs that comprise medullary follicles within the first follicle wave.

*Research Objectives*

1) Backcross the fluorescent reporter and tamoxifen-inducible *Foxl2-cre* alleles onto the SWR inbred strain background for a minimum of six generations, and test the individual construct lines for androgen-induced GC tumour initiation at puberty.

2) Administer tamoxifen to inbred SWR and Line 4-5 female fetuses, and test the influence of this *in utero* tamoxifen exposure on androgen-induced pubertal GC tumour susceptibility.

3) Mate SWR mice with fluorescent reporter and tamoxifen-inducible *Foxl2-cre* alleles, administer tamoxifen to pregnant females at E12.5 to induce a switch from mT expression to mG expression in the first wave of medullary GCs of female fetuses, and administer androgens to female offspring at puberty so as to lineage trace the GC tumour cell of origin.

## 4.2 Materials and Methods

### 4.2.1 Animal Husbandry

#### 4.2.1.1 Animal Housing

Animals were housed as per Section 2.2.1.1.

#### 4.2.1.2 *Amhr2-cre* Mouse Strain

The *Amhr2-cre* mouse strain was backcrossed onto the SWR strain and maintained in a heterozygous state as per Section 3.2.1.3.

#### 4.2.1.3 *mT/mG* Mouse Strain

The 129-*Gt(ROSA)26Sor*$^{tm4(ACTB-tdTomato,-EGFP)Luo}$/J (*mT/mG*) mouse strain was purchased from The Jackson Laboratory (Stock No: 007576; Bar Harbor, ME) and the *Gt(ROSA)26Sor*$^{tm4(ACTB-tdTomato,-EGFP)Luo}$ (*ROSA*$^{mT/mG}$) allele was backcrossed onto the SWR mouse strain. *mT/mG* mice carry a *pCA-mT/mG* construct knocked into the constitutively and ubiquitously expressed *Gt(ROSA)26Sor* (*ROSA*) targeting locus on Chr 6 derived from the (129X1 x 129S1)$F_1$ mouse strain in a 129X1 mouse strain background. The *pCA-mT/mG* construct consists of three components: 1) a ubiquitously expressed chicken *Actb* core promoter with a CMV enhancer (pCA); 2) a floxed mT coding sequence downstream of the pCA promoter; and 3) an mG coding sequence downstream of the mT sequence. Cre-mediated recombination results in the excision of the floxed mT cassette, allowing pCA-driven expression of the mG cassette and therefore EGFP expression with membrane localization in *cre*-expressing tissue(s) (Muzumdar *et al*. 2007).

To determine the GC tumour-supportive action of the (129X1 x 129S1)$F_1$ *ROSA*$^{mT/mG}$ allele and to generate mice used for the experimental cross to determine the GC tumour cell of origin, it was backcrossed onto the SWR inbred strain for six generations ($N_6$, approximately 96.9% SWR background; Silver 1995; Figure 4.2). The presence of SWR alleles at the specific mapped susceptibility *Gct* loci *Gct1*, *Gct2*, *Gct3*, *Gct4*, *Gct5* (*D9Mit17* only), and *Gct6* (*DXamd17*) was confirmed using SSLP DNA markers at $N_4F_1$ prior to further backcrossing onto the SWR inbred strain (Section 4.2.2.3). $N_6F_1$ *ROSA*$^{mT/mG}$ carrier mice were intercrossed and the allele was brought to homozygosity to produce $N_6F_3$ generation SWR.*ROSA*$^{mT/mG/mT/mG}$ mice, which were maintained thereafter as brother-sister matings ($F_3$, $F_4$, etc.). $N_6F_3$ and $N_6F_4$ SWR.*ROSA*$^{mT/mG/mT/mG}$ female mice were examined to confirm that they retained GC tumour susceptibility following pubertal DHEA stimulation (Section 4.2.1.3).

#### 4.2.1.4 *Foxl2-GCE* Mouse Strain

The B6.129P2-*Foxl2*$^{tm1(GFP/cre/ERT2)Pzg}$/J *(Foxl2-GCE*) mouse strain was purchased from The Jackson Laboratory (Stock No: 015854; Bar Harbor, ME) and the *Foxl2*$^{tm1(GFP/cre/ERT2)Pzg}$ (*Foxl2*$^{GCE}$) allele was backcrossed onto the SWR mouse strain. *Foxl2-GCE* mice carry a GCE cassette knocked into exon 1 of the *Foxl2* gene derived from the 129P2/OlaHsd (129P2) mouse strain in a B6J mouse strain background (GUDMAP consortium, #21892; McMahon *et al*. 2008; Harding *et al*. 2011). Notably, native GFP expression is not detectable in *Foxl2-GCE* whole embryo or dissected urogenital sinus samples by direct fluorescence microscopy, and requires immunohistochemical methods for detection (Guo *et al*. 2011).

To assess the extent of native background GFP expression in SWR.*Foxl2*$^{GCE}$ mouse ovaries, to determine the effect of the 129P2 *Foxl2*$^{GCE}$ allele on GC tumourigenesis in a SWR

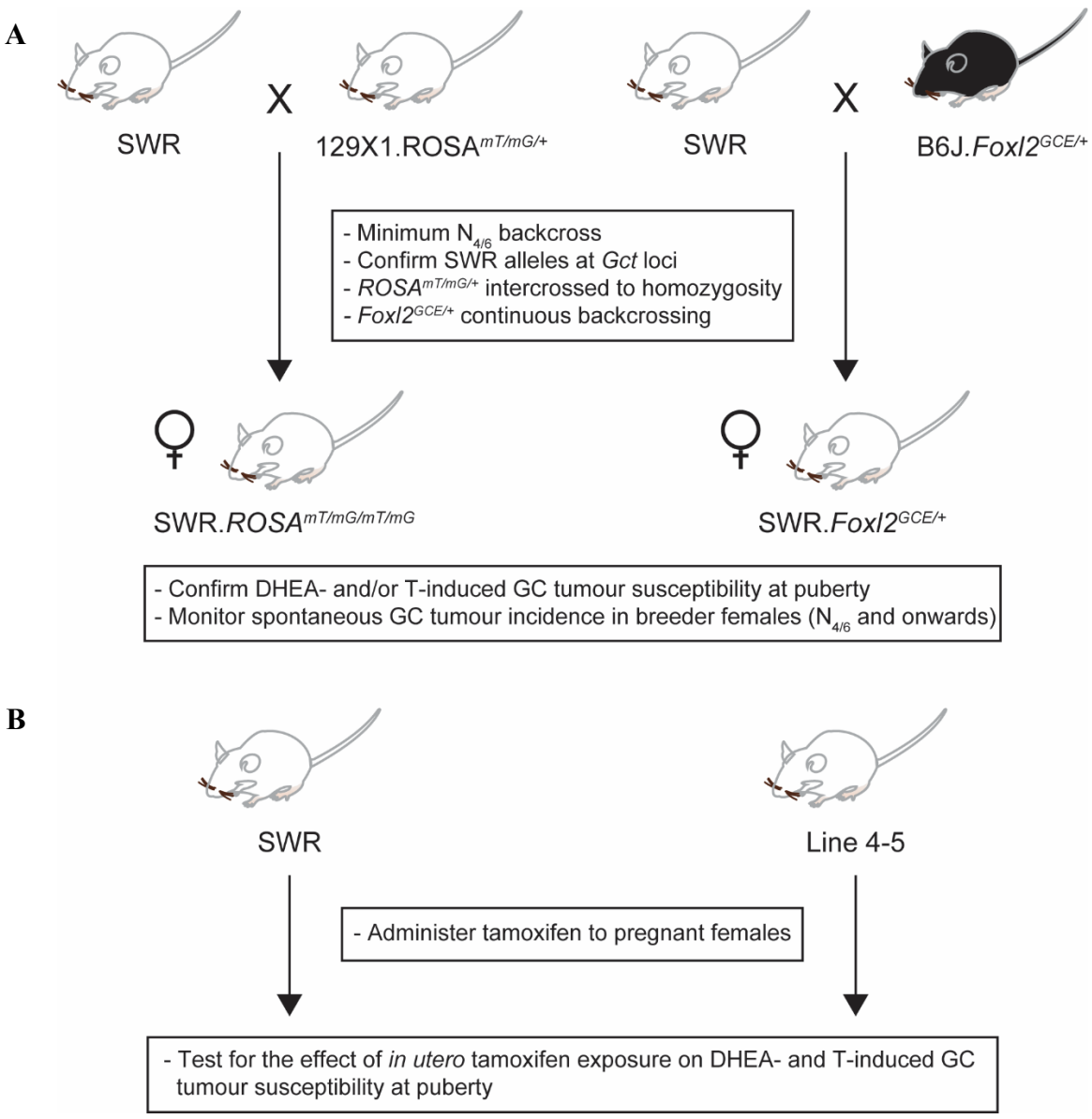


**Figure 4.2 *ROSA*$^{mT/mG}$ and *Foxl2*$^{GCE}$ backcross breeding strategy and experimental outline**

(A) A marker-assisted backcross strategy was employed to indepentently transfer the *ROSA*$^{mT/mG}$ and *Foxl2*$^{GCE}$ alleles onto the SWR strain. Pubertal androgen-induced GC tumour susceptibility was assessed in SWR.*ROSA*$^{mT/mG/mT/mG}$ and SWR.*Foxl2*$^{GCE/+}$ females following a minimum of six or four backcross generations, respectively. Additionally, all SWR.*ROSA*$^{mT/mG/mT/mG}$ and SWR.*Foxl2*$^{GCE/+}$ breeder females were monitored for spontaneous GC tumour incidence from generation $N_6$ or $N_4$ onwards, respectively. (B) Pregnant inbred SWR and Line 4-5 females were administered tamoxifen, and the effect of *in utero* tamoxifen on the GC tumour susceptibility phenotype was tested in female offspring with androgen administration at puberty.

strain background, and to generate mice used for the experimental cross to determine the GC tumour cell of origin, the *Foxl2*$^{GCE}$ allele was backcrossed onto the inbred SWR strain for a minimum of four ($N_4$, approximately 87.5% SWR background; Figure 4.2) and maintained in a heterozygous state, due to the presumed inherent inactivation of the affected *Foxl2* allele as a result of its disruption by the GCE cassette (Guo *et al*. 2011). The presence of SWR alleles at the specific mapped susceptibility *Gct* loci *Gct1*, *Gct2*, *Gct3*, *Gct4*, *Gct5*, and *Gct6* (*DXamd11*) was confirmed using SSLP DNA markers at $N_3F_1$ prior to further and ongoing backcrossing onto the inbred SWR strain for *Foxl2*$^{GCE}$ maintenance (Section 4.2.2.3). $N_4F_1$ through $N_8F_1$ generation SWR.*Foxl2*$^{GCE/+}$ female mice were examined to confirm that they retained GC tumour susceptibility following pubertal DHEA and T stimulation (Section 4.2.1.3). Spontaneous GC tumour incidence in SWR.*Foxl2*$^{GCE/+}$ breeder females was monitored from generation $N_4$ onwards.

#### 4.2.1.5 Experimental Crosses, Timed Matings and Tamoxifen Administration

SWR.*ROSA*$^{mT/mG/mT/mG}$ dams were mated to SWR.*Amhr2*$^{cre/+}$ sires to generate SWR.*ROSA*$^{mT/mG/+}$*Amhr2*$^{+/cre}$ and SWR.*ROSA*$^{mT/mG/+}$*Amhr2*$^{+/+}$ mice for preliminary examinations of GC-specific Cre-mediated mT to mG conversion. SWR.*ROSA*$^{mT/mG/+}$*Foxl2*$^{+/GCE}$ mice were generated by mating SWR.*ROSA*$^{mT/mG/mT/mG}$ dams to SWR.*Foxl2*$^{GCE/+}$ sires overnight. The presence of a vaginal plug on the next morning marked E0.5. Tamoxifen [(Z)-1-(p-dimethylaminoethoxyphenyl)-1,2-diphenyl-1-butene; T5648, Sigma-Aldrich Inc.] was resuspended at 10 mg/mL in a 9:1 ratio solution of 100% ethanol (Commercial Alcohols) to corn oil (President's Choice, Brampton, ON). Pregnant females were injected with a single intraperitoneal (IP) injection of tamoxifen (50 mg/kg body weight, approximately 1.5 mg/mouse)

at E12.5. Pregnant females were also injected with a single IP dose of $P_4$ (4-pregnene-3,20-dione; P3972, Sigma-Aldrich Inc.) in corn oil (10 mg/mL; President's Choice) at approximately half the dose of tamoxifen to decrease the incidence of spontaneous abortion (Nakamura, Nguyen & Mackem 2006). Pups were delivered by Caesarean section at E20.5 as the tamoxifen injection compromised the ability of the mice to have spontaneous vaginal delivery (Zheng *et al*. 2014). Briefly, mothers were killed by cervical dislocation and the uterus and fetal membranes were dissected to expose the pups. Sterile cotton swabs were used to remove amniotic fluid from the mouth and nostrils of the pups and to stimulate breathing. Surrogate mothers were used to nurture the pups. Pregnant inbred SWR and Line 4-5 mice were mated and treated in the same manner as experimental mice; an additional cohort of pregnant SWR females were treated with vehicle (corn oil) only.

#### 4.2.1.6 Surgical Capsule Implantation

Exogenous DHEA or T was administered to female mice at puberty for three purposes: 1) to determine the GC tumour supportive action of the $ROSA^{mT/mG}$ and $Foxl2^{GCE}$ constructs, as well as hemizygosity for *Foxl2*, in a confirmed SWR genetic background prior to the experimental cross to generate SWR.$ROSA^{mT/mG/+}Foxl2^{+/GCE}$ mice; 2) to test the effect of *in utero* tamoxifen administration on androgen-induced GC tumour susceptibility in inbred SWR and Line 4-5 females; and 3) to initiate GC tumours in SWR.$ROSA^{mT/mG/+}Foxl2^{+/GCE}$ mice to determine the GC tumour cell of origin. $N_4F_1$ through $N_8F_1$ generation SWR.$Foxl2^{GCE/+}$, $N_6F_3$ and $N_6F_4$ generation SWR.$ROSA^{mT/mG/mTmG}$, $F_1$ generation SWR.$ROSA^{mT/mG/+}Foxl2^{+/GCE}$, and SWR and Line 4-5 female mice were implanted with DHEA or T capsules as per Sections 2.2.1.3 and 3.2.1.5.

### 4.2.2 Genotyping

#### 4.2.2.1 *Amhr2$^{cre}$*

*Amhr2$^{cre}$* genotyping markers were amplified by multiplex touchdown PCR as per Section 3.2.2.2

#### 4.2.2.2 *ROSA$^{mT/mG}$*

*ROSA$^{mT/mG}$* genotyping markers were amplified by multiplex touchdown PCR using a One*Taq*® GC Reaction Buffer Pack (New England BioLabs® Ltd.) from gDNA extracted from mouse tail samples (Section 2.2.2.1). The following reagents were combined in a 0.2 mL PCR tube (Bio-Rad Laboratories): 6.5375 µL of distilled water, 2.5 µL of 5X One*Taq*® Standard Reaction Buffer, 1.25 µL of One*Taq*® High GC Enhancer, 0.25 µL of 10 mM dNTPs (Invitrogen), 0.30 µL of 10 µM forward primer, 0.20 µL of 10 µM WT reverse primer, 0.40 µL of 10 µM *ROSA$^{mT/mG}$* reverse primer (Integrated DNA Technologies), 0.0625 µL of One*Taq*® DNA polymerase, and 1 µL of gDNA template. A negative control was included with each PCR with distilled water in place of gDNA template. The tubes were placed in a Veriti™ 96-Well Thermal Cycler (Applied Biosystems Inc.) where PCR was performed using the following profile: 94 °C for 5 min; 6 cycles of 95 °C for 15 s, 66 °C-61 °C for 30 s (-1 °C/cycle), and 72 °C for 1 min; 35 cycles of 95 °C for 15 s, 60 °C for 30 s, and 72 °C for 1 min; 72 °C for 10 min. The PCR products were stored at 4 °C until gel electrophoresis. *ROSA$^{mT/mG}$* genotyping primer sequences were obtained from Zong *et al*. 2005 and are shown with their amplicon sizes in Table 4.1. *ROSA$^{mT/mG}$* PCR products were separated by horizontal electrophoresis through a 1% agarose gel as per Section 2.2.2.2 and scored for allele differences as per Table 4.1.

**Table 4.1 *ROSA*$^{mT/mG}$ genotyping primers.** Primer sequences used to amplify the *ROSA*$^{+}$ and *ROSA*$^{mT/mG}$ alleles by multiplex touchdown PCR and the corresponding amplicon lengths are shown.

| Target Allele | Forward Sequence (5′→3′) | Reverse Sequence (5′→3′) | Amplicon (bp) |
|---|---|---|---|
| *ROSA*$^{+}$ | CTCTGCTGCCTCCTGGCTTCT | CGAGGCGGATCACAAGCAATA | 330 |
| *ROSA*$^{mT/mG}$ | CTCTGCTGCCTCCTGGCTTCT | TCAATGGGCGGGGGTCGTT | 250 |

#### 4.2.2.3 *Foxl2*$^{GCE}$

*Foxl2*$^{GCE}$ genotyping markers were amplified by multiplex touchdown PCR using a One*Taq*® GC Reaction Buffer Pack (New England BioLabs® Ltd.) from gDNA extracted from mouse tail samples (Section 2.2.2.1). The following reagents were combined in a 0.2 mL PCR tube (Bio-Rad Laboratories): 6.6875 µL of distilled water, 2.5 µL of 5X One*Taq*® Standard Reaction Buffer, 1.25 µL of One*Taq*® High GC Enhancer, 0.25 µL of 10 mM dNTPs (Invitrogen), 0.25 µL each of 10 µM forward primer, WT reverse primer, and *Foxl2*$^{GCE}$ reverse primer (Integrated DNA Technologies), 0.0625 µL of One*Taq*® DNA polymerase, and 1 µL of gDNA template. A negative control was included with each PCR with distilled water in place of gDNA template. The tubes were placed in a Veriti™ 96-Well Thermal Cycler (Applied Biosystems Inc.) where PCR was performed using the following profile: 94 °C for 2 min; 10 cycles of 94 °C for 20 s, 65 °C-60.5 °C for 15 sec (-0.5 °C/cycle), and 68 °C for 10 sec; 28 cycles of 94 °C for 15 sec, 60 °C for 15 sec, 72 °C for 10 sec; 72 °C for 2 min. The PCR products were stored at 4 °C until gel electrophoresis. *Foxl2*$^{GCE}$ genotyping primer sequences were obtained from Guo *et al*. 2011 and are shown with their allele sizes in Table 4.2. *Foxl2*$^{GCE}$ PCR products were separated by horizontal electrophoresis through a 1% agarose gel as per Section 2.2.2.2 and scored for allele differences as per Table 4.2.

#### 4.2.2.4 SSLPs

SSLPs and their primer sequences were annotated in the MGD (Smith *et al*. 2018) or were identified by the Computational Sciences group at The Jackson Laboratory and designed in-house. SSLP genotyping markers were amplified by PCR using a Master*Taq*™ Kit from gDNA extracted from mouse tail samples as per Section 2.2.2.1. Genotyping marker primer

**Table 4.2 *Foxl2*$^{GCE}$ genotyping primers.** Primer sequences used to amplify the *Foxl2*$^{+}$ and *Foxl2*$^{GCE}$ alleles by multiplex touchdown PCR and the corresponding amplicon lengths are shown.

| Target Allele | Forward Sequence (5′→3′) | Reverse Sequence (5′→3′) | Amplicon (bp) |
|---|---|---|---|
| *Foxl2*$^{+}$ | AGAGAAGAGAGTGAGAGCCG | GAGCGCCACGTACGAGTACG | 335 |
| *Foxl2*$^{GCE}$ | AGAGAAGAGAGTGAGAGCCG | GTCCAGCTCGACCAGGATGG | 221 |

sequences, relative SSLP allele sizes for SWR and 129X1 or B6J, and their genomic locations are shown in Appendix G for mice carrying the *ROSA*$^{mT/mG}$ and *Foxl2*$^{GCE}$ alleles, respectively. SSLP PCR products were separated by horizontal electrophoresis through a 4% agarose gel as per Section 2.2.2.1 and scored for allele differences as per Appendix G.

### 4.2.3 Fluorescent Imaging

#### 4.2.3.1 Tissue Collection and Processing

Mice were euthanized by exposure to $CO_2$ gas at 3 or 8 wk of age, and GC tumour development was assessed by macroscopic examination of the ovaries in mice with present and intact DHEA or T capsules. Ovary pairs and GC tumour samples were collected at necropsy. The tissues were dissected using scissors and tweezers and were fixed in cold 4% paraformaldehyde (PFA; Sigma-Aldrich Inc.) in PBS (pH 7.5) for 24 h at 4 °C, followed by cryoprotection in 30% sucrose (Thermo Fisher Scientific) for 24 h at 4 °C. Samples were embedded in Tissue-Tek® optimal cutting temperature (OCT) compound (Sakura Finetek USA Inc.), and a Leica CM3050 S Research Cryostat (Leica Biosystems Inc.) was used to cut 10 µm tissue sections which were affixed to positively charged Superfrost® Plus Micro Slides (VWR International) and heated overnight in a temperature-controlled oven at 45 °C. Slides were washed three times with 7.5 pH PBS and coverslipped using VECTASHIELD™ HardSet Mounting Medium with DAPI (Vector Laboratories) and allowed to dry flat at RT for 15 min before being transferred to 4 °C. Slides were stored at 4 °C. OCT compound sample embedding and cryosectioning of blocks was performed at the Histology Unit of the Medical Education and Laboratory Support Services of Memorial University of Newfoundland. Slides were processed immediately the day after sectioning.

#### 4.2.3.2 Confocal Microscopy

Fluorescent images were taken with a FluoView FV1000 laser scanning confocal microscope (Olympus, Waltham, MA) in the Confocal Digital Imaging Unit of the Medical Education and Laboratory Support Services of Memorial University of Newfoundland.

### 4.2.4 *Foxl2* Sequencing

The protein coding sequence of the single exon *Foxl2* gene was amplified from gDNA using three primer pairs with overlapping amplicons. *Foxl2* was sequenced from two unique inbred individuals from both the SWR and SJL mouse strains. Additionally, the mouse *Foxl2* coding sequence analogous to that encompassing the c.402C>G *FOXL2* variant observed in human adult GC tumour patients (c.390C; NM_012020.2) was amplified from SWR ovary and GC tumour cDNA using a single primer pair. Unique cDNA samples were prepared from the normal ovaries of one untreated, pubertal SWR female, the normal ovaries of two DHEA-treated SWR females, and three DHEA-induced GC tumours that arose in SWR females. Mice were implanted with DHEA capsules as per Section 2.2.1.3 and necropsied at 4 (untreated) or 5 (DHEA-treated) wk of age as per Section 2.2.1.4. cDNA was reverse transcribed as per Section 2.2.3.3. Primers sequences and their amplicon lengths are shown in Table 4.3. Primers were amplified by PCR and products were electrophoresed, purified, Sanger sequenced and analyzed as per the protocol for SNP genotyping markers (Section 2.2.2.2). Nucleotide sequences were aligned using Clustal Omega (Sievers *et al*. 2011; ebi.ac.uk/Tools/msa/clustalo/).

**Table 4.3 *Foxl2* sequencing primers.** Primer sequences used to amplify overlapping segments of the *Foxl2* gene by PCR, their nucleotide ranges, amplicon lengths, and type of temple input required. Nucleotide ranges are relative to *Foxl2* cDNA bp 1.

| Primer Name | Nucleotide Range | Forward Sequence (5′→3′) | Reverse Sequence (5′→3′) | Amplicon (bp) | Template Input |
|---|---|---|---|---|---|
| Foxl2 1 | -251 – 464 | GGAGAGCTCAGCCAAGAAAA | GAGGACATGTTCGAGAAGGG | 715 | gDNA |
| Foxl2 2 | 293 – 1139 | TCATAGCCAAGTTCCCGTTC | CATTGCTCATACTGGGACCA | 847 | gDNA |
| Foxl2 3 | 933 – +428 | TCACGCACATCATCTGCAC | AAAGAACGTGTCTGGTCGCT | 737 | gDNA |
| Foxl2 cDNA | 267 – 639 | CACTCTGTCCGGCATCTACC | GAACCCCGATTGCAGGTACT | 373 | cDNA |

### 4.2.5 Statistical Analysis

Genotyping and sex ratios were compared by two-tailed z-test, mean pups weaned per litter were compared by one-way ANOVA followed by Tukey's test (*p*-values adjusted for multiple comparisons), and GC tumour frequencies were compared by two-tailed Fisher's exact test using GraphPad Prism version 6.07 for Windows (GraphPad Software). $p < 0.05$ was considered statistically significant. Fertility data is presented as mean pups weaned per litter ± SEM.

## 4.3 Results

### 4.3.1 Generation of SWR.*ROSA*$^{mT/mG/+}$*Foxl2*$^{+/GCE}$ Mice

#### 4.3.1.1 *ROSA*$^{mT/mG}$ and *Foxl2*$^{GCE}$ Construct Lines

The *ROSA*$^{mT/mG}$ and *Foxl2*$^{GCE}$ constructs were successfully backcrossed onto the inbred SWR strain background for a minimum of six generations (approximately 96.9% SWR strain background; Silver 1995), and the presence of SWR alleles was confirmed at mapped *Gct* susceptibility loci. Statistical analysis using the z-test determined that the *Foxl2*$^{GCE}$ allele was recovered at the expected Mendelian frequency during backcrossing onto the SWR strain background ($p = 0.9509$); however, the genotypes observed in the SWR.*ROSA*$^{mT/mG}$ backcross colony deviated significantly from the 1:1 WT-to-heterozygous allele ratio expected for normal litters, with significantly more heterozygous alleles recovered ($p = 0.0169$). No significant deviations from the expected 1:1 male-to-female phenotypic sex ratios were observed in either construct line when analyzed by z-test (SWR.*ROSA*$^{mT/mG}$: $p = 0.6691$ SWR.*Foxl2*$^{GCE}$: $p = 0.8316$). A summary of the phenotypic sex and genotype frequencies observed in the SWR.*ROSA*$^{mT/mG}$ and SWR.*Foxl2*$^{GCE}$ backcross mouse colonies is shown in Table 4.4. No statistically significant reductions in fertility were observed when the average number of pups weaned per litter were compared from the SWR.*ROSA*$^{mT/mG}$ construct line by one-way ANOVA followed by Tukey's test (Figure 4.3); however, SWR dams mated to SWR.*Foxl2*$^{GCE/+}$ sires (SWR x SWR.*Foxl2*$^{GCE/+}$) had significantly more pups weaned per litter ($8.034 \pm 0.2626$) than inbred SWR mice ($6.983 \pm 0.1676$; multiplicity adjusted $p$ value = 0.0093).

Following backcrossing and intercrossing of the SWR.*ROSA*$^{mT/mG}$ allele, we mated SWR.*ROSA*$^{mT/mG/mT/mG}$ dams to SWR.*Amhr2*$^{cre/+}$ sires to generate SWR.*ROSA*$^{mT/mG/+}$*Amhr2*$^{+/cre}$ and SWR.*ROSA*$^{mT/mG/+}$*Amhr2*$^{+/+}$ mice. We examined pubertal ovaries from these mice by

**Table 4.4 Phenotypic sex and genotype frequencies in SWR.*ROSA*$^{mT/mG}$ and SWR.*Foxl2*$^{GCE}$ backcross mouse colonies.**

Phenotypic sex and allele frequencies from SWR.*ROSA*$^{mT/mG}$ and SWR.*Foxl2*$^{GCE}$ backcross breeding colonies are shown. Total cohort sizes are shown in brackets. -: not applicable

| Backcross Colony | Phenotypic Sex | | *ROSA* Alleles | | *Foxl2* Alleles | |
|---|---|---|---|---|---|---|
| | Female | Male | +/+ | +/*mT/mG* | +/+ | +/*Foxl2*$^{GCE}$ |
| SWR.*ROSA*$^{mT/mG}$ | 53.6% (37) | 46.4% (32) | 29.9% (20)[a] | 70.1% (47)[a] | - | - |
| SWR.*Foxl2*$^{GCE}$ | 49.2% (196) | 50.8% (202) | - | - | 49.8% (263) | 50.2% (265) |

[a]Significantly different from the expected 1:1 WT-to-heterozygous allele ratio by z-test ($p = 0.0169$).

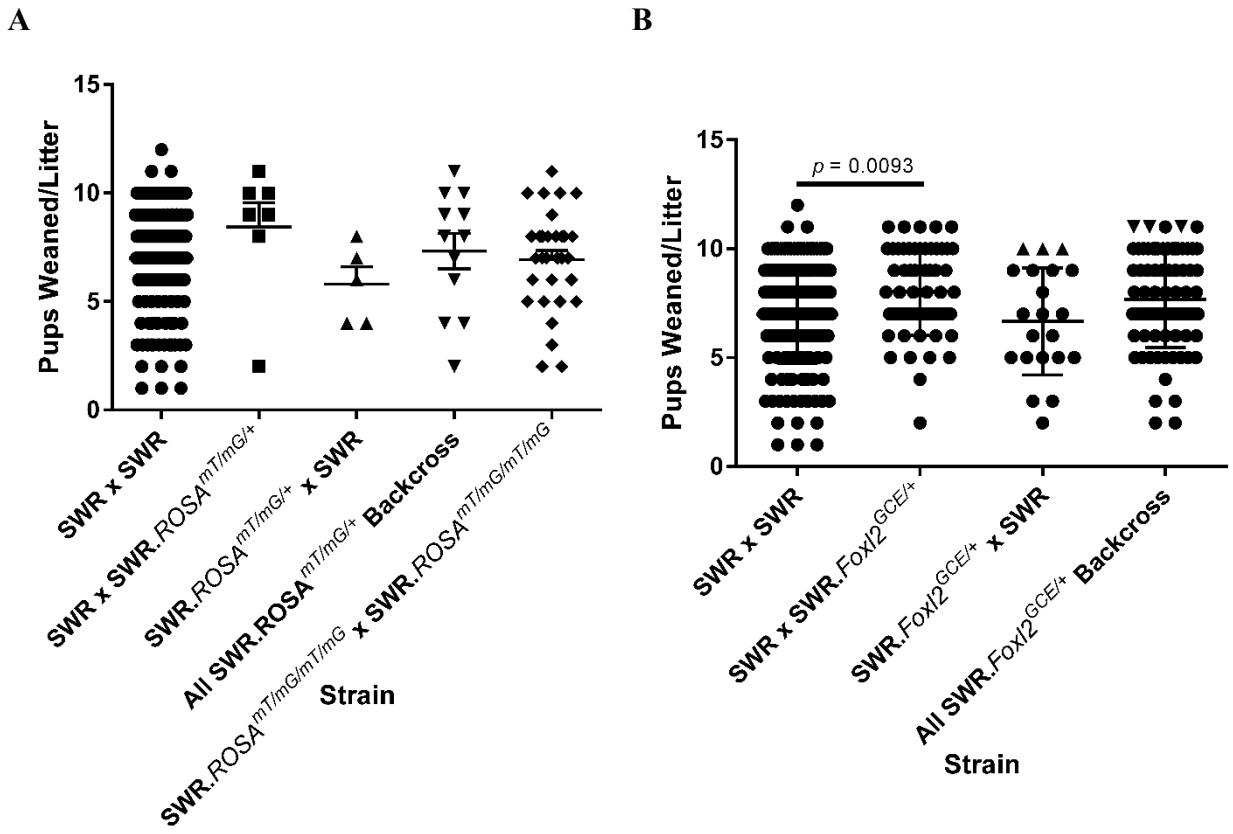


**Figure 4.3 Fertility of SWR.*ROSA*$^{mT/mG}$ and SWR.*Foxl2*$^{GCE}$ female mice**

The average number of pups weaned per litter were compared from the SWR *ROSA*$^{mT/mG}$ and *Foxl*$^{GCE}$ construct lines by one-way ANOVA followed by Tukey's test. No statistically significant differences in fertility were observed in the *ROSA*$^{mT/mG}$ line (A); however, SWR dams mated to SWR.*Foxl2*$^{GCE/+}$ sires (SWR x SWR.*Foxl2*$^{GCE/+}$) had significantly more pups weaned per litter (8.034 ± 0.2626) than inbred SWR mice (6.983 ± 0.1676; multiplicity adjusted $p$ value = 0.0093). Data is presented as mean pups weaned per litter ± SEM.

confocal microscopy as a preliminary examination of GC-specific Cre-mediated mT to mG conversion (Figure 4.4). mT was strongly expressed in ovarian TCs and other stromal tissues, with weaker expression present in GCs. In the presence of an *Amhr2*$^{cre}$ allele, mT was converted to mG in a subset of GCs only.

Female mice carrying homozygous *ROSA*$^{mT/mG/mT/mG}$ or *Foxl2*$^{GCE/+}$ alleles in an SWR inbred strain background were tested for the retention of GC tumour susceptibility following the administration of DHEA at puberty, with an 8 wk endpoint for GC tumour assessment. SWR.*Foxl2*$^{GCE/+}$ females were also tested for GC tumour susceptibility following pubertal T administration. The SWR.*ROSA*$^{mT/mG}$ homozygous construct line was susceptible to GC tumour initiation following pubertal stimulation with DHEA at the 8 wk time point as expected (Table 4.5). Female SWR.*ROSA*$^{mT/mG/mT/mG}$ mice treated with DHEA at puberty developed bilateral GC tumours within 8 wk at a frequency of 10.0% (n = 2). The GC tumours observed in this strain resembled androgen-induced GC tumours found in inbred SWR females when examined macroscopically by H&E (data not shown). No spontaneous GC tumours or other ovarian pathologies were noted in female breeders carrying heterozygous or homozygous *ROSA*$^{mT/mG}$ alleles in an SWR strain background (0/19), and no unexpected breeder deaths were observed in this construct line.

In contrast to the SWR.*ROSA*$^{mT/mG}$ strain, SWR.*Foxl2*$^{GCE/+}$ females were resistant to GC tumour initiation (0.0% GC tumour frequency) when administered either DHEA (n = 60) or T (n = 23) at puberty (Table 4.5). Analyses with Fisher's exact test determined that the GC tumour resistance phenotype in SWR.*Foxl2*$^{GCE/+}$ mice was a significant deviation from those frequencies observed in inbred SWR females administered DHEA (17.6%; Smith 2011; $p = 0.0006$) or fed T in the diet (17.4%; $p = 0.0256$; Tennent, Shultz & Beamer 1993) at puberty ($p < 0.0001$ when

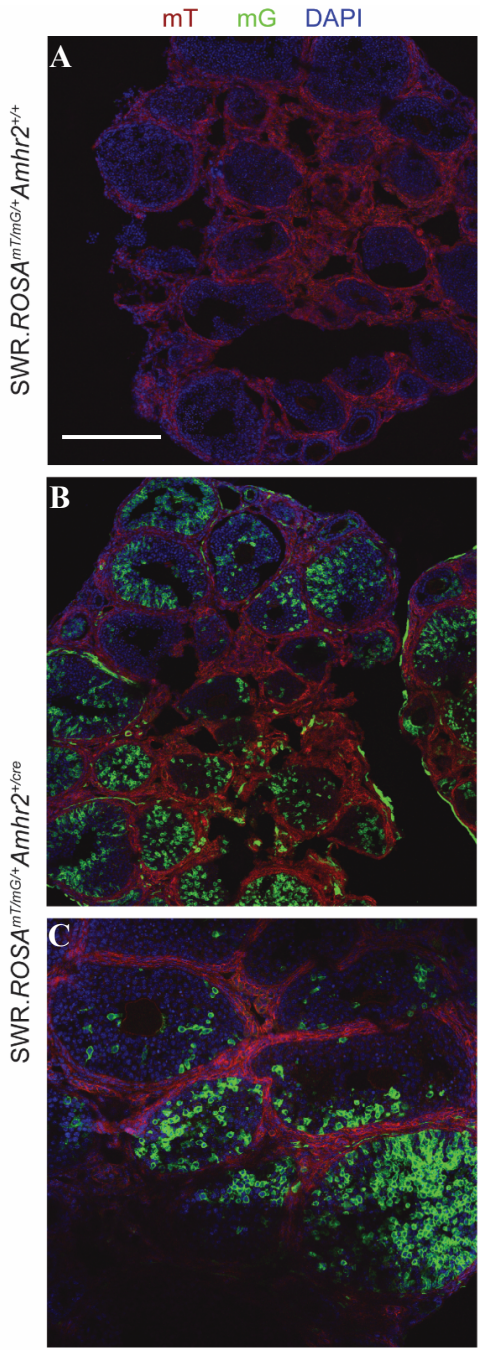


**Figure 4.4 Conversion of mT to mG in pubertal SWR ovarian GCs**

Representative confocal microscopy photos of pubertal ovaries from SWR.*ROSA*$^{mT/mG/+}$*Amhr2*$^{+/+}$ (A) and SWR.*ROSA*$^{mT/mG/+}$*Amhr2*$^{+/cre}$ (B & C) mice. mT is strongly expressed in TCs and other stromal tissues, with weaker expression present in GCs (A). In the presence of an *Amhr2*$^{cre}$ allele, mT is converted to mG in a subset of GCs only (B & C). Magnification: 10X. Scale bar: 500 µm.

**Table 4.5 GC tumour incidence in SWR.*ROSA*$^{mT/mG}$ and SWR.*Foxl2*$^{GCE}$ female mice treated with DHEA or T at puberty.** GC tumour frequencies in 8 wk old mice with homozygous *ROSA*$^{mT/mG}$ alleles or a heterozygous *Foxl2*$^{GCE}$ allele are shown. SWR.*ROSA*$^{mT/mG}$ females were not examined for GC tumour incidence following pubertal T administration. -: not examined

| Strain | DHEA | T |
|---|---|---|
| SWR.*ROSA*$^{mT/mG}$ | 2/20 (10.0%) | - |
| SWR.*Foxl2*$^{GCE}$ | 0/60 (0.0%)[a] | 0/23 (0.0%)[b] |

[a]Significantly different from the GC tumour frequency of SWR females administered DHEA at puberty ($p = 0.0006$; Smith 2011) by Fisher's exact test; [b]Significantly different from the GC tumour frequency of SWR females administered T (dietary supplementation) at puberty ($p = 0.0256$; Tennent *et al*. 1993) by Fisher's exact test.

comparing GC tumour frequencies following administration of any androgen). Steroid sources were not responsible for the loss of the GC tumour phenotype, as the same stocks were used to induce GC tumours in other strains over the same timeframe; further analyses using Fisher's exact test determined that the GC tumour resistance phenotype in SWR.*Foxl2*$^{GCE/+}$ mice was also a significant deviation from those frequencies observed in SWR-derived females over the same timeframe with the same steroid stocks (21.5% in females with AR protein-positive GCs administered DHEA or T; Section 3.3.4.1 and Table 3.10; $p < 0.0001$). Inhibition of GC tumour initiation was independent of the parental origin of the engineered *Foxl2* allele, as proportions of the tested females inherited the *Foxl2*$^{GCE}$ allele paternally (n = 58) or maternally (n = 25). No spontaneous GC tumours or other ovarian pathologies were noted in female breeders in the *Foxl2*$^{GCE}$ continuous backcross breeding colony (0/6), and no unexpected breeder deaths were observed in this construct line.

### 4.3.2 Effects of *in utero* Tamoxifen Exposure on GC Tumour Susceptibility

A cohort of 21 pregnant SWR females were injected with a single IP dose of 50 mg/kg tamoxifen in combination with $P_4$ at E12.5. An additional cohort of four pregnant Line 4-5 females were injected with tamoxifen and $P_4$ using the same paradigm. Finally, a cohort of two pregnant SWR females were treated with corn oil vehicle only at E12.5. Although others have reported that an approximately 1.5 mg dose of tamoxifen in combination with $P_4$ results in efficient recombination without ill effects on pups *in utero* (Nakamura, Nguyen & Mackem 2006), we observed significant toxicity. Of the 21 pregnant SWR females injected with tamoxifen, 20 were subject to Caesarean section at E20.5; one female delivered spontaneously at E20.5 prior to Caesarean section. The majority of pregnant SWR females euthanized at E20.5 (n

= 18) had evidence of fetal and placental remains in the uterus without live pups. Only nine living pups were produced from the two litters born by Caesarean section and the litter that was spontaneously delivered. Among these nine pups were four females, which were implanted with DHEA at puberty. The two pregnant SWR females injected with corn oil vehicle at E12.5 spontaneously delivered litters on E20.5, producing three female pups which were also implanted with DHEA at puberty. In contrast, all of the four pregnant Line 4-5 females injected with tamoxifen were subject to Caesarean section at E20.5, but none produced living pups, precluding an examination of *in utero* tamoxifen administration on GC tumour susceptibility in this resistant congenic strain. Of the four SWR females administered tamoxifen *in utero* and necropsied at 8 wk of age, 50% (n = 2) developed unilateral or bilateral GC tumours following pubertal DHEA administration; 33.3% (n = 1) of the three SWR females administered vehicle only developed unilateral GC tumours following DHEA. A summary of the GC tumour frequencies observed in SWR females following *in utero* tamoxifen or vehicle exposure is shown in Table 4.6.

Nine pregnant SWR.*ROSA*$^{mT/mG/mT/mG}$ females that had been mated to SWR.*Foxl2*$^{GCE/+}$ sires were also injected with tamoxifen and $P_4$ using the same experimental paradigm as SWR and Line 4-5 mice. One female died following injection, whereas Caesarean section of the other eight females revealed evidence of fetal and placental remains in the uterus without live pups. As in the case of the Line 4-5 cohort, this precluded an investigation of the effect of pubertal androgen administration on GC tumour susceptibility in *Foxl2* haploinsufficient females exposed to tamoxifen *in utero*.

**Table 4.6 GC tumour incidence in SWR female mice exposed to 50 mg/kg tamoxifen or vehicle control *in utero* and treated with DHEA at puberty.** Pregnant SWR females were treated with tamoxifen or vehicle at E12.5. GC tumour frequencies from offspring following pubertal DHEA administration in 8 wk old mice are shown.

| Treatment | GC Tumour Incidence |
|---|---|
| Tamoxifen | 2/4 (50%) |
| Vehicle | 1/3 (33.3%) |

### 4.3.3 *Foxl2* Sequencing

Given the loss of the GC tumour phenotype in SWR.*Foxl2*$^{GCE/+}$ females hemizygous for *Foxl2* even in the presence of exogenous androgens, we sequenced the germline and somatic *Foxl2* gene sequences. *Foxl2* resides within the coarsely mapped *Gct5* region (70 Mb in length) on mouse Chr 9, which showed a significant association with GC tumour development in an (SWR x SJL)$F_2$ mapping cross when *Gct5* alleles were donated by the SJL strain (Table 1.2; Beamer *et al*. 1998). The protein coding sequence of the single exon *Foxl2* gene was amplified from SWR and SJL gDNA using three primer pairs with overlapping amplicons. Additionally, the *Foxl2* coding sequence analogous to that encompassing the c.402C>G *FOXL2* variant observed in human adult GC tumour patients (c.390C) was amplified from one untreated, pubertal SWR ovary cDNA sample, two unique SWR ovary cDNA samples from DHEA-treated females, and three unique DHEA-induced GC tumour cDNA samples using a single primer pair. No nucleotide differences between the protein coding sequence gDNA of the SWR and SJL strains, or between either strain and the published B6J mouse reference genome, were identified (Appendix H). Similarly, no nucleotide differences were identified between the untreated or DHEA-treated SWR ovary cDNA samples and the DHEA-induced GC tumour samples in comparison to the published B6J mouse reference genome within the 373 bp amplicon overlapping the sequence analogous to that encompassing the c.402C>G *FOXL2* variant (Appendix I).

## 4.4 Discussion

### 4.4.1 Overview

The restricted window of GC tumour initiation in SWR mice suggests that susceptibility is specific to the GCs of the first follicle wave. The objective of this dissertation chapter was to use an inducible fluorescent reporter system to lineage trace androgen-induced GC tumours so as to pinpoint the GC tumour cell and follicle wave of origin. Although the SWR.*ROSA*$^{mT/mG}$ strain retained GC tumour susceptibility and was useful for fluorescence imaging, the loss of the spontaneous tumour phenotype in SWR mice haploinsufficient for *Foxl2* precluded the completion of the lineage tracing experiment. Furthermore, the high levels of toxicity conferred by tamoxifen prevented a thorough examination of its effects on the spontaneous and androgen-induced GC tumour phenotype in susceptible and resistant mice, as well as in mice hemizygous for *Foxl2*; nonetheless, our preliminary investigation of *in utero* tamoxifen exposure demonstrated that this SERM did not interfere with the pubertal onset of GC tumours in SWR mice.

### 4.4.2 GC Tumour Susceptibility in Engineered SWR Fluorescent Reporter and Cre Strains

The *ROSA*$^{mT/mG}$ and *Foxl2*$^{GCE}$ constructs were backcrossed onto the SWR inbred strain for a minimum of six generations, using marker-assisted progeny selection to achieve approximately 96.9% inbred strain background (Silver 1995). This “speed congenic” approach also ensured a full complement of SWR alleles at important *Gct* loci in SWR.*ROSA*$^{mT/mG}$ and SWR.*Foxl2*$^{GCE}$ mice (Wong 2002). Backcrossing of the *ROSA*$^{mT/mG}$ allele onto the SWR strain was facilitated by the significantly higher frequency of heterozygous pups compared to those

with WT alleles. Importantly, SWR.*ROSA*$^{mT/mG}$ female mice developed GC tumours when administered DHEA at puberty, with a tumour onset timing and macroscopic and microscopic phenotype similar to that observed in androgen-treated inbred SWR mice (Table 4.5). The GC tumour frequency observed in SWR.*ROSA*$^{mT/mG}$ females was not statistically compared to concurrent or historically reported rates, as we were concerned only in ensuring that the SWR construct lines were sensitive to GC tumour development with androgen administration at puberty. *mT/mG* mice carry an engineered fluorescent reporter construct knocked into the Chr 6 *ROSA* targeting locus derived from the (129X1 x 129S1)$F_1$ mouse strain. The presence of this construct and the constitutive expression the fluorescent mT protein in an SWR background had no notable positive or negative influence on the rate of spontaneous GC tumour initiation in *ROSA*$^{mT/mG/+}$ or *ROSA*$^{mT/mG/mTmG}$ breeding colonies, or on the rate of androgen-induced GC tumour initiation in steroid capsule studies of homozygous mice. Although we did not suspect that the fluorescent mT protein or disruption of the endogenous Chr 6 *ROSA* targeting locus – which does not map to any known *Gct* susceptibility loci (Table 1.2) – would influence GC tumour susceptibility, the expression of recombinant fluorescent proteins can produce significant deleterious effects on cell function and metabolomics *in vivo* (Baens *et al*. 2006; Li *et al*. 2013). In addition, the presence of the *ROSA*$^{mT/mG}$ allele did not result in any other spontaneous ovarian pathologies in female breeders or decreases in fertility. Thus, the independent presence of the *ROSA*$^{mT/mG}$ allele did not significantly influence fertility or the expected GC tumour phenotype as has been previously observed, and the choice of fluorescent reporter was appropriate for further experimental crosses prior to lineage tracing the GC tumour cell of origin.

In a stark contrast to all other engineered strains discussed in this dissertation, SWR mice with one copy of the *Foxl2*$^{GCE}$ allele were resistant to GC tumour initiation even in the presence

of exogenous DHEA or T (Table 4.5). GC tumour resistance was not attributable to issues related to steroid sources or parental origin of the engineered *Foxl2* allele, as the same stocks were used to induce GC tumours in other SWR-derived lines over the same timeframe and proportions of the tested females inherited the $Foxl2^{GCE}$ allele paternally or maternally. The presence of the $Foxl2^{GCE}$ allele is therefore tumour-suppressive in the SWR model, although we are not able to determine whether it is *Foxl2* haploinsufficiency or expression of the GCE construct itself that confers GC tumour resistance. We predicted that the presence of only one WT *Foxl2* allele in the GC population would have little to no effect on the GC tumour phenotype – including the restricted window of initiation, tumour histology, and the trait's endocrine sensitivity – based on a number of pieces of published evidence. A normal ovarian appearance and proper specification of the first follicle wave was apparent in the investigation by Mork and colleagues (2012), despite *Foxl2* hemizygosity. In the case of human adult GC tumours, it is an acquired somatic *FOXL2* mutation that likely results in protein activation or gain-of-function that is associated with tumourigenesis, rather than allelic loss (Shah *et al*. 2009). Furthermore, the fact that aggressive human juvenile GC tumours may exhibit absent or reduced *FOXL2* expression suggests a role for FOXL2 as a suppressor of juvenile GC tumour progression and potentially initiation (Kalfa *et al*. 2007). Alternatively, we considered that *Foxl2* haploinsufficiency might instead increase spontaneous and/or androgen-induced GC tumour incidence, given FOXL2's function as an antagonist of the male differentiation pathway. If two copies of *Foxl2* are indeed required for GC tumourigenesis in SWR mice, it would suggest that perturbation of the mechanistic pathway at work in human adult GC tumours also leads to juvenile GC tumour initiation, albeit through a different (i.e. allelic loss) mechanism. Our results and the nature of the somatic *FOXL2* p.Cys134Trp mutation found in adult GC tumours suggests

a potential overarching model, in which both WT germline *FOXL2* alleles and thus normal expression levels in a susceptible population (including mouse strains with $Gct1^{SW}$ alleles), and somatic gain-of-function *FOXL2* mutation in a non-susceptible population, permits GC tumourigenesis. Alternatively, the $Foxl2^{GCE}$ allele may be acting in a dominant negative fashion, resulting in the disruption of normal FOXL2 function. Deletion of the *Foxl2* gene from SWR mice globally or from the ovary using traditional transgenic technology could resolve the effects of *Foxl2* haploinsufficiency versus those imparted by the $Foxl2^{GCE}$ allele.

In contrast to its role in adult ovarian identity maintenance, *Foxl2* is not required for early sex determination in mice (Section 1.1.2.2). Although *Foxl2* supresses male pathway genes, its deletion from the early ovary alone does not cause complete Chr XX female-to-male sex reversal (Schmidt *et al*. 2004; Uda *et al*. 2004; Ottolenghi *et al*. 2005; Garcia-Ortiz *et al*. 2009). However, previous investigations have shown that mice globally haploinsufficient for *Foxl2* demonstrate a number of deviations in gonadal mRNA levels that are consistent with a skew towards initiation of the testis differentiation pathway. Garcia-Ortiz and colleagues (2009) found that at E16.5, as a group, the pro-testis genes *Dmrt1*, *Dhh*, *Fgf9*, *Nr5a1*, and *Sox9* are significantly upregulated in $Foxl2^{+/-}$ ovaries compared to WT ovaries. Similarly, Ottolenghi and colleagues (2005) found that at P1, $Foxl2^{+/-}$ ovaries exhibit lower levels of the pro-ovarian genes *Dax1* and *Fst* and higher levels of *Dhh*, *Fgf9*, *Gata4*, *Nr5a1*, and *Sox9* compared to ovaries from WT littermates. Whereas Garcia-Ortiz and colleagues found the expression of grouped pro-testis genes to be transient, the low levels of *Dax1* and *Fst* and high levels of *Sox9* observed by Ottolenghi *et al*. (2005) persisted until at least P7. At this time, transcript expression patterns – including the aberrant upregulation of fetal ovary development genes, the inhibition of genes associated with early follicle growth and steroidogenesis, and the expression of genes in both WT and *Foxl2*-null but not $Foxl2^{+/-}$

ovaries – suggest that although mice heterozygous for *Foxl2* eventually activate the ovarian differentiation pathway, they do so with a significant delay (Ottolenghi *et al*. 2005; Garcia-Ortiz *et al*. 2009). A delay in normal ovarian FOXL2 function might postpone the onset of pre-GC specification and the subsequent formation of the first follicular wave. As evidence suggests that this wave is the source of the GC tumour cell of origin in the SWR mouse model, an overlap between the delay in FOXL2 action and the window of susceptibility dictated by *Gct1* action could result in inhibition of GC tumour onset, despite the endocrine initiation trigger that occurs via the AR at puberty. Interestingly, strain-specific effects on the timing of primary sex determination and the levels of pro-ovarian gene expression have been reported, suggesting that variability in the onset of this complex process exists and is influenced by genetic factors (Munger *et al*. 2009; Munger *et al*. 2013). Among loci with a genetic contribution to this phenotype is the testis-determining autosomal 1 (*Tda1*) locus on distal Chr 4, which encompasses the *Gct1* locus and has not been resolved (Eicher *et al*. 1996; Munger *et al*. 2009).

That the presence of the $Foxl2^{GCE}$ allele confers GC tumour resistance strongly suggests a role for *Foxl2* in GC tumourigenesis in the SWR mouse model. *Foxl2* resides within the *Gct5* region on mouse Chr 9, which is coarsely mapped and currently spans over 70 Mb. *Gct5* showed a significant association with GC tumour development in an (SWR x SJL)$F_2$ mapping cross when alleles were donated by the SJL strain (Table 1.2; Beamer *et al*. 1998). However, Sanger sequencing revealed that there are no nucleotide differences in the protein coding region sequences of *Foxl2* between SWR and SJL mice or between either strain and the B6J reference sequences (Appendix H). Furthermore, analyses of cDNA sequences from pubertal and DHEA-treated normal SWR ovaries and GC tumours failed to find any nucleotide differences in an amplicon overlapping the *Foxl2* coding sequence analogous to that encompassing the c.402C>G

*FOXL2* variant observed in human adult GC tumour patients (Appendix I). As 1,185 protein coding and RNA genes are present within the current boundaries of *Gct5* (Ensembl BioMart), numerous other candidates other than *Foxl2* have the potential for shared identity with *Gct5*. As *Gct5* is a modifier of spontaneous rather than androgen-induced GC tumourigenesis, and *Gct* alleles from any strain tested to date do not confer complete GC tumour initiation inhibition (as do $Gct1^{CA}$ alleles, for example), resolution of this interval using classical phenotype/genotype methods would require enormous mouse cohort sizes. Rather, whole-transcriptome sequencing may be a more amenable methodology for the resolution of *Gct5* identity.

### 4.4.3 *In utero* Tamoxifen Exposure Permits GC Tumourigenesis

The presence of DHEA-induced GC tumours in inbred SWR mice exposed to tamoxifen *in utero* implies it does not prevent GC tumour initiation in this strain, although low sample sizes precluded statistical analysis of GC tumour incidence rates in females exposed to tamoxifen versus vehicle only. As we could not evaluate the effect of *in utero* tamoxifen exposure on GC tumour susceptibility in Line 4-5 mice or SWR.$Foxl2^{GCE/+}$ females, we could not determine if $Gct1^{SW}$ alleles are a requirement for GC tumour initiation post-tamoxifen exposure or if the inhibition of GC tumourigenesis associated with *Foxl2* haploinsufficiency is overcome by *in utero* tamoxifen. As a SERM, tamoxifen functions as an estrogen receptor antagonist in the breast, but as an agonist in the endometrium, bone, and other tissues (Martinkovich *et al*. 2014). In the hypothalamus, tamoxifen's antagonist activity blocks $E_2$ feedback, resulting in increases in GnRH, FSH, LH and $E_2$ (Figure 1.2), ovulation induction, and the formation of ovarian cysts (Nasu *et al*. 2008). Tamoxifen has also been shown to potentiate FSH-mediated increases in $E_2$ in cultured rodent GCs in a dose-dependent manner (Welsh *et al*. 1984). This data is seemingly

at odds with our current work and previous investigations in the SWR mouse model, which found that short-term pubertal $E_2$ exposure prior to the appearance of pre-neoplastic follicular lesions suppresses GC tumour incidence (Dorward, Shultz & Beamer 2007). The suppression of GC tumour initiation by $E_2$ is thought to occur due to the inhibition of LH release from the anterior pituitary during the pubertal susceptibility window (Section 1.3.1.1). It is possible that as tamoxifen increases LH levels, this pathway to GC tumour initiation may be maintained, even in the presence of high $E_2$ levels. More likely, the short-term elevation in $E_2$ levels induced by tamoxifen at E12.5 has no effect on the pubertal window of endocrine sensitivity that is conferred by androgens and mediated by the AR.

### 4.4.4 Summary

The significant overlap between the first follicular wave and the restricted window of GC tumour susceptibility in SWR mice suggests the GC tumour cell of origin arises from this unique cell population; we therefore proceeded with a high-risk, high-reward strategy to lineage trace the GC tumour cell of origin. We successfully backcrossed the *ROSA*$^{mT/mG}$ fluorescent reporter onto the SWR strain and established an *in utero* tamoxifen administration protocol that, while a considerable technical challenge for fertility maintenance, retained pubertal GC tumour susceptibility. The SWR.*ROSA*$^{mT/mG}$ strain may therefore be a useful resource for tracking spontaneous GC tumour metastases and testing chemotherapeutic and/or biologic treatment agents (e.g. AR antagonists) in the mouse model. In contrast, the loss of the androgen-induced phenotype in SWR.*Foxl2*$^{GCE/+}$ mice meant we could not proceed with our lineage tracing experiment as planned. The loss of this robust, androgen-inducible ovarian phenotype from SWR mice raises a question in regards to the work of Mork and colleagues (2012) and others

employing the engineered *Foxl2*$^{GCE}$ allele in studies of normal ovarian function and follicle wave origins; this strain was also utilized in an investigation of TC lineage specification (Section 1.1.3.2; Liu *et al*. 2015a). Similarly, the effects, if any, of the chimeric *Foxl2-creER*$^{T2}$ construct that maintains *Foxl2* diploid status utilized by Zheng and colleagues (2014) to investigate follicle wave kinetics are unknown. However, the presence of distinct GC differentiation waves and formation of the first follicular cohort as hypothesized by Hirshfield (1992) was evident in both models, and loss of this follicle cohort does not explain the impact of *Foxl2* haploinsufficiency on the GC tumour phenotype in SWR female mice. Although our current data does not allow us to determine whether it is *Foxl2* haploinsufficiency or expression of the GCE construct itself that confers resistance of this sensitive phenotype, our evidence and the known role of *Foxl2* suggests this transcription factor may be required for GC tumour initiation in the SWR mouse model even when *Gct1*$^{SW}$ alleles are present, indicating that the ovarian specification pathway involving *Foxl2* influences, or is influenced by, the activity of the *Gct1* locus.

## 5. Overall Summary

The rarity of juvenile GC tumours in the human population has significantly precluded investigations into the etiology of this pediatric ovarian tumour subtype, whereas the adult-onset phenotype is attributed to an acquired mutation in the GC differentiation marker *FOXL2*. As most attempts at characterizing juvenile-onset GC tumours were conducted prior to the incorporation of *FOXL2* mutation status into the diagnostic paradigm, our current knowledge about the cause, life history, and prognosis of this tumour type is considerably disadvantaged. Resolving the identity of the genetic drivers and endocrine risk factors that contribute to juvenile GC tumour susceptibility is therefore of utmost importance in the era of histological and molecular tumour stratification. The SWR mouse model of GC tumourigenesis is a realistic model for genetically complex and stochastic cancer risk, as well as a recognized model for juvenile GC tumours that appear in pediatric patients. The pursuit of GC tumour susceptibility genes and the dissection of endocrine influences in the mouse will allow for cross-examinations of specific candidate pathways in human juvenile GC tumours, to assist in the elucidation of this unique ovarian tumour subtype's etiology.

The stochastic GC tumour phenotype is driven by the oncogenic action of *Gct1*. As the *Gct1* locus has been a consistently strong genetic prediction across mapping crosses, we anticipated that our genetic analyses of the refined interval would identify a single gene or copy number variant that could be interrogated using classic loss- or gain-of-function analyses in mice. The identity of *Gct1* remains elusive pending further investigations of the c.460-3C>T *Dhrs3* variant's contributions to GC tumour susceptibility. Conversely, our GC-specific AR KO model confirms this steroid hormone receptor is required for GC tumour initiation at puberty,

cementing the *Ar* gene as sharing identity with *Gct4*. Although the window for androgen-induced SWR GC tumourigenesis has been confidently established as overlapping with the pubertal period (Tennent *et al*. 1990), the pathway leading to susceptibility could be initiated *in utero* during differentiation of the GCs comprising the first medullary follicle wave. The action of *Gct1*, for example altered *Dhrs3* transcription resulting in differential retinoid and/or steroid metabolism and signalling, may occur at a critical embryonic window of medullary follicle development. That *Foxl2* haploinsufficiency is associated with a loss of the GC tumour phenotype supports the concept that *Gct1* influence can be modified by a primary factor that dictates GC differentiation and influences early sex specification events, much earlier than the endocrine triggering events that occur at puberty. Thus, influential timing in the SWR model can be segregated into two discrete windows of GC tumour susceptibility versus initiation, driven by *Gct1* action during fetal ovarian development and AR action triggered by the pubertal endocrine environment, respectively (Figure 5.1). Such a scenario is akin to that observed in prostate and breast cancer, in which endocrine stimulation of genetically-susceptible tissues leads to tumour onset. In hindsight, our assumption that the impact of potential *Gct1* ligand (TNF), substrate (RAL) or inducer (RA) was similar to endocrine stimulation and thus influential at the pubertal transition, functional analyses with these molecules with a pubertal treatment paradigm was likely misguided.

An intriguing parallel exists between patterns of ovarian RA signalling, loss of SDSI, and follicle wave activation that is of considerable interest to the SWR model in the context of our current evidence. RA signalling triggers meiotic initiation of female germ cells in an anterior-to-posterior wave-like pattern that originates from the mesonephros at E13.5 (Section 1.1.2.2; Bowles *et al*. 2006; Koubova *et al*. 2006). In addition to its role in meiotic initiation, RA

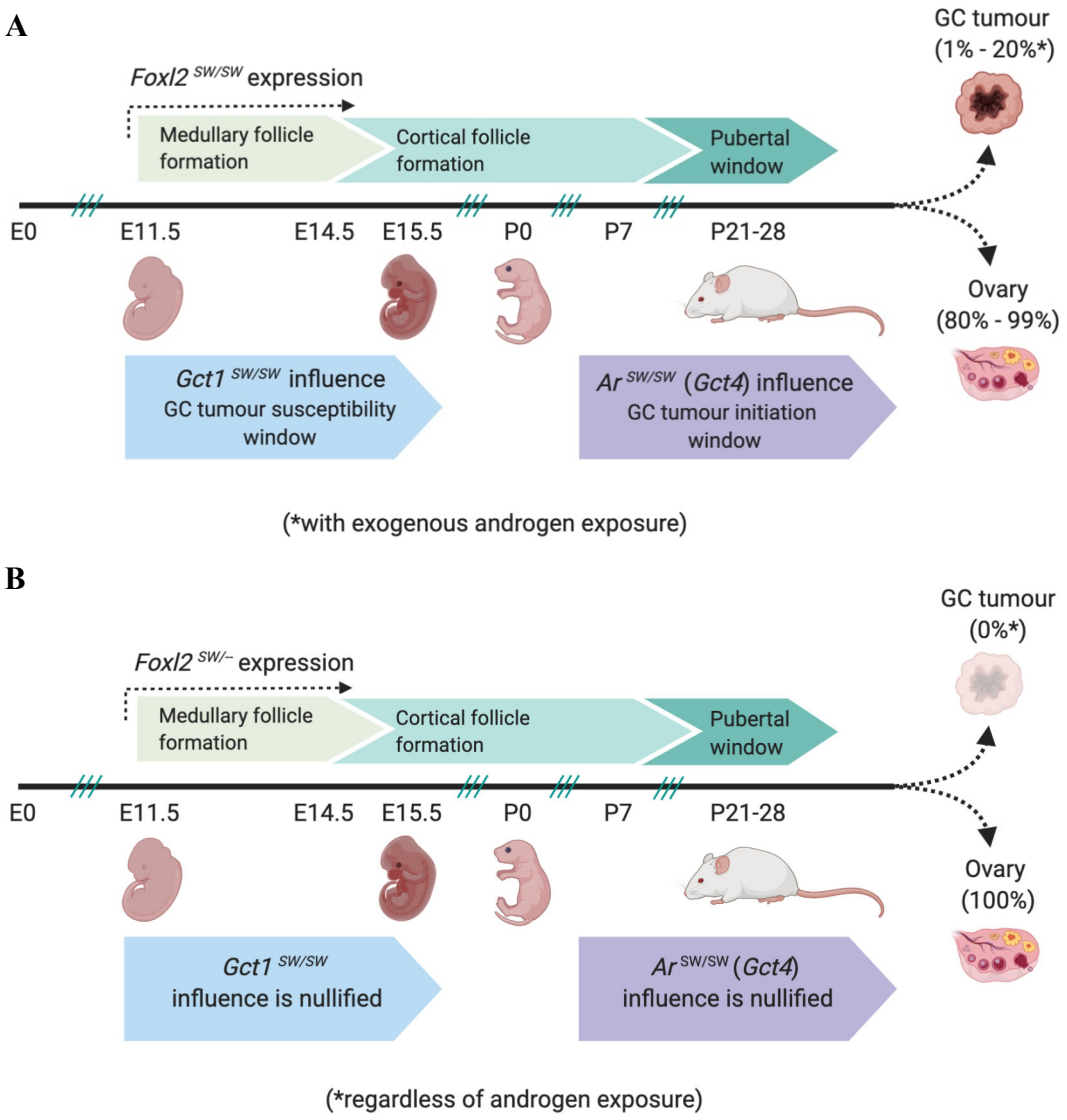
A
GC tumour
(1% - 20%*)
Foxl2 SW/SW expression
Medullary follicle formation
Cortical follicle formation
Pubertal window
E0
E11.5
E14.5
E15.5
P0
P7
P21-28
Ovary
(80% - 99%)
Gct1 SW/SW influence
GC tumour susceptibility window
Ar SW/SW (Gct4) influence
GC tumour initiation window
(*with exogenous androgen exposure)
B
GC tumour
(0%*)
Foxl2 SW/- expression
Medullary follicle formation
Cortical follicle formation
Pubertal window
E0
E11.5
E14.5
E15.5
P0
P7
P21-28
Ovary
(100%)
Gct1 SW/SW
influence is nullified
Ar SW/SW (Gct4)
influence is nullified
(*regardless of androgen exposure)

**Figure 5.1 Summary of the two-stage susceptibility model influencing GC tumourigenesis in SWR female mice**

(A) Establishment of GC tumour susceptibility in the developing ovary requires SWR alleles at the *Gct1* driver, as well as WT levels of *Foxl2* expression, which begins at E11.5. At puberty, GC tumour initiation in genetically susceptible juvenile ovaries requires androgenic signalling from either the first folliculogenesis LH wave or exogenous androgens, which is mediated by *Gct4* (i.e. the AR). The result is spontaneous GC tumour appearance in ≤ 1% of females, or in approximately 20% of females treated with exogenous androgens. (B) The effects of *Gct1* and *Gct4* on GC tumour susceptibility and initiation, respectively, are nullified in the presence of a single *Foxl2* allele, regardless of androgen exposure at puberty.

signalling also accelerates gonadal somatic cell transdifferentiation in at least one mouse model of disturbed adult cell identity maintenance. *Foxl2* and *Dmrt1* mutually antagonize each other to prevent the postnatal transdifferentiation of GCs and Sertoli cells, respectively (Matson & Zarkower 2012). In addition, testicular *Dmrt1* inhibits RA signalling; in its absence, RA signalling activates the expression of pro-ovary genes and promotes transdifferentiation towards the female fate (Minkina *et al*. 2014). As RA signalling is necessary for spermatogenesis, DMRT1 allows for gamete production without unintended Sertoli cell sexual reprogramming. The wave of ovarian RA signalling is preceded by loss of SDSI in almost all Chr XX gonadal supporting cells from E11.5 to E12.0, which also follows an anterior-to-posterior wave-like pattern. As discussed in Section 4.1.1.1, a subset of medullary pre-GCs near the mesonephros and that contribute to the first follicle wave only maintain SDSI until approximately P14; these cells therefore retain sexual bipotentiality, whereas GCs in subsequent cortical follicle waves do not (Hiramatsu *et al*. 2009; Harikae *et al*. 2013). Finally, the formation and activation of the first follicle wave also follows a distinct pattern in the ovary that begins in the medullar anterior-dorsal region and expands into the ovarian periphery (Cordeiro *et al*. 2015); this evidence indicates that the trigger for follicle activation is related to location within the ovary. It is possible that *Gct1* might also follow a restricted pattern of expression and action that coincides with fetal waves of RA signalling, SDSI loss, and first wave follicle activation, which is particularly intriguing given the role of *Dhrs3* in retinoid metabolism. Although we have yet to fully unravel the complexities of GC tumour susceptibility in the SWR mouse model, the validity of the genetic contribution is clear and potentially relevant for pediatric cases of juvenile-onset GC tumours.

# 6. Future Directions

The future directions and goals of this project are interrelated and draw on the results of the chapters of this dissertation as a whole. As the c.460-3C>T *Dhrs3* variant is the primary candidate for *Gct1* identity, ensuing investigations will work to characterize its transcriptional and functional effects. As our lineage tracing experiment was confounded by the sensitivity of the phenotype, other examinations to determine the GC tumour cell of origin should focus on differential gene expression and kinetics of SWR medullary follicles. Following elucidation of the genetic factors influencing susceptibility, the use of available mouse strain resources could be used to characterize GC tumour metastases and investigate treatment modalities.

1) Complete further RNA analyses, such as TOPO cloning, minigene assays, or whole-transcriptome sequencing of the early SWR versus Line 4-5 ovary to characterize *Dhrs3* transcripts; examine endogenous retinoid derivatives and/or retinoid signalling (e.g. *Stra8* levels, etc.) in SWR versus Line 4-5 ovaries.

2) Establish an *in vitro* system (e.g. short-term culture of MEFs isolated from SWR and Line 4-5 embryos) to investigate the c.460-3C>T *Dhrs3* variant and its functional outcome on transcriptional regulation, retinoid metabolism, and steroid biosynthesis.

3) If the c.460-3C>T *Dhrs3* variant has influence on transcriptional profiles, retinoid signalling and/or steroid homeostasis, develop a SNP knock-in mouse model to independently assess GC tumour susceptibility in a tumour-resistant strain(s) (e.g. the B6J reference strain or the Line 4-5 congenic subline, which maintains SWR genome at all loci except for the *Gct1* locus on Chr 4).

4) Assess sexual bipotentiality in the first wave medullary follicle GCs of the SWR ovary using immunohistological measures to test if SDSI is extended in SWR versus Line 4-5 ovaries, for example using kidney capsule ovary transfer to reproductively mature male, isogenic hosts to stimulate sex reversal.

5) Whole-transcriptome sequencing of laser-capture microdissected medullary follicles to identify transcripts with differential expression between SWR and Line 4-5 first wave GCs.

6) Use the SWR.*ROSA*$^{mT/mG}$ and SWR.*Amhr2*$^{cre}$ lines to track spontaneous GC tumour metastases and examine the effects of chemotherapeutic and/or biologic treatment agents (e.g. AR antagonists) in the mouse model.

## 7. References


Abahssain H, Kairouani M, Gherman R, M'rabti H, Errihani H. 2010. Granulosa cell tumor of the ovary and antecedent of adjuvant tamoxifen use for breast cancer. World J Surg Oncol. 8:67,7819-8-67.

Abel MH, Wootton AN, Wilkins V, Huhtaniemi I, Knight PG, Charlton HM. 2000. The effect of a null mutation in the follicle-stimulating hormone receptor gene on mouse reproduction. Endocrinology. 141(5):1795-803.

Abramowicz A, Gos M. 2018. Splicing mutations in human genetic disorders: Examples, detection, and confirmation. J Appl Genet. 59(3):253-68.

Ackert CL, Gittens JE, O'Brien MJ, Eppig JJ, Kidder GM. 2001. Intercellular communication via connexin43 gap junctions is required for ovarian folliculogenesis in the mouse. Dev Biol. 233(2):258-70.

Adams J, Polson DW, Franks S. 1986. Prevalence of polycystic ovaries in women with anovulation and idiopathic hirsutism. Br Med J (Clin Res Ed). 293(6543):355-9.

Adams MK, Belyaeva OV, Wu L, Kedishvili NY. 2014. The retinaldehyde reductase activity of DHRS3 is reciprocally activated by retinol dehydrogenase 10 to control retinoid homeostasis. J Biol Chem. 289(21):14868-80.

Adhikari D, Flohr G, Gorre N, Shen Y, Yang H, Lundin E, Lan Z, Gambello MJ, Liu K. 2009. Disruption of Tsc2 in oocytes leads to overactivation of the entire pool of primordial follicles. Mol Hum Reprod. 15(12):765-70.

Adhikari D, Liu K. 2009. Molecular mechanisms underlying the activation of mammalian primordial follicles. Endocr Rev. 30(5):438-64.

Adhikari D, Zheng W, Shen Y, Gorre N, Hamalainen T, Cooney AJ, Huhtaniemi I, Lan ZJ, Liu K. 2010. Tsc/mTORC1 signaling in oocytes governs the quiescence and activation of primordial follicles. Hum Mol Genet. 19(3):397-410.

Adhikari D, Liu K. 2014. The regulation of maturation promoting factor during prophase I arrest and meiotic entry in mammalian oocytes. Mol Cell Endocrinol. 382(1):480-7.

Ahonen MH, Zhuang YH, Aine R, Ylikomi T, Tuohimaa P. 2000. Androgen receptor and vitamin D receptor in human ovarian cancer: Growth stimulation and inhibition by ligands. Int J Cancer. 86(1):40-6.

Aitken SJ, Presneau N, Khatri B, Flanagan AM, Clarke B, McCluggage WG. 2015. Mutations in IDH1 and IDH2 are not present in sporadic ovarian sex cord-stromal tumours. Histopathology. 66(6):897-8.

Akiyama H, Lyons JP, Mori-Akiyama Y, Yang X, Zhang R, Zhang Z, Deng JM, Taketo MM, Nakamura T, Behringer RR, *et al*. 2004. Interactions between Sox9 and beta-catenin control chondrocyte differentiation. Genes Dev. 18(9):1072-87.

Al-Agha OM, Huwait HF, Chow C, Yang W, Senz J, Kalloger SE, Huntsman DG, Young RH, Gilks CB. 2011. FOXL2 is a sensitive and specific marker for sex cord-stromal tumors of the ovary. Am J Surg Pathol. 35(4):484-94.

Albalat R, Brunet F, Laudet V, Schubert M. 2011. Evolution of retinoid and steroid signaling: Vertebrate diversification from an amphioxus perspective. Genome Biol Evol. 3:985-1005.

Albrecht KH, Eicher EM. 2001. Evidence that sry is expressed in pre-sertoli cells and sertoli and granulosa cells have a common precursor. Dev Biol. 240(1):92-107.

Altschul SF, Gish W, Miller W, Myers EW, Lipman DJ. 1990. Basic local alignment search tool. J Mol Biol. 215(3):403-10.
Amary MF, Damato S, Halai D, Eskandarpour M, Berisha F, Bonar F, McCarthy S, Fantin VR, Straley KS, Lobo S, *et al*. 2011. Ollier disease and maffucci syndrome are caused by somatic mosaic mutations of IDH1 and IDH2. Nat Genet. 43(12):1262-5.
American Cancer Society. 2018. Cancer facts and figures 2018. Atlanta, GA: American Cancer Society.
An P, Rosmond R, Borecki IB, Ukkola O, Rice T, Gagnon J, Rankinen T, Leon AS, Skinner JS, Wilmore JH, *et al*. 2001. Genome-wide linkage scan to detect loci influencing levels of dehydroepiandrosterones in the HERITAGE family study. Metabolism. 50(11):1315-22.
Anderson R, Copeland TK, Scholer H, Heasman J, Wylie C. 2000. The onset of germ cell migration in the mouse embryo. Mech Dev. 91(1-2):61-8.
Anderson RA, Fulton N, Cowan G, Coutts S, Saunders PT. 2007. Conserved and divergent patterns of expression of DAZL, VASA and OCT4 in the germ cells of the human fetal ovary and testis. BMC Dev Biol. 7:136.
Anderson EL, Baltus AE, Roepers-Gajadien HL, Hassold TJ, de Rooij DG, van Pelt AM, Page DC. 2008. Stra8 and its inducer, retinoic acid, regulate meiotic initiation in both spermatogenesis and oogenesis in mice. Proc Natl Acad Sci U S A. 105(39):14976-80.
Anding AL, Wang C, Chang TK, Sliter DA, Powers CM, Hofmann K, Youle RJ, Baehrecke EH. 2018. Vps13D encodes a ubiquitin-binding protein that is required for the regulation of mitochondrial size and clearance. Curr Biol. 28(2):287,295.e6.
Andreu-Vieyra C, Chen R, Matzuk MM. 2007. Effects of granulosa cell-specific deletion of rb in inha-alpha null female mice. Endocrinology. 148(8):3837-49.
Anttonen M, Farkkila A, Tauriala H, Kauppinen M, Maclaughlin DT, Unkila-Kallio L, Butzow R, Heikinheimo M. 2011. Anti-mullerian hormone inhibits growth of AMH type II receptor-positive human ovarian granulosa cell tumor cells by activating apoptosis. Lab Invest. 91(11):1605-14.
Anttonen M, Pihlajoki M, Andersson N, Georges A, L'hote D, Vattulainen S, Farkkila A, Unkila-Kallio L, Veitia RA, Heikinheimo M. 2014. FOXL2, GATA4, and SMAD3 co-operatively modulate gene expression, cell viability and apoptosis in ovarian granulosa cell tumor cells. PLoS One. 9(1):e85545.
Aramaki S, Hayashi K, Kurimoto K, Ohta H, Yabuta Y, Iwanari H, Mochizuki Y, Hamakubo T, Kato Y, Shirahige K, *et al*. 2013. A mesodermal factor, T, specifies mouse germ cell fate by directly activating germline determinants. Dev Cell. 27(5):516-29.
Arnould L, Franco N, Soubeyrand MS, Mege F, Belichard C, Lizard-Nacol S, Collin F. 2002. Breast carcinoma metastasis within granulosa cell tumor of the ovary: Morphologic, immunohistologic, and molecular analyses of the two different tumor cell populations. Hum Pathol. 33(4):445-8.
Auguste A, Chassot AA, Gregoire EP, Renault L, Pannetier M, Treier M, Pailhoux E, Chaboissier MC. 2011. Loss of R-spondin1 and Foxl2 amplifies female-to-male sex reversal in XX mice. Sex Dev. 5(6):304-17.
Auguste A, Bessiere L, Todeschini AL, Caburet S, Sarnacki S, Prat J, D'angelo E, De La Grange P, Ariste O, Lemoine F, *et al*. 2015. Molecular analyses of juvenile granulosa cell tumors bearing AKT1 mutations provide insights into tumor biology and therapeutic leads. Hum Mol Genet. 24(23):6687-98.

Avizienyte E, Loukola A, Roth S, Hemminki A, Tarkkanen M, Salovaara R, Arola J, Butzow R, Husgafvel-Pursiainen K, Kokkola A, *et al*. 1999. LKB1 somatic mutations in sporadic tumors. Am J Pathol. 154(3):677-81.
Baarends WM, Hoogerbrugge JW, Post M, Visser JA, De Rooij DG, Parvinen M, Themmen AP, Grootegoed JA. 1995. Anti-mullerian hormone and anti-mullerian hormone type II receptor messenger ribonucleic acid expression during postnatal testis development and in the adult testis of the rat. Endocrinology. 136(12):5614-22.
Baens M, Noels H, Broeckx V, Hagens S, Fevery S, Billiau AD, Vankelecom H, Marynen P. 2006. The dark side of EGFP: Defective polyubiquitination. PLoS One. 1:e54.
Baerwald AR, Adams GP, Pierson RA. 2012. Ovarian antral folliculogenesis during the human menstrual cycle: A review. Hum Reprod Update. 18(1):73-91.
Bagchi A, Mills AA. 2008. The quest for the 1p36 tumor suppressor. Cancer Res. 68(8):2551-6.
Bagheri-Fam S, Bird AD, Zhao L, Ryan JM, Yong M, Wilhelm D, Koopman P, Eswarakumar VP, Harley VR. 2017. Testis determination requires a specific FGFR2 isoform to repress FOXL2. Endocrinology. 158(11):3832-43.
Bai S, Wei S, Ziober A, Yao Y, Bing Z. 2013. SALL4 and SF-1 are sensitive and specific markers for distinguishing granulosa cell tumors from yolk sac tumors. Int J Surg Pathol. 21(2):121-5.
Baker TG. 1963. A quantitative and cytological study of germ cells in human ovaries. Proc R Soc Lond B Biol S. 158:417-33.
Baker J, Hardy MP, Zhou J, Bondy C, Lupu F, Bellve AR, Efstratiadis A. 1996. Effects of an Igf1 gene null mutation on mouse reproduction. Mol Endocrinol. 10(7):903-18.
Bakker J, Pool CW, Sonnemans M, van Leeuwen FW, Slob AK. 1997. Quantitative estimation of estrogen and androgen receptor-immunoreactive cells in the forebrain of neonatally estrogen-deprived male rats. Neuroscience. 77(3):911-9.
Bakker ST, van de Vrugt HJ, Visser JA, Delzenne-Goette E, van der Wal A, Berns MA, van de Ven M, Oostra AB, de Vries S, Kramer P, *et al*. 2012. Fancf-deficient mice are prone to develop ovarian tumours. J Pathol. 226(1):28-39.
Balchak SK, Marcinkiewicz JL. 1999. Evidence for the presence of tumor necrosis factor alpha receptors during ovarian development in the rat. Biol Reprod. 61(6):1506-12.
Baldeón RL, Weigelt K, de Wit H, Ozcan B, van Oudenaren A, Sempertegui F, Sijbrands E, Grosse L, van Zonneveld AJ, Drexhage HA, *et al*. 2015. Type 2 diabetes monocyte MicroRNA and mRNA expression: Dyslipidemia associates with increased differentiation-related genes but not inflammatory activation. PLoS One. 10(6):e0129421.
Baltus AE, Menke DB, Hu YC, Goodheart ML, Carpenter AE, de Rooij DG, Page DC. 2006. In germ cells of mouse embryonic ovaries, the decision to enter meiosis precedes premeiotic DNA replication. Nat Genet. 38(12):1430-4.
Banner DW, D'Arcy A, Janes W, Gentz R, Schoenfeld HJ, Broger C, Loetscher H, Lesslauer W. 1993. Crystal structure of the soluble human 55 kd TNF receptor-human TNF beta complex: Implications for TNF receptor activation. Cell. 73(3):431-45.
Bannister LA, Reinholdt LG, Munroe RJ, Schimenti JC. 2004. Positional cloning and characterization of mouse mei8, a disrupted allelle of the meiotic cohesin Rec8. Genesis. 40(3):184-94.
Barbaux S, Niaudet P, Gubler MC, Grunfeld JP, Jaubert F, Kuttenn F, Fekete CN, Souleyreau-Therville N, Thibaud E, Fellous M, *et al*. 1997. Donor splice-site mutations in WT1 are responsible for frasier syndrome. Nat Genet. 17(4):467-70.

Barbieri RL, Makris A, Randall RW, Daniels G, Kistner RW, Ryan KJ. 1986. Insulin stimulates androgen accumulation in incubations of ovarian stroma obtained from women with hyperandrogenism. J Clin Endocrinol Metab. 62(5):904-10.
Bardoni B, Zanaria E, Guioli S, Floridia G, Worley KC, Tonini G, Ferrante E, Chiumello G, McCabe ER, Fraccaro M. 1994. A dosage sensitive locus at chromosome Xp21 is involved in male to female sex reversal. Nat Genet. 7(4):497-501.
Barrionuevo F, Bagheri-Fam S, Klattig J, Kist R, Taketo MM, Englert C, Scherer G. 2006. Homozygous inactivation of Sox9 causes complete XY sex reversal in mice. Biol Reprod. 74(1):195-201.
Barrionuevo F, Georg I, Scherthan H, Lécureuil C, Guillou F, Wegner M, Scherer G. 2009. Testis cord differentiation after the sex determination stage is independent of Sox9 but fails in the combined absence of Sox9 and Sox8. Dev Biol. 327(2):301-12.
Barrionuevo FJ, Hurtado A, Kim GJ, Real FM, Bakkali M, Kopp JL, Sander M, Scherer G, Burgos M, Jimenez R. 2016. Sox9 and Sox8 protect the adult testis from male-to-female genetic reprogramming and complete degeneration. Elife. 5:10.7554/eLife.15635.
Bas F, Pescovitz OH, Steinmetz R. 2009. No activating mutations of FSH receptor in four children with ovarian juvenile granulosa cell tumors and the association of these tumors with central precocious puberty. J Pediatr Adolesc Gynecol. 22(3):173-9.
Batista F, Vaiman D, Dausset J, Fellous M, Veitia RA. 2007. Potential targets of FOXL2, a transcription factor involved in craniofacial and follicular development, identified by transcriptomics. Proc Natl Acad Sci U S A. 104(9):3330-5.
Battaglia A, Hoyme HE, Dallapiccola B, Zackai E, Hudgins L, McDonald-McGinn D, Bahi-Buisson N, Romano C, Williams CA, Brailey LL, *et al*. 2008. Further delineation of deletion 1p36 syndrome in 60 patients: A recognizable phenotype and common cause of developmental delay and mental retardation. Pediatrics. 121(2):404-10.
Beamer WG, Hoppe PC, Whitten WK. 1985. Spontaneous malignant granulosa cell tumors in ovaries of young SWR mice. Cancer Res. 45(11):5575-81.
Beamer WG. 1986. Gonadotropin, steroid, and thyroid hormone milieu of young SWR mice bearing spontaneous granulosa cell tumors. J Natl Cancer Inst. 77(5):1117-23.
Beamer WG, Shultz KL, Tennent BJ. 1988. Induction of ovarian granulosa cell tumors in SWXJ-9 mice with dehydroepiandrosterone. Cancer Res. 48(10):2788-92.
Beamer WG, Tennent BJ, Shultz KL, Nadeau JH, Shultz LD, Skow LC. 1988. Gene for ovarian granulosa cell tumor susceptibility, gct, in SWXJ recombinant inbred strains of mice revealed by dehydroepiandrosterone. Cancer Res. 48(18):5092-5.
Beamer WG, Shultz KL, Tennent BJ, Shultz LD. 1993. Granulosa cell tumorigenesis in genetically hypogonadal-immunodeficient mice grafted with ovaries from tumor-susceptible donors. Cancer Res. 53(16):3741-6.
Beamer WG, Shultz KL, Tennent BJ, Nadeau JH, Churchill GA, Eicher EM. 1998. Multigenic and imprinting control of ovarian granulosa cell tumorigenesis in mice. Cancer Res. 58(16):3694-9.
Beamer WG. 2011. Personal communication.
Bedell MA, Brannan CI, Evans EP, Copeland NG, Jenkins NA, Donovan PJ. 1995. DNA rearrangements located over 100 kb 5' of the steel (sl)-coding region in steel-panda and steel-contrasted mice deregulate sl expression and cause female sterility by disrupting ovarian follicle development. Genes. 9(4):455-70.

Behboudi-Gandevani S, Amiri M, Bidhendi Yarandi R, Noroozzadeh M, Farahmand M, Rostami Dovom M, Ramezani Tehrani F. 2017. The risk of metabolic syndrome in polycystic ovary syndrome: A systematic review and meta-analysis. Clin Endocrinol (Oxf).
Behringer RR, Finegold MJ, Cate RL. 1994. Mullerian-inhibiting substance function during mammalian sexual development. Cell. 79(3):415-25.
Belchetz PE, Plant TM, Nakai Y, Keogh EJ, Knobil E. 1978. Hypophysial responses to continuous and intermittent delivery of hypopthalamic gonadotropin-releasing hormone. Science. 202(4368):631-3.
Belyaeva OV, Johnson MP, Kedishvili NY. 2008. Kinetic analysis of human enzyme RDH10 defines the characteristics of a physiologically relevant retinol dehydrogenase. J Biol Chem. 283(29):20299-308.
Belyaeva OV, Adams MK, Wu L, Kedishvili NY. 2017. The antagonistically bifunctional retinoid oxidoreductase complex is required for maintenance of all-trans-retinoic acid homeostasis. J Biol Chem. 292(14):5884-97.
Benayoun BA, Batista F, Auer J, Dipietromaria A, L'Hote D, De Baere E, Veitia RA. 2009. Positive and negative feedback regulates the transcription factor FOXL2 in response to cell stress: Evidence for a regulatory imbalance induced by disease-causing mutations. Hum Mol Genet. 18(4):632-44.
Benayoun BA, Caburet S, Dipietromaria A, Georges A, D'Haene B, Pandaranayaka PJ, L'Hote D, Todeschini AL, Krishnaswamy S, Fellous M, *et al*. 2010. Functional exploration of the adult ovarian granulosa cell tumor-associated somatic FOXL2 mutation p.Cys134Trp (c.402C>G). PLoS One. 5(1):e8789.
Benayoun BA, Georges AB, L'Hote D, Andersson N, Dipietromaria A, Todeschini AL, Caburet S, Bazin C, Anttonen M, Veitia RA. 2011. Transcription factor FOXL2 protects granulosa cells from stress and delays cell cycle: Role of its regulation by the SIRT1 deacetylase. Hum Mol Genet. 20(9):1673-86.
Bendel-Stenzel MR, Gomperts M, Anderson R, Heasman J, Wylie C. 2000. The role of cadherins during primordial germ cell migration and early gonad formation in the mouse. Mech Dev. 91(1-2):143-52.
Benesch M, Lackner H, Pilhatsch A, Gurtl-Lackner B, Schwinger W, Urban C. 2015. Long-term remission in a female with multiple relapsed juvenile granulosa cell tumor. J Pediatr Hematol Oncol. 37(8):e486-9.
Bennett D. 1956. Developmental analysis of a mutation with pleiotropic effects in the mouse. Journal of Morphology. 98(2):199.
Bennett NC, Gardiner RA, Hooper JD, Johnson DW, Gobe GC. 2010. Molecular cell biology of androgen receptor signalling. Int J Biochem Cell Biol. 42(6):813-27.
Bentsi-Barnes IK, Kuo FT, Barlow GM, Pisarska MD. 2010. Human forkhead L2 represses key genes in granulosa cell differentiation including aromatase, P450scc, and cyclin D2. Fertil Steril. 94(1):353-6.
Bergeron L, Perez GI, Macdonald G, Shi L, Sun Y, Jurisicova A, Varmuza S, Latham KE, Flaws JA, Salter JC, *et al*. 1998. Defects in regulation of apoptosis in caspase-2-deficient mice. Genes Dev. 12(9):1304-14.
Bernard P, Sim H, Knower K, Vilain E, Harley V. 2008. Human SRY inhibits beta-catenin-mediated transcription. Int J Biochem Cell Biol. 40(12):2889-900.

Bernard P, Ryan J, Sim H, Czech DP, Sinclair AH, Koopman P, Harley VR. 2012. Wnt signaling in ovarian development inhibits Sf1 activation of Sox9 via the tesco enhancer. Endocrinology. 153(2):901-12.
Bertolino P, Tong WM, Galendo D, Wang ZQ, Zhang CX. 2003. Heterozygous Men1 mutant mice develop a range of endocrine tumors mimicking multiple endocrine neoplasia type 1. Mol Endocrinol. 17(9):1880-92.
Bessière L, Todeschini AL, Auguste A, Sarnacki S, Flatters D, Legois B, Sultan C, Kalfa N, Galmiche L, Veitia RA. 2015. A hot-spot of in-frame duplications activates the oncoprotein AKT1 in juvenile granulosa cell tumors. Ebiomedicine. 2(5):421-31.
Betta P, Bellingeri D. 1985. Androgenic juvenile granulosa cell tumour. case report. Eur J Gynaecol Oncol. 6(1):71-4.
Bevan C, Parker M. 1999. The role of coactivators in steroid hormone action. Exp Cell Res. 253(2):349-56.
Beysen D, Moumne L, Veitia R, Peters H, Leroy BP, De Paepe A, De Baere E. 2008. Missense mutations in the forkhead domain of FOXL2 lead to subcellular mislocalization, protein aggregation and impaired transactivation. Hum Mol Genet. 17(13):2030-8.
Beysen D, De Paepe A, De Baere E. 2009. FOXL2 mutations and genomic rearrangements in BPES. Hum Mutat. 30(2):158-69.
Biason-Lauber A, Konrad D, Meyer M, DeBeaufort C, Schoenle EJ. 2009. Ovaries and female phenotype in a girl with 46,XY karyotype and mutations in the CBX2 gene. Am J Hum Genet. 84(5):658-63.
Bielschowsky M, D'Ath EF. 1973. Spontaneous granulosa cell tumours in mice of strains NZC-B1, NZO-B1, NZY-B1 and NZB-B1. Pathology. 5(4):303-10.
Billig H, Furuta I, Hsueh AJ. 1993. Estrogens inhibit and androgens enhance ovarian granulosa cell apoptosis. Endocrinology. 133(5):2204-12.
Billings SE, Pierzchalski K, Butler Tjaden NE, Pang XY, Trainor PA, Kane MA, Moise AR. 2013. The retinaldehyde reductase DHRS3 is essential for preventing the formation of excess retinoic acid during embryonic development. Faseb j. 27(12):4877-89.
Bingham NC, Verma-Kurvari S, Parada LF, Parker KL. 2006. Development of a steroidogenic factor 1/Cre transgenic mouse line. Genesis. 44(9):419-24.
Binnerts ME, Kim KA, Bright JM, Patel SM, Tran K, Zhou M, Leung JM, Liu Y, Lomas WE,3rd, Dixon M, *et al*. 2007. R-Spondin1 regulates wnt signaling by inhibiting internalization of LRP6. Proc Natl Acad Sci U S A. 104(37):14700-5.
Birk OS, Casiano DE, Wassif CA, Cogliati T, Zhao L, Zhao Y, Grinberg A, Huang S, Kreidberg JA, Parker KL, *et al*. 2000. The LIM homeobox gene Lhx9 is essential for mouse gonad formation. Nature. 403(6772):909-13.
Bishop CE, Whitworth DJ, Qin Y, Agoulnik AI, Agoulnik IU, Harrison WR, Behringer RR, Overbeek PA. 2000. A transgenic insertion upstream of sox9 is associated with dominant XX sex reversal in the mouse. Nat Genet. 26(4):490-4.
Black RA, Rauch CT, Kozlosky CJ, Peschon JJ, Slack JL, Wolfson MF, Castner BJ, Stocking KL, Reddy P, Srinivasan S, *et al*. 1997. A metalloproteinase disintegrin that releases tumour-necrosis factor-alpha from cells. Nature. 385(6618):729-33.
Boerboom D, Paquet M, Hsieh M, Liu J, Jamin SP, Behringer RR, Sirois J, Taketo MM, Richards JS. 2005. Misregulated Wnt/beta-catenin signaling leads to ovarian granulosa cell tumor development. Cancer Res. 65(20):9206-15.

Bogani D, Siggers P, Brixey R, Warr N, Beddow S, Edwards J, Williams D, Wilhelm D, Koopman P, Flavell RA, et al. 2009. Loss of mitogen-activated protein kinase kinase kinase 4 (MAP3K4) reveals a requirement for MAPK signalling in mouse sex determination. PLoS Biol. 7(9):e1000196.
Borghi A, Verstrepen L, Beyaert R. 2016. TRAF2 multitasking in TNF receptor-induced signaling to NF-kappaB, MAP kinases and cell death. Biochem Pharmacol. 116:1-10.
Borman SM, Chaffin CL, Schwinof KM, Stouffer RL, Zelinski-Wooten MB. 2004. Progesterone promotes oocyte maturation, but not ovulation, in nonhuman primate follicles without a gonadotropin surge. Biol Reprod. 71(1):366-73.
Borrelli E, Montmayeur JP, Foulkes NS, Sassone-Corsi P. 1992. Signal transduction and gene control: The cAMP pathway. Crit Rev Oncog. 3(4):321-38.
Borum K. 1961. Oogenesis in the mouse. A study of the meiotic prophase. Exp Cell Res. 24:495-507.
Boulanger L, Pannetier M, Gall L, Allais-Bonnet A, Elzaiat M, Le Bourhis D, Daniel N, Richard C, Cotinot C, Ghyselinck NB, *et al*. 2014. FOXL2 is a female sex-determining gene in the goat. Curr Biol. 24(4):404-8.
Bowles J, Knight D, Smith C, Wilhelm D, Richman J, Mamiya S. 2006. Retinoid signaling determines germ cell fate in mice. Science. 312(5773):596-600.
Boyce AM, Florenzano P, de Castro LF, Collins MT. 1993. Fibrous Dysplasia/McCune-albright syndrome. In: Genereviews((r)). Adam MP, Ardinger HH, Pagon RA, Wallace SE, Bean LJH, Stephens K,Amemiya A, editors. Seattle (WA): University of Washington, Seattle.
Bray JE, Marsden BD, Oppermann U. 2009. The human short-chain dehydrogenase/reductase (SDR) superfamily: A bioinformatics summary. Chem Biol Interact. 178(1-3):99-109.
Breslow NE, Day NE, Tomatis L, Turusov VS. 1974. Associations between tumor types in a large-scale carcinogenesis study of CF-1 mice. J Natl Cancer Inst. 52(1):233-9.
Brickner JH, Fuller RS. 1997. SOI1 encodes a novel, conserved protein that promotes TGN-endosomal cycling of Kex2p and other membrane proteins by modulating the function of two TGN localization signals. J Cell Biol. 139(1):23-36.
Bridges PJ, Koo Y, Kang DW, Hudgins-Spivey S, Lan ZJ, Xu X, DeMayo F, Cooney A, Ko C. 2008. Generation of Cyp17iCre transgenic mice and their application to conditionally delete estrogen receptor alpha (Esr1) from the ovary and testis. Genesis. 46(9):499-505.
Brioude F, Netchine I. 2017. Comment on: Juvenile granulosa cell ovarian tumor in a child with beckwith-wiedemann syndrome. Pediatr Blood Cancer. 64(8):10.1002/pbc.26452. Epub 2017 Jan 11.
Bristol-Gould SK, Kreeger PK, Selkirk CG, Kilen SM, Cook RW, Kipp JL, Shea LD, Mayo KE, Woodruff TK. 2006. Postnatal regulation of germ cells by activin: The establishment of the initial follicle pool. Dev Biol. 298(1):132-48.
Brunak S, Engelbrecht J, Knudsen S. 1991. Prediction of human mRNA donor and acceptor sites from the DNA sequence. J Mol Biol. 220(1):49-65.
Buccione R, Vanderhyden BC, Caron PJ, Eppig JJ. 1990. FSH-induced expansion of the mouse cumulus oophorus in vitro is dependent upon a specific factor(s) secreted by the oocyte. Dev Biol. 138(1):16-25.
Buehr M, McLaren A, Bartley A, Darling S. 1993. Proliferation and migration of primordial germ cells in We/We mouse embryos. Dev Dyn. 198(3):182-9.

Burek M, Duda M, Knapczyk K, Koziorowski M, Slomczynska M. 2007. Tissue-specific distribution of the androgen receptor (AR) in the porcine fetus. Acta Histochem. 109(5):358-65.
Burger HG. 2002. Androgen production in women. Fertil Steril. 77 Suppl 4:S3-5.
Burghen GA, Givens JR, Kitabchi AE. 1980. Correlation of hyperandrogenism with hyperinsulinism in polycystic ovarian disease. J Clin Endocrinol Metab. 50(1):113-6.
Burns KH, Yan C, Kumar TR, Matzuk MM. 2001. Analysis of ovarian gene expression in follicle-stimulating hormone beta knockout mice. Endocrinology. 142(7):2742-51.
Burns KH, Owens GE, Fernandez JM, Nilson JH, Matzuk MM. 2002. Characterization of integrin expression in the mouse ovary. Biol Reprod. 67(3):743-51.
Burns KH, Agno JE, Sicinski P, Matzuk MM. 2003a. Cyclin D2 and p27 are tissue-specific regulators of tumorigenesis in inhibin alpha knockout mice. Mol Endocrinol. 17(10):2053-69.
Burns KH, Agno JE, Chen L, Haupt B, Ogbonna SC, Korach KS, Matzuk MM. 2003b. Sexually dimorphic roles of steroid hormone receptor signaling in gonadal tumorigenesis. Mol Endocrinol. 17(10):2039-52.
Bús D, Buzogany M, Nagy G, Vajda G. 2017. Rare virilizing granulosa cell tumor in an adolescent. Mol Clin Oncol. 6(1):88-90.
Buza N, Wong S, Hui P. 2018. FOXL2 mutation analysis of ovarian sex cord-stromal tumors: Genotype-phenotype correlation with diagnostic considerations. Int J Gynecol Pathol. 37(4):305-15.
Calaminus G, Wessalowski R, Harms D, Gobel U. 1997. Juvenile granulosa cell tumors of the ovary in children and adolescents: Results from 33 patients registered in a prospective cooperative study. Gynecol Oncol. 65(3):447-52.
Caldwell AS, Eid S, Kay CR, Jimenez M, McMahon AC, Desai R, Allan CM, Smith JT, Handelsman DJ, Walters KA. 2015. Haplosufficient genomic androgen receptor signaling is adequate to protect female mice from induction of polycystic ovary syndrome features by prenatal hyperandrogenization. Endocrinology. 156(4):1441-52.
Caldwell ASL, Edwards MC, Desai R, Jimenez M, Gilchrist RB, Handelsman DJ, Walters KA. 2017. Neuroendocrine androgen action is a key extraovarian mediator in the development of polycystic ovary syndrome. Proc Natl Acad Sci U S A. 114(16):E3334-43.
Canadian Cancer Society's Steering Committee on Cancer Statistics. 2019. Canadian cancer statistics 2019. Toronto, ON: Canadian Cancer Society.
Cannon JD, Cherian-Shaw M, Lovekamp-Swan T, Chaffin CL. 2007. Granulosa cell expression of G1/S phase cyclins and cyclin-dependent kinases in PMSG-induced follicle growth. Mol Cell Endocrinol. 264(1-2):6-15.
Capriotti E, Fariselli P. 2017. PhD-SNPg: A webserver and lightweight tool for scoring single nucleotide variants. Nucleic Acids Res. 45(W1):W247-52.
Cara JF, Rosenfield RL. 1988. Insulin-like growth factor I and insulin potentiate luteinizing hormone-induced androgen synthesis by rat ovarian thecal-interstitial cells. Endocrinology. 123(2):733-9.
Cara JF, Fan J, Azzarello J, Rosenfield RL. 1990. Insulin-like growth factor-I enhances luteinizing hormone binding to rat ovarian theca-interstitial cells. J Clin Invest. 86(2):560-5.
Carabatsos MJ, Sellitto C, Goodenough DA, Albertini DF. 2000. Oocyte-granulosa cell heterologous gap junctions are required for the coordination of nuclear and cytoplasmic meiotic competence. Dev Biol. 226(2):167-79.

Cardenas H, Pope WF. 1994. Administration of testosterone during the follicular phase increased the number of corpora lutea in gilts. J Anim Sci. 72(11):2930-5.
Cardenas H, Herrick JR, Pope WF. 2002. Increased ovulation rate in gilts treated with dihydrotestosterone. Reproduction. 123(4):527-33.
Carén H, Djos A, Nethander M, Sjoberg RM, Kogner P, Enstrom C, Nilsson S, Martinsson T. 2011. Identification of epigenetically regulated genes that predict patient outcome in neuroblastoma. BMC Cancer. 11:66,2407-11-66.
Cartegni L, Wang J, Zhu Z, Zhang MQ, Krainer AR. 2003. ESEfinder: A web resource to identify exonic splicing enhancers. Nucleic Acids Res. 31(13):3568-71.
Casagrande JT, Louie EW, Pike MC, Roy S, Ross RK, Henderson BE. 1979. "Incessant ovulation" and ovarian cancer. Lancet. 2(8135):170-3.
Casarini L, Lispi M, Longobardi S, Milosa F, La Marca A, Tagliasacchi D, Pignatti E, Simoni M. 2012. LH and hCG action on the same receptor results in quantitatively and qualitatively different intracellular signalling. PLoS One. 7(10):e46682.
Castrillon DH, Miao L, Kollipara R, Horner JW, DePinho RA. 2003. Suppression of ovarian follicle activation in mice by the transcription factor Foxo3a. Science. 301(5630):215-8.
Cattanach BM, Iddon CA, Charlton HM, Chiappa SA, Fink G. 1977. Gonadotrophin-releasing hormone deficiency in a mutant mouse with hypogonadism. Nature. 269(5626):338-40.
Catteau-Jonard S, Jamin SP, Leclerc A, Gonzales J, Dewailly D, di Clemente N. 2008. Anti-mullerian hormone, its receptor, FSH receptor, and androgen receptor genes are overexpressed by granulosa cells from stimulated follicles in women with polycystic ovary syndrome. J Clin Endocrinol Metab. 93(11):4456-61.
Cerignoli F, Guo X, Cardinali B, Rinaldi C, Casaletto J, Frati L, Screpanti I, Gudas LJ, Gulino A, Thiele CJ, *et al*. 2002. retSDR1, a short-chain retinol dehydrogenase/reductase, is retinoic acid-inducible and frequently deleted in human neuroblastoma cell lines. Cancer Res. 62(4):1196-204.
Chaboissier MC, Kobayashi A, Vidal VI, Lutzkendorf S, van de Kant HJ, Wegner M, de Rooij DG, Behringer RR, Schedl A. 2004. Functional analysis of Sox8 and Sox9 during sex determination in the mouse. Development. 131(9):1891-901.
Chadha S, Rao BR, Slotman BJ, van Vroonhoven CC, van der Kwast TH. 1993. An immunohistochemical evaluation of androgen and progesterone receptors in ovarian tumors. Hum Pathol. 24(1):90-5.
Chadha S, Pache TD, Huikeshoven JM, Brinkmann AO, van der Kwast TH. 1994. Androgen receptor expression in human ovarian and uterine tissue of long-term androgen-treated transsexual women. Hum Pathol. 25(11):1198-204.
Chan FK, Chun HJ, Zheng L, Siegel RM, Bui KL, Lenardo MJ. 2000. A domain in TNF receptors that mediates ligand-independent receptor assembly and signaling. Science. 288(5475):2351-4.
Chang H, Matzuk MM. 2001. Smad5 is required for mouse primordial germ cell development. Mech Dev. 104(1-2):61-7.
Chang H, Gao F, Guillou F, Taketo MM, Huff V, Behringer RR. 2008. Wt1 negatively regulates beta-catenin signaling during testis development. Development. 135(10):1875-85.
Chassot AA, Ranc F, Gregoire EP, Roepers-Gajadien HL, Taketo MM, Camerino G, de Rooij DG, Schedl A, Chaboissier MC. 2008. Activation of beta-catenin signaling by Rspo1 controls differentiation of the mammalian ovary. Hum Mol Genet. 17(9):1264-77.

Chassot AA, Gregoire EP, Lavery R, Taketo MM, de Rooij DG, Adams IR, Chaboissier MC. 2011. RSPO1/beta-catenin signaling pathway regulates oogonia differentiation and entry into meiosis in the mouse fetal ovary. PLoS One. 6(10):e25641.
Chassot AA, Bradford ST, Auguste A, Gregoire EP, Pailhoux E, de Rooij DG, Schedl A, Chaboissier MC. 2012. WNT4 and RSPO1 together are required for cell proliferation in the early mouse gonad. Development. 139(23):4461-72.
Chen YY, Takita J, Chen YZ, Yang HW, Hanada R, Yamamoto K, Hayashi Y. 2003. Genomic structure and mutational analysis of the human KIF1Balpha gene located at 1p36.2 in neuroblastoma. Int J Oncol. 23(3):737-44.
Chen CP, Lin SP, Lee CC, Town DD, Wang W. 2006. Partial trisomy 1p (1p36.22-->pter) and partial monosomy 9p (9p22.2-->pter) associated with achalasia, flexion deformity of the fingers and epilepsy in a girl. Genet Couns. 17(3):301-6.
Chen Y, Jefferson WN, Newbold RR, Padilla-Banks E, Pepling ME. 2007. Estradiol, progesterone, and genistein inhibit oocyte nest breakdown and primordial follicle assembly in the neonatal mouse ovary in vitro and in vivo. Endocrinology. 148(8):3580-90.
Chene G, Ouellet V, Rahimi K, Barres V, Caceres K, Meunier L, Cyr L, De Ladurantaye M, Provencher D, Mes Masson AM. 2015. DNA damage signaling and apoptosis in preinvasive tubal lesions of ovarian carcinoma. Int J Gynecol Cancer. 25(5):761-9.
Cheng G, Weihua Z, Makinen S, Makela S, Saji S, Warner M, Gustafsson JA, Hovatta O. 2002. A role for the androgen receptor in follicular atresia of estrogen receptor beta knockout mouse ovary. Biol Reprod. 66(1):77-84.
Cheng XB, Jimenez M, Desai R, Middleton LJ, Joseph SR, Ning G, Allan CM, Smith JT, Handelsman DJ, Walters KA. 2013. Characterizing the neuroendocrine and ovarian defects of androgen receptor-knockout female mice. Am J Physiol Endocrinol Metab. 305(6):E717-26.
Cheng JC, Klausen C, Leung PC. 2013. Overexpression of wild-type but not C134W mutant FOXL2 enhances GnRH-induced cell apoptosis by increasing GnRH receptor expression in human granulosa cell tumors. PLoS One. 8(1):e55099.
Cheng JC, Chang HM, Qiu X, Fang L, Leung PC. 2014. FOXL2-induced follistatin attenuates activin A-stimulated cell proliferation in human granulosa cell tumors. Biochem Biophys Res Commun. 443(2):537-42.
Cheong ML, Shen J, Huang SH, Chien TY. 2016. Long-term survival in a patient with an advanced ovarian juvenile granulosa cell tumor with para-aortic lymph node metastasis. Taiwan J Obstet Gynecol. 55(6):907-9.
Childs AJ, Anderson RA. 2009. Activin A selectively represses expression of the membrane-bound isoform of kit ligand in human fetal ovary. Fertil Steril. 92(4):1416-9.
Choi Y, Ballow DJ, Xin Y, Rajkovic A. 2008. Lim homeobox gene, lhx8, is essential for mouse oocyte differentiation and survival. Biol Reprod. 79(3):442-9.
Choi Y, Yuan D, Rajkovic A. 2008. Germ cell-specific transcriptional regulator sohlh2 is essential for early mouse folliculogenesis and oocyte-specific gene expression. Biol Reprod. 79(6):1176-82.
Choi JY, Jo MW, Lee EY, Yoon BK, Choi DS. 2010. The role of autophagy in follicular development and atresia in rat granulosa cells. Fertil Steril. 93(8):2532-7.
Chu GC, Dunn NR, Anderson DC, Oxburgh L, Robertson EJ. 2004. Differential requirements for Smad4 in TGFbeta-dependent patterning of the early mouse embryo. Development. 131(15):3501-12.

Chun SY, Billig H, Tilly JL, Furuta I, Tsafriri A, Hsueh AJ. 1994. Gonadotropin suppression of apoptosis in cultured preovulatory follicles: Mediatory role of endogenous insulin-like growth factor I. Endocrinology. 135(5):1845-53.
Chun SY, Eisenhauer KM, Minami S, Billig H, Perlas E, Hsueh AJ. 1996. Hormonal regulation of apoptosis in early antral follicles: Follicle-stimulating hormone as a major survival factor. Endocrinology. 137(4):1447-56.
Chuva de Sousa Lopes SM, van den Driesche S, Carvalho RL, Larsson J, Eggen B, Surani MA, Mummery CL. 2005. Altered primordial germ cell migration in the absence of transforming growth factor beta signaling via ALK5. Dev Biol. 284(1):194-203.
Chuva de Sousa Lopes SM, Hayashi K, Surani MA. 2007. Proximal visceral endoderm and extraembryonic ectoderm regulate the formation of primordial germ cell precursors. BMC Dev Biol. 7:140.
Chuva de Sousa Lopes SM, Hayashi K, Shovlin TC, Mifsud W, Surani MA, McLaren A. 2008. X chromosome activity in mouse XX primordial germ cells. PLoS Genet. 4(2):e30.
Ciftci I, Pirgon MO, Unlu P. 2013. Juvenile granulosa cell tumor and high blood ca-125 levels in children with pseudo-meigs syndrome. Eur J Gen Med. 10(4):232.
Cioni B, Zwart W, Bergman AM. 2018. Androgen receptor moonlighting in the prostate cancer microenvironment. Endocr Relat Cancer. 25(6):R331-49.
Cipriano SC, Chen L, Kumar TR, Matzuk MM. 2000. Follistatin is a modulator of gonadal tumor progression and the activin-induced wasting syndrome in inhibin-deficient mice. Endocrinology. 141(7):2319-27.
Cipriano SC, Chen L, Burns KH, Koff A, Matzuk MM. 2001. Inhibin and p27 interact to regulate gonadal tumorigenesis. Mol Endocrinol. 15(6):985-96.
Clarke TR, Hoshiya Y, Yi SE, Liu X, Lyons KM, Donahoe PK. 2001. Mullerian inhibiting substance signaling uses a bone morphogenetic protein (BMP)-like pathway mediated by ALK2 and induces SMAD6 expression. Mol Endocrinol. 15(6):946-59.
Clarkson J, d'Anglemont de Tassigny X, Moreno AS, Colledge WH, Herbison AE. 2008. Kisspeptin-GPR54 signaling is essential for preovulatory gonadotropin-releasing hormone neuron activation and the luteinizing hormone surge. J Neurosci. 28(35):8691-7.
Cocquet J, Pailhoux E, Jaubert F, Servel N, Xia X, Pannetier M, De Baere E, Messiaen L, Cotinot C, Fellous M, *et al*. 2002. Evolution and expression of FOXL2. J Med Genet. 39(12):916-21.
Coerver KA, Woodruff TK, Finegold MJ, Mather J, Bradley A, Matzuk MM. 1996. Activin signaling through activin receptor type II causes the cachexia-like symptoms in inhibin-deficient mice. Mol Endocrinol. 10(5):534-43.
Colmenares C, Heilstedt HA, Shaffer LG, Schwartz S, Berk M, Murray JC, Stavnezer E. 2002. Loss of the SKI proto-oncogene in individuals affected with 1p36 deletion syndrome is predicted by strain-dependent defects in ski-/- mice. Nat Genet. 30(1):106-9.
Colvin JS, Green RP, Schmahl J, Capel B, Ornitz DM. 2001. Male-to-female sex reversal in mice lacking fibroblast growth factor 9. Cell. 104(6):875-89.
Conlon N, Schultheis AM, Piscuoglio S, Silva A, Guerra E, Tornos C, Reuter VE, Soslow RA, Young RH, Oliva E, *et al*. 2015. A survey of DICER1 hotspot mutations in ovarian and testicular sex cord-stromal tumors. Mod Pathol. 28(12):1603-12.
Cooke PS, Young P, Cunha GR. 1991. Androgen receptor expression in developing male reproductive organs. Endocrinology. 128(6):2867-73.

Cool M, Jolicoeur P. 1999. Elevated frequency of loss of heterozygosity in mammary tumors arising in mouse mammary tumor virus/neu transgenic mice. Cancer Res. 59(10):2438-44.
Cordeiro MH, Kim SY, Ebbert K, Duncan FE, Ramalho-Santos J, Woodruff TK. 2015. Geography of follicle formation in the embryonic mouse ovary impacts activation pattern during the first wave of folliculogenesis. Biol Reprod. 93(4):88.
Couse JF, Hewitt SC, Bunch DO, Sar M, Walker VR, Davis BJ, Korach KS. 1999. Postnatal sex reversal of the ovaries in mice lacking estrogen receptors alpha and beta. Science. 286(5448):2328-31.
Crisponi L, Deiana M, Loi A, Chiappe F, Uda M, Amati P, Bisceglia L, Zelante L, Nagaraja R, Porcu S, *et al*. 2001. The putative forkhead transcription factor FOXL2 is mutated in blepharophimosis/ptosis/epicanthus inversus syndrome. Nat Genet. 27(2):159-66.
Cruickshank E. Investigation of solute carrier SLC25A53 as a candidate ovarian tumour suppressor. St. John's, NL: Memorial University of Newfoundland.
Crum CP, Drapkin R, Miron A, Ince TA, Muto M, Kindelberger DW, Lee Y. 2007. The distal fallopian tube: A new model for pelvic serous carcinogenesis. Curr Opin Obstet Gynecol. 19(1):3-9.
Cunningham F, Amode MR, Barrell D, Beal K, Billis K, Brent S, Carvalho-Silva D, Clapham P, Coates G, Fitzgerald S, *et al*. 2015. Ensembl 2015. Nucleic Acids Res. 43(Database issue):D662-9.
D'Angelo E, Mozos A, Nakayama D, Espinosa I, Catasus L, Munoz J, Prat J. 2011. Prognostic significance of FOXL2 mutation and mRNA expression in adult and juvenile granulosa cell tumors of the ovary. Mod Pathol. 24(10):1360-7.
Danilovich N, Roy I, Sairam MR. 2001. Ovarian pathology and high incidence of sex cord tumors in follitropin receptor knockout (FORKO) mice. Endocrinology. 142(8):3673-84.
Davey RA, Grossmann M. 2016. Androgen receptor structure, function and biology: From bench to bedside. Clin Biochem Rev. 37(1):3-15.
De Cian MC, Pauper E, Bandiera R, Vidal VP, Sacco S, Gregoire EP, Chassot AA, Panzolini C, Wilhelm D, Pailhoux E, *et al*. 2017. Amplification of R-spondin1 signaling induces granulosa cell fate defects and cancers in mouse adult ovary. Oncogene. 36(2):208-18.
De Felici M, Klinger FG, Farini D, Scaldaferri ML, Iona S, Lobascio M. 2005. Establishment of oocyte population in the fetal ovary: Primordial germ cell proliferation and oocyte programmed cell death. Reprod Biomed Online. 10(2):182-91.
De Felici M. 2016. The formation and migration of primordial germ cells in mouse and man. Results Probl Cell Differ. 58:23-46.
De Gendt K, Swinnen JV, Saunders PT, Schoonjans L, Dewerchin M, Devos A, Tan K, Atanassova N, Claessens F, Lécureuil C, *et al*. 2004. A sertoli cell-selective knockout of the androgen receptor causes spermatogenic arrest in meiosis. Proc Natl Acad Sci U S A. 101(5):1327-32.
de Lau W, Barker N, Low TY, Koo BK, Li VS, Teunissen H, Kujala P, Haegebarth A, Peters PJ, van de Wetering M, *et al*. 2011. Lgr5 homologues associate with wnt receptors and mediate R-spondin signalling. Nature. 476(7360):293-7.
de Lau W, Peng WC, Gros P, Clevers H. 2014. The R-spondin/Lgr5/Rnf43 module: Regulator of wnt signal strength. Genes Dev. 28(4):305-16.
Decoster E, Vanhaesebroeck B, Vandenabeele P, Grooten J, Fiers W. 1995. Generation and biological characterization of membrane-bound, uncleavable murine tumor necrosis factor. J Biol Chem. 270(31):18473-8.

Deisenroth C, Itahana Y, Tollini L, Jin A, Zhang Y. 2011. p53-inducible DHRS3 is an endoplasmic reticulum protein associated with lipid droplet accumulation. J Biol Chem. 286(32):28343-56.
Deligeoroglou E, Vrachnis N, Athanasopoulos N, Iliodromiti Z, Sifakis S, Iliodromiti S, Siristatidis C, Creatsas G. 2012. Mediators of chronic inflammation in polycystic ovarian syndrome. Gynecol Endocrinol. 28(12):974-8.
Deringer MK. 1959. Occurrence of tumors, particularly mammary tumors, in agent free strain C3HeB mice. J Natl Cancer Inst. 22(5):995-1002.
Desmet FO, Hamroun D, Lalande M, Collod-Beroud G, Claustres M, Beroud C. 2009. Human splicing finder: An online bioinformatics tool to predict splicing signals. Nucleic Acids Res. 37(9):e67.
Di Carlo A, De Felici M. 2000. A role for E-cadherin in mouse primordial germ cell development. Dev Biol. 226(2):209-19.
Dickie MM. 1954. The use of F1 hybrid and backcross generations to reveal new and/or uncommon tumor types. J Natl Cancer Inst. 15(3):791-9.
Dierich A, Sairam MR, Monaco L, Fimia GM, Gansmuller A, LeMeur M, Sassone-Corsi P. 1998. Impairing follicle-stimulating hormone (FSH) signaling in vivo: Targeted disruption of the FSH receptor leads to aberrant gametogenesis and hormonal imbalance. Proc Natl Acad Sci U S A. 95(23):13612-7.
Dipietromaria A, Benayoun BA, Todeschini AL, Rivals I, Bazin C, Veitia RA. 2009. Towards a functional classification of pathogenic FOXL2 mutations using transactivation reporter systems. Hum Mol Genet. 18(17):3324-33.
Diwan BA, Anderson LM, Ward JM. 1997. Proliferative lesions of oviduct and uterus in CD-1 mice exposed prenatally to tamoxifen. Carcinogenesis. 18(10):2009-14.
Doitsidou M, Reichman-Fried M, Stebler J, Koprunner M, Dorries J, Meyer D, Esguerra CV, Leung T, Raz E. 2002. Guidance of primordial germ cell migration by the chemokine SDF-1. Cell. 111(5):647-59.
Dolci S, Williams DE, Ernst MK, Resnick JL, Brannan CI, Lock LF, Lyman SD, Boswell HS, Donovan PJ. 1991. Requirement for mast cell growth factor for primordial germ cell survival in culture. Nature. 352(6338):809-11.
Dong J, Albertini DF, Nishimori K, Kumar TR, Lu N, Matzuk MM. 1996. Growth differentiation factor-9 is required during early ovarian folliculogenesis. Nature. 383(6600):531-5.
Doree M, Hunt T. 2002. From Cdc2 to Cdk1: When did the cell cycle kinase join its cyclin partner? J Cell Sci. 115(Pt 12):2461-4.
Dorward AM, Shultz KL, Ackert-Bicknell CL, Eicher EM, Beamer WG. 2003. High-resolution genetic map of X-linked juvenile-type granulosa cell tumor susceptibility genes in mouse. Cancer Res. 63(23):8197-202.
Dorward AM, Shultz KL, Horton LG, Li R, Churchill GA, Beamer WG. 2005. Distal chr 4 harbors a genetic locus (Gct1) fundamental for spontaneous ovarian granulosa cell tumorigenesis in a mouse model. Cancer Res. 65(4):1259-64.
Dorward AM, Shultz KL, Beamer WG. 2007. LH analog and dietary isoflavones support ovarian granulosa cell tumor development in a spontaneous mouse model. Endocr Relat Cancer. 14(2):369-79.

Dorward AM, Yaskowiak ES, Smith KN, Stanford KR, Shultz KL, Beamer WG. 2013. Chromosome X loci and spontaneous granulosa cell tumor development in SWR mice: Epigenetics and epistasis at work for an ovarian phenotype. Epigenetics. 8(2):184-91.
Dowling AR, Nedorezov LB, Qiu X, Marino JS, Hill JW. 2013. Genetic factors modulate the impact of pubertal androgen excess on insulin sensitivity and fertility. PLoS One. 8(11):e79849.
Dozois RR, Kempers RD, Dahlin DC, Bartholomeew JG. 1970. Ovarian tumors associated with the peutz-jeghers syndrome. Ann Surg. 172(2):233-8.
Dragovic RA, Ritter LJ, Schulz SJ, Amato F, Thompson JG, Armstrong DT, Gilchrist RB. 2007. Oocyte-secreted factor activation of SMAD 2/3 signaling enables initiation of mouse cumulus cell expansion. Biol Reprod. 76(5):848-57.
Du X, Rosenfield RL, Qin K. 2009. KLF15 is a transcriptional regulator of the human 17beta-hydroxysteroid dehydrogenase type 5 gene. A potential link between regulation of testosterone production and fat stores in women. J Clin Endocrinol Metab. 94(7):2594-601.
Duffy DM, Abdelgadir SE, Stott KR, Resko JA, Stouffer RL, Zelinski-Wooten MB. 1999. Androgen receptor mRNA expression in the rhesus monkey ovary. Endocrine. 11(1):23-30.
Dupe V, Matt N, Garnier JM, Chambon P, Mark M, Ghyselinck NB. 2003. A newborn lethal defect due to inactivation of retinaldehyde dehydrogenase type 3 is prevented by maternal retinoic acid treatment. Proc Natl Acad Sci U S A. 100(24):14036-41.
Dupont S, Krust A, Gansmuller A, Dierich A, Chambon P, Mark M. 2000. Effect of single and compound knockouts of estrogen receptors alpha (ERalpha) and beta (ERbeta) on mouse reproductive phenotypes. Development. 127(19):4277-91.
Durlinger AL, Kramer P, Karels B, de Jong FH, Uilenbroek JT, Grootegoed JA, Themmen AP. 1999. Control of primordial follicle recruitment by anti-mullerian hormone in the mouse ovary. Endocrinology. 140(12):5789-96.
Durlinger AL, Visser JA, Themmen AP. 2002. Regulation of ovarian function: The role of anti-mullerian hormone. Reproduction. 124(5):601-9.
Dutertre M, Gouedard L, Xavier F, Long WQ, di Clemente N, Picard JY, Rey R. 2001. Ovarian granulosa cell tumors express a functional membrane receptor for anti-mullerian hormone in transgenic mice. Endocrinology. 142(9):4040-6.
Edson MA, Nalam RL, Clementi C, Franco HL, Demayo FJ, Lyons KM, Pangas SA, Matzuk MM. 2010. Granulosa cell-expressed BMPR1A and BMPR1B have unique functions in regulating fertility but act redundantly to suppress ovarian tumor development. Mol Endocrinol. 24(6):1251-66.
Eicher EM, Washburn LL, Schork NJ, Lee BK, Shown EP, Xu X, Dredge RD, Pringle MJ, Page DC. 1996. Sex-determining genes on mouse autosomes identified by linkage analysis of C57BL/6J-YPOS sex reversal. Nat Genet. 14(2):206-9.
Ejeskär K, Sjoberg RM, Abel F, Kogner P, Ambros PF, Martinsson T. 2001. Fine mapping of a tumour suppressor candidate gene region in 1p36.2-3, commonly deleted in neuroblastomas and germ cell tumours. Med Pediatr Oncol. 36(1):61-6.
Elia EM, Belgorosky D, Faut M, Vighi S, Pustovrh C, Luigi D, Motta AB. 2009. The effects of metformin on uterine tissue of hyperandrogenized BALB/c mice. Mol Hum Reprod. 15(7):421-32.
Ellsworth BS, Burns AT, Escudero KW, Duval DL, Nelson SE, Clay CM. 2003. The gonadotropin releasing hormone (GnRH) receptor activating sequence (GRAS) is a composite regulatory element that interacts with multiple classes of transcription factors

including smads, AP-1 and a forkhead DNA binding protein. Mol Cell Endocrinol. 206(1-2):93-111.
Ellsworth BS, Egashira N, Haller JL, Butts DL, Cocquet J, Clay CM, Osamura RY, Camper SA. 2006. FOXL2 in the pituitary: Molecular, genetic, and developmental analysis. Mol Endocrinol. 20(11):2796-805.
Elvin JA, Yan C, Wang P, Nishimori K, Matzuk MM. 1999a. Molecular characterization of the follicle defects in the growth differentiation factor 9-deficient ovary. Mol Endocrinol. 13(6):1018-34.
Elvin JA, Clark AT, Wang P, Wolfman NM, Matzuk MM. 1999b. Paracrine actions of growth differentiation factor-9 in the mammalian ovary. Mol Endocrinol. 13(6):1035-48.
Engdahl C, Lagerquist MK, Stubelius A, Andersson A, Studer E, Ohlsson C, Westberg L, Carlsten H, Forsblad-d'Elia H. 2014. Role of androgen and estrogen receptors for the action of dehydroepiandrosterone (DHEA). Endocrinology. 155(3):889-96.
Eppig JJ. 1991. Intercommunication between mammalian oocytes and companion somatic cells. Bioessays. 13(11):569-74.
Eppig JJ. 2001. Oocyte control of ovarian follicular development and function in mammals. Reproduction. 122(6):829-38.
Eppig JJ, O'Brien MJ, Wigglesworth K, Nicholson A, Zhang W, King BA. 2009. Effect of in vitro maturation of mouse oocytes on the health and lifespan of adult offspring. Hum Reprod. 24(4):922-8.
Epping MT, Bernards R. 2006. A causal role for the human tumor antigen preferentially expressed antigen of melanoma in cancer. Cancer Res. 66(22):10639-42.
Evans RM. 1988. The steroid and thyroid hormone receptor superfamily. Science. 240(4854):889-95.
Fan X, Molotkov A, Manabe S, Donmoyer CM, Deltour L, Foglio MH, Cuenca AE, Blaner WS, Lipton SA, Duester G. 2003. Targeted disruption of Aldh1a1 (Raldh1) provides evidence for a complex mechanism of retinoic acid synthesis in the developing retina. Mol Cell Biol. 23(13):4637-48.
Fan HY, Shimada M, Liu Z, Cahill N, Noma N, Wu Y, Gossen J, Richards JS. 2008a. Selective expression of KrasG12D in granulosa cells of the mouse ovary causes defects in follicle development and ovulation. Development. 135(12):2127-37.
Fan HY, Liu Z, Cahill N, Richards JS. 2008b. Targeted disruption of pten in ovarian granulosa cells enhances ovulation and extends the life span of luteal cells. Mol Endocrinol. 22(9):2128-40.
Fan HY, Liu Z, Shimada M, Sterneck E, Johnson PF, Hedrick SM, Richards JS. 2009. MAPK3/1 (ERK1/2) in ovarian granulosa cells are essential for female fertility. Science. 324(5929):938-41.
Fan X, Gabbi C, Kim HJ, Cheng G, Andersson LC, Warner M, Gustafsson JA. 2010. Gonadotropin-positive pituitary tumors accompanied by ovarian tumors in aging female ERbeta-/- mice. Proc Natl Acad Sci U S A. 107(14):6453-8.
Farini D, La Sala G, Tedesco M, De Felici M. 2007. Chemoattractant action and molecular signaling pathways of kit ligand on mouse primordial germ cells. Dev Biol. 306(2):572-83.
Fathalla MF. 1971. Incessant ovulation--a factor in ovarian neoplasia? Lancet. 2(7716):163.
Fauser BC, van Heusden AM. 1997. Manipulation of human ovarian function: Physiological concepts and clinical consequences. Endocr Rev. 18(1):71-106.

Fauser BC, Tarlatzis BC, Rebar RW, Legro RS, Balen AH, Lobo R, Carmina E, Chang J, Yildiz BO, Laven JS, *et al*. 2012. Consensus on women's health aspects of polycystic ovary syndrome (PCOS): The amsterdam ESHRE/ASRM-sponsored 3rd PCOS consensus workshop group. Fertil Steril. 97(1):28,38.e25.
Feil S, Valtcheva N, Feil R. 2009. Inducible cre mice. Methods Mol Biol. 530:343-63.
Felipe F, Bonet ML, Ribot J, Palou A. 2004. Modulation of resistin expression by retinoic acid and vitamin A status. Diabetes. 53(4):882-9.
Feng L, Hernandez RE, Waxman JS, Yelon D, Moens CB. 2010. Dhrs3a regulates retinoic acid biosynthesis through a feedback inhibition mechanism. Dev Biol. 338(1):1-14.
Flaherty L. 1981. Congenic strains. In: The mouse in biomedical research. Foster HL, Small JD,Fox JG, editors. New York: Academic Press. 215-222 p.
Fleming NI, Knower KC, Lazarus KA, Fuller PJ, Simpson ER, Clyne CD. 2010. Aromatase is a direct target of FOXL2: C134W in granulosa cell tumors via a single highly conserved binding site in the ovarian specific promoter. PLoS One. 5(12):e14389.
Folkins AK, Jarboe EA, Saleemuddin A, Lee Y, Callahan MJ, Drapkin R, Garber JE, Muto MG, Tworoger S, Crum CP. 2008. A candidate precursor to pelvic serous cancer (p53 signature) and its prevalence in ovaries and fallopian tubes from women with BRCA mutations. Gynecol Oncol. 109(2):168-73.
Foster JW, Dominguez-Steglich MA, Guioli S, Kwok C, Weller PA, Stevanovic M, Weissenbach J, Mansour S, Young ID, Goodfellow PN. 1994. Campomelic dysplasia and autosomal sex reversal caused by mutations in an SRY-related gene. Nature. 372(6506):525-30.
Fournet N, Weitsman SR, Zachow RJ, Magoffin DA. 1996. Transforming growth factor-beta inhibits ovarian 17 alpha-hydroxylase activity by a direct noncompetitive mechanism. Endocrinology. 137(1):166-74.
Fowler PA, Anderson RA, Saunders PT, Kinnell H, Mason JI, Evans DB, Bhattacharya S, Flannigan S, Franks S, Monteiro A, *et al*. 2011. Development of steroid signaling pathways during primordial follicle formation in the human fetal ovary. J Clin Endocrinol Metab. 96(6):1754-62.
Franks S. 2002. Adult polycystic ovary syndrome begins in childhood. Best Pract Res Clin Endocrinol Metab. 16(2):263-72.
Franks S, McCarthy MI, Hardy K. 2006. Development of polycystic ovary syndrome: Involvement of genetic and environmental factors. Int J Androl. 29(1):278,85; discussion 286-90.
Franks S, Hardy K. 2018. Androgen action in the ovary. Front Endocrinol (Lausanne). 9:452.
Frith CH, Zuna RE, Morgan K. 1981. A morphologic classification and incidence of spontaneous ovarian neoplasms in three strains of mice. J Natl Cancer Inst. 67(3):693-702.
Fuller PJ, Verity K, Shen Y, Mamers P, Jobling T, Burger HG. 1998. No evidence of a role for mutations or polymorphisms of the follicle-stimulating hormone receptor in ovarian granulosa cell tumors. J Clin Endocrinol Metab. 83(1):274-9.
Furuta J, Nobeyama Y, Umebayashi Y, Otsuka F, Kikuchi K, Ushijima T. 2006. Silencing of peroxiredoxin 2 and aberrant methylation of 33 CpG islands in putative promoter regions in human malignant melanomas. Cancer Res. 66(12):6080-6.
Gajecka M, Mackay KL, Shaffer LG. 2007. Monosomy 1p36 deletion syndrome. Am J Med Genet C Semin Med Genet. 145C(4):346-56.

Galas J, Slomczynska M, Knapczyk-Stwora K, Durlej M, Starowicz A, Tabarowski Z, Rutka K, Szoltys M. 2012. Steroid levels and the spatiotemporal expression of steroidogenic enzymes and androgen receptor in developing ovaries of immature rats. Acta Histochem. 114(3):207-16.
Gao Y, Vincent DF, Davis AJ, Sansom OJ, Bartholin L, Li Q. 2016. Constitutively active transforming growth factor beta receptor 1 in the mouse ovary promotes tumorigenesis. Oncotarget. 7(27):40904-18.
Gao Y, Fang X, Vincent DF, Threadgill DW, Bartholin L, Li Q. 2017. Disruption of postnatal folliculogenesis and development of ovarian tumor in a mouse model with aberrant transforming growth factor beta signaling. Reprod Biol Endocrinol. 15(1):94,017-0312-z.
Garcia-Moreno SA, Lin YT, Futtner CR, Salamone IM, Capel B, Maatouk DM. 2019. CBX2 is required to stabilize the testis pathway by repressing wnt signaling. PLoS Genet. 15(5):e1007895.
Garcia-Ortiz JE, Pelosi E, Omari S, Nedorezov T, Piao Y, Karmazin J, Uda M, Cao A, Cole SW, Forabosco A, *et al*. 2009. Foxl2 functions in sex determination and histogenesis throughout mouse ovary development. BMC Dev Biol. 9:36,213X-9-36.
Gasteiger E, Gattiker A, Hoogland C, Ivanyi I, Appel RD, Bairoch A. 2003. ExPASy: The proteomics server for in-depth protein knowledge and analysis. Nucleic Acids Res. 31(13):3784-8.
Gauthier J, Meijer IA, Lessel D, Mencacci NE, Krainc D, Hempel M, Tsiakas K, Prokisch H, Rossignol E, Helm MH, *et al*. 2018. Recessive mutations in >VPS13D cause childhood onset movement disorders. Ann Neurol. 83(6):1089-95.
Geetha P, Nair MK. 2010. Granulosa cell tumours of the ovary. Aust N Z J Obstet Gynaecol. 50(3):216-20.
Geli J, Kiss N, Kogner P, Larsson C. 2010. Suppression of RIZ in biologically unfavourable neuroblastomas. Int J Oncol. 37(5):1323-30.
Georg I, Barrionuevo F, Wiech T, Scherer G. 2012. Sox9 and Sox8 are required for basal lamina integrity of testis cords and for suppression of FOXL2 during embryonic testis development in mice. Biol Reprod. 87(4):99.
Georges A, Auguste A, Bessiere L, Vanet A, Todeschini AL, Veitia RA. 2013. FOXL2: A central transcription factor of the ovary. J Mol Endocrinol. 52(1):R17-33.
Gherman RB, Parker MF, Macri CI. 1994. Granulosa cell tumor of the ovary associated with antecedent tamoxifen use. Obstet Gynecol. 84(4 Pt 2):717-9.
Giknis MLA, Clifford CB. 2005. Spontaneous neoplastic lesions in the crl:CD-1(ICR) mouse in control group from 18 month to 2 year studies. Charles River Laboratories.
Gilks CB. 2010. Molecular abnormalities in ovarian cancer subtypes other than high-grade serous carcinoma. J Oncol. 2010:740968.
Gill A, Jamnongjit M, Hammes SR. 2004. Androgens promote maturation and signaling in mouse oocytes independent of transcription: A release of inhibition model for mammalian oocyte meiosis. Mol Endocrinol. 18(1):97-104.
Gill ME, Hu YC, Lin Y, Page DC. 2011. Licensing of gametogenesis, dependent on RNA binding protein DAZL, as a gateway to sexual differentiation of fetal germ cells. Proc Natl Acad Sci U S A. 108(18):7443-8.
Gocze PM, Beamer WG, de Jong FH, Freeman DA. 1997. Hormone synthesis and responsiveness of spontaneous granulosa cell tumors in (SWR x SWXJ-9) F1 mice. Gynecol Oncol. 65(1):143-8.

Godin I, Deed R, Cooke J, Zsebo K, Dexter M, Wylie CC. 1991. Effects of the steel gene product on mouse primordial germ cells in culture. Nature. 352(6338):807-9.
Golos TG, Strauss JF,3rd, Miller WL. 1987. Regulation of low density lipoprotein receptor and cytochrome P-450scc mRNA levels in human granulosa cells. J Steroid Biochem. 27(4-6):767-73.
Gonzalez-Robayna IJ, Falender AE, Ochsner S, Firestone GL, Richards JS. 2000. Follicle-stimulating hormone (FSH) stimulates phosphorylation and activation of protein kinase B (PKB/Akt) and serum and glucocorticoid-lnduced kinase (sgk): Evidence for A kinase-independent signaling by FSH in granulosa cells. Mol Endocrinol. 14(8):1283-300.
Goodarzi MO, Dumesic DA, Chazenbalk G, Azziz R. 2011. Polycystic ovary syndrome: Etiology, pathogenesis and diagnosis. Nat Rev Endocrinol. 7(4):219-31.
Goulvent T, Ray-Coquard I, Borel S, Haddad V, Devouassoux-Shisheboran M, Vacher-Lavenu MC, Pujade-Laurraine E, Savina A, Maillet D, Gillet G, *et al*. 2016. DICER1 and FOXL2 mutations in ovarian sex cord-stromal tumours: A GINECO group study. Histopathology. 68(2):279-85.
Greenacre CB. 2004. Spontaneous tumors of small mammals. Vet Clin North Am Exot Anim Pract. 7(3):627,51, vi.
Greenfeld CR, Pepling ME, Babus JK, Furth PA, Flaws JA. 2007a. BAX regulates follicular endowment in mice. Reproduction. 133(5):865-76.
Greenfeld CR, Roby KF, Pepling ME, Babus JK, Terranova PF, Flaws JA. 2007b. Tumor necrosis factor (TNF) receptor type 2 is an important mediator of TNF alpha function in the mouse ovary. Biol Reprod. 76(2):224-31.
Grell M, Douni E, Wajant H, Lohden M, Clauss M, Maxeiner B, Georgopoulos S, Lesslauer W, Kollias G, Pfizenmaier K, *et al*. 1995. The transmembrane form of tumor necrosis factor is the prime activating ligand of the 80 kDa tumor necrosis factor receptor. Cell. 83(5):793-802.
Grino PB, Griffin JE, Wilson JD. 1990. Testosterone at high concentrations interacts with the human androgen receptor similarly to dihydrotestosterone. Endocrinology. 126(2):1165-72.
Gruss HJ, Boiani N, Williams DE, Armitage RJ, Smith CA, Goodwin RG. 1994. Pleiotropic effects of the CD30 ligand on CD30-expressing cells and lymphoma cell lines. Blood. 83(8):2045-56.
Gu Y, Runyan C, Shoemaker A, Surani A, Wylie C. 2009. Steel factor controls primordial germ cell survival and motility from the time of their specification in the allantois, and provides a continuous niche throughout their migration. Development. 136(8):1295-303.
Gubbay J, Vivian N, Economou A, Jackson D, Goodfellow P, Lovell-Badge R. 1992. Inverted repeat structure of the sry locus in mice. Proc Natl Acad Sci U S A. 89(17):7953-7.
Gui LM, Joyce IM. 2005. RNA interference evidence that growth differentiation factor-9 mediates oocyte regulation of cumulus expansion in mice. Biol Reprod. 72(1):195-9.
Guibert S, Forne T, Weber M. 2012. Global profiling of DNA methylation erasure in mouse primordial germ cells. Genome Res. 22(4):633-41.
Guigon CJ, Mazaud S, Forest MG, Brailly-Tabard S, Coudouel N, Magre S. 2003. Unaltered development of the initial follicular waves and normal pubertal onset in female rats after neonatal deletion of the follicular reserve. Endocrinology. 144(8):3651-62.
Guo J, McMachon J, Valerius MT, McMahon AP. Foxl2-GCE allele characterization [Internet]; c2011 [cited 2019. Available from: www.gudmap.org/Docs/Mouse_Strains/Foxl2-Strain_characterisation_220311av2.pdf.

Guo M, Zhang H, Bian F, Li G, Mu X, Wen J, Mao G, Teng Z, Xia G, Zhang M. 2012. P4 down-regulates Jagged2 and Notch1 expression during primordial folliculogenesis. Front Biosci (Elite Ed). 4:2631-44.
Haeseleer F, Huang J, Lebioda L, Saari JC, Palczewski K. 1998. Molecular characterization of a novel short-chain dehydrogenase/reductase that reduces all-trans-retinal. J Biol Chem. 273(34):21790-9.
Haeseleer F, Palczewski K. 2000. Short-chain dehydrogenases/reductases in retina. Methods Enzymol. 316:372-83.
Hahn KL, Johnson J, Beres BJ, Howard S, Wilson-Rawls J. 2005. Lunatic fringe null female mice are infertile due to defects in meiotic maturation. Development. 132(4):817-28.
Hajkova P, Ancelin K, Waldmann T, Lacoste N, Lange UC, Cesari F, Lee C, Almouzni G, Schneider R, Surani MA. 2008. Chromatin dynamics during epigenetic reprogramming in the mouse germ line. Nature. 452(7189):877-81.
Ham B, Fernandez MC, D'Costa Z, Brodt P. 2016. The diverse roles of the TNF axis in cancer progression and metastasis. Trends Cancer Res. 11(1):1-27.
Hammes A, Guo JK, Lutsch G, Leheste JR, Landrock D, Ziegler U, Gubler MC, Schedl A. 2001. Two splice variants of the wilms' tumor 1 gene have distinct functions during sex determination and nephron formation. Cell. 106(3):319-29.
Hampton JH, Manikkam M, Lubahn DB, Smith MF, Garverick HA. 2004. Androgen receptor mRNA expression in the bovine ovary. Domest Anim Endocrinol. 27(1):81-8.
Han Y, Xia G, Tsang BK. 2013. Regulation of cyclin D2 expression and degradation by follicle-stimulating hormone during rat granulosa cell proliferation in vitro. Biol Reprod. 88(3):57.
Hannon TS, King DW, Brinkman AD, Steinmetz R, Davis MM, Eugster EA, Pescovitz OH. 2002. Premature thelarche and granulosa cell tumors: A search for FSH receptor and G5alpha activating mutations. J Pediatr Endocrinol Metab. 15 Suppl 3:891-5.
Harding SD, Armit C, Armstrong J, Brennan J, Cheng Y, Haggarty B, Houghton D, Lloyd-MacGilp S, Pi X, Roochun Y, *et al*. 2011. The GUDMAP database--an online resource for genitourinary research. Development. 138(13):2845-53.
Harikae K, Miura K, Kanai Y. 2013. Early gonadogenesis in mammals: Significance of long and narrow gonadal structure. Dev Dyn. 242(4):330-8.
Harikae K, Miura K, Shinomura M, Matoba S, Hiramatsu R, Tsunekawa N, Kanai-Azuma M, Kurohmaru M, Morohashi K, Kanai Y. 2013. Heterogeneity in sexual bipotentiality and plasticity of granulosa cells in developing mouse ovaries. J Cell Sci. 126(Pt 13):2834-44.
Harlow CR, Bradshaw AC, Rae MT, Shearer KD, Hillier SG. 2007. Oestrogen formation and connective tissue growth factor expression in rat granulosa cells. J Endocrinol. 192(1):41-52.
Harris A, Siggers P, Corrochano S, Warr N, Sagar D, Grimes DT, Suzuki M, Burdine RD, Cong F, Koo BK, et al. 2018. ZNRF3 functions in mammalian sex determination by inhibiting canonical WNT signaling. Proc Natl Acad Sci U S A. 115(21):5474-9.
Hartley PS, Bayne RA, Robinson LL, Fulton N, Anderson RA. 2002. Developmental changes in expression of myeloid cell leukemia-1 in human germ cells during oogenesis and early folliculogenesis. J Clin Endocrinol Metab. 87(7):3417-27.
Hawkins JR, Taylor A, Berta P, Levilliers J, Van der Auwera B, Goodfellow PN. 1992. Mutational analysis of SRY: Nonsense and missense mutations in XY sex reversal. Hum Genet. 88(4):471-4.

Hawthorn L, Luce J, Stein L, Rothschild J. 2010. Integration of transcript expression, copy number and LOH analysis of infiltrating ductal carcinoma of the breast. BMC Cancer. 10:460.
Hayashi K, Kobayashi T, Umino T, Goitsuka R, Matsui Y, Kitamura D. 2002a. SMAD1 signaling is critical for initial commitment of germ cell lineage from mouse epiblast. Mech Dev. 118(1-2):99-109.
Hayashi S, Lewis P, Pevny L, McMahon AP. 2002b. Efficient gene modulation in mouse epiblast using a Sox2Cre transgenic mouse strain. Mech Dev. 119 Suppl 1:S97-S101.
Hayes E, Kushnir V, Ma X, Biswas A, Prizant H, Gleicher N, Sen A. 2016. Intra-cellular mechanism of anti-mullerian hormone (AMH) in regulation of follicular development. Mol Cell Endocrinol. 433:56-65.
Hazes B. 1996. The (QxW)3 domain: A flexible lectin scaffold. Protein Sci. 5(8):1490-501.
He WW, Kumar MV, Tindall DJ. 1991. A frame-shift mutation in the androgen receptor gene causes complete androgen insensitivity in the testicular-feminized mouse. Nucleic Acids Res. 19(9):2373-8.
Heilmann-Heimbach S, Herold C, Hochfeld LM, Hillmer AM, Nyholt DR, Hecker J, Javed A, Chew EG, Pechlivanis S, Drichel D, *et al*. 2017. Meta-analysis identifies novel risk loci and yields systematic insights into the biology of male-pattern baldness. Nat Commun. 8:14694.
Heilstedt HA, Burgess DL, Anderson AE, Chedrawi A, Tharp B, Lee O, Kashork CD, Starkey DE, Wu YQ, Noebels JL, *et al*. 2001. Loss of the potassium channel beta-subunit gene, KCNAB2, is associated with epilepsy in patients with 1p36 deletion syndrome. Epilepsia. 42(9):1103-11.
Heilstedt HA, Ballif BC, Howard LA, Kashork CD, Shaffer LG. 2003. Population data suggest that deletions of 1p36 are a relatively common chromosome abnormality. Clin Genet. 64(4):310-6.
Hellwinkel OJ, Bull K, Holterhus PM, Homburg N, Struve D, Hiort O. 1999. Complete androgen insensitivity caused by a splice donor site mutation in intron 2 of the human androgen receptor gene resulting in an exon 2-lacking transcript with premature stop-codon and reduced expression. J Steroid Biochem Mol Biol. 68(1-2):1-9.
Hemminki A, Markie D, Tomlinson I, Avizienyte E, Roth S, Loukola A. 1998. A serine/threonine kinase gene defective in peutz-jeghers syndrome. Nature. 391(6663):184-7.
Henderson SA, Edwards RG. 1968. Chiasma frequency and maternal age in mammals. Nature. 218(5136):22-8.
Henrich KO, Schwab M, Westermann F. 2012. 1p36 tumor suppression--a matter of dosage? Cancer Res. 72(23):6079-88.
Heravi-Moussavi A, Anglesio MS, Cheng SW, Senz J, Yang W, Prentice L, Fejes AP, Chow C, Tone A, Kalloger SE, *et al*. 2012. Recurrent somatic DICER1 mutations in nonepithelial ovarian cancers. N Engl J Med. 366(3):234-42.
Herman C, Chernajovsky Y. 1998. Mutation of proline 211 reduces shedding of the human p75 TNF receptor. J Immunol. 160(5):2478-87.
Hernandez ER, Resnick CE, Holtzclaw WD, Payne DW, Adashi EY. 1988. Insulin as a regulator of androgen biosynthesis by cultured rat ovarian cells: Cellular mechanism(s) underlying physiological and pharmacological hormonal actions. Endocrinology. 122(5):2034-43.
Hernandez Gifford JA, Hunzicker-Dunn ME, Nilson JH. 2009. Conditional deletion of beta-catenin mediated by Amhr2cre in mice causes female infertility. Biol Reprod. 80(6):1282-92.

Hickey TE, Marrocco DL, Gilchrist RB, Norman RJ, Armstrong DT. 2004. Interactions between androgen and growth factors in granulosa cell subtypes of porcine antral follicles. Biol Reprod. 71(1):45-52.
Hild-Petito S, West NB, Brenner RM, Stouffer RL. 1991. Localization of androgen receptor in the follicle and corpus luteum of the primate ovary during the menstrual cycle. Biol Reprod. 44(3):561-8.
Hillier SG, Yong EL, Illingworth PJ, Baird DT, Schwall RH, Mason AJ. 1991. Effect of recombinant activin on androgen synthesis in cultured human thecal cells. J Clin Endocrinol Metab. 72(6):1206-11.
Hillier SG, Whitelaw PF, Smyth CD. 1994. Follicular oestrogen synthesis: The 'two-cell, two-gonadotrophin' model revisited. Mol Cell Endocrinol. 100(1-2):51-4.
Hillier SG, Tetsuka M. 1997. Role of androgens in follicle maturation and atresia. Baillieres Clin Obstet Gynaecol. 11(2):249-60.
Hillier SG, Tetsuka M, Fraser HM. 1997. Location and developmental regulation of androgen receptor in primate ovary. Hum Reprod. 12(1):107-11.
Hillmer AM, Hanneken S, Ritzmann S, Becker T, Freudenberg J, Brockschmidt FF, Flaquer A, Freudenberg-Hua Y, Jamra RA, Metzen C, *et al*. 2005. Genetic variation in the human androgen receptor gene is the major determinant of common early-onset androgenetic alopecia. Am J Hum Genet. 77(1):140-8.
Hilscher B, Hilscher W, Bulthoff-Ohnolz B, Kramer U, Birke A, Pelzer H, Gauss G. 1974. Kinetics of gametogenesis. I. comparative histological and autoradiographic studies of oocytes and transitional prospermatogonia during oogenesis and prespermatogenesis. Cell Tissue Res. 154(4):443-70.
Hiramatsu R, Matoba S, Kanai-Azuma M, Tsunekawa N, Katoh-Fukui Y, Kurohmaru M, Morohashi K, Wilhelm D, Koopman P, Kanai Y. 2009. A critical time window of sry action in gonadal sex determination in mice. Development. 136(1):129-38.
Hirshfield AN, Schmidt WA. 1987. Kinetic aspects of follicular development in the rat. Adv Exp Med Biol. 219:211-36.
Hirshfield AN,. 1991. Development of follicles in the mammalian ovary. Int Rev Cytol. 124:43-101.
Hirshfield AN. 1992. Heterogeneity of cell populations that contribute to the formation of primordial follicles in rats. Biol Reprod. 47(3):466-72.
Hirshfield AN, DeSanti AM. 1995. Patterns of ovarian cell proliferation in rats during the embryonic period and the first three weeks postpartum. Biol Reprod. 53(5):1208-21.
Hoffman BL, Schorge JO, Bradshaw KD, Halvorson LM, Schaffer JI, Corton MM, editors. 2016. Williams gynecology. 3rd ed. McGraw-Hill Education.
Hofmann K, Bucher P. 1996. The UBA domain: A sequence motif present in multiple enzyme classes of the ubiquitination pathway. Trends Biochem Sci. 21(5):172-3.
Honda A, Hirose M, Hara K, Matoba S, Inoue K, Miki H, Hiura H, Kanatsu-Shinohara M, Kanai Y, Kono T, *et al*. 2007. Isolation, characterization, and in vitro and in vivo differentiation of putative thecal stem cells. Proc Natl Acad Sci U S A. 104(30):12389-94.
Horie K, Takakura K, Fujiwara H, Suginami H, Liao S, Mori T. 1992. Immunohistochemical localization of androgen receptor in the human ovary throughout the menstrual cycle in relation to oestrogen and progesterone receptor expression. Hum Reprod. 7(2):184-90.

Horie R, Aizawa S, Nagai M, Ito K, Higashihara M, Ishida T, Inoue J, Watanabe T. 1998. A novel domain in the CD30 cytoplasmic tail mediates NFkappaB activation. Int Immunol. 10(2):203-10.
Houston CS, Opitz JM, Spranger JW, Macpherson RI, Reed MH, Gilbert EF, Herrmann J, Schinzel A. 1983. The campomelic syndrome: Review, report of 17 cases, and follow-up on the currently 17-year-old boy first reported by maroteaux *et al* in 1971. Am J Med Genet. 15(1):3-28.
Hsieh M, Lee D, Panigone S, Horner K, Chen R, Theologis A, Lee DC, Threadgill DW, Conti M. 2007. Luteinizing hormone-dependent activation of the epidermal growth factor network is essential for ovulation. Mol Cell Biol. 27(5):1914-24.
Hsueh AJ, Kawamura K, Cheng Y, Fauser BC. 2015. Intraovarian control of early folliculogenesis. Endocr Rev. 36(1):1-24.
Hu YC, Wang PH, Yeh S, Wang RS, Xie C, Xu Q, Zhou X, Chao HT, Tsai MY, Chang C. 2004. Subfertility and defective folliculogenesis in female mice lacking androgen receptor. Proc Natl Acad Sci U S A. 101(31):11209-14.
Hu J, Boritz E, Wylie W, Douek DC. 2017a. Stochastic principles governing alternative splicing of RNA. PLoS Comput Biol. 13(9):e1005761.
Hu Q, Hong L, Nie M, Wang Q, Fang Y, Dai Y, Zhai Y, Wang S, Yin C, Yang X. 2017b. The effect of dehydroepiandrosterone supplementation on ovarian response is associated with androgen receptor in diminished ovarian reserve women. J Ovarian Res. 10(1):32,017-0326-3.
Huang EJ, Manova K, Packer AI, Sanchez S, Bachvarova RF, Besmer P. 1993. The murine steel panda mutation affects kit ligand expression and growth of early ovarian follicles. Dev Biol. 157(1):100-9.
Huang B, Wang S, Ning Y, Lamb AN, Bartley J. 1999. Autosomal XX sex reversal caused by duplication of SOX9. Am J Med Genet. 87(4):349-53.
Huang CT, Weitsman SR, Dykes BN, Magoffin DA. 2001. Stem cell factor and insulin-like growth factor-I stimulate luteinizing hormone-independent differentiation of rat ovarian theca cells. Biol Reprod. 64(2):451-6.
Huang PL. 2009. A comprehensive definition for metabolic syndrome. Dis Model Mech. 2(5-6):231-7.
Hunter I, Hay CW, Esswein B, Watt K, McEwan IJ. 2018. Tissue control of androgen action: The ups and downs of androgen receptor expression. Mol Cell Endocrinol. 465:27-35.
Ito M, Yokouchi K, Yoshida K, Kano K, Naito K, Miyazaki J, Tojo H. 2006. Investigation of the fate of sry-expressing cells using an in vivo Cre/loxP system. Dev Growth Differ. 48(1):41-7.
Iuchi S. 2001. Three classes of C2H2 zinc finger proteins. Cell Mol Life Sci. 58(4):625-35.
Jameson SA, Lin YT, Capel B. 2012. Testis development requires the repression of Wnt4 by fgf signaling. Dev Biol. 370(1):24-32.
Jameson SA, Natarajan A, Cool J, DeFalco T, Maatouk DM, Mork L, Munger SC, Capel B. 2012. Temporal transcriptional profiling of somatic and germ cells reveals biased lineage priming of sexual fate in the fetal mouse gonad. PLoS Genet. 8(3):e1002575.
Jamieson S, Butzow R, Andersson N, Alexiadis M, Unkila-Kallio L, Heikinheimo M, Fuller PJ, Anttonen M. 2010. The FOXL2 C134W mutation is characteristic of adult granulosa cell tumors of the ovary. Mod Pathol. 23(11):1477-85.

Jamieson S, Fuller PJ. 2012. Molecular pathogenesis of granulosa cell tumors of the ovary. Endocr Rev. 33(1):109-44.
Jamin SP, Arango NA, Mishina Y, Hanks MC, Behringer RR. 2002. Requirement of Bmpr1a for mullerian duct regression during male sexual development. Nat Genet. 32(3):408-10.
Jeays-Ward K, Hoyle C, Brennan J, Dandonneau M, Alldus G, Capel B, Swain A. 2003. Endothelial and steroidogenic cell migration are regulated by WNT4 in the developing mammalian gonad. Development. 130(16):3663-70.
Jefferson WN, Couse JF, Banks EP, Korach KS, Newbold RR. 2000. Expression of estrogen receptor beta is developmentally regulated in reproductive tissues of male and female mice. Biol Reprod. 62(2):310-7.
Jenne DE, Reimann H, Nezu J, Friedel W, Loff S, Jeschke R, Muller O, Back W, Zimmer M. 1998. Peutz-jeghers syndrome is caused by mutations in a novel serine threonine kinase. Nat Genet. 18(1):38-43.
Jeyasuria P, Ikeda Y, Jamin SP, Zhao L, De Rooij DG, Themmen AP, Behringer RR, Parker KL. 2004. Cell-specific knockout of steroidogenic factor 1 reveals its essential roles in gonadal function. Mol Endocrinol. 18(7):1610-9.
Jian X, Boerwinkle E, Liu X. 2014. In silico tools for splicing defect prediction: A survey from the viewpoint of end users. Genet Med. 16(7):497-503.
Jin H, Won M, Park SE, Lee S, Park M, Bae J. 2016. FOXL2 is an essential activator of SF-1-induced transcriptional regulation of anti-mullerian hormone in human granulosa cells. PLoS One. 11(7):e0159112.
John GB, Gallardo TD, Shirley LJ, Castrillon DH. 2008. Foxo3 is a PI3K-dependent molecular switch controlling the initiation of oocyte growth. Dev Biol. 321(1):197-204.
Jordan BK, Mohammed M, Ching ST, Delot E, Chen XN, Dewing P, Swain A, Rao PN, Elejalde BR, Vilain E. 2001. Up-regulation of WNT-4 signaling and dosage-sensitive sex reversal in humans. Am J Hum Genet. 68(5):1102-9.
Jorgez CJ, Klysik M, Jamin SP, Behringer RR, Matzuk MM. 2004. Granulosa cell-specific inactivation of follistatin causes female fertility defects. Mol Endocrinol. 18(4):953-67.
Jorgez CJ, De Mayo FJ, Matzuk MM. 2006. Inhibin alpha-iCre mice: Cre deleter lines for the gonads, pituitary, and adrenal. Genesis. 44(4):183-8.
Jost A. 1953. Problems of fetal endocrinology: The gonadal and hypophyseal hormones. Recent Prog Horm Res. 8:379.
Juengel JL, Heath DA, Quirke LD, McNatty KP. 2006. Oestrogen receptor alpha and beta, androgen receptor and progesterone receptor mRNA and protein localisation within the developing ovary and in small growing follicles of sheep. Reproduction. 131(1):81-92.
Juneja SC, Barr KJ, Enders GC, Kidder GM. 1999. Defects in the germ line and gonads of mice lacking connexin43. Biol Reprod. 60(5):1263-70.
Kaipia A, Chun SY, Eisenhauer K, Hsueh AJ. 1996. Tumor necrosis factor-alpha and its second messenger, ceramide, stimulate apoptosis in cultured ovarian follicles. Endocrinology. 137(11):4864-70.
Kalfa N, Ecochard A, Patte C, Duvillard P, Audran F, Pienkowski C, Thibaud E, Brauner R, Lecointre C, Plantaz D, *et al*. 2006. Activating mutations of the stimulatory g protein in juvenile ovarian granulosa cell tumors: A new prognostic factor? J Clin Endocrinol Metab. 91(5):1842-7.

Kalfa N, Philibert P, Patte C, Ecochard A, Duvillard P, Baldet P, Jaubert F, Fellous M, Sultan C. 2007. Extinction of FOXL2 expression in aggressive ovarian granulosa cell tumors in children. Fertil Steril. 87(4):896-901.
Kalfa N, Meduri G, Philibert P, Patte C, Boizet-Bonhoure B, Thibaut E, Pienkowski C, Jaubert F, Misrahi M, Sultan C. 2010. Unusual virilization in girls with juvenile granulosa cell tumors of the ovary is related to intratumoral aromatase deficiency. Horm Res Paediatr. 74(2):83-91.
Kam RK, Shi W, Chan SO, Chen Y, Xu G, Lau CB, Fung KP, Chan WY, Zhao H. 2013. Dhrs3 protein attenuates retinoic acid signaling and is required for early embryonic patterning. J Biol Chem. 288(44):31477-87.
Kananen K, Markkula M, Rainio E, Su JG, Hsueh AJ, Huhtaniemi IT. 1995. Gonadal tumorigenesis in transgenic mice bearing the mouse inhibin alpha-subunit promoter/simian virus T-antigen fusion gene: Characterization of ovarian tumors and establishment of gonadotropin-responsive granulosa cell lines. Mol Endocrinol. 9(5):616-27.
Karl J, Capel B. 1998. Sertoli cells of the mouse testis originate from the coelomic epithelium. Dev Biol. 203(2):323-33.
Karpova T, Ravichandiran K, Insisienmay L, Rice D, Agbor V, Heckert LL. 2015. Steroidogenic factor 1 differentially regulates fetal and adult leydig cell development in male mice. Biol Reprod. 93(4):83.
Karst AM, Levanon K, Drapkin R. 2011. Modeling high-grade serous ovarian carcinogenesis from the fallopian tube. Proc Natl Acad Sci U S A. 108(18):7547-52.
Kato N, Fukase M, Ono I, Matsumoto K, Okazaki E, Motoyama T. 2001. Sertoli-stromal cell tumor of the ovary: Immunohistochemical, ultrastructural, and genetic studies. Hum Pathol. 32(8):796-802.
Kato S. 2002. Androgen receptor structure and function from knock-out mouse. Clin Pediatr Endocrinol. 11:1-7.
Kato N, Romero M, Catasus L, Prat J. 2004. The STK11/LKB1 peutz-jegher gene is not involved in the pathogenesis of sporadic sex cord-stromal tumors, although loss of heterozygosity at 19p13.3 indicates other gene alteration in these tumors. Hum Pathol. 35(9):1101-4.
Katoh-Fukui Y, Tsuchiya R, Shiroishi T, Nakahara Y, Hashimoto N, Noguchi K, Higashinakagawa T. 1998. Male-to-female sex reversal in M33 mutant mice. Nature. 393(6686):688-92.
Katoh-Fukui Y, Owaki A, Toyama Y, Kusaka M, Shinohara Y, Maekawa M, Toshimori K, Morohashi K. 2005. Mouse polycomb M33 is required for splenic vascular and adrenal gland formation through regulating Ad4BP/SF1 expression. Blood. 106(5):1612-20.
Katoh-Fukui Y, Miyabayashi K, Komatsu T, Owaki A, Baba T, Shima Y, Kidokoro T, Kanai Y, Schedl A, Wilhelm D, *et al*. 2012. Cbx2, a polycomb group gene, is required for sry gene expression in mice. Endocrinology. 153(2):913-24.
Kauff ND, Satagopan JM, Robson ME, Scheuer L, Hensley M, Hudis CA, Ellis NA, Boyd J, Borgen PI, Barakat RR, *et al*. 2002. Risk-reducing salpingo-oophorectomy in women with a BRCA1 or BRCA2 mutation. N Engl J Med. 346(21):1609-15.
Kaur H, Bagga R, Saha SC, Gainder S, Srinivasan R, Adhya AK, Dhaliwal LK. 2009. Juvenile granulosa cell tumor of the ovary presenting with pleural effusion and ascites. Int J Clin Oncol. 14(1):78-81.

Keane TM, Goodstadt L, Danecek P, White MA, Wong K, Yalcin B, Heger A, Agam A, Slater G, Goodson M, *et al*. 2011. Mouse genomic variation and its effect on phenotypes and gene regulation. Nature. 477(7364):289-94.
Kemp B, Silva E, Elnaggar A. 1995. Juvenile granulosa-cell tumor of the ovary - interphase cytogenetics for chromosome-12 and chromosome-x and flow cytometric DNA-ploidy study. Int J Oncol. 7(3):661-5.
Kennedy MK, Willis CR, Armitage RJ. 2006. Deciphering CD30 ligand biology and its role in humoral immunity. Immunology. 118(2):143-52.
Kent J, Wheatley SC, Andrews JE, Sinclair AH, Koopman P. 1996. A male-specific role for SOX9 in vertebrate sex determination. Development. 122(9):2813-22.
Keri RA, Lozada KL, Abdul-Karim FW, Nadeau JH, Nilson JH. 2000. Luteinizing hormone induction of ovarian tumors: Oligogenic differences between mouse strains dictates tumor disposition. Proc Natl Acad Sci USA. 97(1):383-7.
Kezele P, Skinner MK. 2003. Regulation of ovarian primordial follicle assembly and development by estrogen and progesterone: Endocrine model of follicle assembly. Endocrinology. 144(8):3329-37.
Kim JM, Boone DL, Auyeung A, Tsang BK. 1998. Granulosa cell apoptosis induced at the penultimate stage of follicular development is associated with increased levels of fas and fas ligand in the rat ovary. Biol Reprod. 58(5):1170-6.
Kim Y, Kobayashi A, Sekido R, DiNapoli L, Brennan J, Chaboissier MC, Poulat F, Behringer RR, Lovell-Badge R, Capel B. 2006. Fgf9 and Wnt4 act as antagonistic signals to regulate mammalian sex determination. PLoS Biol. 4(6):e187.
Kim SY, Weiss J, Tong M, Laronda MM, Lee EJ, Jameson JL. 2009. Foxl2, a forkhead transcription factor, modulates nonclassical activity of the estrogen receptor-alpha. Endocrinology. 150(11):5085-93.
Kim MS, Hur SY, Yoo NJ, Lee SH. 2010. Mutational analysis of FOXL2 codon 134 in granulosa cell tumour of ovary and other human cancers. J Pathol. 221(2):147-52.
Kim JH, Yoon S, Park M, Park HO, Ko JJ, Lee K, Bae J. 2011. Differential apoptotic activities of wild-type FOXL2 and the adult-type granulosa cell tumor-associated mutant FOXL2 (C134W). Oncogene. 30(14):1653-63.
Kim CH. 2013. Androgen supplementation in IVF. Minerva Ginecol. 65(5):497-504.
Kim MS, Lee SH, Yoo NJ, Lee SH. 2013. DICER1 exons 25 and 26 mutations are rare in common human tumours besides sertoli-leydig cell tumour. Histopathology. 63(3):436-8.
Kim SY, Ebbert K, Cordeiro MH, Romero MM, Whelan KA, Suarez AA, Woodruff TK, Kurita T. 2016. Constitutive activation of PI3K in oocyte induces ovarian granulosa cell tumors. Cancer Res. 76(13):3851-61.
Kindelberger DW, Lee Y, Miron A, Hirsch MS, Feltmate C, Medeiros F, Callahan MJ, Garner EO, Gordon RW, Birch C, *et al*. 2007. Intraepithelial carcinoma of the fimbria and pelvic serous carcinoma: Evidence for a causal relationship. Am J Surg Pathol. 31(2):161-9.
Kinross KM, Montgomery KG, Kleinschmidt M, Waring P, Ivetac I, Tikoo A, Saad M, Hare L, Roh V, Mantamadiotis T, *et al*. 2012. An activating Pik3ca mutation coupled with pten loss is sufficient to initiate ovarian tumorigenesis in mice. J Clin Invest. 122(2):553-7.
Kinsella RJ, Kahari A, Haider S, Zamora J, Proctor G, Spudich G, Almeida-King J, Staines D, Derwent P, Kerhornou A, *et al*. 2011. Ensembl BioMarts: A hub for data retrieval across taxonomic space. Database (Oxford). 2011:bar030.

Kirschner RD, Rother K, Muller GA, Engeland K. 2010. The retinal dehydrogenase/reductase retSDR1/DHRS3 gene is activated by p53 and p63 but not by mutants derived from tumors or EEC/ADULT malformation syndromes. Cell Cycle. 9(11):2177-88.
Kiser PD, Golczak M, Maeda A, Palczewski K. 2012. Key enzymes of the retinoid (visual) cycle in vertebrate retina. Biochim Biophys Acta. 1821(1):137-51.
Knapczyk-Stwora K, Durlej-Grzesiak M, Ciereszko RE, Koziorowski M, Slomczynska M. 2013a. Antiandrogen flutamide affects folliculogenesis during fetal development in pigs. Reproduction. 145(3):265-76.
Knapczyk-Stwora K, Grzesiak M, Duda M, Koziorowski M, Slomczynska M. 2013b. Effect of flutamide on folliculogenesis in the fetal porcine ovary--regulation by kit ligand/c-kit and IGF1/IGF1R systems. Anim Reprod Sci. 142(3-4):160-7.
Knapczyk-Stwora K, Grzesiak M, Slomczynska M. 2013. In utero exposure to the anti-androgen flutamide influences connexin 43 and beta-catenin expression in porcine fetal gonads. Domest Anim Endocrinol. 44(4):185-94.
Knapczyk-Stwora K, Belej A, Grzesiak M, Slomczynska M. 2015. Effect of gestational antiandrogen treatment on Dicer1 expression in the porcine fetal gonads. Acta Histochem. 117(8):725-31.
Knaul JK, Jorg S, Oberbeck-Mueller D, Heinemann E, Scheuermann L, Brinkmann V, Mollenkopf HJ, Yeremeev V, Kaufmann SH, Dorhoi A. 2014. Lung-residing myeloid-derived suppressors display dual functionality in murine pulmonary tuberculosis. Am J Respir Crit Care Med. 190(9):1053-66.
Knaut H, Werz C, Geisler R, Nusslein-Volhard C, Tubingen 2000 Screen Consortium. 2003. A zebrafish homologue of the chemokine receptor Cxcr4 is a germ-cell guidance receptor. Nature. 421(6920):279-82.
Knight PG. 1996. Roles of inhibins, activins, and follistatin in the female reproductive system. Front Neuroendocrinol. 17(4):476-509.
Knight PG, Satchell L, Glister C. 2012. Intra-ovarian roles of activins and inhibins. Mol Cell Endocrinol. 359(1-2):53-65.
Köbel M, Kalloger SE, Huntsman DG, Santos JL, Swenerton KD, Seidman JD, Gilks CB, Cheryl Brown Ovarian Cancer Outcomes Unit of the British Columbia Cancer Agency, Vancouver BC. 2010. Differences in tumor type in low-stage versus high-stage ovarian carcinomas. Int J Gynecol Pathol. 29(3):203-11.
Kogan SC, Hong SH, Shultz DB, Privalsky ML, Bishop JM. 2000. Leukemia initiated by PMLRARalpha: The PML domain plays a critical role while retinoic acid-mediated transactivation is dispensable. Blood. 95(5):1541-50.
Kolehmainen J, Black GC, Saarinen A, Chandler K, Clayton-Smith J, Traskelin AL, Perveen R, Kivitie-Kallio S, Norio R, Warburg M, *et al*. 2003. Cohen syndrome is caused by mutations in a novel gene, COH1, encoding a transmembrane protein with a presumed role in vesicle-mediated sorting and intracellular protein transport. Am J Hum Genet. 72(6):1359-69.
Kommoss S, Gilks CB, Penzel R, Herpel E, Mackenzie R, Huntsman D, Schirmacher P, Anglesio M, Schmidt D, Kommoss F. 2014. A current perspective on the pathological assessment of FOXL2 in adult-type granulosa cell tumours of the ovary. Histopathology. 64(3):380-8.
Koonings PP, Campbell K, Mishell DR, Grimes DA. 1989. Relative frequency of primary ovarian neoplasms: A 10-year review. Obstet Gynecol. 74(6):921-6.

Koopman P, Gubbay J, Vivian N, Goodfellow P, Lovell-Badge R. 1991. Male development of chromosomally female mice transgenic for sry. Nature. 351(6322):117-21.
Koressaar T, Remm M. 2007. Enhancements and modifications of primer design program Primer3. Bioinformatics. 23(10):1289-91.
Kotlar T, Young RH, Albanese C, Crowley WF,Jr, Scully RE, Jameson JL. 1998. Absence of mutations in the FSH receptor in ovarian granulosa cell tumors. J Clin Endocrinol Metab. 83(8):3001-1.
Kotsuji F, Kamitani N, Goto K, Tominaga T. 1990. Bovine theca and granulosa cell interactions modulate their growth, morphology, and function. Biol Reprod. 43(5):726-32.
Koubova J, Douglas BM, Zhou Q, Capel B, Michael DG, David CP. 2006. Retinoic acid regulates sex-specific timing of meiotic initiation in mice. Proc Natl Acad Sci USA. 103(8):2474-9.
Koubova J, Hu YC, Bhattacharyya T, Soh YQ, Gill ME, Goodheart ML, Hogarth CA, Griswold MD, Page DC. 2014. Retinoic acid activates two pathways required for meiosis in mice. PLoS Genet. 10(8):e1004541.
Kousta E, White DM, Franks S. 1997. Modern use of clomiphene citrate in induction of ovulation. Hum Reprod Update. 3(4):359-65.
Krege JH, Hodgin JB, Couse JF, Enmark E, Warner M, Mahler JF, Sar M, Korach KS, Gustafsson JA, Smithies O. 1998. Generation and reproductive phenotypes of mice lacking estrogen receptor beta. Proc Natl Acad Sci U S A. 95(26):15677-82.
Kreidberg JA, Sariola H, Loring JM, Maeda M, Pelletier J, Housman D, Jaenisch R. 1993. WT-1 is required for early kidney development. Cell. 74(4):679-91.
Kriegler M, Perez C, DeFay K, Albert I, Lu SD. 1988. A novel form of TNF/cachectin is a cell surface cytotoxic transmembrane protein: Ramifications for the complex physiology of TNF. Cell. 53(1):45-53.
Krona C, Ejeskar K, Caren H, Abel F, Sjoberg RM, Martinsson T. 2004. A novel 1p36.2 located gene, APITD1, with tumour-suppressive properties and a putative p53-binding domain, shows low expression in neuroblastoma tumours. Br J Cancer. 91(6):1119-30.
Kumar TR, Wang Y, Matzuk MM. 1996. Gonadotropins are essential modifier factors for gonadal tumor development in inhibin-deficient mice. Endocrinology. 137(10):4210-6.
Kumar TR, Wang Y, Lu N, Matzuk MM. 1997. Follicle stimulating hormone is required for ovarian follicle maturation but not male fertility. Nat Genet. 15(2):201-4.
Kumar TR, Palapattu G, Wang P, Woodruff TK, Boime I, Byrne MC, Matzuk MM. 1999. Transgenic models to study gonadotropin function: The role of follicle-stimulating hormone in gonadal growth and tumorigenesis. Mol Endocrinol. 13(6):851-65.
Kumar B, Singh R, Bharathi KV, Himabindu. 2014. Virilizing cystic juvenile granulosa cell tumour of the ovary: A case report. J Clin Diagn Res. 8(4):FD03-4.
Kumari GL, Datta JK, Roy S. 1978. Evidence for a role of androgens in the growth and maturation of ovarian follicles in rats. Horm Res. 9(2):112-20.
Kuo FT, Bentsi-Barnes IK, Barlow GM, Pisarska MD. 2011. Mutant forkhead L2 (FOXL2) proteins associated with premature ovarian failure (POF) dimerize with wild-type FOXL2, leading to altered regulation of genes associated with granulosa cell differentiation. Endocrinology. 152(10):3917-29.
Kurimoto K, Yabuta Y, Ohinata Y, Shigeta M, Yamanaka K, Saitou M. 2008. Complex genome-wide transcription dynamics orchestrated by Blimp1 for the specification of the germ cell lineage in mice. Genes Dev. 22(12):1617-35.

Kurman RJ, Shih I. 2010. The origin and pathogenesis of epithelial ovarian cancer: A proposed unifying theory. Am J Surg Pathol. 34(3):433-43.
Kurman RJ, Shih I. 2011. Molecular pathogenesis and extraovarian origin of epithelial ovarian cancer--shifting the paradigm. Hum Pathol. 42(7):918-31.
Kuroda H, Terada N, Nakayama H, Matsumoto K, Kitamura Y. 1988. Infertility due to growth arrest of ovarian follicles in Sl/Slt mice. Dev Biol. 126(1):71-9.
Kuroda K, Venkatakrishnan R, Salker MS, Lucas ES, Shaheen F, Kuroda M, Blanks A, Christian M, Quenby S, Brosens JJ. 2013. Induction of 11beta-HSD 1 and activation of distinct mineralocorticoid receptor- and glucocorticoid receptor-dependent gene networks in decidualizing human endometrial stromal cells. Mol Endocrinol. 27(2):192-202.
Kusaka M, Katoh-Fukui Y, Ogawa H, Miyabayashi K, Baba T, Shima Y, Sugiyama N, Sugimoto Y, Okuno Y, Kodama R, *et al*. 2010. Abnormal epithelial cell polarity and ectopic epidermal growth factor receptor (EGFR) expression induced in Emx2 KO embryonic gonads. Endocrinology. 151(12):5893-904.
Kwon JS, Tinker A, Pansegrau G, McAlpine J, Housty M, McCullum M, Gilks CB. 2013. Prophylactic salpingectomy and delayed oophorectomy as an alternative for BRCA mutation carriers. Obstet Gynecol. 121(1):14-24.
Labrie F, Luu-The V, Belanger A, Lin SX, Simard J, Pelletier G, Labrie C. 2005. Is dehydroepiandrosterone a hormone? J Endocrinol. 187(2):169-96.
Laguë MN, Paquet M, Fan HY, Kaartinen MJ, Chu S, Jamin SP, Behringer RR, Fuller PJ, Mitchell A, Dore M, *et al*. 2008. Synergistic effects of pten loss and WNT/CTNNB1 signaling pathway activation in ovarian granulosa cell tumor development and progression. Carcinogenesis. 29(11):2062-72.
Lai H, Jia X, Yu Q, Zhang C, Qiao J, Guan Y, Kang J. 2014. High-fat diet induces significant metabolic disorders in a mouse model of polycystic ovary syndrome. Biol Reprod. 91(5):127.
Laird M, Thomson K, Fenwick M, Mora J, Franks S, Hardy K. 2017. Androgen stimulates growth of mouse preantral follicles in vitro: Interaction with follicle-stimulating hormone and with growth factors of the TGFbeta superfamily. Endocrinology. 158(4):920-35.
Laity JH, Dyson HJ, Wright PE. 2000. Molecular basis for modulation of biological function by alternate splicing of the wilms' tumor suppressor protein. Proc Natl Acad Sci U S A. 97(22):11932-5.
Lamas-Pinheiro R, Martins MM, Lobo A, Bom-Sucesso M, Henriques-Coelho T, Estevao-Costa J. 2016. Juvenile granulosa cell ovarian tumor in a child with beckwith-wiedmann syndrome. Pediatr Blood Cancer. 63(4):750-1.
Lamba P, Fortin J, Tran S, Wang Y, Bernard DJ. 2009. A novel role for the forkhead transcription factor FOXL2 in activin A-regulated follicle-stimulating hormone beta subunit transcription. Mol Endocrinol. 23(7):1001-13.
Lan ZJ, Xu X, Cooney AJ. 2004. Differential oocyte-specific expression of cre recombinase activity in GDF-9-iCre, Zp3cre, and Msx2Cre transgenic mice. Biol Reprod. 71(5):1469-74.
Lane DP. 1992. Cancer. p53, guardian of the genome. Nature. 358(6381):15-6.
Lappalainen I, Lopez J, Skipper L, Hefferon T, Spalding JD, Garner J, Chen C, Maguire M, Corbett M, Zhou G, *et al*. 2013. DbVar and DGVa: Public archives for genomic structural variation. Nucleic Acids Res. 41(Database issue):D936-41.

Larizza D, Calcaterra V, Sampaolo P, Lanati G, Brambilla P, Mondello T, Cesari S. 2006. Unusual presentation of juvenile granulosa cell tumor of the ovary. J Endocrinol Invest. 29(7):653-6.
Lavery R, Lardenois A, Ranc-Jianmotamedi F, Pauper E, Gregoire EP, Vigier C, Moreilhon C, Primig M, Chaboissier MC. 2011. XY Sox9 embryonic loss-of-function mouse mutants show complete sex reversal and produce partially fertile XY oocytes. Dev Biol. 354(1):111-22.
Lavery R, Chassot AA, Pauper E, Gregoire EP, Klopfenstein M, de Rooij DG, Mark M, Schedl A, Ghyselinck NB, Chaboissier MC. 2012. Testicular differentiation occurs in absence of R-spondin1 and Sox9 in mouse sex reversals. PLoS Genet. 8(12):e1003170.
LaVoie HA, Garmey JC, Day RN, Veldhuis JD. 1999. Concerted regulation of low density lipoprotein receptor gene expression by follicle-stimulating hormone and insulin-like growth factor I in porcine granulosa cells: Promoter activation, messenger ribonucleic acid stability, and sterol feedback. Endocrinology. 140(1):178-86.
Lawson KA, Hage WJ. 1994. Clonal analysis of the origin of primordial germ cells in the mouse. Ciba found Symp. 182:68,84; discussion 84-91.
Lawson KA, Dunn NR, Roelen BA, Zeinstra LM, Davis AM, Wright CV, Korving JP, Hogan BL. 1999. Bmp4 is required for the generation of primordial germ cells in the mouse embryo. Genes Dev. 13(4):424-36.
Lechowska A, Bilinski S, Choi Y, Shin Y, Kloc M, Rajkovic A. 2011. Premature ovarian failure in nobox-deficient mice is caused by defects in somatic cell invasion and germ cell cyst breakdown. J Assist Reprod Genet. 28(7):583-9.
Lécureuil C, Fontaine I, Crepieux P, Guillou F. 2002. Sertoli and granulosa cell-specific cre recombinase activity in transgenic mice. Genesis. 33(3):114-8.
Lee Y, Miron A, Drapkin R, Nucci MR, Medeiros F, Saleemuddin A, Garber J, Birch C, Mou H, Gordon RW, *et al*. 2007. A candidate precursor to serous carcinoma that originates in the distal fallopian tube. J Pathol. 211(1):26-35.
Lee M, Nam ES, Jung SH, Kim SY, Lee SJ, Yoon JH, Lee NW, Jeon S, Choi JS, Cho CH, *et al*. 2014. 1p36.22 region containing PGD gene is frequently gained in human cervical cancer. J Obstet Gynaecol Res. 40(2):545-53.
Lee BH, Kasparis C, Chen B, Mei H, Edelmann L, Moss C, Weaver DD, Desnick RJ. 2015. Setleis syndrome due to inheritance of the 1p36.22p36.21 duplication: Evidence for lack of penetrance. J Hum Genet. 60(11):717-22.
Legro RS, Driscoll D, Strauss JF,3rd, Fox J, Dunaif A. 1998. Evidence for a genetic basis for hyperandrogenemia in polycystic ovary syndrome. Proc Natl Acad Sci U S A. 95(25):14956-60.
Lehraiki A, Chamaillard C, Krust A, Habert R, Levacher C. 2011. Genistein impairs early testosterone production in fetal mouse testis via estrogen receptor alpha. Toxicol in Vitro. 25(8):1542-7.
Lei L, Spradling AC. 2013. Mouse primordial germ cells produce cysts that partially fragment prior to meiosis. Development. 140(10):2075-81.
Lenie S, Smitz J. 2009. Functional AR signaling is evident in an in vitro mouse follicle culture bioassay that encompasses most stages of folliculogenesis. Biol Reprod. 80(4):685-95.
Leroy X, Augusto D, Leteurtre E, Gosselin B. 2002. CD30 and CD117 (c-kit) used in combination are useful for distinguishing embryonal carcinoma from seminoma. J Histochem Cytochem. 50(2):283-5.

Lesage S, Drouet V, Majounie E, Deramecourt V, Jacoupy M, Nicolas A, Cormier-Dequaire F, Hassoun SM, Pujol C, Ciura S, *et al*. 2016. Loss of VPS13C function in autosomal-recessive parkinsonism causes mitochondrial dysfunction and increases PINK1/Parkin-dependent mitophagy. Am J Hum Genet. 98(3):500-13.
Lewandoski M, Meyers EN, Martin GR. 1997. Analysis of Fgf8 gene function in vertebrate development. Cold Spring Harb Symp Quant Biol. 62:159-68.
Lewis KA, Gray PC, Blount AL, MacConell LA, Wiater E, Bilezikjian LM, Vale W. 2000. Betaglycan binds inhibin and can mediate functional antagonism of activin signalling. Nature. 404(6776):411-4.
Lewis C. 2018. Characterization of spontaneous, juvenile-type granulosa cell tumours from SWR mice. St. John's, NL: Memorial University of Newfoundland.
L'Hôte D, Georges A, Todeschini AL, Kim JH, Benayoun BA, Bae J, Veitia RA. 2012. Discovery of novel protein partners of the transcription factor FOXL2 provides insights into its physiopathological roles. Hum Mol Genet. 21(14):3264-74.
Li Q, Graff JM, O'Connor AE, Loveland KL, Matzuk MM. 2007. SMAD3 regulates gonadal tumorigenesis. Mol Endocrinol. 21(10):2472-86.
Li Q, Pangas SA, Jorgez CJ, Graff JM, Weinstein M, Matzuk MM. 2008a. Redundant roles of SMAD2 and SMAD3 in ovarian granulosa cells in vivo. Mol Cell Biol. 28(23):7001-11.
Li M, Ai JS, Xu BZ, Xiong B, Yin S, Lin SL, Hou Y, Chen DY, Schatten H, Sun QY. 2008b. Testosterone potentially triggers meiotic resumption by activation of intra-oocyte SRC and MAPK in porcine oocytes. Biol Reprod. 79(5):897-905.
Li H, Durbin R. 2009. Fast and accurate short read alignment with burrows-wheeler transform. Bioinformatics. 25(14):1754-60.
Li H, Handsaker B, Wysoker A, Fennell T, Ruan J, Homer N, Marth G, Abecasis G, Durbin R, 1000 Genome Project Data Processing Subgroup. 2009. The sequence Alignment/Map format and SAMtools. Bioinformatics. 25(16):2078-9.
Li R, Brockschmidt FF, Kiefer AK, Stefansson H, Nyholt DR, Song K, Vermeulen SH, Kanoni S, Glass D, Medland SE, et al. 2012. Six novel susceptibility loci for early-onset androgenetic alopecia and their unexpected association with common diseases. PLoS Genet. 8(5):e1002746.
Li H, Wei H, Wang Y, Tang H, Wang Y. 2013. Enhanced green fluorescent protein transgenic expression in vivo is not biologically inert. J Proteome Res. 12(8):3801-8.
Li Y, Zhang L, Hu Y, Chen M, Han F, Qin Y, Chen M, Cui X, Duo S, Tang F, *et al*. 2017. Beta-catenin directs the transformation of testis sertoli cells to ovarian granulosa-like cells by inducing Foxl2 expression. J Biol Chem. 292(43):17577-86.
Lim SS, Davies MJ, Norman RJ, Moran LJ. 2012. Overweight, obesity and central obesity in women with polycystic ovary syndrome: A systematic review and meta-analysis. Hum Reprod Update. 18(6):618-37.
Lin Y, Gill ME, Koubova J, Page DC. 2008. Germ cell-intrinsic and -extrinsic factors govern meiotic initiation in mouse embryos. Science. 322(5908):1685-7.
Lindeman RE, Gearhart MD, Minkina A, Krentz AD, Bardwell VJ, Zarkower D. 2015. Sexual cell-fate reprogramming in the ovary by DMRT1. Curr Biol. 25(6):764-71.
Lindgren V, Waggoner S, Rotmensch J. 1996. Monosomy 22 in two ovarian granulosa cell tumors. Cancer Genet Cytogenet. 89(2):93-7.
Liu CF, Bingham N, Parker K, Yao HH. 2009. Sex-specific roles of beta-catenin in mouse gonadal development. Hum Mol Genet. 18(3):405-17.

Liu CF, Liu C, Yao HH. 2010. Building pathways for ovary organogenesis in the mouse embryo. Curr Top Dev Biol. 90:263-90.
Liu CF, Parker K, Yao HH. 2010. WNT4/beta-catenin pathway maintains female germ cell survival by inhibiting activin betaB in the mouse fetal ovary. PLoS One. 5(4):e10382.
Liu Z, Yang X, Li Z, McMahon C, Sizer C, Barenboim-Stapleton L, Bliskovsky V, Mock B, Ried T, London WB, *et al*. 2011. CASZ1, a candidate tumor-suppressor gene, suppresses neuroblastoma tumor growth through reprogramming gene expression. Cell Death Differ. 18(7):1174-83.
Liu YY, Chen HY, Zhang ML, Tian D, Li S, Lee JY. 2012. Loss of fragile histidine triad and amplification of 1p36.22 and 11p15.5 in primary gastric adenocarcinomas. World J Gastroenterol. 18(33):4522-32.
Liu C, Peng J, Matzuk MM, Yao HH. 2015a. Lineage specification of ovarian theca cells requires multicellular interactions via oocyte and granulosa cells. Nat Commun. 6:6934.
Liu Z, Ren YA, Pangas SA, Adams J, Zhou W, Castrillon DH, Wilhelm D, Richards JS. 2015b. FOXO1/3 and PTEN depletion in granulosa cells promotes ovarian granulosa cell tumor development. Mol Endocrinol. 29(7):1006-24.
Logan DW, Marton TF, Stowers L. 2008. Species specificity in major urinary proteins by parallel evolution. PLoS One. 3(9):e3280.
Long JC, Caceres JF. 2009. The SR protein family of splicing factors: Master regulators of gene expression. Biochem J. 417(1):15-27.
Looyenga BD, Hammer GD. 2007. Genetic removal of Smad3 from inhibin-null mice attenuates tumor progression by uncoupling extracellular mitogenic signals from the cell cycle machinery. Mol Endocrinol. 21(10):2440-57.
Lubahn DB, Joseph DR, Sullivan PM, Willard HF, French FS, Wilson EM. 1988. Cloning of human androgen receptor complementary DNA and localization to the X chromosome. Science. 240(4850):327-30.
Lubahn DB, Moyer JS, Golding TS, Couse JF, Korach KS, Smithies O. 1993. Alteration of reproductive function but not prenatal sexual development after insertional disruption of the mouse estrogen receptor gene. Proc Natl Acad Sci U S A. 90(23):11162-6.
Luchetti CG, Solano ME, Sander V, Arcos ML, Gonzalez C, Di Girolamo G, Chiocchio S, Cremaschi G, Motta AB. 2004. Effects of dehydroepiandrosterone on ovarian cystogenesis and immune function. J Reprod Immunol. 64(1-2):59-74.
Ludbrook LM, Bernard P, Bagheri-Fam S, Ryan J, Sekido R, Wilhelm D, Lovell-Badge R, Harley VR. 2012. Excess DAX1 leads to XY ovotesticular disorder of sex development (DSD) in mice by inhibiting steroidogenic factor-1 (SF1) activation of the testis enhancer of SRY-box-9 (Sox9). Endocrinology. 153(4):1948-58.
Lund SA, Murdoch J, Van Kirk EA, Murdoch WJ. 1999. Mitogenic and antioxidant mechanisms of estradiol action in preovulatory ovine follicles: Relevance to luteal function. Biol Reprod. 61(2):388-92.
Lundova T, Zemanova L, Malcekova B, Skarka A, Stambergova H, Havrankova J, Safr M, Wsol V. 2015. Molecular and biochemical characterisation of human short-chain dehydrogenase/reductase member 3 (DHRS3). Chem Biol Interact. 234:178-87.
Luo X, Ikeda Y, Parker KL. 1994. A cell-specific nuclear receptor is essential for adrenal and gonadal development and sexual differentiation. Cell. 77(4):481-90.
Lyon MF, Hawkes SG. 1970. X-linked gene for testicular feminization in the mouse. Nature. 227(5264):1217-9.

Ma Y, Andrisse S, Chen Y, Childress S, Xue P, Wang Z, Jones D, Ko C, Divall S, Wu S. 2017. Androgen receptor in the ovary theca cells plays a critical role in androgen-induced reproductive dysfunction. Endocrinology. 158(1):98-108.
Maatouk DM, DiNapoli L, Alvers A, Parker KL, Taketo MM, Capel B. 2008. Stabilization of beta-catenin in XY gonads causes male-to-female sex-reversal. Hum Mol Genet. 17(19):2949-55.
Machiela MJ, Grunewald TGP, Surdez D, Reynaud S, Mirabeau O, Karlins E, Rubio RA, Zaidi S, Grossetete-Lalami S, Ballet S, *et al*. 2018. Genome-wide association study identifies multiple new loci associated with ewing sarcoma susceptibility. Nat Commun. 9(1):3184,018-05537-2.
MacLean HE, Warne GL, Zajac JD. 1997. Localization of functional domains in the androgen receptor. J Steroid Biochem Mol Biol. 62(4):233-42.
Magamage MPS, Zengyo M, Moniruzzaman M, Miyano T. 2010. Testosterone induces activation of porcine primordial follicles in vitro. Reprod Med Biol. 10(1):21-30.
Magarelli PC, Zachow RJ, Magoffin DA. 1996. Developmental and hormonal regulation of rat theca-cell differentiation factor secretion in ovarian follicles. Biol Reprod. 55(2):416-20.
Magoffin DA, Weitsman SR. 1994. Insulin-like growth factor-I regulation of luteinizing hormone (LH) receptor messenger ribonucleic acid expression and LH-stimulated signal transduction in rat ovarian theca-interstitial cells. Biol Reprod. 51(4):766-75.
Magoffin DA. 2005. Ovarian theca cell. Int J Biochem Cell Biol. 37(7):1344-9.
Mahakali Zama A, Hudson FP,3rd, Bedell MA. 2005. Analysis of hypomorphic KitlSl mutants suggests different requirements for KITL in proliferation and migration of mouse primordial germ cells. Biol Reprod. 73(4):639-47.
Maillet D, Goulvent T, Rimokh R, Vacher-Lavenu MC, Pautier P, Alexandre J, Pujade-Laurraine E, Devouassoux-Shisheboran M, Treilleux I, Ray-Coquard I, *et al*. 2014. Impact of a second opinion using expression and molecular analysis of FOXL2 for sex cord-stromal tumors. A study of the GINECO group & the TMRO network. Gynecol Oncol. 132(1):181-7.
Mandel H, Shemer R, Borochowitz ZU, Okopnik M, Knopf C, Indelman M, Drugan A, Tiosano D, Gershoni-Baruch R, Choder M, *et al*. 2008. SERKAL syndrome: An autosomal-recessive disorder caused by a loss-of-function mutation in WNT4. Am J Hum Genet. 82(1):39-47.
Mangelsdorf DJ, Thummel C, Beato M, Herrlich P, Schutz G, Umesono K, Blumberg B, Kastner P, Mark M, Chambon P, *et al*. 1995. The nuclear receptor superfamily: The second decade. Cell. 83(6):835-9.
Mansouri-Attia N, James R, Ligon A, Li X, Pangas SA. 2014a. Soy promotes juvenile granulosa cell tumor development in mice and in the human granulosa cell tumor-derived COV434 cell line. Biol Reprod. 91(4):100.
Mansouri-Attia N, Tripurani SK, Gokul N, Piard H, Anderson ML, Eldin K, Pangas SA. 2014b. TGFbeta signaling promotes juvenile granulosa cell tumorigenesis by suppressing apoptosis. Mol Endocrinol. 28(11):1887-98.
Manuylov NL, Smagulova FO, Leach L, Tevosian SG. 2008. Ovarian development in mice requires the GATA4-FOG2 transcription complex. Development. 135(22):3731-43.
Mao B, Wu W, Li Y, Hoppe D, Stannek P, Glinka A, Niehrs C. 2001. LDL-receptor-related protein 6 is a receptor for dickkopf proteins. Nature. 411(6835):321-5.
Mao B, Wu W, Davidson G, Marhold J, Li M, Mechler BM, Delius H, Hoppe D, Stannek P, Walter C, *et al*. 2002. Kremen proteins are dickkopf receptors that regulate Wnt/beta-catenin signalling. Nature. 417(6889):664-7.

Margolin JF, Friedman JR, Meyer WK, Vissing H, Thiesen HJ, Rauscher FJ,3rd. 1994. Kruppel-associated boxes are potent transcriptional repression domains. Proc Natl Acad Sci U S A. 91(10):4509-13.
Mariotti A, Durham J, Frederickson R, Miller R, Butcher F, Mawhinney M. 1987. Actions and interactions of estradiol and retinoic acid in mouse anterior prostate gland. Biol Reprod. 37(4):1023-35.
Mark M, Jacobs H, Oulad-Abdelghani M, Dennefeld C, Feret B, Vernet N, Codreanu CA, Chambon P, Ghyselinck NB. 2008. STRA8-deficient spermatocytes initiate, but fail to complete, meiosis and undergo premature chromosome condensation. J Cell Sci. 121(Pt 19):3233-42.
Marongiu M, Deiana M, Marcia L, Sbardellati A, Asunis I, Meloni A, Angius A, Cusano R, Loi A, Crobu F, *et al*. 2016. Novel action of FOXL2 as mediator of Col1a2 gene autoregulation. Dev Biol. 416(1):200-11.
Martinkovich S, Shah D, Planey SL, Arnott JA. 2014. Selective estrogen receptor modulators: Tissue specificity and clinical utility. Clin Interv Aging. 9:1437-52.
Massagué J. 1998. TGF-beta signal transduction. Annu Rev Biochem. 67:753-91.
Matias-Guiu X, Pons C, Prat J. 1998. Mullerian inhibiting substance, alpha-inhibin, and CD99 expression in sex cord-stromal tumors and endometrioid ovarian carcinomas resembling sex cord-stromal tumors. Hum Pathol. 29(8):840-5.
Matson CK, Murphy MW, Sarver AL, Griswold MD, Bardwell VJ, Zarkower D. 2011. DMRT1 prevents female reprogramming in the postnatal mammalian testis. Nature. 476(7358):101-4.
Matson CK, Zarkower D. 2012. Sex and the singular DM domain: Insights into sexual regulation, evolution and plasticity. Nat Rev Genet. 13(3):163-74.
Matsui Y, Toksoz D, Nishikawa S, Nishikawa S, Williams D, Zsebo K, Hogan BL. 1991. Effect of steel factor and leukaemia inhibitory factor on murine primordial germ cells in culture. Nature. 353(6346):750-2.
Matzuk MM, Finegold MJ, Su JG, Hsueh AJ, Bradley A. 1992. Alpha-inhibin is a tumour-suppressor gene with gonadal specificity in mice. Nature. 360(6402):313-9.
Matzuk MM, Finegold MJ, Mather JP, Krummen L, Lu H, Bradley A. 1994. Development of cancer cachexia-like syndrome and adrenal tumors in inhibin-deficient mice. Proc Natl Acad Sci U S A. 91(19):8817-21.
Mayr D, Kaltz-Wittmer C, Arbogast S, Amann G, Aust DE, Diebold J. 2002. Characteristic pattern of genetic aberrations in ovarian granulosa cell tumors. Mod Pathol. 15(9):951-7.
Mazaud S, Guyot R, Guigon CJ, Coudouel N, Le Magueresse-Battistoni B, Magre S. 2005. Basal membrane remodeling during follicle histogenesis in the rat ovary: Contribution of proteinases of the MMP and PA families. Dev Biol. 277(2):403-16.
McAllister JM, Byrd W, Simpson ER. 1994. The effects of growth factors and phorbol esters on steroid biosynthesis in isolated human theca interna and granulosa-lutein cells in long term culture. J Clin Endocrinol Metab. 79(1):106-12.
McCluggage WG, Maxwell P. 2001. Immunohistochemical staining for calretinin is useful in the diagnosis of ovarian sex cord-stromal tumours. Histopathology. 38(5):403-8.
McConechy MK, Farkkila A, Horlings HM, Talhouk A, Unkila-Kallio L, van Meurs HS, Yang W, Rozenberg N, Andersson N, Zaby K, *et al*. 2016. Molecularly defined adult granulosa cell tumor of the ovary: The clinical phenotype. J Natl Cancer Inst. 108(11):10.1093/jnci/djw134. Print 2016 Nov.

McCoshen JA, McCallion DJ. 1975. A study of the primordial germ cells during their migratory phase in steel mutant mice. Experientia. 31(5):589-90.
McElreavey K, Vilain E, Abbas N, Herskowitz I, Fellous M. 1993. A regulatory cascade hypothesis for mammalian sex determination: SRY represses a negative regulator of male development. Proc Natl Acad Sci U S A. 90(8):3368-72.
McGee EA, Hsu SY, Kaipia A, Hsueh AJ. 1998. Cell death and survival during ovarian follicle development. Mol Cell Endocrinol. 140(1-2):15-8.
McLaren A. 1991. Development of the mammalian gonad: The fate of the supporting cell lineage. Bioessays. 13(4):151-6.
McLaren A, Southee D. 1997. Entry of mouse embryonic germ cells into meiosis. Dev Biol. 187(1):107-13.
McLaren W, Gil L, Hunt SE, Riat HS, Ritchie GR, Thormann A, Flicek P, Cunningham F. 2016. The ensembl variant effect predictor. Genome Biol. 17(1):122,016-0974-4.
McMahon A, Fosten M, Monk M. 1981. Random X-chromosome inactivation in female primordial germ cells in the mouse. J Embryol Exp Morphol. 64:251-8.
McMahon AP, Aronow BJ, Davidson DR, Davies JA, Gaido KW, Grimmond S, Lessard JL, Little MH, Potter SS, Wilder EL, *et al*. 2008. GUDMAP: The genitourinary developmental molecular anatomy project. J Am Soc Nephrol. 19(4):667-71.
McTavish KJ, Nonis D, Hoang YD, Shimasaki S. 2013. Granulosa cell tumor mutant FOXL2C134W suppresses GDF-9 and activin A-induced follistatin transcription in primary granulosa cells. Mol Cell Endocrinol. 372(1-2):57-64.
Medeiros F, Muto MG, Lee Y, Elvin JA, Callahan MJ, Feltmate C, Garber JE, Cramer DW, Crum CP. 2006. The tubal fimbria is a preferred site for early adenocarcinoma in women with familial ovarian cancer syndrome. Am J Surg Pathol. 30(2):230-6.
Mekada K, Abe K, Murakami A, Nakamura S, Nakata H, Moriwaki K, Obata Y, Yoshiki A. 2009. Genetic differences among C57BL/6 substrains. Exp Anim. 58(2):141-9.
Menke DB, Koubova J, Page DC. 2003. Sexual differentiation of germ cells in XX mouse gonads occurs in an anterior-to-posterior wave. Dev Biol. 262(2):303-12.
Mercader J, Granados N, Bonet ML, Palou A. 2008. All-trans retinoic acid decreases murine adipose retinol binding protein 4 production. Cell Physiol Biochem. 22(1-4):363-72.
Merino VF, Cho S, Nguyen N, Sadik H, Narayan A, Talbot C,Jr, Cope L, Zhou XC, Zhang Z, Gyorffy B, *et al*. 2018. Induction of cell cycle arrest and inflammatory genes by combined treatment with epigenetic, differentiating, and chemotherapeutic agents in triple-negative breast cancer. Breast Cancer Res. 20(1):145,018-1068-x.
Merras-Salmio L, Vettenranta K, Mottonen M, Heikinheimo M. 2002. Ovarian granulosa cell tumors in childhood. Pediatr Hematol Oncol. 19(3):145-56.
Mescher AL. 2018. Junqueira's basic histology: Text and atlas. 15th ed. McGraw-Hill Education.
Metzler MA, Sandell LL. 2016. Enzymatic metabolism of vitamin A in developing vertebrate embryos. Nutrients. 8(12):10.3390/nu8120812.
Midorikawa Y, Yamamoto S, Tsuji S, Kamimura N, Ishikawa S, Igarashi H, Makuuchi M, Kokudo N, Sugimura H, Aburatani H. 2009. Allelic imbalances and homozygous deletion on 8p23.2 for stepwise progression of hepatocarcinogenesis. Hepatology. 49(2):513-22.
Migeon BR, Brown TR, Axelman J, Migeon CJ. 1981. Studies of the locus for androgen receptor: Localization on the human X chromosome and evidence for homology with the tfm locus in the mouse. Proc Natl Acad Sci U S A. 78(10):6339-43.

Miller WL. 1988. Molecular biology of steroid hormone synthesis. Endocr Rev. 9(3):295-318.
Mills AM, Chinn Z, Rauh LA, Dusenbery AC, Whitehair RM, Saks E, Duska LR. 2019. Emerging biomarkers in ovarian granulosa cell tumors. Int J Gynecol Cancer. 29(3):560-5.
Mingels MJ, Roelofsen T, van der Laak JA, de Hullu JA, van Ham MA, Massuger LF, Bulten J, Bol M. 2012. Tubal epithelial lesions in salpingo-oophorectomy specimens of BRCA-mutation carriers and controls. Gynecol Oncol. 127(1):88-93.
Minkina A, Matson CK, Lindeman RE, Ghyselinck NB, Bardwell VJ, Zarkower D. 2014. DMRT1 protects male gonadal cells from retinoid-dependent sexual transdifferentiation. Dev Cell. 29(5):511-20.
Mintz B, Russell ES. 1957. Gene-induced embryological modifications of primordial germ cells in the mouse. J Exp Zool. 134(2):207-37.
Minucci S, Monestiroli S, Giavara S, Ronzoni S, Marchesi F, Insinga A, Diverio D, Gasparini P, Capillo M, Colombo E, *et al*. 2002. PML-RAR induces promyelocytic leukemias with high efficiency following retroviral gene transfer into purified murine hematopoietic progenitors. Blood. 100(8):2989-95.
Mir SS, Richter BW, Duckett CS. 2000. Differential effects of CD30 activation in anaplastic large cell lymphoma and hodgkin disease cells. Blood. 96(13):4307-12.
Mitchell AL, Attwood TK, Babbitt PC, Blum M, Bork P, Bridge A, Brown SD, Chang HY, El-Gebali S, Fraser MI, *et al*. 2019. InterPro in 2019: Improving coverage, classification and access to protein sequence annotations. Nucleic Acids Res. 47(D1):D351-60.
Miura K, Murata C, Harikae K, Suzuki H, Kanai-Azuma M, Kurohmaru M, Tsunekawa N, Kanai Y. 2017. Defects in the first wave of folliculogenesis in mouse XO ovaries. J Reprod Dev. 63(3):333-8.
Miura K, Harikae K, Nakaguchi M, Imaimatsu K, Hiramatsu R, Tomita A, Hirate Y, Kanai-Azuma M, Kurohmaru M, Ogura A, *et al*. 2019. Molecular and genetic characterization of partial masculinization in embryonic ovaries grafted into male nude mice. PLoS One. 14(3):e0212367.
Miyamoto N, Yoshida M, Kuratani S, Matsuo I, Aizawa S. 1997. Defects of urogenital development in mice lacking Emx2. Development. 124(9):1653-64.
Miyamoto Y, Taniguchi H, Hamel F, Silversides DW, Viger RS. 2008. A GATA4/WT1 cooperation regulates transcription of genes required for mammalian sex determination and differentiation. BMC Mol Biol. 9:44,2199-9-44.
Mizusaki H, Kawabe K, Mukai T, Ariyoshi E, Kasahara M, Yoshioka H, Swain A, Morohashi K. 2003. Dax-1 (dosage-sensitive sex reversal-adrenal hypoplasia congenita critical region on the X chromosome, gene 1) gene transcription is regulated by wnt4 in the female developing gonad. Mol Endocrinol. 17(4):507-19.
MMRRC UNC – Genotyping Protocol [Internet]: University of North Carolina, Chapel Hill; c2013 [cited 2019. Available from: www.med.unc.edu/mmrrc/files/2017/12/MMRRC-Center-Protocol-14245.pdf.
Molitch ME, Schimmer BP. 2018. Chapter 42: Introduction to endocrinology: The hypothalamic-pituitary axis. In: Goodman and Gilman's: The pharmacological basis of therapeutics. Brunton LL, Hilal-Dandan R,Knollmann BC, editors. 13th ed. McGraw-Hill Education.
Möller M, Flachsbart F, Till A, Thye T, Horstmann RD, Meyer CG, Osei I, van Helden PD, Hoal EG, Schreiber S, *et al*. 2010. A functional haplotype in the 3'untranslated region of

TNFRSF1B is associated with tuberculosis in two african populations. Am J Respir Crit Care Med. 181(4):388-93.
Molyneaux KA, Stallock J, Schaible K, Wylie C. 2001. Time-lapse analysis of living mouse germ cell migration. Dev Biol. 240(2):488-98.
Molyneaux KA, Zinszner H, Kunwar PS, Schaible K, Stebler J, Sunshine MJ, O'Brien W, Raz E, Littman D, Wylie C, *et al*. 2003. The chemokine SDF1/CXCL12 and its receptor CXCR4 regulate mouse germ cell migration and survival. Development. 130(18):4279-86.
Mom CH, Engelen MJ, Willemse PH, Gietema JA, ten Hoor KA, de Vries EG, van der Zee AG. 2007. Granulosa cell tumors of the ovary: The clinical value of serum inhibin A and B levels in a large single center cohort. Gynecol Oncol. 105(2):365-72.
Moons DS, Jirawatnotai S, Tsutsui T, Franks R, Parlow AF, Hales DB, Gibori G, Fazleabas AT, Kiyokawa H. 2002. Intact follicular maturation and defective luteal function in mice deficient for cyclin- dependent kinase-4. Endocrinology. 143(2):647-54.
Moore RK, Otsuka F, Shimasaki S. 2003. Molecular basis of bone morphogenetic protein-15 signaling in granulosa cells. J Biol Chem. 278(1):304-10.
Morais da Silva S, Hacker A, Harley V, Goodfellow P, Swain A, Lovell-Badge R. 1996. Sox9 expression during gonadal development implies a conserved role for the gene in testis differentiation in mammals and birds. Nat Genet. 14(1):62-8.
Moran LJ, Misso ML, Wild RA, Norman RJ. 2010. Impaired glucose tolerance, type 2 diabetes and metabolic syndrome in polycystic ovary syndrome: A systematic review and meta-analysis. Hum Reprod Update. 16(4):347-63.
Mori T, Suzuki A, Nishimura T, Kambegawa A. 1977. Evidence for androgen participation in induced ovulation in immature rats. Endocrinology. 101(2):623-6.
Mork L, Maatouk DM, McMahon JA, Guo JJ, Zhang P, McMahon AP, Capel B. 2012. Temporal differences in granulosa cell specification in the ovary reflect distinct follicle fates in mice. Biol Reprod. 86(2):37.
Morrison LJ, Marcinkiewicz JL. 2002. Tumor necrosis factor alpha enhances oocyte/follicle apoptosis in the neonatal rat ovary. Biol Reprod. 66(2):450-7.
Moss ML, Jin SL, Milla ME, Bickett DM, Burkhart W, Carter HL, Chen WJ, Clay WC, Didsbury JR, Hassler D, *et al*. 1997. Cloning of a disintegrin metalloproteinase that processes precursor tumour-necrosis factor-alpha. Nature. 385(6618):733-6.
Mowa CN, Iwanaga T. 2000. Differential distribution of oestrogen receptor-alpha and -beta mRNAs in the female reproductive organ of rats as revealed by in situ hybridization. J Endocrinol. 165(1):59-66.
Mroz K, Carrel L, Hunt PA. 1999. Germ cell development in the XXY mouse: Evidence that X chromosome reactivation is independent of sexual differentiation. Dev Biol. 207(1):229-38.
Mudge JM, Armstrong SD, McLaren K, Beynon RJ, Hurst JL, Nicholson C, Robertson DH, Wilming LG, Harrow JL. 2008. Dynamic instability of the major urinary protein gene family revealed by genomic and phenotypic comparisons between C57 and 129 strain mice. Genome Biol. 9(5):R91,2008-9-5-r91. Epub 2008 May 28.
Munger SC, Aylor DL, Syed HA, Magwene PM, Threadgill DW, Capel B. 2009. Elucidation of the transcription network governing mammalian sex determination by exploiting strain-specific susceptibility to sex reversal. Genes Dev. 23(21):2521-36.
Munger SC, Natarajan A, Looger LL, Ohler U, Capel B. 2013. Fine time course expression analysis identifies cascades of activation and repression and maps a putative regulator of mammalian sex determination. PLoS Genet. 9(7):e1003630.

Munir I, Yen HW, Geller DH, Torbati D, Bierden RM, Weitsman SR, Agarwal SK, Magoffin DA. 2004. Insulin augmentation of 17alpha-hydroxylase activity is mediated by phosphatidyl inositol 3-kinase but not extracellular signal-regulated kinase-1/2 in human ovarian theca cells. Endocrinology. 145(1):175-83.
Munirajan AK, Ando K, Mukai A, Takahashi M, Suenaga Y, Ohira M, Koda T, Hirota T, Ozaki T, Nakagawara A. 2008. KIF1Bbeta functions as a haploinsufficient tumor suppressor gene mapped to chromosome 1p36.2 by inducing apoptotic cell death. J Biol Chem. 283(36):24426-34.
Murray AA, Gosden RG, Allison V, Spears N. 1998. Effect of androgens on the development of mouse follicles growing in vitro. J Reprod Fertil. 113(1):27-33.
Musgrove EA, Caldon CE, Barraclough J, Stone A, Sutherland RL. 2011. Cyclin D as a therapeutic target in cancer. Nat Rev Cancer. 11(8):558-72.
Muzumdar MD, Tasic B, Miyamichi K, Li L, Luo L. 2007. A global double-fluorescent cre reporter mouse. Genesis. 45(9):593-605.
Nagaraja AK, Agno JE, Kumar TR, Matzuk MM. 2008. Luteinizing hormone promotes gonadal tumorigenesis in inhibin-deficient mice. Mol Cell Endocrinol. 294(1-2):19-28.
Nagaraja AK, Middlebrook BS, Rajanahally S, Myers M, Li Q, Matzuk MM, Pangas SA. 2010. Defective gonadotropin-dependent ovarian folliculogenesis and granulosa cell gene expression in inhibin-deficient mice. Endocrinology. 151(10):4994-5006.
Nakamura T, Takio K, Eto Y, Shibai H, Titani K, Sugino H. 1990. Activin-binding protein from rat ovary is follistatin. Science. 247(4944):836-8.
Nakamura E, Nguyen MT, Mackem S. 2006. Kinetics of tamoxifen-regulated cre activity in mice using a cartilage-specific CreER(T) to assay temporal activity windows along the proximodistal limb skeleton. Dev Dyn. 235(9):2603-12.
Nakashima N, Young RH, Scully RE. 1984. Androgenic granulosa cell tumors of the ovary. A clinicopathologic analysis of 17 cases and review of the literature. Arch Pathol Lab Med. 108(10):786-91.
Narkwichean A, Jayaprakasan K, Maalouf WE, Hernandez-Medrano JH, Pincott-Allen C, Campbell BK. 2014. Effects of dehydroepiandrosterone on in vivo ovine follicular development. Hum Reprod. 29(1):146-54.
Nasu K, Takai N, Nishida M, Narahara H. 2008. Tumorigenic effects of tamoxifen on the female genital tract. Clin Med Pathol. 1:17-34.
Naz RK, Zhu X, Menge AC. 1997. Expression of tumor necrosis factor-alpha and its receptors type I and type II in human oocytes. Mol Reprod Dev. 47(2):127-33.
Nestler JE, Jakubowicz DJ, de Vargas AF, Brik C, Quintero N, Medina F. 1998. Insulin stimulates testosterone biosynthesis by human thecal cells from women with polycystic ovary syndrome by activating its own receptor and using inositolglycan mediators as the signal transduction system. J Clin Endocrinol Metab. 83(6):2001-5.
Ng A, Tan S, Singh G, Rizk P, Swathi Y, Tan TZ, Huang RY, Leushacke M, Barker N. 2014. Lgr5 marks stem/progenitor cells in ovary and tubal epithelia. Nat Cell Biol. 16(8):745-57.
Nicol L, Bishop SC, Pong-Wong R, Bendixen C, Holm LE, Rhind SM, McNeilly AS. 2009. Homozygosity for a single base-pair mutation in the oocyte-specific GDF9 gene results in sterility in thoka sheep. Reproduction. 138(6):921-33.
Nicol B, Yao HH. 2015. Gonadal identity in the absence of pro-testis factor SOX9 and pro-ovary factor beta-catenin in mice. Biol Reprod. 93(2):35.

Nicol B, Grimm SA, Gruzdev A, Scott GJ, Ray MK, Yao HH. 2018. Genome-wide identification of FOXL2 binding and characterization of FOXL2 feminizing action in the fetal gonads. Hum Mol Genet. 27(24):4273-87.
Nicol B, Grimm SA, Chalmel F, Lecluze E, Pannetier M, Pailhoux E, Dupin-De-Beyssat E, Guiguen Y, Capel B, Yao HH. 2019. RUNX1 maintains the identity of the fetal ovary through an interplay with FOXL2. Nat Commun. 10(1):5116,019-13060-1.
Niederreither K, Subbarayan V, Dolle P, Chambon P. 1999. Embryonic retinoic acid synthesis is essential for early mouse post-implantation development. Nat Genet. 21(4):444-8.
Niehrs C. 2012. The complex world of WNT receptor signalling. Nat Rev Mol Cell Biol. 13(12):767-79.
Nielsen ME, Rasmussen IA, Kristensen SG, Christensen ST, Mollgard K, Wreford Andersen E, Byskov AG, Yding Andersen C. 2011. In human granulosa cells from small antral follicles, androgen receptor mRNA and androgen levels in follicular fluid correlate with FSH receptor mRNA. Mol Hum Reprod. 17(1):63-70.
Nilsson EE, Stanfield J, Skinner MK. 2006. Interactions between progesterone and tumor necrosis factor-alpha in the regulation of primordial follicle assembly. Reproduction. 132(6):877-86.
Nilsson EE, Schindler R, Savenkova MI, Skinner MK. 2011. Inhibitory actions of anti-mullerian hormone (AMH) on ovarian primordial follicle assembly. PLoS One. 6(5):e20087.
Nippoldt TB, Reame NE, Kelch RP, Marshall JC. 1989. The roles of estradiol and progesterone in decreasing luteinizing hormone pulse frequency in the luteal phase of the menstrual cycle. J Clin Endocrinol Metab. 69(1):67-76.
Nishi Y, Yanase T, Mu Y, Oba K, Ichino I, Saito M, Nomura M, Mukasa C, Okabe T, Goto K, *et al*. 2001. Establishment and characterization of a steroidogenic human granulosa-like tumor cell line, KGN, that expresses functional follicle-stimulating hormone receptor. Endocrinology. 142(1):437-45.
Nishimura T, Nishida N, Komeda T, Fukuda Y, Ikai I, Yamaoka Y, Nakao K. 2006. Genome-wide semiquantitative microsatellite analysis of human hepatocellular carcinoma: Discrete mapping of smallest region of overlap of recurrent chromosomal gains and losses. Cancer Genet Cytogenet. 167(1):57-65.
Niwa K, Yano R, Mori S, Yamaguchi Y, Narikawa N, Tanaka T. 2013. Androgenic adult granulosa cell tumor with secondary amenorrhea and elevated luteinizing hormone. Pathol Discov. 1(9):1-9.
Nixon VL, Levasseur M, McDougall A, Jones KT. 2002. Ca(2+) oscillations promote APC/C-dependent cyclin B1 degradation during metaphase arrest and completion of meiosis in fertilizing mouse eggs. Curr Biol. 12(9):746-50.
Nogales FF, Musto ML, Saez AI, Robledo M, Palacios J, Aneiros J. 2004. Multifocal intrafollicular granulosa cell tumor of the ovary associated with an unusual germline p53 mutation. Mod Pathol. 17(7):868-73.
Nomelini RS, Micheletti ARM, Adad SJ, Murta EFC. 2007. Androgenic juvenile granulosa cell tumor of the ovary with cystic presentation: A case report. Eur J Gynaecol Oncol. 28(3):236-8.
Nonis D, McTavish KJ, Shimasaki S. 2013. Essential but differential role of FOXL2wt and FOXL2C134W in GDF-9 stimulation of follistatin transcription in co-operation with Smad3 in the human granulosa cell line COV434. Mol Cell Endocrinol. 372(1-2):42-8.

Notini AJ, Davey RA, McManus JF, Bate KL, Zajac JD. 2005. Genomic actions of the androgen receptor are required for normal male sexual differentiation in a mouse model. J Mol Endocrinol. 35(3):547-55.
Novotny MV. 2003. Pheromones, binding proteins and receptor responses in rodents. Biochem Soc Trans. 31(Pt 1):117-22.
O'Brien MJ, Pendola JK, Eppig JJ. 2003. A revised protocol for in vitro development of mouse oocytes from primordial follicles dramatically improves their developmental competence. Biol Reprod. 68(5):1682-6.
Oflazoglu E, Grewal IS, Gerber H. 2009. Targeting CD30/CD30L in oncology and autoimmune and inflammatory diseases. Adv Exp Med Biol. 647:174-85.
Ohinata Y, Payer B, O'Carroll D, Ancelin K, Ono Y, Sano M, Barton SC, Obukhanych T, Nussenzweig M, Tarakhovsky A, *et al*. 2005. Blimp1 is a critical determinant of the germ cell lineage in mice. Nature. 436(7048):207-13.
Ohinata Y, Ohta H, Shigeta M, Yamanaka K, Wakayama T, Saitou M. 2009. A signaling principle for the specification of the germ cell lineage in mice. Cell. 137(3):571-84.
Oler G, Camacho CP, Hojaij FC, Michaluart P,Jr, Riggins GJ, Cerutti JM. 2008. Gene expression profiling of papillary thyroid carcinoma identifies transcripts correlated with BRAF mutational status and lymph node metastasis. Clin Cancer Res. 14(15):4735-42.
Olopade OI, Wei M. 2003. FANCF methylation contributes to chemoselectivity in ovarian cancer. Cancer Cell. 3(5):417-20.
Omari S, Waters M, Naranian T, Kim K, Perumalsamy AL, Chi M, Greenblatt E, Moley KH, Opferman JT, Jurisicova A. 2015. Mcl-1 is a key regulator of the ovarian reserve. Cell Death Dis. 6:e1755.
Orisaka M, Tajima K, Mizutani T, Miyamoto K, Tsang BK, Fukuda S, Yoshida Y, Kotsuji F. 2006. Granulosa cells promote differentiation of cortical stromal cells into theca cells in the bovine ovary. Biol Reprod. 75(5):734-40.
Ottolenghi C, Veitia R, Quintana-Murci L, Torchard D, Scapoli L, Souleyreau-Therville N, Beckmann J, Fellous M, McElreavey K. 2000. The region on 9p associated with 46,XY sex reversal contains several transcripts expressed in the urogenital system and a novel doublesex-related domain. Genomics. 64(2):170-8.
Ottolenghi C, Omari S, Garcia-Ortiz JE, Uda M, Crisponi L, Forabosco A, Pilia G, Schlessinger D. 2005. Foxl2 is required for commitment to ovary differentiation. Hum Mol Genet. 14(14):2053-62.
Ottolenghi C, Pelosi E, Tran J, Colombino M, Douglass E, Nedorezov T, Cao A, Forabosco A, Schlessinger D. 2007. Loss of Wnt4 and Foxl2 leads to female-to-male sex reversal extending to germ cells. Hum Mol Genet. 16(23):2795-804.
Ozaki R, Kuroda K, Ikemoto Y, Ochiai A, Matsumoto A, Kumakiri J, Kitade M, Itakura A, Muter J, Brosens JJ, *et al*. 2017. Reprogramming of the retinoic acid pathway in decidualizing human endometrial stromal cells. PLoS One. 12(3):e0173035.
Ozisik G, Achermann JC, Jameson JL. 2002. The role of SF1 in adrenal and reproductive function: Insight from naturally occurring mutations in humans. Mol Genet Metab. 76(2):85-91.
Padmos RC, Schloot NC, Beyan H, Ruwhof C, Staal FJ, de Ridder D, Aanstoot HJ, Lam-Tse WK, de Wit H, de Herder C, *et al*. 2008. Distinct monocyte gene-expression profiles in autoimmune diabetes. Diabetes. 57(10):2768-73.

Pailhoux E, Vigier B, Chaffaux S, Servel N, Taourit S, Furet JP, Fellous M, Grosclaude F, Cribiu EP, Cotinot C, *et al*. 2001. A 11.7-kb deletion triggers intersexuality and polledness in goats. Nat Genet. 29(4):453-8.

Pang TP, Clarke MV, Ghasem-Zadeh A, Lee NK, Davey RA, MacLean HE. 2012. A physiological role for androgen actions in the absence of androgen receptor DNA binding activity. Mol Cell Endocrinol. 348(1):189-97.

Pangas SA, Jorgez CJ, Matzuk MM. 2004. Growth differentiation factor 9 regulates expression of the bone morphogenetic protein antagonist gremlin. J Biol Chem. 279(31):32281-6.

Pangas SA, Li X, Robertson EJ, Matzuk MM. 2006. Premature luteinization and cumulus cell defects in ovarian-specific Smad4 knockout mice. Mol Endocrinol. 20(6):1406-22.

Pangas SA, Li X, Umans L, Zwijsen A, Huylebroeck D, Gutierrez C, Wang D, Martin JF, Jamin SP, Behringer RR, *et al*. 2008. Conditional deletion of Smad1 and Smad5 in somatic cells of male and female gonads leads to metastatic tumor development in mice. Mol Cell Biol. 28(1):248-57.

Pannetier M, Fabre S, Batista F, Kocer A, Renault L, Jolivet G, Mandon-Pepin B, Cotinot C, Veitia R, Pailhoux E. 2006. FOXL2 activates P450 aromatase gene transcription: Towards a better characterization of the early steps of mammalian ovarian development. J Mol Endocrinol. 36(3):399-413.

Pansuriya TC, van Eijk R, d'Adamo P, van Ruler MA, Kuijjer ML, Oosting J, Cleton-Jansen AM, van Oosterwijk JG, Verbeke SL, Meijer D, *et al*. 2011. Somatic mosaic IDH1 and IDH2 mutations are associated with enchondroma and spindle cell hemangioma in ollier disease and maffucci syndrome. Nat Genet. 43(12):1256-61.

Park JY, Su YQ, Ariga M, Law E, Jin SL, Conti M. 2004. EGF-like growth factors as mediators of LH action in the ovulatory follicle. Science. 303(5658):682-4.

Park SY, Tong M, Jameson JL. 2007. Distinct roles for steroidogenic factor 1 and desert hedgehog pathways in fetal and adult leydig cell development. Endocrinology. 148(8):3704-10.

Park M, Shin E, Won M, Kim JH, Go H, Kim HL, Ko JJ, Lee K, Bae J. 2010. FOXL2 interacts with steroidogenic factor-1 (SF-1) and represses SF-1-induced CYP17 transcription in granulosa cells. Mol Endocrinol. 24(5):1024-36.

Park M, Suh DS, Lee K, Bae J. 2014. Positive cross talk between FOXL2 and antimullerian hormone regulates ovarian reserve. Fertil Steril. 102(3):847,855.e1.

Parma P, Radi O, Vidal V, Chaboissier MC, Dellambra E, Valentini S, Guerra L, Schedl A, Camerino G. 2006. R-spondin1 is essential in sex determination, skin differentiation and malignancy. Nat Genet. 38(11):1304-9.

Parrott JA, Skinner MK. 1999. Kit-ligand/stem cell factor induces primordial follicle development and initiates folliculogenesis. Endocrinology. 140(9):4262-71.

Passon N, Bregant E, Sponziello M, Dima M, Rosignolo F, Durante C, Celano M, Russo D, Filetti S, Damante G. 2015. Somatic amplifications and deletions in genome of papillary thyroid carcinomas. Endocrine. 50(2):453-64.

Pelletier G. 2000. Localization of androgen and estrogen receptors in rat and primate tissues. Histol Histopathol. 15(4):1261-70.

Peluso JJ, Steger RW. 1978. Role of FSH in regulating granulosa cell division and follicular atresia in rats. J Reprod Fertil. 54(2):275-8.

Peng XR, Hsueh AJ, LaPolt PS, Bjersing L, Ny T. 1991. Localization of luteinizing hormone receptor messenger ribonucleic acid expression in ovarian cell types during follicle development and ovulation. Endocrinology. 129(6):3200-7.
Pepling ME, Spradling AC. 1998. Female mouse germ cells form synchronously dividing cysts. Development. 125(17):3323-8.
Pepling ME, Spradling AC. 2001. Mouse ovarian germ cell cysts undergo programmed breakdown to form primordial follicles. Dev Biol. 234(2):339-51.
Pepling ME, Sundman EA, Patterson NL, Gephardt GW, Medico L,Jr, Wilson KI. 2010. Differences in oocyte development and estradiol sensitivity among mouse strains. Reproduction. 139(2):349-57.
Peral B, San Millan JL, Castello R, Moghetti P, Escobar-Morreale HF. 2002. Comment: The methionine 196 arginine polymorphism in exon 6 of the TNF receptor 2 gene (TNFRSF1B) is associated with the polycystic ovary syndrome and hyperandrogenism. J Clin Endocrinol Metab. 87(8):3977-83.
Perets R, Drapkin R. 2016. It's totally tubular....riding the new wave of ovarian cancer research. Cancer Res. 76(1):10-7.
Perez GI, Robles R, Knudson CM, Flaws JA, Korsmeyer SJ, Tilly JL. 1999. Prolongation of ovarian lifespan into advanced chronological age by bax-deficiency. Nat Genet. 21(2):200-3.
Pertea M, Lin X, Salzberg SL. 2001. GeneSplicer: A new computational method for splice site prediction. Nucleic Acids Res. 29(5):1185-90.
Petkov PM, Ding Y, Cassell MA, Zhang W, Wagner G, Sargent EE, Asquith S, Crew V, Johnson KA, Robinson P, *et al*. 2004. An efficient SNP system for mouse genome scanning and elucidating strain relationships. Genome Res. 14(9):1806-11.
Pierce JG, Parsons TF. 1981. Glycoprotein hormones: Structure and function. Annu Rev Biochem. 50:465-95.
Pierucci-Alves F, Clark AM, Russell LD. 2001. A developmental study of the desert hedgehog-null mouse testis. Biol Reprod. 65(5):1392-402.
Pisarska MD, Bae J, Klein C, Hsueh AJ. 2004. Forkhead l2 is expressed in the ovary and represses the promoter activity of the steroidogenic acute regulatory gene. Endocrinology. 145(7):3424-33.
Plon SE, Pirics ML, Nuchtern J, Hicks J, Russell H, Agrawal S, Zbuk K, Eng C, Hegde M, Chin EL. 2008. Multiple tumors in a child with germ-line mutations in TP53 and PTEN. N Engl J Med. 359(5):537-9.
Postel-Vinay S, Veron AS, Tirode F, Pierron G, Reynaud S, Kovar H, Oberlin O, Lapouble E, Ballet S, Lucchesi C, *et al*. 2012. Common variants near TARDBP and EGR2 are associated with susceptibility to ewing sarcoma. Nat Genet. 44(3):323-7.
Pötter T, Wedemeyer N, van Dulmen A, Kohnlein W, Gohde W. 2001. Identification of a deletion hotspot on distal mouse chromosome 4 by YAC fingerprinting. Mutat Res. 476(1-2):29-42.
Pradeep PK, Li X, Peegel H, Menon KM. 2002. Dihydrotestosterone inhibits granulosa cell proliferation by decreasing the cyclin D2 mRNA expression and cell cycle arrest at G1 phase. Endocrinology. 143(8):2930-5.
Purdie DM, Christopher JB, Siskind V, Penelope MW, Adèle CG. 2003. Ovulation and risk of epithelial ovarian cancer. Int J Cancer. 104(2):228-32.

Quan L, Dittmar A, Zhou Y, Hutson A, Stassen AP, Demant P. 2012. Susceptibility loci affecting ERBB2/neu-induced mammary tumorigenesis in mice. Genes Chromosomes Cancer. 51(7):631-43.
Quigley CA, Evans BA, Simental JA, Marschke KB, Sar M, Lubahn DB, Davies P, Hughes IA, Wilson EM, French FS. 1992. Complete androgen insensitivity due to deletion of exon C of the androgen receptor gene highlights the functional importance of the second zinc finger of the androgen receptor in vivo. Mol Endocrinol. 6(7):1103-12.
Quigley CA, De Bellis A, Marschke KB, el-Awady MK, Wilson EM, French FS. 1995. Androgen receptor defects: Historical, clinical, and molecular perspectives. Endocr Rev. 16(3):271-321.
Quirk SM, Cowan RG, Harman RM. 2006. The susceptibility of granulosa cells to apoptosis is influenced by oestradiol and the cell cycle. J Endocrinol. 189(3):441-53.
Rabie Z. 2015. The chr X-linked Gct6 locus: A granulosa cell tumor suppressor in mice. St. John's, NL: Memorial University of Newfoundland.
Racine C, Rey R, Forest MG, Louis F, Ferre A, Huhtaniemi I, Josso N, di Clemente N. 1998. Receptors for anti-mullerian hormone on leydig cells are responsible for its effects on steroidogenesis and cell differentiation. Proc Natl Acad Sci U S A. 95(2):594-9.
Radany EH, Hong K, Kesharvarzi S, Lander ES, Bishop JM. 1997. Mouse mammary tumor virus/v-ha-ras transgene-induced mammary tumors exhibit strain-specific allelic loss on mouse chromosome 4. Proc Natl Acad Sci U S A. 94(16):8664-9.
Rajanahally S, Agno JE, Nalam RL, Weinstein MB, Loveland KL, Matzuk MM, Li Q. 2010. Genetic evidence that SMAD2 is not required for gonadal tumor development in inhibin-deficient mice. Reprod Biol Endocrinol. 8:69,7827-8-69.
Rajareddy S, Reddy P, Du C, Liu L, Jagarlamudi K, Tang W, Shen Y, Berthet C, Peng SL, Kaldis P, *et al*. 2007. p27kip1 (cyclin-dependent kinase inhibitor 1B) controls ovarian development by suppressing follicle endowment and activation and promoting follicle atresia in mice. Mol Endocrinol. 21(9):2189-202.
Rajkovic A, Stephanie AP, Ballow D, Suzumori N, Martin MM. 2004. NOBOX deficiency disrupts early folliculogenesis and oocyte-specific gene expression. Science. 305(5687):1157-9.
Rampoldi L, Dobson-Stone C, Rubio JP, Danek A, Chalmers RM, Wood NW, Verellen C, Ferrer X, Malandrini A, Fabrizi GM, *et al*. 2001. A conserved sorting-associated protein is mutant in chorea-acanthocytosis. Nat Genet. 28(2):119-20.
Rana K, Davey RA, Zajac JD. 2014. Human androgen deficiency: Insights gained from androgen receptor knockout mouse models. Asian J Androl. 16(2):169-77.
Ransohoff JD, Wei Y, Khavari PA. 2018. The functions and unique features of long intergenic non-coding RNA. Nat Rev Mol Cell Biol. 19(3):143-57.
Rao MC, Midgley AR,Jr, Richards JS. 1978. Hormonal regulation of ovarian cellular proliferation. Cell. 14(1):71-8.
Rastetter RH, Bernard P, Palmer JS, Chassot AA, Chen H, Western PS, Ramsay RG, Chaboissier MC, Wilhelm D. 2014. Marker genes identify three somatic cell types in the fetal mouse ovary. Dev Biol. 394(2):242-52.
Rebbeck TR, Lynch HT, Neuhausen SL, Narod SA, Van't Veer L, Garber JE, Evans G, Isaacs C, Daly MB, Matloff E, *et al*. 2002. Prophylactic oophorectomy in carriers of BRCA1 or BRCA2 mutations. N Engl J Med. 346(21):1616-22.

Reddy P, Shen L, Ren C, Boman K, Lundin E, Ottander U, Lindgren P, Liu YX, Sun QY, Liu K. 2005. Activation of akt (PKB) and suppression of FKHRL1 in mouse and rat oocytes by stem cell factor during follicular activation and development. Dev Biol. 281(2):160-70.
Reddy P, Liu L, Adhikari D, Jagarlamudi K, Rajareddy S, Shen Y, Du C, Tang W, Hamalainen T, Peng SL, *et al*. 2008. Oocyte-specific deletion of pten causes premature activation of the primordial follicle pool. Science. 319(5863):611-3.
Reddy P, Adhikari D, Zheng W, Liang S, Hamalainen T, Tohonen V, Ogawa W, Noda T, Volarevic S, Huhtaniemi I, *et al*. 2009. PDK1 signaling in oocytes controls reproductive aging and lifespan by manipulating the survival of primordial follicles. Hum Mol Genet. 18(15):2813-24.
Redon R, Rio M, Gregory SG, Cooper RA, Fiegler H, Sanlaville D, Banerjee R, Scott C, Carr P, Langford C, *et al*. 2005. Tiling path resolution mapping of constitutional 1p36 deletions by array-CGH: Contiguous gene deletion or "deletion with positional effect" syndrome? J Med Genet. 42(2):166-71.
Reitsma W, de Bock GH, Oosterwijk JC, Bart J, Hollema H, Mourits MJ. 2013. Support of the 'fallopian tube hypothesis' in a prospective series of risk-reducing salpingo-oophorectomy specimens. Eur J Cancer. 49(1):132-41.
Ren Y, Suzuki H, Jagarlamudi K, Golnoski K, McGuire M, Lopes R, Pachnis V, Rajkovic A. 2015. Lhx8 regulates primordial follicle activation and postnatal folliculogenesis. BMC Biol. 13:39,015-0151-3.
Rentzsch P, Witten D, Cooper GM, Shendure J, Kircher M. 2019. CADD: Predicting the deleteriousness of variants throughout the human genome. Nucleic Acids Res. 47(D1):D886-94.
Rescigno P, Cerillo I, Ruocco R, Condello C, De Placido S, Pensabene M. 2013. New hypothesis on pathogenesis of ovarian cancer lead to future tailored approaches. Biomed Res Int. 2013:852839.
Rey R, Josso N, Racine C. 2000. Sexual differentiation. In: Endotext. Feingold KR, Anawalt B, Boyce A, Chrousos G, Dungan K, Grossman A, Hershman JM, Kaltsas G, Koch C, Kopp P, *et al*., editors. South Dartmouth (MA): MDText.com, Inc.
Reynolds N, Collier B, Bingham V, Gray NK, Cooke HJ. 2007. Translation of the synaptonemal complex component Sycp3 is enhanced in vivo by the germ cell specific regulator dazl. Rna. 13(7):974-81.
Rice S, Ojha K, Whitehead S, Mason H. 2007. Stage-specific expression of androgen receptor, follicle-stimulating hormone receptor, and anti-mullerian hormone type II receptor in single, isolated, human preantral follicles: Relevance to polycystic ovaries. J Clin Endocrinol Metab. 92(3):1034-40.
Richards JS. 1979. Hormonal control of ovarian follicular development: A 1978 perspective. Recent Prog Horm Res. 35:343-73.
Richards JS, Hedin L, Caston L. 1986. Differentiation of rat ovarian thecal cells: Evidence for functional luteinization. Endocrinology. 118(4):1660-8.
Richards JS, Russell DL, Ochsner S, Hsieh M, Doyle KH, Falender AE, Lo YK, Sharma SC. 2002a. Novel signaling pathways that control ovarian follicular development, ovulation, and luteinization. Recent Prog Horm Res. 57:195-220.
Richards JS, Sharma SC, Falender AE, Lo YH. 2002b. Expression of FKHR, FKHRL1, and AFX genes in the rodent ovary: Evidence for regulation by IGF-I, estrogen, and the gonadotropins. Mol Endocrinol. 16(3):580-99.

Richards JS, Liu Z, Shimada M. 2008. Immune-like mechanisms in ovulation. Trends Endocrinol Metab. 19(6):191-6.
Richards JS, Fan HY, Liu Z, Tsoi M, Lague MN, Boyer A, Boerboom D. 2012. Either kras activation or pten loss similarly enhance the dominant-stable CTNNB1-induced genetic program to promote granulosa cell tumor development in the ovary and testis. Oncogene. 31(12):1504-20.
Risma KA, Clay CM, Nett TM, Wagner T, Yun J, Nilson JH. 1995. Targeted overexpression of luteinizing hormone in transgenic mice leads to infertility, polycystic ovaries, and ovarian tumors. Proc Natl Acad Sci USA. 92(5):1322-6.
Robker RL, Richards JS. 1998. Hormone-induced proliferation and differentiation of granulosa cells: A coordinated balance of the cell cycle regulators cyclin D2 and p27Kip1. Mol Endocrinol. 12(7):924-40.
Roby KF, Son DS, Terranova PF. 1999. Alterations of events related to ovarian function in tumor necrosis factor receptor type I knockout mice. Biol Reprod. 61(6):1616-21.
Rogers MF, Shihab HA, Mort M, Cooper DN, Gaunt TR, Campbell C. 2018. FATHMM-XF: Accurate prediction of pathogenic point mutations via extended features. Bioinformatics. 34(3):511-3.
Rogozin IB, Milanesi L. 1997. Analysis of donor splice sites in different eukaryotic organisms. J Mol Evol. 45(1):50-9.
Rojas V, Hirshfield KM, Ganesan S, Rodriguez-Rodriguez L. 2016. Molecular characterization of epithelial ovarian cancer: Implications for diagnosis and treatment. Int J Mol Sci. 17(12):10.3390/ijms17122113.
Romero S, Smitz J. 2010. Exposing cultured mouse ovarian follicles under increased gonadotropin tonus to aromatizable androgens influences the steroid balance and reduces oocyte meiotic capacity. Endocrine. 38(2):243-53.
Rosario R, Wilson M, Cheng WT, Payne K, Cohen PA, Fong P, Shelling AN. 2013. Adult granulosa cell tumours (GCT): Clinicopathological outcomes including FOXL2 mutational status and expression. Gynecol Oncol. 131(2):325-9.
Rosario R, Cohen PA, Shelling AN. 2014. The role of FOXL2 in the pathogenesis of adult ovarian granulosa cell tumours. Gynecol Oncol. 133(2):382-7.
Rosen MP, Cedars MI. 2018. Chapter 13: Female reproductive endocrinology and infertility. In: Greenspan's basic and clinical endocrinology. Gardner DG, Shoback D, editors. 10th ed. McGraw-Hill Education.
Rosenfield RL, Ehrmann DA. 2016. The pathogenesis of polycystic ovary syndrome (PCOS): The hypothesis of PCOS as functional ovarian hyperandrogenism revisited. Endocr Rev. 37(5):467-520.
Rouiller-Fabre V, Carmona S, Merhi RA, Cate R, Habert R, Vigier B. 1998. Effect of anti-mullerian hormone on sertoli and leydig cell functions in fetal and immature rats. Endocrinology. 139(3):1213-20.
Roybal LL, Hambarchyan A, Meadows JD, Barakat NH, Pepa PA, Breen KM, Mellon PL, Coss D. 2014. Roles of binding elements, FOXL2 domains, and interactions with cJUN and SMADs in regulation of FSHbeta. Mol Endocrinol. 28(10):1640-55.
Rucker EB,3rd, Dierisseau P, Wagner KU, Garrett L, Wynshaw-Boris A, Flaws JA, Hennighausen L. 2000. Bcl-x and bax regulate mouse primordial germ cell survival and apoptosis during embryogenesis. Mol Endocrinol. 14(7):1038-52.

Rutkowski K, Sowa P, Rutkowska-Talipska J, Kuryliszyn-Moskal A, Rutkowski R. 2014. Dehydroepiandrosterone (DHEA): Hypes and hopes. Drugs. 74(11):1195-207.
Saitou M, Barton SC, Surani MA. 2002. A molecular programme for the specification of germ cell fate in mice. Nature. 418(6895):293-300.
Sakurai T, Iguchi T, Moriwaki K, Noguchi M. 1995. The *ter* mutation first causes primordial germ cell deficiency in *ter/ter* mouse embryos at 8 days of gestation. Dev Growth Differ. 37:293-302.
Salustri A, Yanagishita M, Hascall VC. 1990. Mouse oocytes regulate hyaluronic acid synthesis and mucification by FSH-stimulated cumulus cells. Dev Biol. 138(1):26-32.
Salvetti NR, Alfaro NS, Velazquez MM, Amweg AN, Matiller V, Diaz PU, Ortega HH. 2012. Alteration in localization of steroid hormone receptors and coregulatory proteins in follicles from cows with induced ovarian follicular cysts. Reproduction. 144(6):723-35.
Salvi S, Bonafè M, Bravaccini S. 2019. Androgen receptor in breast cancer: A wolf in sheep's clothing? A lesson from prostate cancer. Semin Cancer Biol.
Sandell LL, Sanderson BW, Moiseyev G, Johnson T, Mushegian A, Young K, Rey JP, Ma JX, Staehling-Hampton K, Trainor PA. 2007. RDH10 is essential for synthesis of embryonic retinoic acid and is required for limb, craniofacial, and organ development. Genes Dev. 21(9):1113-24.
Sander V, Luchetti CG, Solano ME, Elia E, Di Girolamo G, Gonzalez C, Motta AB. 2006. Role of the N, N'-dimethylbiguanide metformin in the treatment of female prepuberal BALB/c mice hyperandrogenized with dehydroepiandrosterone. Reproduction. 131(3):591-602.
Santamaria D, Ortega S. 2006. Cyclins and CDKS in development and cancer: Lessons from genetically modified mice. Front Biosci. 11:1164-88.
Sasson R, Winder N, Kees S, Amsterdam A. 2002. Induction of apoptosis in granulosa cells by TNF alpha and its attenuation by glucocorticoids involve modulation of bcl-2. Biochem Biophys Res Commun. 294(1):51-9.
Saunders CM, Larman MG, Parrington J, Cox LJ, Royse J, Blayney LM, Swann K, Lai FA. 2002. PLC zeta: A sperm-specific trigger of ca(2+) oscillations in eggs and embryo development. Development. 129(15):3533-44.
Schlisio S, Kenchappa RS, Vredeveld LC, George RE, Stewart R, Greulich H, Shahriari K, Nguyen NV, Pigny P, Dahia PL, *et al*. 2008. The kinesin KIF1Bbeta acts downstream from EglN3 to induce apoptosis and is a potential 1p36 tumor suppressor. Genes Dev. 22(7):884-93.
Schmidt D, Ovitt CE, Anlag K, Fehsenfeld S, Gredsted L, Treier AC, Treier M. 2004. The murine winged-helix transcription factor Foxl2 is required for granulosa cell differentiation and ovary maintenance. Development. 131(4):933-42.
Schneider DT, Janig U, Calaminus G, Gobel U, Harms D. 2003. Ovarian sex cord-stromal tumors--a clinicopathological study of 72 cases from the kiel pediatric tumor registry. Virchows Arch. 443(4):549-60.
Schofield DE, Fletcher JA. 1992. Trisomy 12 in pediatric granulosa-stromal cell tumors. demonstration by a modified method of fluorescence in situ hybridization on paraffin-embedded material. Am J Pathol. 141(6):1265-9.
Schrader KA, Gorbatcheva B, Senz J, Heravi-Moussavi A, Melnyk N, Salamanca C, Maines-Bandiera S, Cooke SL, Leung P, Brenton JD, *et al*. 2009. The specificity of the FOXL2 c.402C>G somatic mutation: A survey of solid tumors. PLoS One. 4(11):e7988.

Schultz KA, Pacheco MC, Yang J, Williams GM, Messinger Y, Hill DA, Dehner LP, Priest JR. 2011. Ovarian sex cord-stromal tumors, pleuropulmonary blastoma and DICER1 mutations: A report from the international pleuropulmonary blastoma registry. Gynecol Oncol. 122(2):246-50.
Schumer ST, Cannistra SA. 2003. Granulosa cell tumor of the ovary. J Clin Oncol. 21(6):1180-9.
Schwenk F, Baron U, Rajewsky K. 1995. A cre-transgenic mouse strain for the ubiquitous deletion of loxP-flanked gene segments including deletion in germ cells. Nucleic Acids Res. 23(24):5080-1.
Scully RE. 1987. Classification of human ovarian tumors. Environ Health Perspect. 73:15-25.
Scully RE, Young RH, Clement PB. 1998. Tumors of the ovary, maldeveloped gonads, fallopian tube, and broad ligament. 3rd ed. Washington DC: Armed Forces Institute of Pathology.
Seki Y, Hayashi K, Itoh K, Mizugaki M, Saitou M, Matsui Y. 2005. Extensive and orderly reprogramming of genome-wide chromatin modifications associated with specification and early development of germ cells in mice. Dev Biol. 278(2):440-58.
Seki Y, Yamaji M, Yabuta Y, Sano M, Shigeta M, Matsui Y, Saga Y, Tachibana M, Shinkai Y, Saitou M. 2007. Cellular dynamics associated with the genome-wide epigenetic reprogramming in migrating primordial germ cells in mice. Development. 134(14):2627-38.
Sekido R, Bar I, Narvaez V, Penny G, Lovell-Badge R. 2004. SOX9 is up-regulated by the transient expression of SRY specifically in sertoli cell precursors. Dev Biol. 274(2):271-9.
Sekido R, Lovell-Badge R. 2008. Sex determination involves synergistic action of SRY and SF1 on a specific Sox9 enhancer. Nature. 453(7197):930-4.
Sen A, Hammes SR. 2010. Granulosa cell-specific androgen receptors are critical regulators of ovarian development and function. Mol Endocrinol. 24(7):1393-403.
Sen A, Prizant H, Light A, Biswas A, Hayes E, Lee HJ, Barad D, Gleicher N, Hammes SR. 2014. Androgens regulate ovarian follicular development by increasing follicle stimulating hormone receptor and microRNA-125b expression. Proc Natl Acad Sci U S A. 111(8):3008-13.
Senapathy P, Shapiro MB, Harris NL. 1990. Splice junctions, branch point sites, and exons: Sequence statistics, identification, and applications to genome project. Methods Enzymol. 183:252-78.
Seong E, Insolera R, Dulovic M, Kamsteeg EJ, Trinh J, Bruggemann N, Sandford E, Li S, Ozel AB, Li JZ, *et al*. 2018. Mutations in VPS13D lead to a new recessive ataxia with spasticity and mitochondrial defects. Ann Neurol. 83(6):1075-88.
Shah SP, Köbel M, Senz J, Morin RD, Clarke BA, Wiegand KC, Leung G, Zayed A, Mehl E, Kalloger SE, *et al*. 2009. Mutation of FOXL2 in granulosa-cell tumors of the ovary. N Engl J Med. 360(26):2719-29.
Shashi V, Golden WL, von Kap C, Andersen WA, Gaffey MJ. 1994. Interphase fluorescence in situ hybridization for trisomy 12 on archival ovarian sex cord-stromal tumors. Gynecol Oncol. 55(3):349-54.
Shaw PA, Rouzbahman M, Pizer ES, Pintilie M, Begley H. 2009. Candidate serous cancer precursors in fallopian tube epithelium of BRCA1/2 mutation carriers. Mod Pathol. 22(9):1133-8.
Shen JH, Ingraham HA. 2002. Regulation of the orphan nuclear receptor steroidogenic factor 1 by sox proteins. Mol Endocrinol. 16(3):529-40.

Shen M, Liu Z, Li B, Teng Y, Zhang J, Tang Y, Sun SC, Liu H. 2014. Involvement of FoxO1 in the effects of follicle-stimulating hormone on inhibition of apoptosis in mouse granulosa cells. Cell Death Dis. 5:e1475.
Shen M, Jiang Y, Guan Z, Cao Y, Sun SC, Liu H. 2016. FSH protects mouse granulosa cells from oxidative damage by repressing mitophagy. Sci Rep. 6:38090.
Shen M, Jiang Y, Guan Z, Cao Y, Li L, Liu H, Sun SC. 2017. Protective mechanism of FSH against oxidative damage in mouse ovarian granulosa cells by repressing autophagy. Autophagy. 13(8):1364-85.
Sherry ST, Ward MH, Kholodov M, Baker J, Phan L, Smigielski EM, Sirotkin K. 2001. dbSNP: The NCBI database of genetic variation. Nucleic Acids Res. 29(1):308-11.
Shih I, Kurman RJ. 2004. Ovarian tumorigenesis: A proposed model based on morphological and molecular genetic analysis. Am J Pathol. 164(5):1511-8.
Shiina H, Matsumoto T, Sato T, Igarashi K, Miyamoto J, Takemasa S, Sakari M, Takada I, Nakamura T, Metzger D, *et al*. 2006. Premature ovarian failure in androgen receptor-deficient mice. Proc Natl Acad Sci U S A. 103(1):224-9.
Shou W, Woodruff TK, Matzuk MM. 1997. Role of androgens in testicular tumor development in inhibin-deficient mice. Endocrinology. 138(11):5000-5.
Sicinski P, Donaher JL, Geng Y, Parker SB, Gardner H, Park MY, Robker RL, Richards JS, McGinnis LK, Biggers JD, *et al*. 1996. Cyclin D2 is an FSH-responsive gene involved in gonadal cell proliferation and oncogenesis. Nature. 384(6608):470-4.
Sievers F, Wilm A, Dineen D, Gibson TJ, Karplus K, Li W, Lopez R, McWilliam H, Remmert M, Soding J, *et al*. 2011. Fast, scalable generation of high-quality protein multiple sequence alignments using clustal omega. Mol Syst Biol. 7:539.
Siiteri PK, Murai JT, Hammond GL, Nisker JA, Raymoure WJ, Kuhn RW. 1982. The serum transport of steroid hormones. Recent Prog Horm Res. 38:457-510.
Silver LM. 1995. Mouse genetics: Concepts and applications. New York: Oxford University Press.
Silverman LA, Gitelman SE. 1996. Immunoreactive inhibin, müllerian inhibitory substance, and activin as biochemical markers for juvenile granulosa cell tumors. J Pediatr. 129(6):918-21.
Sim NL, Kumar P, Hu J, Henikoff S, Schneider G, Ng PC. 2012. SIFT web server: Predicting effects of amino acid substitutions on proteins. Nucleic Acids Res. 40(Web Server issue):W452-7.
Simon AM, Goodenough DA, Li E, Paul DL. 1997. Female infertility in mice lacking connexin 37. Nature. 385(6616):525-9.
Simon MM, Mallon AM, Howell GR, Reinholdt LG. 2012. High throughput sequencing approaches to mutation discovery in the mouse. Mamm Genome. 23(9-10):499-513.
Simon MM, Greenaway S, White JK, Fuchs H, Gailus-Durner V, Wells S, Sorg T, Wong K, Bedu E, Cartwright EJ, *et al*. 2013. A comparative phenotypic and genomic analysis of C57BL/6J and C57BL/6N mouse strains. Genome Biol. 14(7):R82,2013-14-7-r82.
Sironi M, Menozzi G, Riva L, Cagliani R, Comi GP, Bresolin N, Giorda R, Pozzoli U. 2004. Silencer elements as possible inhibitors of pseudoexon splicing. Nucleic Acids Res. 32(5):1783-91.
Slomczyńska M, Duda M, Slęzak K. 2001. The expression of androgen receptor, cytochrome P450 aromatase and FSH receptor mRNA in the porcine ovary. Folia Histochem Cytobiol. 39(1):9-13.

Slomczyńska M, Tabarowski Z. 2001. Localization of androgen receptor and cytochrome P450 aromatase in the follicle and corpus luteum of the porcine ovary. Anim Reprod Sci. 65(1-2):127-34.
Smith JT, Clifton DK, Steiner RA. 2006. Regulation of the neuroendocrine reproductive axis by kisspeptin-GPR54 signaling. Reproduction. 131(4):623-30.
Smith JT, Popa SM, Clifton DK, Hoffman GE, Steiner RA. 2006. Kiss1 neurons in the forebrain as central processors for generating the preovulatory luteinizing hormone surge. J Neurosci. 26(25):6687-94.
Smith KN. 2011. Positional cloning of the *Gct1* granulosa cell tumour susceptibility locus in SWR inbred mice. Memorial University of Newfoundland.
Smith KN, Halfyard SJ, Yaskowiak ES, Shultz KL, Beamer WG, Dorward AM. 2013. Fine map of the *Gct1* spontaneous ovarian granulosa cell tumor locus. Mamm Genome. 24(1-2):63-71.
Smith P, Wilhelm D, Rodgers RJ. 2014. Development of mammalian ovary. J Endocrinol. 221(3):R145-61.
Smith CL, Blake JA, Kadin JA, Richardson JE, Bult CJ, Mouse Genome Database Group. 2018. Mouse genome database (MGD)-2018: Knowledgebase for the laboratory mouse. Nucleic Acids Res. 46(D1):D836-42.
Son DS, Arai KY, Roby KF, Terranova PF. 2004. Tumor necrosis factor alpha (TNF) increases granulosa cell proliferation: Dependence on c-jun and TNF receptor type 1. Endocrinology. 145(3):1218-26.
Soyal SM, Amleh A, Dean J. 2000. FIGalpha, a germ cell-specific transcription factor required for ovarian follicle formation. Development. 127(21):4645-54.
Spandidos A, Wang X, Wang H, Dragnev S, Thurber T, Seed B. 2008. A comprehensive collection of experimentally validated primers for polymerase chain reaction quantitation of murine transcript abundance. BMC Genomics. 9:633.
Spandidos A, Wang X, Wang H, Seed B. 2010. PrimerBank: A resource of human and mouse PCR primer pairs for gene expression detection and quantification. Nucleic Acids Res. 38(Database issue):D792-9.
Spears N, Murray AA, Allison V, Boland NI, Gosden RG. 1998. Role of gonadotrophins and ovarian steroids in the development of mouse follicles in vitro. J Reprod Fertil. 113(1):19-26.
Sprang SR. 1997. G protein mechanisms: Insights from structural analysis. Annu Rev Biochem. 66:639-78.
Stallock J, Molyneaux K, Schaible K, Knudson CM, Wylie C. 2003. The pro-apoptotic gene bax is required for the death of ectopic primordial germ cells during their migration in the mouse embryo. Development. 130(26):6589-97.
Steffensen LL, Ernst EH, Amoushahi M, Ernst E, Lykke-Hartmann K. 2018. Transcripts encoding the androgen receptor and IGF-related molecules are differently expressed in human granulosa cells from primordial and primary follicles. Front Cell Dev Biol. 6:85.
Stocco DM, Clark BJ. 1996. Regulation of the acute production of steroids in steroidogenic cells. Endocr Rev. 17(3):221-44.
Stocco C, Telleria C, Gibori G. 2007. The molecular control of corpus luteum formation, function, and regression. Endocr Rev. 28(1):117-49.

Su YQ, Wigglesworth K, Pendola FL, O'Brien MJ, Eppig JJ. 2002. Mitogen-activated protein kinase activity in cumulus cells is essential for gonadotropin-induced oocyte meiotic resumption and cumulus expansion in the mouse. Endocrinology. 143(6):2221-32.
Su YQ, Wu X, O'Brien MJ, Pendola FL, Denegre JN, Matzuk MM, Eppig JJ. 2004a. Synergistic roles of BMP15 and GDF9 in the development and function of the oocyte-cumulus cell complex in mice: Genetic evidence for an oocyte-granulosa cell regulatory loop. Dev Biol. 276(1):64-73.
Su AI, Wiltshire T, Batalov S, Lapp H, Ching KA, Block D, Zhang J, Soden R, Hayakawa M, Kreiman G, *et al*. 2004b. A gene atlas of the mouse and human protein-encoding transcriptomes. Proc Natl Acad Sci U S A. 101(16):6062-7.
Sugimoto M, Abe K. 2007. X chromosome reactivation initiates in nascent primordial germ cells in mice. PLoS Genet. 3(7):e116.
Suzuki T, Sasano H, Kimura N, Tamura M, Fukaya T, Yajima A, Nagura H. 1994. Immunohistochemical distribution of progesterone, androgen and oestrogen receptors in the human ovary during the menstrual cycle: Relationship to expression of steroidogenic enzymes. Hum Reprod. 9(9):1589-95.
Suzuki H, Tsuda M, Kiso M, Saga Y. 2008. Nanos3 maintains the germ cell lineage in the mouse by suppressing both bax-dependent and -independent apoptotic pathways. Dev Biol. 318(1):133-42.
Swain A, Narvaez V, Burgoyne P, Camerino G, Lovell-Badge R. 1998. Dax1 antagonizes sry action in mammalian sex determination. Nature. 391(6669):761-7.
Sybert VP, McCauley E. 2004. Turner's syndrome. N Engl J Med. 351(12):1227-38.
Szoltys M, Slomczyńska M. 2000. Changes in distribution of androgen receptor during maturation of rat ovarian follicles. Exp Clin Endocrinol Diabetes. 108(3):228-34.
Takasawa K, Kashimada K, Pelosi E, Takagi M, Morio T, Asahara H, Schlessinger D, Mizutani S, Koopman P. 2014. FOXL2 transcriptionally represses Sf1 expression by antagonizing WT1 during ovarian development in mice. Faseb j. 28(5):2020-8.
Taketo T, Merchant-Larios H, Koide SS. 1984. Induction of testicular differentiation in the fetal mouse ovary by transplantation into adult male mice. Proc Soc Exp Biol Med. 176(2):148-53.
Taketo T, Merchant-Larios H. 1986. Gonadal sex reversal of fetal mouse ovaries following transplantation into adult mice. Prog Clin Biol Res. 217A:171-4.
Tam PP, Snow MH. 1981. Proliferation and migration of primordial germ cells during compensatory growth in mouse embryos. J Embryol Exp Morphol. 64:133-47.
Tanaka T, Kato T, Ohmichi M. 2012. Granulosa cell tumor of the ovary after long-term use of tamoxifen and toremifene. J Obstet Gynaecol Res. 38(12):1379-84.
Tanaka SS, Nakane A, Yamaguchi YL, Terabayashi T, Abe T, Nakao K, Asashima M, Steiner KA, Tam PP, Nishinakamura R. 2013. Dullard/Ctdnep1 modulates WNT signalling activity for the formation of primordial germ cells in the mouse embryo. PLoS One. 8(3):e57428.
Tartaglia LA, Pennica D, Goeddel DV. 1993. Ligand passing: The 75-kDa tumor necrosis factor (TNF) receptor recruits TNF for signaling by the 55-kDa TNF receptor. J Biol Chem. 268(25):18542-8.
Tarumi W, Tsukamoto S, Okutsu Y, Takahashi N, Horiuchi T, Itoh MT, Ishizuka B. 2012. Androstenedione induces abnormalities in morphology and function of developing oocytes, which impairs oocyte meiotic competence. Fertil Steril. 97(2):469-76.

Tavassoli FA, Mooney E, Gersell DJ, McCluggage WG, Konishi I, Fujii S, Kiyokawa T, Schwartz P, Kubik-Huch RA, Roth LM. 2003. Sex cord-stromal tumours. In: Pathology and genetics of tumours of the breast and female genital organs. Tassavoli FA, Devilee P, editors. Lyon: IARC.
Tennent BJ, Shultz KL, Sundberg JP, Beamer WG. 1990. Ovarian granulosa cell tumorigenesis in SWR-derived F1 hybrid mice: Preneoplastic follicular abnormality and malignant disease progression. Am J Obstet Gynecol. 163(2):625-34.
Tennent BJ, Shultz KL, Beamer WG. 1993. Genetic susceptibility for C19 androgen induction of ovarian granulosa cell tumorigenesis in SWXJ strains of mice. Cancer Res. 53(5):1059-63.
Terranova PF. 1997. Potential roles of tumor necrosis factor-alpha in follicular development, ovulation, and the life span of the corpus luteum. Domest Anim Endocrinol. 14(1):1-15.
Thayer KA, Foster PM. 2007. Workgroup report: National toxicology program workshop on hormonally induced reproductive tumors - relevance of rodent bioassays. Environ Health Perspect. 115(9):1351-6.
The Rotterdam ESHRE/ASRM-sponsored PCOS consensus workshop group. 2004. Revised 2003 consensus on diagnostic criteria and long-term health risks related to polycystic ovary syndrome (PCOS). Hum Reprod. 19(1):41-7.
Till A, Rosenstiel P, Krippner-Heidenreich A, Mascheretti-Croucher S, Croucher PJ, Schafer H, Scheurich P, Seegert D, Schreiber S. 2005. The met-196 -> arg variation of human tumor necrosis factor receptor 2 (TNFR2) affects TNF-alpha-induced apoptosis by impaired NF-kappaB signaling and target gene expression. J Biol Chem. 280(7):5994-6004.
Tillmann T, Kamino K, Mohr U. 2000. Incidence and spectrum of spontaneous neoplasms in male and female CBA/J mice. Exp Toxicol Pathol. 52(3):221-5.
Toda K, Takeda K, Okada T, Akira S, Saibara T, Kaname T, Yamamura K, Onishi S, Shizuta Y. 2001. Targeted disruption of the aromatase P450 gene (Cyp19) in mice and their ovarian and uterine responses to 17beta-oestradiol. J Endocrinol. 170(1):99-111.
Todeschini AL, Dipietromaria A, L'hote D, Boucham FZ, Georges AB, Pandaranayaka PJ, Krishnaswamy S, Rivals I, Bazin C, Veitia RA. 2011. Mutational probing of the forkhead domain of the transcription factor FOXL2 provides insights into the pathogenicity of naturally occurring mutations. Hum Mol Genet. 20(17):3376-85.
Tomaselli S, Megiorni F, De Bernardo C, Felici A, Marrocco G, Maggiulli G, Grammatico B, Remotti D, Saccucci P, Valentini F, *et al*. 2008. Syndromic true hermaphroditism due to an R-spondin1 (RSPO1) homozygous mutation. Hum Mutat. 29(2):220-6.
Tomizuka K, Horikoshi K, Kitada R, Sugawara Y, Iba Y, Kojima A, Yoshitome A, Yamawaki K, Amagai M, Inoue A, *et al*. 2008. R-spondin1 plays an essential role in ovarian development through positively regulating wnt-4 signaling. Hum Mol Genet. 17(9):1278-91.
Tone AA. 2017. Taking the tube: From normal fallopian tube epithelium to ovarian high-grade serous carcinoma. Clin Obstet Gynecol. 60(4):697-710.
Tremblay KD, Dunn NR, Robertson EJ. 2001. Mouse embryos lacking Smad1 signals display defects in extra-embryonic tissues and germ cell formation. Development. 128(18):3609-21.
Trombly DJ, Woodruff TK, Mayo KE. 2009. Suppression of notch signaling in the neonatal mouse ovary decreases primordial follicle formation. Endocrinology. 150(2):1014-24.
Truman AM, Tilly JL, Woods DC. 2017. Ovarian regeneration: The potential for stem cell contribution in the postnatal ovary to sustained endocrine function. Mol Cell Endocrinol. 445:74-84.

Tsuda M, Sasaoka Y, Kiso M, Abe K, Haraguchi S, Kobayashi S, Saga Y. 2003. Conserved role of nanos proteins in germ cell development. Science. 301(5637):1239-41.
Turner OC, Keefe RG, Sugawara I, Yamada H, Orme IM. 2003. SWR mice are highly susceptible to pulmonary infection with mycobacterium tuberculosis. Infect Immun. 71(9):5266-72.
Uda M, Ottolenghi C, Crisponi L, Garcia JE, Deiana M, Kimber W, Forabosco A, Cao A, Schlessinger D, Pilia G. 2004. Foxl2 disruption causes mouse ovarian failure by pervasive blockage of follicle development. Hum Mol Genet. 13(11):1171-81.
Ueno S, Maruki Y, Nakamura M, Tomemori Y, Kamae K, Tanabe H, Yamashita Y, Matsuda S, Kaneko S, Sano A. 2001. The gene encoding a newly discovered protein, chorein, is mutated in chorea-acanthocytosis. Nat Genet. 28(2):121-2.
Uhlenhaut NH, Jakob S, Anlag K, Eisenberger T, Sekido R, Kress J, Treier AC, Klugmann C, Klasen C, Holter NI, *et al*. 2009. Somatic sex reprogramming of adult ovaries to testes by FOXL2 ablation. Cell. 139(6):1130-42.
UniProt Consortium. 2019. UniProt: A worldwide hub of protein knowledge. Nucleic Acids Res. 47(D1):D506-15.
Untergasser A, Cutcutache I, Koressaar T, Ye J, Faircloth BC, Remm M, Rozen SG. 2012. Primer3--new capabilities and interfaces. Nucleic Acids Res. 40(15):e115.
Vainio S, Heikkila M, Kispert A, Chin N, McMahon AP. 1999. Female development in mammals is regulated by wnt-4 signalling. Nature. 397(6718):405-9.
van den Berg-Bakker CA, Hagemeijer A, Franken-Postma EM, Smit VT, Kuppen PJ, van Ravenswaay Claasen HH, Cornelisse CJ, Schrier PI. 1993. Establishment and characterization of 7 ovarian carcinoma cell lines and one granulosa tumor cell line: Growth features and cytogenetics. Int J Cancer. 53(4):613-20.
van der Heul-Nieuwenhuijsen L, Padmos RC, Drexhage RC, de Wit H, Berghout A, Drexhage HA. 2010. An inflammatory gene-expression fingerprint in monocytes of autoimmune thyroid disease patients. J Clin Endocrinol Metab. 95(4):1962-71.
van Meurs HS, van Lonkhuijzen LR, Limpens J, van der Velden J, Buist MR. 2014. Hormone therapy in ovarian granulosa cell tumors: A systematic review. Gynecol Oncol. 134(1):196-205.
Vang R, Herrmann ME, Tavassoli FA. 2004. Comparative immunohistochemical analysis of granulosa and sertoli components in ovarian sex cord-stromal tumors with mixed differentiation: Potential implications for derivation of sertoli differentiation in ovarian tumors. Int J Gynecol Pathol. 23(2):151-61.
Varani S, Elvin JA, Yan C, DeMayo J, DeMayo FJ, Horton HF, Byrne MC, Matzuk MM. 2002. Knockout of pentraxin 3, a downstream target of growth differentiation factor-9, causes female subfertility. Mol Endocrinol. 16(6):1154-67.
Varma G, Varma R, Huang H, Pryshchepava A, Groth J, Fleming D, Nowak NJ, McQuaid D, Conroy J, Mahoney M, *et al*. 2005. Array comparative genomic hybridisation (aCGH) analysis of premenopausal breast cancers from a nuclear fallout area and matched cases from western new york. Br J Cancer. 93(6):699-708.
Vassal G, Flamant F, Caillaud JM, Demeocq F, Nihoul-Fekete C, Lemerle J. 1988. Juvenile granulosa cell tumor of the ovary in children: A clinical study of 15 cases. J Clin Oncol. 6(6):990-5.
Velayos-Baeza A, Vettori A, Copley RR, Dobson-Stone C, Monaco AP. 2004. Analysis of the human VPS13 gene family. Genomics. 84(3):536-49.

Veldhuis JD. 1988. Follicle-stimulating hormone regulates low density lipoprotein metabolism by swine granulosa cells. Endocrinology. 123(3):1660-7.
Vendola KA, Zhou J, Adesanya OO, Weil SJ, Bondy CA. 1998. Androgens stimulate early stages of follicular growth in the primate ovary. J Clin Invest. 101(12):2622-9.
Vendola K, Zhou J, Wang J, Famuyiwa OA, Bievre M, Bondy CA. 1999. Androgens promote oocyte insulin-like growth factor I expression and initiation of follicle development in the primate ovary. Biol Reprod. 61(2):353-7.
Vidal VP, Chaboissier MC, de Rooij DG, Schedl A. 2001. Sox9 induces testis development in XX transgenic mice. Nat Genet. 28(3):216-7.
Vincent SD, Dunn NR, Sciammas R, Shapiro-Shalef M, Davis MM, Calame K, Bikoff EK, Robertson EJ. 2005. The zinc finger transcriptional repressor Blimp1/Prdm1 is dispensable for early axis formation but is required for specification of primordial germ cells in the mouse. Development. 132(6):1315-25.
Visser JA. 2003. AMH signaling: From receptor to target gene. Mol Cell Endocrinol. 211(1-2):65-73.
Visser JA, de Jong FH, Laven JS, Themmen AP. 2006. Anti-mullerian hormone: A new marker for ovarian function. Reproduction. 131(1):1-9.
Wagner T, Wirth J, Meyer J, Zabel B, Held M, Zimmer J, Pasantes J, Bricarelli FD, Keutel J, Hustert E, *et al*. 1994. Autosomal sex reversal and campomelic dysplasia are caused by mutations in and around the SRY-related gene SOX9. Cell. 79(6):1111-20.
Wagner EJ, Garcia-Blanco MA. 2001. Polypyrimidine tract binding protein antagonizes exon definition. Mol Cell Biol. 21(10):3281-8.
Wahl EC, Aronson J, Liu L, Fowlkes JL, Thrailkill KM, Bunn RC, Skinner RA, Miller MJ, Cockrell GE, Clark LM, *et al*. 2010a. Restoration of regenerative osteoblastogenesis in aged mice: Modulation of TNF. J Bone Miner Res. 25(1):114-23.
Wahl EC, Aronson J, Liu L, Skinner RA, Miller MJ, Cockrell GE, Fowlkes JL, Thrailkill KM, Bunn RC, Ronis MJ, *et al*. 2010b. Direct bone formation during distraction osteogenesis does not require TNFalpha receptors and elevated serum TNFalpha fails to inhibit bone formation in TNFR1 deficient mice. Bone. 46(2):410-7.
Waldstreicher J, Santoro NF, Hall JE, Filicori M, Crowley WF,Jr. 1988. Hyperfunction of the hypothalamic-pituitary axis in women with polycystic ovarian disease: Indirect evidence for partial gonadotroph desensitization. J Clin Endocrinol Metab. 66(1):165-72.
Wallach D, Engelmann H, Nophar Y, Aderka D, Kemper O, Hornik V, Holtmann H, Brakebusch C. 1991. Soluble and cell surface receptors for tumor necrosis factor. Agents Actions Suppl. 35:51-7.
Walters KA, Allan CM, Jimenez M, Lim PR, Davey RA, Zajac JD, Illingworth P, Handelsman DJ. 2007. Female mice haploinsufficient for an inactivated androgen receptor (AR) exhibit age-dependent defects that resemble the AR null phenotype of dysfunctional late follicle development, ovulation, and fertility. Endocrinology. 148(8):3674-84.
Walters KA, Allan CM, Handelsman DJ. 2008. Androgen actions and the ovary. Biol Reprod. 78(3):380-9.
Walters KA, McTavish KJ, Seneviratne MG, Jimenez M, McMahon AC, Allan CM, Salamonsen LA, Handelsman DJ. 2009. Subfertile female androgen receptor knockout mice exhibit defects in neuroendocrine signaling, intraovarian function, and uterine development but not uterine function. Endocrinology. 150(7):3274-82.

Walters KA, Middleton LJ, Joseph SR, Hazra R, Jimenez M, Simanainen U, Allan CM, Handelsman DJ. 2012. Targeted loss of androgen receptor signaling in murine granulosa cells of preantral and antral follicles causes female subfertility. Biol Reprod. 87(6):151.
Walters KA, Handelsman DJ. 2018. Role of androgens in the ovary. Mol Cell Endocrinol. 465:36-47.
Wan Y, Larson DR. 2018. Splicing heterogeneity: Separating signal from noise. Genome Biol. 19(1):86,018-1467-4.
Wang ZJ, Churchman M, Campbell IG, Xu WH, Yan ZY, McCluggage WG, Foulkes WD, Tomlinson IP. 1999. Allele loss and mutation screen at the peutz-jeghers (LKB1) locus (19p13.3) in sporadic ovarian tumours. Br J Cancer. 80(1-2):70-2.
Wang H, Andoh K, Hagiwara H, Xiaowei L, Kikuchi N, Abe Y, Yamada K, Fatima R, Mizunuma H. 2001. Effect of adrenal and ovarian androgens on type 4 follicles unresponsive to FSH in immature mice. Endocrinology. 142(11):4930-6.
Wang Y, Asselin E, Tsang BK. 2002. Involvement of transforming growth factor alpha in the regulation of rat ovarian X-linked inhibitor of apoptosis protein expression and follicular growth by follicle-stimulating hormone. Biol Reprod. 66(6):1672-80.
Wang X, Seed B. 2003. A PCR primer bank for quantitative gene expression analysis. Nucleic Acids Res. 31(24):e154.
Wang Z, Niu W, Wang Y, Teng Z, Wen J, Xia G, Wang C. 2015a. Follistatin288 regulates germ cell cyst breakdown and primordial follicle assembly in the mouse ovary. PLoS One. 10(6):e0129643.
Wang F, Pan J, Liu Y, Meng Q, Lv P, Qu F, Ding GL, Klausen C, Leung PC, Chan HC, *et al*. 2015b. Alternative splicing of the androgen receptor in polycystic ovary syndrome. Proc Natl Acad Sci U S A. 112(15):4743-8.
Wang RS, Chang HY, Kao SH, Kao CH, Wu YC, Yeh S, Tzeng CR, Chang C. 2015c. Abnormal mitochondrial function and impaired granulosa cell differentiation in androgen receptor knockout mice. Int J Mol Sci. 16(5):9831-49.
Wang H, Guo J, Jiang J, Wu W, Chang X, Zhou H, Li Z, Zhao J. 2017. New genes associated with rheumatoid arthritis identified by gene expression profiling. Int J Immunogenet. 44(3):107-13.
Wang S, Yu J, Jones JW, Pierzchalski K, Kane MA, Trainor PA, Xavier-Neto J, Moise AR. 2018. Retinoic acid signaling promotes the cytoskeletal rearrangement of embryonic epicardial cells. Faseb j. 32(7):3765-81.
Ware VC. 1982. The role of androgens in follicular development in the ovary. I. A quantitative analysis of oocyte ovulation. J Exp Zool. 222(2):155-67.
Watson RH, Roy WJJ, Davis M, Hitchcock A, Campbell IG. 1997. Loss of heterozygosity at the alpha-inhibin locus on chromosome 2q is not a feature of human granulosa cell tumors. Gynecol Oncol. 65(3):387-90.
Wayne CM, Fan HY, Cheng X, Richards JS. 2007. Follicle-stimulating hormone induces multiple signaling cascades: Evidence that activation of rous sarcoma oncogene, RAS, and the epidermal growth factor receptor are critical for granulosa cell differentiation. Mol Endocrinol. 21(8):1940-57.
Weaver DD, Norby AR, Rosenfeld JA, Proud VK, Spangler BE, Ming JE, Chisholm E, Zackai EH, Lee BH, Edelmann L, *et al*. 2015. Chromosome 1p36.22p36.21 duplications/triplication causes setleis syndrome (focal facial dermal dysplasia type III). Am J Med Genet A. 167A(5):1061-70.

Webb SJ, Geoghegan TE, Prough RA, Michael Miller KK. 2006. The biological actions of dehydroepiandrosterone involves multiple receptors. Drug Metab Rev. 38(1-2):89-116.
Weil SJ, Vendola K, Zhou J, Adesanya OO, Wang J, Okafor J, Bondy CA. 1998. Androgen receptor gene expression in the primate ovary: Cellular localization, regulation, and functional correlations. J Clin Endocrinol Metab. 83(7):2479-85.
Weil S, Vendola K, Zhou J, Bondy CA. 1999. Androgen and follicle-stimulating hormone interactions in primate ovarian follicle development. J Clin Endocrinol Metab. 84(8):2951-6.
Weitsman SR, Magoffin DA. 1995. Transforming growth factor-alpha inhibition of luteinizing hormone-stimulated androgen production by ovarian theca-interstitial cells: Mechanism of action. Endocrine. 3(6):415-20.
Welsh TH,Jr, Jia XC, Jones PB, Zhuang LZ, Hsueh AJ. 1984. Disparate effects of triphenylethylene antiestrogens on estrogen and progestin biosyntheses by cultured rat granulosa cells. Endocrinology. 115(4):1275-82.
Welt CK, Duran JM. 2014. Genetics of polycystic ovary syndrome. Semin Reprod Med. 32(3):177-82.
Wessalowski R, Spaar HJ, Pape H, Willers R, Harms D, Gobel U. 1995. Successful liver treatment of a juvenile granulosa cell tumor in a 4-year-old child by regional deep hyperthermia, systemic chemotherapy, and irradiation. Gynecol Oncol. 57(3):417-22.
Western PS, Miles DC, van den Bergen JA, Burton M, Sinclair AH. 2008. Dynamic regulation of mitotic arrest in fetal male germ cells. Stem Cells. 26(2):339-47.
Wijgerde M, Ooms M, Hoogerbrugge JW, Grootegoed JA. 2005. Hedgehog signaling in mouse ovary: Indian hedgehog and desert hedgehog from granulosa cells induce target gene expression in developing theca cells. Endocrinology. 146(8):3558-66.
Wilhelm D, Englert C. 2002. The wilms tumor suppressor WT1 regulates early gonad development by activation of Sf1. Genes Dev. 16(14):1839-51.
Wilhelm D, Hiramatsu R, Mizusaki H, Widjaja L, Combes AN, Kanai Y, Koopman P. 2007. SOX9 regulates prostaglandin D synthase gene transcription in vivo to ensure testis development. J Biol Chem. 282(14):10553-60.
Wilhelm D, Washburn LL, Truong V, Fellous M, Eicher EM, Koopman P. 2009. Antagonism of the testis- and ovary-determining pathways during ovotestis development in mice. Mech Dev. 126(5-6):324-36.
Will CL, Luhrmann R. 2011. Spliceosome structure and function. Cold Spring Harb Perspect Biol. 3(7):10.1101/cshperspect.a003707.
Willis D, Franks S. 1995. Insulin action in human granulosa cells from normal and polycystic ovaries is mediated by the insulin receptor and not the type-I insulin-like growth factor receptor. J Clin Endocrinol Metab. 80(12):3788-90.
Willis D, Mason H, Gilling-Smith C, Franks S. 1996. Modulation by insulin of follicle-stimulating hormone and luteinizing hormone actions in human granulosa cells of normal and polycystic ovaries. J Clin Endocrinol Metab. 81(1):302-9.
Wilson CM, McPhaul MJ. 1996. A and B forms of the androgen receptor are expressed in a variety of human tissues. Mol Cell Endocrinol. 120(1):51-7.
Witkowski L, Mattina J, Schonberger S, Murray MJ, Choong CS, Huntsman DG, Reis-Filho JS, McCluggage WG, Nicholson JC, Coleman N, *et al*. 2013. DICER1 hotspot mutations in non-epithelial gonadal tumours. Br J Cancer. 109(10):2744-50.

Wong GT. 2002. Speed congenics: Applications for transgenic and knock-out mouse strains. Neuropeptides. 36(2-3):230-6.
Wong JJ, Au AY, Ritchie W, Rasko JE. 2016. Intron retention in mRNA: No longer nonsense: Known and putative roles of intron retention in normal and disease biology. Bioessays. 38(1):41-9.
Woodruff TK, Shea LD. 2007. The role of the extracellular matrix in ovarian follicle development. Reprod Sci. 14(8 Suppl):6-10.
Wu YQ, Heilstedt HA, Bedell JA, May KM, Starkey DE, McPherson JD, Shapira SK, Shaffer LG. 1999. Molecular refinement of the 1p36 deletion syndrome reveals size diversity and a preponderance of maternally derived deletions. Hum Mol Genet. 8(2):313-21.
Wu CH, Yang JG, Yang JJ, Lin YM, Tsai HD, Lin CY, Kuo PL. 2010. Androgen excess down-regulates connexin43 in a human granulosa cell line. Fertil Steril. 94(7):2938-41.
Wu S, Divall S, Nwaopara A, Radovick S, Wondisford F, Ko C, Wolfe A. 2014. Obesity-induced infertility and hyperandrogenism are corrected by deletion of the insulin receptor in the ovarian theca cell. Diabetes. 63(4):1270-82.
Xu H, Beasley MD, Warren WD, van der Horst GT, McKay MJ. 2005. Absence of mouse REC8 cohesin promotes synapsis of sister chromatids in meiosis. Dev Cell. 8(6):949-61.
Xu J, Gridley T. 2013. Notch2 is required in somatic cells for breakdown of ovarian germ-cell nests and formation of primordial follicles. BMC Biol. 11:13,7007-11-13.
Xu Y, Li X, Wang H, Xie P, Yan X, Bai Y, Zhang T. 2016. Hypermethylation of CDH13, DKK3 and FOXL2 promoters and the expression of EZH2 in ovary granulosa cell tumors. Mol Med Rep. 14(3):2739-45.
Xu HY, Zhang HX, Xiao Z, Qiao J, Li R. 2019. Regulation of anti-mullerian hormone (AMH) in males and the associations of serum AMH with the disorders of male fertility. Asian J Androl. 21(2):109-14.
Yabuta Y, Kurimoto K, Ohinata Y, Seki Y, Saitou M. 2006. Gene expression dynamics during germline specification in mice identified by quantitative single-cell gene expression profiling. Biol Reprod. 75(5):705-16.
Yalcin B, Wong K, Agam A, Goodson M, Keane TM, Gan X, Nellaker C, Goodstadt L, Nicod J, Bhomra A, *et al*. 2011. Sequence-based characterization of structural variation in the mouse genome. Nature. 477(7364):326-9.
Yamaguchi S, Kimura H, Tada M, Nakatsuji N, Tada T. 2005. Nanog expression in mouse germ cell development. Gene Expr Patterns. 5(5):639-46.
Yamaji M, Seki Y, Kurimoto K, Yabuta Y, Yuasa M, Shigeta M, Yamanaka K, Ohinata Y, Saitou M. 2008. Critical function of Prdm14 for the establishment of the germ cell lineage in mice. Nat Genet. 40(8):1016-22.
Yamamoto Y, Kuwahara A, Taniguchi Y, Yamasaki M, Tanaka Y, Mukai Y, Yamashita M, Matsuzaki T, Yasui T, Irahara M. 2015. Tumor necrosis factor alpha inhibits ovulation and induces granulosa cell death in rat ovaries. Reprod Med Biol. 14(3):107-15.
Yan C, Wang P, DeMayo J, DeMayo FJ, Elvin JA, Carino C, Prasad SV, Skinner SS, Dunbar BS, Dube JL, *et al*. 2001. Synergistic roles of bone morphogenetic protein 15 and growth differentiation factor 9 in ovarian function. Mol Endocrinol. 15(6):854-66.
Yang MY, Fortune JE. 2006. Testosterone stimulates the primary to secondary follicle transition in bovine follicles in vitro. Biol Reprod. 75(6):924-32.
Yang JL, Zhang CP, Li L, Huang L, Ji SY, Lu CL, Fan CH, Cai H, Ren Y, Hu ZY, *et al*. 2010. Testosterone induces redistribution of forkhead box-3a and down-regulation of growth and

differentiation factor 9 messenger ribonucleic acid expression at early stage of mouse folliculogenesis. Endocrinology. 151(2):774-82.
Yang L, Lin C, Jin C, Yang JC, Tanasa B, Li W, Merkurjev D, Ohgi KA, Meng D, Zhang J, *et al*. 2013. lncRNA-dependent mechanisms of androgen-receptor-regulated gene activation programs. Nature. 500(7464):598-602.
Yang M, Li J, An Y, Zhang S. 2015. Effects of androgen on immunohistochemical localization of androgen receptor and connexin 43 in mouse ovary. Tissue Cell. 47(5):526-32.
Yang S, Wang J, Brand DD, Zheng SG. 2018. Role of TNF-TNF receptor 2 signal in regulatory T cells and its therapeutic implications. Front Immunol. 9:784.
Yao HH, Whoriskey W, Capel B. 2002. Desert Hedgehog/Patched 1 signaling specifies fetal leydig cell fate in testis organogenesis. Genes Dev. 16(11):1433-40.
Yao HH, Matzuk MM, Jorgez CJ, Menke DB, Page DC, Swain A, Capel B. 2004. Follistatin operates downstream of Wnt4 in mammalian ovary organogenesis. Dev Dyn. 230(2):210-5.
Yazawa T, Kawabe S, Kanno M, Mizutani T, Imamichi Y, Ju Y, Matsumura T, Yamazaki Y, Usami Y, Kuribayashi M, *et al*. 2013. Androgen/androgen receptor pathway regulates expression of the genes for cyclooxygenase-2 and amphiregulin in periovulatory granulosa cells. Mol Cell Endocrinol. 369(1-2):42-51.
Ye J, Coulouris G, Zaretskaya I, Cutcutache I, Rozen S, Madden TL. 2012. Primer-BLAST: A tool to design target-specific primers for polymerase chain reaction. BMC Bioinformatics. 13:134,2105-13-134.
Yeh S, Tsai MY, Xu Q, Mu XM, Lardy H, Huang KE, Lin H, Yeh SD, Altuwaijri S, Zhou X, *et al*. 2002. Generation and characterization of androgen receptor knockout (ARKO) mice: An in vivo model for the study of androgen functions in selective tissues. Proc Natl Acad Sci U S A. 99(21):13498-503.
Yeo G, Burge CB. 2004. Maximum entropy modeling of short sequence motifs with applications to RNA splicing signals. J Comput Biol. 11(2-3):377-94.
Ying SY. 1988. Inhibins, activins, and follistatins: Gonadal proteins modulating the secretion of follicle-stimulating hormone. Endocr Rev. 9(2):267-93.
Ying Y, Liu XM, Marble A, Lawson KA, Zhao GQ. 2000. Requirement of Bmp8b for the generation of primordial germ cells in the mouse. Mol Endocrinol. 14(7):1053-63.
Ying Y, Zhao GQ. 2001. Cooperation of endoderm-derived BMP2 and extraembryonic ectoderm-derived BMP4 in primordial germ cell generation in the mouse. Dev Biol. 232(2):484-92.
Yoshida H, Takakura N, Kataoka H, Kunisada T, Okamura H, Nishikawa SI. 1997. Stepwise requirement of c-kit tyrosine kinase in mouse ovarian follicle development. Dev Biol. 184(1):122-37.
Yoshino O, McMahon HE, Sharma S, Shimasaki S. 2006. A unique preovulatory expression pattern plays a key role in the physiological functions of BMP-15 in the mouse. Proc Natl Acad Sci U S A. 103(28):10678-83.
Young RH, Welch WR, Dickersin GR, Scully RE. 1982. Ovarian sex cord tumor with annular tubules: Review of 74 cases including 27 with peutz-jeghers syndrome and four with adenoma malignum of the cervix. Cancer. 50(7):1384-402.
Young RH, Dickersin GR, Scully RE. 1984. Juvenile granulosa cell tumor of the ovary. A clinicopathological analysis of 125 cases. Am J Surg Pathol. 8(8):575-96.
Young RH. 2005. Sex cord-stromal tumors of the ovary and testis: Their similarities and differences with consideration of selected problems. Mod Pathol. 18 Suppl 2:S81-98.

Youngren KK, Coveney D, Peng X, Bhattacharya C, Schmidt LS, Nickerson ML, Lamb BT, Deng JM, Behringer RR, Capel B, *et al*. 2005. The ter mutation in the dead end gene causes germ cell loss and testicular germ cell tumours. Nature. 435(7040):360-4.
Yu M, Wang J, Liu W, Qin J, Zhou Q, Wang Y, Huang H, Chen W, Ma C. 2014. Effects of tamoxifen on the sex determination gene and the activation of sex reversal in the developing gonad of mice. Toxicology. 321:89-95.
Yu M, Liu W, Wang J, Qin J, Wang Y, Wang Y. 2015. Effects of tamoxifen on autosomal genes regulating ovary maintenance in adult mice. Environ Sci Pollut Res Int. 22(24):20234-44.
Yuan C, Gao C, Qian Y, Liu Y, Jiang SW, Cui Y, Liu J. 2015. Polymorphism of CAG and GGN repeats of androgen receptor gene in women with polycystic ovary syndrome. Reprod Biomed Online. 31(6):790-8.
Zachow RJ, Magoffin DA. 1995. Granulosa cell modulation of luteinizing hormone-dependent androgen production by ovarian theca-interstitial cells: A temporal switch from suppression to augmentation stimulated by follicle-stimulating hormone in vitro. Biol Reprod. 53(4):758-65.
Zachow RJ, Weitsman SR, Magoffin DA. 1997. Hepatocyte growth factor regulates ovarian theca-interstitial cell differentiation and androgen production. Endocrinology. 138(2):691-7.
Zannoni GF, Improta G, Petrillo M, Pettinato A, Scambia G, Fraggetta F. 2016. FOXL2 molecular status in adult granulosa cell tumors of the ovary: A study of primary and metastatic cases. Oncol Lett. 12(2):1159-63.
Zerbino DR, Achuthan P, Akanni W, Amode MR, Barrell D, Bhai J, Billis K, Cummins C, Gall A, Giron CG, *et al*. 2018. Ensembl 2018. Nucleic Acids Res. 46(D1):D754-61.
Zhang MQ. 1998. Statistical features of human exons and their flanking regions. Hum Mol Genet. 7(5):919-32.
Zhang H, Vollmer M, De Geyter M, Litzistorf Y, Ladewig A, Durrenberger M, Guggenheim R, Miny P, Holzgreve W, De Geyter C. 2000. Characterization of an immortalized human granulosa cell line (COV434). Mol Hum Reprod. 6(2):146-53.
Zhang H, Zhai Y, Hu Z, Wu C, Qian J, Jia W, Ma F, Huang W, Yu L, Yue W, *et al*. 2010. Genome-wide association study identifies 1p36.22 as a new susceptibility locus for hepatocellular carcinoma in chronic hepatitis B virus carriers. Nat Genet. 42(9):755-8.
Zhang H, Risal S, Gorre N, Busayavalasa K, Li X, Shen Y, Bosbach B, Brannstrom M, Liu K. 2014. Somatic cells initiate primordial follicle activation and govern the development of dormant oocytes in mice. Curr Biol. 24(21):2501-8.
Zhang Y, Xu Y, Kuai Y, Wang S, Xue Q, Shang J. 2016. Effect of testosterone on the Connexin37 of sexual mature mouse cumulus oocyte complex. J Ovarian Res. 9(1):82,016-0290-3.
Zhang S, Liu Y, Zheng Z, Zeng X, Liu D, Wang C, Ting K. 2018. MicroRNA-223 suppresses osteoblast differentiation by inhibiting DHRS3. Cell Physiol Biochem. 47(2):667-79.
Zhao H, Sun Z, Wang J, Huang H, Kocher JP, Wang L. 2014. CrossMap: A versatile tool for coordinate conversion between genome assemblies. Bioinformatics. 30(7):1006-7.
Zheng B, Fiumara P, Li YV, Georgakis G, Snell V, Younes M, Vauthey JN, Carbone A, Younes A. 2003. MEK/ERK pathway is aberrantly active in hodgkin disease: A signaling pathway shared by CD30, CD40, and RANK that regulates cell proliferation and survival. Blood. 102(3):1019-27.

Zheng W, Zhang H, Gorre N, Risal S, Shen Y, Liu K. 2014. Two classes of ovarian primordial follicles exhibit distinct developmental dynamics and physiological functions. Hum Mol Genet. 23(4):920-8.
Zhou J, Kumar TR, Matzuk MM, Bondy C. 1997. Insulin-like growth factor I regulates gonadotropin responsiveness in the murine ovary. Mol Endocrinol. 11(13):1924-33.
Zhu JQ, Zhu L, Liang XW, Xing FQ, Schatten H, Sun QY. 2010. Demethylation of LHR in dehydroepiandrosterone-induced mouse model of polycystic ovary syndrome. Mol Hum Reprod. 16(4):260-6.
Zlotogora J, Sagi M, Cohen T. 1983. The blepharophimosis, ptosis, and epicanthus inversus syndrome: Delineation of two types. Am J Hum Genet. 35(5):1020-7.
Zolfaghari R, Chen Q, Ross AC. 2012. DHRS3, a retinal reductase, is differentially regulated by retinoic acid and lipopolysaccharide-induced inflammation in THP-1 cells and rat liver. Am J Physiol Gastrointest Liver Physiol. 303(5):G578-88.
Zong H, Espinosa JS, Su HH, Muzumdar MD, Luo L. 2005. Mosaic analysis with double markers in mice. Cell. 121(3):479-92.

# 8. Appendices

## Appendix A: Statement of Co-Authorship and Contributions

Figure 2.8 is published in adapted form in Mammalian Genome (Smith *et al*. 2013; 24(1-2):63-71). I appear as first author, followed by Sarah Halfyard, Dr. Edward Yaskowiak, Kathryn Shultz, Dr. Wesley Beamer, and Dr. Ann Dorward. All work in this dissertation was completed by the author with the exception of the following contributions, which will be acknowledged by co-authorship on future manuscripts:

NGS Sample Preparation

The gDNA used in the NGS analysis of the *Gct1* interval was extracted from mouse kidneys and tested for integrity by Dr. Edward Yaskowiak, a Research Associate in the Dorward laboratory.

CNV Analysis

Kayleigh Maxwell, an undergraduate medical student at Memorial University of Newfoundland, conducted aCGH data analysis using Agilent Feature Extraction Software and Agilent Genomic Workbench Software as part of an Undergraduate Medical Student Research Project entitled “Copy Number Variation (CNV) Analysis in a Spontaneous Mouse Ovarian Tumour Model”.

AR Protein IHC Protocol

The AR protein IHC protocol was optimized by Elizabeth Chia, a Research Assistant in the Dorward laboratory.

**Appendix B: NGS quality metric definitions**

| Metric Name | Definition |
|---|---|
| Allele frequency (AF1) | Expectation maximization estimate of the site allele frequency of the strongest non-reference allele; AF1 values of 1 indicate homozygotes, whereas AF1 values < 1 indicate heterozygotes |
| Consensus quality | Positive consensus quality scores equal the Phred-scaled probability of there being two or more different alleles, whereas negative consensus quality scores equal the minus Phred-scaled probability of all chromosomes being identical; a positive consensus quality indicates heterozygotes, whereas a negative consensus quality indicates homozygotes |
| DP4 | The number of 1) forward reference alleles, 2) reverse reference alleles, 3) forward non-reference alleles, and 4) reverse non-reference alleles used in variant calling; the sum can be smaller than the read depth because low-quality bases are not counted |
| Genotype quality | The probability that the genotype call is wrong under the condition that the site is being variant |
| Mapping quality | The Phred-scaled probability of the alignment being correct |
| Read depth | The number of reads covering or bridging the position |

**Appendix C: *In silico* program prediction inputs and interpretations.** Score interpretations were retrieved from Jian, Boerwinkle & Liu 2014 or the respective program websites and/or references (Section 2.2.3.2). GRCh37: Genome Reference Consortium Human Build 37; GRCh38: Genome Reference Consortium Human Build 38

| Prediction Program Type | Program | Assembly Interrogated | Score Interpretation |
|---|---|---|---|
| Splice site | GeneSplicer | GRCh38 | Scores below the splice site threshold (0) are abolished/absent |
| | Human Splicing Finder | GRCh37 | Higher scores imply a more potential splice site; scores below the splice site threshold (65) are abolished/absent |
| | MaxEntScan | GRCh38 | Higher scores imply a higher probability of the sequence being a true splice site; scores below the splice site threshold (0) are abolished/absent |
| | NetGene2 | GRCh38 | Higher scores imply a higher confidence of a true splice site |
| | SpliceSiteFinder-like | GRCh38 | Scores below the splice site threshold (70) are abolished/absent |
| | SpliceView | GRCm38 | Higher scores imply a more similar splice site sequence with the consensus sequence |
| Splicing regulatory element | ESEFinder | GRCh38 | Scores below the binding threshold (SRSF1: 1.956; SRSF2: 2.383; SRSF5: 2.670) are abolishsed/absent |
| | Branch points | GRCh37 | Scores below the branch point threshold (67) are abolished/absent |
| | hnRNP motifs | GRCh37 | Scores below the binding threshold (65.476) are abolished/absent |
| | Silencer motifs | GRCh37 | Scores below the binding threshold (60) are abolished/absent |
| Non-coding | CADD | GRCh38 | Scores between 10 to 20 are between the 1% and 10% most deleterious possible substitutions in the human genome |
| | *FATHMM-XF* | GRCh38 | Scores greater than 0.5 are pathogenic; scores closest to the extremes (0 or 1) are the highest confidence predictions that yield the highest accuracy |
| | PhD-SNP[g] | GRCh37 | Scores greater than 0.5 are pathogenic |

**Appendix D: Intronic candidate gene variants and their quality metrics.** Variants in red text were not pursued as they did not meet the minimum requirements for empirical validation.

| Gene | Location on Chr 4 (bp) | Reference Allele | Alternate Allele | Number of Samples | Average Read Depth | Average DP4 | Average Genotype Quality | Average Mapping Quality | Average Consensus Quality |
|---|---|---|---|---|---|---|---|---|---|
| *Dhrs3* | 144,895,554 | A | G | 3 | 25.7X | 0,0,13,10 | 171 | 43.7 | -96.0 |
| | 144,895,848 | AC | ACGC | 2 | 5.5X | 0,0,0,2.5 | 15.0 | 25.0 | -42.0 |
| | 144,895,920 | A | G | 2 | 13.5X | 2.5,0,7.5,0 | 73.1 | 28.5 | -14.0 |
| | 144,895,922 | A | G | 2 | 13.5X | 2.5,0,7.5,0 | 72.1 | 28.5 | -13.0 |
| | 144,895,928 | A | G | 2 | 19.0X | 3,0,7.5,0 | 73.5 | 28.5 | -7.0 |
| | 144,895,936 | A | G | 3 | 15.0X | 2.3,0,8,0 | 59.4 | 28.7 | -12.4 |
| | 144,898,026 | C | T | 3 | 50.3X | 0,0,31.7,17.3 | 222.0 | 60.0 | -174.3 |
| | 144,899,520 | G | A | 3 | 37.0X | 0,0,15,21 | 149.3 | 59.7 | -135.0 |
| | 144,900,470 | T | C | 3 | 39.3X | 0,0,18,19.7 | 222.0 | 58.0 | -140.0 |
| | 144,900,669 | GAGAAGAAGAAG | GAGAAGAAGAAGAAG | 2 | 9.5X | 0,0,5,2.5 | 122.3 | 46.0 | -57.0 |
| | 144,901,872 | G | A | 3 | 68.3X | 0,0,28.3,31.7 | 192.0 | 59.7 | -208.0 |
| | 144,902,233 | G | A | 3 | 38.7X | 0,0,21,14.7 | 177.0 | 60.0 | -134.0 |
| | 144,910,330 | C | T | 3 | 19.3X | 0,0,10.3,8 | 126.0 | 60.0 | -82.0 |
| | 144,917,378 | G | C | 3 | 47.7X | 0,0,17,30 | 222.0 | 60.0 | -168.3 |
| | 144,919,838 | C | T | 3 | 65.3X | 0.7,0.3,37.3,26.3 | 203.3 | 60.0 | -185.3 |
| *Vps13d* | 145,008,075 | G | T | 3 | 13.0X | 0,0,3.3,9.3 | 213.0 | 60.0 | -65.0 |
| | 145,018,055 | TCCC | TCC | 2 | 29.5X | 0,0,0.5,2 | 32.4 | 60.0 | -42.0 |

| Gene | Location on Chr 4 (bp) | Reference Allele | Alternate Allele | Number of Samples | Average Read Depth | Average DP4 | Average Genotype Quality | Average Mapping Quality | Average Consensus Quality |
|---|---|---|---|---|---|---|---|---|---|
| | 145,027,494 | T | TTCCTGGCAGATGATTGGTGGCTGTGTGTGG | 1 | 20.0X | 0,0,4,0 | 41.0 | 27.0 | -46.5 |
| | 145,044,633 | A | ACT | 1 | 2.0X | 0,0,0,2 | 14.4 | 29.0 | -40.5 |
| | 145,071,222 | C | T | 3 | 27.3X | 0,0,10,16.7 | 222.0 | 58.3 | -107.0 |
| | 145,089,880 | TG | T | 1 | 6.0X | 0,0,1,1 | 4.91 | 29.0 | -40.5 |
| | 145,111,456 | G | A | 1 | 6.0X | 0,0,0,3 | 20.0 | 29.0 | -36.0 |
| | 145,111,460 | G | A | 1 | 4.0X | 0,0,0,3 | 11.1 | 29.0 | -33.0 |
| | 145,111,462 | G | A | 1 | 4.0X | 0,0,0,2 | 11.1 | 29.0 | -33.0 |
| | 145,111,464 | G | A | 1 | 4.0X | 0,0,0,2 | 9.31 | 29.0 | -33.0 |
| | 145,115,338 | AG | A | 1 | 6.0X | 0,0,3,0 | 5.77 | 60.0 | -43.5 |
| | 145,129,450 | GAA | GA | 1 | 6.0X | 0,0,0,3 | 30.4 | 42.0 | -43.5 |
| | 145,166,463 | T | C | 3 | 7.7X | 0,0,4.3,3 | 135.5 | 37.0 | -49.0 |
| *Tnfrsf1b* | 145,237,143 | C | T | 3 | 33.3X | 0,0,16.3,15.3 | 222.0 | 59.3 | -122.0 |
| *Tnfrsf8* | 145,282,619 | AGG | AG | 1 | 6.0X | 0,0,2,0 | 23.2 | 60.0 | -40.5 |
| | 145,282,758 | G | T | 3 | 17.7X | 0,0,10.3,10.3 | 176.0 | 54.0 | -79.0 |
| | 145,308,667 | G | T | 3 | 10.0X | 0,0,6.3,3.7 | 120.7 | 58.3 | -57.0 |

**Appendix E: aCGH metric value ranges and definitions**

| Metric Name | Value Range | | | Definition |
|---|---|---|---|---|
| | Excellent | Good | Evaluate | |
| IsGoodGrid | > 1 | NA | < 1 | Tracks the automatic grid-finding of Feature Extraction |
| AnyColorPrcntFeatNonUnifOL | < 1 | 1 to 5 | > 5 | The percentage of features that are feature non-uniformity outliers in either channel |
| DerivativeL_R_Spread | < 0.20 | 0.20 to 0.30 | > 0.30 | The standard deviation of the probe-to-probe difference of the log ratios; smaller values indicate less noise in the biological samples |
| gRepro | 0 to 0.05 | 0.05 to 0.20 | < 0 or > 0.20 | The probes of replicates used to calculate a variation coefficient for the green channel |
| g_BGNoise | < 5 | 5 to 15 | >15 | The standard deviation of the signals on the negative controls for the green channel; an estimate of the background noise of the signal |
| g_Signal2Noise | > 100 | 30 to 100 | <30 | The ratio of signal intensity to background noise for the green channel |
| g_SignalIntensity | > 150 | 50 to 150 | <50 | The relative intensity of the signal produced by probes for the green channel |
| rRepro | 0 to 0.05 | 0.05 to 0.20 | < 0 or > 0.20 | The probes of replicates used to calculate a variation coefficient for the red channel |
| r_BGNoise | < 5 | 5 to 15 | > 15 | The standard deviation of the signals on the negative controls for the red channel; an estimate of the background noise of the signal |
| r_Signal2Noise | > 100 | 30 to 100 | < 30 | The ratio of signal intensity to background noise for the red channel |
| r_SignalIntensity | > 150 | 50 to 150 | < 50 | The relative intensity of the signal produced by probes for the red channel |
| LogRatioImbalance | -0.26 to 0.26 | -0.75 to -0.26; 0.26 to 0.75 | < -0.75 or > 0.75 | Calculates the amount of amplifications versus deletions per chromosome to determine if there is an imbalance that falls out of normal expectations |

**Appendix F: Body weight and body weight-relative organ weights of mice at necropsy following *in vivo* functional analyses.** Data is presented as mean ± SEM.

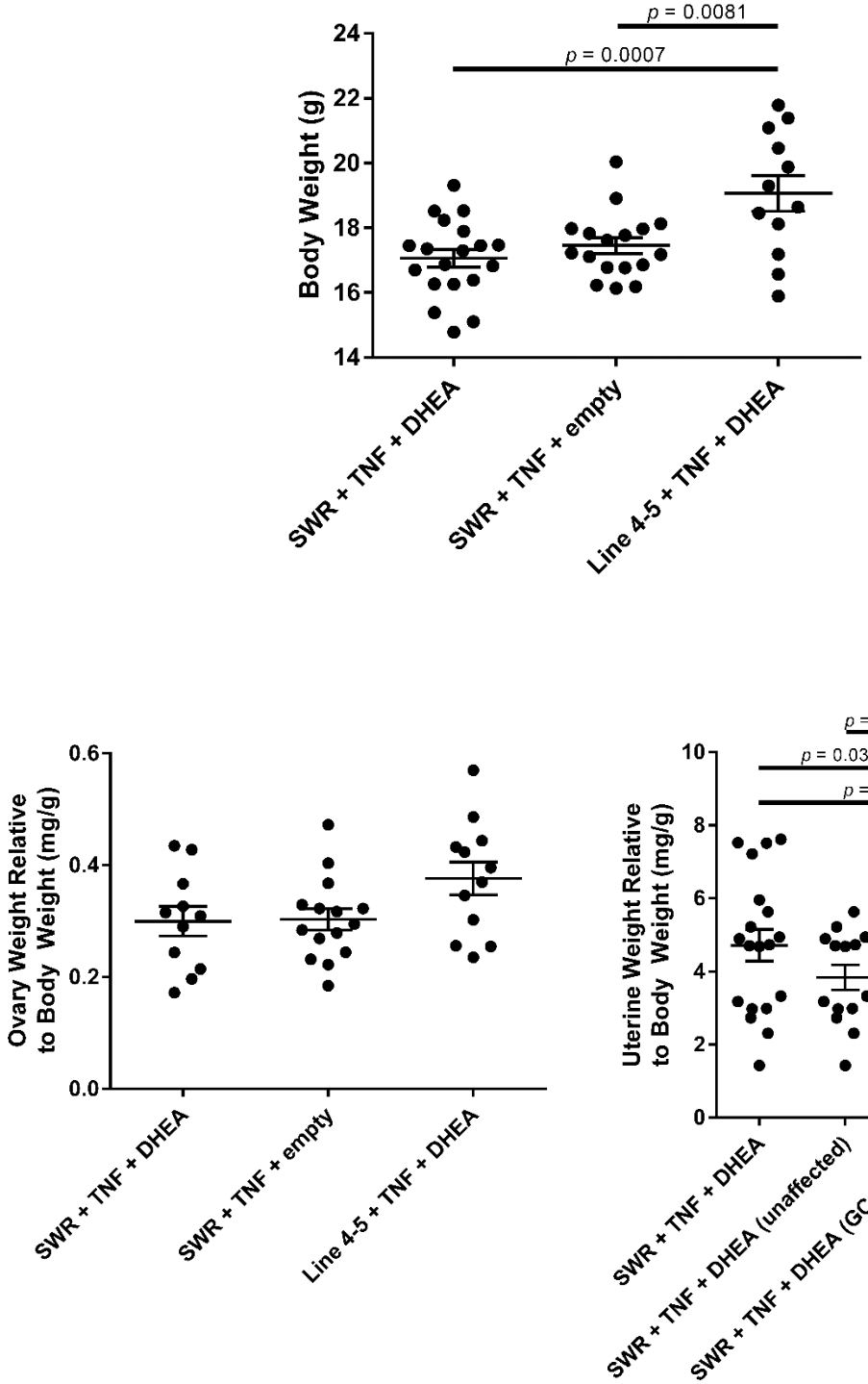

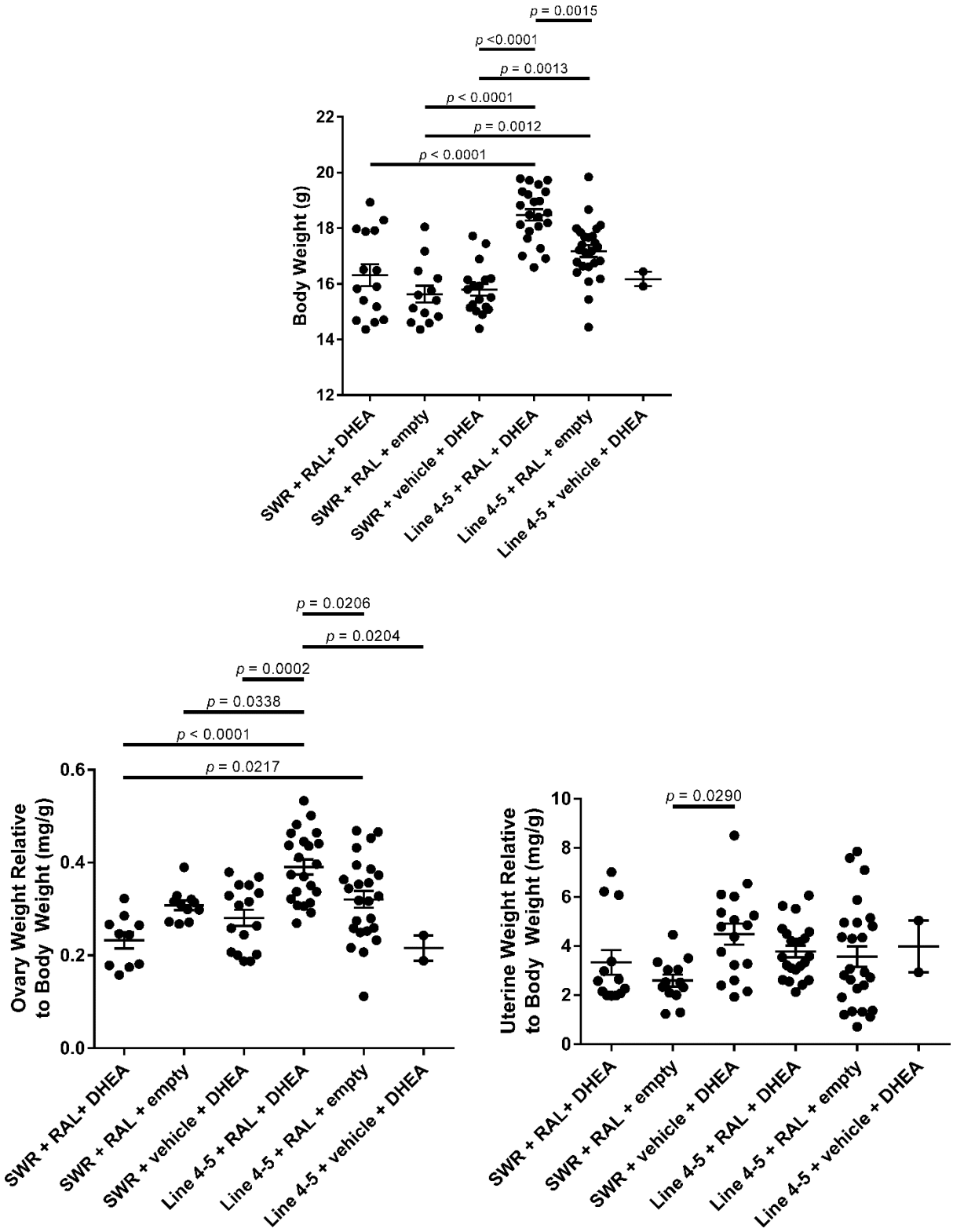
p = 0.0015
p <0.0001
p = 0.0013
p < 0.0001
p = 0.0012
p < 0.0001
Body Weight (g)
22
20
18
16
14
12
SWR + RAL+ DHEA
SWR + RAL + empty
SWR + vehicle + DHEA
Line 4-5 + RAL + DHEA
Line 4-5 + RAL + empty
Line 4-5 + vehicle + DHEA
p = 0.0206
p = 0.0204
p = 0.0002
p = 0.0338
p < 0.0001
p = 0.0217
Ovary Weight Relative to Body Weight (mg/g)
0.6
0.4
0.2
0.0
SWR + RAL+ DHEA
SWR + RAL + empty
SWR + vehicle + DHEA
Line 4-5 + RAL + DHEA
Line 4-5 + RAL + empty
Line 4-5 + vehicle + DHEA
p = 0.0290
Uterine Weight Relative to Body Weight (mg/g)
10
8
6
4
2
0
SWR + RAL+ DHEA
SWR + RAL + empty
SWR + vehicle + DHEA
Line 4-5 + RAL + DHEA
Line 4-5 + RAL + empty
Line 4-5 + vehicle + DHEA

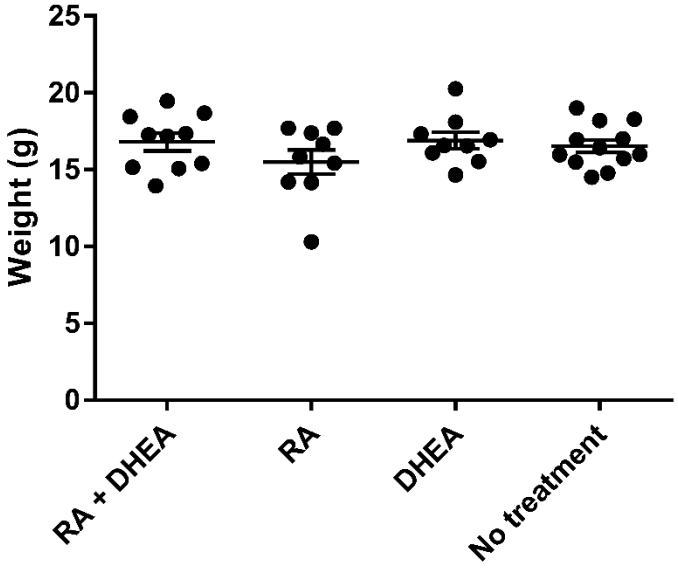
Weight (g)
25
20
15
10
5
0
RA + DHEA
RA
DHEA
No treatment

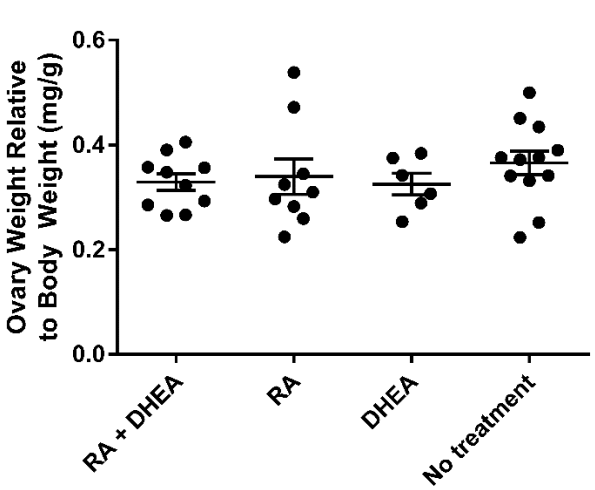
Ovary Weight Relative to Body Weight (mg/g)
0.6
0.4
0.2
0.0
RA + DHEA
RA
DHEA
No treatment

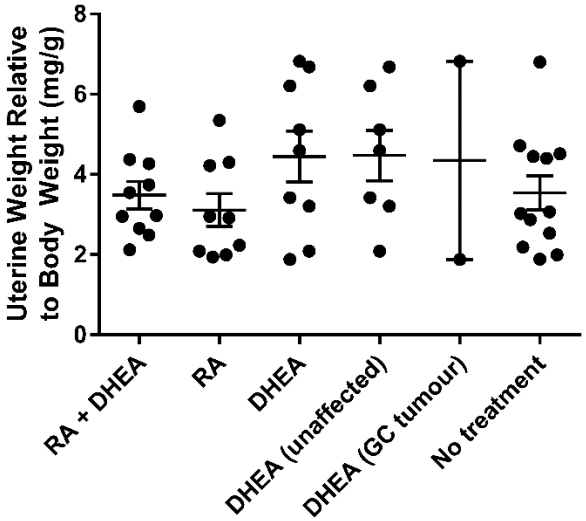
Uterine Weight Relative to Body Weight (mg/g)
8
6
4
2
0
RA + DHEA
RA
DHEA
DHEA (unaffected)
DHEA (GC tumour)
No treatment

**Appendix G: Backcross SSLP genotyping markers.** Primer sequences used to amplify SSLPs for marker-assisted backcrossing of the *Ar*$^{flox}$, *Amhr2*$^{cre}$, *Foxl2*$^{GCE}$, and *ROSA*$^{mT/mG}$ alleles by PCR and their associated *Gct* susceptibility loci, Chr and genomic location, and relative SSLP allele sizes are shown. Data is from Ensembl release 95 (January 2019; Zerbino *et al*. 2018). Relative SSLP sizes were determined from horizontal agarose gel electrophoresis. 129: 129X1 allele; B6: B6J/B6N allele

| Marker Symbol | Forward Sequence (5′→3′) | Reverse Sequence (5′→3′) | Locus Name | Chr and Start of Amplified Region (bp) | Relative SSLP Allele Size |
|---|---|---|---|---|---|
| *D4Mit232* | GCGTCACCACACTGCTCTT | ACTCAGAGTCCCCTGGCC | *Gct1* | 4:145,057,656 | SW < 129, B6 |
| *D12Mit172* | AACTGAAATCGCATTACAAAACC | TAATATTGCGAGTTAGAAATGACCA | *Gct2* | 12:46,113,902 | SW < 129, B6 |
| *D15Mit133* | GTGTGTTTTGTTCTTTGTAGGTGC | TTCCCATACATGTGTAAATGTGC | *Gct3* | 15:64,537,747 | SW < 129, B6 |
| *DXMit96* | CATGTCAATTGGGATCTTTGG | AGGAGCAAATCCAACCTGG | *Gct4* | X:99,231,474 | SW > 129, B6 |
| *D9Mit21* | TATAGTCCATTGTGGCAGAGGAGT | CAGTCCCTGGTTAATAACAACAAC | *Gct5* | 9:57,684,209 | SW < B6 |
| *D9Mit17* | GCCAAGGCTGTCTCTTAGCC | GAGAGAAGGGTTCTGGGCAG | *Gct5* | 9:115,121,809 | SW < 129, B6 |
| *DXamd17* | ACTTGTCCTGTGGCTCCTTT | GATATGCCTGTAATCTCAACACC | *Gct6* | X:137,052,777 | SW > 129 |
| *DXamd22* | CCTTCCCTCTCACTGTGTCC | AATGCCATGGTTTTGCTCAT | *Gct6* | X:137,088,324 | SW > B6 |
| *DXamd11* | AGCAACTGAGGTGGGAGTTG | ACGCAAATATGTGCACGAGT | *Gct6* | X:137,761,427 | SW > B6 |

**Appendix H: Alignment of the SWR, SJL, and B6J *Foxl2* gDNA protein coding consensus nucleotide sequences.** *: identities

```
B6J     ATGATGGCCAGCTACCCCGAGCCCGAAGACACGGCGGGGACCCTGCTGGCTCCGGAGAGC    60
SJL     ATGATGGCCAGCTACCCCGAGCCCGAAGACACGGCGGGGACCCTGCTGGCTCCGGAGAGC    60
SWR     ATGATGGCCAGCTACCCCGAGCCCGAAGACACGGCGGGGACCCTGCTGGCTCCGGAGAGC    60
        ************************************************************

B6J     GGACGCGCAGTCAAAGAGGCCGAGGCGTCGCCGCCGAGTCCCGGCAAGGGAGGCGGGACA    120
SJL     GGACGCGCAGTCAAAGAGGCCGAGGCGTCGCCGCCGAGTCCCGGCAAGGGAGGCGGGACA    120
SWR     GGACGCGCAGTCAAAGAGGCCGAGGCGTCGCCGCCGAGTCCCGGCAAGGGAGGCGGGACA    120
        ************************************************************

B6J     ACACCGGAGAAACCAGACCCCGCGCAGAAGCCCCCGTACTCGTACGTGGCGCTCATCGCC    180
SJL     ACACCGGAGAAACCAGACCCCGCGCAGAAGCCCCCGTACTCGTACGTGGCGCTCATCGCC    180
SWR     ACACCGGAGAAACCAGACCCCGCGCAGAAGCCCCCGTACTCGTACGTGGCGCTCATCGCC    180
        ************************************************************

B6J     ATGGCGATCCGCGAGAGCGCCGAGAAGAGGCTCACTCTGTCCGGCATCTACCAGTACATC    240
SJL     ATGGCGATCCGCGAGAGCGCCGAGAAGAGGCTCACTCTGTCCGGCATCTACCAGTACATC    240
SWR     ATGGCGATCCGCGAGAGCGCCGAGAAGAGGCTCACTCTGTCCGGCATCTACCAGTACATC    240
        ************************************************************

B6J     ATAGCCAAGTTCCCGTTCTACGAGAAGAACAAGAAGGGCTGGCAGAATAGCATCCGCCAC    300
SJL     ATAGCCAAGTTCCCGTTCTACGAGAAGAACAAGAAGGGCTGGCAGAATAGCATCCGCCAC    300
SWR     ATAGCCAAGTTCCCGTTCTACGAGAAGAACAAGAAGGGCTGGCAGAATAGCATCCGCCAC    300
        ************************************************************

B6J     AACCTCAGCCTCAACGAGTGCTTCATCAAGGTGCCGCGCGAGGGCGGCGGCGAGCGCAAG    360
SJL     AACCTCAGCCTCAACGAGTGCTTCATCAAGGTGCCGCGCGAGGGCGGCGGCGAGCGCAAG    360
SWR     AACCTCAGCCTCAACGAGTGCTTCATCAAGGTGCCGCGCGAGGGCGGCGGCGAGCGCAAG    360
        ************************************************************

B6J     GGCAACTACTGGACGCTCGACCCGGCCTGCGAGGACATGTTCGAGAAGGGCAACTACCGG    420
SJL     GGCAACTACTGGACGCTCGACCCGGCCTGCGAGGACATGTTCGAGAAGGGCAACTACCGG    420
SWR     GGCAACTACTGGACGCTCGACCCGGCCTGCGAGGACATGTTCGAGAAGGGCAACTACCGG    420
        ************************************************************

B6J     CGCCGCCGCCGCATGAAGCGGCCCTTCCGGCCGCCGCCCGCTCACTTCCAGCCCGGCAAG    480
SJL     CGCCGCCGCCGCATGAAGCGGCCCTTCCGGCCGCCGCCCGCTCACTTCCAGCCCGGCAAG    480
SWR     CGCCGCCGCCGCATGAAGCGGCCCTTCCGGCCGCCGCCCGCTCACTTCCAGCCCGGCAAG    480
        ************************************************************

B6J     GGGCTCTTCGGGAGCGGAGGAGCGGCGGGTGGCTGCGGCGTGCCCGGAGCTGGGGCCGAT    540
SJL     GGGCTCTTCGGGAGCGGAGGAGCGGCGGGTGGCTGCGGCGTGCCCGGAGCTGGGGCCGAT    540
SWR     GGGCTCTTCGGGAGCGGAGGAGCGGCGGGTGGCTGCGGCGTGCCCGGAGCTGGGGCCGAT    540
        ************************************************************

B6J     GGCTATGGCTACCTGGCGCCACCCAAGTACCTGCAATCGGGGTTCCTCAACAACTCCTGG    600
SJL     GGCTATGGCTACCTGGCGCCACCCAAGTACCTGCAATCGGGGTTCCTCAACAACTCCTGG    600
SWR     GGCTATGGCTACCTGGCGCCACCCAAGTACCTGCAATCGGGGTTCCTCAACAACTCCTGG    600
        ************************************************************


B6J     CCCCTGCCGCAGCCTCCCTCGCCCATGCCCTACGCCTCCTGCCAGATGGCGGCGGCTGCG    660
SJL     CCCCTGCCGCAGCCTCCCTCGCCCATGCCCTACGCCTCCTGCCAGATGGCGGCGGCTGCG    660
SWR     CCCCTGCCGCAGCCTCCCTCGCCCATGCCCTACGCCTCCTGCCAGATGGCGGCGGCTGCG    660
```

```
        ************************************************************

B6J     GCGGCCGCTGCTGCAGCCGCTGCAGCCGCCGGCCCGGGCAGCCCCGGTGCAGCCGCGGTG       720
SJL     GCGGCCGCTGCTGCAGCCGCTGCAGCCGCCGGCCCGGGCAGCCCCGGTGCAGCCGCGGTG       720
SWR     GCGGCCGCTGCTGCAGCCGCTGCAGCCGCCGGCCCGGGCAGCCCCGGTGCAGCCGCGGTG       720
        ************************************************************

B6J     GTCAAGGGGCTGGCGGGCCCCGCCGCCTCCTACGGGCCGTACTCGCGCGTGCAGAGCATG       780
SJL     GTCAAGGGGCTGGCGGGCCCCGCCGCCTCCTACGGGCCGTACTCGCGCGTGCAGAGCATG       780
SWR     GTCAAGGGGCTGGCGGGCCCCGCCGCCTCCTACGGGCCGTACTCGCGCGTGCAGAGCATG       780
        ************************************************************

B6J     GCGCTGCCTCCGGGCGTCGTGAACTCCTACAACGGCCTGGGGGGCCCTCCTGCCGCACCA       840
SJL     GCGCTGCCTCCGGGCGTCGTGAACTCCTACAACGGCCTGGGGGGCCCTCCTGCCGCACCA       840
SWR     GCGCTGCCTCCGGGCGTCGTGAACTCCTACAACGGCCTGGGGGGCCCTCCTGCCGCACCA       840
        ************************************************************

B6J     CCGCCGCCGCCACCGCCGCCGCACCCTCACCCGCACCCTCACGCACATCATCTGCACGCG       900
SJL     CCGCCGCCGCCACCGCCGCCGCACCCTCACCCGCACCCTCACGCACATCATCTGCACGCG       900
SWR     CCGCCGCCGCCACCGCCGCCGCACCCTCACCCGCACCCTCACGCACATCATCTGCACGCG       900
        ************************************************************

B6J     GCCGCTGCGCCCCCGCCAGCCCCGCCACACCACGGGGCTGCCGCGCCTCCCCCGGGTCAG       960
SJL     GCCGCTGCGCCCCCGCCAGCCCCGCCACACCACGGGGCTGCCGCGCCTCCCCCGGGTCAG       960
SWR     GCCGCTGCGCCCCCGCCAGCCCCGCCACACCACGGGGCTGCCGCGCCTCCCCCGGGTCAG       960
        ************************************************************

B6J     CTCAGTCCCGCCAGCCCGGCCACCGCCGCGCCCCCGGCACCCGCGCCCACGAGCGCGCCC      1020
SJL     CTCAGTCCCGCCAGCCCGGCCACCGCCGCGCCCCCGGCACCCGCGCCCACGAGCGCGCCC      1020
SWR     CTCAGTCCCGCCAGCCCGGCCACCGCCGCGCCCCCGGCACCCGCGCCCACGAGCGCGCCC      1020
        ************************************************************

B6J     GGCCTGCAGTTCGCCTGCGCCCGGCAACCCGAGCTCGCCATGATGCATTGCTCATACTGG      1080
SJL     GGCCTGCAGTTCGCCTGCGCCCGGCAACCCGAGCTCGCCATGATGCATTGCTCATACTGG      1080
SWR     GGCCTGCAGTTCGCCTGCGCCCGGCAACCCGAGCTCGCCATGATGCATTGCTCATACTGG      1080
        ************************************************************

B6J     GACCACGACAGCAAGACGGGCGCGCTGCACTCGCGTCTGGATCTCTGA  1128
SJL     GACCACGACAGCAAGACGGGCGCGCTGCACTCGCGTCTGGATCTCTGA  1128
SWR     GACCACGACAGCAAGACGGGCGCGCTGCACTCGCGTCTGGATCTCTGA  1128
        ********************************************
```

**Appendix I: Alignment of the SWR and B6J *Foxl2* cDNA consensus nucleotide sequences.**

*: identities. DHEA: DHEA-treated SWR normal ovary; GC tumour: DHEA-induced SWR GC tumour; untreated: untreated, pubertal SWR normal ovary

```
B6J           CACTCTGTCCGGCATCTACCAGTACATCATAGCCAAGTTCCCGTTCTACGAGAAGAACAA 60
Untreated     CACTCTGTCCGGCATCTACCAGTACATCATAGCCAAGTTCCCGTTCTACGAGAAGAACAA 60
DHEA          CACTCTGTCCGGCATCTACCAGTACATCATAGCCAAGTTCCCGTTCTACGAGAAGAACAA 60
GC Tumour     CACTCTGTCCGGCATCTACCAGTACATCATAGCCAAGTTCCCGTTCTACGAGAAGAACAA 60
              ************************************************************

B6J           GAAGGGCTGGCAGAATAGCATCCGCCACAACCTCAGCCTCAACGAGTGCTTCATCAAGGT 120
Untreated     GAAGGGCTGGCAGAATAGCATCCGCCACAACCTCAGCCTCAACGAGTGCTTCATCAAGGT 120
DHEA          GAAGGGCTGGCAGAATAGCATCCGCCACAACCTCAGCCTCAACGAGTGCTTCATCAAGGT 120
GC Tumour     GAAGGGCTGGCAGAATAGCATCCGCCACAACCTCAGCCTCAACGAGTGCTTCATCAAGGT 120
              ************************************************************

B6J           GCCGCGCGAGGGCGGCGGCGAGCGCAAGGGCAACTACTGGACGCTCGACCCGGCCTGCGA 180
Untreated     GCCGCGCGAGGGCGGCGGCGAGCGCAAGGGCAACTACTGGACGCTCGACCCGGCCTGCGA 180
DHEA          GCCGCGCGAGGGCGGCGGCGAGCGCAAGGGCAACTACTGGACGCTCGACCCGGCCTGCGA 180
GC Tumour     GCCGCGCGAGGGCGGCGGCGAGCGCAAGGGCAACTACTGGACGCTCGACCCGGCCTGCGA 180
              ************************************************************

B6J           GGACATGTTCGAGAAGGGCAACTACCGGCGCCGCCGCCGCCGCATGAAGCGGCCCTTCCGGCC 240
Untreated     GGACATGTTCGAGAAGGGCAACTACCGGCGCCGCCGCCGCCGCATGAAGCGGCCCTTCCGGCC 240
DHEA          GGACATGTTCGAGAAGGGCAACTACCGGCGCCGCCGCCGCCGCATGAAGCGGCCCTTCCGGCC 240
GC Tumour     GGACATGTTCGAGAAGGGCAACTACCGGCGCCGCCGCCGCCGCATGAAGCGGCCCTTCCGGCC 240
              ************************************************************

B6J           GCCGCCCGCTCACTTCCAGCCCGGCAAGGGGCTCTTCGGGAGCGGAGGAGCGGCGGGTGG 300
Untreated     GCCGCCCGCTCACTTCCAGCCCGGCAAGGGGCTCTTCGGGAGCGGAGGAGCGGCGGGTGG 300
DHEA          GCCGCCCGCTCACTTCCAGCCCGGCAAGGGGCTCTTCGGGAGCGGAGGAGCGGCGGGTGG 300
GC Tumour     GCCGCCCGCTCACTTCCAGCCCGGCAAGGGGCTCTTCGGGAGCGGAGGAGCGGCGGGTGG 300
              ************************************************************

B6J           CTGCGGCGTGCCCGGAGCTGGGGCCGATGGCTATGGCTACCTGGCGCCACCCAAGTACCT 360
Untreated     CTGCGGCGTGCCCGGAGCTGGGGCCGATGGCTATGGCTACCTGGCGCCACCCAAGTACCT 360
DHEA          CTGCGGCGTGCCCGGAGCTGGGGCCGATGGCTATGGCTACCTGGCGCCACCCAAGTACCT 360
GC Tumour     CTGCGGCGTGCCCGGAGCTGGGGCCGATGGCTATGGCTACCTGGCGCCACCCAAGTACCT 360
              ************************************************************

B6J           GC         362
Untreated     GC         362
DHEA          GC         362
GC Tumour     GC         362
              **
```